



**Influence of Leading Edge Oscillatory Blowing
on Time-Accurate Dynamic Store Separation**

THESIS

Saunders, Ryan G., 2d Lt, USAF
AFIT-ENY-MS-19-M-244

**DEPARTMENT OF THE AIR FORCE
AIR UNIVERSITY**

AIR FORCE INSTITUTE OF TECHNOLOGY

Wright-Patterson Air Force Base, Ohio

DISTRIBUTION STATEMENT A
APPROVED FOR PUBLIC RELEASE; DISTRIBUTION UNLIMITED.

The views expressed in this document are those of the author and do not reflect the official policy or position of the United States Air Force, the United States Department of Defense or the United States Government. This material is declared a work of the U.S. Government and is not subject to copyright protection in the United States.

AFIT-ENY-MS-19-M-244

INFLUENCE OF LEADING EDGE OSCILLATORY BLOWING ON
TIME-ACCURATE DYNAMIC STORE SEPARATION

THESIS

Presented to the Faculty
Department of Aeronautics and Astronautics
Graduate School of Engineering and Management
Air Force Institute of Technology
Air University
Air Education and Training Command
in Partial Fulfillment of the Requirements for the
Degree of Master of Science (Aerospace Engineering)

Saunders, Ryan G., BS

2d Lt, USAF

21 March 2019

DISTRIBUTION STATEMENT A
APPROVED FOR PUBLIC RELEASE; DISTRIBUTION UNLIMITED.

AFIT-ENY-MS-19-M-244

INFLUENCE OF LEADING EDGE OSCILLATORY BLOWING ON
TIME-ACCURATE DYNAMIC STORE SEPARATION

THESIS

Saunders, Ryan G., BS
2d Lt, USAF

Committee Membership:

Dr. Mark F. Reeder
Chair

Dr. Donald L. Kunz
Member

Lt Col Jacob A. Freeman
Member

Abstract

The primary objective of this research is to support the static and dynamic characterization and the time-accurate dynamic load data acquisition of store separation from a cavity with leading edge oscillatory blowing. Developing an understanding of, and potentially controlling, pitch bifurcation of a store release is a motivation for this research. The apparatus and data acquisition system was used in a two-part experiment to collect both static and dynamic testing data in the AFIT low speed wind tunnel in speeds of 60, 100, and 120 mph, from Reynolds numbers varying from 5.5×10^4 to 4.6×10^5 , depending on reference length and tunnel speed. An ATI Nano25 6-DOF force and moment sensor was used to produce time-accurate force and moment measurements. Common aerodynamic trends were observed in the comparison of trials with different store model sizes and angles of attack which align with established aerodynamic analysis. The 5 Hz oscillatory flow control, using multiple flow control approaches, had a direct impact on the forces experienced by the mission store and a 5 Hz pattern in the data was observed in static positions as well as before and after store release. Data collected for the normal force, pitch moment, and axial force coefficients depict the aerodynamic loads of a store release from a cavity environment with a developed shear layer. Phase manipulation of relative linear motor positions allowed for data collection under varying store release conditions and timings. A 180° out of phase phenomena was observed in the normal force coefficient in cases where the position of the motor was also 180° out of phase.

I would first like to thank my mother and father for generally providing support and guidance throughout this trial. Their unconditional love has given me strength over the years. I would also like to thank my siblings, close friends, and loved ones for their understanding, advice, and support in this challenge.

Acknowledgements

Lt Saunders would like to extend gratitude to his thesis advisor, Dr. Mark Reeder, for providing guidance and insight throughout the thesis writing process. Dr. Reeder supplied valuable knowledge involving the concepts, mechanisms, and significance of this research. Lt Saunders would like to thank the committee members for this thesis for taking the time to provide feedback and additional guidance. Lt Saunders would also like to acknowledge the efforts of Capt Matt Wood, USMC, who conducted previous research on the same topic. His work resulted in a great reference and starting point for this research. Finally, Lt Saunders would like to personally thank Mr. Josh DeWitt of the AFIT labs for going above and beyond in helping with the research. Without Mr. DeWitt's assistance, completing the data collection would not have been possible.

Saunders, Ryan G.

Table of Contents

	Page
Abstract	iv
Acknowledgements	vi
List of Figures	x
List of Tables	xxxi
List of Symbols	xxxiv
List of Abbreviations	xxxvi
I. Introduction	1
1.1 Background and Motivation	1
1.2 Problem Statement	2
1.3 Methodology	3
1.4 Limitations	5
1.5 Overview of Subsequent Chapters	5
II. Literature Review	7
2.1 Chapter Overview	7
2.2 Cavity Aeroacoustics	7
2.2.1 History of the Aeroacoustic Environment	7
2.2.2 Classifications of Cavities	12
2.3 Open Flow Phenomena	13
2.4 Store Separation Effects	15
2.5 Oscillatory Blowing	18
2.6 Dynamic Wind Tunnel Testing	20
2.7 Configuration of Rigs	22
2.8 Experimental Measurements	23
2.9 Chapter Summary	24
III. Methodology	25
3.1 Introduction	25
3.2 AFIT Wind Tunnel	25
3.3 Linear Motion Apparatus	26
3.3.1 Design Overview	26
3.3.2 Rig Configurations	27
3.3.3 Motor Control System	27
3.4 Experimental Models	29

	Page
3.4.1 3D Printer Rapid Prototyping	29
3.4.2 Piston and Sleeve Design	30
3.4.3 Leading Edge Blowing Devices	31
3.4.4 Support Sting	34
3.4.5 Angle of Attack Base Plate	36
3.4.6 Mission Store Model	38
3.5 Wind Tunnel Apparatuses and Mechanical Components	42
3.5.1 Freestream Apparatus	42
3.5.2 Cavity Apparatus	42
3.5.3 Linear Motor	43
3.5.4 Controller	44
3.5.5 Controller Programming and Operation	45
3.5.6 Nano25 Force and Torque Transducer	46
3.6 Overview of Experimental Setup	49
3.7 Phase I: Static Wind Tunnel Tests	50
3.7.1 Trials and Variables	50
3.7.2 Post Processing Phase I	52
3.7.3 Repeatability of Static Trials	56
3.8 Phase II: Dynamic Wind Tunnel Tests	60
3.8.1 Trials and Variables	60
3.8.2 Triggering the Trajectory Motion	60
3.8.3 Timing of Mission Store Release	61
3.8.4 Post Processing Phase II	64
3.8.5 Repeatability of Dynamic Trials	66
3.9 Reynolds number	70
3.10 Summary	71
IV. Results and Analysis	73
4.1 Overview of Results and Analysis	73
4.2 Phase I : Static Wind Tunnel Testing	74
4.2.1 Freestream Apparatus Data Analysis	74
4.2.2 Cavity Apparatus Data Analysis	92
4.2.3 Cavity Apparatus with Flow Control	113
4.3 Phase II: Dynamic Mission Store Release	126
4.3.1 Tare Example	126
4.3.2 Normal Force Coefficient Trajectory Analysis	128
4.3.3 Pitch Moment Coefficient Trajectory Analysis	139
4.3.4 Axial Force Coefficient Trajectory Analysis	143
4.3.5 Comparison of Flow Control Devices	148
4.4 Summary of Results	152

	Page
V. Conclusions and Recommendations	154
5.1 Scope of Testing.....	154
5.2 Summary of Results	155
5.3 Significance of Research	157
5.4 Recommendation for future testing	158
Appendix A. Test Matrices	161
Appendix B. Additional Experimental Data	170
Appendix C. Galil and Matlab Code	383
Appendix D. Drawings of Models	448
Bibliography	452

List of Figures

Figure		Page
1	Fully assembled cavity representing the modified SUU-41 pod [8].	4
2	Typical Oscillation Cycle [13]	10
3	An example of the pressure magnitudes as a function of distance from the leading edge data, a pseudopiston analogy [14]	11
4	Depictions of the different flow field types based upon the varying dimensions of L/D [18]	13
5	Cavity flow feedback loop depiction	14
6	Illustration of how the quasi-steady assumption of CTS neither captures the time-dependent forces of the unsteady shear layer, nor allows for accurate prediction of store separation [20]	16
7	The effect of release time on trajectory based upon a 3-dimensional CFD model [24]	17
8	AFIT Wind Tunnel (Not to Scale) [8]	26
9	Freestream apparatus inside the AFIT low-speed wind tunnel	28
10	Cavity apparatus inside the AFIT low-speed wind tunnel	29
11	Piston for the leading edge blower [8]	30
12	Cylinder for the leading edge blower and support mount [8]	31
13	Example of the channel of the slot sliding onto the sleeve. [8]	32
14	Example of a fluidic diode opening. [8]	33
15	Internal view of the slot leading edge blower [8]	33
16	Internal view of the Diode 2 leading edge blower [8]	34

Figure		Page
17	Flat portion of vertical rod	35
18	Flat portion of vertical rod which allows for the rod to be secured to the linear motor	36
19	Mounting block connecting the vertical rod and the linear motor, and the arrows show how the height of the rod can easily be adjusted	37
20	Side view of angle of attack plate showing the top screw that secures the plate to the rod	39
21	Angle of attack plate (furthest left) secured to both the Nano25 sensor and the mission store model	40
22	Small mission store model length of 9 inches and diameter of 1.3 inches	40
23	Large mission store model length of 12 inches and diameter of 1.7 inches	41
24	3D printed piece that holds the linear motor wires to the side of the cavity so the wires don't hit the vertical rod and impacting the force measurements	43
25	SRS-003-04-003-01 Linear Motor used for the experimental study [8]	44
26	Galil DMC-4020 dual-axis motion controller [8]	45
27	Direction of measurements made by the Nano25 sensor [8]	48
28	Direction of measurements made by the Nano25 sensor [8]	49
29	Calibration matrix of Nano25 model FTI-15790 [8]	49
30	Lowest position of mission store in the cavity apparatus	52
31	Shear layer, or midpoint, position of mission store in the cavity apparatus	53
32	Highest position of mission store in the cavity apparatus	54
33	Example of matlab filtering and a normal force coefficient plot. The coefficient value is plotted by the blue line and filtered data is plotted by the red line	56

Figure		Page
34	Static normal force repeatability, large model, 10° AoA, tare and mean.....	57
35	Repeatability of static normal force coefficients at 10° AoA in the cavity apparatus, large model, all wind speeds.....	59
36	Representation of the verification of encoder positions using a high speed camera.....	63
37	Encoder position plots verifying the release positions of both linear motors.	64
38	Phantom Mirolab 3a10 high speed camera used to record trials.....	65
39	Tare plots of Normal Force, before data alignment on the left and after data alignment on the right.....	66
40	Dynamic normal force repeatability, large model, 10° AoA, tare and mean	67
41	Repeatability of dynamic normal force coefficients at 10° AoA in the cavity apparatus, large model, all wind speeds, all are the first release timing.....	69
42	Graphs of normal force and axial force coefficients in the freestream apparatus, small model, 10°, all wind speeds.....	78
43	Graphs of pitch moment coefficient and standard deviations of coefficients in the freestream apparatus, small model, 10°, all wind speeds	79
44	Comparison of the difference in wind speeds of the normal force coefficient for the freestream apparatus, small model.....	80
45	Comparison of the difference in wind speeds of the normal force coefficient for the freestream apparatus, large model	81
46	Comparison of the difference model sizes at 0 AoA of the normal force coefficient for the freestream apparatus, 60 mph.....	84

Figure		Page
47	Comparison of the difference model sizes at 0 AoA of the normal force coefficient for the freestream apparatus, 100 mph	85
48	Comparison of the difference model sizes at 0° AoA of the pitch moment coefficient for the freestream apparatus, 60 mph	87
49	Comparison of the difference model sizes at 10° AoA of the pitch moment coefficient for the freestream apparatus, 60 mph	88
50	Comparison of the difference model sizes at 0° AoA of the pitch moment coefficient for the freestream apparatus, 60 mph	90
51	Comparison of the difference model sizes at 10° AoA of the pitch moment coefficient for the freestream apparatus, 60 mph	91
52	Example of tare and tared data for force coefficients of the small model at 10° AoA in the cavity apparatus, 60 mph	93
53	Axial Force Coefficient, cavity apparatus, large model, 10° AoA, 120 mph, shear position, tare	94
54	Example of filtered coefficients for all coefficients of the small model at 10° AoA in the cavity apparatus, 60 mph	95
55	All coefficients at all wind speeds for the small model at 10° AoA in the cavity apparatus, in cavity position	99
56	All coefficients at all wind speeds for the small model at 10° AoA in the cavity apparatus, shear position	102
57	All coefficients at all wind speeds for the small model at 10° AoA in the cavity apparatus, outside cavity position	105
58	All wind speeds for the small model at 10° AoA in the cavity apparatus, all cavity positions. The “freestream” label in the figure actually means the “out of cavity” position	107

Figure	Page
59	Comparison of normal force coefficients with different model sizes at 0° AoA, 120 mph, all positions 110
60	Comparison of normal force coefficients with different model sizes at 0° AoA, 120 mph, all positions 112
61	All positions for the small model at 10° AoA in the cavity apparatus, 120 mph, with flow control 115
62	All wind speeds for the small model at 10° AoA in the cavity apparatus, all cavity position, flow control. The “freestream” label in the figure actually means the “out of cavity” position 118
63	Comparison of the difference model sizes at 0° AoA of the normal force coefficient, cavity apparatus, all positions, 120 mph. The “freestream” label in the figure actually means the “out of cavity” position 121
64	Comparison of different model sizes at 10° AoA of the normal force coefficient, cavity apparatus, all positions, 120 mph. The “freestream” label in the figure actually means the “out of cavity” position 122
65	Comparison of normal force coefficients with flow control devices at 10° AoA, small model, 120 mph, all positions. The “freestream” label in the figure actually means the “out of cavity” position 124
66	Comparison of normal force coefficients with flow control devices at 10° AoA, large model, 120 mph, all positions. The “freestream” label in the figure actually means the “out of cavity” position 125
67	Examples of dynamic tared data of all coefficients for the small model at 10° AoA in the cavity apparatus 127
68	Axial Force Coefficient, cavity apparatus, small model, 10° AoA, slot, 120 mph, tare 128
69	Normal Force Coefficient, cavity apparatus, small model, 10 degrees angle of attack, slot, 120 mph 129

Figure		Page
70	Comparison of dynamic normal force coefficients with different model sizes at 0° AoA, 120 mph, all release timings	132
71	Comparison of dynamic normal force coefficients with different model sizes at 10° AoA, 120 mph, all release timings	133
72	Zoomed, filtered values for normal force coefficients of all four timings, small model, 10° AoA, 120 mph, slot	137
73	Zoomed, filtered values for normal force coefficients of all four timings, large model, 10° AoA, 120 mph, slot	138
74	Pitch Moment Coefficient, cavity apparatus, small model, 10 degrees angle of attack, slot, 120 mph	139
75	Comparison of dynamic normal force coefficients with different model sizes at 0° AoA, 120 mph, all release timings	141
76	Comparison of dynamic normal force coefficients with different model sizes at 10° AoA, 120 mph, all release timings	142
77	Axial Force Coefficient, cavity apparatus, small model, 10 degrees angle of attack, slot, 120 mph	143
78	Comparison of dynamic normal force coefficients with different model sizes at 0° AoA, 120 mph, all release timings	145
79	Zoomed, filtered values for normal force coefficients of all four timings, large model, 10° AoA, 120 mph, slot	147
80	Comparison of dynamic normal force coefficients with flow control devices at 10° AoA, large model, 60 mph, all release timings	150
81	Comparison of dynamic normal force coefficients with flow control devices at 10° AoA, large model, 120 mph, all release timings	151
82	Drawing of heights of models measured from the floor of the cavity, "In Cavity" position	171

Figure		Page
83	Drawing of heights of models measured from the floor of the cavity, “Shear Layer” position	172
84	Drawing of heights of models measured from the floor of the cavity, “Out of Cavity” position	173
85	Small model at 0° AoA of the pitch moment and axial force coefficients for the freestream apparatus, 100 MPH	174
86	Small model at 10° AoA of the pitch moment and axial force coefficients for the freestream apparatus, 100 MPH	175
87	Large model at 0° AoA of the pitch moment and axial force coefficients for the freestream apparatus, 100 MPH	176
88	Large model at 10° AoA of the pitch moment and axial force coefficients for the freestream apparatus, 100 MPH	177
89	Large model at 10° AoA of the pitch moment and axial force coefficients for the freestream apparatus, 120 MPH	178
90	Small model at 0° AoA of the pitch moment and axial force coefficients for the cavity apparatus, 60 MPH	179
91	Small model at 0° AoA of the pitch moment and axial force coefficients for the cavity apparatus, 100 MPH	180
92	Small model at 0° AoA of the pitch moment and axial force coefficients for the cavity apparatus, 120 MPH	181
93	Small model at 0° AoA of the normal force coefficients for the cavity apparatus, 60 MPH and 100 MPH	182
94	Large model at 0° AoA of the pitch moment and axial force coefficients for the cavity apparatus, 60 MPH	183
95	Large model at 0° AoA of the pitch moment and axial force coefficients for the cavity apparatus, 100 MPH	184
96	Large model at 0° AoA of the pitch moment and axial force coefficients for the cavity apparatus, 120 MPH	185
97	Large model at 0° AoA of the normal force coefficients for the cavity apparatus, 60 MPH and 100 MPH	186

Figure		Page
98	Large model at 10° AoA of the pitch moment and axial force coefficients for the cavity apparatus, 60 MPH	187
99	Large model at 10° AoA of the pitch moment and axial force coefficients for the cavity apparatus, 100 MPH	188
100	Large model at 10° AoA of the pitch moment and axial force coefficients for the cavity apparatus, 120 MPH	189
101	Large model at 10° AoA of the normal force coefficients for the cavity apparatus, 60 MPH and 100 MPH	190
102	Small model at 0° AoA of the pitch moment and normal force coefficients for various positions, slot, 60 MPH	191
103	Small model at 0° AoA of the pitch moment and axial force coefficients for various positions, flow control, slot, 100 MPH	192
104	Small model at 0° AoA of the pitch moment and axial force coefficients for various positions, flow control, slot, 120 MPH	193
105	Small model at 0° AoA of the normal force coefficient for various positions, flow control, slot, 100 MPH and 120 MPH	194
106	Small model at 10° AoA of the pitch moment and normal force coefficients for various positions, flow control, slot, 60 MPH	195
107	Small model at 10° AoA of the pitch moment and normal force coefficients for various positions, flow control, slot, 100 MPH	196
108	Small model at 10° AoA of the pitch moment and axial force coefficients for various positions, flow control, slot, 120 MPH	197
109	Normal Force Coefficient, all positions, flow control, small model, 10° AoA, slot, 120 MPH	198
110	Large model at 0° AoA of the pitch moment and normal force coefficients for various positions, flow control, slot, 60 MPH	199

Figure		Page
111	Large model at 0° AoA of the pitch moment and axial force coefficients for various positions, flow control, slot, 100 MPH	200
112	Large model at 0° AoA of the pitch moment and axial force coefficients for various positions, flow control, slot, 120 MPH	201
113	Large model at 0° AoA of the normal force coefficient for various positions, flow control, slot, 100 MPH and 120 MPH	202
114	Large model at 10° AoA of the pitch moment and normal force coefficients for various positions, flow control, slot, 60 MPH	203
115	Large model at 10° AoA of the pitch moment and axial force coefficients for various positions, flow control, slot, 100 MPH	204
116	Large model at 10° AoA of the pitch moment and axial force coefficients for various positions, flow control, slot, 120 MPH	205
117	Large model at 10° AoA of the normal force coefficients for various positions, flow control, slot, 100 MPH and 120 MPH	206
118	Small model at 0° AoA of the pitch moment and normal force coefficients for various positions, flow control, diode 2, 60 MPH	207
119	Small model at 0° AoA of the pitch moment and axial force coefficients for various positions, flow control, diode 2, 100 MPH	208
120	Small model at 0° AoA of the pitch moment and axial force coefficients for various positions, flow control, diode 2, 120 MPH	209
121	Small model at 0° AoA of the normal force coefficient for various positions, flow control, diode 2, 100 MPH and 120 MPH	210

Figure		Page
122	Small model at 10° AoA of the pitch moment and normal force coefficients for various positions, flow control, diode 2, 60 MPH	211
123	Small model at 10° AoA of the pitch moment and normal force coefficients for various positions, flow control, diode 2, 100 MPH	212
124	Small model at 10° AoA of the pitch moment and axial force coefficients for various positions, flow control, diode 2, 120 MPH	213
125	Normal Force Coefficient, all positions, flow control, small model, 10° AoA, diode 2, 120 MPH	214
126	Large model at 0° AoA of the pitch moment and normal force coefficients for various positions, flow control, diode 2, 60 MPH	215
127	Large model at 0° AoA of the pitch moment and axial force coefficients for various positions, flow control, diode 2, 100 MPH	216
128	Large model at 0° AoA of the pitch moment and axial force coefficients for various positions, flow control, diode 2, 120 MPH	217
129	Large model at 0° AoA of the normal force coefficient for various positions, flow control, diode 2, 100 MPH and 120 MPH	218
130	Large model at 10° AoA of the pitch moment and normal force coefficients for various positions, flow control, diode 2, 60 MPH	219
131	Large model at 10° AoA of the pitch moment and normal force coefficients for various positions, flow control, diode 2, 100 MPH	220
132	Large model at 10° AoA of the pitch moment and axial force coefficients for various positions, flow control, diode 2, 120 MPH	221
133	Normal Force Coefficient, all positions, flow control, large model, 10° AoA, diode 2, 120 MPH	222

Figure	Page
134	Small model at 0° AoA of the pitch moment and normal force coefficients, dynamic release, slot, 60 MPH 223
135	Small model at 0° AoA of the pitch moment and axial force coefficients, dynamic release, slot, 100 MPH 224
136	Normal Force Coefficient, dynamic release, small model, 0° AoA, slot, 100 MPH 225
137	Small model at 10° AoA of the pitch moment and normal force coefficients, dynamic release, slot, 60 MPH 226
138	Small model at 10° AoA of the pitch moment and normal force coefficients, dynamic release, slot, 100 MPH 227
139	Small model at 0° AoA of the pitch moment and normal force coefficients, dynamic release, diode 2, 60 MPH 228
140	Small model at 0° AoA of the pitch moment and normal force coefficients, dynamic release, diode 2, 100 MPH 229
141	Small model at 0° AoA of the pitch moment and normal force coefficients, dynamic release, diode 2, 120 MPH 230
142	Normal Force Coefficient, dynamic release, small model, 0° AoA, diode 2, 100 MPH 231
143	Small model at 10° AoA of the pitch moment and normal force coefficients, dynamic release, diode 2, 60 MPH 232
144	Small model at 10° AoA of the pitch moment and normal force coefficients, dynamic release, diode 2, 100 MPH 233
145	Small model at 10° AoA of the pitch moment and normal force coefficients, dynamic release, diode 2, 120 MPH 234
146	Normal Force Coefficient, dynamic release, small model, 10° AoA, diode 2, 100 MPH 235
147	Large model at 0° AoA of the pitch moment and normal force coefficients, dynamic release, slot, 60 MPH 236

Figure	Page
148	Large model at 0° AoA of the pitch moment and normal force coefficients, dynamic release, slot, 100 MPH 237
149	Pitch Moment Coefficient, dynamic release, large model, 10° AoA, slot, 60 MPH 238
150	Large model at 0° AoA of the pitch moment and normal force coefficients, dynamic release, diode 2, 60 MPH 239
151	Large model at 0° AoA of the pitch moment and normal force coefficients, dynamic release, diode 2, 100 MPH 240
152	Large model at 0° AoA of the pitch moment and normal force coefficients, dynamic release, diode 2, 120 MPH 241
153	Large model at 0° AoA of the pitch moment and normal force coefficients, dynamic release, diode 2, 120 MPH 242
154	Large model at 10° AoA of the pitch moment and normal force coefficients, dynamic release, diode 2, 100 MPH 243
155	Large model at 10° AoA of the pitch moment and normal force coefficients, dynamic release, diode 2, 120 MPH 244
156	Repeatability of static coefficients, large model, 10° AoA, diode 2, 0 MPH, 10 trials 246
157	Repeatability of static coefficients, in cavity position, 10° AoA, diode 2, 120 MPH 247
158	Repeatability of static coefficients, shear position, 10° AoA, diode 2, 120 MPH 248
159	Repeatability of static coefficients, out of cavity position, 10° AoA, diode 2, 120 MPH 249
160	Repeatability of dynamic coefficients, large model, 10° AoA, diode 2, 0 MPH, 10 trials 250
161	Repeatability of dynamic coefficients, large model, 10° AoA, diode 2, 60 MPH, 10 trials 251
162	Repeatability of dynamic coefficients, large model, 10° AoA, diode 2, 60 MPH, 10 trials 252

Figure		Page
163	Repeatability of dynamic coefficients, large model, 10° AoA, diode 2, 100 MPH, 10 trials	253
164	Repeatability of dynamic coefficients, large model, 10° AoA, diode 2, 120 MPH, 10 trials	254
165	Small model at 10° AoA of the normal force coefficient, 120 MPH, tare	256
166	Small model at 10° AoA of the pitch moment and normal force coefficients, 120 MPH, tare	257
167	Small model at 10° AoA of the pitch moment coefficient, 120 MPH, tare	258
168	Small model at 10° AoA of the Axial Force coefficient, 120 MPH, tare	259
169	Small model at 10° AoA of the axial force and normal force coefficients, 120 MPH, tare	260
170	Small model at 10° AoA of the normal force coefficient, 120 MPH, slot, tare	261
171	Small model at 10° AoA of the pitch moment coefficient, 120 MPH, slot, tare	262
172	Small model at 10° AoA of the pitch moment and axial force coefficients, 120 MPH, slot, tare	263
173	Small model at 10° AoA of the axial force coefficient, 120 MPH, slot, tare	264
174	Large model at 10° AoA of the normal force coefficient, 120 MPH, tare	266
175	Large model at 10° AoA of the pitch moment and normal force coefficients, 120 MPH, tare	267
176	Large model at 10° AoA of the pitch moment coefficient, 120 MPH, tare	268
177	Large model at 10° AoA of the Axial Force coefficient, 120 MPH, tare	269

Figure		Page
178	Large model at 10° AoA of the axial force and normal force coefficients, 120 MPH, tare	270
179	Large model at 10° AoA of the normal force coefficient, 120 MPH, slot, tare	271
180	Large model at 10° AoA of the pitch moment coefficient, 120 MPH, slot, tare	272
181	Large model at 10° AoA of the pitch moment and axial force coefficients, 120 MPH, slot, tare	273
182	Large model at 10° AoA of the axial force coefficient, 120 MPH, slot, tare	274
183	Small model at 10° AoA of the normal force coefficient, release times one and two, 120 MPH, tare	276
184	Small model at 10° AoA of the normal force coefficient, release times three and four, 120 MPH, tare	277
185	Small model at 10° AoA of the pitch moment coefficient, release times one and two, 120 MPH, tare	278
186	Small model at 10° AoA of the pitch moment coefficient, release times three and four, 120 MPH, tare	279
187	Small model at 10° AoA of the axial force coefficient, release times one and two, 120 MPH, tare	280
188	Small model at 10° AoA of the axial force coefficient, release times three and four, 120 MPH, tare	281
189	Large model at 10° AoA of the normal force coefficient, release times one and two, 120 MPH, tare	283
190	Large model at 10° AoA of the normal force coefficient, release times three and four, 120 MPH, tare	284
191	Large model at 10° AoA of the pitch moment coefficient, release times one and two, 120 MPH, tare	285
192	Large model at 10° AoA of the pitch moment coefficient, release times three and four, 120 MPH, tare	286

Figure		Page
193	Large model at 10° AoA of the axial force coefficient, release times one and two, 120 MPH, tare	287
194	Large model at 10° AoA of the axial force coefficient, release times three and four, 120 MPH, tare	288
195	Small model at 10° AoA of the normal force coefficient, 120 MPH, individual trial	289
196	Small model at 10° AoA of the pitch moment and normal force coefficients, 120 MPH, individual trial	290
197	Small model at 10° AoA of the pitch moment coefficient, 120 MPH, individual trial	291
198	Small model at 10° AoA of the Axial Force coefficient, 120 MPH, individual trial	292
199	Small model at 10° AoA of the axial force and normal force coefficients, 120 MPH, individual trial	293
200	Small model at 10° AoA of the normal force coefficient, 120 MPH, slot, individual trial	294
201	Small model at 10° AoA of the pitch moment coefficient, 120 MPH, slot, individual trial	295
202	Small model at 10° AoA of the pitch moment and axial force coefficients, 120 MPH, slot, individual trial	296
203	Small model at 10° AoA of the axial force coefficient, 120 MPH, slot, individual trial	297
204	Large model at 10° AoA of the normal force coefficient, 120 MPH, individual trial	298
205	Large model at 10° AoA of the pitch moment and normal force coefficients, 120 MPH, individual trial	299
206	Large model at 10° AoA of the pitch moment coefficient, 120 MPH, individual trial	300
207	Large model at 10° AoA of the Axial Force coefficient, 120 MPH, individual trial	301

Figure		Page
208	Large model at 10° AoA of the axial force and normal force coefficients, 120 MPH, individual trial	302
209	Large model at 10° AoA of the normal force coefficient, 120 MPH, slot, individual trial	303
210	Large model at 10° AoA of the pitch moment coefficient, 120 MPH, slot, individual trial	304
211	Large model at 10° AoA of the pitch moment and axial force coefficients, 120 MPH, slot, individual trial	305
212	Large model at 10° AoA of the axial force coefficient, 120 MPH, slot, individual trial	306
213	Small model at 10° AoA of the normal force coefficient, release times one and two, 120 MPH, individual trial	307
214	Small model at 10° AoA of the normal force coefficient, release times three and four, 120 MPH, individual trial	308
215	Small model at 10° AoA of the pitch moment coefficient, release times one and two, 120 MPH, individual trial	309
216	Small model at 10° AoA of the pitch moment coefficient, release times three and four, 120 MPH, individual trial	310
217	Small model at 10° AoA of the axial force coefficient, release times one and two, 120 MPH, individual trial	311
218	Small model at 10° AoA of the axial force coefficient, release times three and four, 120 MPH, individual trial	312
219	Large model at 10° AoA of the normal force coefficient, release times one and two, 120 MPH, individual trial	313
220	Large model at 10° AoA of the normal force coefficient, release times three and four, 120 MPH, individual trial	314
221	Large model at 10° AoA of the pitch moment coefficient, release times one and two, 120 MPH, individual trial	315
222	Large model at 10° AoA of the pitch moment coefficient, release times three and four, 120 MPH, individual trial	316

Figure		Page
223	Large model at 10° AoA of the axial force coefficient, release times one and two, 120 MPH, individual trial	317
224	Large model at 10° AoA of the axial force coefficient, release times three and four, 120 MPH, individual trial	318
225	Small model at 0° AoA of the normal force coefficient, 120 MPH, tare	320
226	Small model at 0° AoA of the pitch moment and normal force coefficients, 120 MPH, tare	321
227	Small model at 0° AoA of the pitch moment coefficient, 120 MPH, tare	322
228	Small model at 0° AoA of the Axial Force coefficient, 120 MPH, tare	323
229	Small model at 0° AoA of the axial force and normal force coefficients, 120 MPH, tare	324
230	Small model at 0° AoA of the normal force coefficient, 120 MPH, slot, tare	325
231	Small model at 0° AoA of the pitch moment coefficient, 120 MPH, slot, tare	326
232	Small model at 0° AoA of the pitch moment and axial force coefficients, 120 MPH, slot, tare.....	327
233	Small model at 0° AoA of the axial force coefficient, 120 MPH, slot, tare.....	328
234	Large model at 0° AoA of the normal force coefficient, 120 MPH, tare	330
235	Large model at 0° AoA of the pitch moment and normal force coefficients, 120 MPH, tare	331
236	Large model at 0° AoA of the pitch moment coefficient, 120 MPH, tare	332
237	Large model at 0° AoA of the Axial Force coefficient, 120 MPH, tare	333

Figure	Page
238	Large model at 0° AoA of the axial force and normal force coefficients, 120 MPH, tare 334
239	Large model at 0° AoA of the normal force coefficient, 120 MPH, slot, tare 335
240	Large model at 0° AoA of the pitch moment coefficient, 120 MPH, slot, tare 336
241	Large model at 0° AoA of the pitch moment and axial force coefficients, 120 MPH, slot, tare 337
242	Large model at 0° AoA of the axial force coefficient, 120 MPH, slot, tare 338
243	Small model at 0° AoA of the normal force coefficient, release times one and two, 120 MPH, tare 340
244	Small model at 0° AoA of the normal force coefficient, release times three and four, 120 MPH, tare 341
245	Small model at 0° AoA of the pitch moment coefficient, release times one and two, 120 MPH, tare 342
246	Small model at 0° AoA of the pitch moment coefficient, release times three and four, 120 MPH, tare 343
247	Small model at 0° AoA of the axial force coefficient, release times one and two, 120 MPH, tare 344
248	Small model at 0° AoA of the axial force coefficient, release times three and four, 120 MPH, tare 345
249	Large model at 0° AoA of the normal force coefficient, release times one and two, 120 MPH, tare 347
250	Large model at 0° AoA of the normal force coefficient, release times three and four, 120 MPH, tare 348
251	Large model at 0° AoA of the pitch moment coefficient, release times one and two, 120 MPH, tare 349
252	Large model at 0° AoA of the pitch moment coefficient, release times three and four, 120 MPH, tare 350

Figure		Page
253	Large model at 0° AoA of the axial force coefficient, release times one and two, 120 MPH, tare	351
254	Large model at 0° AoA of the axial force coefficient, release times three and four, 120 MPH, tare	352
255	Small model at 0° AoA of the normal force coefficient, 120 MPH, individual trial	353
256	Small model at 0° AoA of the pitch moment and normal force coefficients, 120 MPH, individual trial	354
257	Small model at 0° AoA of the pitch moment coefficient, 120 MPH, individual trial	355
258	Small model at 0° AoA of the Axial Force coefficient, 120 MPH, individual trial	356
259	Small model at 0° AoA of the axial force and normal force coefficients, 120 MPH, individual trial	357
260	Small model at 0° AoA of the normal force coefficient, 120 MPH, slot, individual trial	358
261	Small model at 0° AoA of the pitch moment coefficient, 120 MPH, slot, individual trial	359
262	Small model at 0° AoA of the pitch moment and axial force coefficients, 120 MPH, slot, individual trial	360
263	Small model at 0° AoA of the axial force coefficient, 120 MPH, slot, individual trial	361
264	Large model at 0° AoA of the normal force coefficient, 120 MPH, individual trial	362
265	Large model at 0° AoA of the pitch moment and normal force coefficients, 120 MPH, individual trial	363
266	Large model at 0° AoA of the pitch moment coefficient, 120 MPH, individual trial	364
267	Large model at 0° AoA of the Axial Force coefficient, 120 MPH, individual trial	365

Figure	Page
268	Large model at 0° AoA of the axial force and normal force coefficients, 120 MPH, individual trial 366
269	Large model at 0° AoA of the normal force coefficient, 120 MPH, slot, individual trial 367
270	Large model at 0° AoA of the pitch moment coefficient, 120 MPH, slot, individual trial 368
271	Large model at 0° AoA of the pitch moment and axial force coefficients, 120 MPH, slot, individual trial 369
272	Large model at 0° AoA of the axial force coefficient, 120 MPH, slot, individual trial 370
273	Small model at 0° AoA of the normal force coefficient, release times one and two, 120 MPH, individual trial 371
274	Small model at 0° AoA of the normal force coefficient, release times three and four, 120 MPH, individual trial 372
275	Small model at 0° AoA of the pitch moment coefficient, release times one and two, 120 MPH, individual trial 373
276	Small model at 0° AoA of the pitch moment coefficient, release times three and four, 120 MPH, individual trial 374
277	Small model at 0° AoA of the axial force coefficient, release times one and two, 120 MPH, individual trial 375
278	Small model at 0° AoA of the axial force coefficient, release times three and four, 120 MPH, individual trial 376
279	Large model at 0° AoA of the normal force coefficient, release times one and two, 120 MPH, individual trial 377
280	Large model at 0° AoA of the normal force coefficient, release times three and four, 120 MPH, individual trial 378
281	Large model at 0° AoA of the pitch moment coefficient, release times one and two, 120 MPH, individual trial 379
282	Large model at 0° AoA of the pitch moment coefficient, release times three and four, 120 MPH, individual trial 380

Figure		Page
283	Large model at 0° AoA of the axial force coefficient, release times one and two, 120 MPH, individual trial	381
284	Large model at 0° AoA of the axial force coefficient, release times three and four, 120 MPH, individual trial	382
285	Drawing of Mounting Block for vertical rod and linear motor	449
286	Drawing of Tapered Rod for vertical rod and linear motor	450
287	Drawing of Simple Rod for vertical rod and linear motor	451

List of Tables

Table		Page
1	Nano-25 Calibration Specifications [6]	47
2	Nano-25 Single-Axis Overload [6]	48
3	“In Cavity” position heights of model from the cavity floor in inches	51
4	“Shear Layer” position heights of model from the cavity floor in inches	51
5	“Out of Cavity” position heights of model from the cavity floor in inches	51
6	“Out of Cavity” position heights of model from the top lip of the cavity in inches	51
7	Example portion of the Phase 1 test matrix portion. Sample of different variables used in the full matrix.	53
8	Repeatability of static normal force coefficients at various positions in the cavity apparatus, large model.	58
9	Example portion of the Phase 2 test matrix portion. Sample of different variables used in the full matrix.	60
10	Repeatability of dynamic normal force coefficients at 10° AoA with flow control devices, large model, all wind speeds	67
11	Phase 1 Reynolds Numbers	70
12	Phase 2 Reynolds Numbers	71
13	Filtered values for small and large models at various wind speeds at 10° AoA in the freestream apparatus.	77
14	Values used in calculation of error bars for coefficient values, freestream	77
15	Filtered values for small and large models at various wind speeds at 0° AoA in the freestream apparatus.	83

Table		Page
16	Filtered values for small at various wind speeds and positions at 10° AoA in the cavity apparatus, Part 1	98
17	Filtered values for small at various wind speeds and positions at 10° AoA in the cavity apparatus, Part 2	98
18	Filtered values for 120 mph with both model sizes and angles of attack in various positions in the cavity apparatus, Part 1	109
19	Filtered values for 120 mph with both model sizes and angles of attack in various positions in the cavity apparatus, Part 2	111
20	Filtered values for 120 mph with both model sizes and angles of attack in various positions in the cavity apparatus, Part3	111
21	Filtered values for the small model at 10° AoA in various positions in the cavity apparatus with flow control and slot, Part 1	116
22	Filtered values for the small model at 10° AoA in various positions in the cavity apparatus with flow control and slot, Part 2	116
23	Filtered values for various models and angles of attack at 120 mph in various positions in the cavity apparatus with flow control and slot, Part 1	120
24	Filtered values for various models and angles of attack at 120 mph in various positions in the cavity apparatus with flow control and slot, Part 2	120
25	Normal Force Coefficient comparison of Flow Control Devices with Flow Control	123
26	Mean Filtered values of all four release timings for various models and angles of attack at 120 mph with slot, before and after release	131
27	Mean Filtered values of all four release timings for various flow control devices and wind speeds at 10° AoA with large model, before and after release, Part 1	149

Table		Page
28	Mean Filtered values of all four release timings for various flow control devices and wind speeds at 10° AoA with large model, before and after release, Part 2	149
29	Filtered values of lift coefficients for all four release timings for various flow control devices at 120 mph with large model at 10° AoA, before and after release	152
30	Phase 1 Full Test Matrix Part 1, no flow control	162
31	Phase 1 Full Test Matrix Part 2, no flow control	163
32	Phase 1 Full Test Matrix Part 3, with flow control	164
33	Phase 1 Full Test Matrix Part 4, with flow control	165
34	Phase 2 Full Test Matrix Part 1	166
35	Phase 2 Full Test Matrix Part 2	167
36	Phase 2 Full Test Matrix Part 3	168
37	Phase 2 Full Test Matrix Part 4	169

List of Symbols

Symbol	Page
x/L	Non-Dimensional Position 4
α_k	Constant of Proportionality (Karamcheti) 7
L	Cavity Length 7
f	Cavity Frequency 7
S	Strouhal Number 8
$\frac{L}{U}$	Non-Dimensional Scaling Parameter 8
m	Integer Mode Number 8
M_∞	Freestream Mach Number 8
U_∞	Freestream Velocity 8
n	Empirical Constant 8
K	Empirical Constant 8
$\frac{L}{D}$	Length-to-Depth Ratio 9
λ	Adiabatic Exponent 9
T_c	Static Temperature 9
T_0	Static Temperature 9
T_∞	Freestream Temperature 9
a_c	Speed of Sound for the Cavity 9
a_∞	Static Freestream Speed of Sound 9
γ	Ratio of Specific Heats 9
F_x	Force in x-direction 46
F_y	Force in y-direction 46
T_z	Torque in z-direction 46

Symbol	Page
F_z	Force in z-direction 46
T_x	Torque in x-direction 46
T_y	Torque in y-direction 46
C_N	Normal Force Coefficient 56
N	Normal Force 57
ρ	Density 73
V_∞	Velocity 73
D	Diameter 73
C_D	Drag Coefficient 76
C_L	Lift Coefficient 76
C_m	Pitch Moment Coefficient 85
C_A	Axial Force Coefficient 88
$C_{N1,filtered}$	Normal Force Coefficient for the First Release Timing 134
$C_{N3,filtered}$	Normal Force Coefficient for the Third Release Timing 134
$C_{N2,filtered}$	Normal Force Coefficient for the Second Release Timing 134
$C_{N4,filtered}$	Normal Force Coefficient for the Fourth Release Timing 134
$C_{A1,filtered}$	Axial Force Coefficient for the First Release Timing 145
$C_{A3,filtered}$	Axial Force Coefficient for the Third Release Timing 145
$C_{A2,filtered}$	Axial Force Coefficient for the Second Release Timing 146
$C_{A4,filtered}$	Axial Force Coefficient for the Fourth Release Timing 146

List of Abbreviations

Abbreviation	Page
DOF	Degrees of Freedom iv
USAF	United States Air Force 1
AFIT	Air Force Institute of Technology 2
LMA	Linear Motor Apparatus 3
DAQ	Data Acquisition System 3
AoA	Angle of Attack 4
NI	National Instruments 5
CTS	Captive Trajectory System 15
CANs	Combined Asymptotic and Numerical Analysis 16
AFSEO	Air Force SEEK EAGLE Office 17
CFD	Computational Fluid Dynamics 17
WPAFB	Wright Patterson Air Force Base 25
FDM	Fused Deposition Modeling 29
PLA	Polylactic Acid 29
US	United States 38
L/D	Length-to-Depth Ratio 42
GDK	Galil Design Kit 46
AIAA	The American Institute of Aeronautics and Astronautics 47
ATI	ATI Industrial Automation 48
Re	Reynolds Number 70
DOF	Degrees of Freedom 1

INFLUENCE OF LEADING EDGE OSCILLATORY BLOWING ON TIME-ACCURATE DYNAMIC STORE SEPARATION

I. Introduction

1.1 Background and Motivation

Increasing the operational efficiency of weapons employed in hostile environments is a high priority of the United States Air Force (USAF). In recent history, the USAF has made a move to smaller and internally stored weapons, especially for fighter aircraft. Maintaining a low radar cross section signature, and thus a low observable air vehicle, is desirable so the aircraft is less detectable by the enemy. An internal weapons bay has a reduced load out but yields a low observable profile (reduced radar cross section) [1]. Also, aircraft can carry a greater number of weapons if the weapons are smaller, increasing the quantity of targets that can be engaged per sortie [1]. The newer attack aircraft in the United States, such as the P-8A, F-22 and, most recently, the F-35 employ weapons delivery from bomb bays [2]. The effects of this design element have not been fully explored and the impact on weapon release can sometimes be challenging to predict. Thus, it is important to understand the sensitivity of the flow field effects on the internally loaded weapon within a few feet from the carriage [1].

When using an internal weapons bay, several issues arise with the weapon release. The aeroacoustic environment formed by the cavity is unsteady. The mission stores are subject to this unsteady flow and strong acoustic loads [2]. The unsteadiness originates from the presence of a self-reinforced acoustic resonance phenomenon in

conjunction with a robust free shear layer instability [2]. Pressure fluctuations and acoustic resonance that stem from this unsteady flow can impart high dynamic loads on the weapon stores while in motion. These dynamic loads can also fatigue the cavity structure as well as impact the release trajectory from aircraft bays. Unsteady and un-suppressed pressure levels reach up to 180 dB and can lead to structural fatigue of bulkheads and even failure of weapon components [2]. Strong acoustic resonance can, in dramatic cases, lead to instant changes in direction of normal forces from ‘in to’ to ‘out of’ the weapons bay; this is called “pitch bifurcation” [2]. In general, it is possible that strongly time-dependent flow might affect mission store release. For smaller and lighter weapons, this could impact its safe release and effectiveness [3].

The time-dependency of cavity flow is a matter of concern for current data acquisition. Since typical wind tunnel data consists of time averaged store loads, common store separation analysis cannot detect a sensitivity to timing of the store release[4]. Also, the workload and cost associated with a specific project increase dramatically for the testing of multiple configurations. Mitigation of the workload and cost can be accomplished with the implementation of dynamic wind tunnel testing which also provides time-accurate data. Previous research conducted in the Air Force Institute of Technology, AFIT, low-speed wind tunnel emphasized the importance of collecting such data in order to characterize of dynamic loads during mission store release [5] [6].

1.2 Problem Statement

The goal of the current study is to support the static and dynamic characterization and the time-accurate dynamic load data acquisition in a low-speed wind tunnel. Oscillatory blowing was applied at the leading edge to emulate, to an extent, the strong time-dependent flow in a transonic environment, where Rossiter tones prevail. Both

static and dynamic testing data in the AFIT low speed wind tunnel were collected at speeds of 60, 100, and 120 mph, with different model sizes and angles of attack, to produce time-accurate force and moment measurements. Actuation of the Linear Motor Apparatus, LMA, accomplished a vertical store release trajectory. The data was analyzed to determine the nature of the effects of strong oscillatory flow of load profiles as the store progresses through the free shear layer.

1.3 Methodology

This experimental setup includes a vertically oriented linear motor inside the AFIT low-speed wind tunnel and was used to create a realistic release trajectory. The mission store model was supported by a shaft connected to the base apparatus in the freestream tests. In the cavity tests, the store was supported by the same shaft which was embedded in the cavity apparatus and passed through a linear bearing in the floor of the cavity to provide additional stability. The trajectory commands are written in a Galil code format. The dynamic test trajectories will only include a vertical linear translation that will represent the store separation. The motion is limited to a linear translation to simplify the analysis and to attempt to isolate the aerodynamic effects of the oscillatory blowing.

Attached to the linear motor and the mission store model was a Nano25 force and moment sensor. When this sensor experiences aerodynamic loads in the x-, y-, and z- directions, analog voltage signals are sent to the Data Acquisition System, DAQ, and processed using LabVIEW software. Initial runs at rest will capture inertial effects and were used to tare subsequent runs. Post processing, including converting files from LabVIEW into .csv files and importing them into Matlab, will yield time-accurate force and moment data for all runs completed.

The runs that were completed involve two main parts. The first part will involve

static testing of various conditions in both a freestream environment and various positions using the cavity apparatus. This will characterize the aerodynamic loads experienced by the mission store. In the second part, the characterization of the dynamic loading on the mission store was completed in the cavity environment by varying the angle of attack (AoA) and having an oscillatory blowing of 5 Hz. The cavity apparatus consists of a modified SUU-41 pod, pictured in Figure 1, designated as WASSP developed by Probst [7]. To allow for sufficient shear layer growth, the mission store model will have a starting position of $x/L = 0.55$ from the front of the cavity. The initial vertical position was 0.5 inches below the cavity lip line and a final position of 9.0 inches above the cavity lip line and moved backwards. These tests will involve wind tunnel speeds at 60, 100, and 120 mph, angles of attack at 0.0° and 10.0° , two mission store sizes with a 1.3 inches and a 1.7 inches diameter model, and other variables to extensively characterize the static and dynamic loads experienced by the store.

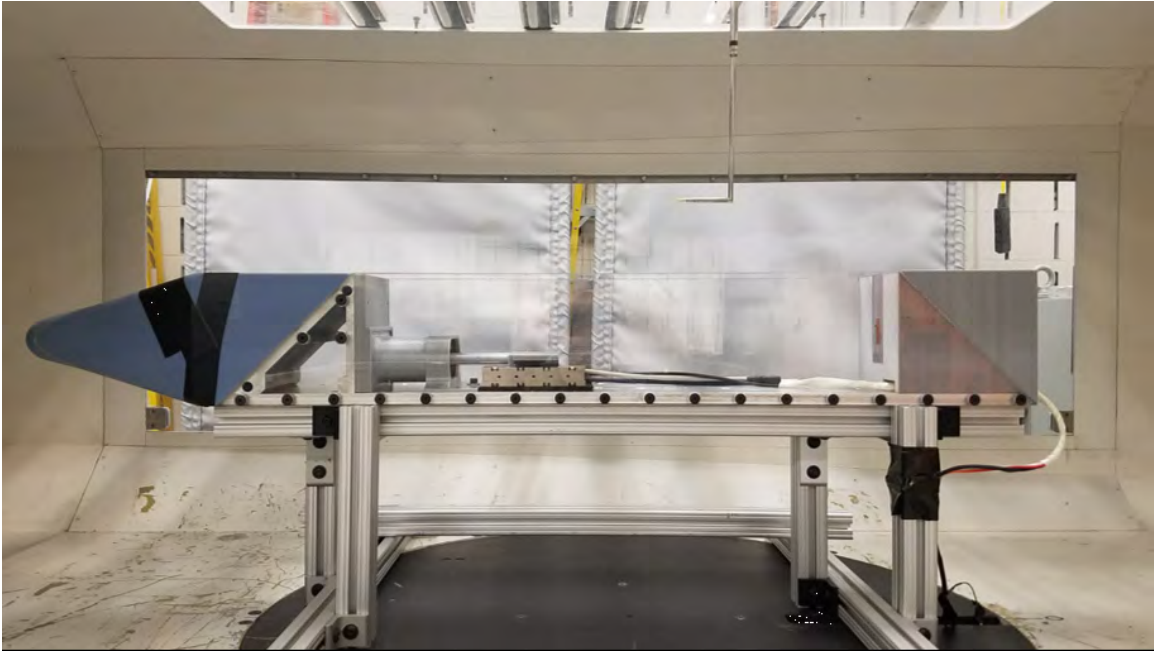


Figure 1: Fully assembled cavity representing the modified SUU-41 pod [8].

The prescribed motion was conducted by the linear motor apparatus in two configurations, a freestream apparatus and a cavity apparatus. Both configurations will be described in Chapter III. The linear motors are coupled with a National Instruments, (NI), DAQ and a Nano25 force and moment sensor for data collection. The force and moment sensor can be used on the model with the LMA to gather all necessary data by using the method described by Sellers [6].

1.4 Limitations

The physical limitations of the experimental setup involve the range of motion of the vertical linear motor, the operating rate of the oscillating linear motor, and the conservative approach taken may limit the loading of the sensor and the capability of consistently obtaining time-accurate data. The operational setup limits the movement trajectory to prescribed motion only. Also, the store protrudes from the cavity for multiple angle of attack trials which limits the accuracy of the results and forces a lack of accuracy at the beginning of the store release. For the oscillating linear motor to achieve a 100 percent duty cycle, it was restricted to only 5.0 Hz. A conservative approach to testing led to relatively low loading of the force and moment sensor and left room for error and noise accumulation. The capability of consistently obtaining time-accurate data is an underlying theme in this research. Several precautions were taken in the operational set up to reduce the amount of noise in the data collected.

1.5 Overview of Subsequent Chapters

The arrangement of the succeeding chapters is as follows. Chapter II addresses a literature review of experimental measurements, dynamic wind tunnel testing, cavity aeroacoustic environments, store effects, reference frames and coordinate transformations, and previous research on active flow control devices. Chapter III explains

equipment and system setup, methodology for data acquisition, the Nano25 sensor, and post processing methods of using data acquisition in conjunction with specific sensors. Chapter IV provides experimental results for select tests of the mission store in the freestream and cavity environments of varying store sizes, wind speeds, angles of attack, and release timings. Experimental results for the effects of all variables on the mission store model are described by the acquisition of quantitative data from aerodynamic force and moment measurements. Chapter V outlines conclusions obtained on the characterization of static and dynamic loading on the mission store model, the identification of repeatable patterns in the normal forces during store motion seen for various store initialization positions, and time-accurate force and moment measurements of the LMA performance.

II. Literature Review

2.1 Chapter Overview

This chapter summarizes the history of exploration regarding the aeroacoustic environment within a cavity and the classification of cavities. Open flow phenomena and store separation effects within the cavity are described. The definition of different rig configurations is also provided. Finally, the importance of the data acquisition of time-accurate dynamic wind tunnel data and time-accurate experimental measurements are also discussed.

2.2 Cavity Aeroacoustics

2.2.1 History of the Aeroacoustic Environment.

Initial investigation into the challenging acoustic environment generated by subsonic and supersonic flow past a cavity began in the 1950s by Karamcheti. These experiments involved Schlieren methodology and the use of hot wire anemometers. Karamcheti measured the strong acoustic field generated by a cavity and measured the frequency by varying the cavity length gradually while maintaining the flow at constant free stream Mach and stagnation temperature. The frequency is inversely proportional to the cavity length as seen in Equation 2.1. With α_k being the constant of proportionality in units of velocity, L as the cavity length, and f as the cavity frequency. The observations indicated that there is a minimum cavity length required to generate acoustic noise. This length is affected by the boundary layer type, the size of the cavity, and the free stream velocity [9].

$$f = \alpha_k * \frac{1}{L} \tag{2.1}$$

Different tones are generated in the cavity when the flow is laminar compared to turbulent. The laminar case produces a single dominant frequency while the turbulent produces two frequencies of equal strength; both also develop harmonic frequencies in the cavity [9].

Karamcheti was able to compare the intensity of the acoustic field using the Strouhal number, S . This number is a non-dimensional scaling parameter that relates the velocity, $\frac{L}{U}$, to the “vortex shedding frequency of an oscillating flow mechanism and a characteristic dimension” [8]. Karamcheti used this number in Equation 2.2 to show that as speed increased, the acoustic field grew in intensity; as cavity length increased, the acoustic field decreased in intensity. However, he was unable to calculate the cavity frequency with precision based on the flow field conditions [8].

$$S = f * \frac{L}{U} \tag{2.2}$$

Based on previous work, J.E. Rossiter researched how unsteady pressure fluctuations around the cavity portray both periodic and random components. In an attempt to build on Karamcheti's work, he explored a calculation of cavity frequency [8]. Rossiter empirically derived the formula for cavity frequency (f), shown in Equation 2.5. This equation is based on observations of the secondary frequencies of the cavity following a family of curves while the dominant frequencies can appear to jump in value as they shift between families of curves [10]. Rossiter uses the integer mode number, m , which demonstrates the frequency ranges between jumps [11]. In Equation 2.4 and 2.5, M_∞ is the freestream Mach number, U_∞ is the freestream velocity, L is the cavity length, n is an empirical constant and the phase delay between acoustic wave and new vortex, and K is an empirical constant for the ratio of convective velocity of vortices to freestream velocity [8].

$$S = \frac{f * L}{U_\infty} \quad (2.3)$$

$$\frac{f * L}{U_\infty} = \frac{m - n}{\frac{1}{K + M_\infty}} \quad (2.4)$$

$$f = \frac{(m - n) * U_\infty}{\frac{1}{K + M_\infty} * L} \quad (2.5)$$

It was subsequently found that since Rossiter assumes the speed of sound in the free stream and in the cavity are equivalent, Rossiter's formula produces error at low Mach and significantly increases error above Mach 1.5 [12]. To further refine these empirical formulas, experiments in 1971 found how to estimate the speed of sound in the cavity. Heller, Holmes, and Covert used a cavity with a Length-to-Depth Ratio, $\frac{L}{D}$, varying from 4.0 to 7.0 and Mach ranging from 0.8 to 3.0. Heller et al. used a combination of a thermocouple and piezoelectric microphones to capture the distribution of unsteady pressures within the cavity and the cavity temperature [12]. This allowed for the calculation of the speed of sound using Equation 2.6 with λ being the adiabatic exponent, T_c being the static temperature, T_0 being the stagnation temperature, T_∞ being the freestream temperature, a_c being the speed of sound for the cavity, and a_∞ being the static free stream speed of sound [12].

$$a_c = a_\infty * [1 + \frac{T_c - T_\infty}{T_0 - T_\infty}(\lambda - 0.5)^{0.5}] \quad (2.6)$$

Heller et al. continued to modify Rossiter's formula to account for the error at higher Mach caused by the speed of sound assumption mentioned before [12]. The introduction of the ratio of specific heats, γ , led to Equation 2.7 [8]. This change allowed for more effective prediction, over a greater range of Mach numbers, of the potential oscillation frequencies for a shallow cavity [12].

$$f = \frac{(m - n)}{\left[\frac{1}{K} + \left(\frac{M_\infty}{1 + \frac{\gamma - 1}{2} M_\infty^2} \right)^{1/2} \right]} \frac{U_\infty}{L} \quad (2.7)$$

In 1975, experimental research began regarding the physical mechanisms involving pressure fluctuations in shallow rectangular cavity flow as well as evaluating devices capable of suppressing those fluctuations [13]. Heller and Bliss observed periodic addition and removal of mass at the trailing edge of the cavity [8] named the pseudopiston effect because of the periodic nature. This effect creates waves that travel forward from the rear of the cavity, reflect at the front wall, and then travel back to the rear wall [8]. The pseudopiston effect generates unsteady motion in the shear layer which completes the feedback loop and allows for more mass addition and removal towards the trailing edge [13]. Figure 2 depicts the six-step process involving this effect presented by Heller and Bliss.

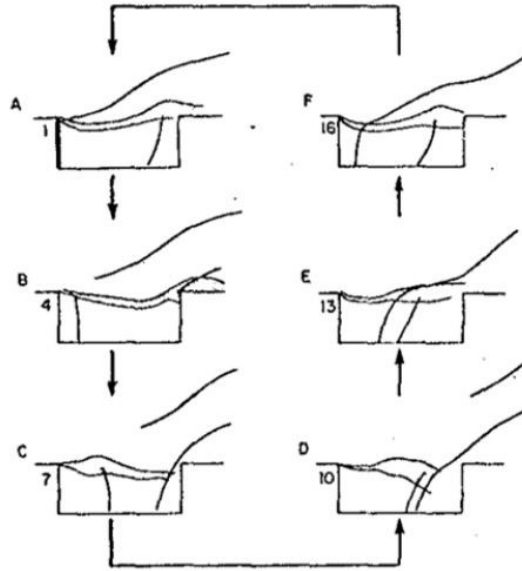


Figure 2: Typical Oscillation Cycle [13]

The pseudopiston effect observation inspired a simple analytical internal wave

structure model for the cavity. With this model, Heller and Bliss could accurately present the peak pressure magnitudes as a function of distance along the cavity from the leading edge [13]. An analogy can be seen in Figure 3 [14]. Although Heller and Bliss did not present an equation for this model, they claimed the calculations were repeatable for different L/D ratios and frequencies, and the experimental mode shapes agreed qualitatively with the model [8].

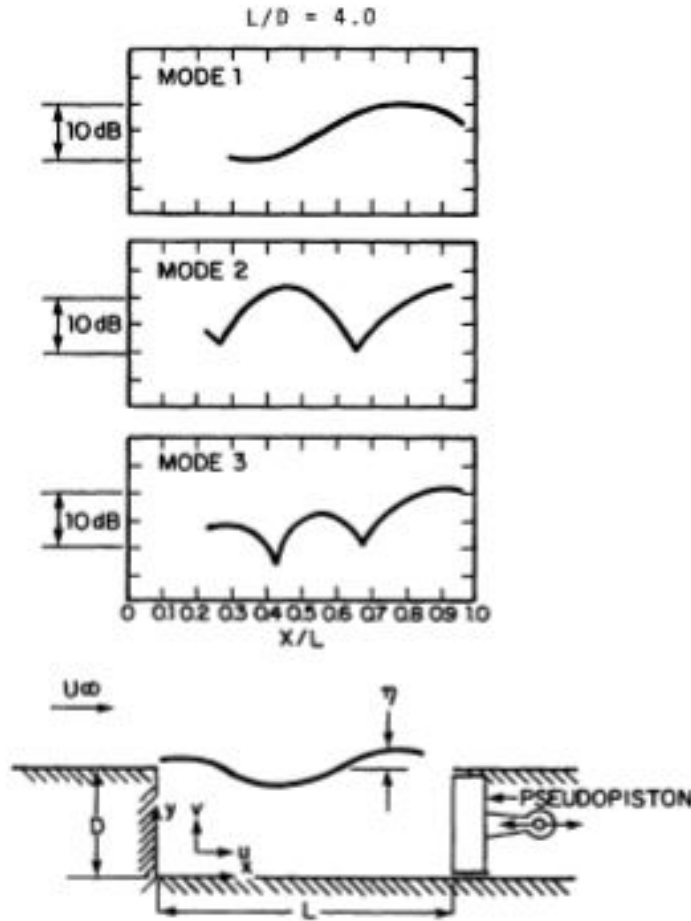


Figure 3: An example of the pressure magnitudes as a function of distance from the leading edge data, a pseudopiston analogy [14]

Almost thirty years after Karamcheti's initial investigations into the aerodynamic effects, Rockwell and Naudascher created a matrix, to categorize self-sustaining oscillations. While they knew that the mechanisms of the oscillations were practically a

combination of different types, they categorized these oscillations into three groups. First, there is a fluid dynamic source where the instability of the flow cause oscillations. Second, there is fluid resonance, where resonant wave effects influence the oscillations. Lastly, there is fluid elastic, where the motion of a solid boundary may be coupled to the oscillations [15]. Though this matrix does not account for a turbulent free shear layer, it categorizes the quasi-two-dimensional flow of the oscillations. The aeroacoustic effects within a cavity were designated in this manner, but the categorization of cavities still needed to be addressed.

Although the frequency of tones in cavities is well-predicted by the modified Rossiter equation, amplitudes remain difficult to determine. One important factor, very relevant to the current research, is that the amplitude of the acoustic tones increases dramatically as freestream Mach number increases from low subsonic ($M_\infty = 0.1$) to transonic conditions.

2.2.2 Classifications of Cavities.

There are two main types of cavity flow, open and closed cavity flow [16], as well as a transitional phase in between. These types can be classified based on the L/D of the cavity and some qualitative characteristics of the shear layer. An open cavity flow typically corresponds to $L/D < 10.0$. The boundary layer separates at the leading edge so that the shear layer flows over, or bridges, the cavity. The shear layer interacts with the rear wall of the cavity which generates acoustic waves which travel up through the cavity as shown in Figure 4a [17]. Contrarily, closed cavity flow typically occurs for $L/D > 13.0$. The shear layer, for this classification, expands over the leading edge of the cavity, impinges on the floor of the cavity, then exits the cavity before the rear wall as shown in Figure 4b [17]. The transitional classification between open and closed occurs for L/D around 12.0. For this classification, the flow

is on the verge of changing from closed to open as shown in Figure 4c and Figure 4d [16]. The switch from transitional to closed is highly dependent on Mach number and cavity configuration. As the width-to-depth ratio increases, the range of L/D over which transitional flow occurs at a given Mach number also increases [18] [19] .

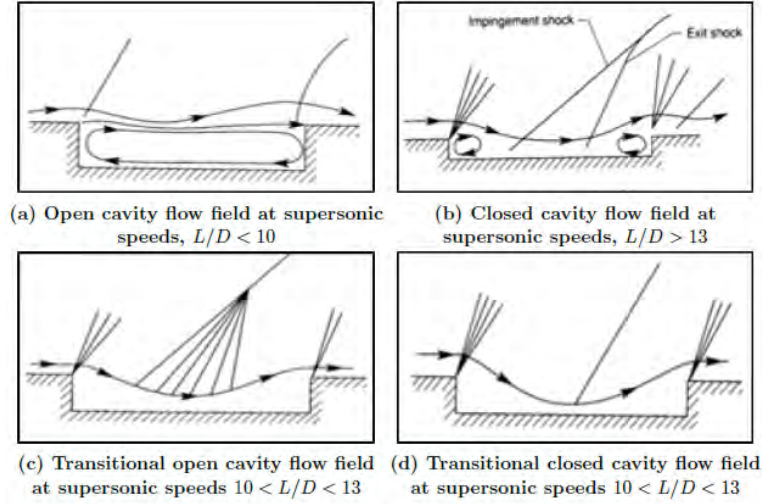


Figure 4: Depictions of the different flow field types based upon the varying dimensions of L/D [18]

2.3 Open Flow Phenomena

The latest generation of fighters have weapon bays that are generally classified as open cavities [20]. To gain a better understanding of the physical process that occurs within a weapon bay, a brief discussion of open cavity phenomena is required. Acoustic waves generated can perturb the shear layer which can create tones significantly larger in amplitude than the broadband fluctuations [10]. The shear layer interacts with the rear wall which creates cavity resonance in an open cavity flow field. The mechanisms for cavity resonance have been summarized in four steps: the amplification phase, the interaction phase, the feedback phase, and the receptivity phase [21]. A depiction of this feedback loop can be seen in Figure 5.

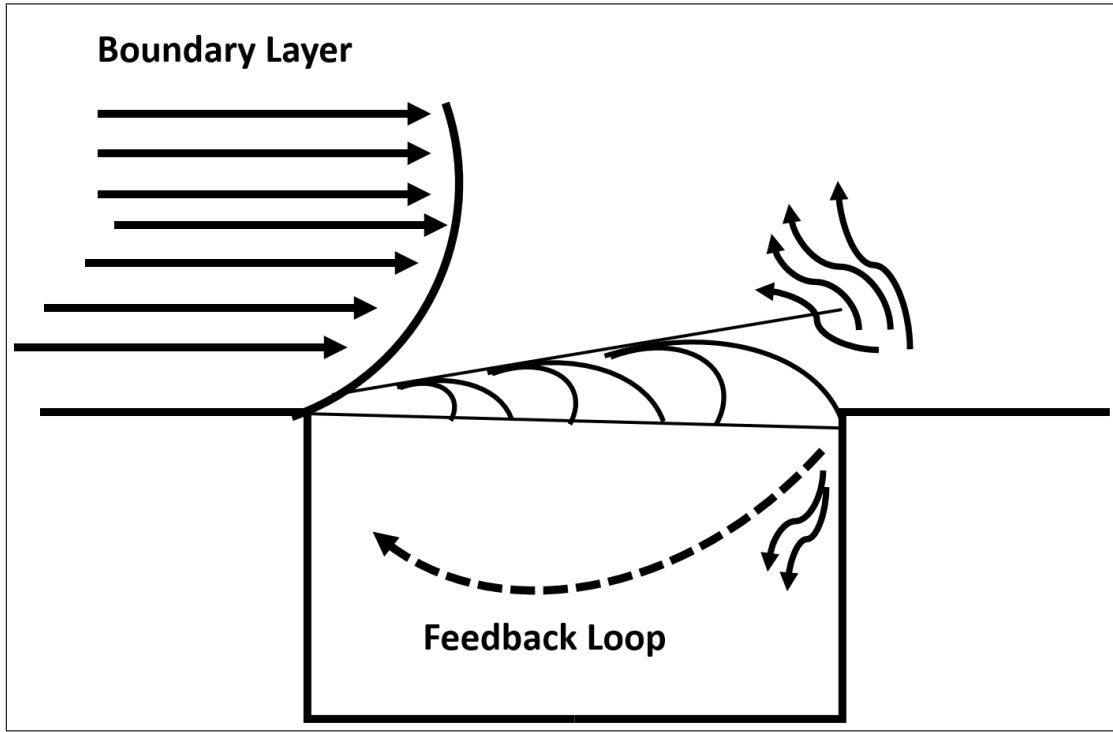


Figure 5: Cavity flow feedback loop depiction

Amplification is the growth of vertical instabilities in the free shear layer as they travel aft from the leading edge of the cavity. Interaction begins at the rear of the wall when the large vertical structures impinge on the trailing edge and produce periodic acoustic instabilities. Feedback results from the acoustic instabilities propagating upstream. Finally, receptivity is when the flow reaches the upstream end of the cavity where the acoustic waves excite disturbances in the shear layer resulting in the shedding of new vortices [21]. This feedback mechanism creates a defined resonance consisting of high-amplitude tones which are a function of the freestream conditions and cavity geometry [21].

Pressure gradients also develop and impact the cavity environment. Pressure coefficients over the cavity floor are slightly positive and relatively uniform with the exception of a small adverse gradient occurring ahead of the rear face that is caused by the shear layer impinging on the outer edge of the rear face [16]. This phenomenon

can impact a store separation greatly and is important to consider.

2.4 Store Separation Effects

While there are many challenges associated with cavity acoustics, the most salient point for the current research is that a strong oscillatory flow can develop. In cavity flow, dynamic loads of up to 180 dB can be caused by acoustic resonance and pressure fluctuations and can lead to structural fatigue of the cavity [3]. These fatigue and aerodynamic effects are magnified with the push to smaller weapons bay and more advanced munitions and electronics in the cavity [8]. Additionally, the highly oscillatory flow-field can negatively affect the safe departure and accurate delivery of munitions [3].

Unsteady flow is a known characteristic of cavity flow since the common use of weapons bays over seventy years ago. Recent store design has inspired a greater study of unsteady flow caused by the cavity. Trends in store design may lead to more sensitivity toward the unsteady aerodynamics [8]. These trends include decreased store aerodynamic stability which increases glide time, folded fins and wings for increased packing density, and smaller and lighter munitions [20].

Much of the current separation trajectory analysis revolves around the release of an external store. The Captive Trajectory System (CTS) uses a store placed on a sting positioned in the flow field to acquire force and moment measurements. These data are time-averaged and historically provide the correct level of fidelity for external clearance situations [20]. This type of test does not account for the unsteadiness resulting from a cavity in the flow field. The CTS is limited in fully predicting mission store trajectory from an internal weapons bay [8]. This unsteady component, linked to strong acoustic resonance, can lead to a change in sign of normal forces from positive to negative, into and out of the bay. A potentially extreme example

of this has been described as pitch bifurcation [20]. The change in direction shows a time-dependent aspect of weapons release which cannot be represented accurately which is shown in Figure 6. Accurate modeling of the unsteadiness in store separation introduced by the flow from the cavity requires a different approach than the CTS. The method involving acquiring time-averaged values and assuming quasi-steady flow cannot be used to measure the stores sensitivity to small perturbations resulting from the shear layer [8].

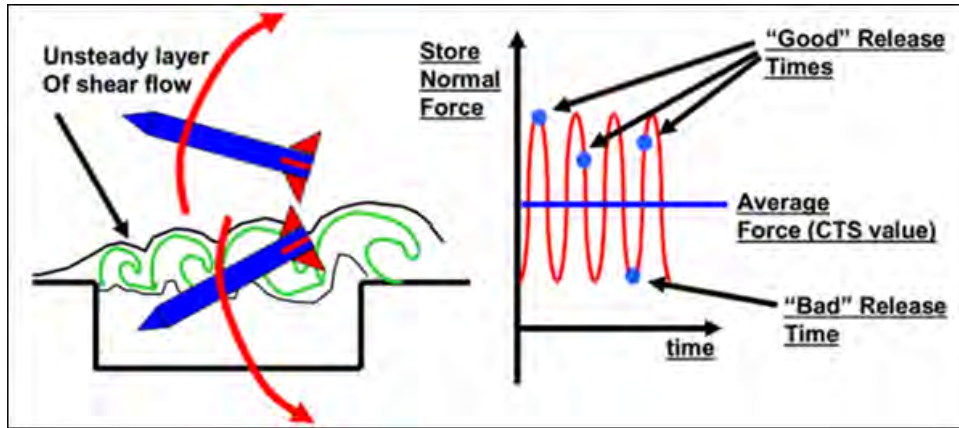


Figure 6: Illustration of how the quasi-steady assumption of CTS neither captures the time-dependent forces of the unsteady shear layer, nor allows for accurate prediction of store separation [20]

A model that explores the sensitivity of a mission store to the unsteady shear layer resulting from flow over a cavity is the Combined Asymptotic and Numerical Analysis (CANs) [4]. This model is theoretical and divides the store separation into three individual phases. These include when the store is in the cavity, when the store crosses through the shear layer, and when the store is outside the cavity [22]. This model assumes “slender body theory, asymptotic methods, and a steady inviscid shear layer” [8]. It provides theoretical evidence that the pitching behavior on release of the cavity depends on how the store enters into the shear layer. This model establishes evidence on a mission store’s sensitivity to the unsteady shear layer. This

time-sensitive nature resulting from the unsteady shear layer necessitates exploration of time-accurate models. The Air Force SEEK EAGLE Office (AFSEO) modeled dynamic GBU-12 separations from a deep weapons bay after a mishap involving a GBU-12 striking the tail of a B-52 upon release [23]. This model of pitch bifurcation used a fully viscous, time-accurate CFD model and held all initial conditions constant except the time of release. The results of these cases, replicated in Figure 7, show that each store followed a different path and orientation, and each store demonstrated the effect of the unsteady shear layer on the release trajectory [8].

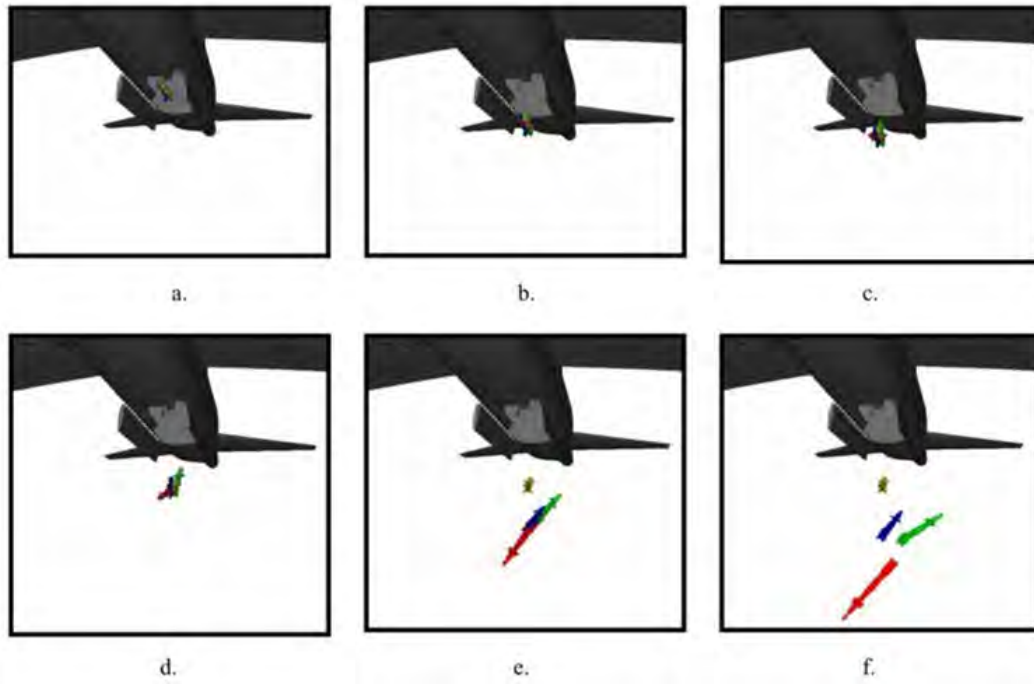


Figure 7: The effect of release time on trajectory based upon a 3-dimensional CFD model [24]

The correlation between the force and moment acting on a mission store, and the acoustic modes in the cavity, have a strong significance in the trajectory of the store. CFD research conducted using OVERFLOW 2.1 explored this effect on four configurations of the store location within a cavity of $L/D = 4.5$ at Mach 0.95 [25]. It was found that regardless of the position of the store, including the case of an empty

cavity, the acoustic response was fundamentally the same. This research implies that store separation research can be simplified to characterizing an empty cavity although the time-accurate prediction of the store trajectory would still need to be analyzed using dynamic wind tunnel testing.

Certain key factors influence the store separation process more than others. Varying the total impulse of a mission store results in a direct impact on the initial linear and angular velocities. Variables including the moment arm of the release mechanism are directly proportional to the total impulse while the moment of inertia of the store is inversely proportional. Similarly, dynamic pressures are proportional to the aerodynamic forces and moments experienced by the mission store. Anything that adjusts the velocity of the center of gravity of the store can alter the release and trajectory. “Lightweight, unstable, low-drag stores are especially likely to present separation problems” [26]. The trajectories of a heavier store are less impacted by changes in release conditions and is more stable and predictable. Additionally, the effects on the mission store are lessened when the dynamic pressure is lower. Certain factors don’t directly impact or have little impact on the forces and moments experienced by the store.

2.5 Oscillatory Blowing

Cavity resonance is a complicated phenomenon. As described in the Section 2.3, when the cavity is defined as an open cavity, the shear layer, formed at the front of the cavity, reattaches at the aft wall and acts as an acoustic source in this region. Acoustic waves travel in the cavity and force the shear layer at the front of the cavity. These instabilities affect the formation of large-scale vortical structures that in turn form a feedback loop when they reach the aft wall of the cavity. It should be noted that in subsonic flow, the acoustic waves also travel outside the cavity [27].

Active flow control of flow-induced cavity oscillations has been investigated by the USAF and other institutions for many years due to its adaptability across a wide range of flight conditions [28]. The general purpose of active flow control is to suppress cavity oscillation by providing external energy to the flow field over an open cavity [27]. In contrast, passive flow control typically uses geometric modifications to alter the flow field. In traditional passive flow control no external energy is added and the effect cannot be adjusted without altering the flow conditions or changing the physical device. Compared to this control technique, active flow control, in many scenarios, provides additional opportunities to investigate or leverage different effects in research or in application. Active flow control also has the categorization of open-loop or closed-loop control. Closed loop control involves a feedback loop where a sensor collects information or a flow quantity is estimated which is then used to modify the control. This has many advantages but can be difficult to implement. Open loop control, contrarily, implies no feedback loop [27].

The effectiveness of active flow control and oscillatory forcing of the flow field has been evaluated over the years. As early as 1997 it was found that open loop sinusoidal forcing at the leading edge of the cavity was able to suppress cavity fluctuations. A sinusoidal forcing seeds the shear layer with instabilities and disturbances large enough to prevent the natural growth of cavity disturbances. This disrupts the feedback loop of the acoustic resonance. Oscillation is used in multiple forms involving either mass injection or flow deflection. Both methods have commonly been experimented at frequencies up to 100 Hz. One particular experiment by Shaw in 1998 found that, in his specific experiment, a low oscillation of 5 Hz provided maximum suppression of the cavity fluctuations. Certain blowing configurations have been manually optimized to investigate the effectiveness of suppression in supersonic flow because shock dynamics are dominant factors. Contrarily, at subsonic speeds, the most effective mechanism is

the alteration of the shear layer stability characteristics. At these lower speeds, lower frequency forcing appears to have a greater impact on the flow characteristics than at higher speeds [27].

Additionally, for mass injection cases in a cavity environment, it was found that normal mass injection is more effective in suppression than tangential mass injection. The normal mass injection disrupts the shear layer more and has a greater influence on the pressure fluctuations when the flow reaches the aft wall of the cavity downstream. With tangential mass injection, the momentum in the stream-wise direction is influenced and has different effects unrelated to the suppression of natural cavity fluctuations [27].

Very recently, three-dimensional blowing has been investigated by Zhang in the effort of suppressing cavity flow oscillations. Significant reductions of fluctuating pressures were observed for an open cavity. The span-wise wavelike structures generated by the flow control disrupts the shear layer and inhibits the growth of larger vortical structures. These experiments span from subsonic to transonic cavity flow conditions. Simulations were also conducted which agreed with the experimental results [29]. This topic provides a great area of research that is still being investigated in 2-dimensional and 3-dimensional blowing situations. Regardless of the type of active open-loop flow control used, active flow control is attractive in many scenarios because of its relative simplicity and flexibility in different flow conditions and environments.

2.6 Dynamic Wind Tunnel Testing

Many aircraft use internal weapons bays to reduce the radar cross section and drag [20]. Typical wind tunnel testing cannot identify the unsteady aerodynamic effects since the data collected is static and time-averaged [4]. For mission store clearance, the USAF current test method is the Captive Trajectory System (CTS).

This system collects time-averaged data for externally carried stores where the flow is non-separated and relatively steady [20]. In the current method, separation caused by the cavity flow has a negative impact on the effectiveness of reliable data collection for internal weapons bay [20]. The cavity flow effects created by opening the internal weapons bay complicates the store separation and necessitates dynamic testing to accurately detect the effect of the flow on a moving store [2].

Dynamic wind tunnel testing would be a good experimental way to measure store separation effects [30]. Through this testing, the goal is to acquire aerodynamic forces and moments about a specific location, as well as dynamic pressure and model attitude [30]. Testing dynamically helps evaluate aircraft stability and control for air vehicle research [31]. Acquisition rates must allow for proper data collection in these trials. In certain cases where aerodynamic effects have a lower impact on the model, have a frequency up to 50 Hz. Other cases prove to have a higher frequency such as 500 Hz [4]. The acquisition rate used in a certain experiment depends on the effects desired to be observed and the time-resolution desired. This method of testing is important for acquiring accurate separation effects and for determining the safety and effectiveness of the separation, especially with new aircraft and new internally released stores [2].

Difficulties arise when measuring loads for a store in motion. Damping vibration and energy dissipation have the potential of impacting the recorded data when the sensor is externally excited [32]. Many sensors also experience creep in the resistive material, sometimes called relaxation of the material, which can cause output drift [33]. Additionally, this can negatively affect the repeatability of certain tests [34]. In this experiment, there is an interface between the sensor and the model made of a plastic material. A set of screws connects the sensor to the model and apparatus. This causes the sensor to have a small amount of flexibility which can increase the

noise level in the recorded data. The dynamic recording of force and moment measurements introduces complications for the sensor that must be taken into account when analyzing the data.

2.7 Configuration of Rigs

The configuration of model and apparatus that holds the model can vary in style based on the type of motion being used in the wind tunnel. Three main configurations include a free-flying wind tunnel model, a free-motion rig, and a forced-motion rig [35]. The LMA is a forced-motion rig with a prescribed trajectory the mission store model follows while the force and moment measurements are taken. While the LMA will have a vertical trajectory, other apparatuses, including some in the AFIT low-speed wind tunnel, offer additional options for curved trajectories. Forced-motion rigs have been used in the past to explore aerodynamic characteristics of transport aircraft configurations undergoing different roll, pitch, and yaw maneuvers [36].

Likewise, the CTS is a forced-motion rig and pursues the store separation test and analysis capability [37] and seeks the maximum trajectory angles as a function of the distance from the carriage (the trajectory envelope). Using measurements at multiple locations and the integration of translational and rotational acceleration, the CTS can compute angular velocities, positions, and orientations [5]. Mechanical limitations restrict the capability of getting fully time-accurate trajectory models since it is finding time-averaged data [4]. The value of the CTS modeling excels in quasi-steady situations but lacks in usefulness when used to try to find the effects of unsteady flow, especially due to cavity effects. The need for dynamic wind tunnel testing becomes apparent when seeking time-accurate measurements for this unsteady flow [?].

Free-motion test rigs allow at least 1-DOF and are used to characterize aerody-

dynamic performance as the model undergoes pitching, rolling, and yawing. This is hard to effectively execute, especially in a small or restricted wind tunnel area. It would require being able to feed the encoder positions back into the trajectory modeling. This configuration is not used because of the program and coding as well as the space required. Similarly, free-flying wind tunnel models produce high fidelity measurements because there are no rigs in the wind tunnel that affect the flow surrounding the model. Since the model is free-flying, a large space is typically required for the model to be able to move around without contacting the edges of the wind tunnel. Larger tunnels have been used in previous tests [5].

2.8 Experimental Measurements

Properly measuring the aerodynamic forces and moments is critical to the characterization and quantification of aircraft performance [38]. For dynamic wind tunnel testing, there is an emphasis on time-accurate data collection and characterization. In this experiment, force and moment data are collected for both freestream flow and cavity flow in the low speed AFIT wind tunnel. Flow around the open cavity is unsteady and can have a significant effect on store separation trajectories [4]. To measure this effect, a Nano25 sensor (a 6-component transducer) is used. This sensor works by using strain gauges attached to the internal structure of the sensor [6]. As forces or moments are applied to the Nano25, the strain gauges flex and change the voltage output. This combined with a signal condition has the ability to detect changes in values above any noise produced [30]. This sensor has been successfully used in limited research of mission store dynamics in a wind tunnel environment including oscillatory pitching movement, complex store release trajectories, and complex cavity environments [6] [5] [8]. This data acquisition facilitates time-accurate measurements up to 70 Hz [39].

To record time-accurate force and moment data using the LMA setup, a taring process was used to capture the true aerodynamics [5]. As the force and moment balance travels along a prescribed trajectory, the inertial effects generated by its own mass will affect the data collected. This effect can be accounted for using the taring procedure. The taring procedure involves running the trial when the wind tunnel velocity is set to zero mph. These measurements can be subtracted from the recorded trials with the wind tunnel on to get the effects of the trajectory on the model in the wind [40].

The linear motor apparatus requires the use of forced-motion for all completed tests. The rig takes trajectory data from a Galil file and, at the correct point in time relative to the oscillating linear motor, moves the vertical rod to transport the mission store model through the shear layer and out of the cavity. During this motion, the DAQ automatically documents the encoder positions [8]. Verification of this trajectory and timing of the release can be accomplished two ways. First, the analysis of the encoder position data can depict the position of both motors relative to each other when the store is released. Second, the use of a high speed camera can visually track both motors and their relative positions [8]. With the verification data, the tests can be repeated with varying parameters to explore and identify different trends.

2.9 Chapter Summary

This chapter explored the history of cavity aeroacoustics, store separation effects, classification of cavities, open flow phenomena, and the importance of dynamic wind tunnel testing and time-accurate data acquisition. It also discussed the differences in potential rig configurations, including the forced-motion test rig, and introduced additional time-accurate experimental measurement techniques.

III. Methodology

3.1 Introduction

This chapter develops the methodology for analyzing the impact of dynamic wind tunnel testing on two different sized mission store models using the AFIT low-speed wind tunnel and the linear motion apparatus. The materials and equipment used as well as the procedures and processes for executing this experiment are included below.

3.2 AFIT Wind Tunnel

The AFIT wind tunnel, located in Building 644 at WPAFB, is an open circuit design wind tunnel. This means that the flow pulled into the wind tunnel comes from atmospheric conditions and the air flowing out returns to those atmospheric conditions. It provides consistent and accurate flow speeds for consistent tunnel tests. The wind tunnel has the capability of reaching wind speeds of up to 150 mph and can facilitate tests for both static and dynamic tests. The flow is controlled by a LabVIEW interface. The actual test section is 44 inches wide by 31 inches tall and additional dimensions are shown in Figure 8. This test section is accessed by plexi-glass doors on both sides and the upper surface of the test section. There are panels in the doors that allow for additional instrumentation and apparatuses to be in the wind tunnel while still maintaining a quality seal. This provides numerous capabilities for tests and trials.

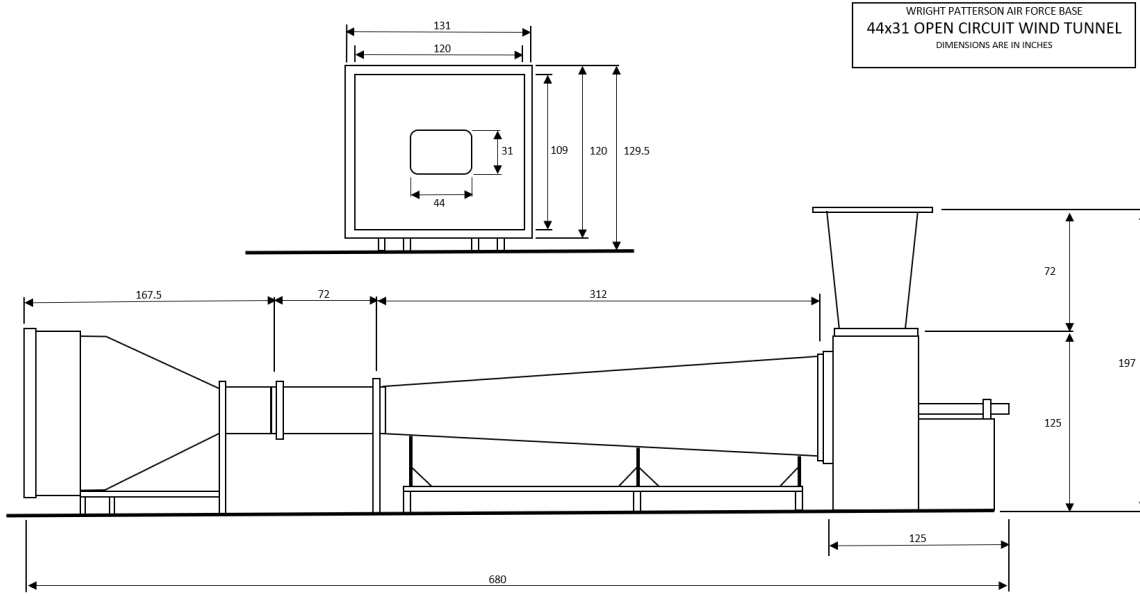


Figure 8: AFIT Wind Tunnel (Not to Scale) [8]

3.3 Linear Motion Apparatus

3.3.1 Design Overview.

The linear motion apparatus (LMA) in the AFIT low-speed wind tunnel lab is used in two configurations, the freestream and cavity apparatuses. The initial cavity apparatus was created in previous research but the design has been improved with the intent to reduce noise and increase the signal-to-noise ratio [8]. A linear motor was attached in the vertical orientation. Multiple sting rods were designed to fit into the motor as well as the weapon store, though only one was used in this experiment. In the cavity apparatus, explained further in this chapter, these rods fit through a linear bearing and only serve the purpose of maneuvering the store vertically. The linear bearing is an addition to previous iterations of the cavity apparatus used in research and is expected to reduce vibration levels and stiffen the system. This should raise the resonance frequency of the system. Also in the cavity set up is a horizontally oriented linear motor, connected to a piston head. This motor pushes air through a

chamber and through openings, described as a “slot” for one design and “fluid diode” for others. These openings inject the air into the freestream just upstream of the front edge of the cavity. This disrupts the flow and the shear layer created by the front lip of the cavity. The motor oscillates at a particular frequency of 5 Hz and generates pulses of air at the same frequency at the front of the cavity. The data was collected through a Nano25 force and moment sensor attached to the weapon store. With this apparatus, many variables can be tested and compared to facilitate the experimentation and analysis of dynamic wind tunnel testing in the AFIT low-speed wind tunnel.

3.3.2 Rig Configurations.

There are two main configurations used for the collection of data in this research. First, the freestream setup can be seen in Figure 9. This configuration allows for the collection of force and moment data affecting the weapon store just from the aerodynamic effects of the wind speed. Second, the cavity setup can be seen in Figure 10. This configuration allows for the collection of force and moment data affecting the weapon store from the effects of the cavity as well as flow control device. Also, in this configuration, the store can be positioned outside the cavity and stationary with the horizontal oscillating motor to collect targeted data in the freestream or inside the disrupted shear layer.

3.3.3 Motor Control System.

The linear motors in the LMA are both controlled by Galil code on the lab computer. The operator sends instructions via an Ethernet cable into the controller. The controller is a DMC-4020 and is discussed in the cavity and mechanical components section. The controller sends the instructions through cables to each individual motor



Figure 9: Freestream apparatus inside the AFIT low-speed wind tunnel

that move to the desired position at the desired time. Phasing between the two linear motors was incorporated into the study. The vertical motor was actuated when the horizontal motor was at different positions, creating different results in the forces and moments.

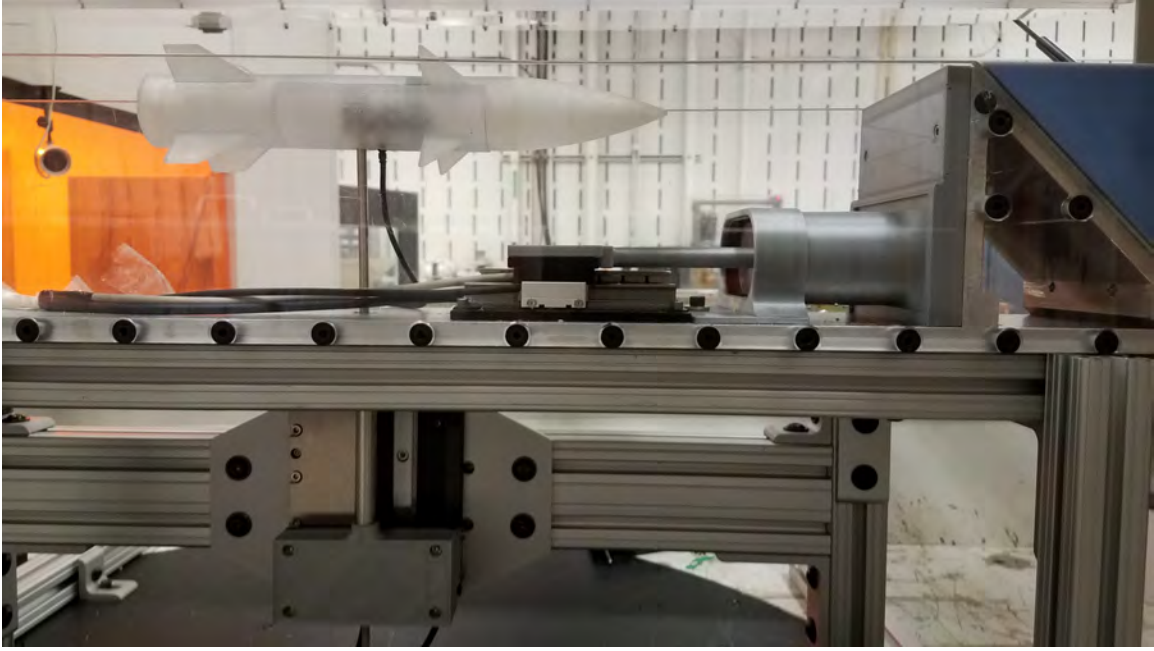


Figure 10: Cavity apparatus inside the AFIT low-speed wind tunnel

3.4 Experimental Models

3.4.1 3D Printer Rapid Prototyping.

In this research, 3D printing was used extensively for rapid prototyping of the mission store models. The two main 3D printers used were the Ultimaker 2+ and the Ultimaker 3. The Ultimaker 2+ used fused deposition modeling (FDM) technology with a single-extrusion print head [41]. The Ultimaker 3 used FDM with a dual extrusion print head [42]. The benefit of the Ultimaker 3 over the Ultimaker 2+ is the capability of building a model or structure with two different materials. A $0.40mm$ nozzle was used for all builds in this experimental study. The material used in these 3D printers for the fabrication of flow control devices was polylactic acid (PLA) chosen for its high print speed, high resolution, good tensile strength, and surface quality [43].

3.4.2 Piston and Sleeve Design.

The piston and sleeve design used in the experiment were the same as those used for Wood's research [8]. These designs are shown in Figures 11 and 12. The piston head uses two ring grooves holding rubber gaskets for a tighter seal and is attached to the linear motor with a mount. With the piston positioned just inside the sleeve, the volume of air that is pushed through the flow control device is $22.37in^3$. Dimensions and additional drawings for these devices can be seen in Wood's research [8]. The piston is attached to the horizontally oriented linear motor laying on the bottom surface of the cavity. The oscillating linear motor achieves mass injection at the leading edge of the cavity. Oscillation of this motor is conducted at 5 Hz. This was determined as the optimum oscillation rate for the analysis of the forces and moments with the current sensor. To minimize wear and improve the seal, the cylinder was lined with three-inch-wide Kapton tape and lubricated. This aspect of the apparatus is unchanged from that used in reference [8].

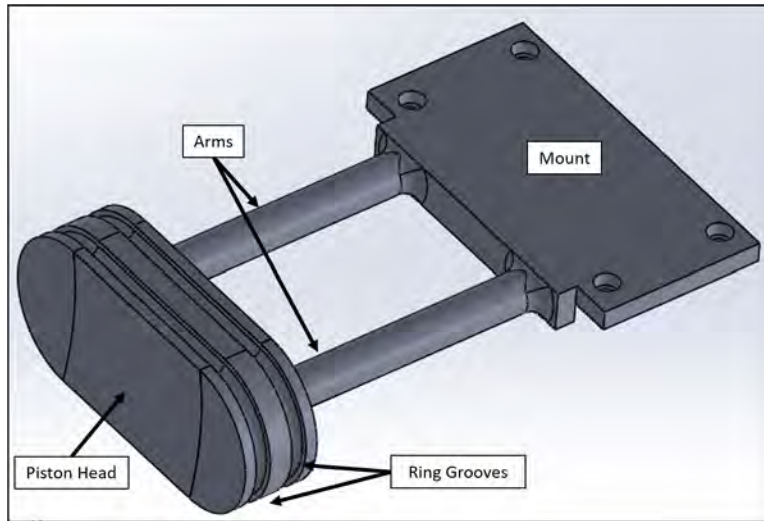


Figure 11: Piston for the leading edge blower [8]

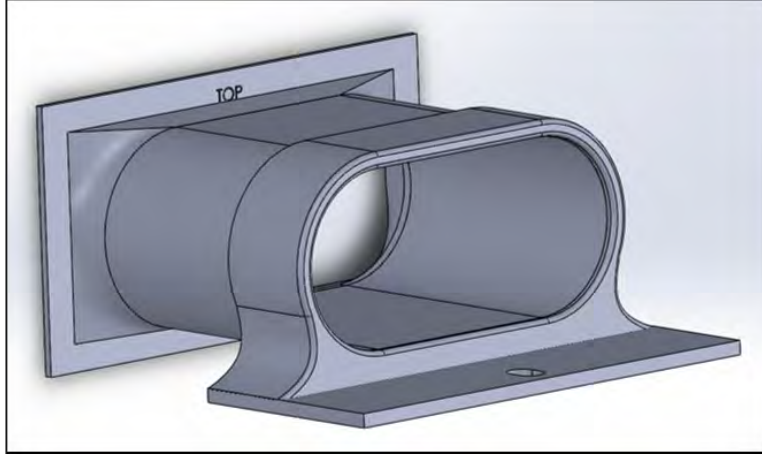


Figure 12: Cylinder for the leading edge blower and support mount [8]

3.4.3 Leading Edge Blowing Devices.

The device positioned at the front of the cavity and connected to the horizontal oscillating linear motor is called a leading edge blowing device. There were two main devices used as variables in this research the slot and diode, both previously developed [8]. Both devices used a channel and two holes to allow for securing of the device to the cavity wall. The channel that connects to the sleeve is shown in Figure 13. Figure 14 shows the internal view of a fluidic diode opening and a depiction of the flow path in a diode. The opening at the top is neither normal or tangential to the flow and introduces a three-dimensional aspect of the flow similar to research conducted by Zhang [29]. The leftmost image is a side-view of the diode. The center image depicts the curve of outer channels with respect to flow direction. The right image show the curve of central channel with respect to the flow direction.

The slot is a rectangular opening with a width of 4.03 inches and depth of 0.25 inches and an exit area of $1.007in^2$ that allows for the passage of air in both directions, in and out. This leading edge blowing device is the same as used in Wood's research and is shown in Figure 15 [8]. Diode 2 is a specific fluidic diode which uses specific geometry to produce different blowing effects. The two outer channels have a width

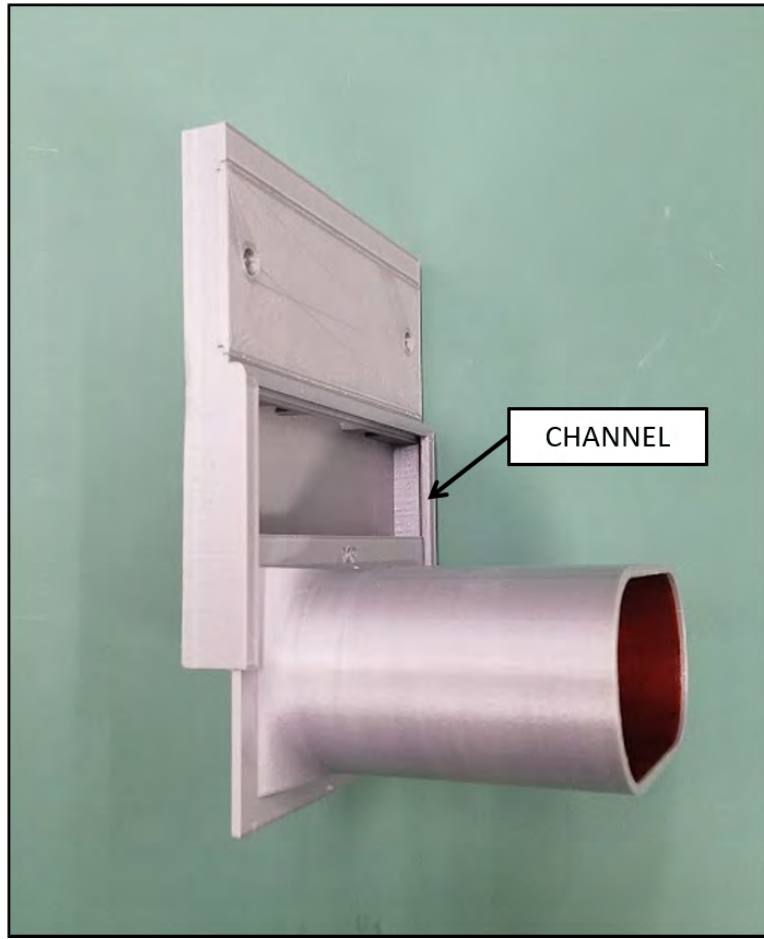


Figure 13: Example of the channel of the slot sliding onto the sleeve. [8]

and depth of 0.5 inches by 0.25 inches, respectively. This particular diode makes it more difficult to push air out of the two peripheral openings and less difficult to push air out of the central opening. Subsequently, the path outward has less resistance through the center channel and more resistance through the channels on either side. Further analysis and research on fluidic diodes and specifications for this particular diode are explained in previous research conducted by Wood [8]. This leading edge blowing device is shown in Figure 16.

All leading edge blowing devices for this study have a channel at the base of the device, under the main chambers that have dimensions of 5.05 inches x 2.53 inches

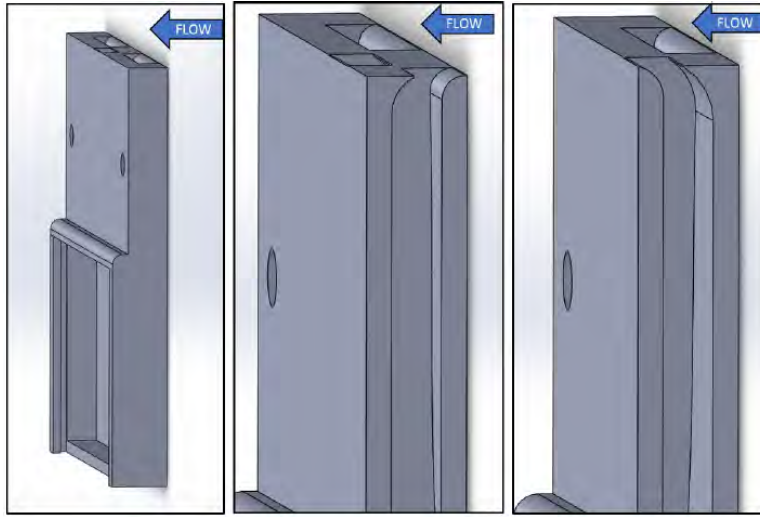


Figure 14: Example of a fluidic diode opening. [8]

x 0.37 inches and a volume of $4.72in^3$. As mentioned in the previous section, the sleeve with the piston inside has a volume of $22.37in^3$. This amount of air is pushed through the channel and through the main chambers of the respective flow control device during every stroke of the horizontally oriented motor.

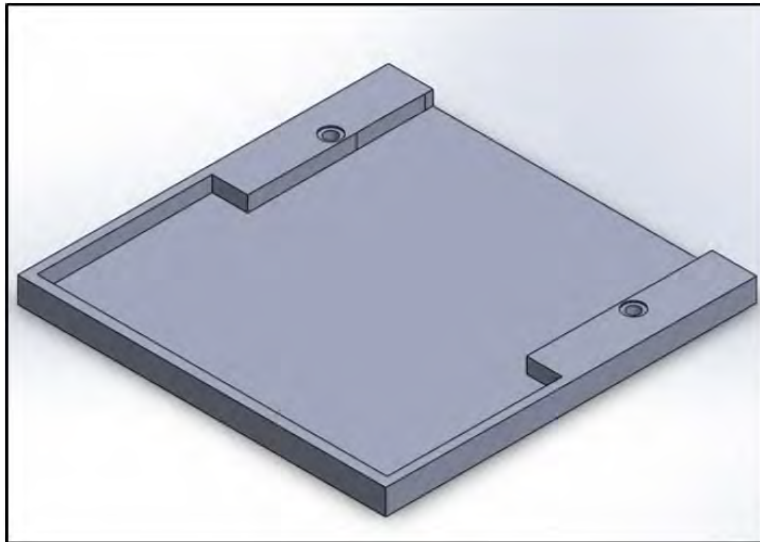


Figure 15: Internal view of the slot leading edge blower [8]

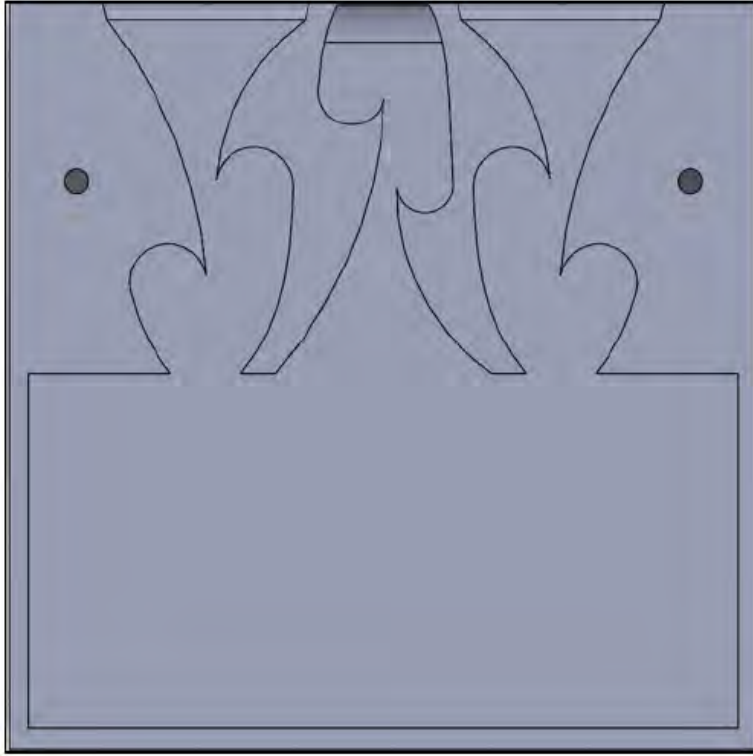


Figure 16: Internal view of the Diode 2 leading edge blower [8]

3.4.4 Support Sting.

The mission store model is connected to a second linear motor positioned vertically which allows for the store release from the cavity. The model starts in a position below the lip of the cavity and ends completely out of the cavity. This motor is attached underneath the floor of the cavity and put through a 0.5625-inch hole at $\frac{x}{L} = 0.55$. Prior work used a sting fabricated from optical rods and had multiple parts. A new rod was made to stiffen the structure. It was fabricated using a steel rod which is 12 inches long and is tapered from 0.5 inches diameter to 0.15 inches diameter starting halfway up the rod. A portion at the bottom was shaved flat which secures the rod to the linear motor by using two screws that create friction on the surface of the flat portion. The rod can be moved up and down by a couple inches and affixed to the linear motor. The rod can be seen in Figure 17 and the flat portion can be seen in

the zoomed Figure 18. The sting is also threaded through a linear bearing with an inside diameter of 0.5 inches. The bearing was set in the drilled hole in the floor of the cavity and was included to stiffen the structure further.



Figure 17: Flat portion of vertical rod

The vertical rod is connected to the linear motor through a mounting block that was 3D printed. This piece can be seen in Figure 19. A hole through the block allows for the rod to slide through the entire piece, and the flat portion of the rod allows

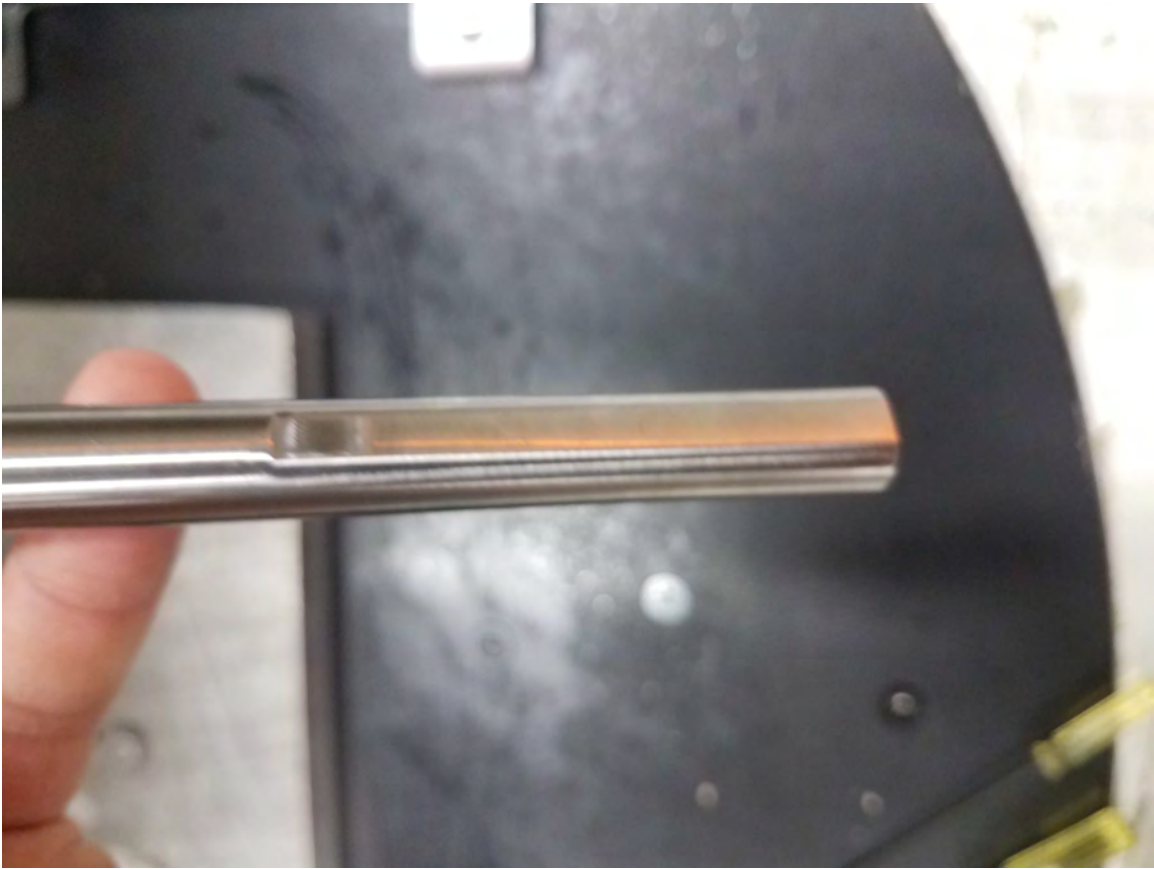


Figure 18: Flat portion of vertical rod which allows for the rod to be secured to the linear motor

for screws to pass through the block and secure the rod. The arrows in the figure show how the height of the rod can be changed by loosening the two screws. A similar mounting block was used in previous research, but this block was designed to be more lightweight and allow for the easy adjustment of the rod height. The adjustability is new to this version. The drawing for this can be found in Appendix D.

3.4.5 Angle of Attack Base Plate.

In order to connect the mission store model to both the Nano25 sensor and the support sting, a 3D printed interface was created to sit on top of the vertical support sting. This plate screws securely into the rod. To reduce noise picked up by the

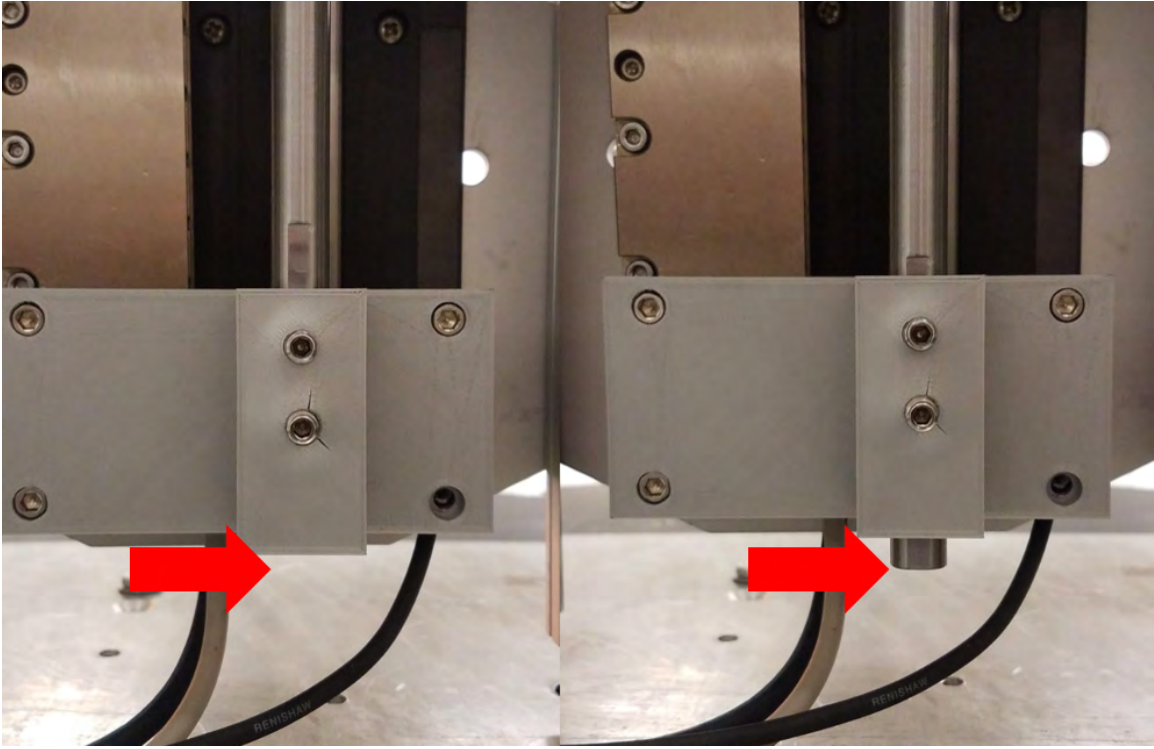


Figure 19: Mounting block connecting the vertical rod and the linear motor, and the arrows show how the height of the rod can easily be adjusted

sensor, two screws were used, one on top and one in the axial direction in relation to the cavity length. The top view of the plate attached to the rod is shown in Figure 20. These holes were tapped into the posts. When screwed in, rotation of the model is prevented so the accurate reading of forces and moments can be achieved. The plate attaches to the Nano25 using three screws with small plastic washers which provide the alignment for the Nano25 and the store model. The plate screwed into the Nano25 and the mission store is shown in Figure 21. Multiple plates with varying angles of attack were printed in both 0° and 10° with diameter of 0.984 inches and width of 0.591 inches. The plates do not come into contact with the inner diameter of the store model.

3.4.6 Mission Store Model.

There were two geometrically-similar models of different scale used in this experiment. One model had a diameter of 1.3 inches and length of 9.25 inches while the other had a diameter of 1.7 inches and length of 12 inches. The models represent generic stores with canards, fins, and an ogive-cylinder shape and do not conform to the specific geometry of any US weapons system. The smaller model was previously used in experiments by Bower [5] and Wood [8] and the larger model was adapted from the smaller one and is unique to this research. The purpose of having a larger model size is to change the scale of the experiment while keeping the freestream conditions consistent. The length of the large model is half of the length of the cavity. Different effects could be identified using a different scale model relative to the cavity length. Also, it is convenient to conduct parametric studies. Finally, this also verifies the measurement approach. The Nano25 sensors are positioned at $\frac{x}{L} = 0.5$ along the model. There is an interface access plate with deliberately designed holes to allow for different angles of attack. The models were made using the Stratasys 3D printer with plastic as the model material. The small and large models can be seen in Figure 22 and Figure 23 respectively. Specifications and drawings for these models are included in Appendix D.

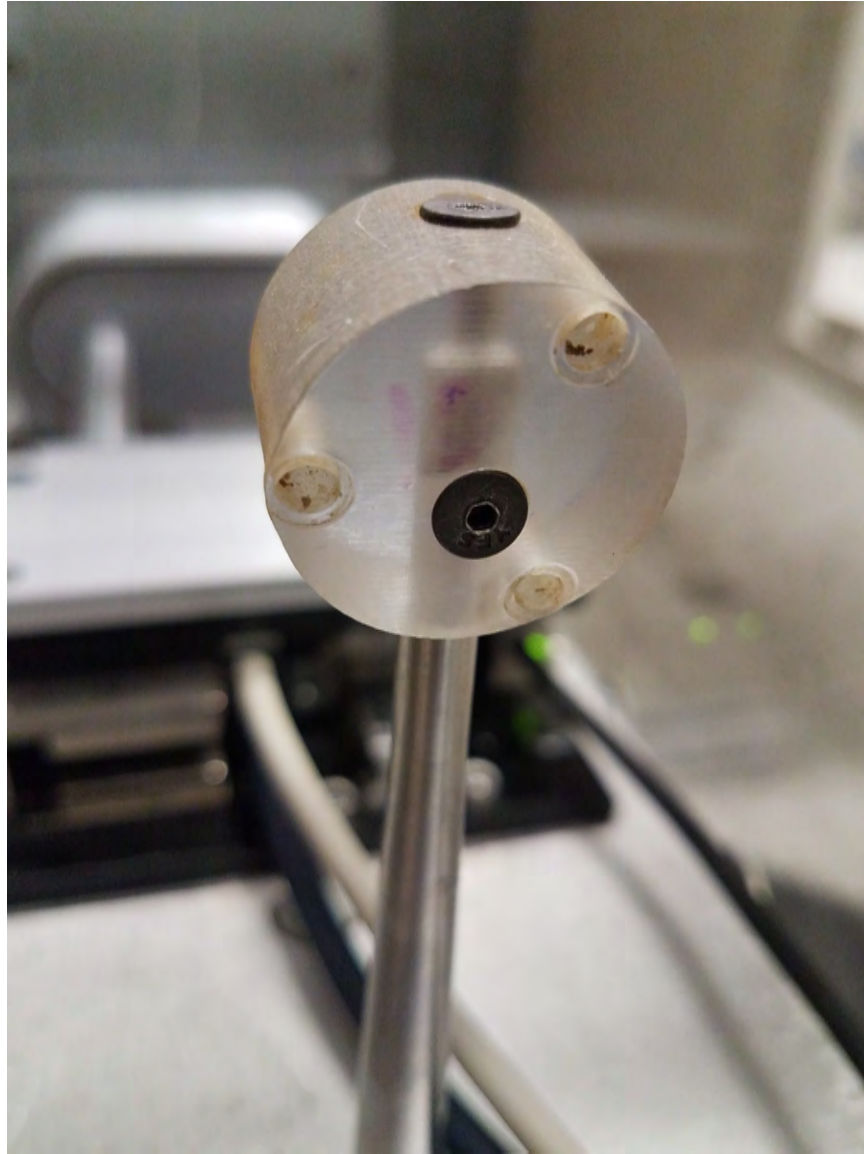


Figure 20: Side view of angle of attack plate showing the top screw that secures the plate to the rod



Figure 21: Angle of attack plate (furthest left) secured to both the Nano25 sensor and the mission store model

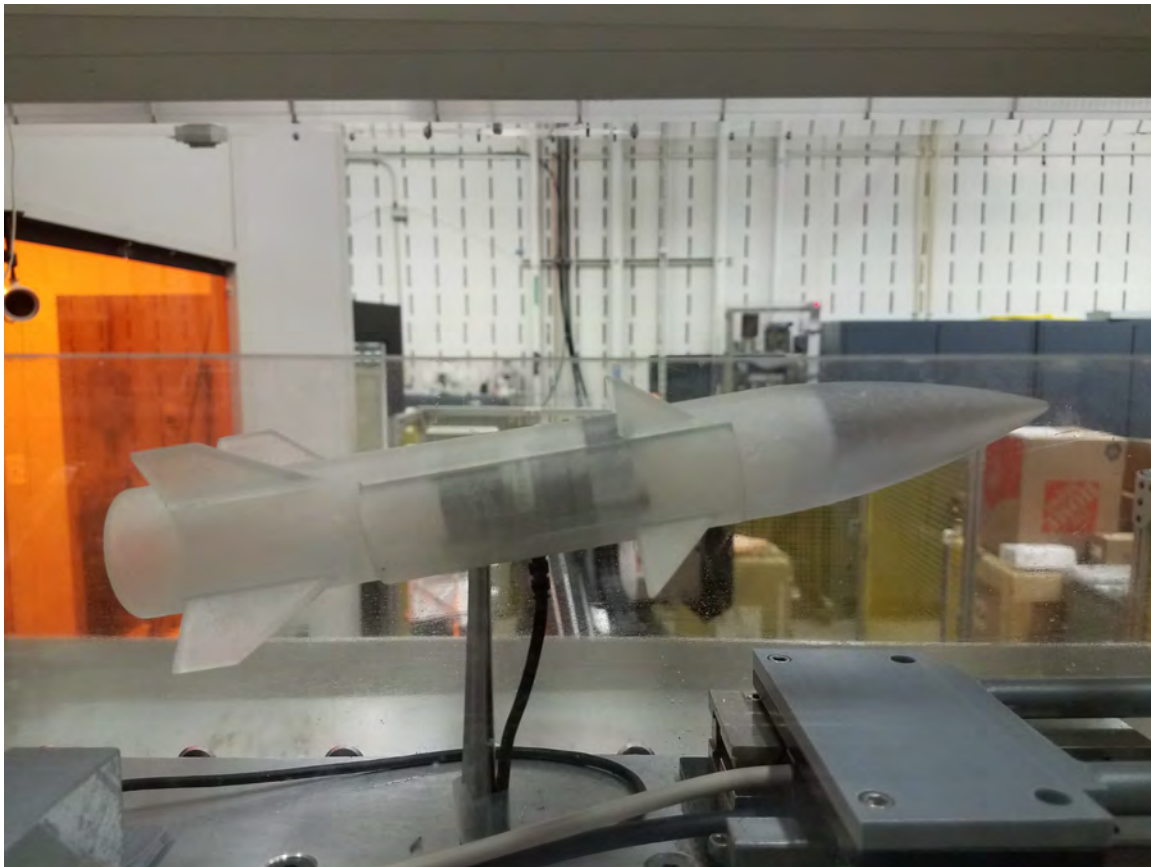


Figure 22: Small mission store model length of 9 inches and diameter of 1.3 inches



Figure 23: Large mission store model length of 12 inches and diameter of 1.7 inches

3.5 Wind Tunnel Apparatuses and Mechanical Components

3.5.1 Freestream Apparatus.

The freestream apparatus consists of the rig configuration described earlier in this chapter and shown in Figure 9. The vertically oriented linear motor is attached to a structure of 80/20 aluminum that is securely attached to the base of the wind tunnel test section. A rod extends vertically with an angle of attack base plate at the top which is also secured to the mission store model. In this position, the Nano25 sensor inside the mission store model can record force and moment data for the freestream without being influenced by a cavity or other apparatuses. This baseline data shows how regular freestream wind speeds affect the forces and moments that are imparted on the mission store model. In this mounting, the missile model was maintained 8 inches from the structure to collect freestream data and not the flow interrupted by the base of the apparatus.

3.5.2 Cavity Apparatus.

The cavity apparatus used in this research can be seen in Figure 10. The cavity is 24 inches long, $5\frac{3}{8}$ inches deep, and $5\frac{3}{8}$ inches wide with a length-to-depth ratio (L/D) of 4.465. The cavity dimensions are based on the SUU-41 pod utilized in flight tests described in reference [44]. This is the same cavity model used in research by Bower [5], and Wood [8]. The cavity apparatus is connected to a base constructed of 80/20 aluminum and securely attached to the base of the wind tunnel test section. The 80/20 structure also secures a vertically oriented linear motor that moves the mission store model. At the rear of the cavity there is a rectangular channel of dimensions 1.5 x 0.5 inches through which the cords for the horizontally oriented linear motor and the Nano25 can pass without significantly disrupting the flow elsewhere within the cavity. There is also a small plastic 3D printed part that confines the electrical

cords to the side of the cavity shown in Figure 24. The dimensions for this are 1.5 inches high, 3.2 inches long, and 1.1 inches wide. The thin part at the bottom that makes contact with the bottom of the cavity is 1 inch long and 0.15 inches high. This approach prevents the cords from interfering with the vertical rod which would create unwanted noise in the force and moment data.

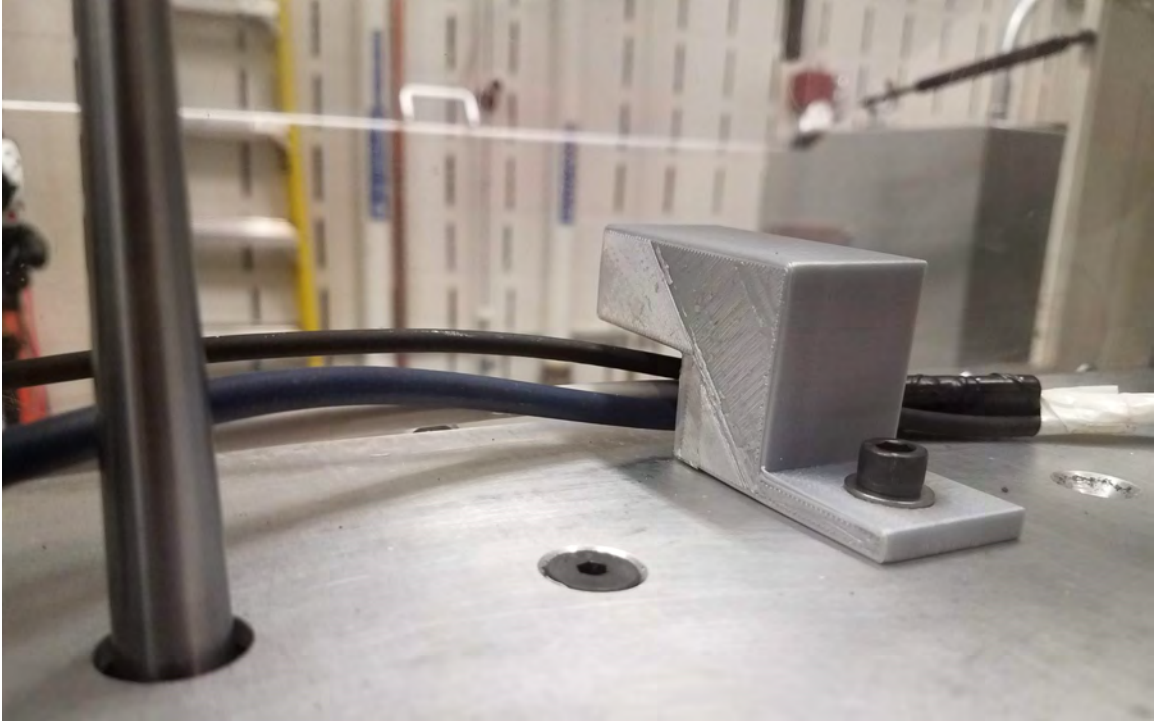


Figure 24: 3D printed piece that holds the linear motor wires to the side of the cavity so the wires don't hit the vertical rod and impacting the force measurements

3.5.3 Linear Motor.

The linear motors used in this experiment are brushless motors shown in Figure 25 and were supplied by H2W Technologies, Incorporated. This particular model is an SRS-003-04-003-01 low-profile single-rail linear motor and has dimensions of 5.3 x 5.3 inches. There are four tapped holes, one in every corner, to allow the motor to be secured to any apparatus. The stroke length of this model is 3 inches and it can

generate 2.7lbs continuous force and 10.7lbs peak force. Finally, the LM13 encoder is a contactless linear magnetic system with a resolution of 1.0 micrometer [45]. Two of these motors were used in the experiment, one in the vertical orientation which drove the store out of the cavity, and one in the horizontal orientation which provided disruption in the freestream.



Figure 25: SRS-003-04-003-01 Linear Motor used for the experimental study [8]

3.5.4 Controller.

The Galil DMC-4020 is the controller used in this experiment to operate the linear motors. The controller, shown in Figure 26, can execute point to point positioning, jogging, and sinusoidal modes of motion. It contains the amplifier that can drive motors at 20-80 VDC and up to 10 Amps continuous. The amplifier can also drive motors up to 15 Amps peak and protects against over/under voltage and over-current as well as short-circuit protection [46]. The controller accepts encoder inputs up to 22.0 MHz and provides servo update rates of 16 kHz [47]. An important feature is the multi-axis control which allows for synchronization of the motors, and this attribute plays a key role in the second phase of this experiment [8]. The controller interfaces through an Ethernet port labeled Ethernet 0 on the controller. The main processor

of the controller is RAM and Flash capable which can do live execution or download a batch of commands for later execution [46].

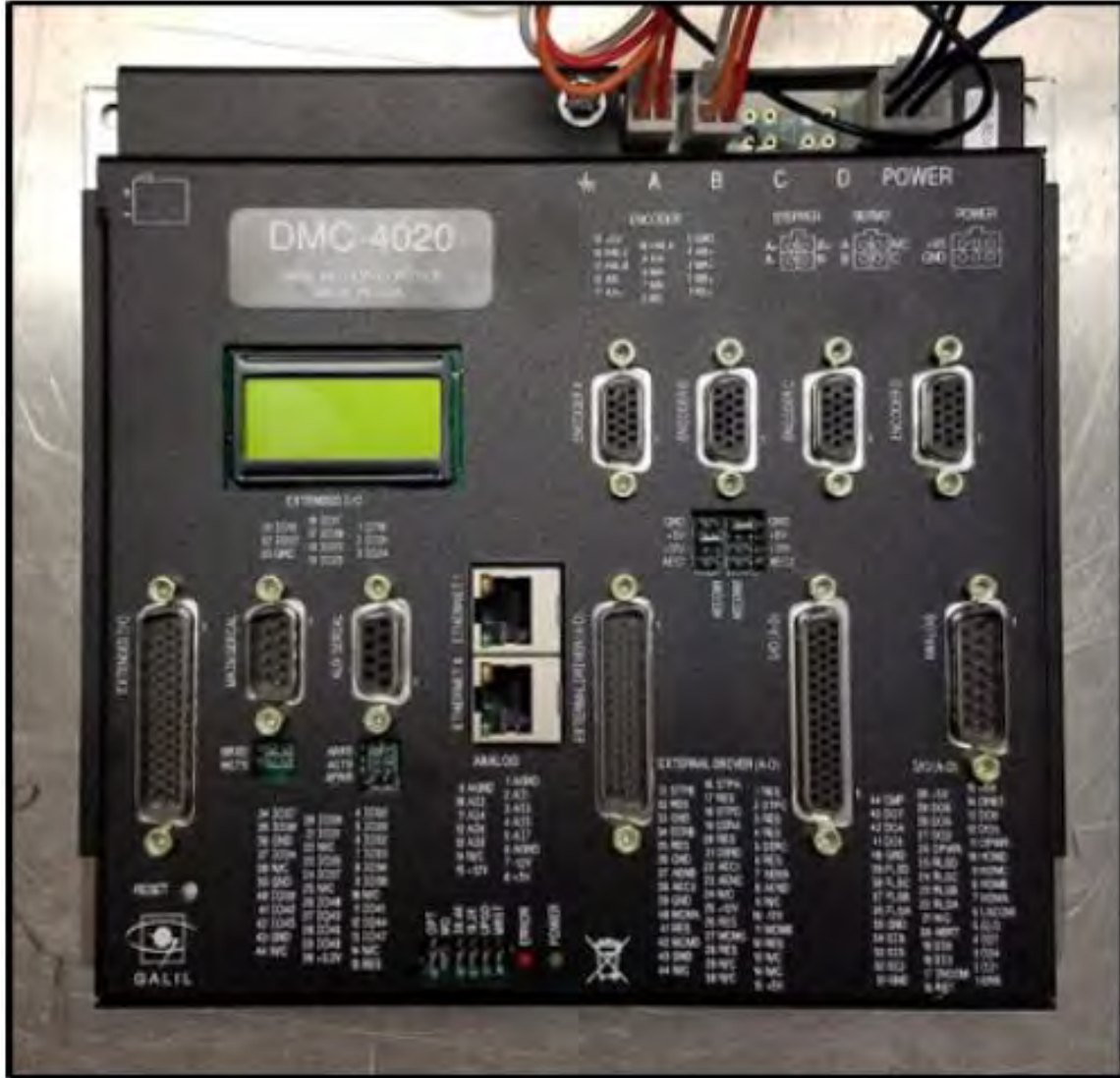


Figure 26: Galil DMC-4020 dual-axis motion controller [8]

3.5.5 Controller Programming and Operation.

For operation of the Galil controller, power is provided by an Acopian linear regulated power supply which outputs both AC and DC in a single output. To drive the linear motor, the amplifier converts the ± 10 Volts signal to current. A green light

is illuminated on the encoder portion of the linear motor and a green light labeled PWR is illuminated on the controller when power is supplied to the system. The linear motors are plugged into the encoder power slots labeled A and B. All code refers to the horizontally oriented motor as A and the vertically oriented motor as B. Then VGA cords from the motors are plugged into the Encoder A and Encoder B positions, respectively.

All programming for this system was made in the Galil Design Kit (GDK) software package. This package includes a terminal, program editor, scope, and has auto-tuner capabilities. The Galil code consists of two ASCII uppercase characters followed by an applicable argument [46]. The capability of the controller extends to interpreting conditional statements to loop required commands or for positional based triggers such as those used in phase two of the experiment. Each motor requires an initialization code to be executed before additional commands are sent. The initialization code used for the motors in this experiment can be found in the Galil section of Appendix C. Further instructions on this programming and the creation of an initialization code can be found in the work by Wood [8].

3.5.6 Nano25 Force and Torque Transducer.

The sensor used in this experiment is a six-component wind tunnel balance. The ATI Nano25 force and torque transducer characterizes loads and moments acting on the aerodynamic body. Wind tunnel balances traditionally acquire time-averaged values but the Nano25 is a piezoresistive sensor is effective for time-accurate data. The Nano25 is 0.984 inches in diameter, 0.85 inches in height, and weighs 0.14 pounds [48]. It has the capability of accurately measuring forces and moments well over 25 pounds force. The manufacturer cites a resonant frequency of 3600 Hz for F_x , F_y , and T_z , and 3800 Hz for F_z , T_x , and T_y [48]. Each Nano25 was delivered with a unique

signal conditioner box both with serial number FTI-15790.

The sensor measures forces in the x-, y-, z- axes (F_x, F_y, F_z) and torques about the x-, y-, z-axes (T_x, T_y, T_z). F_{xy} and T_{xy} denote any combination of forces and torques in the x- and y- directions respectively. The Nano25 balance outputs in imperial units. Two tables with the specifications of the sensor can be seen in Tables 1 and 2. Figure 27 shows how the right hand rule matches with the directions of the measurements. The coordinate system is transformed to be in accordance with AIAA Nomenclature and Axis Systems for Aerodynamic Wind Tunnel Testing Guide as shown in Figure 28 and using equation 3.1 [8].

It should be noted that the pitch moment is recorded with reference to the face of the sensor which is placed at $\frac{x}{L} = 0.5$ on each model. Also, the axial force is recorded with reference to the front face of the sensor.

$$\begin{bmatrix} F_{x_{Nano25}} \\ F_{y_{Nano25}} \\ F_{z_{Nano25}} \\ T_{x_{Nano25}} \\ T_{y_{Nano25}} \\ T_{z_{Nano25}} \end{bmatrix} = \begin{bmatrix} A_{z_b} \\ A_{y_b} \\ A_{x_b} \\ T_{x_b} \\ T_{y_b} \\ T_{z_b} \end{bmatrix} = \begin{bmatrix} -N \\ Y \\ -A \\ l \\ m \\ n \end{bmatrix} \quad (3.1)$$

	Sensing Ranges	Resolution
Fx, Fy	25.0 lb_f	1/224 lb_f
Fz	100.0 lb_f	3/224 lb_f
Tx, Ty	25.0 $lb_f - in$	1/160 $lb_f - in$
Tz	25.0 $lb_f - in$	1/320 $lb_f - in$

Table 1: Nano-25 Calibration Specifications [6]

The Nano25 balance produces analog voltages recorded using LabVIEW program and saved as .lvm files. Matlab code post-processes the voltages and can produce

Single-Axis Overload	
F _{xy}	$\pm 520.0 \text{ lb}_f$
F _z	$\pm 1600.0 \text{ lb}_f$
T _{xy}	$\pm 380.0 \text{ lb}_f - in$
T _z	$\pm 560.0 \text{ lb}_f - in$

Table 2: Nano-25 Single-Axis Overload [6]

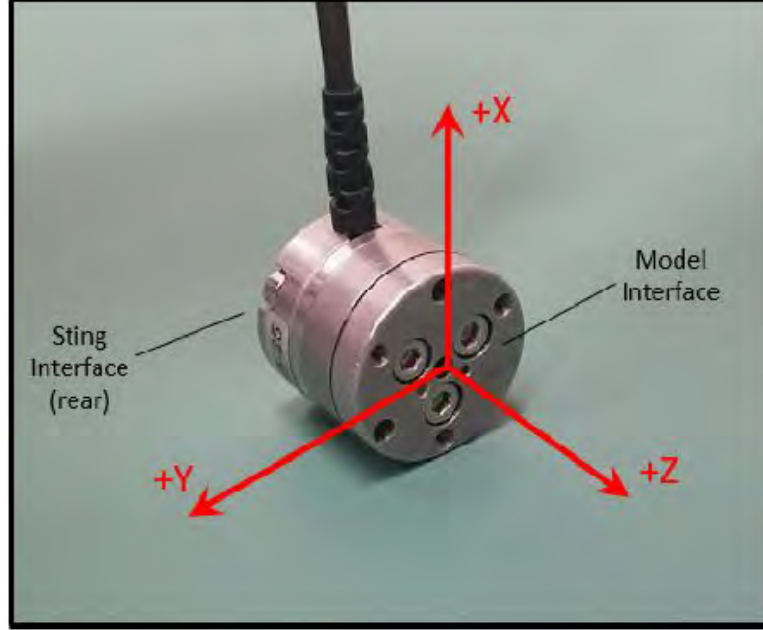


Figure 27: Direction of measurements made by the Nano25 sensor [8]

time-accurate forces and moments. Post processing requires a calibration matrix which is unique to each Nano25 and provided by ATI. The calibration matrix for this Nano25 sensor is shown in Figure 29. This sensor was used by Sellers [49], Bower [5], and Wood [8] to collect data at rates up to 1000.0 Hz for a wing oscillating at 1.5 Hz.

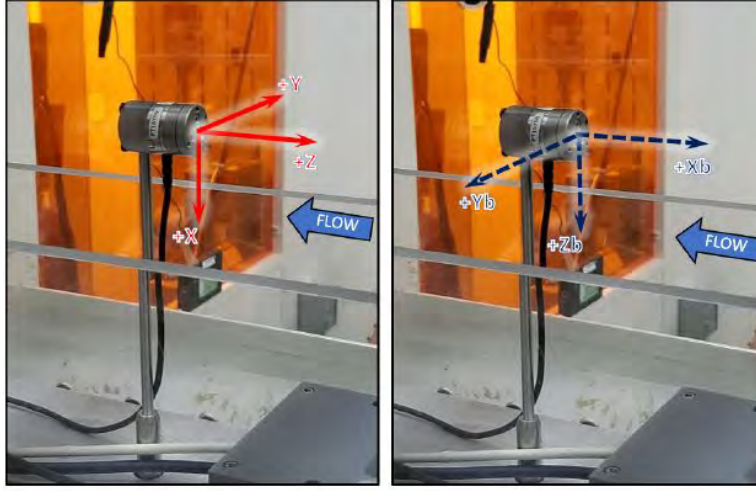


Figure 28: Direction of measurements made by the Nano25 sensor [8]

0.01666	-0.00399	-0.31744	2.98746	0.42269	-3.00593
0.17884	-3.47015	-0.14035	1.72288	-0.31903	1.75159
5.26167	-0.04467	5.59050	0.20559	5.32144	-0.10468
0.07209	-1.22529	2.09820	0.72446	-2.13718	0.63742
-2.40927	0.01016	1.39990	-1.01331	0.98241	1.08087
0.03166	-1.11580	0.14224	-1.09552	0.16628	-1.10239

Figure 29: Calibration matrix of Nano25 model FTI-15790 [8]

3.6 Overview of Experimental Setup

The experiment was expanded into two major phases. First, wind tunnel testing was executed with the model placed statically in both the freestream flow and at various heights in the cavity apparatus. The model was attached to a shaft and a linear motor that was used for the second phase. The collection of force and moment data were accomplished using the Nano25 sensor which is connected to the mission store model. The second phase involved dynamic wind tunnel testing of the mission store being released from the cavity. This was accomplished using the linear motor and the vertical shaft. As the model is drawn out of the cavity on a simulated release

trajectory, force and moment data were collected using the Nano25 sensor. Additional information regarding the execution of the experiment and post processing of the data is provided in the following sections. Repeatability of the trials are discussed in the respective sections.

3.7 Phase I: Static Wind Tunnel Tests

3.7.1 Trials and Variables.

The static wind tunnel tests conducted consist of both freestream and cavity trials. Many variables within this experiment have been changed to analyze different phenomena and impacts of each variable. These variables include changing the angle of attack between 0° and 10° , the store sizes of geometrically similar models at 9.25 inches and 12 inches, wind tunnel speeds of 0, 60, 100, and 120 mph, and three different positions with the cavity apparatus. The static test positions in the cavity apparatus include in the cavity, as low as the linear motor can go, in the shear layer created by the front lip of the cavity, and out of the cavity at the max height the linear motor goes. The heights of the model measured from the cavity floor for the “in cavity”, “shear layer”, “out of cavity” positions, with dimensions in inches to clarify the setup, are shown in Tables 3, 4, and 5, respectively. Recall the full cavity dimensions are 24 inches long, $5\frac{3}{8}$ inches deep, and $5\frac{3}{8}$ inches wide with a length-to-depth ratio of 4.465. Additionally, the heights of the models in the “out of cavity” position measured from the top lip of the cavity are shown in Table 6. These positions are depicted in Figures 30, 31, and 32, respectively. Illustrations of these positions and measurements are shown in Figures 82, 83, and 84 in Appendix B.

A portion of the test matrix for Phase I is shown below in Table 7 and the full test matrix is shown in Appendix A. Each variation of variables resulted in another completed trial and data collected. As discussed earlier in the chapter, the data

Point of Measurement	Small 0 AoA L = 9.25in D = 1.3in	Large 0 AoA L = 12in D = 1.7in	Small 10 AoA L = 9.25in D = 1.3in	Large 10 AoA L = 12in D = 1.7in
Front of Model	3.9	3.85	4.85	5
Vertical Rod	3.25	3	3.25	3
Back of Model	3.25	3	2.75	2.25

Table 3: “In Cavity” position heights of model from the cavity floor in inches

Point of Measurement	Small 0 AoA L = 9.25in D = 1.3in	Large 0 AoA L = 12in D = 1.7in	Small 10 AoA L = 9.25in D = 1.3in	Large 10 AoA L = 12in D = 1.7in
Front of Model	5.4	5.35	6.35	6.5
Vertical Rod	4.75	4.5	4.75	4.5
Back of Model	4.75	4.5	4.25	3.75

Table 4: “Shear Layer” position heights of model from the cavity floor in inches

Point of Measurement	Small 0 AoA L = 9.25in D = 1.3in	Large 0 AoA L = 12in D = 1.7in	Small 10 AoA L = 9.25in D = 1.3in	Large 10 AoA L = 12in D = 1.7in
Front of Model	6.9	6.85	7.85	8
Vertical Rod	6.25	6	6.25	6
Back of Model	6.25	6	5.75	5.25

Table 5: “Out of Cavity” position heights of model from the cavity floor in inches

Point of Measurement	Small 0 AoA L = 9.25in D = 1.3in	Large 0 AoA L = 12in D = 1.7in	Small 10 AoA L = 9.25in D = 1.3in	Large 10 AoA L = 12in D = 1.7in
Front of Model	1.55	1.5	2.5	2.65
Vertical Rod	0.9	0.65	0.9	0.65
Back of Model	0.9	0.65	0.4	-0.10

Table 6: “Out of Cavity” position heights of model from the top lip of the cavity in inches

collection was made possible by the NI DAQ system. The files for each trial were taken and post processed with LabVIEW and Matlab.

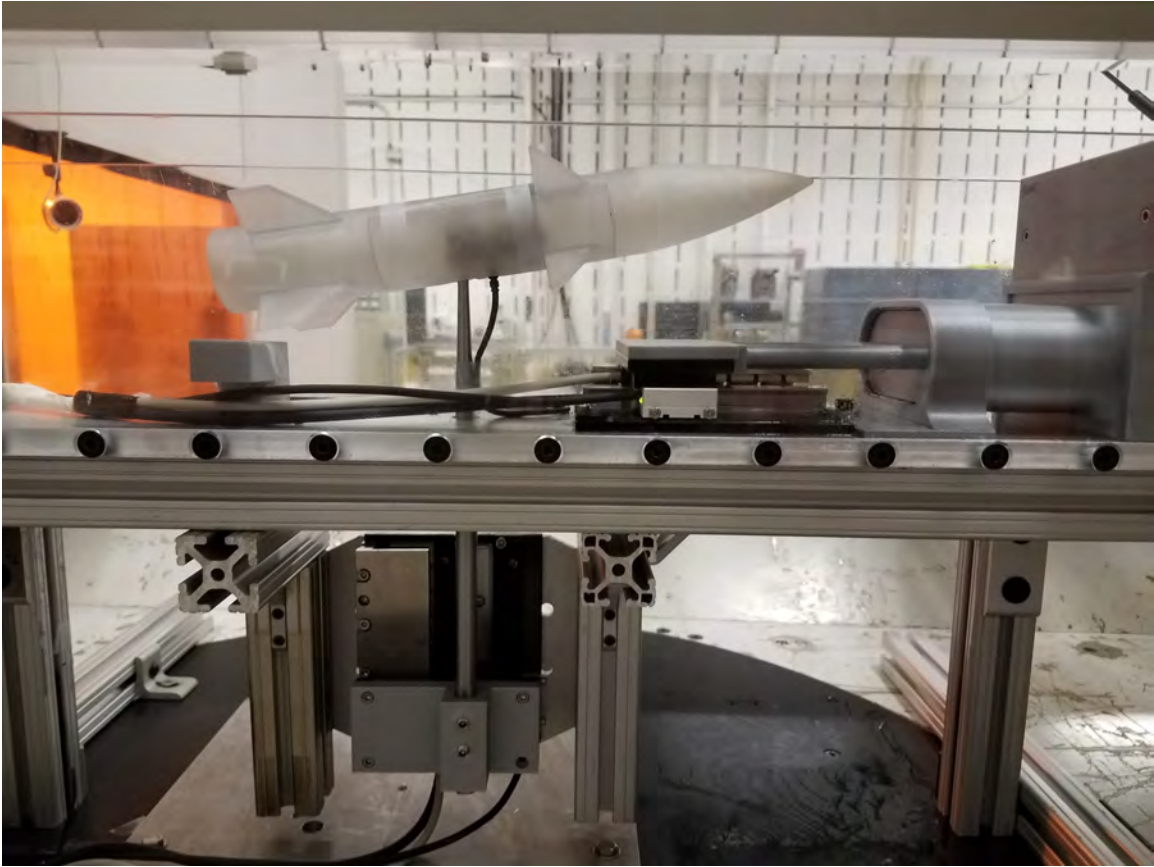


Figure 30: Lowest position of mission store in the cavity apparatus

3.7.2 Post Processing Phase I.

The LabVIEW files that each trial was recorded in were converted into .csv files in Microsoft Excel. After conversion, these files could be imported into Matlab. The files contain vectors for time, and six vectors for voltage data in each of the six force and moment directions. The vector of voltage data is multiplied by the calibration matrix to calculate the forces and torques as shown in Equation 3.2. The code executed to import the data into Matlab involves a for loop, reading the data from a .csv file, taking a two-second portion of the data, and making a time vector. The code used is as follows:

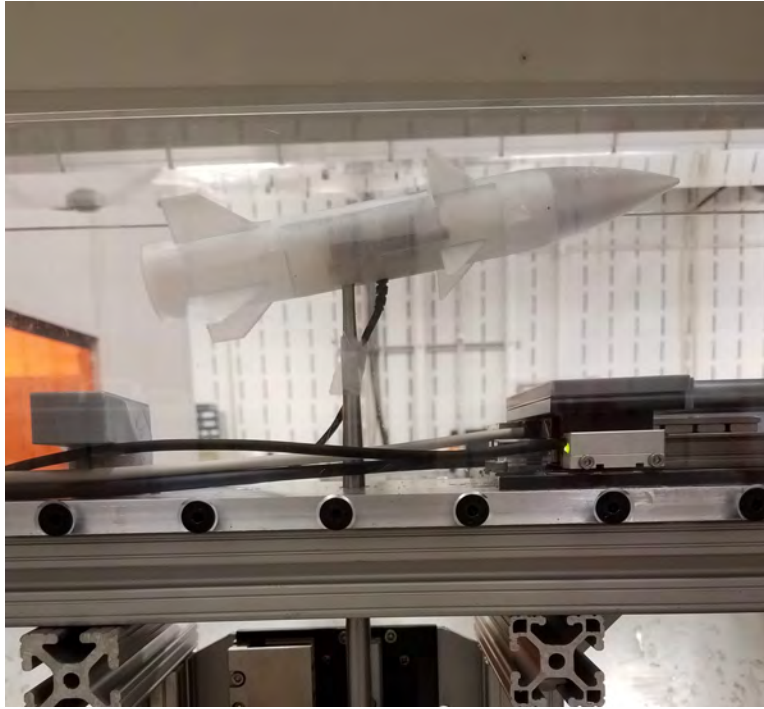


Figure 31: Shear layer, or midpoint, position of mission store in the cavity apparatus

Apparatus	Model	AoA ($^{\circ}$)	Speed (mph)	Position
Freestream	Large	0	60	Out of Cavity
Freestream	Large	0	100	Out of Cavity
Freestream	Large	0	120	Out of Cavity
Freestream	Large	10	60	Out of Cavity
Freestream	Large	10	100	Out of Cavity
Freestream	Large	10	120	Out of Cavity
Cavity	Small	0	60	In Cavity
Cavity	Small	0	60	Shear Layer
Cavity	Small	0	60	Out of Cavity
Cavity	Small	0	100	In Cavity
Cavity	Small	0	100	Shear Layer
Cavity	Small	0	100	Out of Cavity
Cavity	Small	0	120	In Cavity
Cavity	Small	0	120	Shear Layer
Cavity	Small	0	120	Out of Cavity

Table 7: Example portion of the Phase 1 test matrix portion. Sample of different variables used in the full matrix.

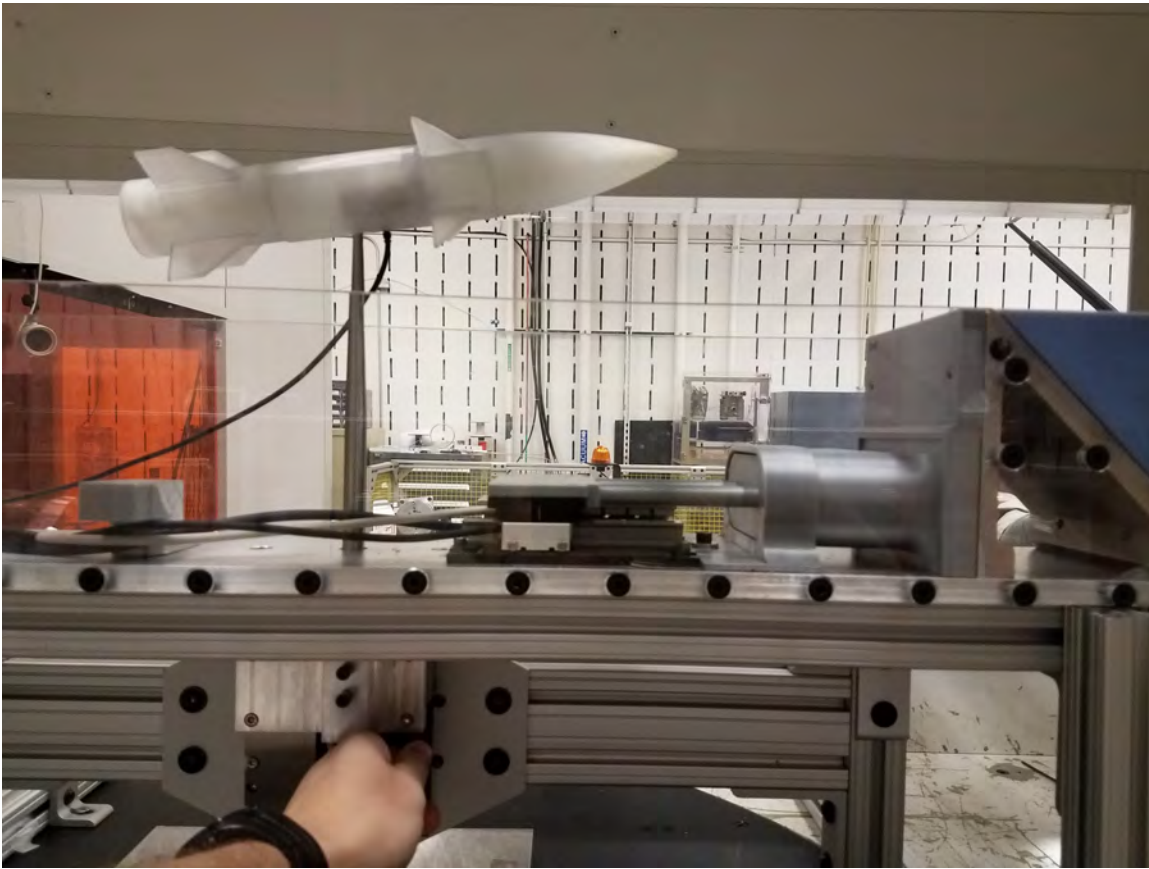


Figure 32: Highest position of mission store in the cavity apparatus

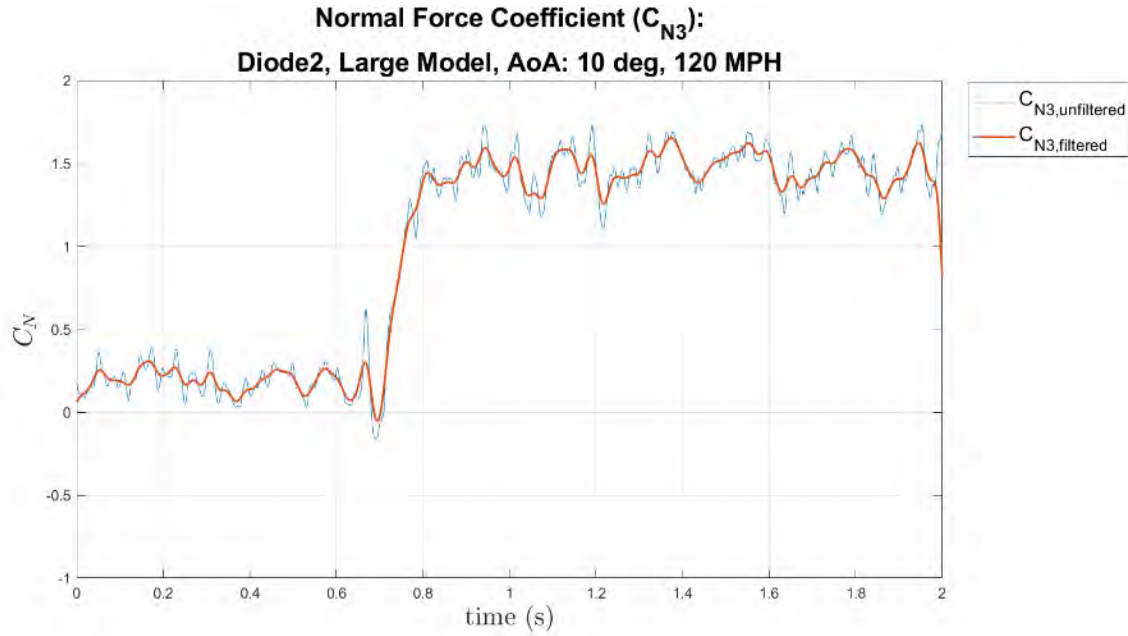
DATA IMPORT MATLAB CODE:

```
for i = 1:length(x1)
    voltage{i}.import1 = csvread(filename1{i});
    voltage{i}.use1 = voltage{i}.import1(end-x1(i):end-x2(i),:);
    voltage{i}.time1 = voltage{i}.use1(:,1);
    voltage{i}.encodera1 = voltage{i}.use1(:,8)/10^5;
    voltage{i}.encoderb1 = voltage{i}.use1(:,9)/10^5;
    voltage{i}.encoderb1 = voltage{i}.encoderb1/div1(i);
end
```

$$\begin{bmatrix} F_x \\ F_y \\ F_z \\ T_x \\ T_y \\ T_z \end{bmatrix} = \begin{bmatrix} 0.01666 & \cdots & -3.00593 \\ \vdots & \ddots & \vdots \\ 0.03166 & \cdots & -1.10239 \end{bmatrix} \begin{bmatrix} V_{Fx} \\ V_{Fy} \\ V_{Fz} \\ V_{Tx} \\ V_{Ty} \\ V_{Tz} \end{bmatrix} \quad (3.2)$$

Filtering was required to clarify some traits of the data. The process for the coding of the filter is described in Wood's research and supported by observations in Bowers research [8]. An analog cutoff frequency filter in LabVIEW was used in the data collection at 30 Hz. The time required for the maneuver to release the store, approximately $0.15\text{sec} \pm 0.05\text{sec}$, and the desired observable frequency being 5 Hz both were factors in choosing the filter specifications. The frequency of 15 Hz makes it more difficult to measure what is exactly happening during the motion because the motion itself is on the same order of magnitude. Then a digital cutoff frequency filter in Matlab was used to provide further clarity. This time the cutoff frequency was set at 15 Hz, about half of the analog one which smoothed the data to match the original data very well. This is a FIR filter. The Matlab code and an example of the result of the filtering are shown in Figure 33.

Emphasized plots are shown in the results and analysis chapter and include normal force, pitch moment, and axial forces experienced by the mission store. The Matlab code used for the static tests in the freestream apparatus as well as the cavity apparatus can be seen in Appendix C. Reynolds number information is included in the Phase II.



```

Fs = 1000; % sample rate in Hz +
cof = 15; % cutoff frequency in Hz
order = 60; % -th Order of lowpas filter
Fnorm = cof/(Fs/2); % Normalized frequency

for i = 1:length(x1)
    df = designfilt('lowpassfir','FilterOrder',order,'CutoffFrequency',Fnorm);
    Delay = mean(grpdelay(df)); % filter delay in samples
    filtered{i}.CN = filter(df,[voltage{i}.CN; zeros(Delay,1)]); % Delay zeros concatenated with the input data
    filtered{i}.CN = filtered{i}.CN(Delay+1:end); % Shift data to compensate for delay
    filtered{i}.CY = filter(df,[voltage{i}.CY; zeros(Delay,1)]); filtered{i}.CY = filtered{i}.CY(Delay+1:end);
    filtered{i}.CA = filter(df,[voltage{i}.CA; zeros(Delay,1)]); filtered{i}.CA = filtered{i}.CA(Delay+1:end);
    filtered{i}.Cl = filter(df,[voltage{i}.Cn; zeros(Delay,1)]); filtered{i}.Cl = filtered{i}.Cl(Delay+1:end);
    filtered{i}.Cm = filter(df,[voltage{i}.Cm; zeros(Delay,1)]); filtered{i}.Cm = filtered{i}.Cm(Delay+1:end);
    filtered{i}.Cn = filter(df,[voltage{i}.Cl; zeros(Delay,1)]); filtered{i}.Cn = filtered{i}.Cn(Delay+1:end);

```

Figure 33: Example of matlab filtering and a normal force coefficient plot. The coefficient value is plotted by the blue line and filtered data is plotted by the red line

3.7.3 Repeatability of Static Trials.

Repeatability trials were conducted to test the precision of the recorded measurements for various static trials. First, ten tare trials were recorded to see the impact of recording different tare trials in the same conditions. These trials were conducted with the large model in the out-of-cavity position. Figure 34 shows the normal force coefficient, C_N , of ten tare trials in varying gradients of grey and the mean of those trials in blue. The average value of the mean vector was a nominal

value of $N = -0.392\text{ lbf}$ which is the weight of the large model and accompanying apparatus on the Nano25 sensor. This value was added to the trials. All ten trials fell in between $C_N = -0.008$ and $N = 0.008\text{ lbf}$ with a difference of only 0.016. The average value, after subtracting the mean, of the tare trials lies around zero with a standard deviation of 0.00015. This means that the precision of the recorded data is very high with only small differences in the recorded data from trial to trial.

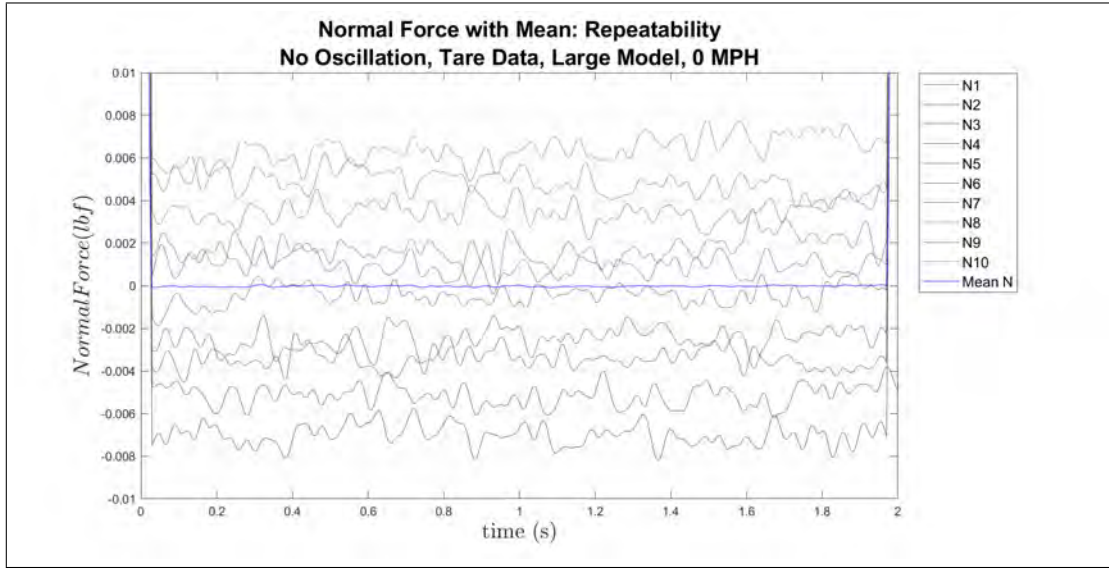


Figure 34: Static normal force repeatability, large model, 10° AoA, tare and mean

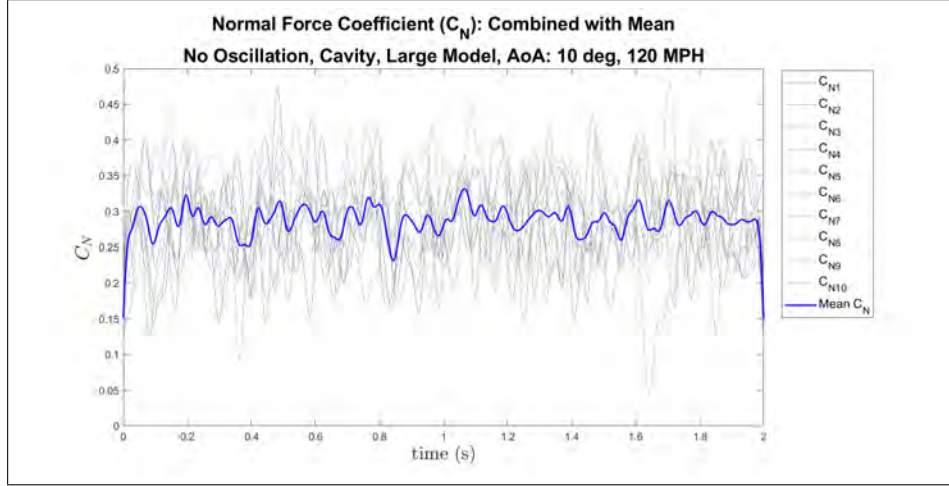
Additional repeatability trials were conducted for the large model at 10° AoA and 120 mph in all three positions in the cavity apparatus and shown in Figure 35. The flow control device was not turned on for these trials. Again, the ten trials for each case are in varying gradients of grey and the mean is in blue. The mean is $\overline{C}_N = 0.289$ for the in-cavity position shown in Figure 35a with a standard deviation of 0.0163. The mean is $\overline{C}_N = 1.015$ for the shear layer position shown in Figure 35b with a standard deviation of 0.021. Finally, the mean is $\overline{C}_N = 1.662$ for the out of cavity position shown in Figure 35c with a standard deviation of 0.015. These are consistent with the values presented above in this phase of the research. While there are some

differences between specific recorded trials with the same conditions, the deviation from the mean is at maximum only 0.15.

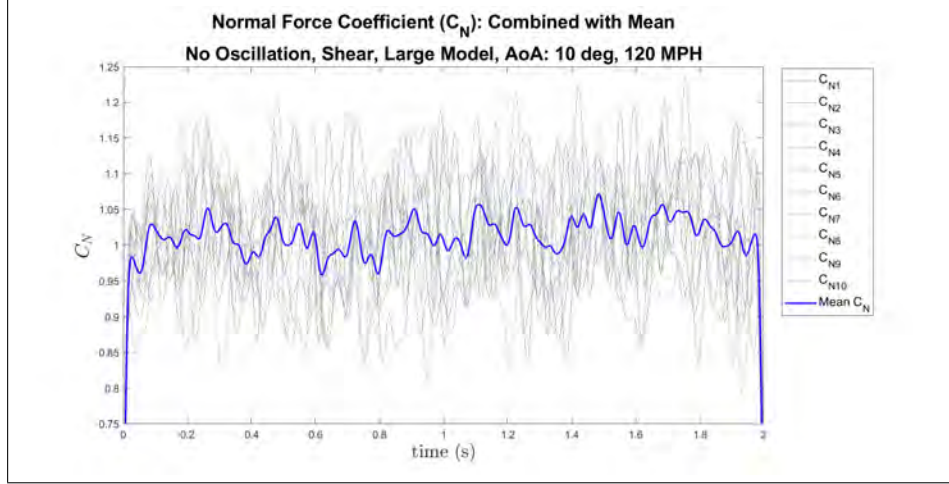
All of these values for the static repeatability trials can be seen in Table 8. The standard deviations for the trials are relatively low, especially for the tare trial. The standard deviation for the shear layer is higher than the other two positions. The trends for the normal force coefficient are clear, with a drastic increase in normal force coefficient when the mission store is released from the cavity. The precision overall for each trial is relatively high.

Model	Angle(Deg)	Speed (mph)	Position	\bar{C}_N Before	std dev
Large	0	0	Out Cavity	-4.684	0.0001
Large	10	120	In cavity	0.289	0.016
Large	10	120	Shear Layer	1.015	0.021
Large	10	120	Out Cavity	1.662	0.015

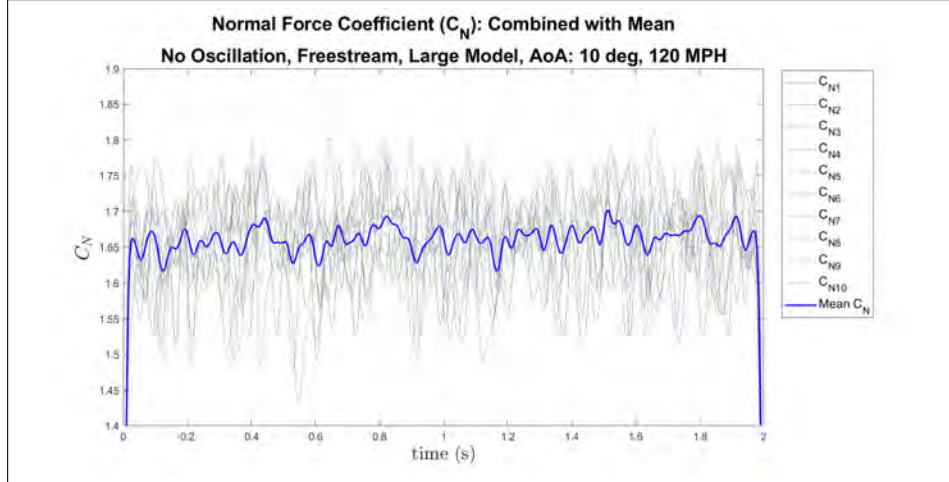
Table 8: Repeatability of static normal force coefficients at various positions in the cavity apparatus, large model



(a) Static repeatability, large model, 10° AoA, 120 mph, in cavity position, 10 trials and mean



(b) Static repeatability, large model, 10° AoA, 120 mph, shear layer position, 10 trials and mean



(c) Static repeatability, large model, 10° AoA, 120 mph, out of cavity position, 10 trials and mean

Figure 35: Repeatability of static normal force coefficients at 10° AoA in the cavity apparatus, large model, all wind speeds

3.8 Phase II: Dynamic Wind Tunnel Tests

3.8.1 Trials and Variables.

Many variables within this experiment have been changed to analyze different phenomena and impacts of each variable. These variables include changing the angle of attack between 0 and 10°, the weapon store size at a 9 inches and 12 inches, wind tunnel speed between 60, 100, and 120 mph, two different fluidic diode variations, and finally the timing of the weapon release relative to the horizontally oriented motor position. A sample table of the test matrix for this phase is included below in Table 9 and the full test matrix is shown in Appendix A.

Model	FC Device	AoA (°)	Speed (mph)	Release Timing
Small	Slot	10	120	Release Time 1
Small	Slot	10	120	Release Time 2
Small	Slot	10	120	Release Time 3
Small	Slot	10	120	Release Time 4
Small	Diode 2	0	60	Release Time 1
Small	Diode 2	0	60	Release Time 2
Small	Diode 2	0	60	Release Time 3
Small	Diode 2	0	60	Release Time 4
Large	Slot	10	120	Release Time 1
Large	Slot	10	120	Release Time 2
Large	Slot	10	120	Release Time 3
Large	Slot	10	120	Release Time 4
Large	Diode 2	0	60	Release Time 1
Large	Diode 2	0	60	Release Time 2
Large	Diode 2	0	60	Release Time 3
Large	Diode 2	0	60	Release Time 4

Table 9: Example portion of the Phase 2 test matrix portion. Sample of different variables used in the full matrix.

3.8.2 Triggering the Trajectory Motion.

The dual-axis DMC-4020 Controller can use conditional statements to allow for the positional triggering of the vertically oriented linear motor based on the horizontally

oriented linear motor. An “IF” statement can trigger the actuation of the vertically oriented motor when the horizontally oriented motor is at any one of the four desired positions described in the next subsection. The basis for the conditional statements are described in Wood’s research [8]. The triggering conditions were changed slightly to achieve the desired positions. Galil code used in this experiment is included in Appendix C. The Galil code also triggers the saving of the data just before the vertically oriented motor triggers. This allows for each data file to be a similar size and capture the desired point in time before, during, and after the mission store release. An example of the Galil code for initialization of the linear motor is shown below.

```
INITIALIZATION GALIL CODE
BA B; 'initializes B motor
BMB=30720;
TLB=6.75;
TKB=9;
ERB=10000;
AUB=1;
OEB=1;
BZB=4;
MTB=1;
KDB=350;
KPB=20;
KIB=2;
AMB;
```

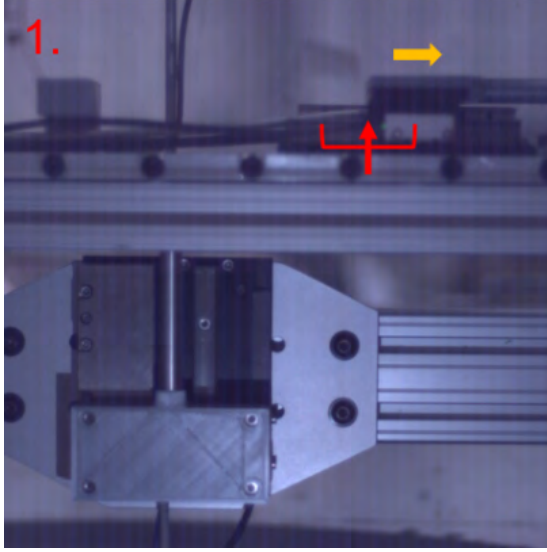
3.8.3 Timing of Mission Store Release.

The horizontal motion of the first linear motor compresses the gas in the compartment. The air exits upward through the flow control device when the motor moves in the direction toward the front of the cavity. The air is drawn in through the slot or diode when the motor moves in the opposite direction. These actions cause cyclic disruptions in the flow at the front lip of the cavity. The device, in turn, introduces

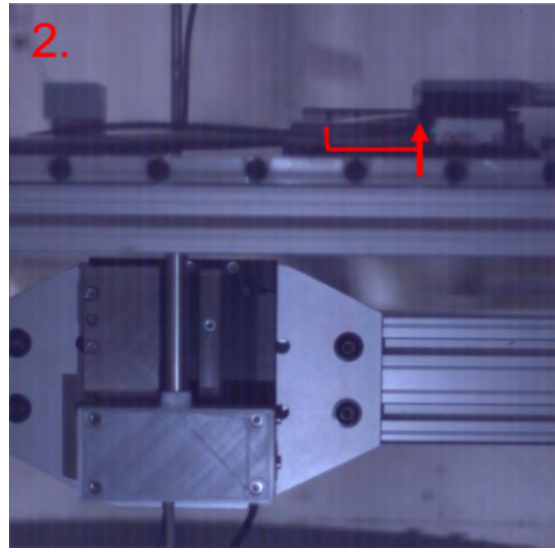
an opportunity to release the mission store at a specific time within the cycle. In this testing phase, four different phases were explored. The first position is when the horizontally oriented motor is all the way forward on the forward stroke. The second position is at the midpoint of the stroke length on the back stroke, when the motor is moving toward the rear of the cavity. The third position is when the motor is all the way back, as far from the front as possible. Finally, the fourth position is at the midpoint of the stroke length when the motor is moving forward toward the front of the cavity. The basis for these four release times are to cover a full cycle with even increments. The vortices were not timed or measured to determine these timings. A depiction of these timings are shown in Figure 36.

Following the work of Wood, these release times were verified in two ways, first with the encoder positions recorded and second with high speed camera footage. The encoder positions were recorded as vectors in the same fashion that time and all forces and moments were. The vectors were taken, plotted in Matlab, and compared to each other. The motion of the horizontally oriented motor is plotted as a sine wave with the minimum point being the back stroke where the motor is furthest back and the maximum point being the forward stroke where the motor is most forward. The time at which the vertically oriented motor release begins is represented with a vertical line on the plots shown in Figure 37. Encoder A shows the 5 Hz oscillation in the position of the motor. These plots verified that the vertically oriented motor, which moves the store, was activated at the proper time.

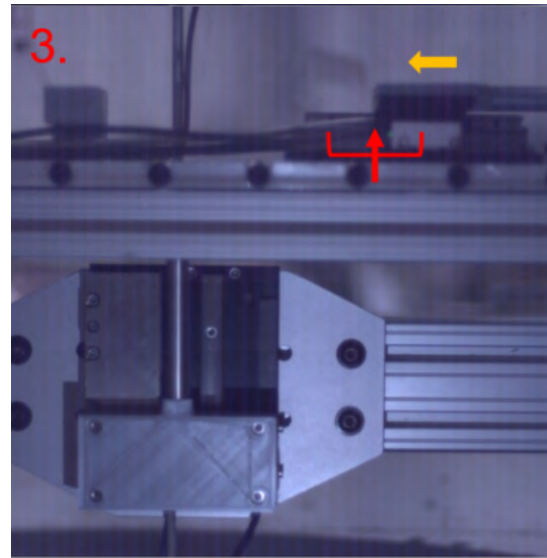
A Phantom Mirolab 3a10 high-speed digital camera was used to capture footage of the mission store release relative to the position of the horizontally oriented motors. Each trial was recorded and analyzed to make sure the footage matched the encoder verification. The point at which the vertically oriented motor releases for each case is shown in Figure 38. These pictures verify that the release points match the desired



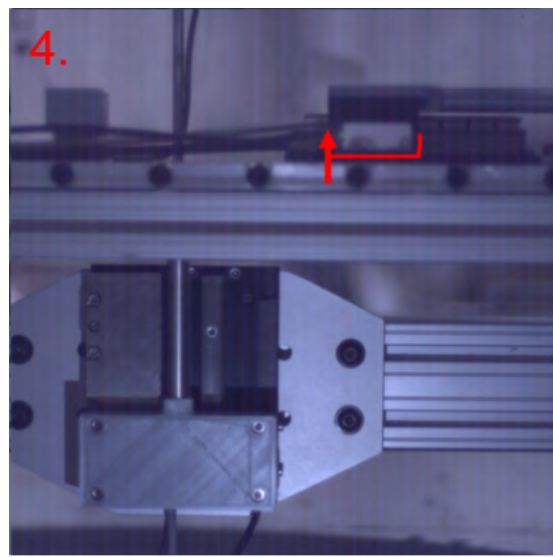
(a) First release time, moved half way along the track on the retracting stroke



(b) Second release time, moved all the way retracted back along the motor track



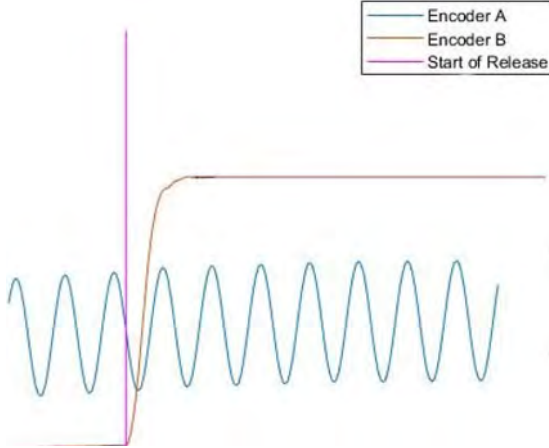
(c) Third release time, moved half way along the track on the forward stroke



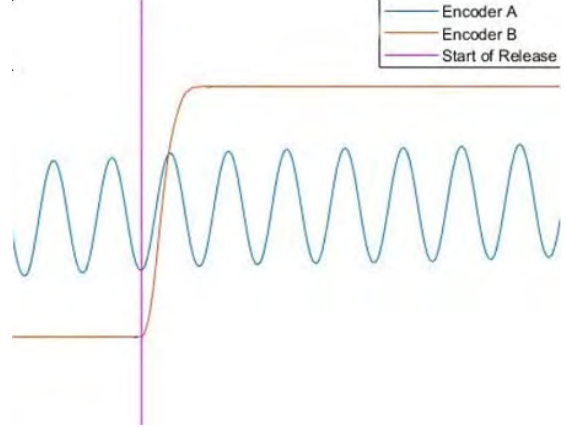
(d) Fourth release time, moved all the way moved forward along the motor track

Figure 36: Representation of the verification of encoder positions using a high speed camera.

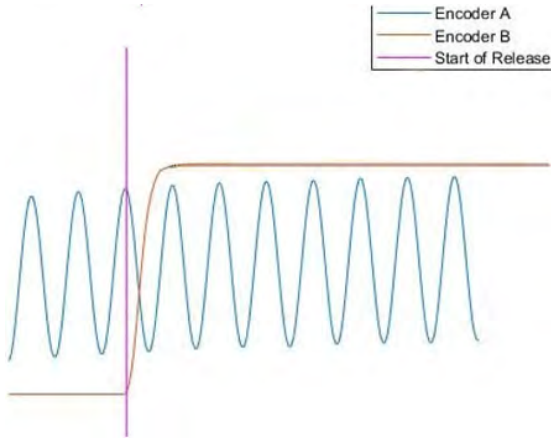
points in time as well as match with the encoder verification.



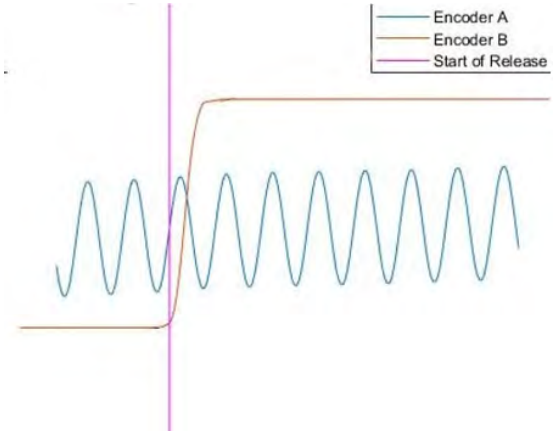
(a) First release time, moved half way along the track on the retracting stroke



(b) Second release time, moved all the way retracted back along the motor track



(c) Third release time, moved half way along the track on the forward stroke



(d) Fourth release time, moved all the way moved forward along the motor track

Figure 37: Encoder position plots verifying the release positions of both linear motors.

3.8.4 Post Processing Phase II.

Recorded data in the experiment included additional forces and moments from the trajectory motion and noise in the wind tunnel. In order to account for inertial effects, a tare file was generated for each trial run with different variables by running the test at 0 mph inside the wind tunnel. Furthermore, the DMC-4020 controller outputs a digital trigger that begins and ends the data collection at the desired times. The timing of this trigger resulted in variations of up to 0.15 seconds. This led to the

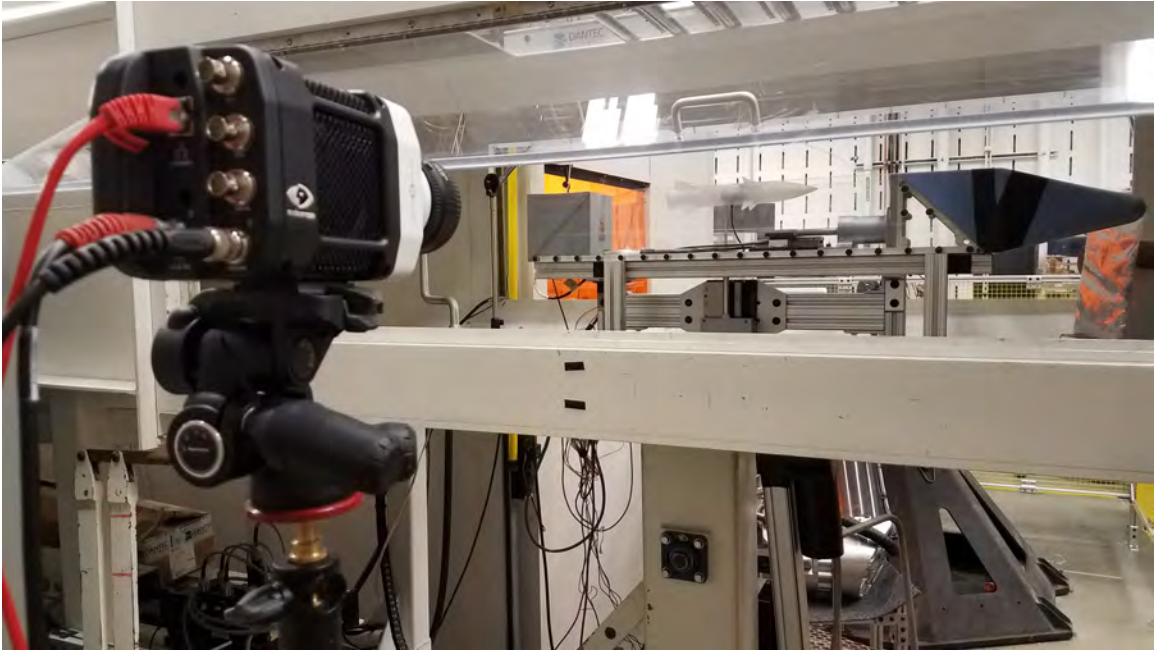


Figure 38: Phantom Mirolab 3a10 high speed camera used to record trials

requirement of aligning each file with the respective tare file for each case in the experiment. This alignment was achieved objectively within $\pm 0.002 \text{ sec}$. Both files for a given trial were plotted on the same figure. The spike in forces as the mission store is released in the tare file was used as a reference point and the spike in the file at speed was shifted to match the tare data. Then the tare data was subtracted from the data collected with the wind speed on. This allowed for the forces and moments generated as a result of the wind, the cavity environment, and the shear layer to be presented properly [8]. Figure 39 shows the plots generated before and after the alignment of the data on the left and right, respectively.

The filtering and importing process were the same as in Phase I using the same Matlab codes. Emphasized plots produced by the Matlab code include normal force, pitch moment, and axial force plots. All of the plots and analysis can be seen in the results and analysis section. The Matlab code used for the dynamic release tests can be seen in Appendix C.

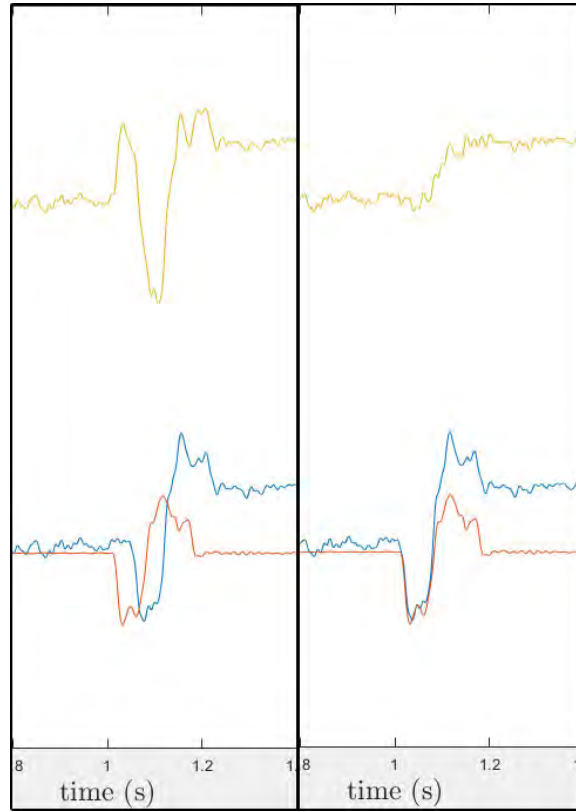


Figure 39: Tare plots of Normal Force, before data alignment on the left and after data alignment on the right

3.8.5 Repeatability of Dynamic Trials.

3.8.5.1 Repeatability of Tare.

Repeatability trials were completed for the dynamic trials exhibited in Phase II of the experiment. These trials take the normal force coefficient in the two seconds surrounding the store release event. First, a tare trial was recorded ten times and compared in Figure 40. The ten trials are different gradients of grey while the mean of those trials is shown in blue. This was the only repeatability trial run with flow control off. The average value of the mean vector was a nominal value of $N = -0.392\text{ lbf}$ which is the weight of the large model and accompanying apparatus on the Nano25 sensor. This value was added to the trials. Before the release the average value is

stable at zero with a standard deviation of 0.00009. After the release, the mean becomes $\bar{C}_N = -0.001$ with a standard deviation of 0.0007. Both of these match the mean of the static trials. During the release period, multiple trials are more visible in the grey colors. The minimum peak of the mean trial goes to $N = -1.24$ and the maximum peak is $C_N = 1.03$. The ten trials range between $C_N = -1.37$ and $C_N = 1.23$ so there is a maximum difference of only 0.2 at any given point compared to the mean. This shows the precision of the recorded tare data.

All of the values for the normal force coefficient before and after release for the repeatability trials at all wind speeds are shown in Table 10.

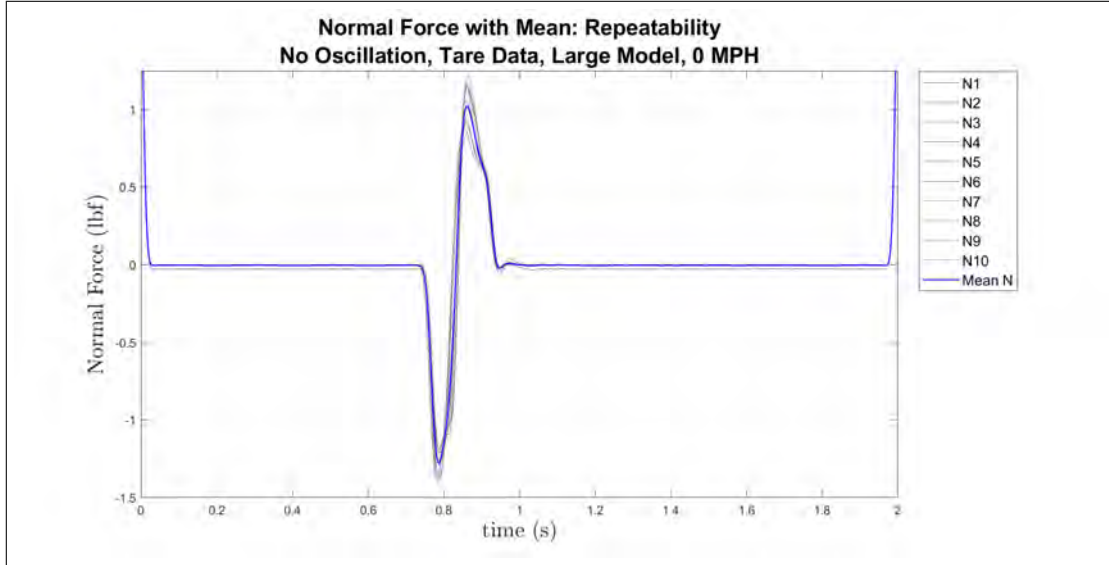


Figure 40: Dynamic normal force repeatability, large model, 10° AoA, tare and mean

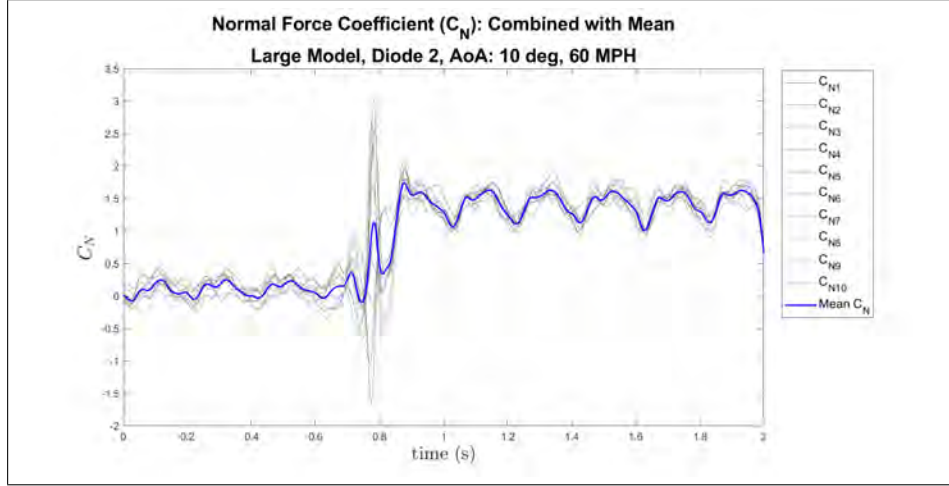
FC Device	Speed (mph)	\bar{C}_N Before	std dev	\bar{C}_N After	std dev
No FC	0	-4.729	0.001	-4.729	0.001
Diode 2	60	0.107	0.084	1.406	0.169
Diode 2	100	0.155	0.029	1.490	0.078
Diode 2	120	0.160	0.031	1.494	0.061

Table 10: Repeatability of dynamic normal force coefficients at 10° AoA with flow control devices, large model, all wind speeds

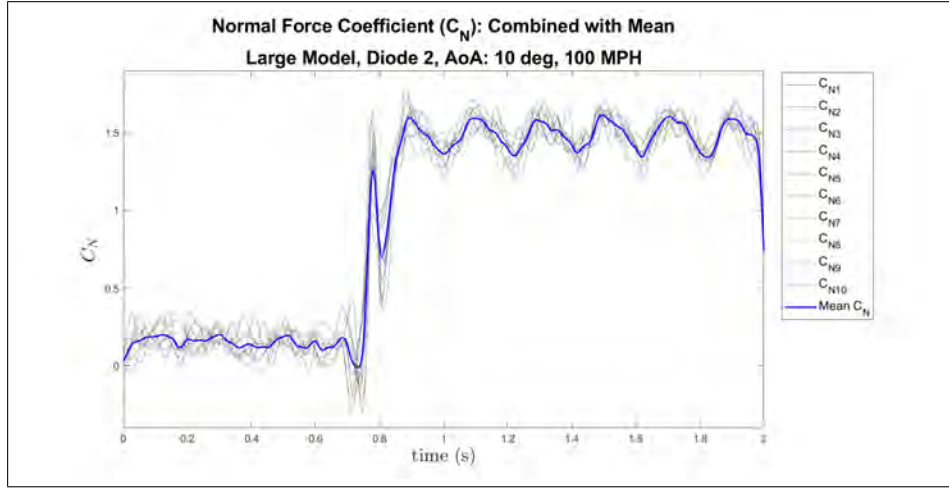
3.8.5.2 Average Normal Force Coefficients.

Additional trials were conducted ten times in different wind speeds and the normal force coefficients can be seen in Figure 41. These are all cases using the large mode, diode 2, and are placed at 10° AoA. Again, the ten trials are designated with different gradients of grey while the mean is colored blue. The 60 mph case, seen in Figure 41a, shows a mean of $\overline{C}_N = 0.107$ before the release and $\overline{C}_N = 1.406$ after release with standard deviations of 0.0842 and 0.17, respectively. The individual trials have a maximum peak at around $C_N = 3.0$ and a minimum peak at around $C_N = -1.6$. The 100 mph case, shown in Figure 41b, has a mean of $\overline{C}_N = 0.155$ before the release and $\overline{C}_N = 1.490$ after the release with standard deviations of 0.029 and 0.078, respectively. The maximum peak is around $C_N = 1.8$ while the minimum peak is around $C_N = -0.8$. Finally, the 120 mph case, shown in Figure 41c, has a mean of $\overline{C}_N = 0.160$ before release and $\overline{C}_N = 1.494$ after release with standard deviations of 0.031 and 0.061, respectively. The max peak is around $C_N = 1.75$ and the min peak is around $C_N = -1.25$.

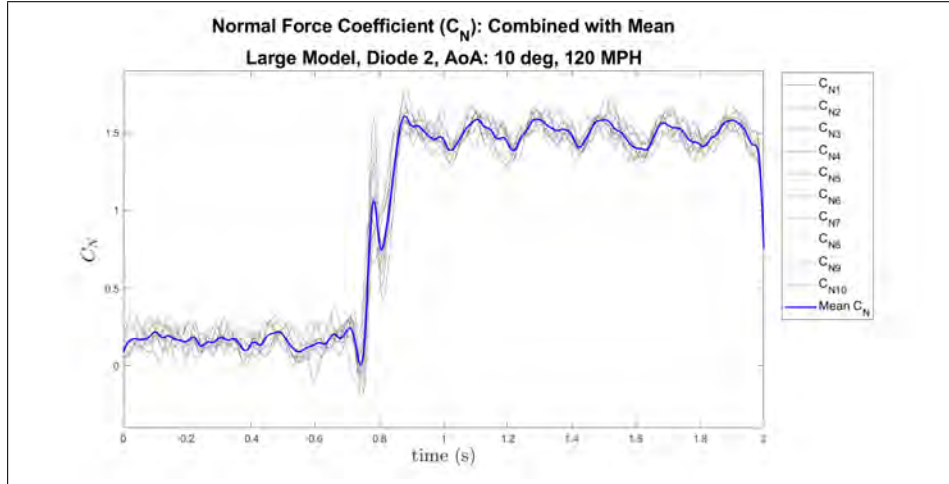
All of the coefficient values can be seen in Table 10. In terms of trends, as the wind speed increases, the coefficients both before and after release modestly increase, and the standard deviations decrease consistently. This is accounted for by the Reynolds number effects. Each case shows a very clear 5 Hz oscillation after the store release. The 60 mph also has a clear 5 Hz oscillation before, but the 100 mph and 120 mph cases are slightly less obvious. Also, one oscillation can be seen at each wind speed during the release of the store. Also, a clear oscillation during the release period is observed in all cases. This shows the effect of the flow control on the release. This data shows the precision of the recorded data and the repeatability of the trials.



(a) Dynamic repeatability, large model, 10° AoA, 60 mph, 10 trials and mean



(b) Dynamic repeatability, large model, 10° AoA, 100 mph, 10 trials and mean



(c) Dynamic repeatability, large model, 10° AoA, 120 mph, 10 trials and mean

Figure 41: Repeatability of dynamic normal force coefficients at 10° AoA in the cavity apparatus, large model, all wind speeds, all are the first release timing

3.9 Reynolds number

Air pressure and temperature at the time of collection were used to calculate the Reynolds number for each case. Two characteristic lengths were used to produce two different Reynolds numbers for each case. The first characteristic length was the diameter of the mission store model, 1.3 inches for the small model and 1.7 inches for the large model. The second characteristic length used was the depth of the cavity which was 5.37 inches. The specific gas constant was $287.05 \frac{K}{kgK}$. Table 11 shows the Reynolds numbers for cases in Phase I for both apparatuses and Table 12 shows the Reynolds numbers for cases in Phase II. With varied wind speeds, Re varied from 5.47×10^4 to 1.45×10^5 with the model diameter as the characteristic length, and varied from 2.28×10^5 to 4.58×10^5 with the cavity depth as the characteristic length. Each doubles because the tunnel speed doubles. The table for all of the Reynolds numbers and the Matlab code used for this calculation is included in Appendix C.

Model	AoA (°)	Speed (mph)	Re Model Diameter	Re Cavity Depth
Small	0	60	5.47E+04	2.28E+05
Small	0	100	9.12E+04	3.80E+05
Small	0	120	1.09E+05	4.56E+05
Small	10	60	5.47E+04	2.28E+05
Small	10	100	9.12E+04	3.80E+05
Small	10	120	1.09E+05	4.56E+05
Large	0	60	7.20E+04	2.28E+05
Large	0	100	1.20E+05	3.80E+05
Large	0	120	1.44E+05	4.55E+05
Large	10	60	7.20E+04	2.28E+05
Large	10	100	1.20E+05	3.80E+05
Large	10	120	1.44E+05	4.55E+05

Table 11: Phase 1 Reynolds Numbers

Model	Device	AoA (°)	Speed (mph)	Re Model Diameter	Re Cavity Depth
Small	Slot	0	60	5.50E+04	2.29E+05
Small	Slot	0	100	9.17E+04	3.82E+05
Small	Slot	0	120	1.10E+05	4.58E+05
Small	Slot	10	60	5.50E+04	2.29E+05
Small	Slot	10	100	9.17E+04	3.82E+05
Small	Slot	10	120	1.10E+05	4.58E+05
Small	Diode 2	0	60	5.50E+04	2.29E+05
Small	Diode 2	0	100	9.17E+04	3.82E+05
Small	Diode 2	0	120	1.10E+05	4.58E+05
Small	Diode 2	10	60	5.50E+04	2.29E+05
Small	Diode 2	10	100	9.17E+04	3.82E+05
Small	Diode 2	10	120	1.10E+05	4.58E+05
Large	Slot	0	60	7.25E+04	2.29E+05
Large	Slot	0	100	1.21E+05	3.82E+05
Large	Slot	0	120	1.45E+05	4.58E+05
Large	Slot	10	60	7.25E+04	2.29E+05
Large	Slot	10	100	1.21E+05	3.82E+05
Large	Slot	10	120	1.45E+05	4.58E+05
Large	Diode 2	0	60	7.25E+04	2.29E+05
Large	Diode 2	0	100	1.21E+05	3.82E+05
Large	Diode 2	0	120	1.45E+05	4.58E+05
Large	Diode 2	10	60	7.25E+04	2.29E+05
Large	Diode 2	10	100	1.21E+05	3.82E+05
Large	Diode 2	10	120	1.45E+05	4.58E+05

Table 12: Phase 2 Reynolds Numbers

3.10 Summary

The equipment and apparatuses in the experiment are detailed throughout Sections 3.2 - 3.5.6. The experiment execution and post processing were described in Sections 3.6 - 3.9. In Phase I, static tests were completed using both the freestream and cavity apparatuses. The mission store models were subjected to wind speeds ranging from 60 to 120 mph with variables including angle of attack, mission store size, and position in the cavity environment. The positions within the cavity present include inside the cavity, in the shear layer produced by the front lip of the cavity, and

above the shear layer in the freestream above the cavity. Post processing of this data involved Matlab code and filtering to produce a clear result. In Phase II, dynamic tests were completed using the cavity apparatus. Variables from the still tests were included in addition to varying the fluidic diodes, which pushes air out at the front of the cavity to disrupt the shear layer, and the release times based on the relative positions of the vertically and horizontally oriented linear motors. Four different release times within a cycle were executed to try to identify any differences in forces and moments experienced by the aerodynamic body, specifically normal force, pitch moment, and axial force were examined closely for trends. The post processing for this phase also included filtering with the addition of aligning and taring the data to produce clearer results. The test matrices for both phases are included in this chapter and the plots and results are analyzed in the next chapter.

IV. Results and Analysis

4.1 Overview of Results and Analysis

The data in this research involves subtracting the tare from raw force and moment data. In principle, one could compute all six components, but herein the focus is the normal force coefficient, pitch moment coefficient, and axial force coefficient. The normal force coefficient will be most emphasized in the following chapter and was calculated using Equation 4.1, with ρ as the density, V_∞ as the velocity, and D as the model diameter.

$$C_N = \frac{F_x}{\frac{1}{2}\rho V_\infty^2 (\frac{\pi}{4} D^2)} \quad (4.1)$$

The experiment and analysis was broken into two main phases. Phase I consists of static testing both in the freestream apparatus and the cavity apparatus. The freestream apparatus data was collected in one orientation, in the freestream flow, while the cavity apparatus used three different vertical positions of the model. The three positions were in the cavity, in the shear layer just above the lip of the cavity, and at the max height in the flow out of the cavity. Figures including single normal force coefficient examples, tare examples, and combined figures for several trials are all displayed and discussed in this phase. Some figures have residual values that are influenced by the filtering process at the beginning and end of each data collection sequence. Trends among the data are analyzed and discussed.

Phase II consists of dynamic testing of the mission store release from the cavity in a vertical trajectory. Many variables were adjusted to analyze different effects on the release including multiple release times relative to the position of the horizontally oriented linear motor. In this phase, the mission store model goes through a simulated weapon release, and the loads are captured in two-second long sequences

and compared. Similar figures to Phase I are used and discussed in this phase. The artifact from filtering can also be seen in several figures and can be ignored for the purposes of data analysis.

It should be noted that the pitch moment and axial force were recorded at position $\frac{x}{L} = 0.5$ on each model. Also, part of the calculation of the pitch moment coefficient in research conducted by Wood was corrected herein. A negative sign was neglected but must be accounted for due to the orientation of the Nano25 sensor in the wind tunnel. Therefore, all of the pitch-moment values calculated in the prior work must be corrected. The analysis code was also corrected for this research. It should also be stated that all standard deviations are in units of lb_f for the normal and axial forces and units of $lb_f - in$ for the pitch moment.

4.2 Phase I : Static Wind Tunnel Testing

4.2.1 Freestream Apparatus Data Analysis.

Data presented in this section were collected in the freestream apparatus at varying wind speeds, angles of attack, and mission store sizes. All cases were collected in the freestream with no obstructions (i.e. no cavity apparatus) in the test section so the mission store is only acted on by the incoming wind. This data serves the purpose of being a baseline for the forces and moments experienced by the mission store in the wind tunnel setting. Notable features of these figures include a relatively low amount of noise. Since there are no obstructions, minimal turbulence is experienced by the store and data is more stable. Emphasis is placed on trials including the 10° AoA because the forces and moments experienced by the store are more prominent and can be analyzed more efficiently. Additionally, initial trials made in the freestream cases later determined which trials to narrow in on and which collection frequency and low pass filter to use. These decisions were initially made through trial and error.

The time traces throughout Phase I are presented in this fashion to provide a comparison to later analysis in Phase II. The dynamic release of the store in Phase II require time traces to properly analyze the effects of the forces and moments on the store. Therefore, it is easy to provide the time traces for the static trials to directly compare and analyze the effects of dynamic trials. Additional analysis in the form of average values for the coefficients throughout Phase I are provided.

4.2.1.1 Normal Force Coefficient.

The normal force coefficient, C_N , was used for these trials because of the importance it holds in store release and it serves as an identifier for any interesting or important phenomena in the forces experienced by the mission store. In the freestream apparatus, both the small and large model sizes were used with an angle of attack of 10° at wind speeds of 60, 100, and 120 mph. This data is presented in Figure 44 for the small model and Figure 45 for the large model. These figures represent the baseline expected normal force coefficients for all these cases in the freestream flow at their respective wind speeds.

Certain trends become apparent through the comparison of the same model size with varying wind speeds. In Figure 44a for the 60 mph case, the mean coefficient is $\bar{C}_N = 1.540$ with a standard deviation of 0.041. In the 100 mph case, shown in Figure 44b, the mean is $\bar{C}_N = 1.481$ and the standard deviation of 0.033. Next, the 120 mph case, shown in Figure 44c, shows the same trend with a low standard deviation at 0.033 and the mean at $\bar{C}_N = 1.473$. A similar trend is displayed in the large model figures, Figure 45a, with the 60 mph case mean of $\bar{C}_N = 1.514$ and standard deviation of 0.032. Then the 100 mph and 120 mph cases are shown in Figures 45b and 45c respectively. They have a mean of $\bar{C}_N = 1.558$ and $\bar{C}_N = 1.554$ and standard deviations of 0.037 and 0.031, respectively. These values suggest a

near-independence of Reynolds number at higher tunnel speeds.

In the 10° AoA cases, lower levels of fluctuations are observed in the 120 mph case compared to the 60 mph case. In general, the higher the air speed, the lower the standard deviation. There are a few exceptions in the recorded data, however. Finally the drag, C_D , and lift, C_L , coefficients were calculated using Equation 4.2 and 4.3, respectively, using the mean values for the applicable coefficients. The drag coefficient increases and the lift coefficient decreases with an increase in wind speed. The values for all of the coefficients for these cases are shown in Table 13, and Figures 42 and 43. The normal force and axial force coefficients should lie generally flat and on top of each other. The scales on the graphs are small so it looks like they do not coincide.

$$C_D = C_N * \cos(\alpha) - C_A * \sin(\alpha) \quad (4.2)$$

$$C_L = C_N * \sin(\alpha) + C_A * \cos(\alpha) \quad (4.3)$$

To determine the error, the partial derivatives for the normal force, pitch moment, and axial force coefficients were computed using Equations 4.4 - 4.6. Only the errors in the forces and moments collected due to the sensor and error in the wind speed were addressed in this calculation. These values were used in Equations 4.7 - 4.9 to find the magnitude of the error bars for the respective coefficients. The error in the sensor measurements was determined based on factory specifications and the error in the velocity was determined to be $\delta V = 1.0 \text{ mph}$. The calculated values for these are shown in Table 14. The error bars are shown in the plots mentioned above.

$$\frac{dC_N}{dF_x} = \frac{1}{\frac{1}{2}\rho V_\infty^2 (\frac{\pi}{4}D^2)} \text{ and } \frac{dC_N}{dV_\infty} = \frac{-2F_x}{\frac{1}{2}\rho V_\infty^3 (\frac{\pi}{4}D^2)} \quad (4.4)$$

$$\frac{dC_m}{dT_y} = \frac{1}{\frac{1}{2}\rho V_\infty^2 (\frac{\pi}{4}D^3)} \text{ and } \frac{dC_m}{dV_\infty} = \frac{-2T_y}{\frac{1}{2}\rho V_\infty^3 (\frac{\pi}{4}D^3)} \quad (4.5)$$

$$\frac{dC_A}{dF_z} = \frac{1}{\frac{1}{2}\rho V_\infty^2 (\frac{\pi}{4}D^2)} \text{ and } \frac{dC_A}{dV_\infty} = \frac{-2F_z}{\frac{1}{2}\rho V_\infty^3 (\frac{\pi}{4}D^2)} \quad (4.6)$$

$$dC_N = \sqrt{\left(\frac{dC_N}{dF_x} * dF_x\right)^2 + \left(\frac{dC_N}{dV_\infty} * dV_\infty\right)^2} \quad (4.7)$$

$$dC_m = \sqrt{\left(\frac{dC_m}{dT_y} * dT_y\right)^2 + \left(\frac{dC_m}{dV_\infty} * dV_\infty\right)^2} \quad (4.8)$$

$$dC_A = \sqrt{\left(\frac{dC_A}{dF_z} * dF_z\right)^2 + \left(\frac{dC_A}{dV_\infty} * dV_\infty\right)^2} \quad (4.9)$$

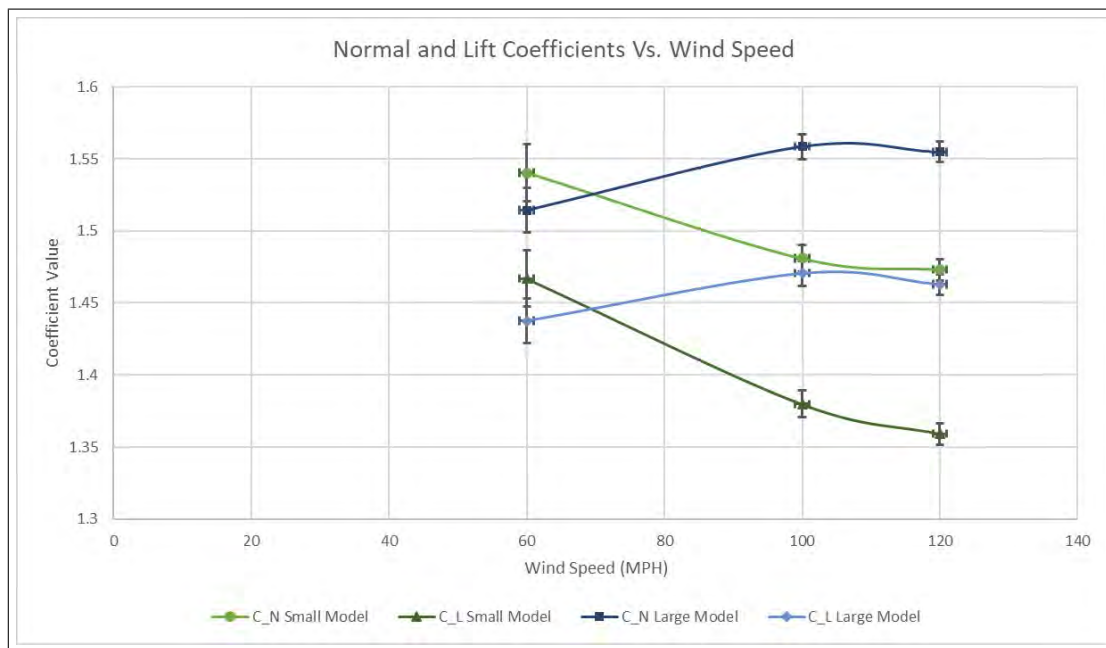
Model	Speed (mph)	N (lb_f)	std dev	C_N	std dev	m ($lb_f - in$)	std dev	C_m	std dev
Small	60	0.126	0.003	1.540	0.041	-0.0004	0.0006	-0.042	0.077
Small	100	0.335	0.008	1.481	0.033	-0.003	0.001	-0.114	0.056
Small	120	0.479	0.011	1.473	0.034	-0.005	0.002	-0.132	0.057
Large	60	0.211	0.005	1.514	0.033	-0.004	0.001	-0.201	0.073
Large	100	0.602	0.014	1.559	0.037	-0.014	0.005	-0.248	0.097
Large	120	0.864	0.018	1.555	0.032	-0.019	0.006	-0.252	0.082

Model	Speed (mph)	A (lb_f)	std dev	C_A	std dev	C_D	C_L
Small	60	0.024	0.009	0.288	0.121	0.552	1.467
Small	100	0.102	0.014	0.453	0.064	0.703	1.379
Small	120	0.171	0.021	0.527	0.067	0.775	1.359
Large	60	0.043	0.011	0.309	0.079	0.568	1.438
Large	100	0.143	0.036	0.371	0.092	0.636	1.471
Large	120	0.218	0.043	0.393	0.0766	0.657	1.463

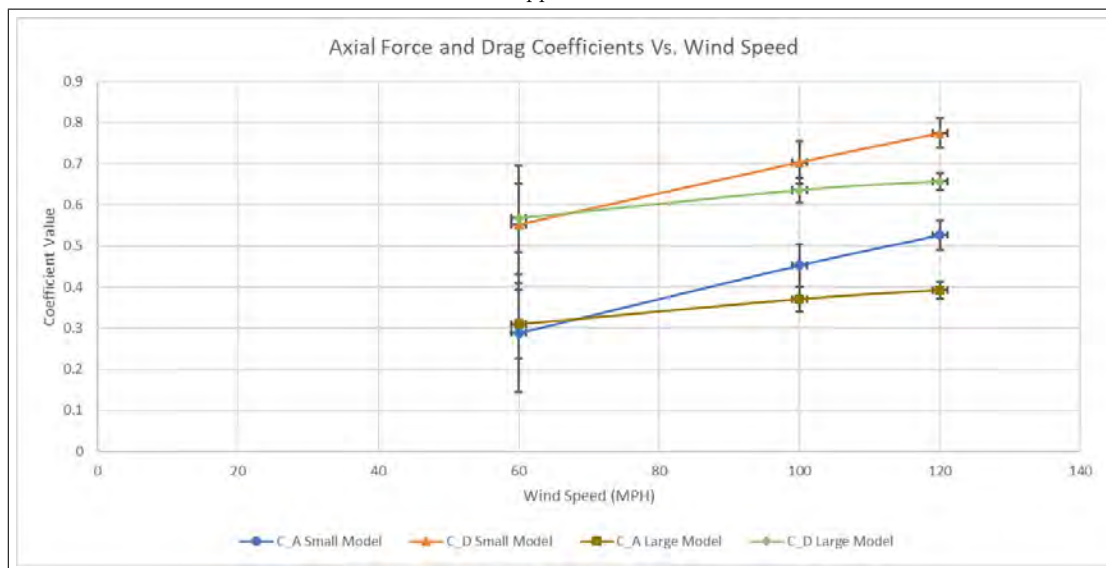
Table 13: Filtered values for small and large models at various wind speeds at 10° AoA in the freestream apparatus

Model	Speed (mph)	$\frac{dC_N}{dN}$	$\frac{dC_N}{dv}$	dC_N	$\frac{dC_m}{dm}$	$\frac{dC_m}{dV}$	dC_m	$\frac{dC_A}{dA}$	$\frac{dC_A}{dV}$	dC_A
Small	60	2.87	-0.03	0.017	86.84	0.002	0.013	2.87	-0.005	0.029
Small	100	1.03	-0.02	0.008	31.32	0.004	0.005	1.03	-0.005	0.010
Small	120	0.72	-0.01	0.006	21.78	0.004	0.004	0.72	-0.005	0.007
Large	60	1.68	-0.03	0.013	38.89	0.012	0.007	1.68	-0.005	0.017
Large	100	0.61	-0.02	0.007	14.04	0.009	0.004	0.61	-0.004	0.006
Large	120	0.42	-0.01	0.005	9.76	0.007	0.003	0.42	-0.003	0.004

Table 14: Values used in calculation of error bars for coefficient values, freestream

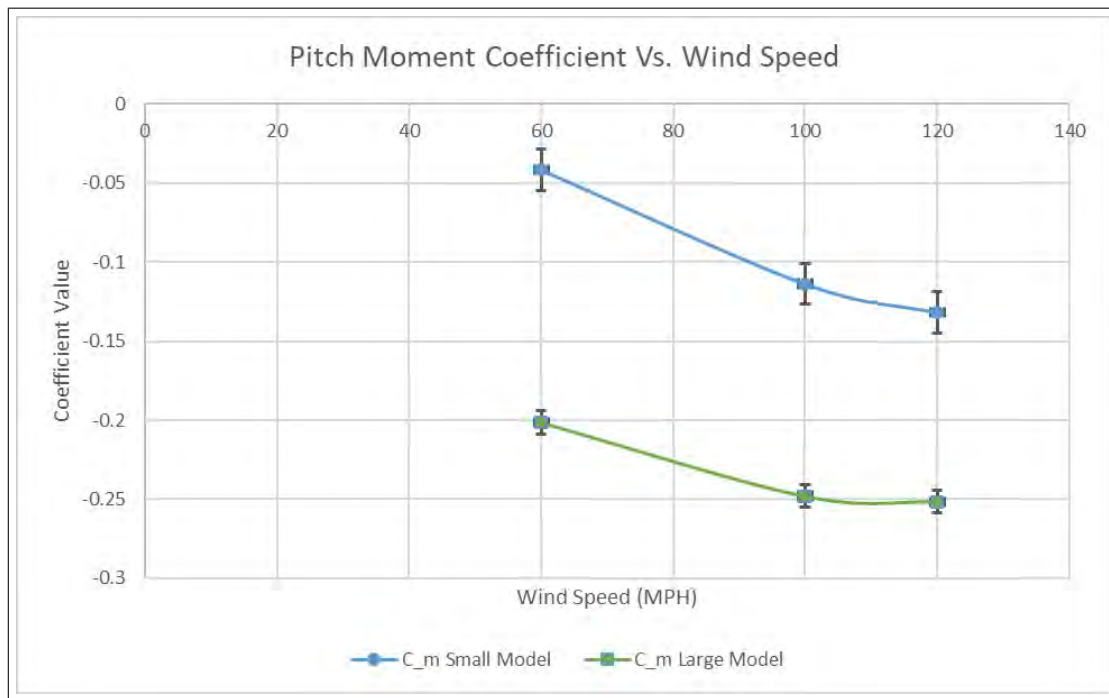


(a) Graph of normal force coefficient values for the small model at 10° AoA at various wind speeds in the freestream apparatus

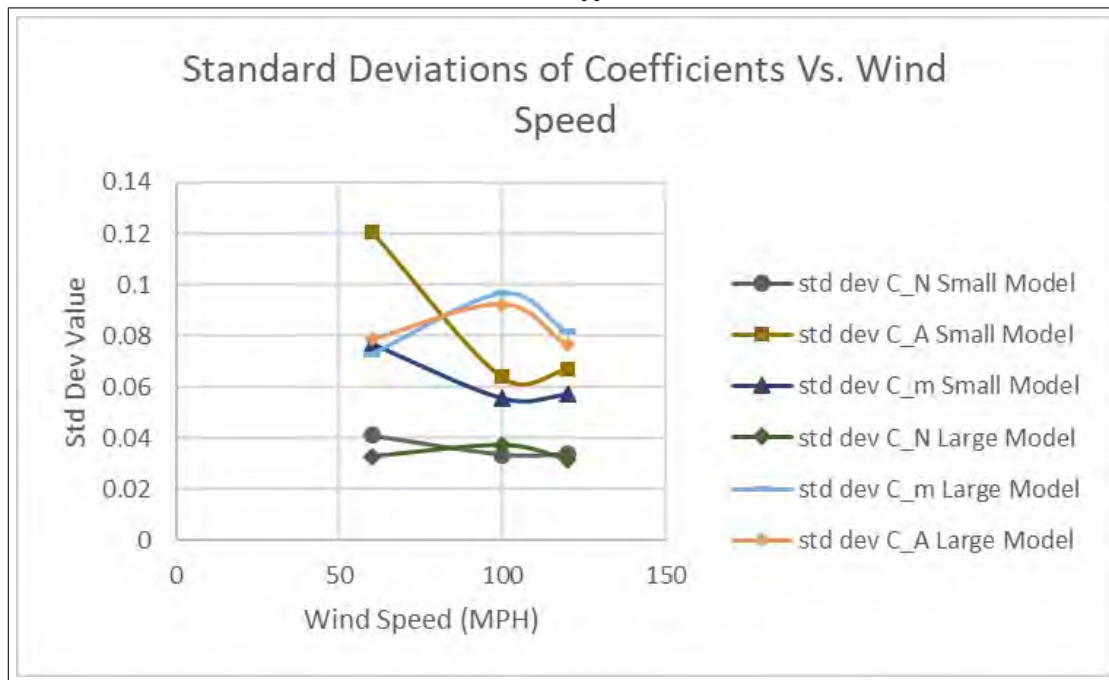


(b) Graph of axial force coefficient values for the small model at 10° AoA at various wind speeds in the freestream apparatus

Figure 42: Graphs of normal force and axial force coefficients in the freestream apparatus, small model, 10° , all wind speeds

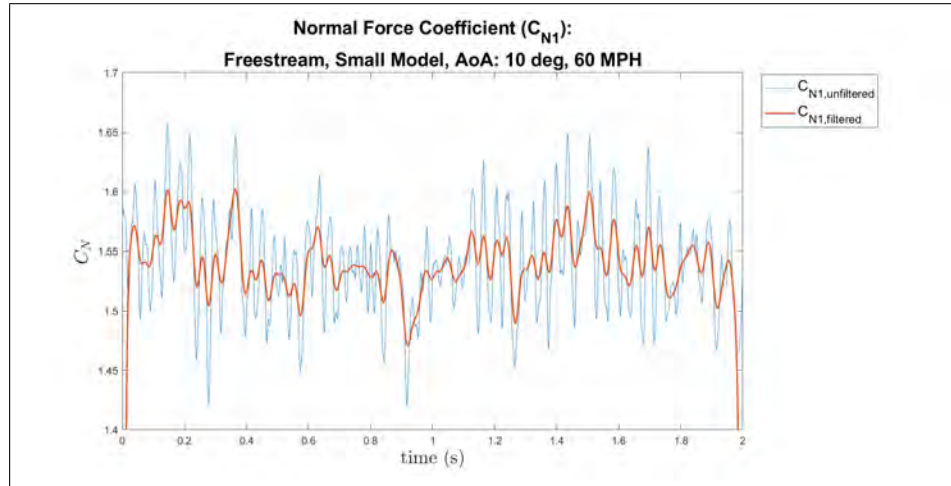


(a) Graph of pitch moment coefficient values for the small model at 10° AoA at various wind speeds in the freestream apparatus

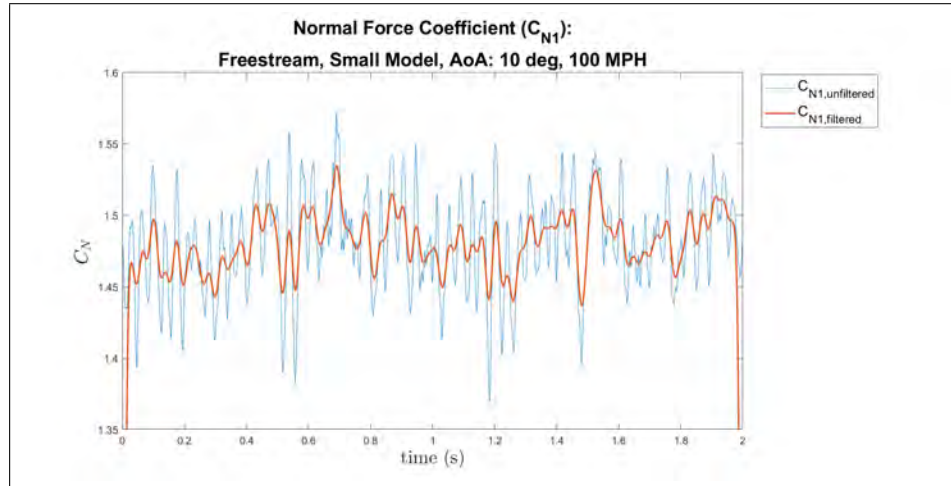


(b) Graph of standard deviations for all coefficients for the small model at 10° AoA at various wind speeds in the freestream apparatus

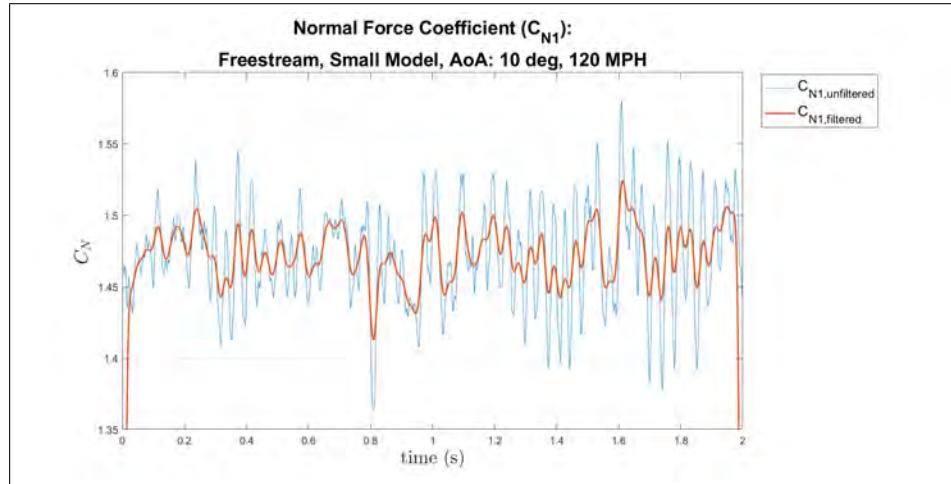
Figure 43: Graphs of pitch moment coefficient and standard deviations of coefficients in the freestream apparatus, small model, 10°, all wind speeds



(a) Normal Force Coefficient, freestream apparatus, small model, 10° AoA, 60 mph

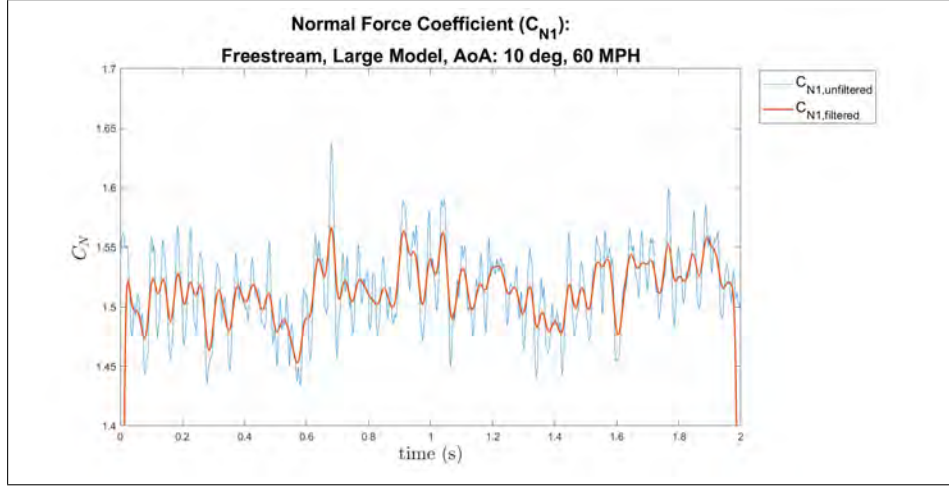


(b) Normal Force Coefficient, freestream apparatus, small model, 10° AoA, 100 mph

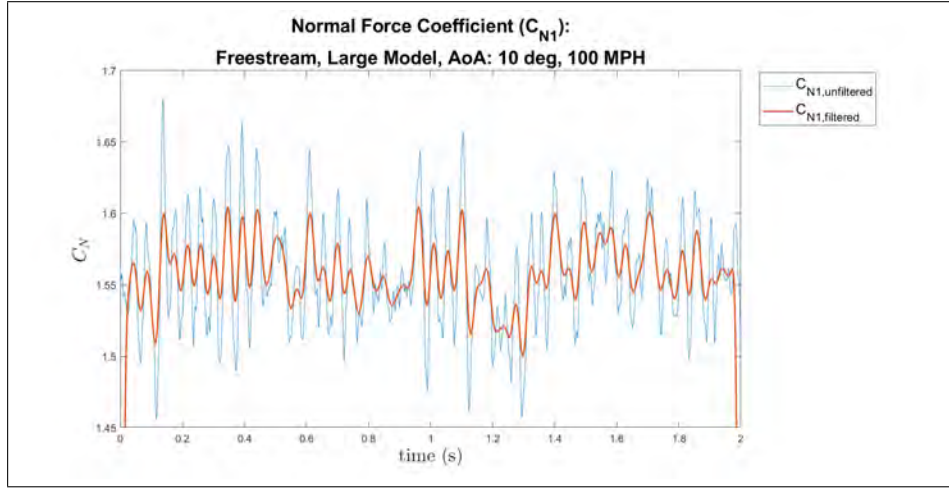


(c) Normal Force Coefficient, freestream apparatus, small model, 10° AoA, 120 mph

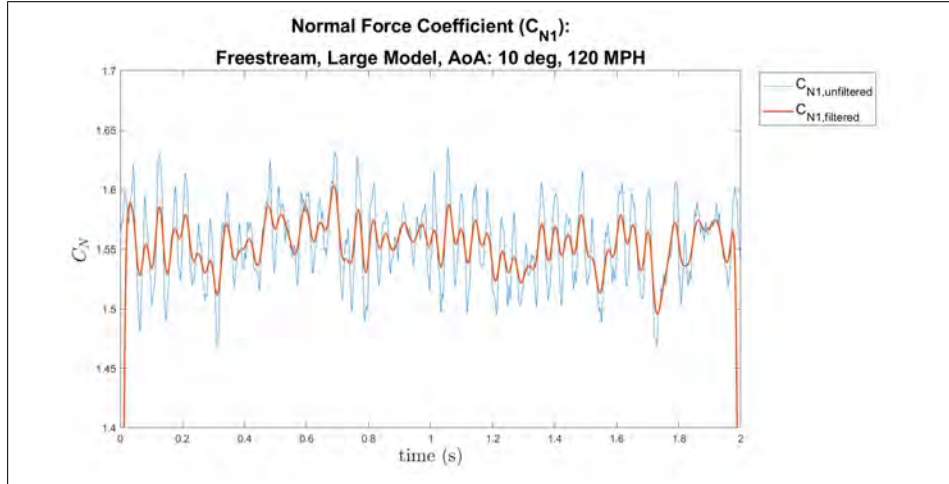
Figure 44: Comparison of the difference in wind speeds of the normal force coefficient for the freestream apparatus, small model



(a) Normal Force Coefficient, freestream apparatus, large model, 10° AoA, 60 mph



(b) Normal Force Coefficient, freestream apparatus, large model, 10° AoA, 100 mph



(c) Normal Force Coefficient, freestream apparatus, large model, 10° AoA, 120 mph

Figure 45: Comparison of the difference in wind speeds of the normal force coefficient for the freestream apparatus, large model

Data was also collected in the freestream apparatus for cases with an angle of attack of 0° . These cases will prove to be less interesting in terms of trends being very apparent and worthy of note. Figures 46a and 47a show the small model cases for 60 and 100 mph respectively. The 60 mph case shows a normal force coefficient mean of $\overline{C}_N = 0.352$ with a standard deviation of 0.038, while the 100 mph case has a mean of $\overline{C}_N = 0.174$ and a standard deviation of 0.028. The large model cases for 60 and 100 mph shown in Figures 46b and 47b, respectively. These cases actually demonstrate slightly negative normal force coefficient values with means of $\overline{C}_N = -0.0531$ and $\overline{C}_N = -0.0722$ and standard deviations of 0.031 and 0.023, respectively. The standard deviations are all calculated using the filtered values.

A difference of about 1.5 in the value of the normal force coefficient corresponds to about a 10° change in the model orientation. This means that a change of 0.15 corresponds to a 1° change. The mean values recorded in these trials suggest a range from a change of 0.5° to 2° while the model is supposed to be in a 0° AoA orientation. This could be caused by the interference from the electrical cords moving in the wind or several other factors.

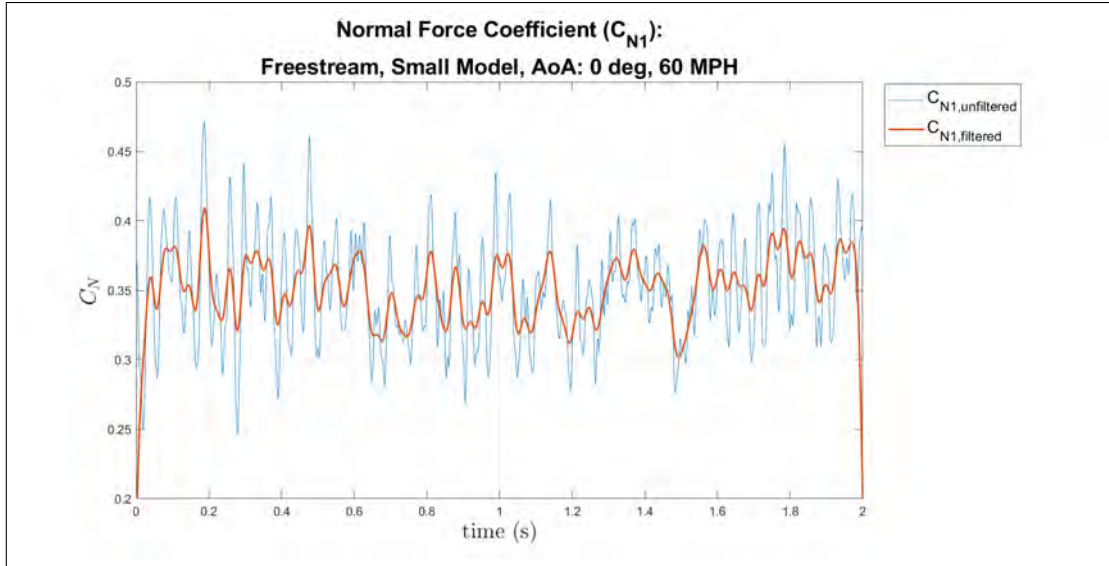
In these nominal 0° AoA cases, as the speed increases, the normal force coefficient decreases, the standard deviation decreases for every coefficient, the drag coefficient increases slightly, and the lift coefficient decreases slightly. These values as well as the normal and axial forces and pitch moment values can be seen in Table 15. These trends are the same as those in the 10° AoA cases.

Model	Speed (mph)	N (lb_f)	std dev	C_N	std dev
Small	60	0.029	0.003	0.352	0.038
Small	100	0.039	0.006	0.174	0.028
Large	60	-0.007	0.004	-0.053	0.031
Large	100	-0.028	0.009	-0.072	0.023

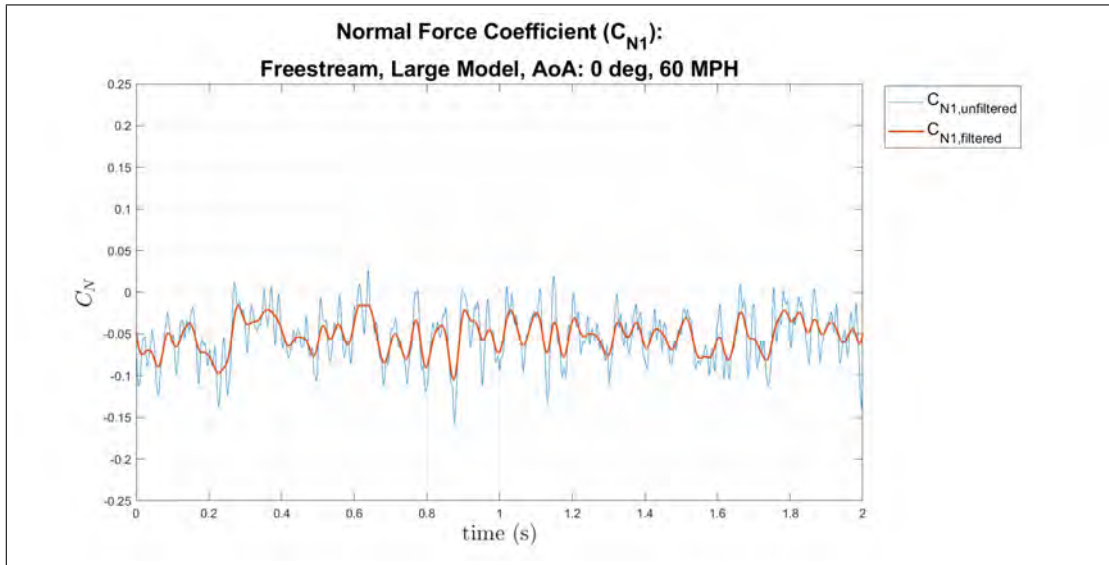
Model	Speed (mph)	m ($lb_f - in$)	std dev	C_m	std dev
Small	60	0.000	0.001	0.009	0.099
Small	100	-0.0003	0.002	-0.012	0.066
Large	60	0.005	0.002	0.246	0.085
Large	100	0.011	0.005	0.209	0.084

Model	Speed (mph)	A (lb_f)	std dev	C_A	std dev	C_D	C_L
Small	60	0.049	0.013	0.602	0.160	0.654	0.242
Small	100	0.200	0.019	0.886	0.087	0.903	0.017
Large	60	0.048	0.014	0.342	0.099	0.328	-0.112
Large	100	0.144	0.033	0.371	0.085	0.353	-0.136

Table 15: Filtered values for small and large models at various wind speeds at 0° AoA in the freestream apparatus

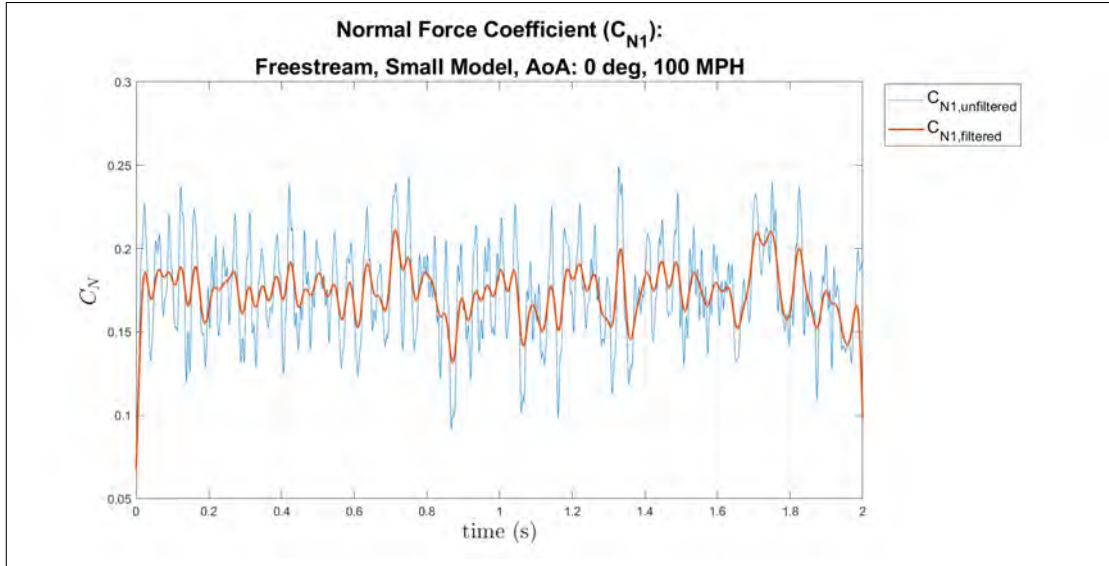


(a) Normal Force Coefficient, freestream apparatus, small model, 0° AoA, 60 mph

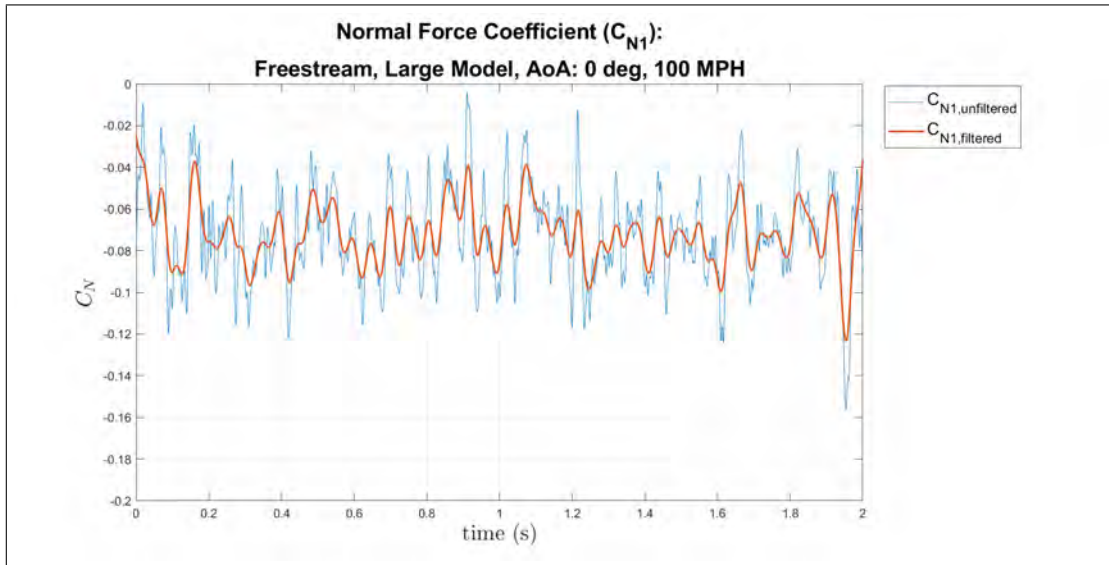


(b) Normal Force Coefficient, freestream apparatus, large model, 0° AoA, 60 mph

Figure 46: Comparison of the difference model sizes at 0 AoA of the normal force coefficient for the freestream apparatus, 60 mph



(a) Normal Force Coefficient, freestream apparatus, small model, 0° AoA, 100 mph



(b) Normal Force Coefficient, freestream apparatus, large model, 0° AoA, 100 mph

Figure 47: Comparison of the difference model sizes at 0 AoA of the normal force coefficient for the freestream apparatus, 100 mph

4.2.1.2 Pitch Moment Coefficient.

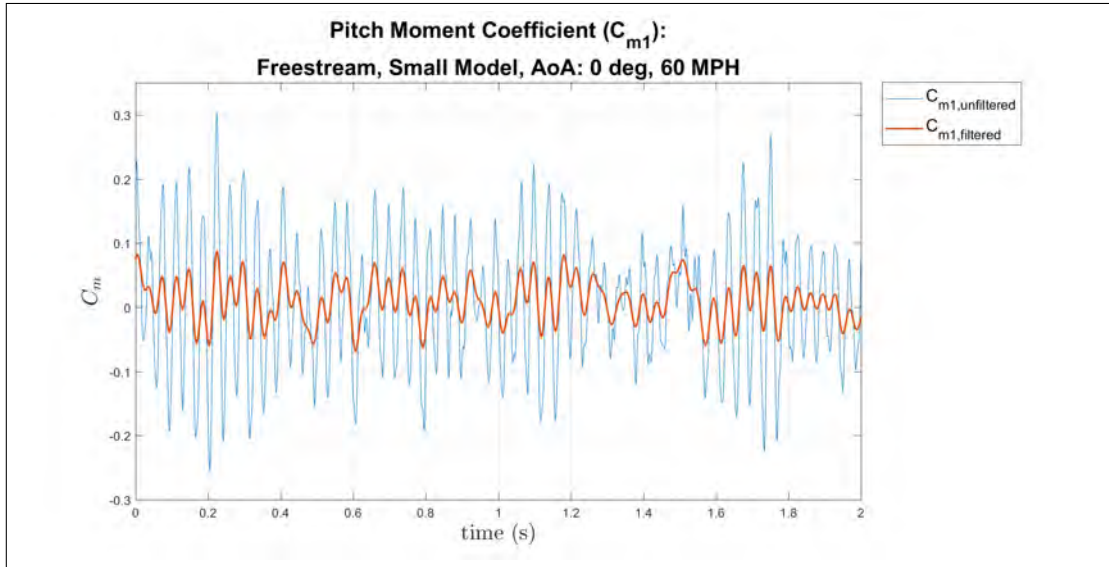
The pitch moment coefficient, C_m , allows a glance at the moments experienced by the mission store in the flow upon release. In all tests, the pitch moment is measured about the face of the Nano25 sensor, where it was attached to the mission store body

located at $\frac{x}{L} = 0.5$ for both models. The pitch moment was measured in the same trials as all of the normal force coefficients and presented as the filtered coefficients. Below in Figures 48 and 49 are four cases including the small and large model sizes as well as a 0 and 10° AoA for the 60 mph case. Both the filtered and unfiltered data is presented. These figures represent the baseline expected pitch moment coefficients in the freestream flow. Figure 48a and Figure 48b compare the 0° AoA case for the small and large models respectively. At 0° both models are symmetrical and normal to the flow, so the absolute values of the coefficient are relatively low. The small model exhibits this with a mean of $\overline{C}_m = 0.0092$ and a standard deviation of 0.099. The large model shows lower mean of $\overline{C}_m = 0.246$ and a standard deviation of 0.085. This lower value could be caused by the length of the large model disrupting the flow and having a greater effect along the length of the body.

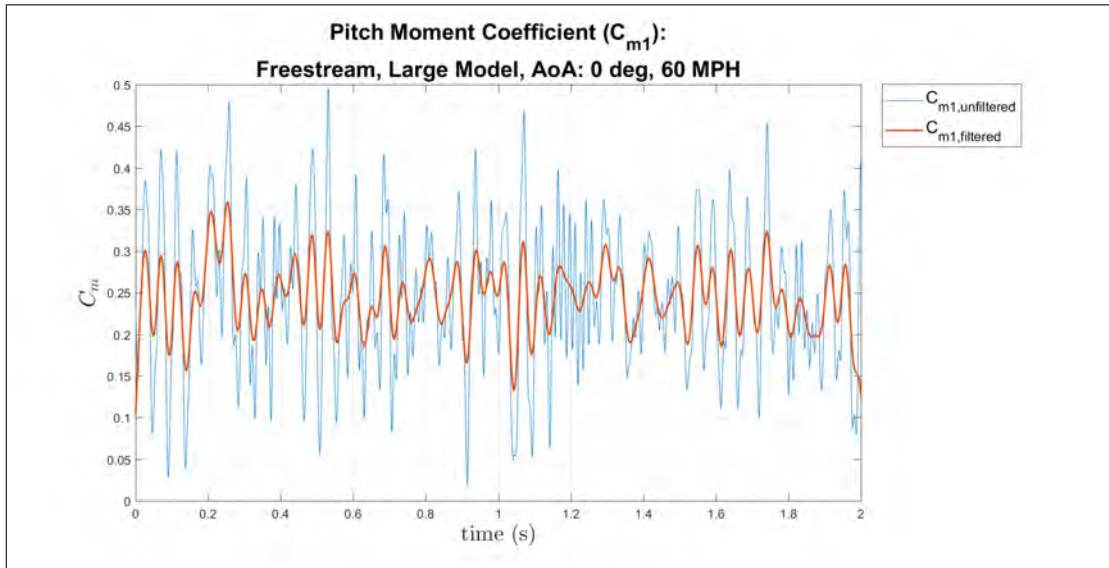
Comparison between the small and large models for the 10° case can be seen in Figures 49a and 49b respectively. These cases have a greater, and positive value because of the orientation of the model. There is a greater cross sectional area normal to the flow which increases the moment coefficient about the face of the Nano25 sensor. The small model case has a mean of $\overline{C}_m = -0.041$ and a standard deviation of 0.07 and the large model case has a mean of 0.39 and a standard deviation of 0.1. Since the large model has a greater surface area, it makes sense the moment coefficient is larger. The standard deviation is also significantly larger which could also be attributed to the larger surface area.

The values for the pitch moment coefficient were given in Tables 13 as shown in the normal force coefficient section. As wind speed increases, the pitch moment coefficient decreases and the standard deviation decreases with one exception. With an increases in angle of attack, the pitch moment coefficient turns negative. In the 10° AoA case, since the aft section of the model has a tail, the flow pushes against it

and applies a nose-up moment on the model which is in the negative sense for C_m .

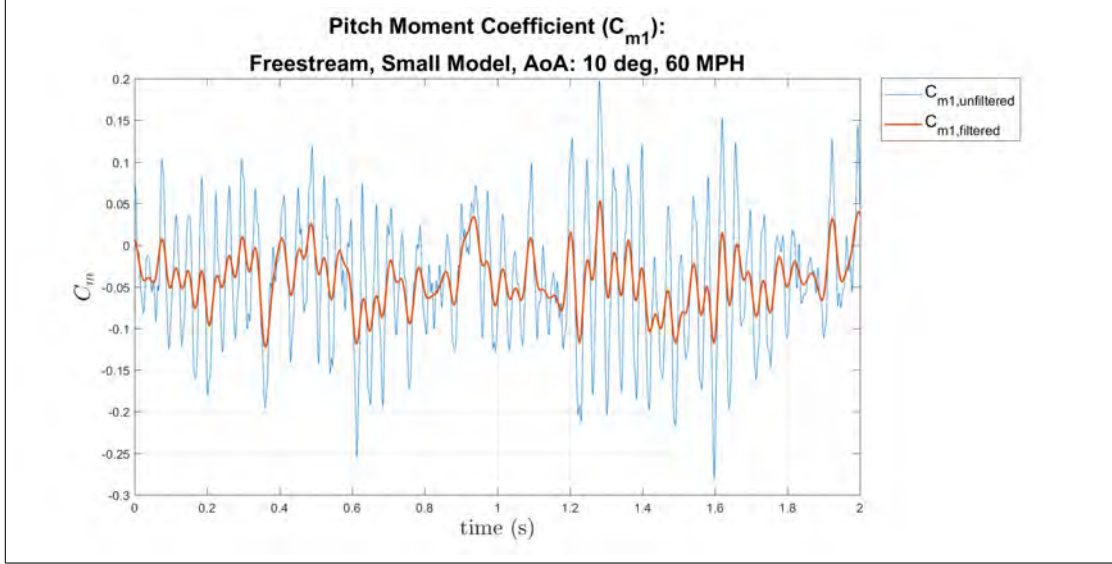


(a) Pitch Moment Coefficient, freestream apparatus, small model, 0° AoA, 60 mph

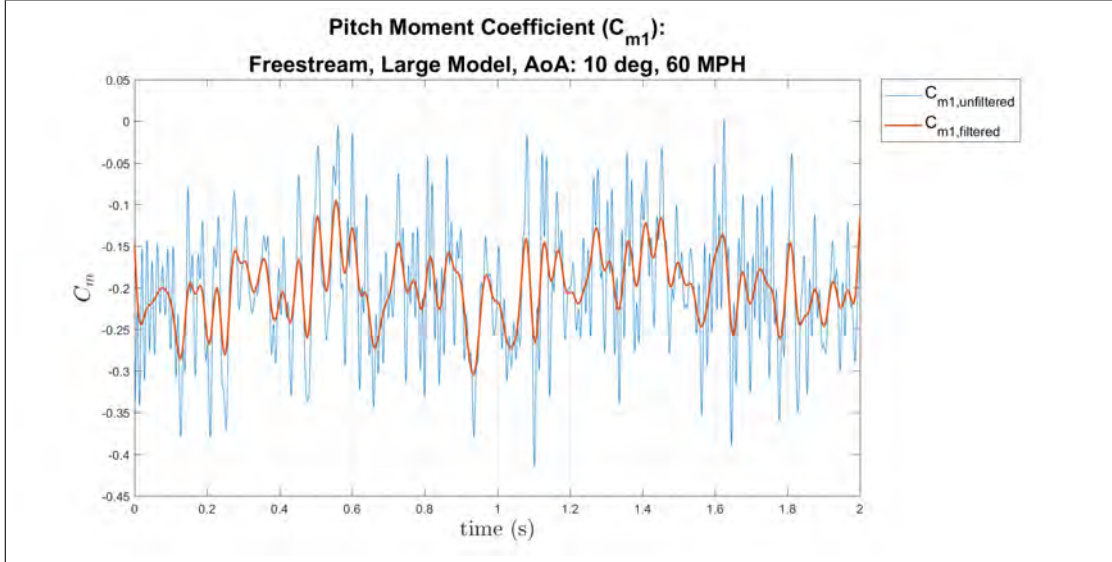


(b) Pitch Moment Coefficient, freestream apparatus, large model, 0° AoA, 60 mph

Figure 48: Comparison of the difference model sizes at 0° AoA of the pitch moment coefficient for the freestream apparatus, 60 mph



(a) Pitch Moment Coefficient, freestream apparatus, small model, 10° AoA, 60 mph



(b) Pitch Moment Coefficient, freestream apparatus, large model, 10° AoA, 60 mph

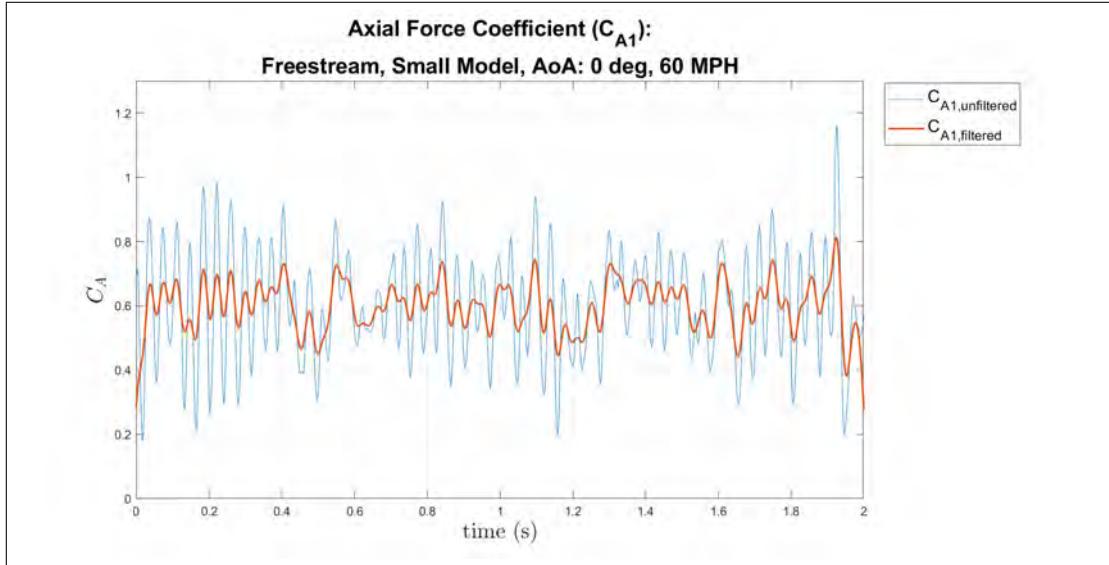
Figure 49: Comparison of the difference model sizes at 10° AoA of the pitch moment coefficient for the freestream apparatus, 60 mph

4.2.1.3 Axial Force Coefficient.

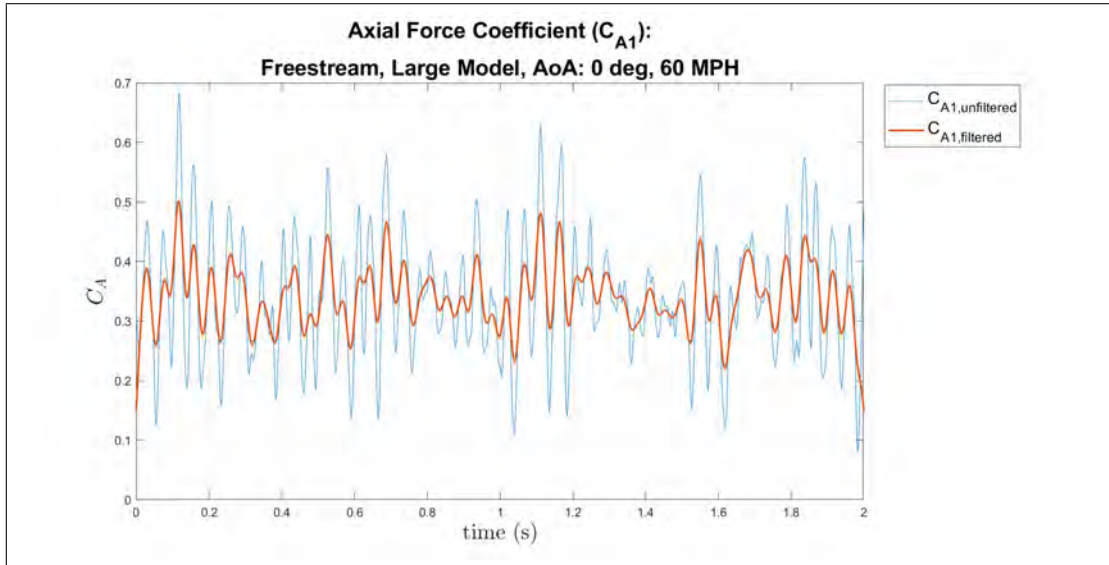
The axial force coefficient, C_A , was another component force collected in all of the trials. The axial force was collected in reference to the face of the Nano25 force and moment sensor. In the 10° AoA cases, the Nano25 sensor was also angled at 10°

along with the model so the data presented is the angled values. The comparison between the small and large models at 60 mph and 0 and 10° can be seen in Figures 50 and 51, respectively. Both the unfiltered and filtered data are shown. The mean axial force coefficient for the small model at 0°, shown in Figure 50a, is $\overline{C}_A = 0.602$ with a standard deviation of 0.16. The large model at 0°, shown in Figure 50b, has a mean of $\overline{C}_A = 0.342$ with a standard deviation of 0.099. The mean of the small model at 10°, shown in Figure 51a, is $\overline{C}_A = 0.288$ with a standard deviation of 0.12. The mean for the large model, shown in Figure 51b, is $\overline{C}_A = 0.309$ and a standard deviation of 0.079.

As the wind speed increases, the axial force coefficient increases, the standard deviation decreases with one exception. With an increase in angle of attack, both the axial force coefficient and the standard deviation decreases. This could be caused by the orientation of the sensor and how the force is recorded relative to the angle of the sensor. Again, the frequency observed in these examples is about 15 Hz which is the cutoff frequency for the filter. These trends are seen in Tables 13 and 15 as shown in the other sections.

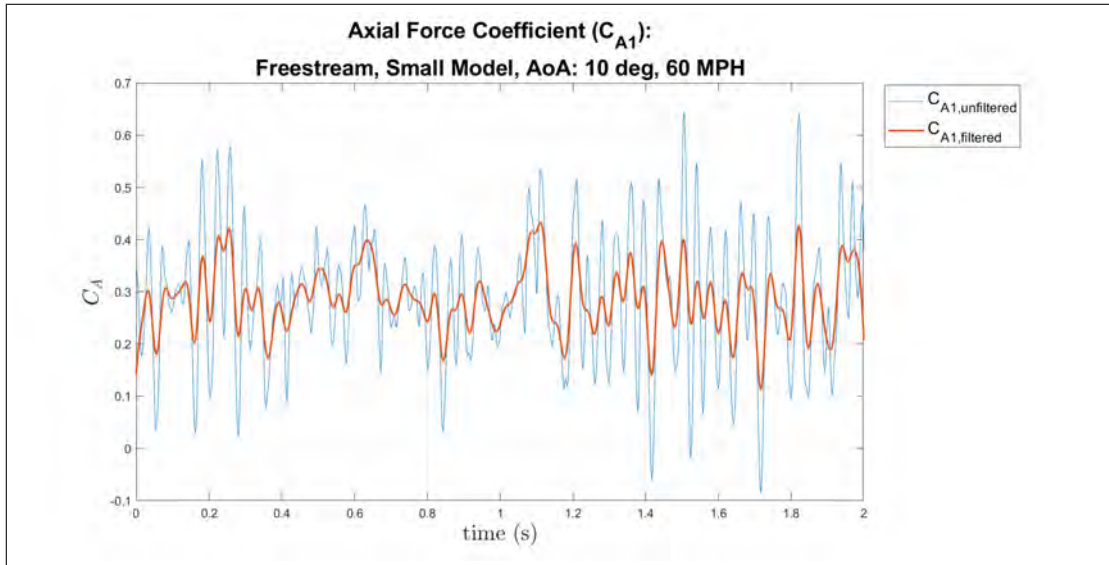


(a) Axial Force Coefficient, freestream apparatus, small model, 0° AoA, 60 mph

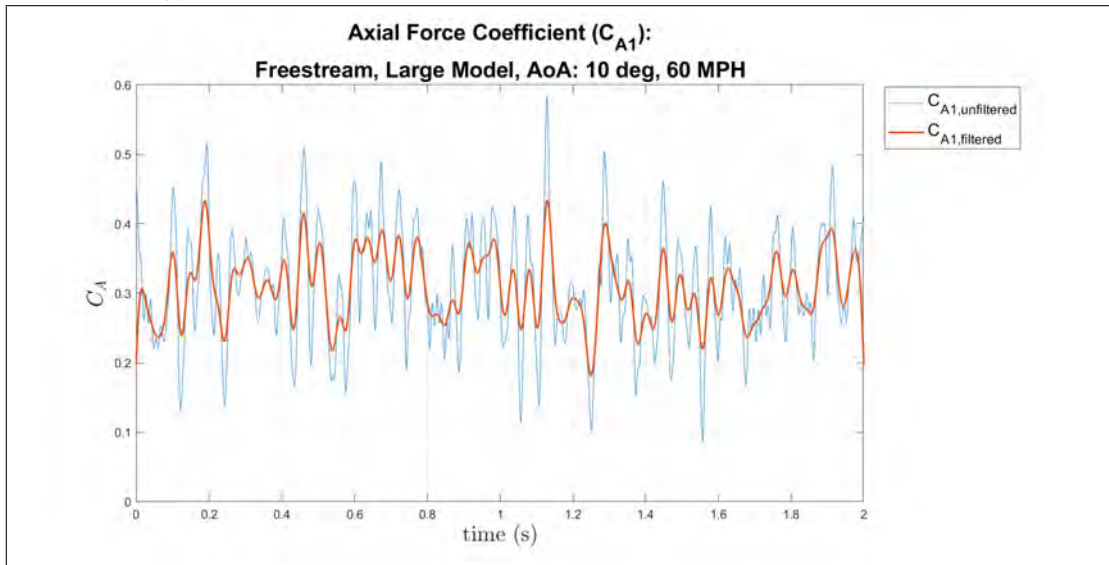


(b) Axial Force Coefficient, freestream apparatus, large model, 0° AoA, 60 mph

Figure 50: Comparison of the difference model sizes at 0° AoA of the pitch moment coefficient for the freestream apparatus, 60 mph



(a) Axial Force Coefficient, freestream apparatus, small model, 10° AoA, 60 mph



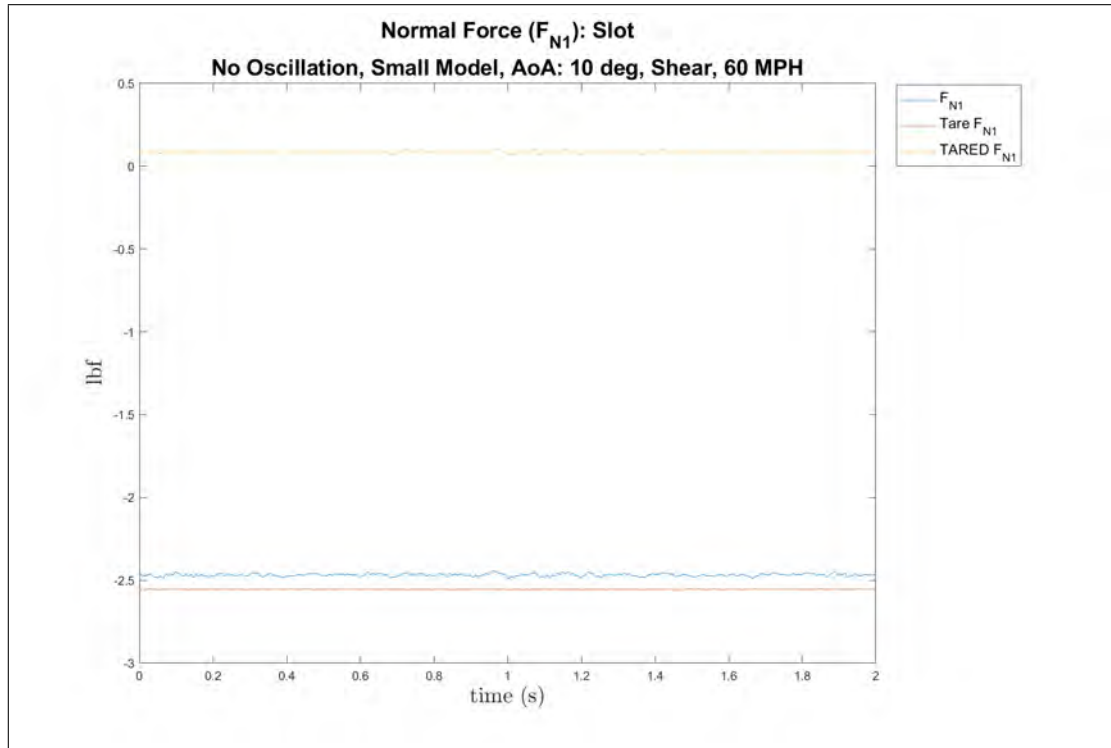
(b) Axial Force Coefficient, freestream apparatus, large model, 10° AoA, 60 mph

Figure 51: Comparison of the difference model sizes at 10° AoA of the pitch moment coefficient for the freestream apparatus, 60 mph

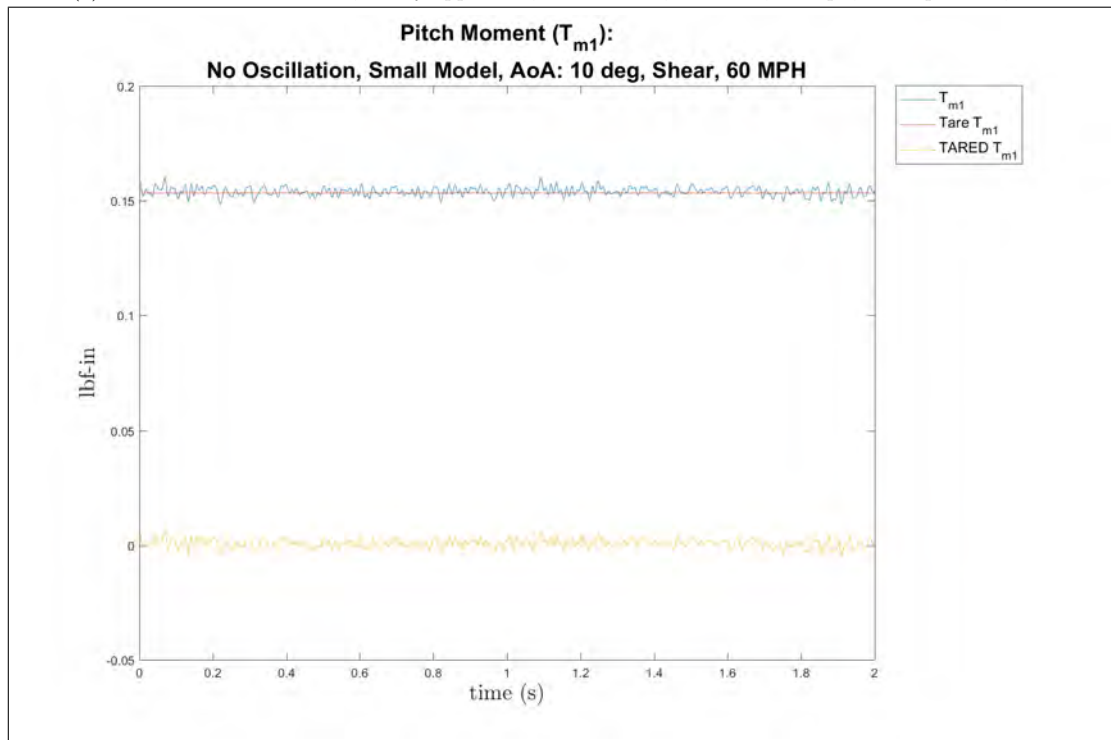
4.2.2 Cavity Apparatus Data Analysis.

4.2.2.1 Tare Example.

The data collected in the cavity apparatus, with no oscillation of the flow control device, were taken and tared in every trial. Every trial that was taken with the wind tunnel on had the data subtracted by a trial taken at 0 mph to account for the apparatus and additional noise. An example of the data, the tare data, and the tared data are plotted together for multiple coefficients in Figure 52. Figure 52a shows the tared data for the normal force at 60 mph in the shear layer position of the cavity apparatus. Figure 52b presents the tared data for the pitch moment while Figure 53 shows the tared data for the axial force. This was the process used to create all of the tared data used to calculate the coefficients of interest. One tare file was created for every trial that had different conditions and used for every wind speed collected with those conditions. These files were recorded before the low speed runs.



(a) Normal Force Coefficient, cavity apparatus, small model, 10° AoA, 60 mph, shear position, tare



(b) Pitch Moment Coefficient, cavity apparatus, large model, 10° AoA, 100 mph, shear position, tare

Figure 52: Example of tare and tared data for force coefficients of the small model at 10° AoA in the cavity apparatus, 60 mph

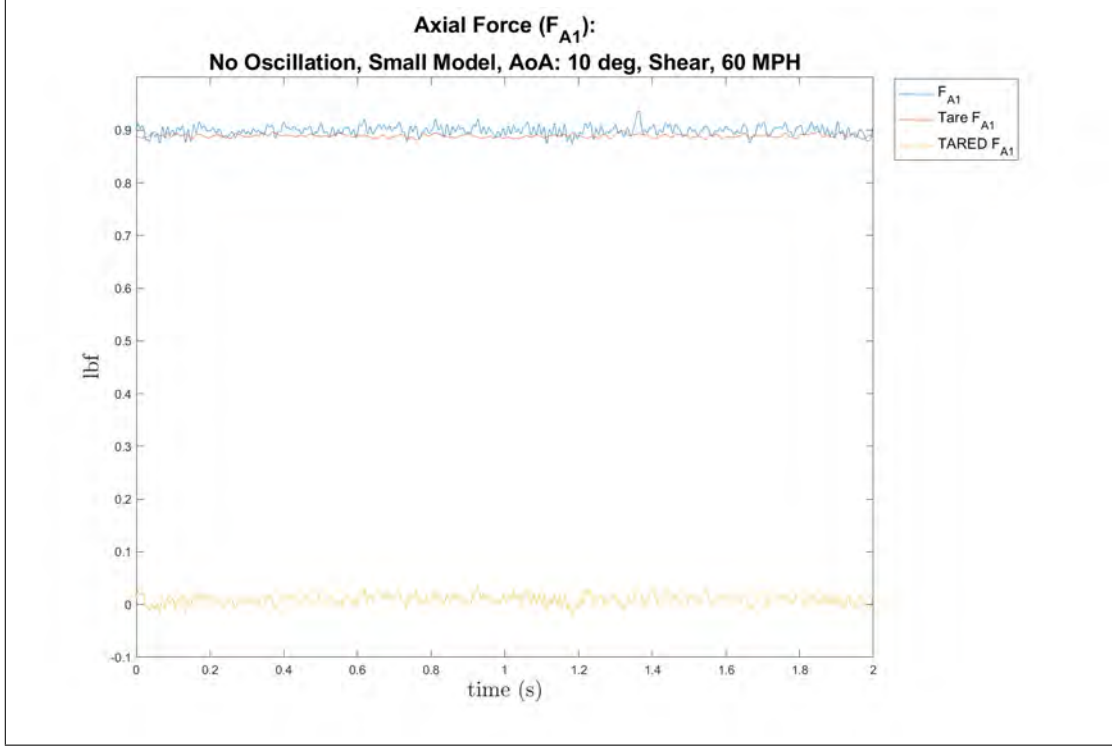
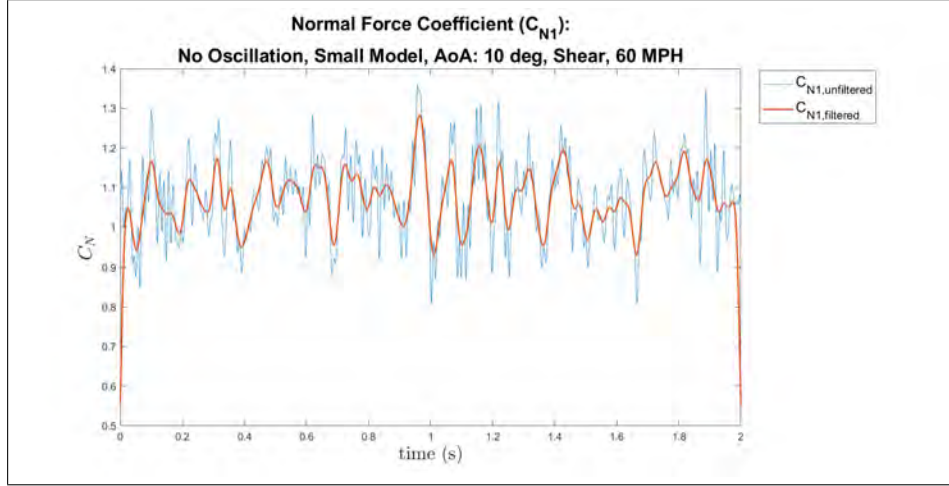


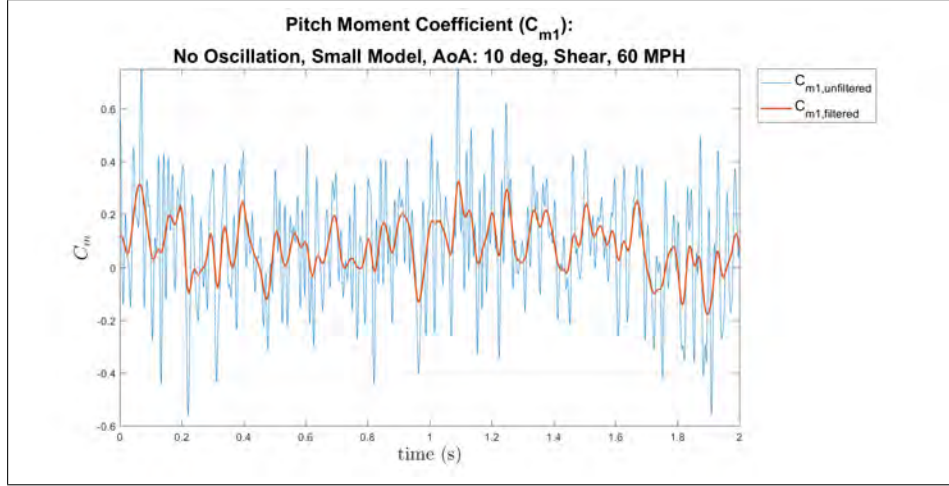
Figure 53: Axial Force Coefficient, cavity apparatus, large model, 10° AoA, 120 mph, shear position, tare

4.2.2.2 Force and Moment Coefficients Example.

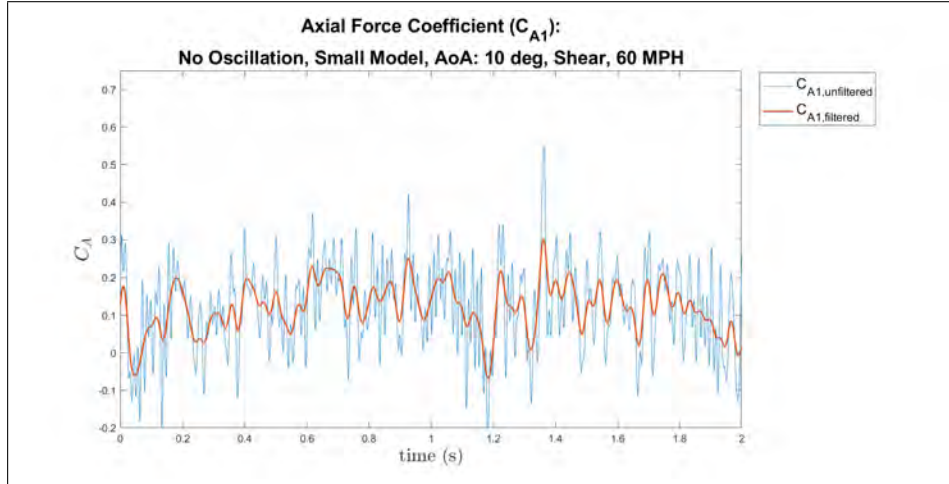
The data presented in this research is in the form of the normal force, pitch moment, and axial force coefficients. In addition to showing “unfiltered” data, which in practice did use a 30 Hz low-pass hardware filter, results for a 15 Hz low-pass filter are also shown to clarify trends. Figure 54 shows examples of individual trials recorded for all three coefficients. The trial shown is the small model at 10° AoA at 60 mph in the cavity apparatus at the shear layer position. This figure serves the purpose of showing how the coefficients were filtered individually, and this data is taken and combined with other trials to analyze trends later in the section.



(a) Normal Force Coefficient, cavity apparatus, small model, 10° AoA, 60 mph, shear position



(b) Pitch Moment Coefficient, cavity apparatus, small model, 10° AoA, 60 mph, shear position



(c) Axial Force Coefficient, cavity apparatus, small model, 10° AoA, 60 mph, shear position

Figure 54: Example of filtered coefficients for all coefficients of the small model at 10° AoA in the cavity apparatus, 60 mph

4.2.2.3 In-Cavity Position Values.

All of the cases in Figure 55 involve the small model at 10° AoA, statically placed at the “in-cavity” position. All of the values for every wind speed can be seen in Tables 16 and 17.

Figure 55a shows the values of the normal force coefficient for all three wind speeds. The 60 mph case oscillates and has a mean and standard deviation of $\overline{C}_N = 0.035$ and 0.10, the 100 mph case is $\overline{C}_N = 0.184$ and 0.083, and the 120 mph case is $\overline{C}_N = 0.132$ and 0.086. By increasing the wind speed, the normal force coefficient increases then decreases at a certain point while the standard deviation decreases then increases. These trends are different than other trends because of the nature of the position inside the cavity. While in the “in cavity” position, there is a lot of turbulence and disruption of the flow in the cavity. The model is not directly acted upon by the freestream, so the loads on the model are much lower than the freestream case in Figure 44. This makes the trends of the coefficients less clear than in other positions and other cases. Additionally, the values of the normal coefficient are relatively low compared to other positions which will be shown next. This can also be attributed to the position of the model inside the cavity.

Figure 55b shows the pitch moment coefficient for the same trials. Here, the proportionality of an increase of speed with an increase in the coefficient is not observed. The values for every wind speed lie on top of each other and oscillate just under zero, around $C_m = -0.218$ to $C_m = -0.271$. In this context, a positive moment is consistent with a nose-pitch out of the cavity. The standard deviations range from 0.21 to 0.27. These values are positive because of the position of the model under the lip of the cavity. This would cause the wind to flow downward before it interacts with the model. The coefficient starts off higher in the 60 mph case, decreases in the 100 mph case, then increases again in the 120 mph case.

Figure 55c shows the axial force coefficient for the same trials. The 60 mph case has a mean and standard deviation of $\overline{C}_A = 0.485$ and 0.12, the 100 mph case is $\overline{C}_A = 0.171$ and 0.069, and the 120 mph case is $\overline{C}_A = 0.275$ and 0.073. This trend is the opposite of the one seen in the normal force coefficient. An increase in wind speed could cause a greater portion of the flow to go over the cavity and not pass through the shear layer. This would cause less flow to interact with the model, causing a lower axial force coefficient. Additionally, the decrease in standard deviation with an increase in speed is observed.

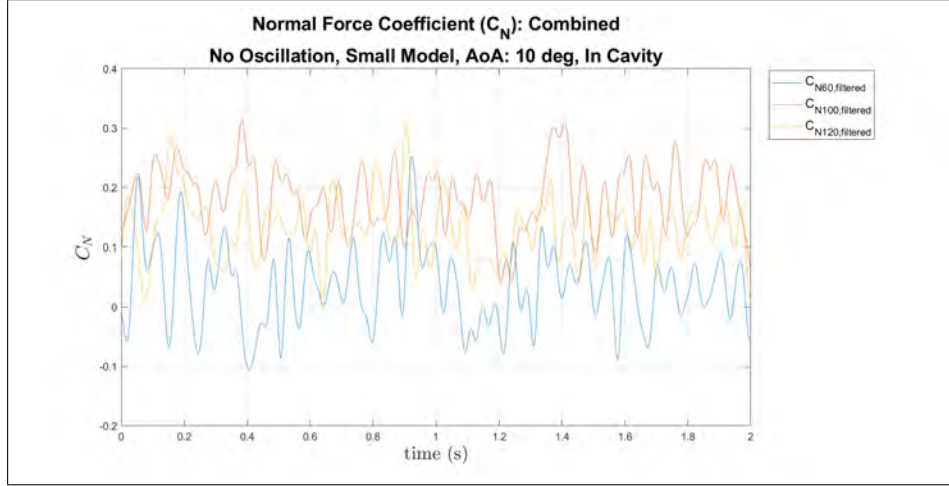
As mentioned before, the nature of the position of the cavity makes the trends seen in the values of the coefficient less clear than in other positions. In general, as the wind speed increases, the normal force coefficient increases then begins to decrease at 120 mph. The pitch moment coefficient decreases initially then increases. The axial force coefficient decreases then increases again. All of the standard deviations decrease then increase slightly. Finally, the drag coefficient decreases then increases while the lift coefficient increases then decreases. These trends are visible in the tables in this section. These trends match the expectations of a higher signal-to-noise ratio in higher air speeds. Additionally, these trends are identified with data recorded from only three air speeds so caution must be taken in drawing general conclusions. Many of these trends observed are unique to the “in-cavity” cases because of the position of the model relative to the shear layer and the flow outside the cavity.

Speed (mph)	Position	N (lb_f)	std dev	C_N	std dev	m ($lb_f - in$)	std dev	C_m	std dev
60	In Cavity	0.003	0.008	0.085	0.104	-0.002	0.002	0.230	0.268
60	Shear Layer	0.087	0.008	1.077	0.096	-0.001	0.002	0.081	0.205
60	Out Cavity	0.117	0.007	1.449	0.089	0.003	0.002	-0.383	0.183
100	In Cavity	0.041	0.019	0.184	0.083	-0.005	0.005	0.218	0.214
100	Shear Layer	0.231	0.019	1.034	0.083	-0.001	0.003	0.026	0.132
100	Out Cavity	0.348	0.017	1.557	0.078	0.008	0.003	-0.334	0.123
120	In Cavity	0.042	0.028	0.132	0.086	0.009	0.008	0.271	0.215
120	Shear Layer	0.330	0.026	1.026	0.081	0.001	0.004	0.032	0.124
120	Out Cavity	0.492	0.024	1.530	0.076	-0.012	0.004	-0.333	0.121

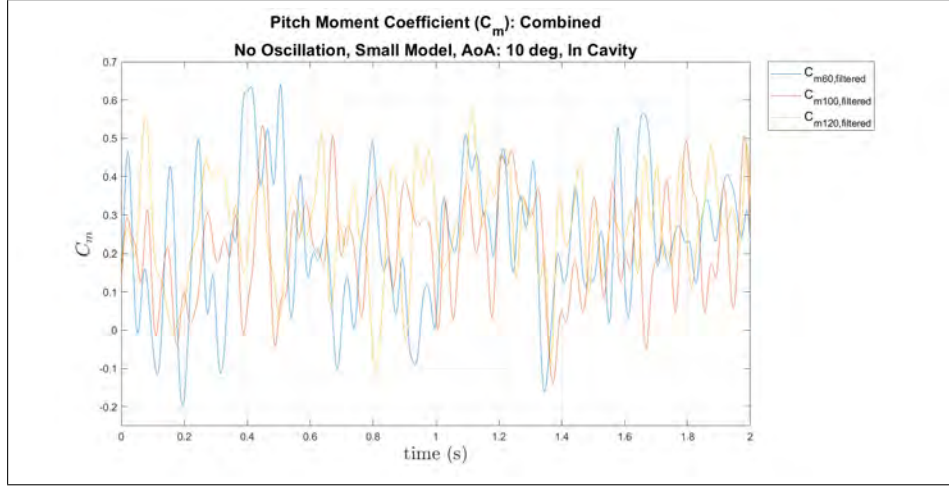
Table 16: Filtered values for small at various wind speeds and positions at 10° AoA in the cavity apparatus, Part 1

Speed (mph)	Position	A (lb_f)	std dev	C_A	std dev	C_D	C_L
60	In Cavity	0.039	0.010	0.485	0.124	0.484	-0.049
60	Shear Layer	0.009	0.009	0.122	0.112	0.308	1.039
60	Out Cavity	0.071	0.009	0.878	0.107	1.116	1.275
100	In Cavity	0.038	0.015	0.171	0.069	0.201	0.151
100	Shear Layer	0.069	0.016	0.308	0.073	0.483	0.964
100	Out Cavity	0.177	0.014	0.794	0.061	1.052	1.366
120	In Cavity	0.088	0.024	0.275	0.073	0.294	0.082
120	Shear Layer	0.107	0.023	0.333	0.071	0.507	0.953
120	Out Cavity	0.258	0.023	0.801	0.071	1.054	1.368

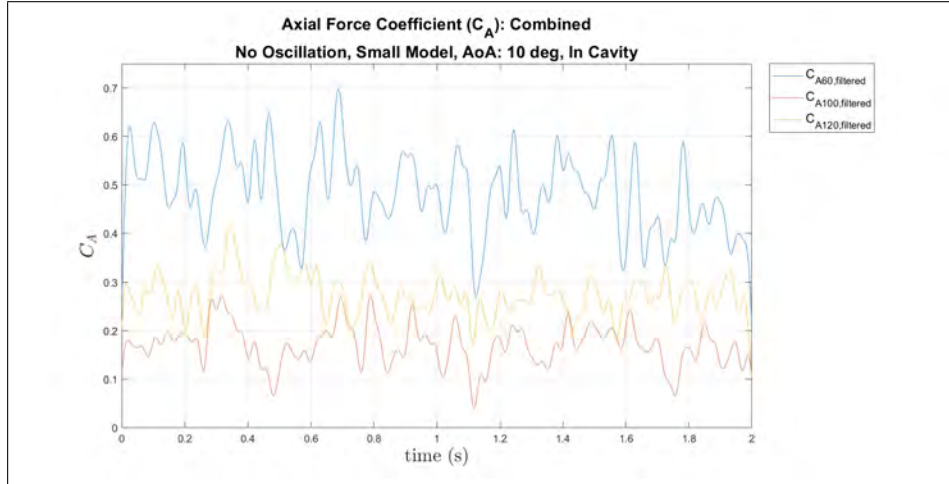
Table 17: Filtered values for small at various wind speeds and positions at 10° AoA in the cavity apparatus, Part 2



(a) Normal Force Coefficient, cavity apparatus, small model, 10° AoA, all speeds, in cavity position



(b) Pitch Moment Coefficient, cavity apparatus, small model, 10° AoA, all speeds, in cavity position



(c) Axial Force Coefficient, cavity apparatus, small model, 10° AoA, all speeds, in cavity position

Figure 55: All coefficients at all wind speeds for the small model at 10° AoA in the cavity apparatus, in cavity position

4.2.2.4 Shear Layer Position Values.

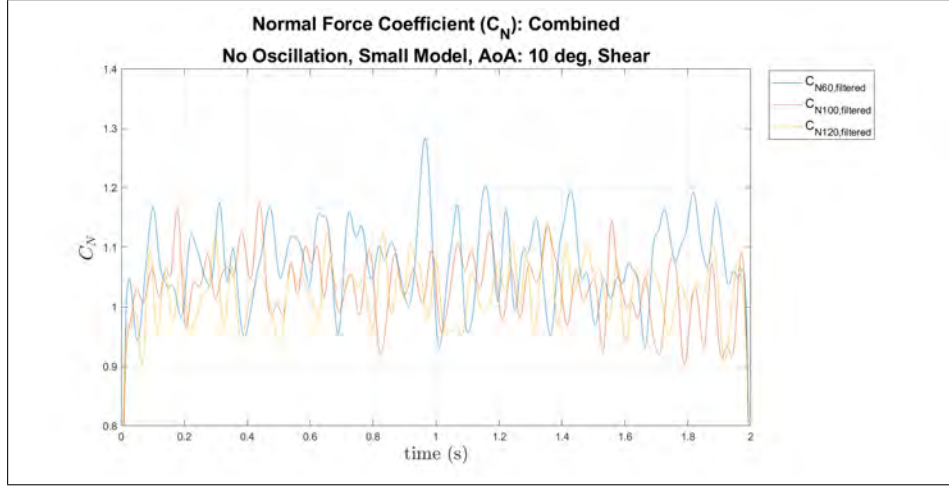
All of the cases in Figure 56 involve the small model at 10° AoA, statically placed at the “shear layer” position. Figure 56a shows the normal force coefficient. The trends for the normal force coefficient in the shear layer are more clear than inside the cavity. The coefficient values for all wind speeds, however, all lie almost on top of each other with means of $\overline{C}_N = 1.076$, $\overline{C}_N = 1.034$, and $\overline{C}_N = 1.026$ for the 60 mph, 100 mph, and 120 mph cases respectively. The standard deviations for these trials are 0.097, 0.083, and 0.081 respectively. With an increase in wind speed, the normal force coefficients and the standard deviations both decrease slightly.

The pitch moment coefficient shows a more complicated trend in Figure 56b. The 100 mph and 120 mph cases lie almost on top of each other. The mean for the coefficient decreases at 100 mph then increases at 120 mph. The mean values and standard deviations for the 60 mph, 100 mph, and 120 mph cases are $\overline{C}_m = 0.081$, $\overline{C}_m = 0.026$, and $\overline{C}_m = 0.032$, and 0.21, 0.13, and 0.12 respectively. Compared to the position within the cavity, this indicated a situation of nearly neutral stability for the moment about $\frac{x}{L} = 0.5$.

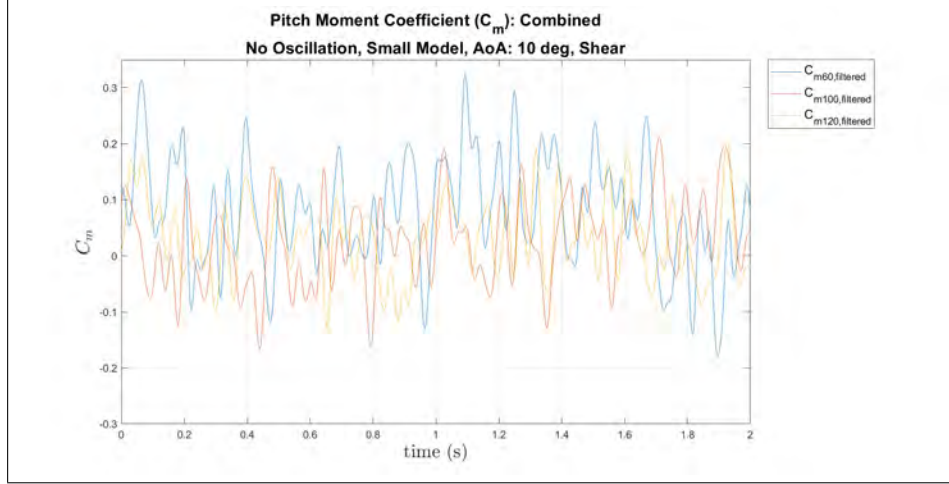
The axial force coefficient, shown in Figure 56c, presents a clearer and simpler trend. As the wind speed increases, the axial force coefficient increases and the standard deviation decreases. These values for the 60 mph, 100 mph, and 120 mph cases are $\overline{C}_A = 0.122$, $\overline{C}_A = 0.308$, and $\overline{C}_A = 0.333$, with standard deviations of 0.11, 0.073, and 0.071 respectively.

In terms of trends, as the wind speed increases, the normal force coefficient decreases, the axial force coefficient increases, the pitch moment coefficient decreases then increases, the drag coefficient increases, the lift coefficient decreases, and all the standard deviations decrease. Compared to the “in cavity” position, the normal force coefficient increases, the pitch moment coefficient decreases, the axial force coeffi-

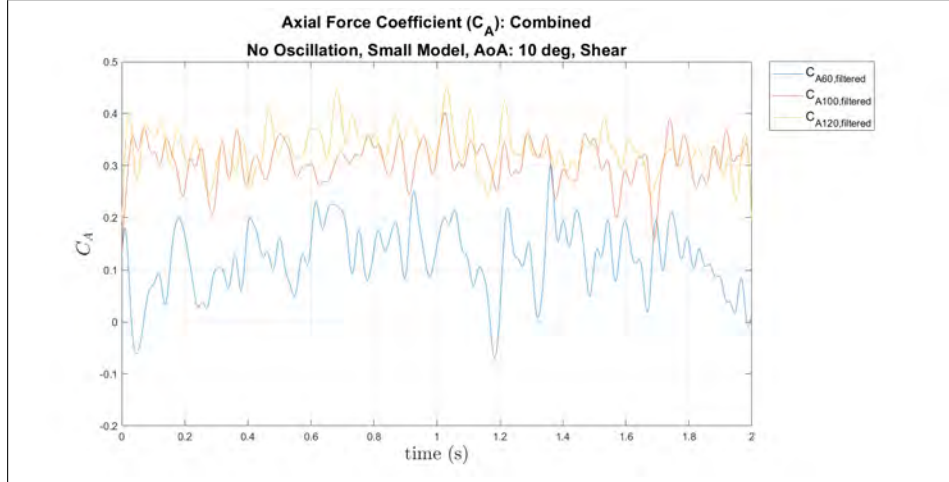
cient and drag coefficients both decrease which is an anomaly, and the lift coefficient increases. All of the values can be seen in Tables 16 and 17.



(a) Normal Force Coefficient, cavity apparatus, small model, 10° AoA, all speeds, shear position



(b) Pitch Moment Coefficient, cavity apparatus, small model, 10° AoA, all speeds, shear position



(c) Axial Force Coefficient, cavity apparatus, small model, 10° AoA, all speeds, shear position

Figure 56: All coefficients at all wind speeds for the small model at 10° AoA in the cavity apparatus, shear position

4.2.2.5 Out of Cavity Position Values.

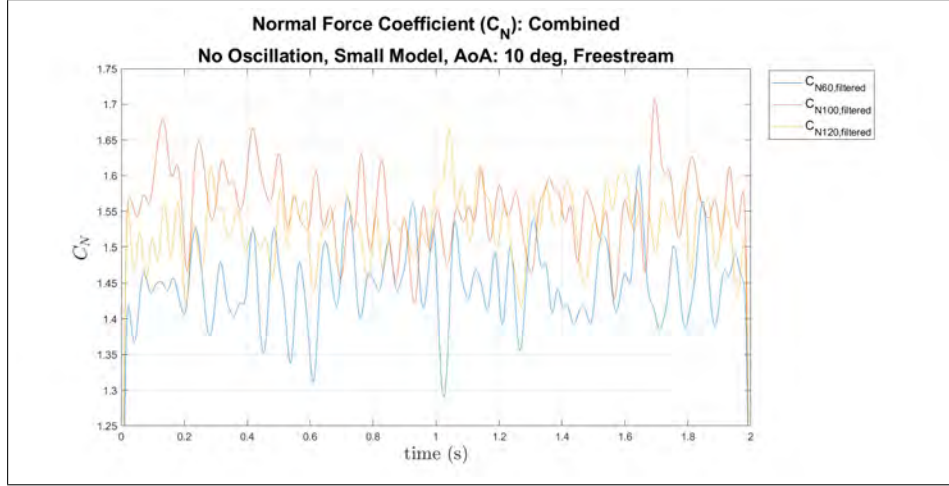
All of the cases in Figure 57 involve the small model at 10° AoA, statically placed at the “out-of-cavity position. All of these figures have a labeling of “freestream” on the image, but it is not the true freestream flow as seen in the freestream apparatus. These cases are merely out of the cavity, above the shear layer, as far as the linear motor would extend. The normal force coefficient can be seen in Figure 57a. The coefficient increases at 100 mph then decreases again at 120 mph. The standard deviation on the other hand just simply decreases. The 60 mph case mean is $\overline{C}_N = 1.449$ with a standard deviation of 0.089, the 100 mph case has a mean of $\overline{C}_N = 1.557$ with a standard deviation of 0.078, and the 120 mph case has a mean of $\overline{C}_N = 1.530$ with a standard deviation of 0.076.

Figure 57b shows the pitch moment coefficient for this position. The values of this coefficient increase with an increase in wind speed while the standard deviations decrease. These values lie almost on top of each other. The means and standard deviations are $\overline{C}_m = -0.383$ and 0.18 for the 60 mph, $\overline{C}_m = -0.334$ and 0.12 for the 100 mph case, and $\overline{C}_m = -0.332$ and 0.12 for the 120 mph.

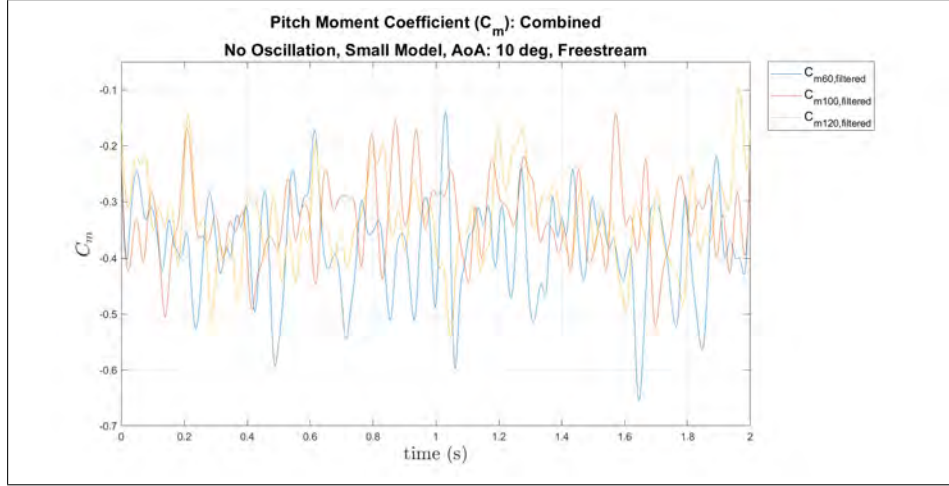
Finally, Figure 57c portrays the axial force coefficients. These show the opposite trend to the normal force coefficient. Both the axial force coefficient and the standard deviations initially decreases then slightly increases. The 60 mph case has a mean of $\overline{C}_A = 0.878$ with a standard deviation of 0.11, the 100 mph case has a mean of $\overline{C}_A = 0.794$ with a standard deviation of 0.061, and the 120 mph case has a mean of $\overline{C}_A = 0.801$ with a standard deviation of 0.071.

In terms of trends, the normal force coefficient increases then decreases, the pitch moment coefficient increases, the axial force coefficient and drag coefficient decreases then increases, and the lift coefficient increases. Compared to the other positions, the normal force coefficient increased, the pitch moment coefficient decreased, the axial

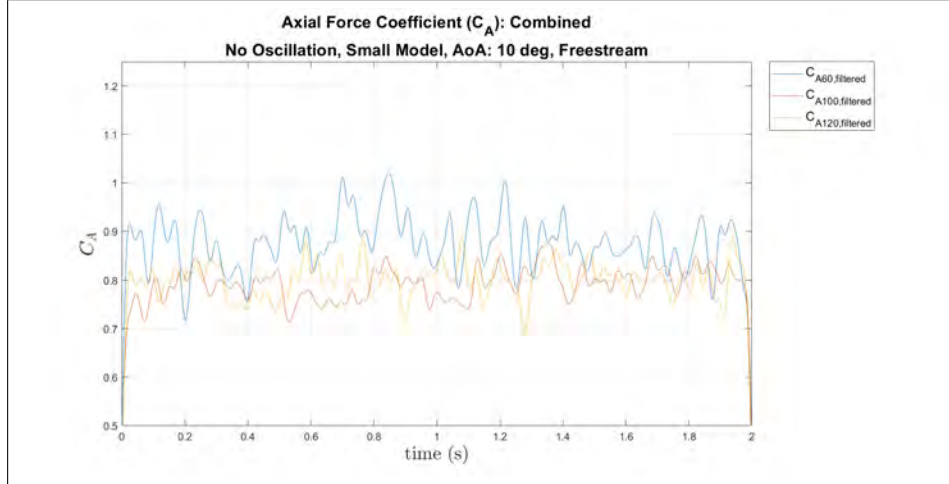
force coefficient increased, the drag coefficient increased, the lift coefficient increased and the standard deviations all decreased. All of the values can be seen in Tables 16 and 17.



(a) Normal Force Coefficient, cavity apparatus, small model, 10° AoA, out of cavity position



(b) Pitch Moment Coefficient, cavity apparatus, small model, 10° AoA, out of cavity position



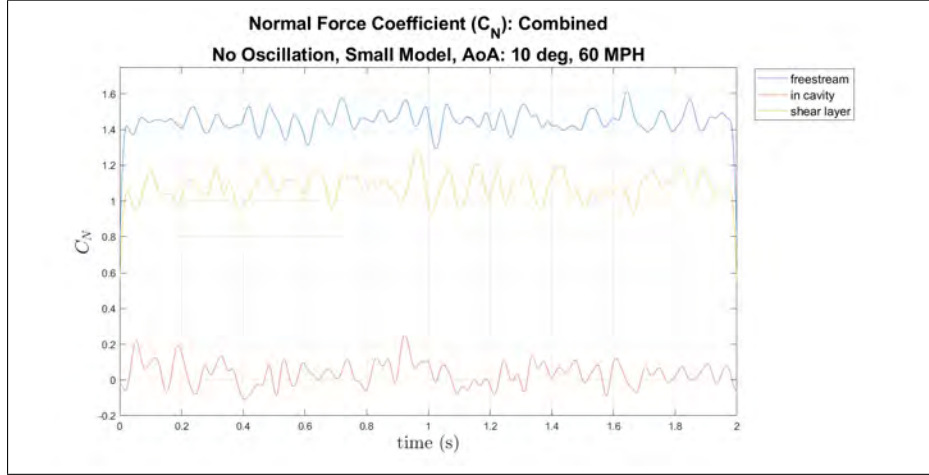
(c) Axial Force Coefficient, cavity apparatus, small model, 10° AoA, out of cavity position

Figure 57: All coefficients at all wind speeds for the small model at 10° AoA in the cavity apparatus, outside cavity position

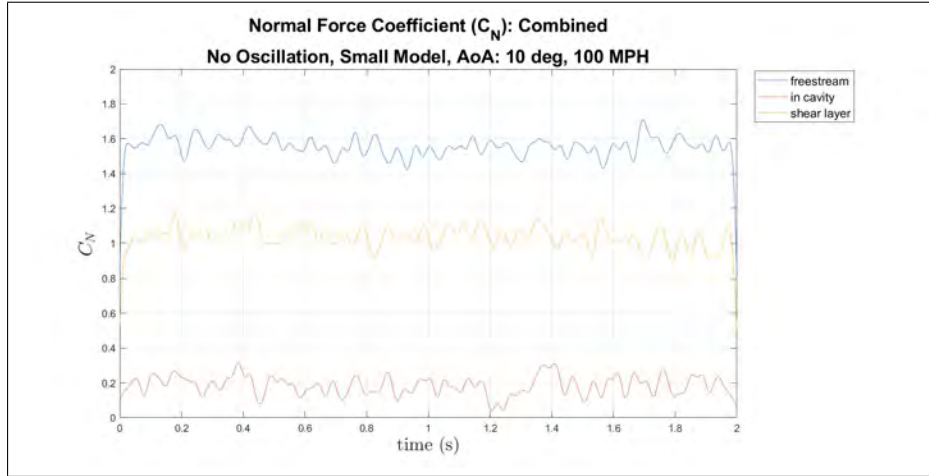
4.2.2.6 Comparison of C_N at Different Positions and Speeds.

Figure 58 compares the small model, 10° AoA case at all speeds. Figure 58a shows the 60 mph case, Figure 58b shows the 100 mph case, and Figure 58c shows the 120 mph case. The out of cavity position in these figures is labeled as the “freestream” but is really only the max height of the linear motor. These figures compare the filtered normal force coefficients for all three positions in the cavity apparatus. The means are all listed in Tables 16 and 17 and each position is explained in the respective sections.

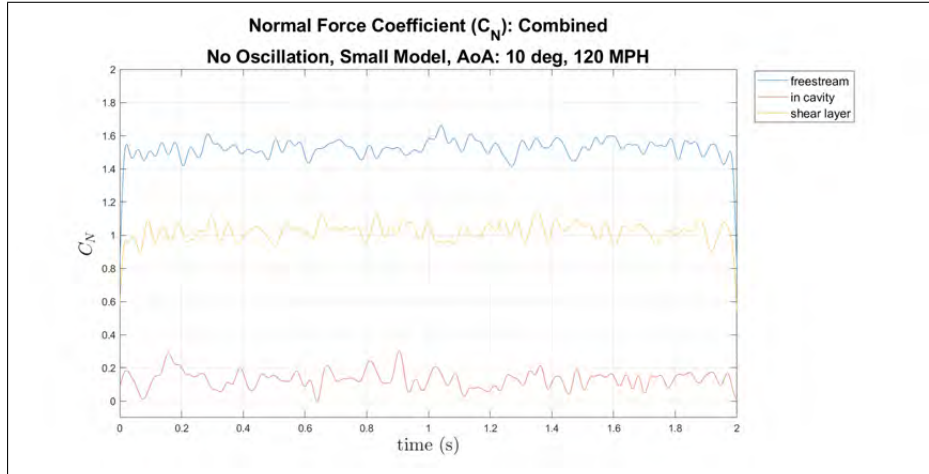
The normal force coefficient increases when the model is raised out of the cavity. This is observed in all cases and is very clear as seen by the three lines in the figures. Also, the coefficient increases as the wind speed increases, with the only notable exception being in the shear layer position.



(a) Normal Force Coefficient, cavity apparatus, small model, 10° AoA, 60 mph, all positions



(b) Normal Force Coefficient, cavity apparatus, small model, 10° AoA, 100 mph, all positions



(c) Normal Force Coefficient, cavity apparatus, small model, 10° AoA, 120 mph, all positions

Figure 58: All wind speeds for the small model at 10° AoA in the cavity apparatus, all cavity positions. The “freestream” label in the figure actually means the “out of cavity” position

4.2.2.7 Comparison of Model Sizes and AoA.

Figure 59 shows the normal force coefficient at 0° AoA for the small and large models. Figure 59a shows the small model cases for all positions. In these cases the normal force coefficients lay approximately coincident and they are slightly negative oscillating at approximately $C_N = -0.1$. The “out-of-cavity” case is slightly higher at about $C_N = -0.07$. The values increase from “in-cavity” to “out-of-cavity” which makes sense because the flow speed experienced by the model is increasing. The slightly negative value is caused by the orientation of the model with the nose normal to the flow. With an AoA of 0° , the forces experienced by the model are minimal. Figure 59b shows the large model cases at 0° AoA. A similar trend is seen with most of the data coincident but range from $C_N = -0.015$ in the cavity to $C_N = 0.047$ out of the cavity. The large model experiences slightly greater forces because of the greater surface area normal to the flow.

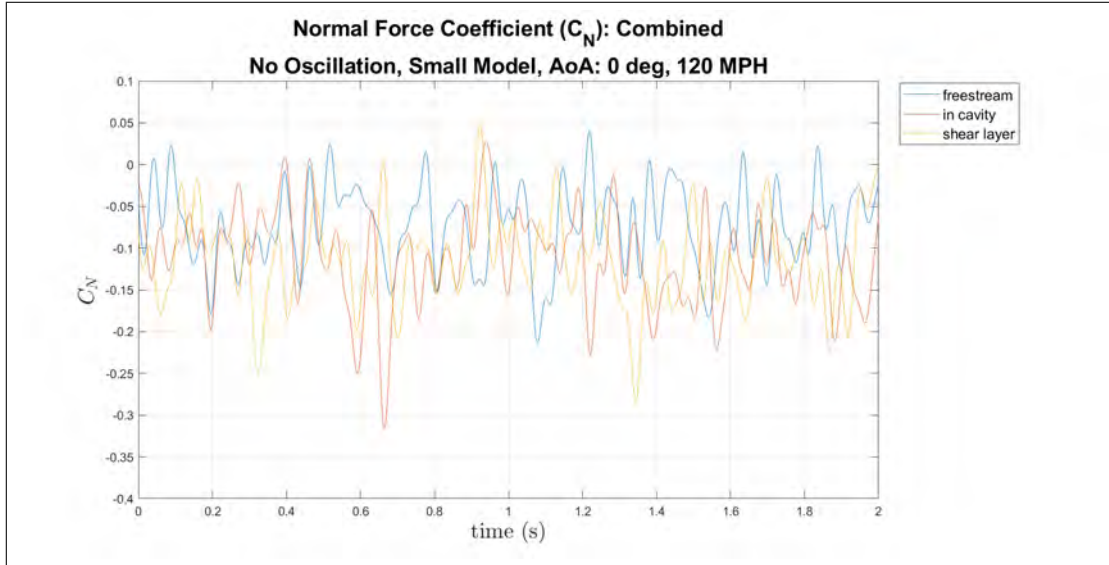
Figure 60 shows the normal force coefficient at 10° AoA for the small and large models. Figure 60a shows the small model cases for all positions. The normal force coefficients in these cases are much more pronounced than in the 0° case. The coefficient mean in the cavity is still small at $\overline{C}_N = 0.13$ with a standard deviation of 0.087. When the model is placed in the shear layer, the coefficient mean jumps to $\overline{C}_N = 1.03$ with a standard deviation of 0.081. Then the mean is $\overline{C}_N = 1.53$ for the out of cavity position with a standard deviation of 0.076. The “in-cavity” and “out-of-cavity” values are significant because they are seen in later trials with flow control and dynamic cases. Also, the distinction between the positions is clear and the increase in normal force coefficient is large. A similar trend is seen in Figure 60b which shows the large model in the same trials. In each position in the cavity apparatus, the large model cases are slightly lower than the small model cases. The coefficient means are $\overline{C}_N = -0.12$ in the cavity, $\overline{C}_N = 0.85$ in the shear layer, and

$\overline{C}_N = 1.45$ out of the cavity with standard deviations of 0.094, 0.092, and 0.095, respectively. There is a difference of less than 0.05 to 0.25 between the coefficients of each case.

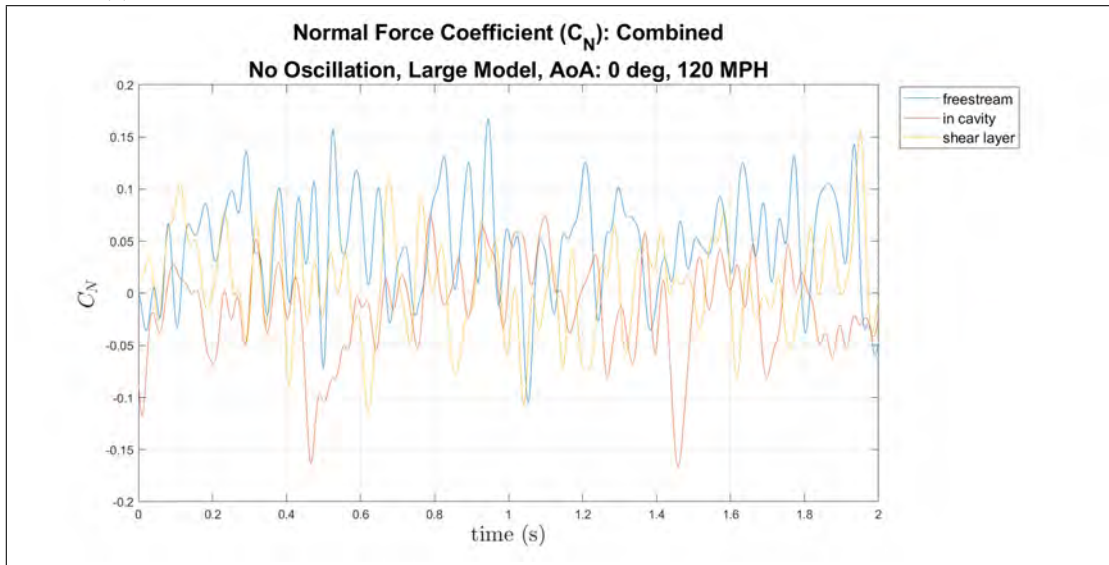
All values for these cases at 120 mph including the other coefficients can be seen in Tables 18, 19, and 20. In terms of trends for the normal force coefficient, for the 0° AoA cases, most of the trials oscillate around just under zero because of the model orientation. The large model has slightly greater values. The standard deviations for the small model are almost equal while the standard deviations for the large model trials vary greatly. For the 10° AoA cases, the coefficients are much greater. The small model has slightly higher coefficient values but the standard deviations are slightly lower than the large model trials.

Model	AoA ($^\circ$)	Position	N (lb_f)	std dev	C_N	std dev
Small	0	In Cavity	-0.036	0.028	-0.111	0.087
Small	0	Shear Layer	-0.037	0.027	-0.114	0.083
Small	0	Out Cavity	-0.023	0.028	-0.073	0.086
Small	10	In Cavity	0.042	0.028	0.132	0.086
Small	10	Shear Layer	0.330	0.026	1.026	0.081
Small	10	Out Cavity	0.492	0.024	1.530	0.076
Large	0	In Cavity	-0.008	0.036	-0.015	0.065
Large	0	Shear Layer	0.005	0.041	0.009	0.075
Large	0	Out Cavity	0.026	0.046	0.047	0.084
Large	10	In Cavity	-0.068	0.051	-0.125	0.094
Large	10	Shear Layer	0.469	0.050	0.855	0.092
Large	10	Out Cavity	0.795	0.052	1.449	0.095

Table 18: Filtered values for 120 mph with both model sizes and angles of attack in various positions in the cavity apparatus, Part 1



(a) Normal Force Coefficient, cavity apparatus, small model, 0° AOA, 120 mph, all positions



(b) Normal Force Coefficient, cavity apparatus, large model, 0° AOA, 120 mph, all positions

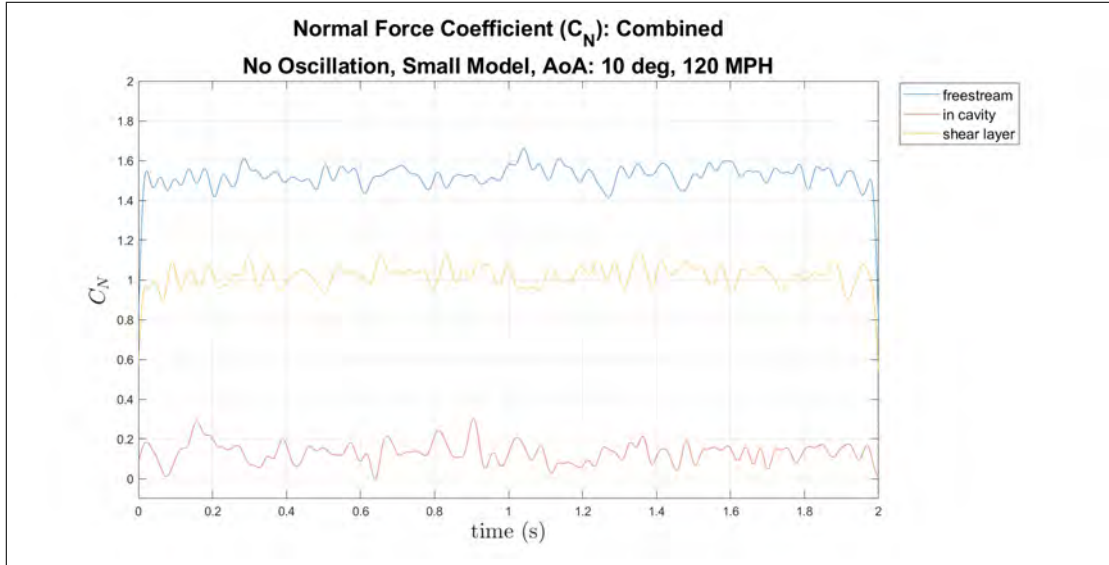
Figure 59: Comparison of normal force coefficients with different model sizes at 0° AoA, 120 mph, all positions

Model	AoA (°)	Position	m ($lb_f - in$)	std dev	C_m	std dev
Small	0	In Cavity	0.009	0.006	-0.276	0.174
Small	0	Shear Layer	-0.008	0.005	0.243	0.145
Small	0	Out Cavity	-0.003	0.005	0.085	0.131
Small	10	In Cavity	0.009	0.008	0.271	0.215
Small	10	Shear Layer	0.001	0.004	0.032	0.146
Small	10	Out Cavity	-0.012	0.004	-0.333	0.121
Large	0	In Cavity	0.001	0.013	0.017	0.161
Large	0	Shear Layer	-0.031	0.013	-0.394	0.163
Large	0	Out Cavity	-0.021	0.015	-0.268	0.179
Large	10	In Cavity	0.079	0.020	1.022	0.026
Large	10	Shear Layer	-0.002	0.016	-0.023	0.209
Large	10	Out Cavity	-0.014	0.017	-0.182	0.221

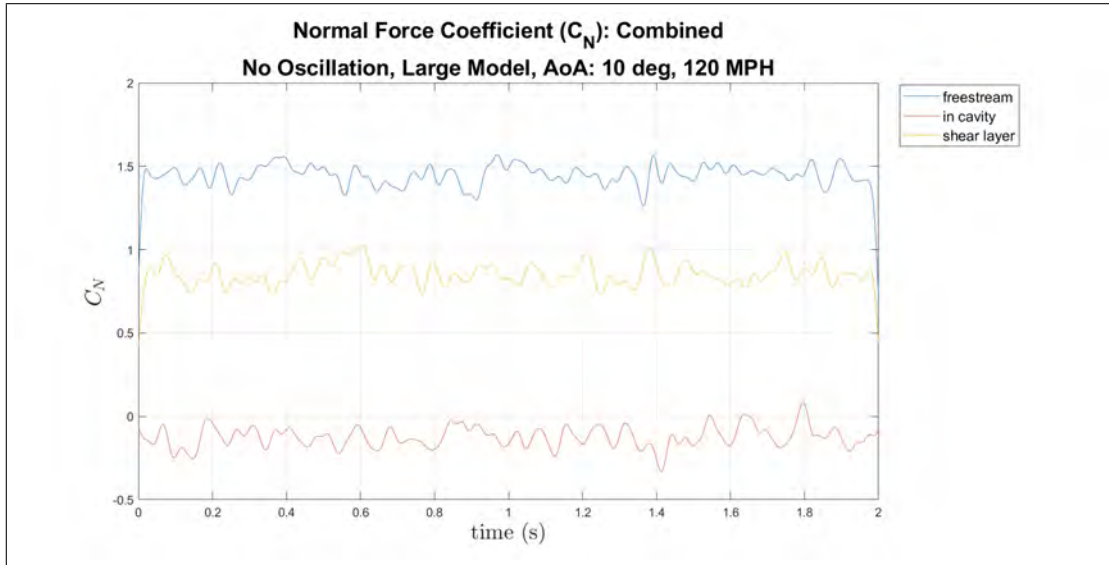
Table 19: Filtered values for 120 mph with both model sizes and angles of attack in various positions in the cavity apparatus, Part 2

Model	AoA (°)	Position	A (lb_f)	std dev	C_A	std dev	C_D	C_L
Small	0	In Cavity	0.030	0.024	0.095	0.076	0.095	-0.111
Small	0	Shear Layer	0.154	0.024	0.483	0.073	0.483	-0.114
Small	0	Out Cavity	0.211	0.024	0.657	0.074	0.657	-0.073
Small	10	In Cavity	0.088	0.024	0.275	0.073	0.435	0.082
Small	10	Shear Layer	0.107	0.023	0.333	0.071	0.507	0.953
Small	10	Out Cavity	0.258	0.023	0.801	0.071	1.054	1.368
Large	0	In Cavity	0.089	0.031	0.162	0.057	0.162	-0.015
Large	0	Shear Layer	0.261	0.036	0.476	0.065	0.476	0.009
Large	0	Out Cavity	0.372	0.039	0.677	0.072	0.677	0.047
Large	10	In Cavity	0.041	0.056	0.075	0.102	0.052	-0.136
Large	10	Shear Layer	0.126	0.033	0.230	0.059	0.375	0.802
Large	10	Out Cavity	0.294	0.046	0.536	0.083	0.779	1.335

Table 20: Filtered values for 120 mph with both model sizes and angles of attack in various positions in the cavity apparatus, Part3



(a) Normal Force Coefficient, cavity apparatus, small model, 10° AOA, 120 mph, all positions



(b) Normal Force Coefficient, cavity apparatus, large model, 10° AOA, 120 mph, all positions

Figure 60: Comparison of normal force coefficients with different model sizes at 0° AoA, 120 mph, all positions

4.2.3 Cavity Apparatus with Flow Control.

This portion of the experiment consists of static tests with the flow control device activated. The horizontally oriented linear motor oscillates at a frequency of 5 Hz, disrupting the flow and the shear layer. Air from the flow at the front lip of the cavity is drawn in and pushed out of the flow control device placed at the front of the cavity. The majority of cases used the slot for the flow control device, but some were also acquired with “diode 2”. A comparison to the diode is made in this section.

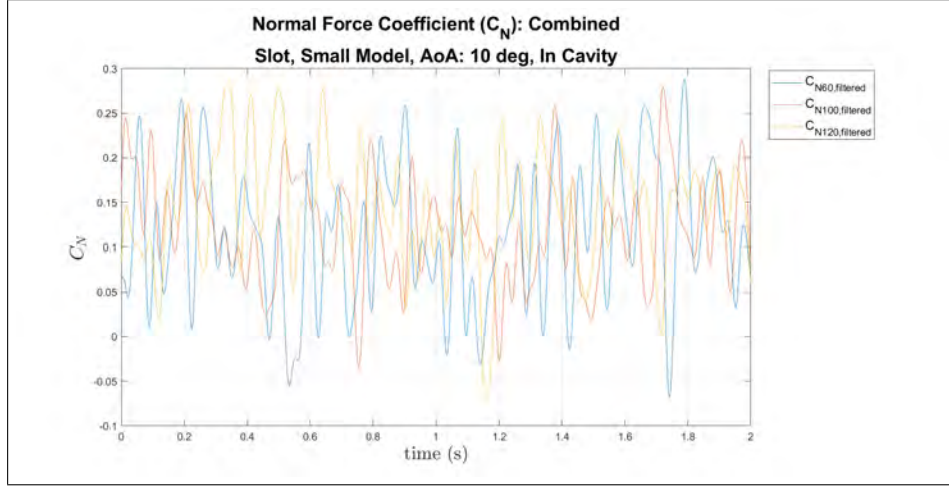
4.2.3.1 Comparison of Cavity Positions with Flow Control.

A comparison of different positions in the cavity apparatus for the small model at 10° AoA, with the flow control operating, is portrayed in Figure 61. In the cavity, shown in Figure 61a, the normal force coefficients for 60 mph, 100 mph, and 120 mph lie approximately on top of each other around $C_N = 0.116$ to $C_N = 0.147$ with standard deviations of 0.12, 0.09, and 0.097 respectively. Values are relatively low and are comparable to the “in-cavity” position without flow control. In this position there is still not a clear frequency shown in the coefficient at any wind speed.

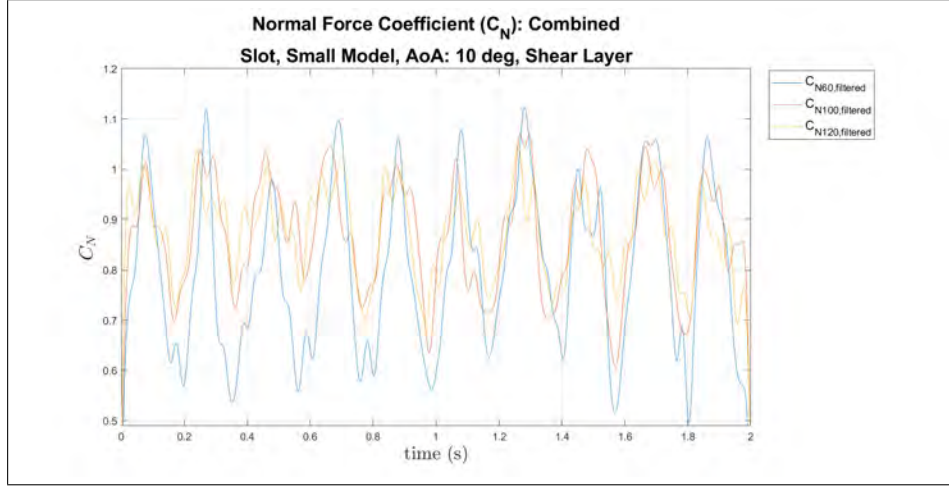
In the shear layer position, shown in Figure 61b, it is clear that the force coefficient indicates a frequency consistent with the flow control. The mean coefficients are very close to each other with the mean of $C_N = 0.797$ for the 60 mph case and approximately $C_N = 0.87$ for the 100 mph and 120 mph cases. The standard deviations are 0.19, 0.13, and 0.11 respectively. These have a greater amplitude than in the cavity position and greater standard deviations which makes sense because the shear layer is oscillating. The oscillation is clearly 5 Hz as shown by the troughs of the wave at approximately $time = 0.2sec$, $time = 0.4sec$, $time = 0.6sec$, $time = 0.8sec$, and $time = 1.0sec$. This result is significant and in that it validates the use of the Nano25 for measuring cyclic forces at 5 Hz. Finally, in Figure 61c, the out of cavity case re-

flects the same trends as the shear layer case but the trials have means of $C_N = 1.417$, $C_N = 1.448$, and $C_N = 1.479$, with standard deviations of 0.17, 0.12, 0.10, for the 60 mph, 100 mph, and 120 mph cases respectively. The standard deviations are slightly less than in the shear layer but the coefficient values are much greater. The 5 Hz frequency is also clear in the out of cavity position.

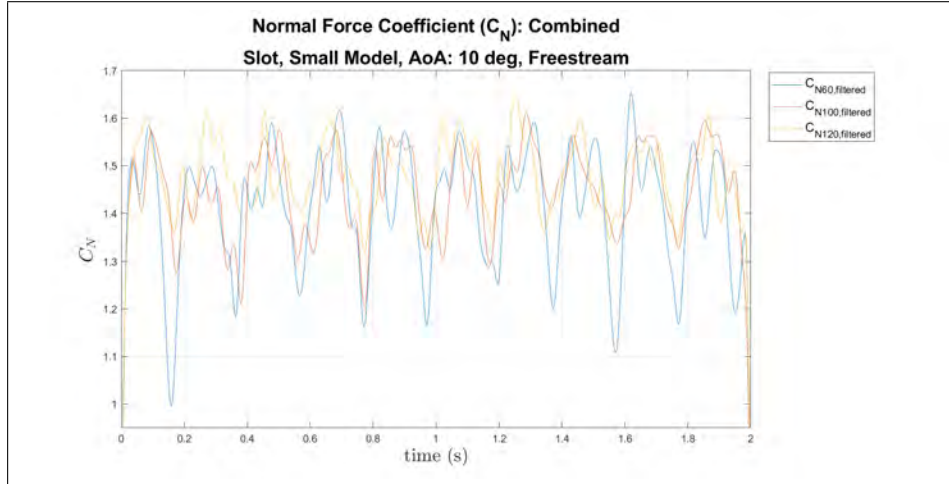
In terms of trends, when the wind speed increases, the normal force coefficient increases and the standard deviations increase, with the exception of the standard deviations in the shear layer position. Also, the coefficient value drastically increases when the store is moved out of the cavity. Additionally, A clear 5 Hz oscillation frequency is observed in both the shear layer and out of cavity positions for all wind speeds, while the oscillation in the cavity position is less clear. A table with all of the values for every coefficient can be seen in Tables 21 and 22. Compared to the cases without flow control, the values follow the same trends. The differences in normal force coefficient is about 33% to 36% for “in-cavity”, 15% to 25% for “shear layer”, and 2% to 6% for “out-of-cavity”. The standard deviations for these values have a change of 9% to 12%, 41% to 61%, and 36% to 49% respectively. The differences in axial force coefficient is about 2% to 5% for “in-cavity”, 5% to 18% for “shear layer”, and 4% to 28% for “out-of-cavity”. The standard deviations for these values have a change of 0% to 8%, 10% to 52%, and 4% to 38% respectively.



(a) Normal Force Coefficient, small model, 10° AoA, 120 mph, in cavity position, flow control



(b) Normal Force Coefficient, small model, 10° AoA, 120 mph, shear layer position, flow control



(c) Normal Force Coefficient, small model, 10° AoA, 120 mph, out of cavity position, flow control

Figure 61: All positions for the small model at 10° AoA in the cavity apparatus, 120 mph, with flow control

FC Device	Speed (mph)	Position	C_N	std dev	C_m	std dev
Slot	60	In Cavity	0.116	0.117	0.069	0.294
Slot	60	Shear Layer	0.797	0.191	0.007	0.266
Slot	60	Out Cavity	1.417	0.167	-0.193	0.336
Slot	100	In Cavity	0.123	0.090	0.127	0.237
Slot	100	Shear Layer	0.870	0.134	0.071	0.166
Slot	100	Out Cavity	1.448	0.116	-0.283	0.192
Slot	120	In Cavity	0.145	0.097	0.179	0.222
Slot	120	Shear Layer	0.873	0.114	0.114	0.130
Slot	120	Out Cavity	1.479	0.104	-0.262	0.171

Table 21: Filtered values for the small model at 10° AoA in various positions in the cavity apparatus with flow control and slot, Part 1

FC Device	Speed (mph)	Position	C_A	std dev	C_L	C_D
Slot	60	In Cavity	0.475	0.134	0.488	0.032
Slot	60	Shear Layer	0.131	0.124	0.267	0.762
Slot	60	Out Cavity	0.843	0.102	1.076	1.249
Slot	100	In Cavity	0.182	0.075	0.199	0.089
Slot	100	Shear Layer	0.186	0.112	0.334	0.825
Slot	100	Out Cavity	0.303	0.084	0.549	1.374
Slot	120	In Cavity	0.267	0.073	0.288	0.096
Slot	120	Shear Layer	0.396	0.104	0.541	0.791
Slot	120	Out Cavity	0.573	0.081	0.821	1.657

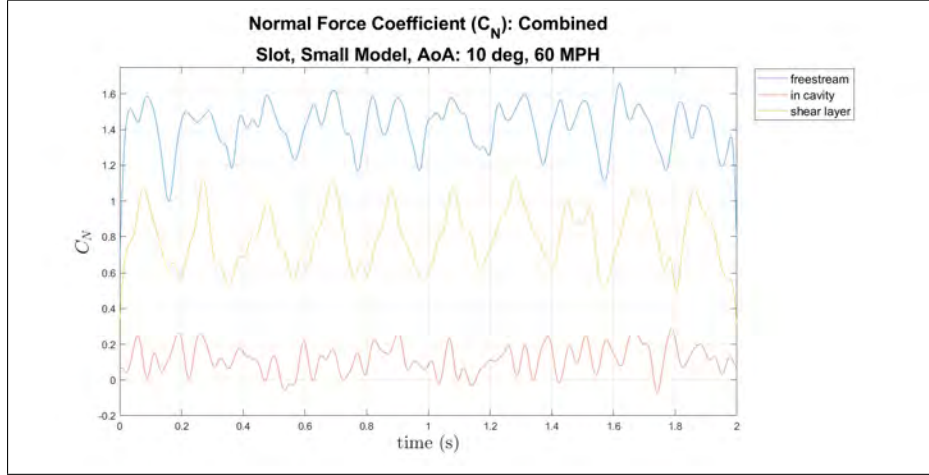
Table 22: Filtered values for the small model at 10° AoA in various positions in the cavity apparatus with flow control and slot, Part 2

4.2.3.2 Comparison of Positions at Different Speeds with Flow Control.

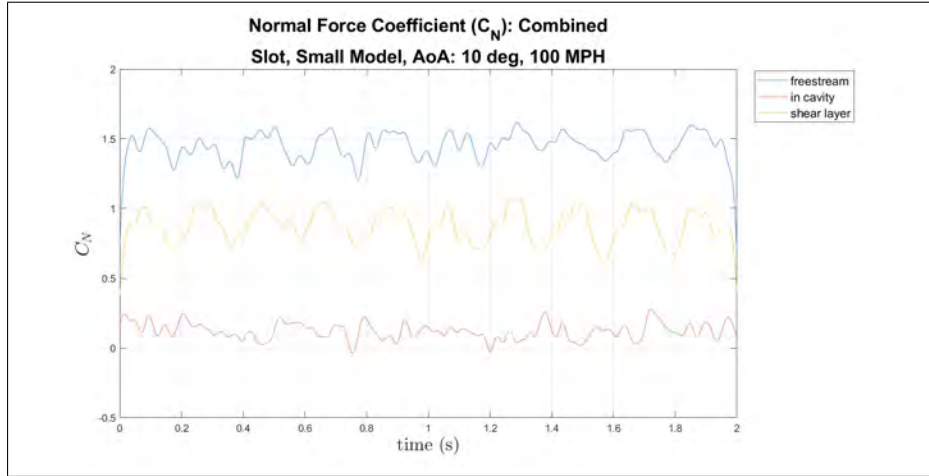
A comparison of trials involving all wind speeds and static positions in the cavity with the flow control on is shown in Figure 62. These scenarios directly compare to the plots shown in Figure 58 which has the same scenarios but without flow control. Figure 62a shows the 60 mph case, Figure 62b shows the 100 mph case, but the main comparison should be made with the 120 mph case shown in Figure 62c. The trials in these figures are the same in the last section, and the coefficients are numerated

in Tables 21 and 22.

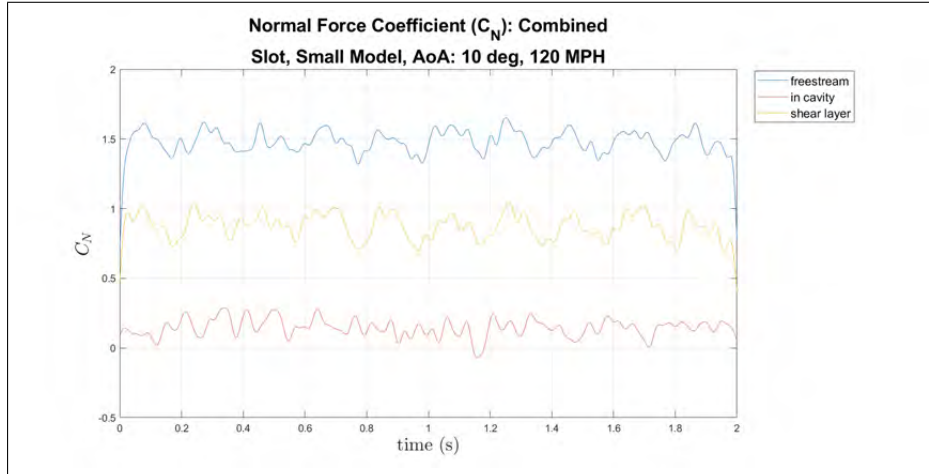
All of these cases in the shear layer and out of cavity positions show a clear 5 Hz signal which was generated by the flow control device. This pattern can be seen at all wind speeds. The in cavity case has a far less distinct frequency. This absence of a 5 Hz signal in the cavity position verifies that the oscillation is caused by the flow and not created by mechanical vibration. The cases from 60 mph to 120 mph for the in cavity position have a frequency ranging from approximately 5 to 15 Hz. The flow control device still has some impact on the normal force coefficient compared to the trials without flow control. The flow control device does not greatly change the average values of each coefficient, but the oscillation frequency is directly impacted. The trends are the same for the last section. The standard deviations decrease when the wind speed increases.



(a) Normal Force Coefficient, small model, 10° AoA, 60 mph, all positions, flow control



(b) Normal Force Coefficient, small model, 10° AoA, 100 mph, all positions, flow control



(c) Normal Force Coefficient, small model, 10° AoA, 120 mph, all positions, flow control

Figure 62: All wind speeds for the small model at 10° AoA in the cavity apparatus, all cavity position, flow control. The “freestream” label in the figure actually means the “out of cavity” position

4.2.3.3 Comparison of Model Sizes and AoA with Flow Control.

This section compares the impact of model size and angle of attack on the normal force coefficient at 120 mph with the 0° AoA shown in Figure 63 and the 10° AoA in Figure 64. These cases are with flow control on using the “slot” device. The small model at 0° shown in Figure 63a and the large model case shown in Figure 63b portray a similar trend as without flow control. The values of the normal force coefficient all lie on top of each other with the average values just below zero. This is expected because of the orientation of the models at 0° AoA and the low amount of surface area normal to the flow. The difference between these trials and the ones without flow control is the 5 Hz oscillation which is discernible in many of the subfigures. The “in-cavity” trials for the small model is the easiest to see with peaks at $time = 0.2sec$ and every $0.2sec$ after that. This is caused by the orientation of the model as well. This same oscillation is seen in the large model case by the line at approximately the same time positions. The values of the coefficients, when comparing the different positions, are nearly unchanged.

Figure 64a shows the small model case at 10° AoA, and is the same as Figure 62c, while Figure 64b shows the large model case at 10° AoA. These cases clearly show the effects of different positions in the cavity apparatus on the normal force coefficient. The large model coefficients have average values that are slightly lower than the small model case. Additionally the standard deviation is slightly greater than in the small model case.

The means of all of the coefficient values including the normal force coefficient can be seen in Tables 23 and 24. In terms of trends, the normal force coefficient increases when the model moves out of the cavity for all cases except the large model at 0° AoA. The standard deviations for these cases vary but they are higher in the shear layer and out of cavity positions. Also, the coefficient drastically increases from the

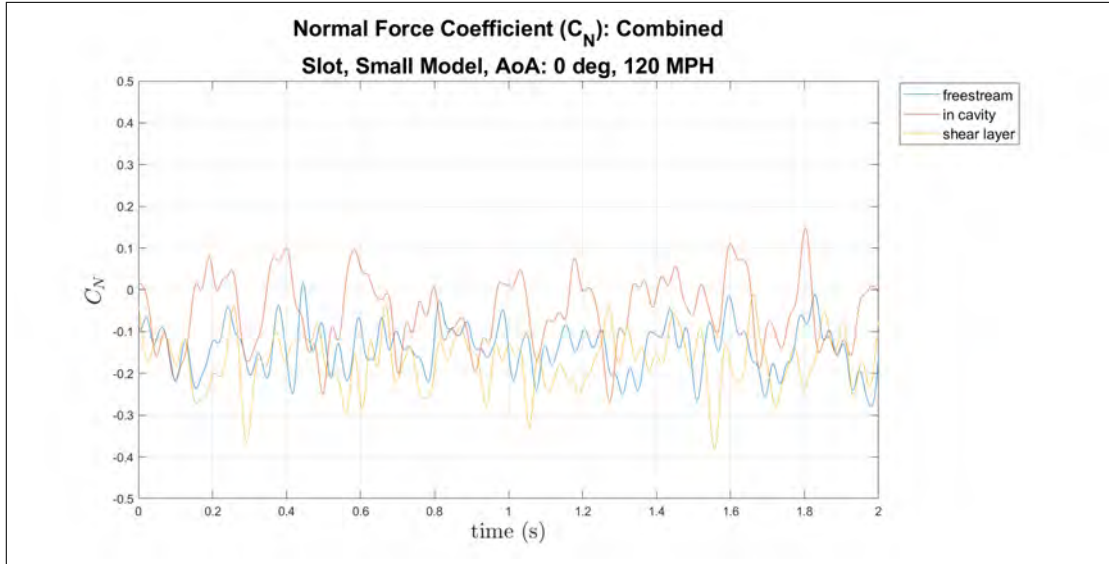
0° AoA to the 10° AoA. The standard deviations do not have a clear trend for this comparison. The large model coefficient values are slightly less than the small model values. The standard deviations for the large model are also slightly lower for most cases.

Model	AoA (°)	Position	C_N	std dev	C_m	std dev
Small	0	In Cavity	-0.051	0.113	0.196	0.214
Small	0	Shear Layer	-0.171	0.105	-0.158	0.019
Small	0	Out of Cavity	-0.141	0.099	-0.108	0.173
Small	10	In Cavity	0.145	0.097	0.179	0.222
Small	10	Shear Layer	0.873	0.114	0.114	0.130
Small	10	Out of Cavity	1.479	0.104	-0.262	0.171
Large	0	In Cavity	0.016	0.088	0.049	0.174
Large	0	Shear Layer	-0.047	0.075	-0.280	0.196
Large	0	Out of Cavity	-0.007	0.097	-0.257	0.242
Large	10	In Cavity	0.134	0.092	0.016	0.271
Large	10	Shear Layer	0.786	0.098	0.014	0.204
Large	10	Out of Cavity	1.380	0.124	-0.17	0.243

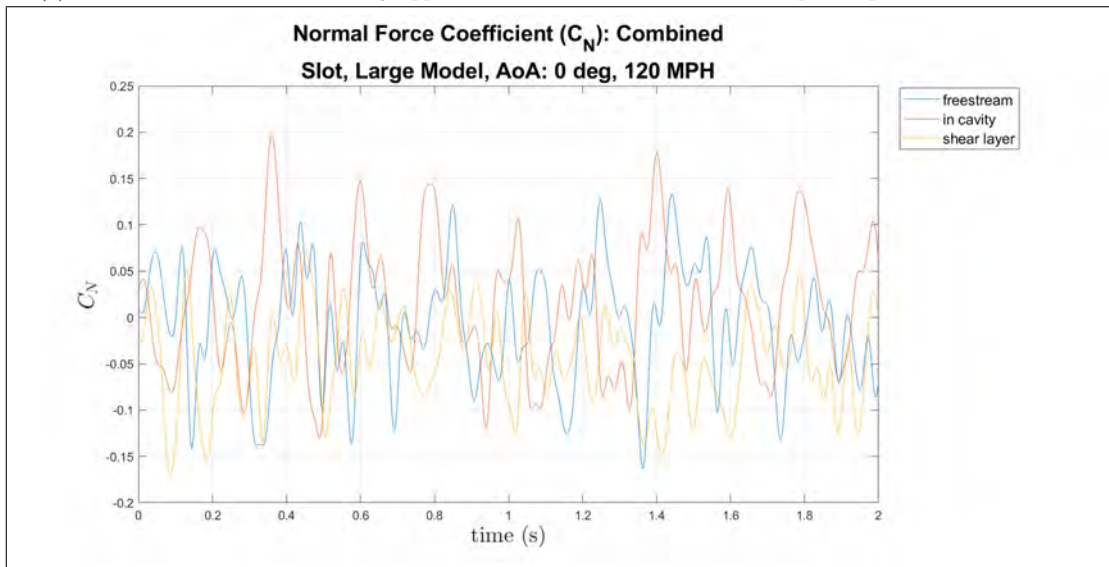
Table 23: Filtered values for various models and angles of attack at 120 mph in various positions in the cavity apparatus with flow control and slot, Part 1

Model	AoA (°)	Position	C_A	std dev	C_D	C_L
Small	0	In Cavity	0.188	0.097	0.188	-0.171
Small	0	Shear Layer	0.534	0.091	0.534	-0.171
Small	0	Out of Cavity	0.757	0.083	0.757	-0.141
Small	10	In Cavity	0.267	0.073	0.288	0.096
Small	10	Shear Layer	0.396	0.104	0.541	0.791
Small	10	Out of Cavity	0.573	0.081	0.821	1.657
Large	0	In Cavity	0.109	0.067	0.109	0.016
Large	0	Shear Layer	0.397	0.070	0.397	-0.047
Large	0	Out of Cavity	0.616	0.080	0.616	-0.007
Large	10	In Cavity	0.102	0.096	0.102	0.134
Large	10	Shear Layer	0.282	0.068	0.282	0.786
Large	10	Out of Cavity	0.563	0.077	0.563	1.380

Table 24: Filtered values for various models and angles of attack at 120 mph in various positions in the cavity apparatus with flow control and slot, Part 2

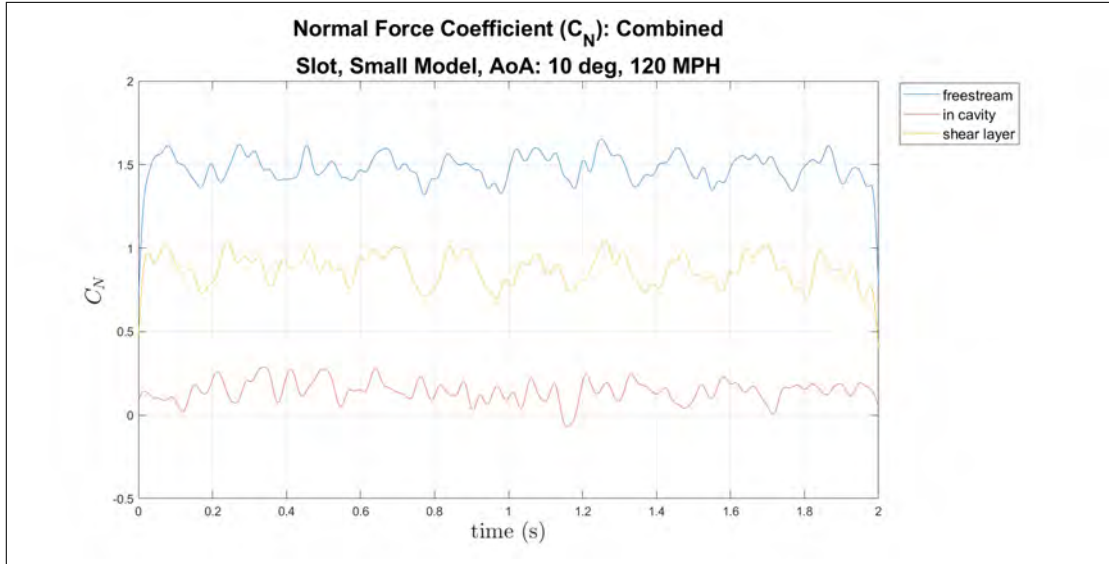


(a) Normal Force Coefficient, cavity apparatus, small model, 0° AOA, 120 mph, all positions, flow control

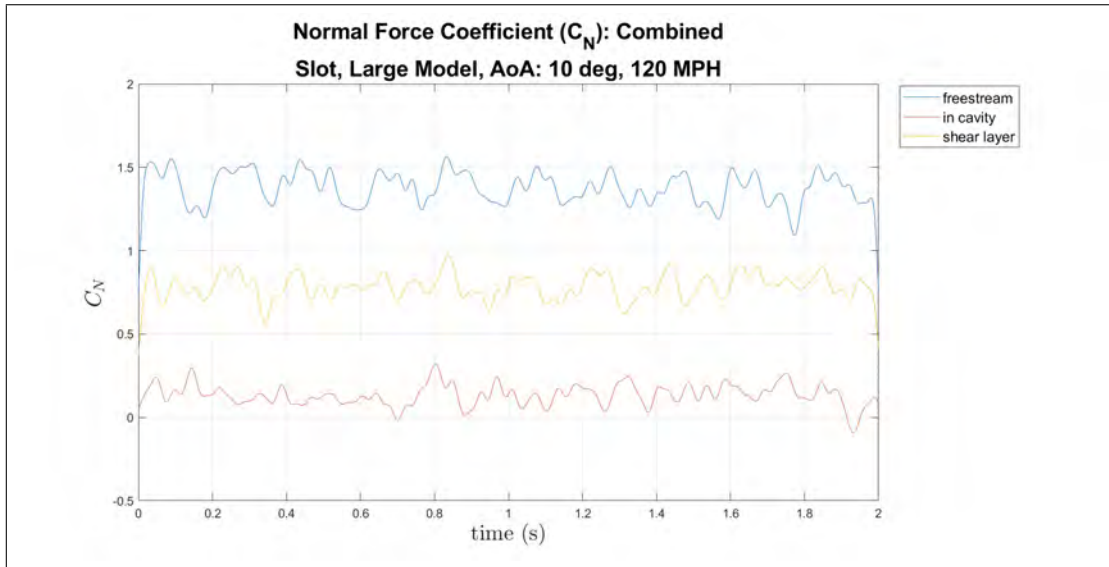


(b) Normal Force Coefficient, cavity apparatus, large model, 0° AOA, 120 mph, all positions, flow control

Figure 63: Comparison of the difference model sizes at 0° AoA of the normal force coefficient, cavity apparatus, all positions, 120 mph. The “freestream” label in the figure actually means the “out of cavity” position



(a) Normal Force Coefficient, cavity apparatus, small model, 10° AOA, 120 mph, all positions, flow control



(b) Normal Force Coefficient, cavity apparatus, large model, 10° AOA, 120 mph, all positions, flow control

Figure 64: Comparison of different model sizes at 10° AoA of the normal force coefficient, cavity apparatus, all positions, 120 mph. The “freestream” label in the figure actually means the “out of cavity” position

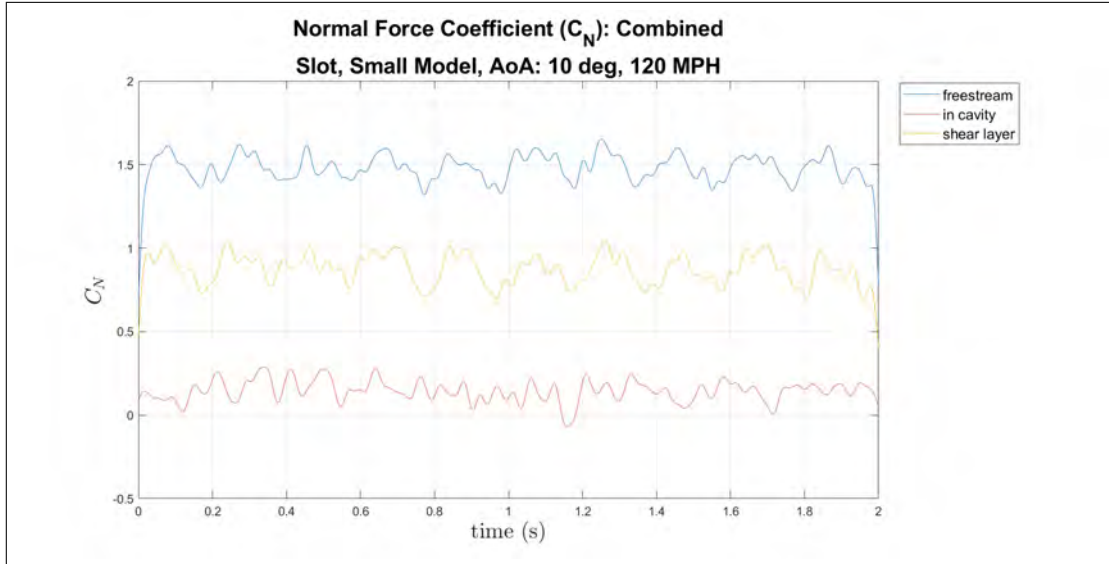
4.2.3.4 Comparison of Flow Control Devices.

A comparison of the effects of different flow control devices was made with both models at 10° AoA and 120 mph. The small model cases are shown in Figure 65 and the large model cases are shown in Figure 66. Figure 65a portrays the slot case for the small model and Figure 65b portrays the diode 2 case. Meanwhile, Figure 66a shows the slot case for the large model and Figure 66b shows the diode 2 case. These cases all exhibit the same trends of previous trials in terms of showing the 5 Hz signal and having coefficients at the expected values for the respective positions of the model.

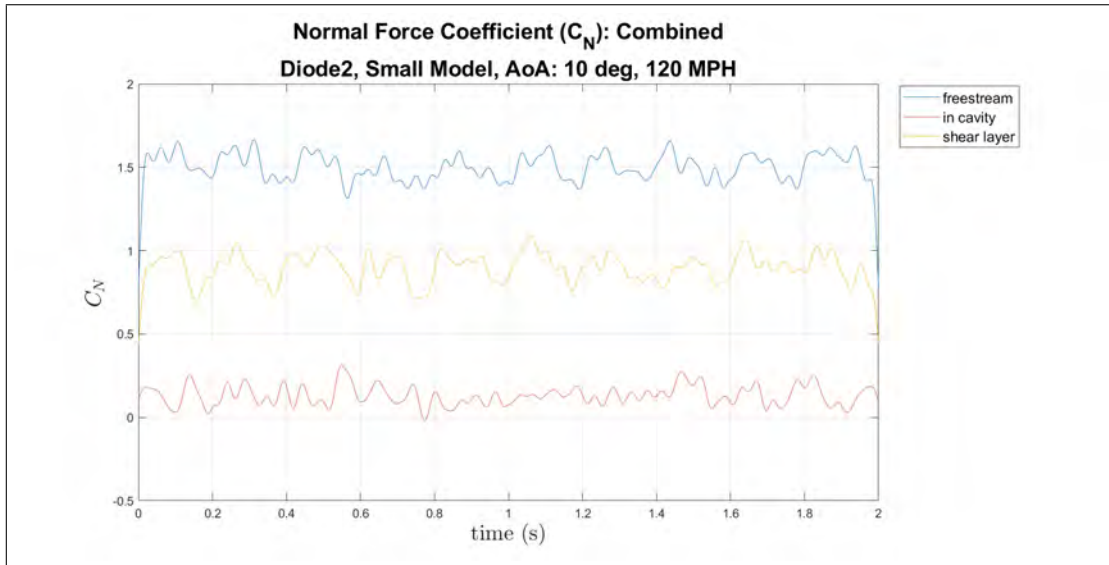
The values of the coefficients and the standard deviation for each trial are numerated in Table 25. Between the means of each position in the cavity, the difference in value when comparing the different model sizes and flow control devices is only 1 to 6%. The diode makes the means of every position consistently higher except for the small model in the cavity. The standard deviations are within 10% of each other but are extremely similar. There is no strong trend indicating which flow control device has a higher standard deviation.

NFC Means	Cavity	std dev	Shear Layer	std dev	Out of Cavity	std dev
Small Model Slot	0.14	0.09	0.87	0.11	1.48	0.10
Small Model Diode	0.13	0.09	0.89	0.10	1.50	0.11
Large Model Slot	0.13	0.09	0.78	0.09	1.38	0.12
Large Model Diode	0.15	0.08	0.84	0.11	1.44	0.11

Table 25: Normal Force Coefficient comparison of Flow Control Devices with Flow Control

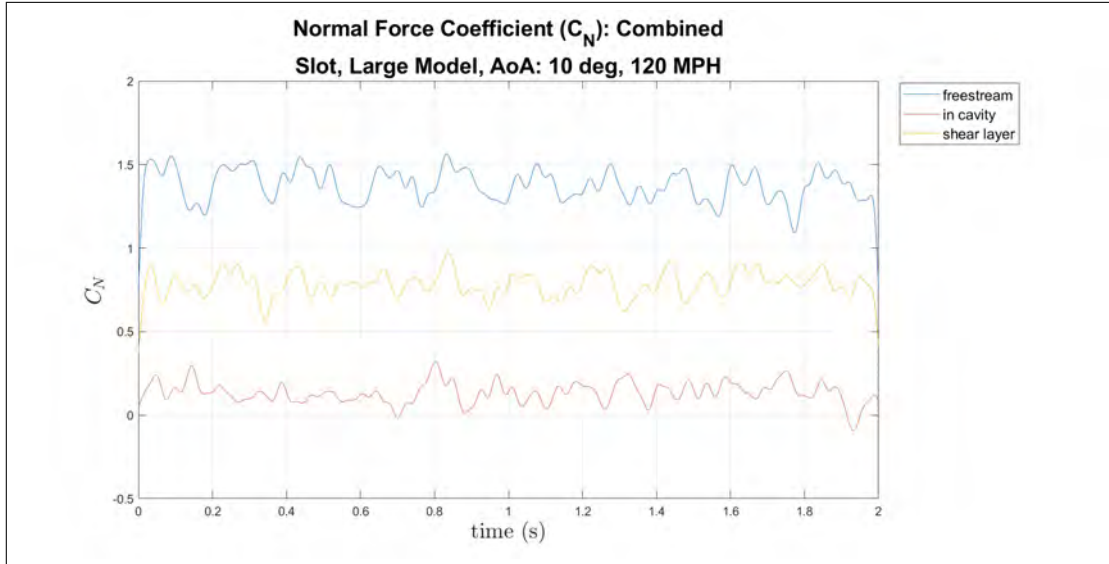


(a) Normal Force Coefficient, cavity apparatus, small model, 10° AOA, 120 mph, slot, all positions

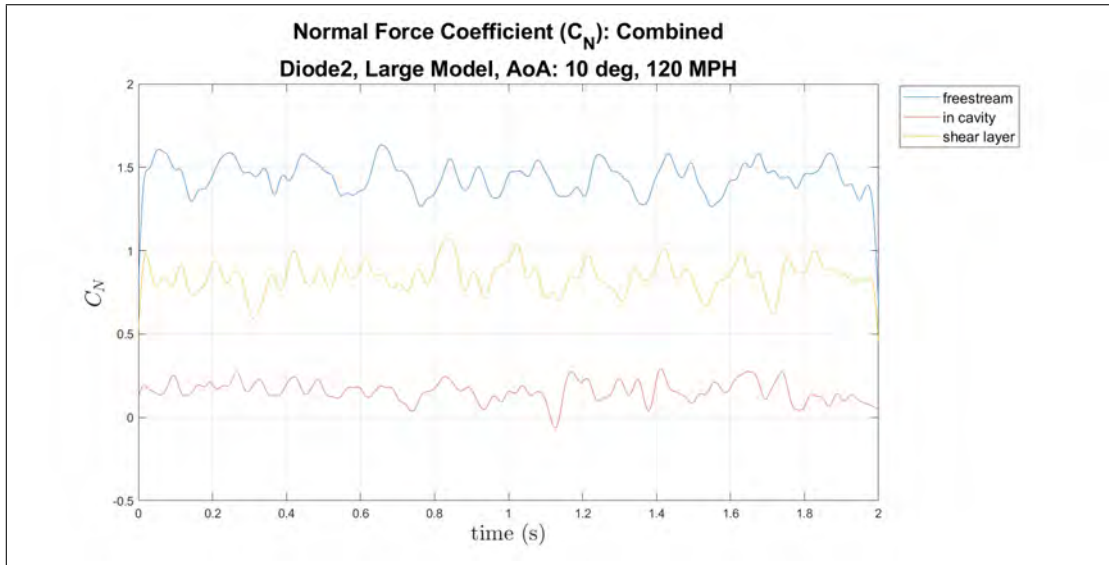


(b) Normal Force Coefficient, cavity apparatus, small model, 10° AOA, 120 mph, diode2 , all positions

Figure 65: Comparison of normal force coefficients with flow control devices at 10° AoA, small model, 120 mph, all positions. The “freestream” label in the figure actually means the “out of cavity” position



(a) Normal Force Coefficient, cavity apparatus, large model, 10° AOA, 120 mph, slot, all positions



(b) Normal Force Coefficient, cavity apparatus, large model, 10° AOA, 120 mph, diode2, all positions

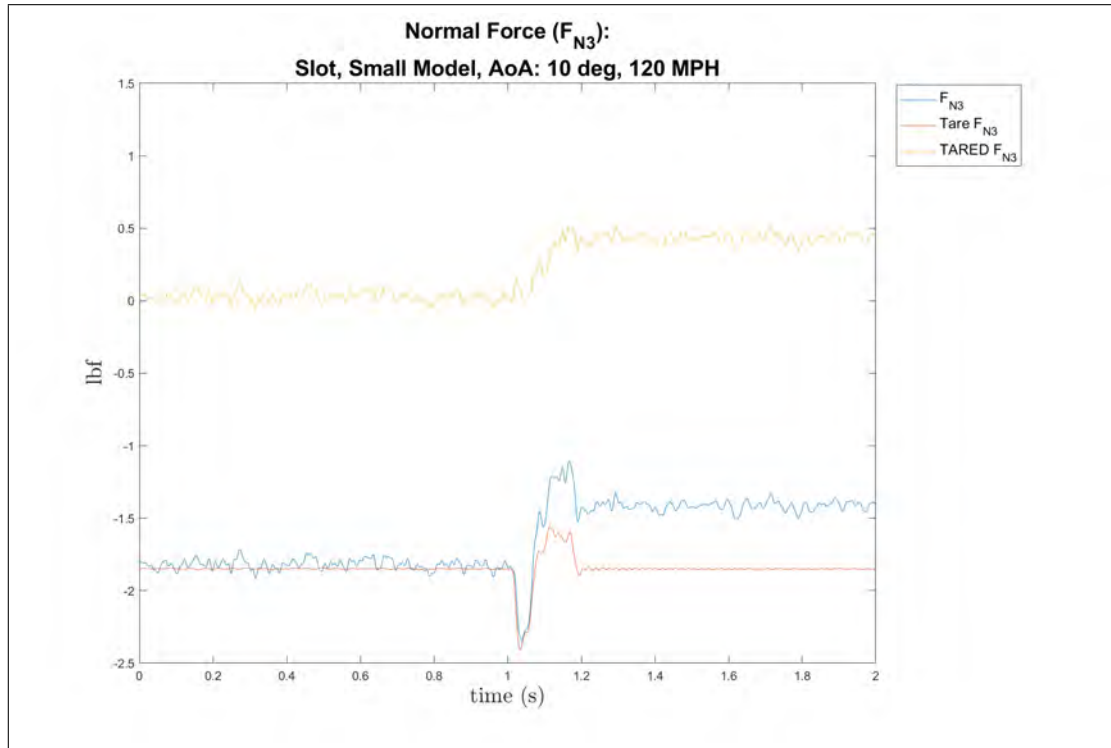
Figure 66: Comparison of normal force coefficients with flow control devices at 10° AoA, large model, 120 mph, all positions. The “freestream” label in the figure actually means the “out of cavity” position

4.3 Phase II: Dynamic Mission Store Release

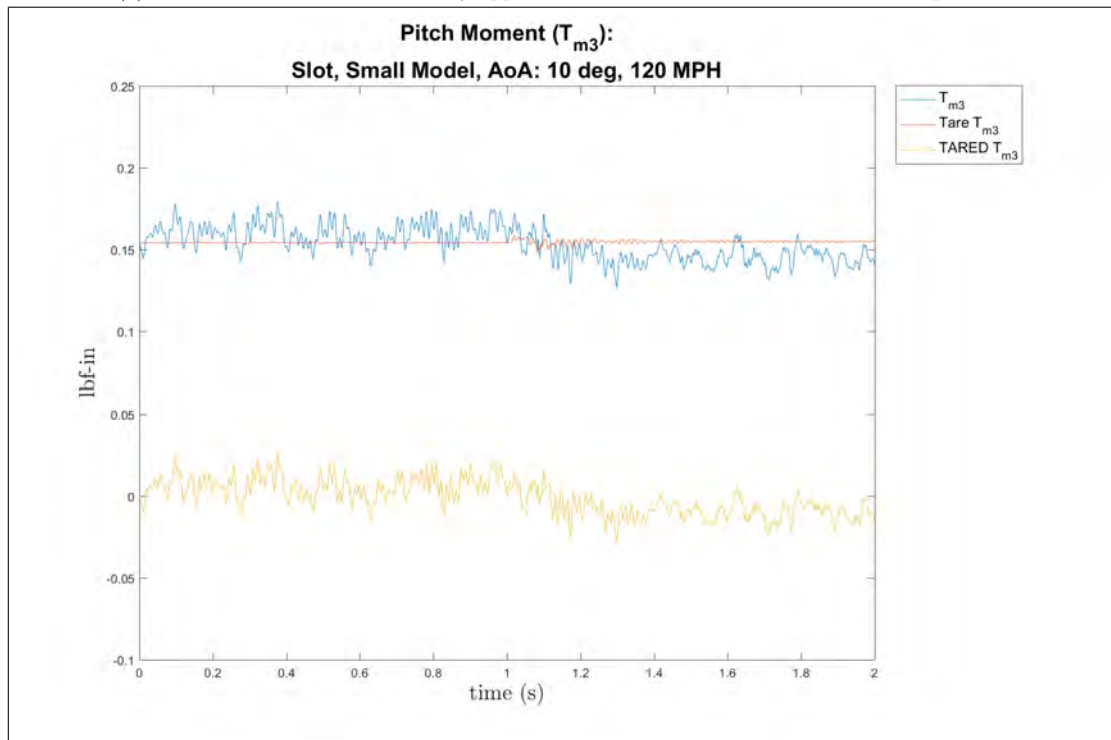
The figures shown in this section show the data recorded in the dynamic trials. The data recorded is in two-second windows and captures the moment of the model releasing from the cavity. An emphasis of these trials was collecting the effects on the normal force coefficient in order to identify any trends that could be beneficial in predicting the “pitch bifurcation” phenomena.

4.3.1 Tare Example.

Tare trials were recorded for every variable change in order to properly get tared data once recorded. The procedure for this was explained in Chapter III, Section 3.8.4. The tare example for the normal force and axial force in the dynamic trials are shown in Figure 67. Figure 67b shows the normal force coefficient while Figures 67a and 68 show the pitch moment and axial force coefficients, respectively. These examples show the tare files in red, the trial at wind speed in blue, and the tared file in yellow. The impact of the movement on the mission store model can be seen at 0 mph and 120 mph. This figure is just an example to show the process of taring the data for the dynamic trials.



(a) Normal Force Coefficient, cavity apparatus, small model, 10° AoA, slot, 120 mph, tare



(b) Pitch Moment Coefficient, cavity apparatus, small model, 10° AoA, slot, 120 mph, tare

Figure 67: Examples of dynamic tared data of all coefficients for the small model at 10° AoA in the cavity apparatus

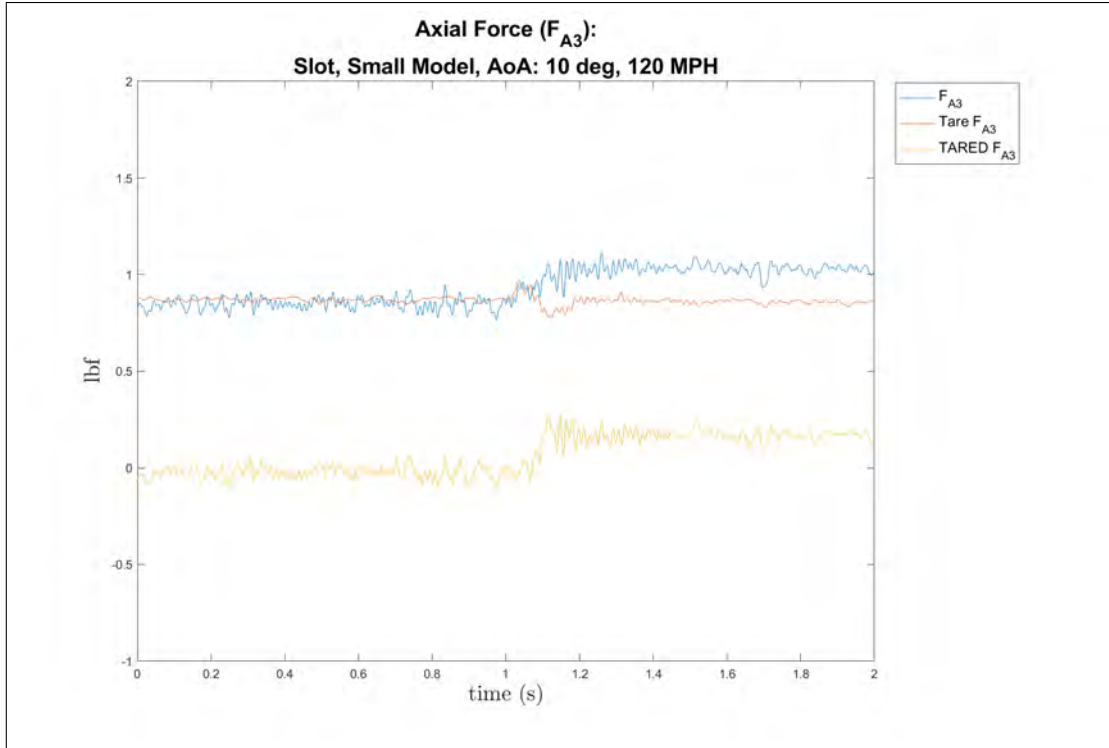


Figure 68: Axial Force Coefficient, cavity apparatus, small model, 10° AoA, slot, 120 mph, tare

4.3.2 Normal Force Coefficient Trajectory Analysis.

4.3.2.1 Coefficient Example.

An example of the digital filter, detailed in Section 3.7.2 of a dynamic trial is shown in Figure 69 with the normal force coefficient. The tared data is in blue and the filtered coefficient is in red. This example of the normal force coefficient also shows the impact of the mission store upon release. The model experiences the coefficient value in the cavity, then jumps to the value experienced out of the cavity as described in the static cases with flow control. The comparisons in the dynamic section of the chapter will describe correlations between the effects of different variables on the model release. All of the data presented, unless otherwise stated, is the digitally filtered data (15 Hz). Analysis of these figures is done before and after the release.

Some additional analysis on the small window of release, which may be of the most interest, is explored.

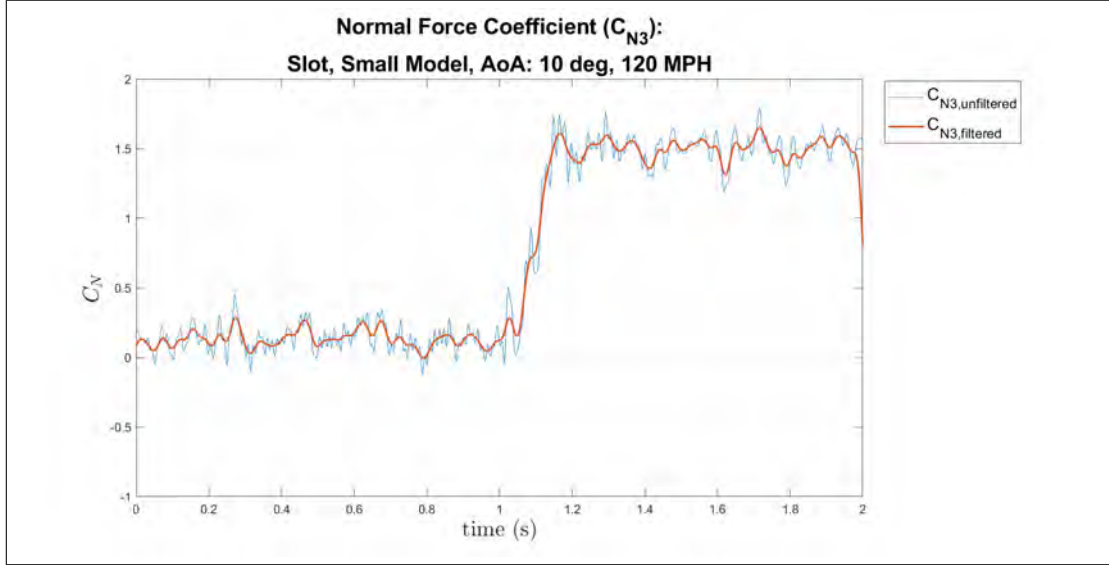


Figure 69: Normal Force Coefficient, cavity apparatus, small model, 10 degrees angle of attack, slot, 120 mph

4.3.2.2 C_N comparison of Model Sizes and AoA.

The dynamic trials with both models at 0° AoA and 120 mph for the normal force coefficient are shown in Figure 70. Figure 70a shows the small model. The coefficient starts oscillating with a mean of $C_N = -0.041$ and standard deviation of 0.11 in the cavity position. The large jump that begins at $time = 1sec$ is the beginning of the store release. This release lasts in between $0.15sec$ and $0.2sec$. Then, once the model reaches the out of cavity position, the mean is $\overline{C}_N = -0.121$ with a standard deviation of 0.10. The four trials shown are the four different release timings explained in Chapter III. There is no discernible difference in the release timing for this case. Figure 70b shows the large model case at 0° AoA. The mean values for before and after the release are $\overline{C}_N = 0.024$ and $\overline{C}_N = -0.00091$ while the standard deviations are 0.079 and 0.096 respectively. A similar trend is seen before and after the store release

with the mean decreasing slightly. The 5 Hz signal can be seen in each individual case. Zoomed in figures of these cases are shown later in this subsection.

The 10° AoA cases for the normal force coefficients of the dynamic trials are seen in Figure 71. The effect of the mission store is more pronounced in these trials. Figure 71a shows the small model case. Before the release the mean of the coefficient is $\bar{C}_N = 0.129$ and is $\bar{C}_N = 1.485$ after release with standard deviations of 0.096 and 0.104 respectively. These values are consistent with the static trials at the respective positions in the cavity apparatus. Also, the 5 Hz signal is prevalent both before and after the release in all release timing trials. Additionally, during the release period, which is approximately 0.15sec in length, a full period of an oscillation can be seen. With the 5 Hz signal, an oscillation occurs every 0.2sec so it makes sense that one oscillation is seen during the store release which is approximately the same length of time. Figure 71b shows the large model case for the same trial. The mean values for before and after the release are $\bar{C}_N = 0.160$ and $\bar{C}_N = 1.394$ while the standard deviations are 0.098 and 0.11 respectively. The same trends are seen in the large model case in terms of the mean normal force coefficient before and after release, the visible 5 Hz oscillation, and the oscillation seen during the duration of the store release. In this case, however, the oscillation is slightly less pronounced. This could be caused by the size of the model causing the flow to have a lesser impact during release.

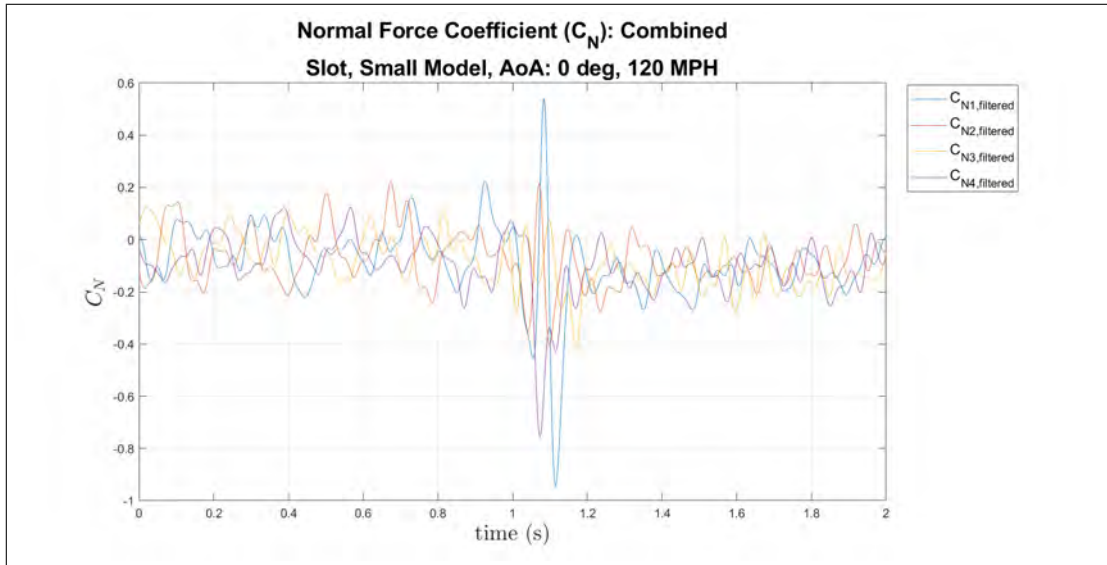
All of the mean values for all coefficients of the four release timings both before and after release can be seen in Table 26. In terms of trends, the large model has a slightly lower normal force coefficient than the small model cases. An increase in angle of attack drastically increases the coefficient after store release. The standard deviations have no discernible trend between the models, angles of attack, or before and after release which is surprising. The 5 Hz oscillation is observed in all trials but

is offset between the four release timings.

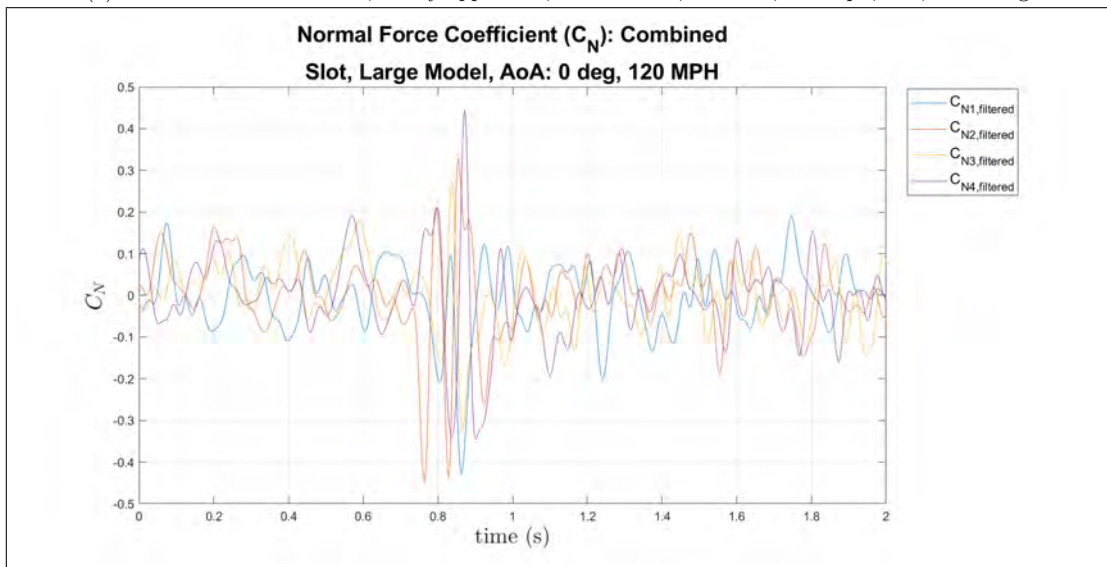
Model	AoA ($^{\circ}$)	Release	C_N	std dev	C_m	std dev
Small	0	Before	-0.042	0.110	0.174	0.206
Small	0	After	-0.121	0.100	-0.093	0.179
Small	10	Before	0.129	0.096	0.188	0.232
Small	10	After	1.485	0.104	-0.260	0.185
Large	0	Before	0.024	0.079	0.014	0.187
Large	0	After	-0.001	0.097	-0.265	0.224
Large	10	Before	0.160	0.098	0.018	0.274
Large	10	After	1.394	0.114	-0.176	0.228

Model	AoA ($^{\circ}$)	Release	C_A	std dev	C_D	C_L
Small	0	Before	0.134	0.082	0.134	-0.042
Small	0	After	0.732	0.094	0.699	-0.247
Small	10	Before	0.063	0.082	0.085	0.116
Small	10	After	0.511	0.093	0.761	1.374
Large	0	Before	0.056	0.074	0.056	0.025
Large	0	After	0.575	0.075	0.573	-0.001
Large	10	Before	0.059	0.102	0.086	0.147
Large	10	After	0.532	0.083	0.766	1.280

Table 26: Mean Filtered values of all four release timings for various models and angles of attack at 120 mph with slot, before and after release

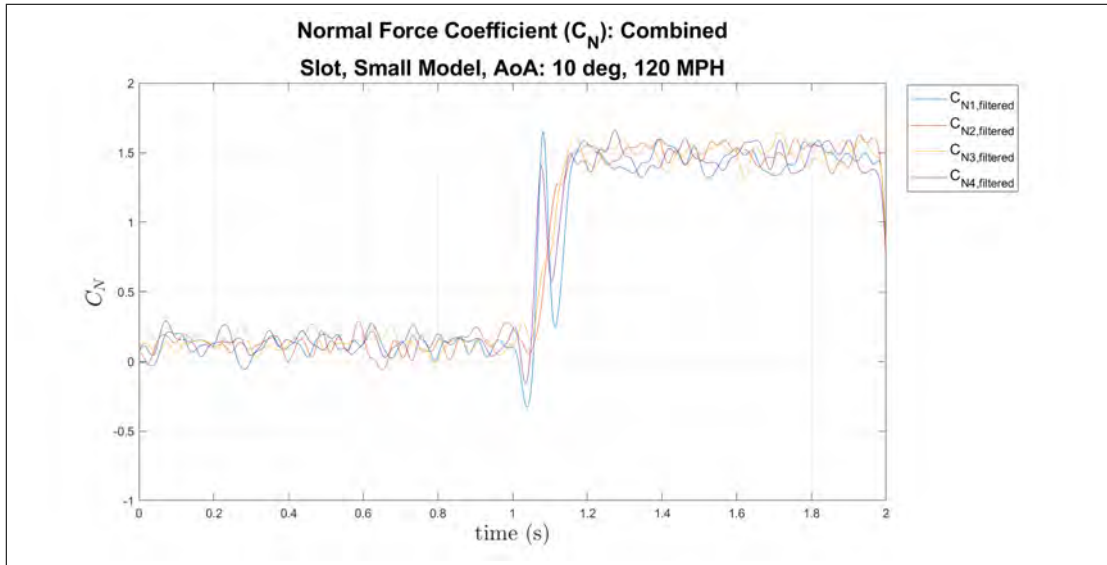


(a) Normal Force Coefficient, cavity apparatus, small model, 0° AOA, 120 mph, slot, all timings

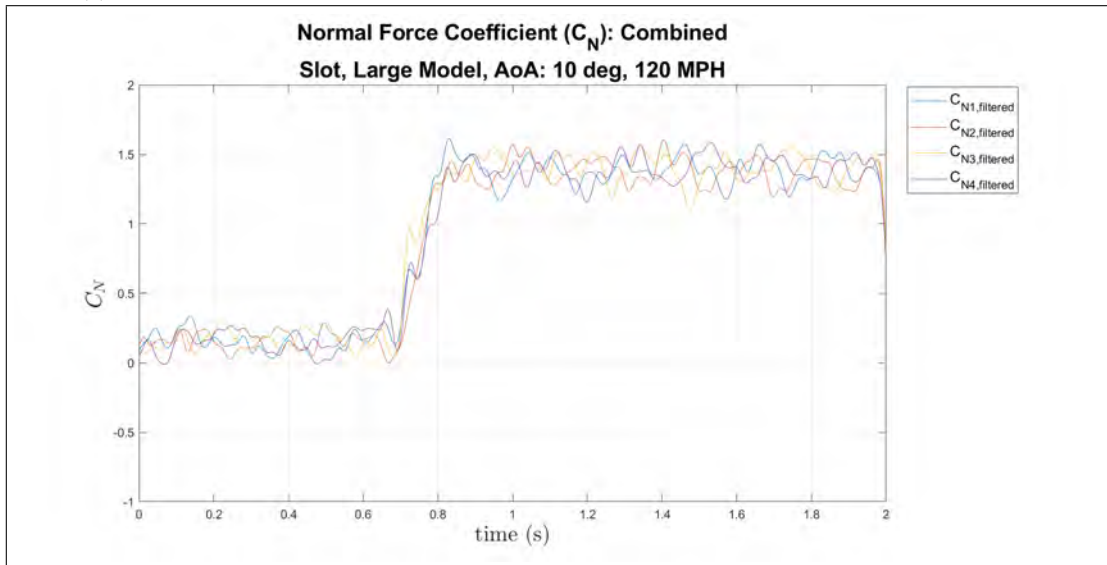


(b) Normal Force Coefficient, cavity apparatus, large model, 0° AOA, 120 mph, slot, all timings

Figure 70: Comparison of dynamic normal force coefficients with different model sizes at 0° AoA, 120 mph, all release timings



(a) Normal Force Coefficient, cavity apparatus, small model, 10° AOA, 120 mph, slot, all timings



(b) Normal Force Coefficient, cavity apparatus, large model, 10° AOA, 120 mph, slot, all timings

Figure 71: Comparison of dynamic normal force coefficients with different model sizes at 10° AoA, 120 mph, all release timings

The zoomed in portions of the 10° and 120 mph cases are shown in Figure 72 for the small model and Figure 73 for the large model. Portions of the full file are shown to represent before, during, and after the release of the mission store. Figure 72a shows the zoomed in small model case before the release. The significance of this is that an offset can be seen between the four release timings which is expected. Trial one and trial three are out of phase by 180° in terms of the position of the horizontally oriented linear motor. This phase manipulation is clearly represented in the normal force coefficient at $time = 0.275sec$ and $time = 0.46$. At these times, it is most apparent that $C_{N1,filtered}$ is opposite from $C_{N3,filtered}$. Additionally, $C_{N2,filtered}$ is 180° out of phase from $C_{N4,filtered}$ which is apparent at $time = 0.4sec$ and $time = 0.58$. These two trials are less clearly out of phase all the time. In terms of all four release times, the phase of each is not perfectly aligned with the others. There are specific times, however, that can provide a glimpse at the overall trends. At times of $time = 0.35sec$, $time = 0.54sec$, and $time = 0.59sec$, the peaks of the coefficients are shown in order from one to four or looping back from four to one then continuing the pattern. Other notable times such as $time = 0.3sec$ and $time = 0.42sec$, the second and third trials are swapped. These show the inconsistency of the pattern between all four release times. Figure 72c shows the portion of the same trial, after the release of the store. Similar trends are seen in this figure compared to before the release. $C_{N1,filtered}$ is opposite from $C_{N3,filtered}$ at $time = 1.72sec$ and $time = 1.79sec$ while $C_{N2,filtered}$ is opposite from $C_{N4,filtered}$ at $time = 1.57sec$ and $time = 1.75sec$. There are no times when all four release times line up in order but some notable times when the peaks of one and four are swapped are at $time = 1.6sec$, $time = 1.67sec$, and $time = 1.78sec$. These still show the effect of the release time is significant.

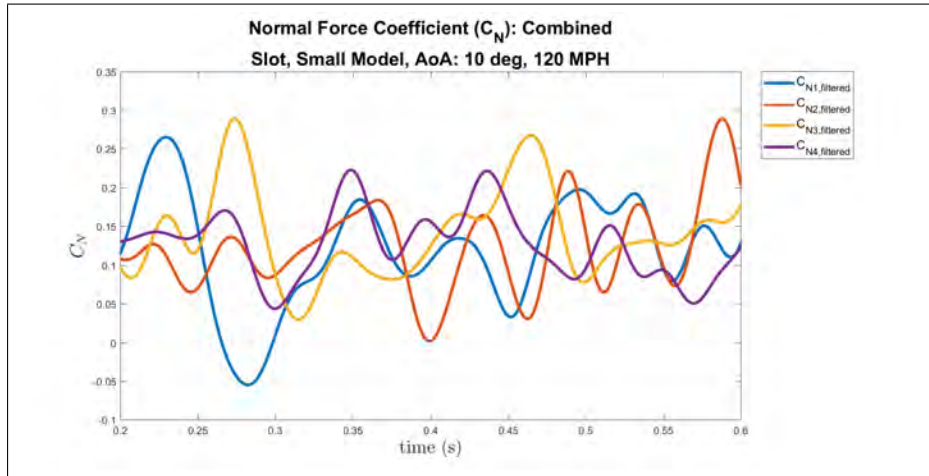
The zoomed in large case is shown in Figure 73. Figure 73a shows the before release portion of the data. $C_{N1,filtered}$ is opposite from $C_{N3,filtered}$ as seen at $time = 0.23sec$,

$time = 0.35sec$, $time = 0.5sec$, and $time = 0.57sec$. $C_{N2,filtered}$ is 180° out of phase from $C_{N4,filtered}$ at $time = 0.25sec$, $time = 0.31sec$, $time = 0.45sec$, and $time = 0.5$. Comparing all four release times to each other, there are two points, $time = 0.34sec$ and $time = 0.4sec$, where the peaks are offset in order. Notable times when the second and third release times are swapped are $time = 0.49sec$ and $time = 0.57sec$. Figure 73c shows the portion of the data file after the store release. In this figure, $C_{N1,filtered}$ is opposite from $C_{N3,filtered}$ at $time = 1.47sec$, $time = 1.57sec$, $time = 1.61sec$, and $time = 1.75sec$ while $C_{N2,filtered}$ is 180° out of phase from $C_{N4,filtered}$ at $time = 1.53sec$, $time = 1.65sec$, and $time = 1.73sec$. These figures repeat the trends shown in the small model figures for before and after the store release.

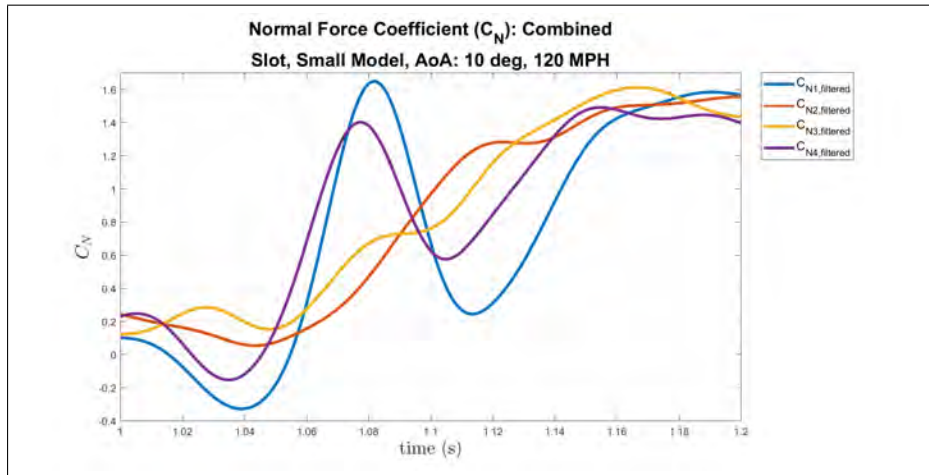
The period of time during the release of the store are also presented in these figures. Figure 72b shows the small model release period. The significance of this figure is in the analysis of both the oscillation seen during the release and the order of the four release times. For $C_{N1,filtered}$ and $C_{N4,filtered}$, there clearly is a full oscillation or two shown in the value of the coefficient. The significance of this is that the flow control directly affects the forces acting on the mission store during the actual release of the model. In terms of the order of the four release times, there is a clear difference in the peaks and troughs of the oscillations. At $time = 1.04sec$ it can be seen that the minimums of each trough are in order starting from the fourth trial, looping back to the first, then continuing with the second then third release time. This phenomena is also seen in the troughs at $time = 1.15sec$ and the peaks at $time = 1.16sec$. Figure 73b shows the same conditions during the large store release. In this figure, at least one full oscillation is shown in three of the four release times. The peaks of these oscillations all line up near $time = 0.73sec$. The alignment of the four release times are less clear in this figure than the small model case. The troughs of the

four release times line up in order at $time = 1.67sec$. There are no other points at which the release times line up well, however. Comparing the small model release to the large model release, the small case has more variations in coefficient values. The release coefficient ranges from $C_N = -0.35$ to $C_N = 1.62$ while the large ranges from $C_N = 0.1$ to $C_N = 1.61$. This variation could be caused by the sensitivity of the sensor. The loads are smaller in the small model case while the amount of noise stays the same. This means that the impact of the noise on the data is greater in the small model case. This is consistent with expectations.

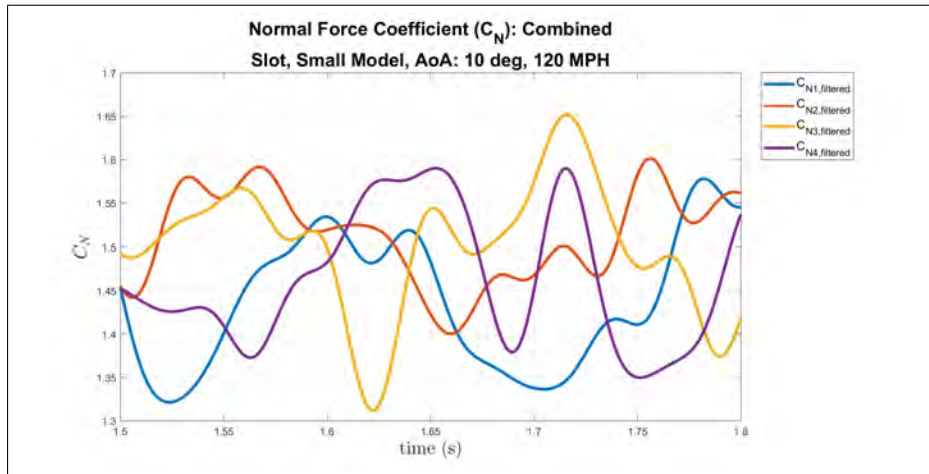
In terms of trends, a 5 Hz oscillation is seen before and after the store release in every trial. Also, there is a clear oscillation in the normal force coefficients during the period of release in at least a few release times in each trial. Finally, the zoomed in figures show that $C_{N1,filtered}$ is frequently 180° out of phase from $C_{N3,filtered}$ as are $C_{N2,filtered}$ and $C_{N4,filtered}$. This is expected because the horizontally oriented linear motor oscillates such that those trials are opposite from each other. It is still apparent that the change in release time has a direct effect on the forces experienced by the mission store upon release.



(a) Zoomed NFC, small model, 10° AoA, 120 mph, slot, before release

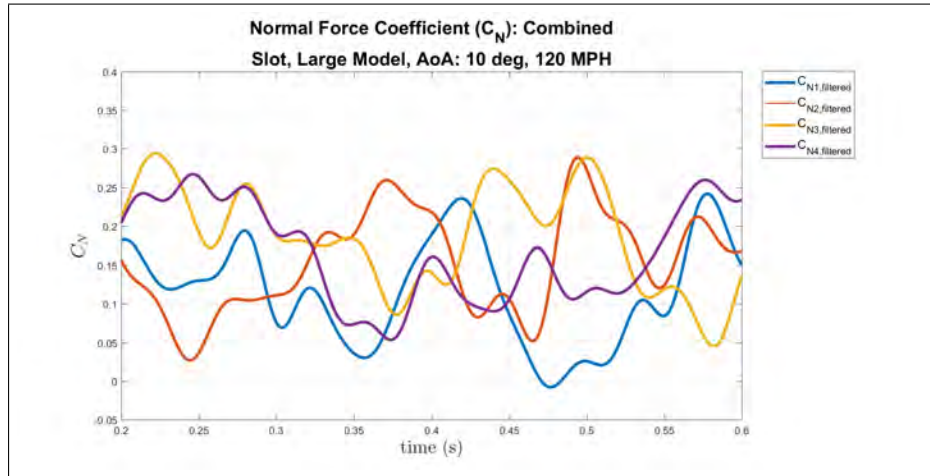


(b) Zoomed NFC, small model, 10° AoA, 120 mph, slot, during release

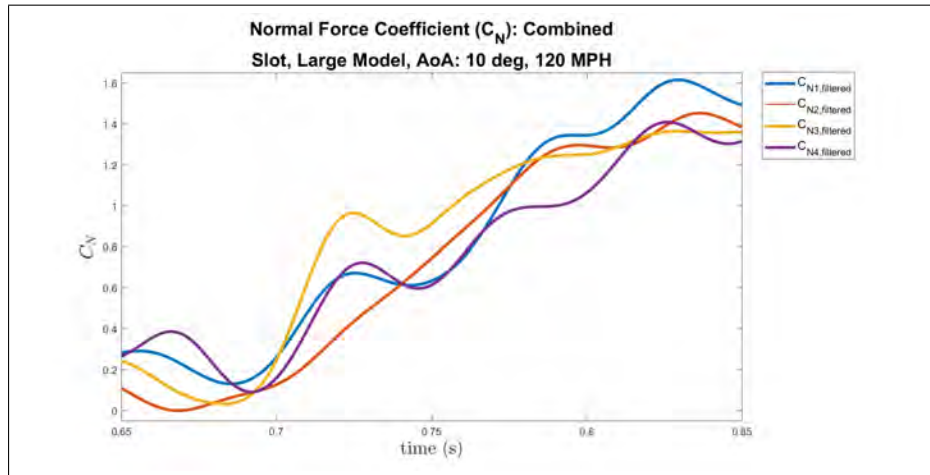


(c) Zoomed NFC, small model, 10° AoA, 120 mph, slot, after release

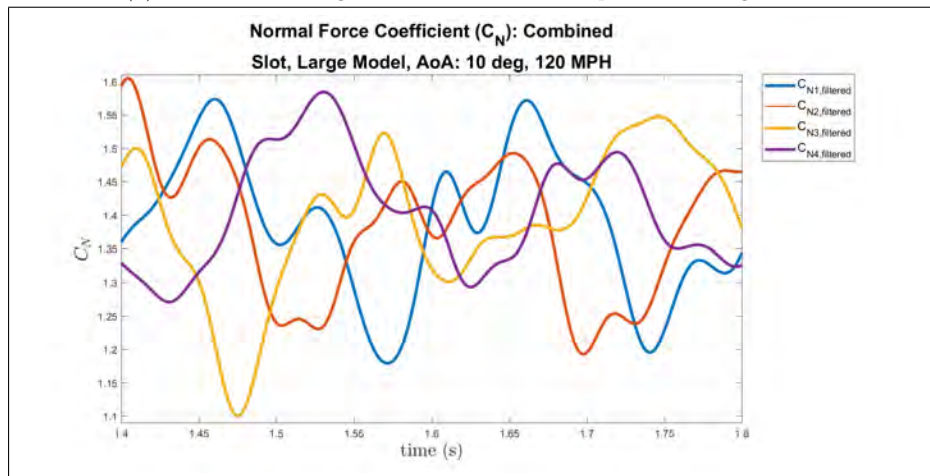
Figure 72: Zoomed, filtered values for normal force coefficients of all four timings, small model, 10° AoA, 120 mph, slot



(a) Zoomed NFC, large model, 10° AoA, 120 mph, slot, before release



(b) Zoomed NFC, large model, 10° AoA, 120 mph, slot, during release



(c) Zoomed NFC, large model, 10° AoA, 120 mph, slot, after release

Figure 73: Zoomed, filtered values for normal force coefficients of all four timings, large model, 10° AoA, 120 mph, slot

4.3.3 Pitch Moment Coefficient Trajectory Analysis.

4.3.3.1 Coefficient Example.

The digital filtering was also applied to the pitch moment coefficient. Figure 74 shows one example, in the same way that the normal force coefficient was done. The store release can be seen at $time = 1.0sec$ when the coefficient changes drastically over the period of about $0.15sec$. This is a single trial that is plotted individually. The change in coefficient is not as great as that shown in the normal force coefficient, but the change is still distinct. After the mission store release, the pitch moment turns negative for every trial conducted. Additional pitch moment coefficient plots in the next section show multiple release timings on the same figure.

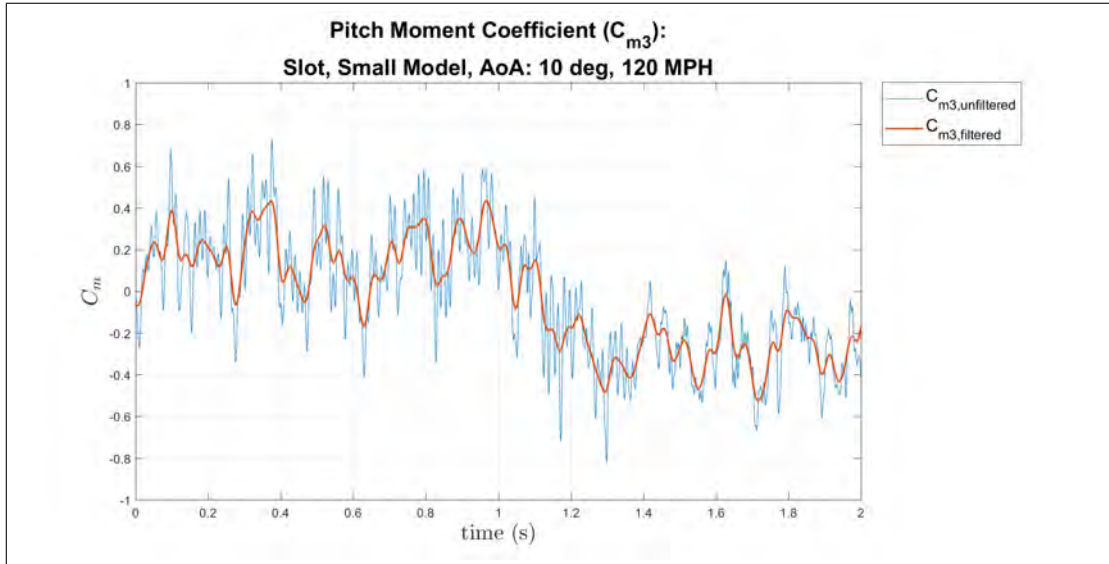


Figure 74: Pitch Moment Coefficient, cavity apparatus, small model, 10 degrees angle of attack, slot, 120 mph

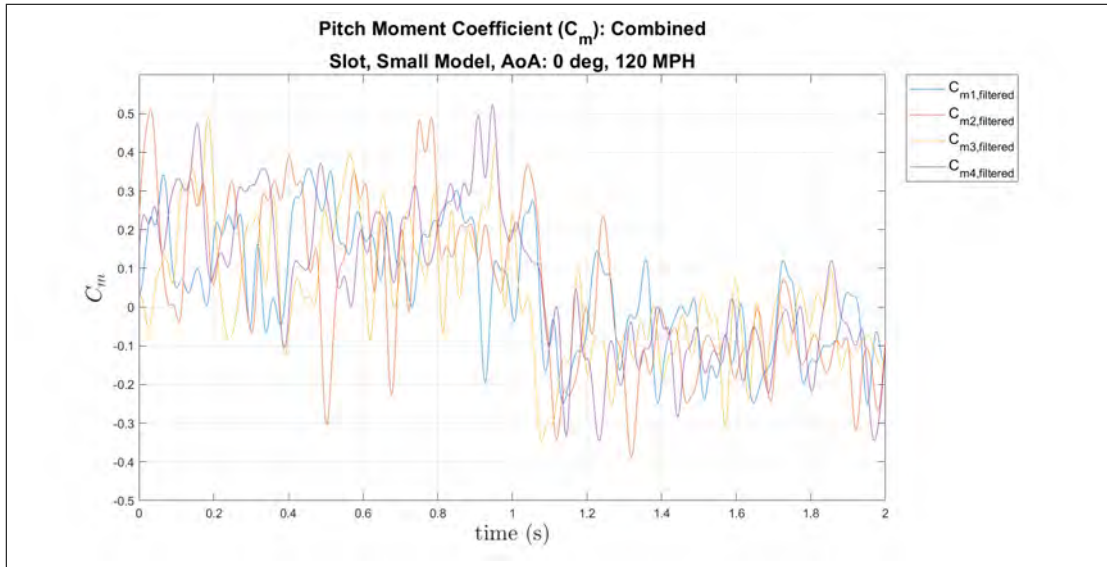
4.3.3.2 C_m comparison of Model Sizes and AoA.

The same trials that were discussed in the normal force coefficient section are discussed in this section. Figure 75 shows the 0° AoA cases at 120 mph for both models. In the small model case, shown in Figure 75a, displays the small change

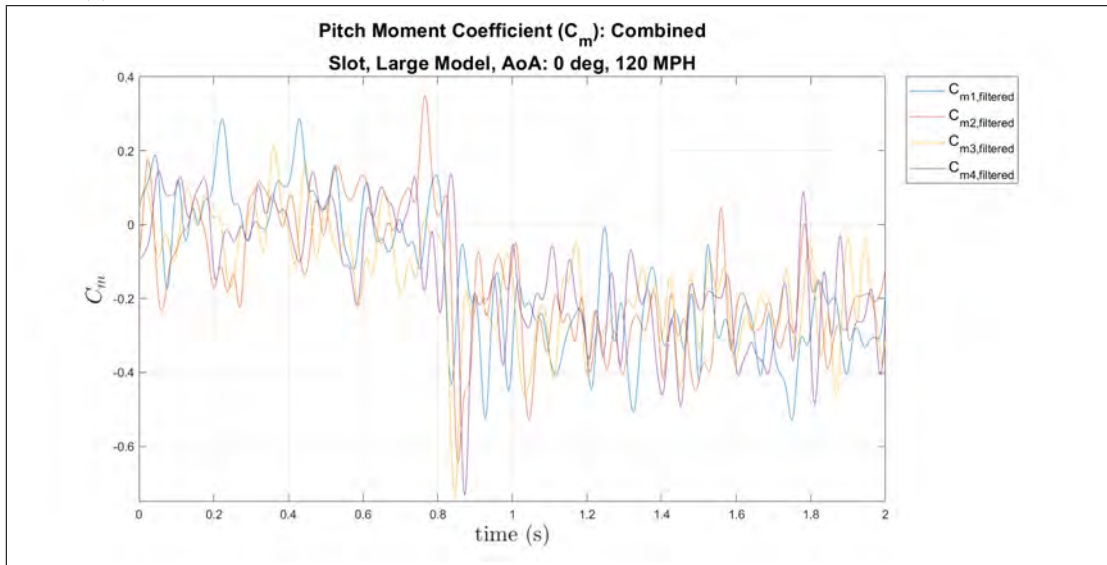
in the coefficient upon release. Before store release, the mean of the coefficient is $\overline{C}_m = 0.174$ while after release the mean is $\overline{C}_m = -0.0931$ with standard deviations of 0.21 and 0.18 respectively. Similar to the normal force coefficient, the 5 Hz oscillation is visible in every trial and the peaks are offset by a portion of the period because they are all different release times. Figure 75b shows the large model case. The mean goes from $\overline{C}_m = 0.014$ to $\overline{C}_m = -0.265$ with standard deviations of 0.18 and 0.22 respectively. These values are slightly lower than the small model case. Additionally, the effect of the release is slightly greater with the hump at the end of the release going down to $C_m = -0.6$ in three of the runs. It should be noted that the precision limit of these measurements is $2\sigma_x$.

The 10° AoA trials are shown in Figure 76. The small model case in Figure 76a shows a similar trend but with more drastic values. The mean before the release is $\overline{C}_M = 0.188$ and the mean after is $\overline{C}_m = -0.260$ with standard deviations of 0.23 and 0.18 respectively. The release begins at *time* = 1.1sec. The large model case in Figure 76b has a less clear decrease with the mean before being $\overline{C}_m = 0.0176$ and the mean after being $\overline{C}_m = -0.176$ with standard deviations of 0.27 and 0.23 respectively. In this figure the release began at *time* = 0.8sec.

All of the mean values for the four release timings of these trials, both before and after release, can be seen in Tables 26. In terms of trends, the pitch moment coefficient is always negative after the release. Increasing the angle of attack decreases the coefficient values in the small model case but increases them in the large model case. Increasing the model size decreases the pitch moment coefficient with one exception. The standard deviations have no discernible trends between the different angles of attack and model sizes.

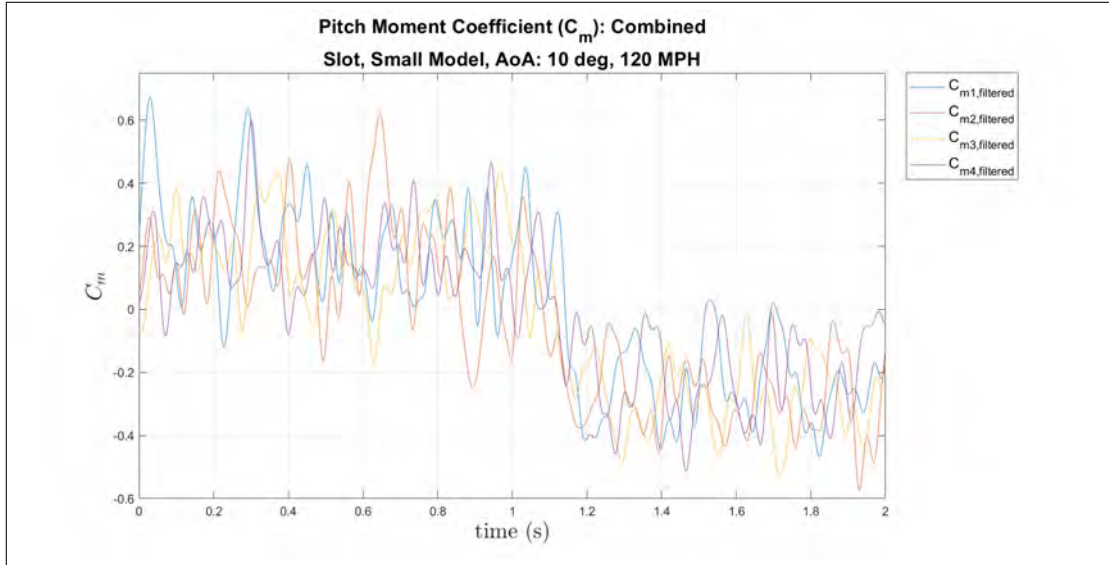


(a) Pitch Moment Coefficient, cavity apparatus, small model, 0° AOA, 120 mph, slot, all timings

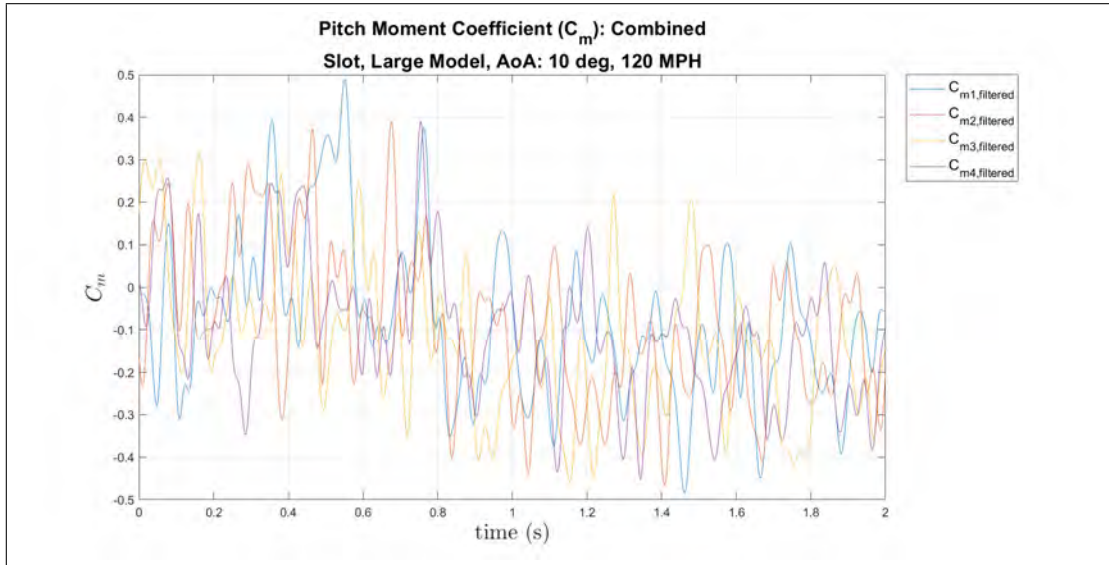


(b) Pitch Moment Coefficient, cavity apparatus, large model, 0° AOA, 120 mph, slot, all timings

Figure 75: Comparison of dynamic normal force coefficients with different model sizes at 0° AoA, 120 mph, all release timings



(a) Pitch Moment Coefficient, cavity apparatus, small model, 10° AOA, 120 mph, slot, all timings



(b) Pitch Moment Coefficient, cavity apparatus, large model, 10° AOA, 120 mph, slot, all timings

Figure 76: Comparison of dynamic normal force coefficients with different model sizes at 10° AoA, 120 mph, all release timings

4.3.4 Axial Force Coefficient Trajectory Analysis.

4.3.4.1 Coefficient Example.

The final main coefficient looked at in this research is the axial force coefficient. The dynamic cases for the same conditions as mentioned in the previous two coefficient sections are shown here. The coefficient example is shown in Figure 77. Here, the same digital filtering process was conducted. The jump in coefficient upon release is more significant than the pitch moment coefficient. All four release timing are plotted on top of each other in other figures in this section. This coefficient is less emphasized in this research because of the lower resolution and lower loads in the axial direction. As mentioned before, when the sensor is at an angle, the axial force is measured relative to that.

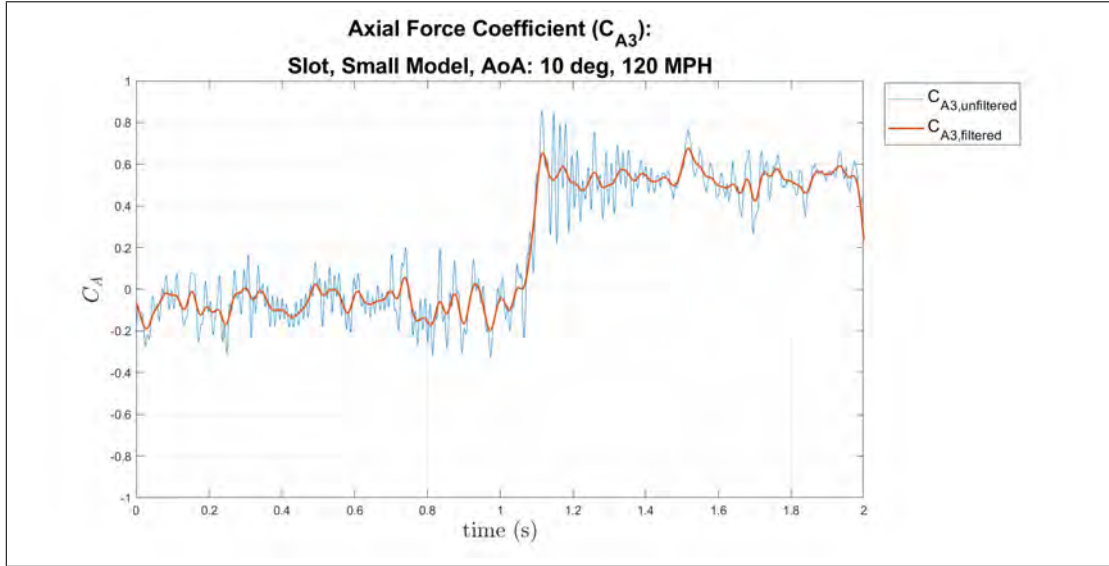


Figure 77: Axial Force Coefficient, cavity apparatus, small model, 10 degrees angle of attack, slot, 120 mph

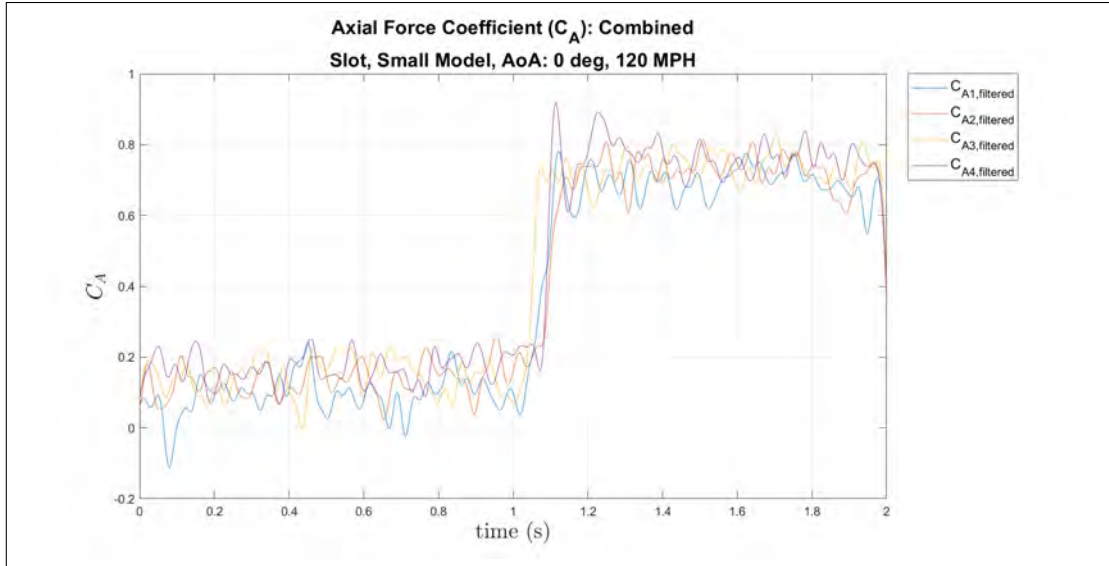
4.3.4.2 C_A comparison of Model Sizes and AoA.

The axial force coefficient during the dynamic release for both models at 0° AoA and 120 mph is shown in Figure 78. The mean for the small model, in Figure 78a, is

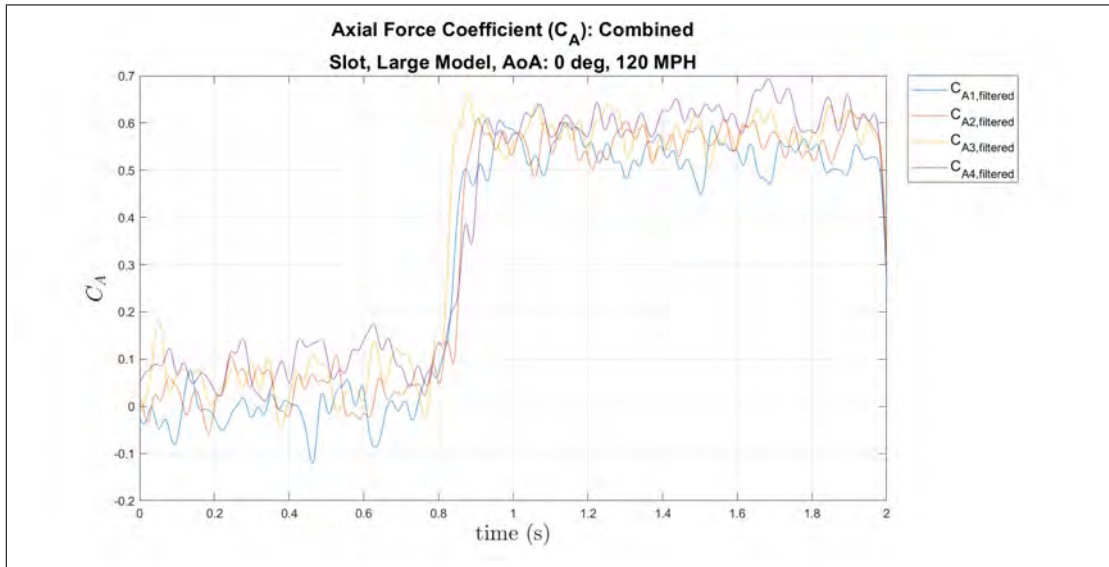
$\overline{C}_A = 0.134$ before release and $\overline{C}_A = 0.731$ after release with standard deviations of 0.082 and 0.094 respectively. A 5 Hz signal is observable but the four release timings are offset so the peaks do not line up. There is no discernible pattern between the four release timing during the release period. Most cases end the release around $C_A = 0.75$ but one goes up to $C_A = 0.9$, though this is probably just an anomaly. Additionally, the period during release seems to just increase drastically, uninfluenced by the flow control as was the normal force coefficient.

The large model case, in Figure 78b, has a slightly lower mean at $\overline{C}_A = 0.056$ before release and $\overline{C}_A = 0.575$ after release with standard deviations of 0.074 and 0.075 respectively. The oscillation of 5 Hz is still apparent in these cases. There is only a distinct oscillation in the middle of the release in one of the four cases, the rest are like the small model case.

All of the mean values for the four release timings of these trials, both before and after release, can be seen in Tables 26. The coefficient drastically increases upon release with no oscillation in the middle of the release or effect from the flow control. The 5 Hz oscillation is seen in all cases and is offset from each other.



(a) Axial Force Coefficient, cavity apparatus, small model, 0° AOA, 120 mph, slot, all timings



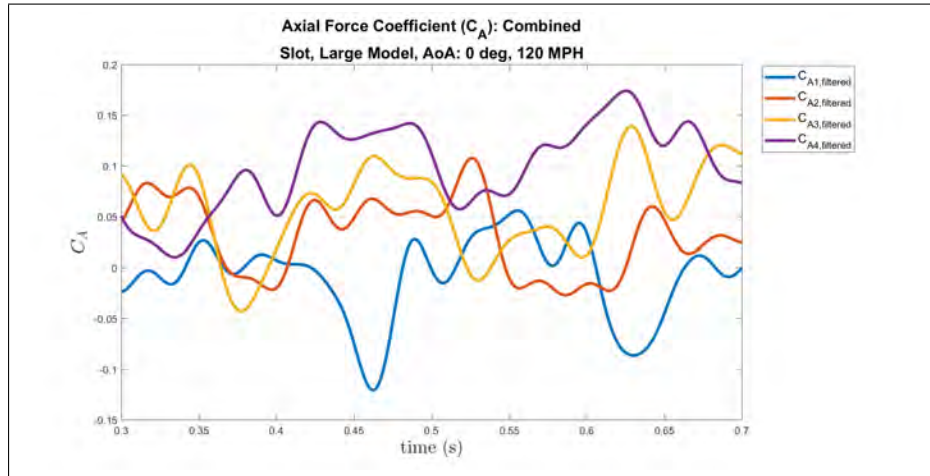
(b) Axial Force Coefficient, cavity apparatus, large model, 0° AOA, 120 mph, slot, all timings

Figure 78: Comparison of dynamic normal force coefficients with different model sizes at 0° AoA, 120 mph, all release timings

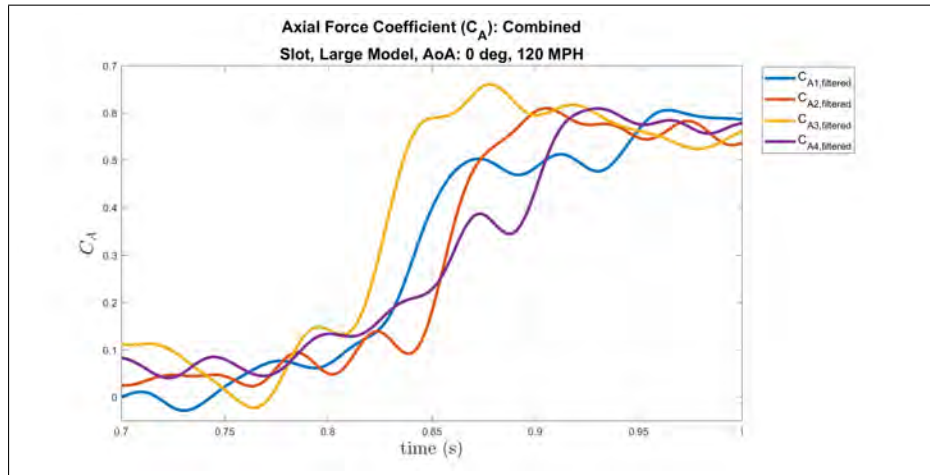
The zoomed in portions of the large model case are shown in Figure 79 to allow further analysis of the effect of the four release timings. Similar to the normal force coefficients, the release times that are 180° out of phase from each other have coefficient values that are also 180° out of phase. Figure 79a shows the oscillation before the release of the store. In this figure, $C_{A1,filtered}$ is opposite from $C_{A3,filtered}$ at $time = 0.32sec$,

$time = 0.46sec$, $time = 0.57sec$, $time = 0.63sec$, and $time = 0.69sec$. $C_{A2,filtered}$ is opposite from $C_{A4,filtered}$ at $time = 0.37sec$, $time = 0.53sec$, $time = 0.64sec$, and $time = 0.67sec$. In terms of all four release times compared to each other, the order of the release times line up, in reverse order, at the peaks at $time = 0.35sec$ and $time = 0.62sec$ and the troughs at $time = 0.65sec$. Figure 79c shows the oscillation after the release of the store. In this figure, $C_{A1,filtered}$ is opposite from $C_{A3,filtered}$ at $time = 1.49sec$, $time = 1.58sec$, $time = 1.63sec$, $time = 1.68sec$, and $time = 1.72sec$. $C_{A2,filtered}$ is opposite from $C_{A4,filtered}$ at $time = 1.44sec$, $time = 1.56sec$, $time = 1.63sec$, and $time = 1.72sec$. In terms of all four release times compared to each other, the order of the release times line up at the peaks at $time = 1.55sec$ and $time = 1.65sec$. These findings show the effect of the release time on the axial force experienced by the mission store before and after release.

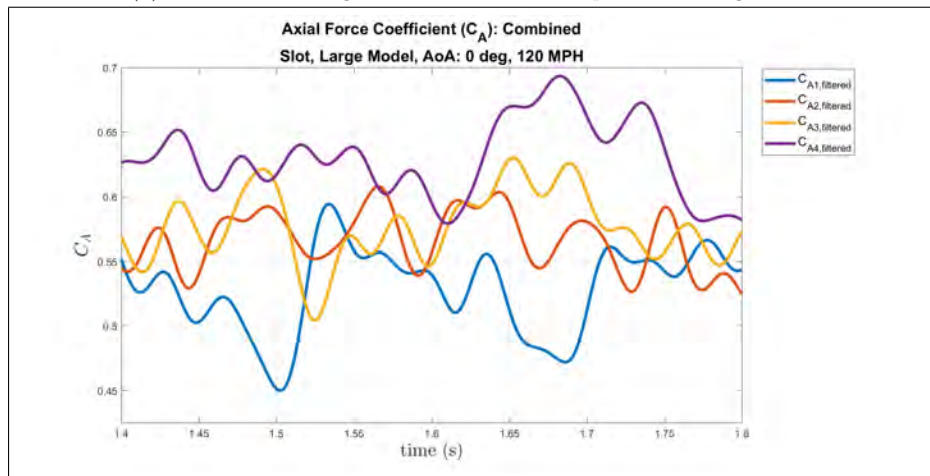
Figure 79b shows the axial force coefficient of the store during the period of release. A full oscillation that was seen in the normal force coefficient can only be seen in one case for the axial force coefficient. It can be seen that $C_{A1,filtered}$ is opposite from $C_{A3,filtered}$ at $time = 0.79sec$, and after the release at $time = 0.87sec$. The order of the release does not line up in order from the first release time to the fourth release time. Additionally, there is no clear trend based on the maxima or minima of each individual release time. During the release period, the order of oscillation at the beginning of release is not maintained through the duration of the release until after release. The order of oscillation immediately after release is different than immediately before.



(a) Zoomed AFC, large model, 0° AoA, 120 mph, slot, before release



(b) Zoomed AFC, large model, 0° AoA, 120 mph, slot, during release



(c) Zoomed AFC, large model, 0° AoA, 120 mph, slot, after release

Figure 79: Zoomed, filtered values for normal force coefficients of all four timings, large model, 10° AoA, 120 mph, slot

4.3.5 Comparison of Flow Control Devices.

A comparison of the normal force coefficients and the changes based on the flow control device are described in this section. All of these trials are with the large model at two wind speeds. The 60 mph case is shown in Figure 80. For the slot case, in Figure 80a, the mean before is $\overline{C}_N = 0.152$ and the mean after release is $\overline{C}_N = 1.40$ with standard deviations of 0.14 and 0.19 respectively. The lowest a case goes is $C_N = -0.6$ during the release but only goes up to $C_N = 1.65$ after. The diode 2 case, in Figure 80b, is very similar with the mean before at $\overline{C}_N = 0.11$ and $\overline{C}_N = 1.38$ after release with standard deviations of 0.15 and 0.21 respectively. The coefficient has a minimum of $C_N = -1.05$ and a maximum of $C_N = 2.1$ during the release period. Both cases have a clear 5 Hz signal shown before and after each release. Also, an oscillation in the duration of the release is seen in almost every trial. Additionally, the offset of period caused by the change in release time is very clear after release. The troughs in the oscillations alternate colors clearly.

The 120 mph cases are presented in Figure 81. Similar trends are shown in these figures compared to the 60 mph case. The 120 mph slot case is shown in Figure 81a. The mean before is $\overline{C}_N = 0.16$ and the mean after release is $\overline{C}_N = 1.394$ with standard deviations of 0.098 and 0.11 respectively. The minima and maxima in these cases are not nearly as drastic as the 60 mph case as seen in the figures. The diode 2 case is shown in Figure 81b. The mean for this case before release is $\overline{C}_N = 0.16$ and is $\overline{C}_N = 1.463$ after release with standard deviations of 0.091 and 0.11 respectively. Again, both cases show the 5 Hz oscillation and a small oscillation during the actual release of the model.

The average values for all four release timings for these cases are shown in Tables 27 and 28. In terms of trends, as the wind speed increases, the normal force coefficient typically increases and the standard deviations decrease. The difference between the

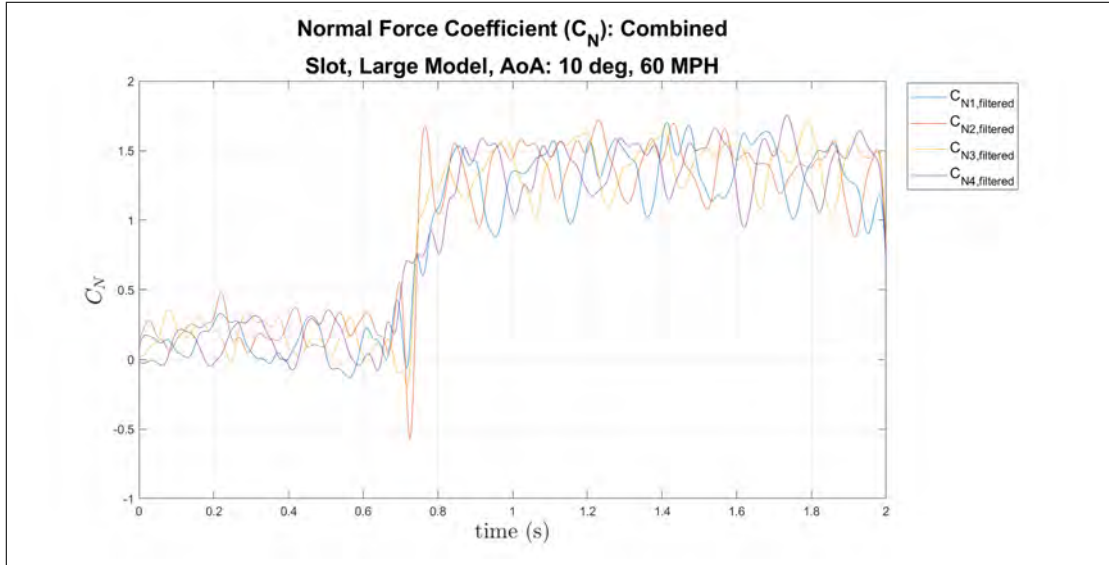
flow control devices is unclear, the mean values are all about the same. The standard deviations for the diode are higher in the 60 mph case but about the same in the 120 mph case. The 5 Hz oscillation is clear in every case and an oscillation during the release period is observed in almost every case. Finally, with an increase in speed, the minima and maxima of the coefficient during the release period become much less dramatic. Additionally, Table 29 shows the lift coefficients for both diodes with the large model at 10° AoA and 120 mph. These values show that the diode 2 consistently produces higher lift for the mission store model after release. This observation is consistent with research conducted by Wood [8].

Model	AoA (°)	Position	C_N	std dev	C_m	std dev
Slot	60	Before	0.152	0.138	0.121	0.391
Slot	60	After	1.403	0.199	-0.368	0.469
Slot	120	Before	0.160	0.098	0.018	0.274
Slot	120	After	1.394	0.114	-0.176	0.228
Diode 2	60	Before	0.114	0.146	0.219	0.433
Diode 2	60	After	1.383	0.213	-0.165	0.537
Diode 2	120	Before	0.160	0.091	0.078	0.288
Diode 2	120	After	1.463	0.112	-0.232	0.241

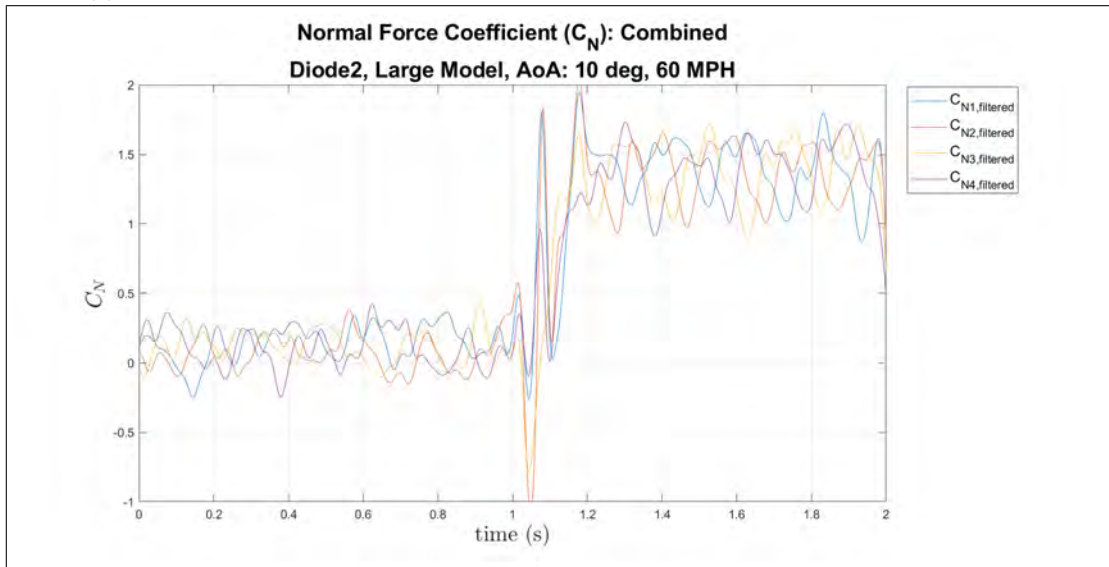
Table 27: Mean Filtered values of all four release timings for various flow control devices and wind speeds at 10° AoA with large model, before and after release, Part 1

Model	AoA (°)	Position	C_N	std dev	C_m	std dev
Slot	60	Before	0.041	0.127	0.067	0.142
Slot	60	After	0.236	0.147	0.476	1.340
Slot	120	Before	0.059	0.102	0.0863	0.147
Slot	120	After	0.532	0.083	0.766	1.280
Diode 2	60	Before	0.039	0.156	0.058	0.105
Diode 2	60	After	0.226	0.178	0.463	1.323
Diode 2	120	Before	0.039	0.112	0.067	0.151
Diode 2	120	After	0.459	0.086	0.706	1.362

Table 28: Mean Filtered values of all four release timings for various flow control devices and wind speeds at 10° AoA with large model, before and after release, Part 2

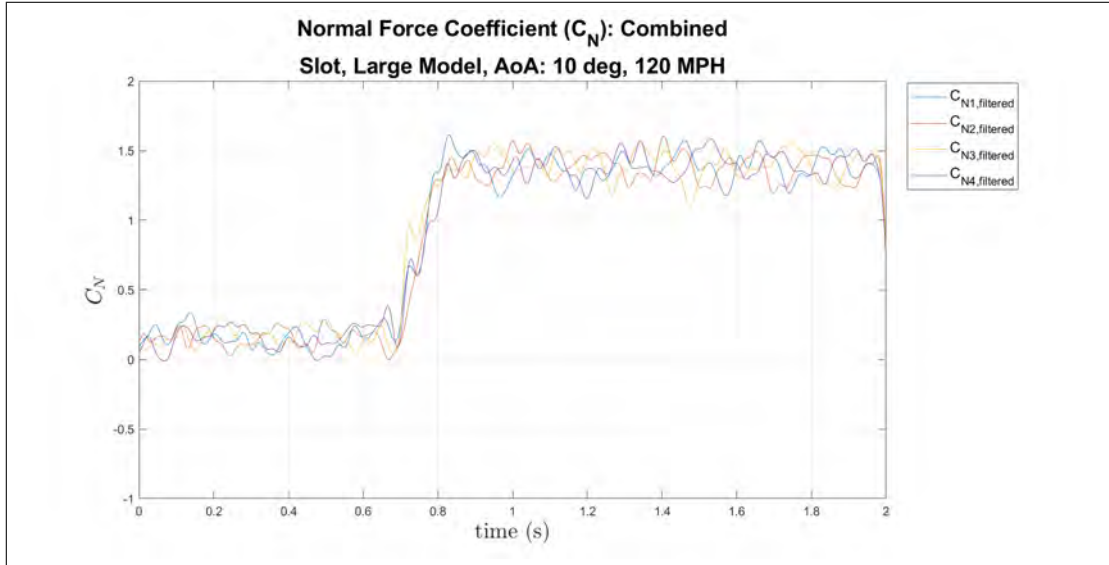


(a) Normal Force Coefficient, cavity apparatus, large model, 10° AOA, 60 mph, slot, all timings

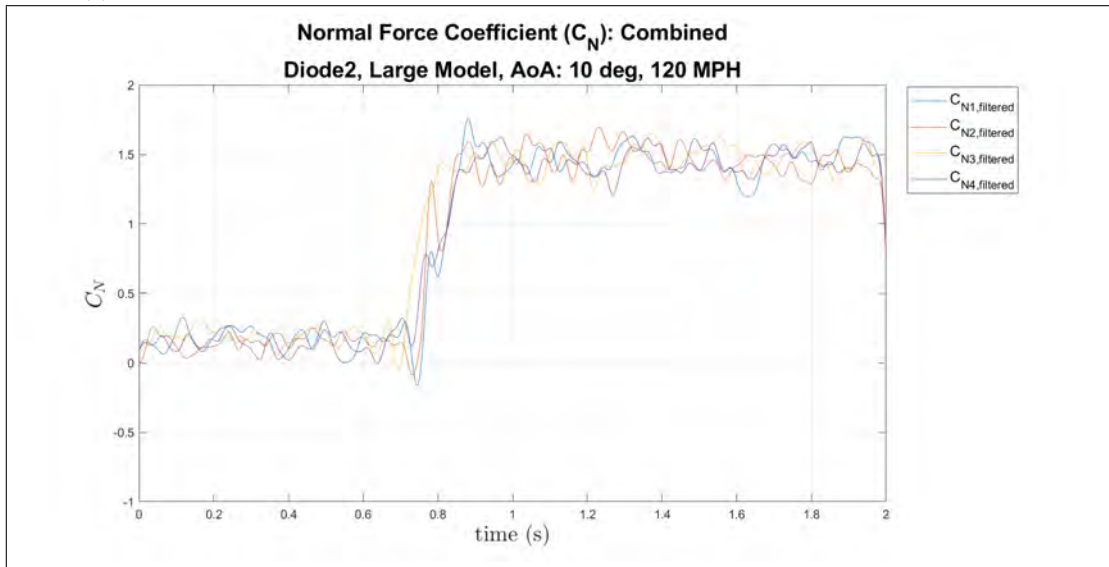


(b) Normal Force Coefficient, cavity apparatus, large model, 10° AOA, 60 mph, diode 2, all timings

Figure 80: Comparison of dynamic normal force coefficients with flow control devices at 10° AoA, large model, 60 mph, all release timings



(a) Normal Force Coefficient, cavity apparatus, large model, 10° AOA, 120 mph, slot, all timings



(b) Normal Force Coefficient, cavity apparatus, large model, 10° AOA, 120 mph, diode 2, all timings

Figure 81: Comparison of dynamic normal force coefficients with flow control devices at 10° AoA, large model, 120 mph, all release timings

Model	Speed (mph)	Release	Release	C_L slot	C_L diode 2
Large	120	Time 1	Before	0.138	0.153
Large	120	Time 2	Before	0.151	0.146
Large	120	Time 3	Before	0.155	0.179
Large	120	Time 4	Before	0.146	0.125
Large	120	Time 1	After	1.282	1.375
Large	120	Time 2	After	1.270	1.364
Large	120	Time 3	After	1.279	1.364
Large	120	Time 4	After	1.289	1.344

Table 29: Filtered values of lift coefficients for all four release timings for various flow control devices at 120 mph with large model at 10° AoA, before and after release

4.4 Summary of Results

In this chapter the static experimental data was presented in Phase I and dynamic experimental data was shown in Phase II. Data collected using the Nano25 force and moment sensor are shown in various plots. Tare plots and individual coefficients are shown as examples of how the process of taring the data was conducted. Figures showing the normal force coefficient, pitch moment coefficient, and axial force coefficient were presented for analysis. An emphasis was placed on the analysis of the normal force coefficient. Drag and lift coefficients were also calculated and included in most tables, but were not discussed extensively.

First, in Phase I, trials were conducted with the freestream apparatus with the small and large models at various angles of attack in wind speeds of 60 mph, 100 mph, and 120 mph. Next, the cavity apparatus was used to collect data in the cavity, in the shear layer, and out of the cavity. Baseline data was collected in these static trials and was used to compare the addition of flow control and dynamic store release.

The last part of Phase I consisted of the same cavity apparatus trials in all three positions, but this time with flow control turned on. The effects of the flow control were isolated and directly compared to the static cases. A 5 Hz oscillating signal is

clear in most of the coefficients and most of the positions. The trends are less clear in the cavity because the shear layer disrupts the flow and the mission store model is less impacted.

Finally, Phase II was conducted completing trials of dynamic store release with different variables and different coordinated release times. Flow control was turned on for these trials as well. The 5 Hz signal was visible in every case both before and after release. At least one full oscillation was observed during the period of release for almost every trial. When zoomed in, an offset was observed between the four release times. The release times that were 180° out of phase frequently shown having that same effect in the values of the coefficient. Additionally, the four release times were shown to line up in the expected order many times in several trials. Extremely clear trends cannot be attributed to the offset of coefficients due to the release times, but it can definitely be concluded that the difference in release times affects the forces and moments experienced by the mission store.

V. Conclusions and Recommendations

The primary purpose of this research was to analyze the impact of varying flow conditions on the understanding of time-dependent store release from a cavity in a flow field. This was achieved by using the linear motor apparatus to support the static and dynamic characterization and the time-accurate dynamic load data acquisition of a mission store in the freestream as well as in store separation. Two leading edge oscillatory blowing devices were used in flow control to influence the flow and characterize the effects on the force and moments experienced by the mission store model. The leading edge oscillatory blowing enabled the testing in a low-speed tunnel even though the effects of fluctuating flow are much more pronounced at transonic conditions. The synchronization of the position of the oscillatory motor and the singular vertical store release trajectory in the cavity apparatus was altered to produce data results for four different release timings. The Nano25 6-DOF force and moment sensor was used in conjunction with the specified cavity in the AFIT low speed wind tunnel to acquire time-accurate measurements and the data was analyzed for identifiable trends.

5.1 Scope of Testing

The scope of testing was very broad. The data collected required a tare which accounted for inertial effects for a moving store model. Tare plots and individual coefficients are shown throughout Chapter IV as examples of how the process of taring the data was conducted. The data were acquired at 1000 Hz and filtered with a low-pass analog filter set to 30 Hz initially then also a 15 Hz low-pass digital filter. The coefficients for normal force, pitch moment, and axial force were presented for analysis. Drag and lift coefficients were also calculated and discussed. The analysis

emphasized the impact on the normal force coefficient. Additionally, the effects of multiple variables on the coefficients were compared. A small and large model were used at 0° and 10° AoA and in wind speeds of 60 mph, 100 mph, and 120 mph. Different positions were used in the static trials of Phase I and different release timings were used in the dynamic trials of Phase II. The oscillatory blowing flow control devices used in this research included the slot and a fluidic diode referred to as diode 2, or simply diode. These are the same referenced and used in Wood’s research [8].

Repeatability trials were conducted for the static and dynamic trials. The tare trials conducted showed relatively low standard deviations. The other trials showed standard deviations expected of the respective trials. The trends discussed in every case become more apparent when the mean of ten trials was taken. The precision of the ten trials is very high which shows the experiments are repeatable. For the dynamic trials, the 5 Hz oscillation is very clear before and after release. Additionally, the full period of an oscillation is observed during the release of the store.

5.2 Summary of Results

Baseline data were collected in the static freestream and certain trends were observed. An increase in wind speed, with only a few exceptions, causes a mild increase in C_N and lift coefficient, decrease in C_m , increase in C_A and drag coefficient, and a decrease in standard deviation. Additionally, comparing the different geometrically similar models, the values of the coefficients are alike which is expected. Overall, the similarities of the values in the freestream demonstrate that the data aligns with expectations and validates the approach taken to recording and analyzing the data.

Additional static baseline data were gathered in the cavity environment. Similar effects are seen when comparing the “in-cavity” position to the “shear layer” and “out-of-cavity” position. The 0° cases show a decrease in normal force and lift co-

efficients and produce less clear trends overall. With an increase in angle of attack, the normal force and lift coefficients increase, the pitch moment coefficient decreases, and the standard deviations decrease. The trends inside the cavity are consistent with expectations since the store is shielded from the freestream. The trends appear clearer when the model enters the shear layer and the “out-of-cavity” positions. The standard deviations also increase while in the shear layer compared to the other positions which was anticipated. The normal force coefficients for the large model are consistently lower than, but approximately equivalent with the small model values. All of this static data can serve as a reference in future work.

The second part of Phase I involved similar trials, but with flow control at a 5 Hz oscillation. These trials exhibit the same trends as the static trials without flow control but with addition of a visible 5 Hz oscillation in the coefficient values. This clear oscillation also serves to validate the methods of data acquisition used. With an increase in wind speed, the standard deviations typically increase except the trials in the shear layer position. They also increase in the “out-of-cavity” position compared to in the cavity. In most trials, in the shear layer and “out-of-cavity” positions, a clear 5 Hz oscillation is visible in the normal force and axial forces. The “in-cavity” position yielded a less obvious oscillation, because the flow is disrupted by the cavity. Changing the flow control device does not significantly change the average values of each coefficient, but the diode makes the average values at every position consistently higher except for the small model in the cavity. Additionally, when comparing the flow control devices, it became apparent that the diode produced consistently, but only slightly, higher lift coefficients in the shear layer and “out-of-cavity” positions. This could be caused by the diode adding momentum by directing air flow in the streamwise direction, while the slot configuration directs the air directly upwards at the lip of the cavity. This echoes trends seen in Wood’s research.

Finally, Phase II was conducted completing trials of dynamic store release with different variables and different coordinated release times. Flow control was turned on for these trials as well. The 5 Hz signal was visible in every case which shows the impact of the flow control on the normal forces. A slight increase in the normal force and lift coefficients was observed for the diode compared to the slot device, which agrees with trends acknowledged in Phase I. Comparing the geometrically similar models, with a 25% decrease in model size, a consistently greater response was recorded for the effects of the release. Also, the oscillation during release is more obvious in the small model case.

An offset was observed, in Phase II, between the four release times based on the period of the oscillation and the synchronization of the motors. The average values before and after the store release were analyzed and were found to directly compare with the static cases at the respective positions. The pitch moment coefficient always turned negative after release while the normal force and axial force coefficient both increased dramatically. During the period of release, for the 10° AoA cases, a full period of the oscillation is visible in the normal force coefficient. Release times that are offset by 180° in the position of the horizontally oriented motor also show a 180° offset at many points of the coefficient data. Additionally, when comparing all four release times to each other, the proper order of release times is seen several times before and after release of the mission store. Though this effect was not as evident in some trials, this indicates a direct effect of the release time on the forces and moments experienced by the store upon release.

5.3 Significance of Research

The major significance of this research is showing the time-accurate force and moment data can be collected with a fine enough accuracy to differentiate the effects of

different variables on the force and moments observed by the mission store model. The two variables with the most potential are the flow control devices and the synchronized release timings. The leading edge oscillatory blowing devices in the low speed wind tunnel have the ability to force the shear layer at a desired frequency in an attempt to mimic the dominant frequencies seen in transonic and supersonic flow fields. The use of two different sizes of geometrically similar models provides insight into the scaling of these forces and the impact of the research in different environments with different conditions. The release timings proved to force an offset in the normal force and axial force coefficients and in some cases were identified in the proper sequence. This could be leveraged to prevent a pitch bifurcation during the release of the mission store.

Additionally, much of the static recorded data can serve as a baseline to inform the findings of future work. All six forces and moments were collected using the Nano25 6-DOF sensor. This research only explored the normal forces, pitch moments, and axial forces. Secondary trends could be identified in the other forces and moments that provide more insight into the effects of flow control and synchronized release timings on the pitch bifurcation possibility in the store release.

5.4 Recommendation for future testing

The fluidic diodes showed promise in affecting the forces and moments experienced by the store model through flow control. Initial investigations into the effects of different diodes was conducted in Wood's research. Certain trends were confirmed in this research. The simplicity of these devices and lack of moving parts, further discussed in previous research by Wood, provides good reason to explore more possibilities using them. Specifically analyzing the impact of different diodes in different scenarios more in depth could provide more information on the impact on the forces and moments. Moreover, there is room for diode refinement, exploring the ability to

encourage flow in a certain direction and the full capability of influencing the shear layer.

Alternate methods of influencing the shear layer and mimicking the cavity environment could also be investigated. Specifically, the modified actuator referenced by Wood which could achieve oscillatory blowing of up to 750 Hz using pressurized air. This, however, might prove a challenge to synchronize with the store release with the current apparatuses in the AFIT low speed wind tunnel. An easier method would be to change the blowing frequency and observe different effects. Another approach could be investigating continuous blowing.

More complex store separation trajectories could be explored with the 6-DOF Motion Test Apparatus currently residing in the AFIT low speed wind tunnel. A vertical release limits the analysis greatly but a more realistic store release could provide additional insight into the dynamic characterization of the store release from a cavity environment. Also this would also allow for the release to begin at different positions of the cavity.

To immediately continue this research, analysis of the other three forces and moments of the same collected data could be conducted. Trends could potentially be identified and provide greater understanding into the effects of each variable on the store release. This could also be a great starting point for improving the release apparatus or using the robot arm mentioned above to do additional testing.

Another beneficial path of investigation could be observing the effects in a higher Reynolds number environment. The pressure fluctuations were investigated in a low speed wind tunnel and the oscillations were artificial, but the effects could be observed naturally in transonic or supersonic flow with a faster release apparatus.

Finally, conducting more thorough research on the effects of the release timing could prove to be valuable. Isolating the effects of the release timing through more

careful and consistent trials could help show a more clear effect. Finding a way to quantitatively compare the offset of the different release times could prove valuable. Conducting multiple trials with each release time, calculating a mean for each, then directly comparing the four release times could be the first step in further investigations.

Appendix A. Test Matrices

Index of Figures in Appendix A

Full Test Matrices	(pg 160)
Phase 1 Test Matrices	(pg 160)
Phase 2 Test Matrices	(pg 164)

Full Test Matrices

Phase 1 Test Matrices

Apparatus	Model	AoA (°)	Speed (mph)	Position
Freestream	Small	0	60	Out Cavity
Freestream	Small	0	100	Out Cavity
Freestream	Small	0	120	Out Cavity
Freestream	Small	10	60	Out Cavity
Freestream	Small	10	100	Out Cavity
Freestream	Small	10	120	Out Cavity
Freestream	Large	0	60	Out Cavity
Freestream	Large	0	100	Out Cavity
Freestream	Large	0	120	Out Cavity
Freestream	Large	10	60	Out Cavity
Freestream	Large	10	100	Out Cavity
Freestream	Large	10	120	Out Cavity
Cavity	Small	0	60	In Cavity
Cavity	Small	0	60	Shear Layer
Cavity	Small	0	60	Out Cavity
Cavity	Small	0	100	In Cavity
Cavity	Small	0	100	Shear Layer
Cavity	Small	0	100	Out Cavity
Cavity	Small	0	120	In Cavity
Cavity	Small	0	120	Shear Layer
Cavity	Small	0	120	Out Cavity
Cavity	Small	10	60	In Cavity
Cavity	Small	10	60	Shear Layer
Cavity	Small	10	60	Out Cavity
Cavity	Small	10	100	In Cavity
Cavity	Small	10	100	Shear Layer
Cavity	Small	10	100	Out Cavity
Cavity	Small	10	120	In Cavity
Cavity	Small	10	120	Shear Layer
Cavity	Small	10	120	Out Cavity

Table 30: Phase 1 Full Test Matrix Part 1, no flow control

Apparatus	Model	AoA ($^{\circ}$)	Speed (mph)	Position
Cavity	Large	0	60	In Cavity
Cavity	Large	0	60	Shear Layer
Cavity	Large	0	60	Out Cavity
Cavity	Large	0	100	In Cavity
Cavity	Large	0	100	Shear Layer
Cavity	Large	0	100	Out Cavity
Cavity	Large	0	120	In Cavity
Cavity	Large	0	120	Shear Layer
Cavity	Large	0	120	Out Cavity
Cavity	Large	10	60	In Cavity
Cavity	Large	10	60	Shear Layer
Cavity	Large	10	60	Out Cavity
Cavity	Large	10	100	In Cavity
Cavity	Large	10	100	Shear Layer
Cavity	Large	10	100	Out Cavity
Cavity	Large	10	120	In Cavity
Cavity	Large	10	120	Shear Layer
Cavity	Large	10	120	Out Cavity

Table 31: Phase 1 Full Test Matrix Part 2, no flow control

Model	FC Device	AoA ($^{\circ}$)	Speed (mph)	Position
Small	Slot	0	60	In Cavity
Small	Slot	0	60	Shear Layer
Small	Slot	0	60	out Cavity
Small	Slot	0	100	In Cavity
Small	Slot	0	100	Shear Layer
Small	Slot	0	100	out Cavity
Small	Slot	0	120	In Cavity
Small	Slot	0	120	Shear Layer
Small	Slot	0	120	out Cavity
Small	Slot	10	60	In Cavity
Small	Slot	10	60	Shear Layer
Small	Slot	10	60	out Cavity
Small	Slot	10	100	In Cavity
Small	Slot	10	100	Shear Layer
Small	Slot	10	100	out Cavity
Small	Slot	10	120	In Cavity
Small	Slot	10	120	Shear Layer
Small	Slot	10	120	out Cavity
Small	Diode 2	0	60	In Cavity
Small	Diode 2	0	60	Shear Layer
Small	Diode 2	0	60	out Cavity
Small	Diode 2	0	100	In Cavity
Small	Diode 2	0	100	Shear Layer
Small	Diode 2	0	100	out Cavity
Small	Diode 2	0	120	In Cavity
Small	Diode 2	0	120	Shear Layer
Small	Diode 2	0	120	out Cavity
Small	Diode 2	10	60	In Cavity
Small	Diode 2	10	60	Shear Layer
Small	Diode 2	10	60	out Cavity
Small	Diode 2	10	100	In Cavity
Small	Diode 2	10	100	Shear Layer
Small	Diode 2	10	100	out Cavity
Small	Diode 2	10	120	In Cavity
Small	Diode 2	10	120	Shear Layer
Small	Diode 2	10	120	out Cavity

Table 32: Phase 1 Full Test Matrix Part 3, with flow control

Model	FC Device	AoA ($^{\circ}$)	Speed (mph)	Position
Large	Slot	0	60	In Cavity
Large	Slot	0	60	Shear Layer
Large	Slot	0	60	out Cavity
Large	Slot	0	100	In Cavity
Large	Slot	0	100	Shear Layer
Large	Slot	0	100	out Cavity
Large	Slot	0	120	In Cavity
Large	Slot	0	120	Shear Layer
Large	Slot	0	120	out Cavity
Large	Slot	10	60	In Cavity
Large	Slot	10	60	Shear Layer
Large	Slot	10	60	out Cavity
Large	Slot	10	100	In Cavity
Large	Slot	10	100	Shear Layer
Large	Slot	10	100	out Cavity
Large	Slot	10	120	In Cavity
Large	Slot	10	120	Shear Layer
Large	Slot	10	120	out Cavity
Large	Diode 2	0	60	In Cavity
Large	Diode 2	0	60	Shear Layer
Large	Diode 2	0	60	out Cavity
Large	Diode 2	0	100	In Cavity
Large	Diode 2	0	100	Shear Layer
Large	Diode 2	0	100	out Cavity
Large	Diode 2	0	120	In Cavity
Large	Diode 2	0	120	Shear Layer
Large	Diode 2	0	120	out Cavity
Large	Diode 2	10	60	In Cavity
Large	Diode 2	10	60	Shear Layer
Large	Diode 2	10	60	out Cavity
Large	Diode 2	10	100	In Cavity
Large	Diode 2	10	100	Shear Layer
Large	Diode 2	10	100	out Cavity
Large	Diode 2	10	120	In Cavity
Large	Diode 2	10	120	Shear Layer
Large	Diode 2	10	120	out Cavity

Table 33: Phase 1 Full Test Matrix Part 4, with flow control

Phase 2 Test Matrices

Model	FC Device	AoA ($^{\circ}$)	Speed (mph)	Release Timing
Small	Slot	0	60	Release Time 1
Small	Slot	0	60	Release Time 2
Small	Slot	0	60	Release Time 3
Small	Slot	0	60	Release Time 4
Small	Slot	0	100	Release Time 1
Small	Slot	0	100	Release Time 2
Small	Slot	0	100	Release Time 3
Small	Slot	0	100	Release Time 4
Small	Slot	0	120	Release Time 1
Small	Slot	0	120	Release Time 2
Small	Slot	0	120	Release Time 3
Small	Slot	0	120	Release Time 4
Small	Slot	10	60	Release Time 1
Small	Slot	10	60	Release Time 2
Small	Slot	10	60	Release Time 3
Small	Slot	10	60	Release Time 4
Small	Slot	10	100	Release Time 1
Small	Slot	10	100	Release Time 2
Small	Slot	10	100	Release Time 3
Small	Slot	10	100	Release Time 4
Small	Slot	10	120	Release Time 1
Small	Slot	10	120	Release Time 2
Small	Slot	10	120	Release Time 3
Small	Slot	10	120	Release Time 4

Table 34: Phase 2 Full Test Matrix Part 1

Model	FC Device	AoA ($^{\circ}$)	Speed (mph)	Release Timing
Small	Diode 2	0	60	Release Time 1
Small	Diode 2	0	60	Release Time 2
Small	Diode 2	0	60	Release Time 3
Small	Diode 2	0	60	Release Time 4
Small	Diode 2	0	100	Release Time 1
Small	Diode 2	0	100	Release Time 2
Small	Diode 2	0	100	Release Time 3
Small	Diode 2	0	100	Release Time 4
Small	Diode 2	0	120	Release Time 1
Small	Diode 2	0	120	Release Time 2
Small	Diode 2	0	120	Release Time 3
Small	Diode 2	0	120	Release Time 4
Small	Diode 2	10	60	Release Time 1
Small	Diode 2	10	60	Release Time 2
Small	Diode 2	10	60	Release Time 3
Small	Diode 2	10	60	Release Time 4
Small	Diode 2	10	100	Release Time 1
Small	Diode 2	10	100	Release Time 2
Small	Diode 2	10	100	Release Time 3
Small	Diode 2	10	100	Release Time 4
Small	Diode 2	10	120	Release Time 1
Small	Diode 2	10	120	Release Time 2
Small	Diode 2	10	120	Release Time 3
Small	Diode 2	10	120	Release Time 4

Table 35: Phase 2 Full Test Matrix Part 2

Model	FC Device	AoA ($^{\circ}$)	Speed (mph)	Release Timing
Large	Slot	0	60	Release Time 1
Large	Slot	0	60	Release Time 2
Large	Slot	0	60	Release Time 3
Large	Slot	0	60	Release Time 4
Large	Slot	0	100	Release Time 1
Large	Slot	0	100	Release Time 2
Large	Slot	0	100	Release Time 3
Large	Slot	0	100	Release Time 4
Large	Slot	0	120	Release Time 1
Large	Slot	0	120	Release Time 2
Large	Slot	0	120	Release Time 3
Large	Slot	0	120	Release Time 4
Large	Slot	10	60	Release Time 1
Large	Slot	10	60	Release Time 2
Large	Slot	10	60	Release Time 3
Large	Slot	10	60	Release Time 4
Large	Slot	10	100	Release Time 1
Large	Slot	10	100	Release Time 2
Large	Slot	10	100	Release Time 3
Large	Slot	10	100	Release Time 4
Large	Slot	10	120	Release Time 1
Large	Slot	10	120	Release Time 2
Large	Slot	10	120	Release Time 3
Large	Slot	10	120	Release Time 4

Table 36: Phase 2 Full Test Matrix Part 3

Model	FC Device	AoA ($^{\circ}$)	Speed (mph)	Release Timing
Large	Slot	0	60	Release Time 1
Large	Slot	0	60	Release Time 2
Large	Slot	0	60	Release Time 3
Large	Slot	0	60	Release Time 4
Large	Slot	0	100	Release Time 1
Large	Slot	0	100	Release Time 2
Large	Slot	0	100	Release Time 3
Large	Slot	0	100	Release Time 4
Large	Slot	0	120	Release Time 1
Large	Slot	0	120	Release Time 2
Large	Slot	0	120	Release Time 3
Large	Slot	0	120	Release Time 4
Large	Slot	10	60	Release Time 1
Large	Slot	10	60	Release Time 2
Large	Slot	10	60	Release Time 3
Large	Slot	10	60	Release Time 4
Large	Slot	10	100	Release Time 1
Large	Slot	10	100	Release Time 2
Large	Slot	10	100	Release Time 3
Large	Slot	10	100	Release Time 4
Large	Slot	10	120	Release Time 1
Large	Slot	10	120	Release Time 2
Large	Slot	10	120	Release Time 3
Large	Slot	10	120	Release Time 4

Table 37: Phase 2 Full Test Matrix Part 4

Appendix B. Additional Experimental Data

Index of Figures in Appendix B

Additional Illustrations	(pg 169)
Position Heights Illustrations	(pg 169)
Phase I: Freestream Apparatus	(pg 172)
Pitch Moment and Axial Force Coefficients	(pg 172)
Phase I: Cavity Apparatus	(pg 177)
Normal Force, Pitch Moment, and Axial Force Coefficients	(pg 177)
Phase I: Cavity Apparatus with Flow Control	(pg 189)
Normal Force, Pitch Moment, and Axial Force Coefficients	(pg 189)
Phase II: Dynamic Store Release	(pg 221)
Normal Force, Pitch Moment, and Axial Force Coefficients	(pg 221)
Repeatability Trials	(pg 243)
Normal Force, Pitch Moment, and Axial Force Coefficients	(pg 243)
Tare Examples 10 Degrees	(pg 253)
Normal Force, Pitch Moment, and Axial Force Coefficients	(pg 253)
Individual Examples 10 Degrees	(pg 287)
Normal Force, Pitch Moment, and Axial Force Coefficients	(pg 287)
Tare Examples 0 Degrees	(pg 317)
Normal Force, Pitch Moment, and Axial Force Coefficients	(pg 317)
Individual Examples 0 Degrees	(pg 351)
Normal Force, Pitch Moment, and Axial Force Coefficients	(pg 351)

Additional Illustrations

Position Heights Illustrations

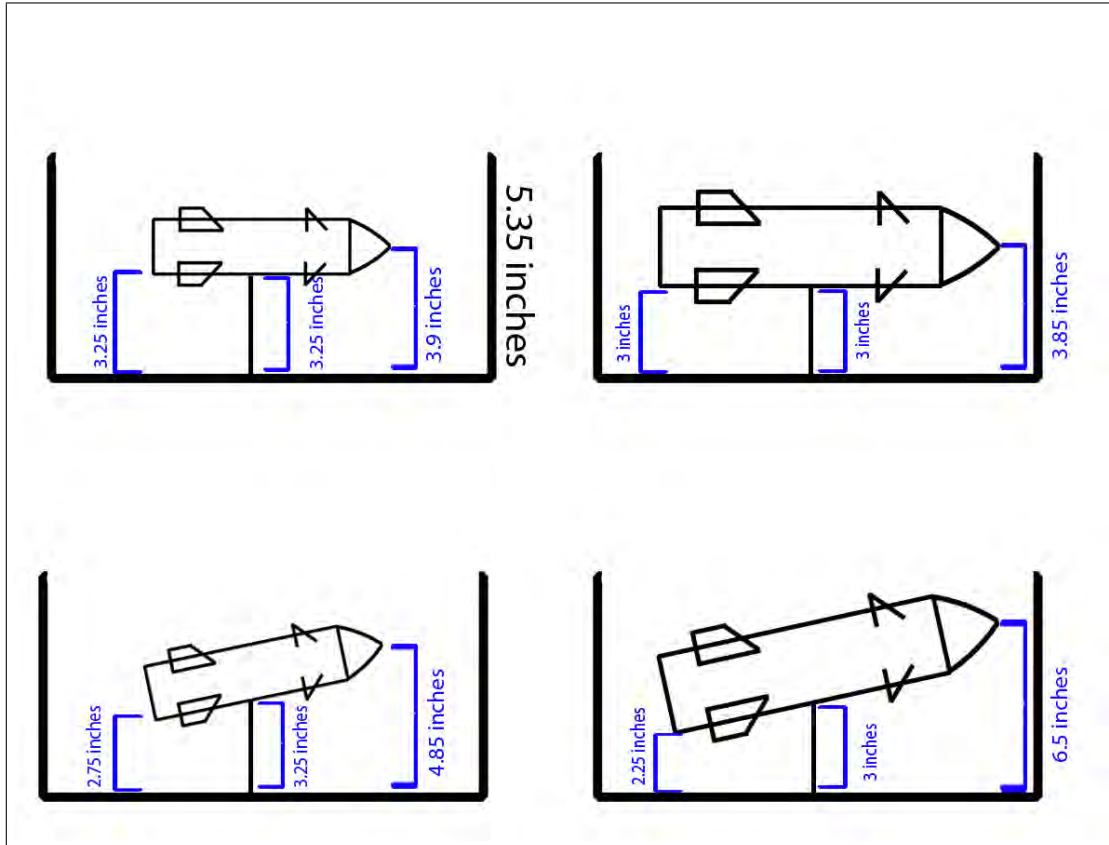


Figure 82: Drawing of heights of models measured from the floor of the cavity, "In Cavity" position

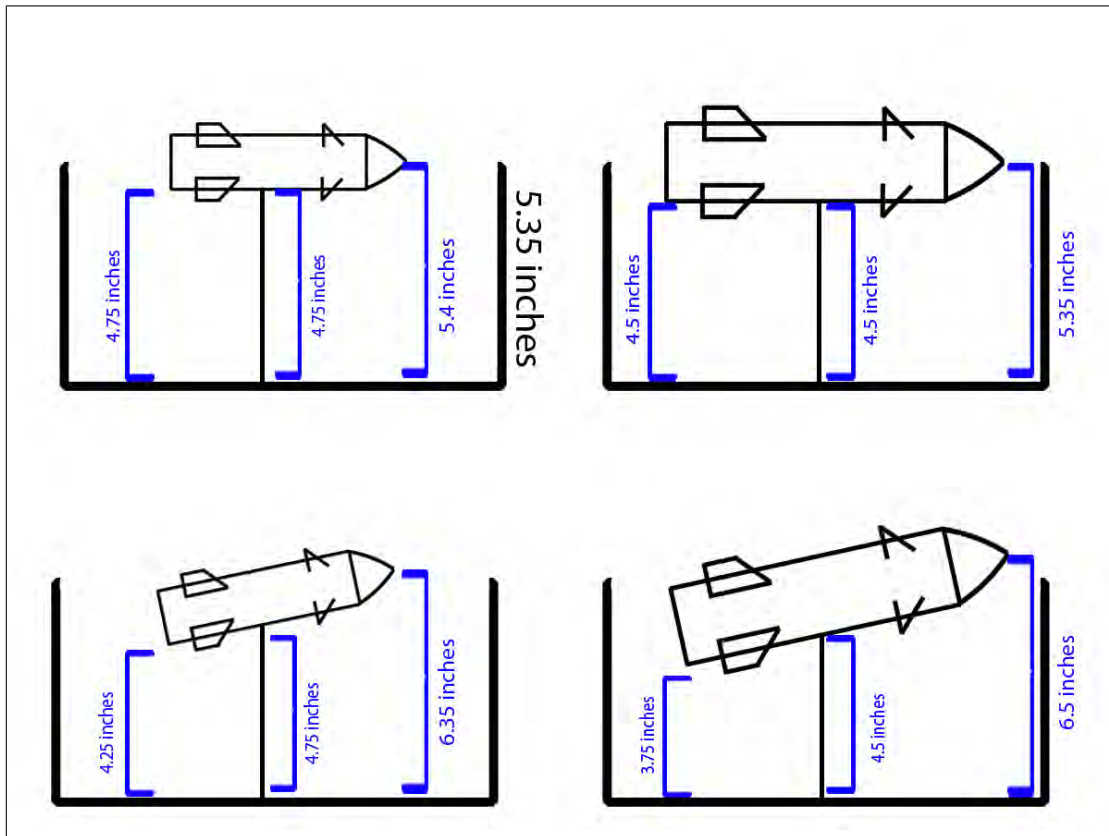


Figure 83: Drawing of heights of models measured from the floor of the cavity, "Shear Layer" position

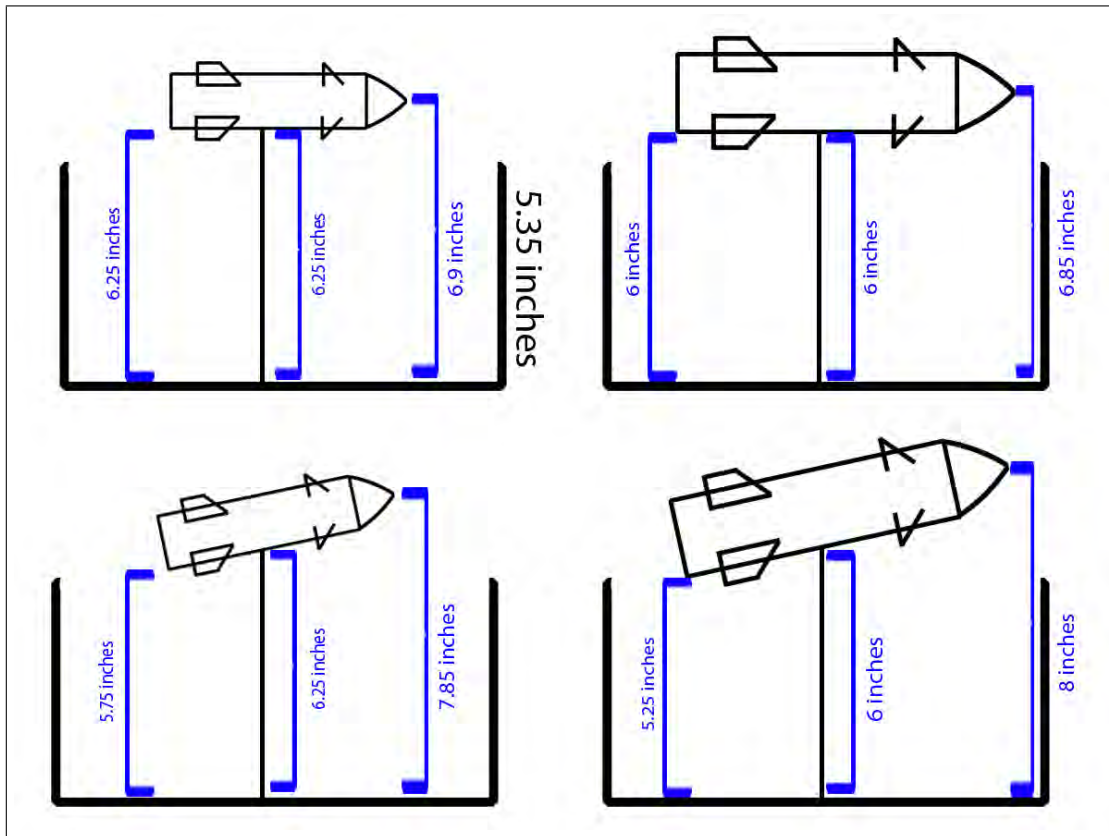
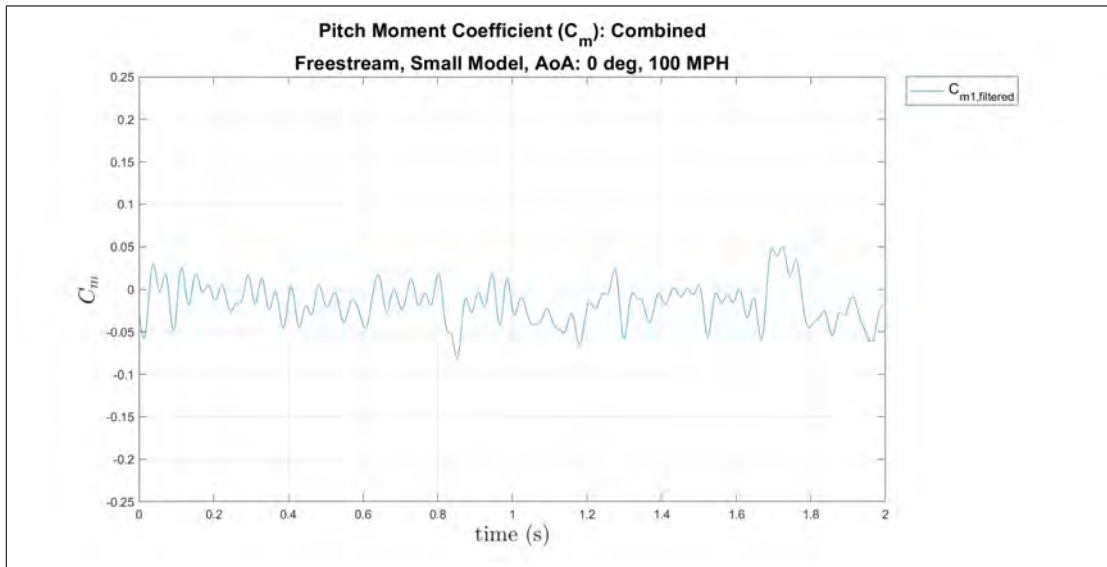


Figure 84: Drawing of heights of models measured from the floor of the cavity, “Out of Cavity” position

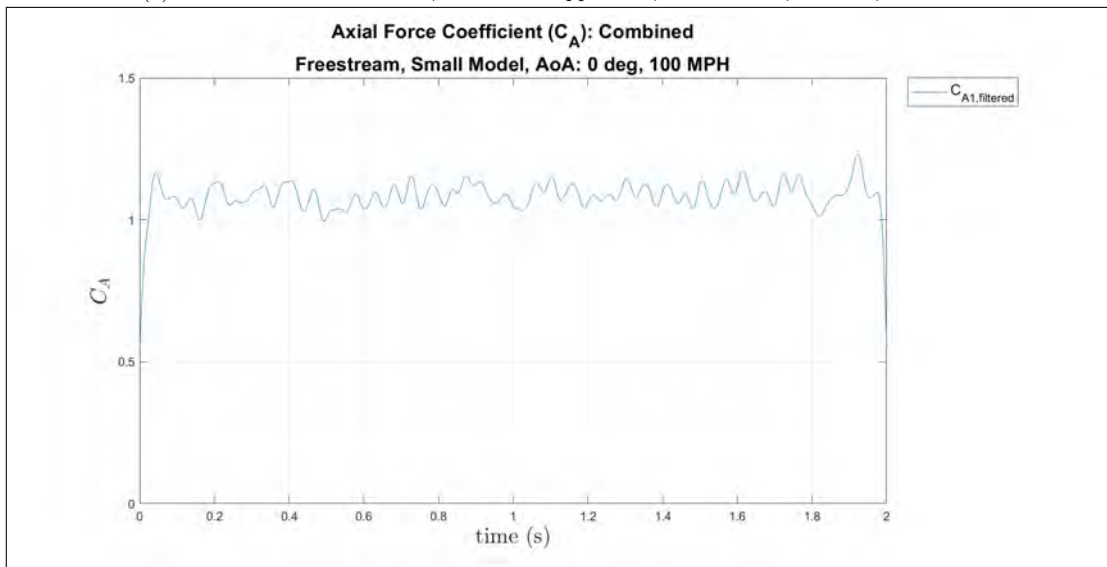
Phase I: Freestream Apparatus

Pitch Moment and Axial Force Coefficients

Small Model, 0° AoA, 100 MPH



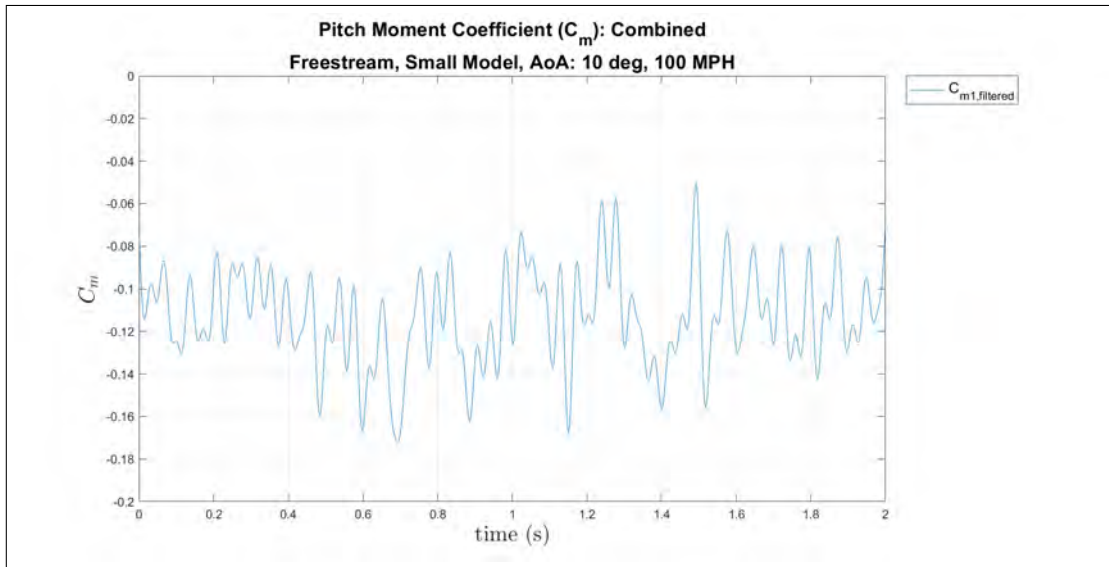
(a) Pitch Moment Coefficient, freestream apparatus, small model, 0° AoA, 100 MPH



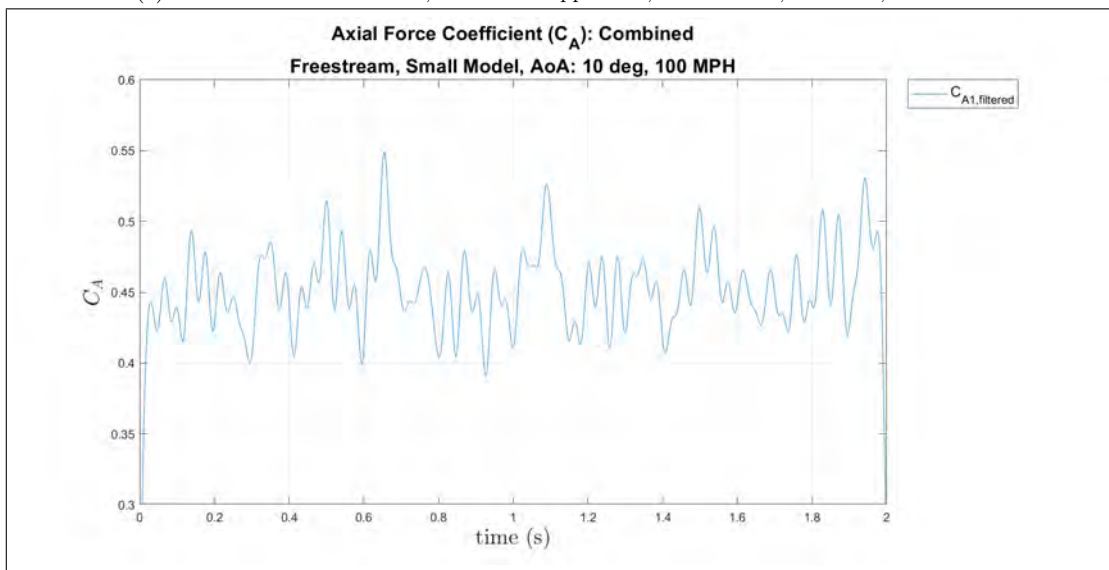
(b) Axial Force Coefficient, freestream apparatus, small model, 0° AoA, 100 MPH

Figure 85: Small model at 0° AoA of the pitch moment and axial force coefficients for the freestream apparatus, 100 MPH

Small Model, 10° AoA, 100 MPH



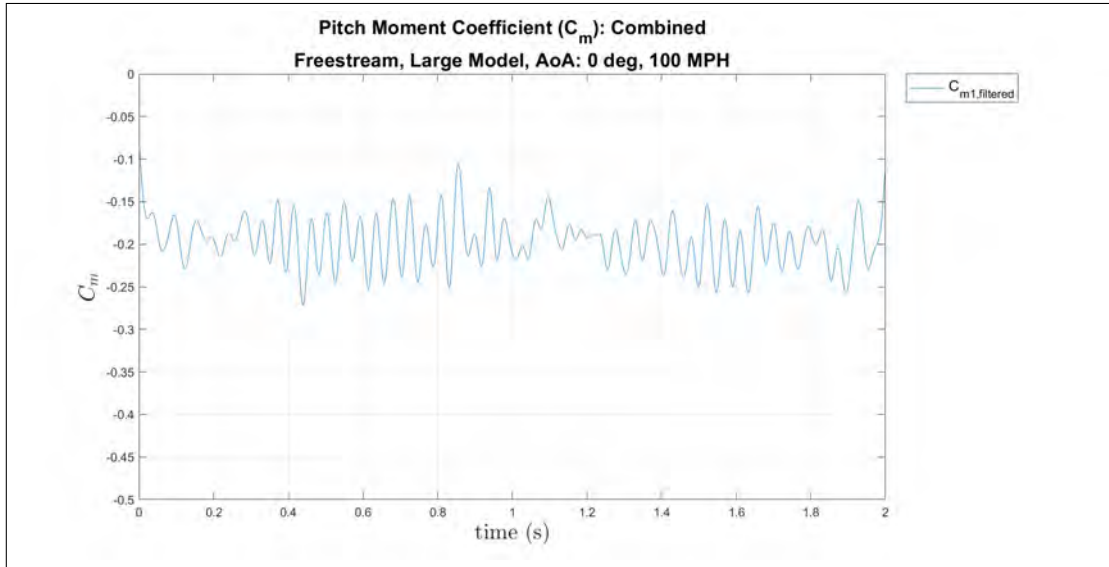
(a) Pitch Moment Coefficient, freestream apparatus, small model, 10° AoA, 100 MPH



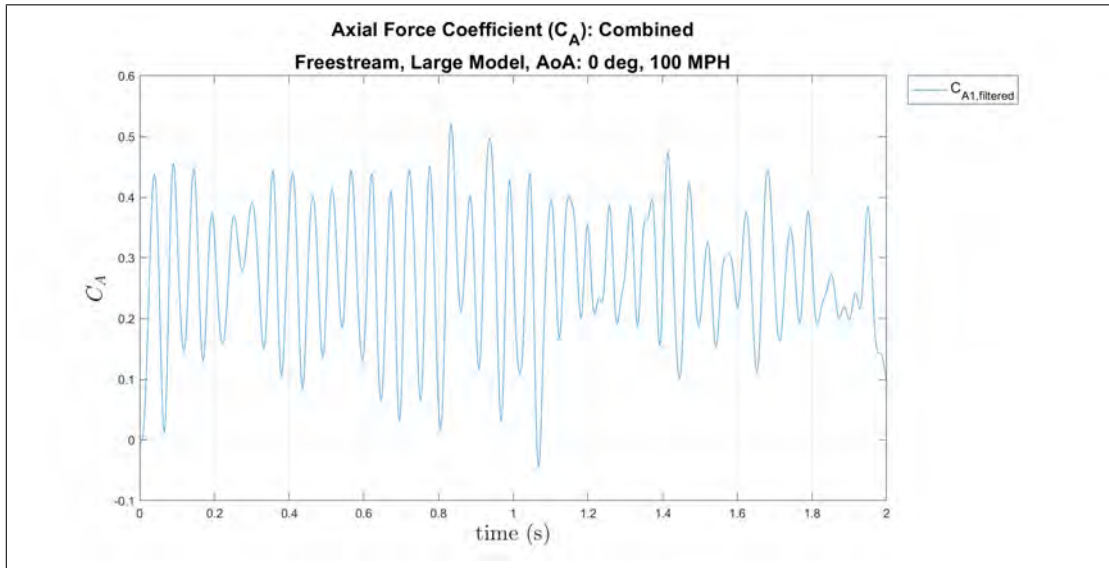
(b) Axial Force Coefficient, freestream apparatus, small model, 10° AoA, 100 MPH

Figure 86: Small model at 10° AoA of the pitch moment and axial force coefficients for the freestream apparatus, 100 MPH

Large Model, 0° AoA, 100 MPH



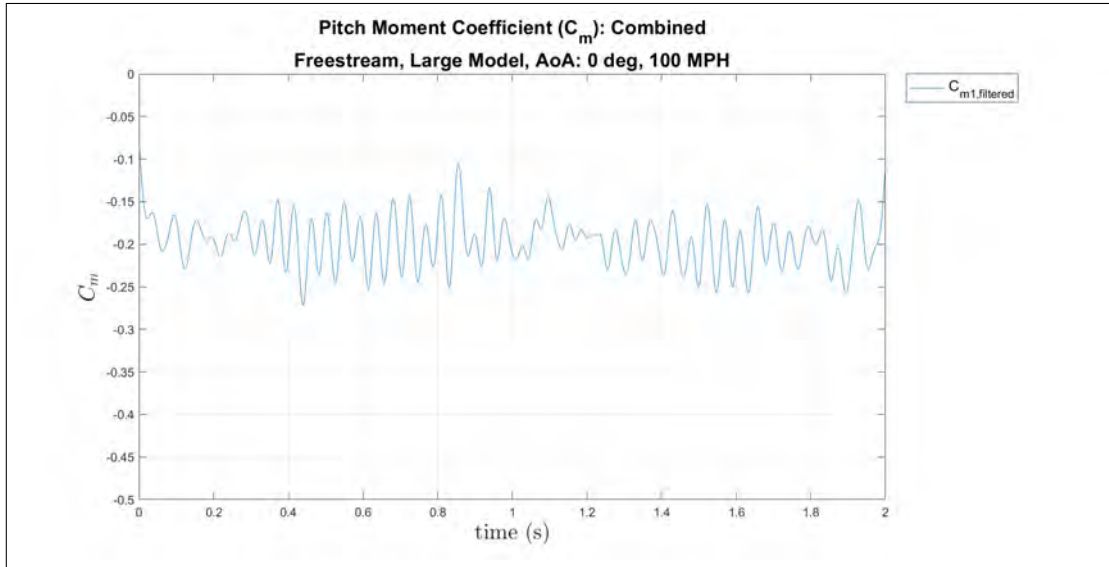
(a) Pitch Moment Coefficient, freestream apparatus, large model, 0° AoA, 100 MPH



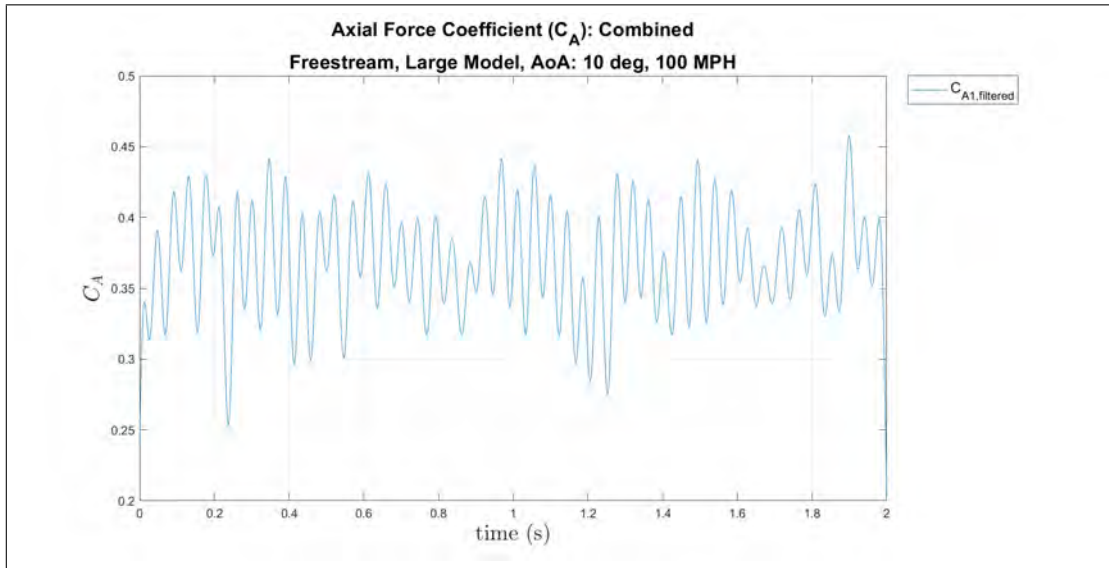
(b) Axial Force Coefficient, freestream apparatus, large model, 0° AoA, 100 MPH

Figure 87: Large model at 0° AoA of the pitch moment and axial force coefficients for the freestream apparatus, 100 MPH

Large Model, 10° AoA, 100 MPH



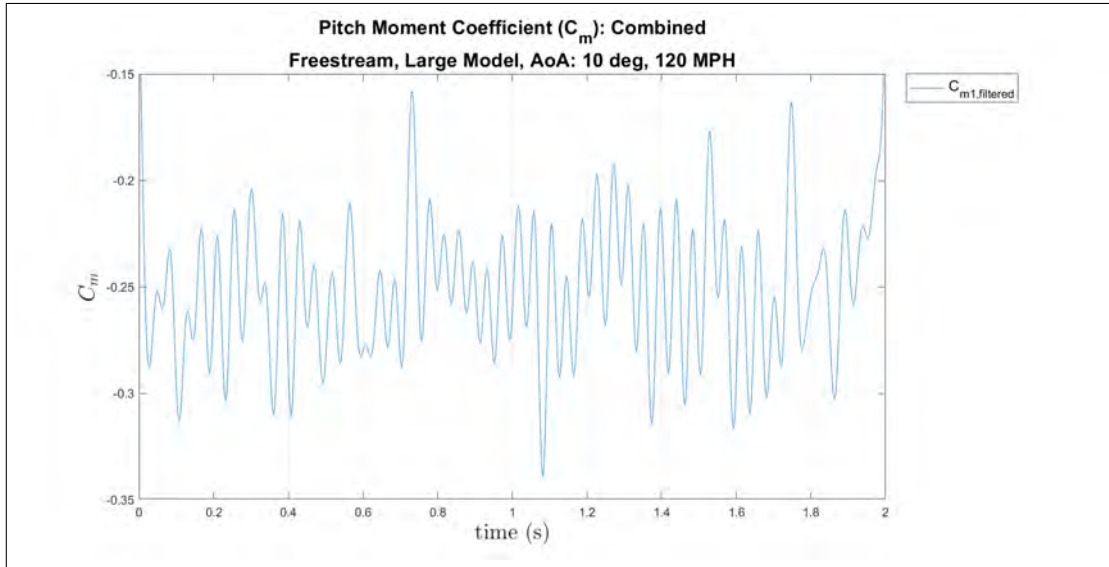
(a) Pitch Moment Coefficient, freestream apparatus, large model, 10° AoA, 100 MPH



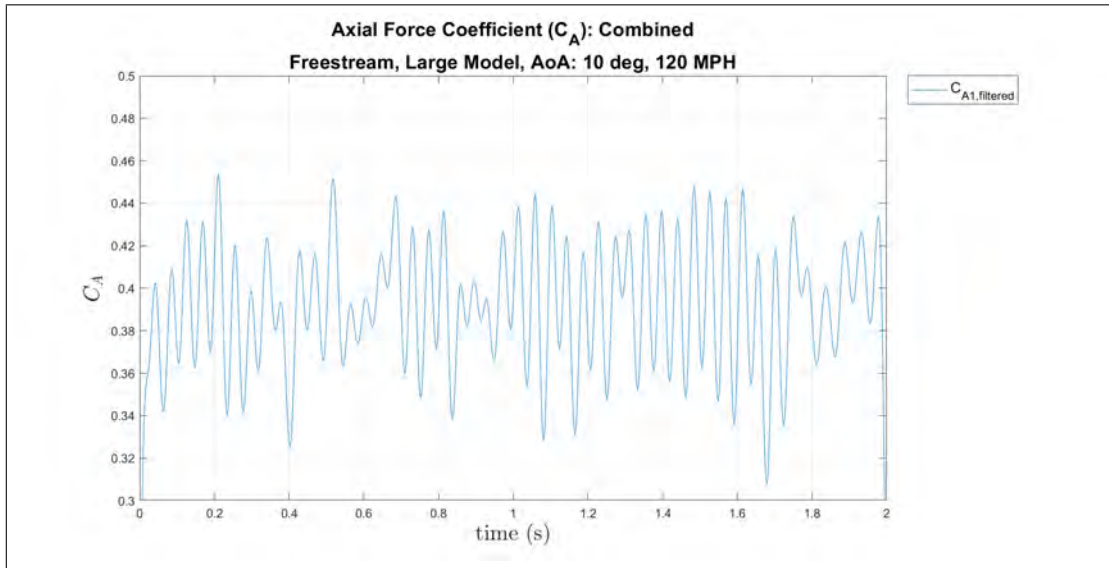
(b) Axial Force Coefficient, freestream apparatus, large model, 10° AoA, 100 MPH

Figure 88: Large model at 10° AoA of the pitch moment and axial force coefficients for the freestream apparatus, 100 MPH

Large Model, 10° AoA, 120 MPH



(a) Pitch Moment Coefficient, freestream apparatus, large model, 10° AoA, 120 MPH



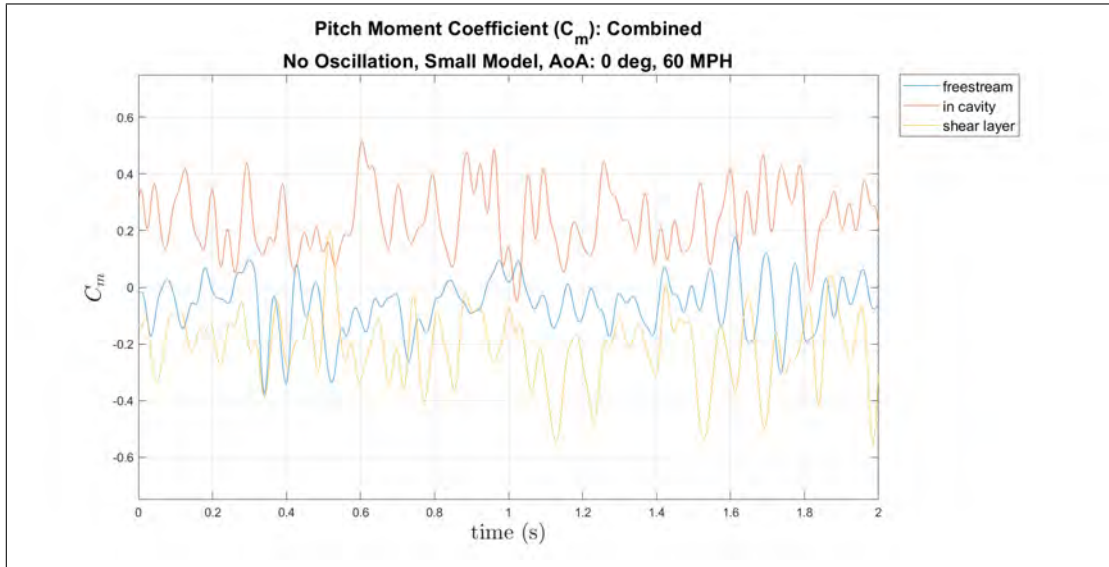
(b) Axial Force Coefficient, freestream apparatus, large model, 10° AoA, 120 MPH

Figure 89: Large model at 10° AoA of the pitch moment and axial force coefficients for the freestream apparatus, 120 MPH

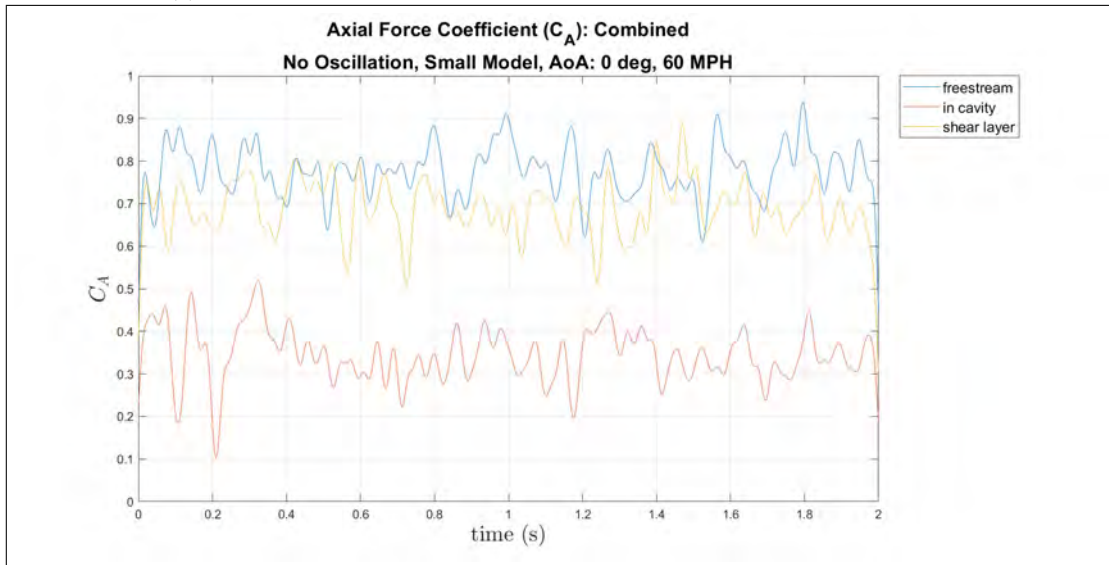
Phase I: Cavity Apparatus

Normal Force, Pitch Moment, and Axial Force Coefficients

Small Model, 0° AoA

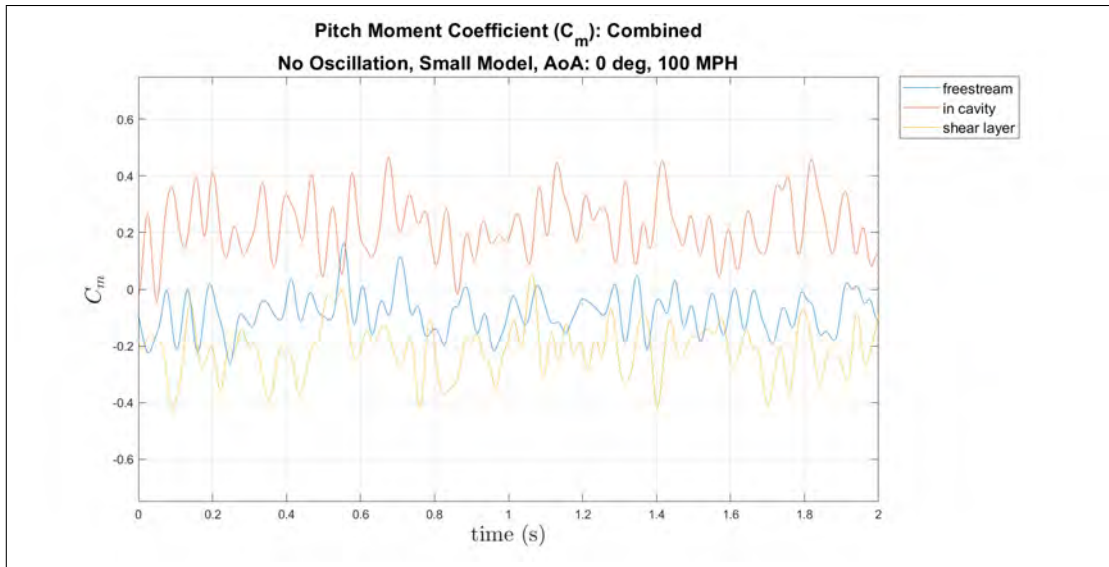


(a) Pitch Moment Coefficient, cavity apparatus, small model, 0° AoA, 60 MPH

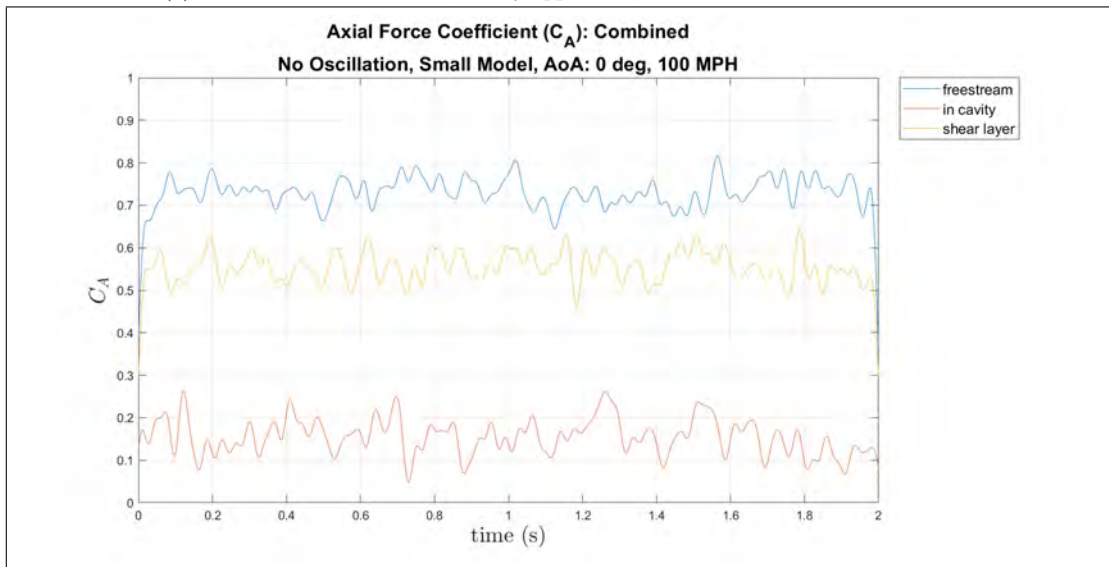


(b) Axial Force Coefficient, cavity apparatus, small model, 0° AoA, 60 MPH

Figure 90: Small model at 0° AoA of the pitch moment and axial force coefficients for the cavity apparatus, 60 MPH

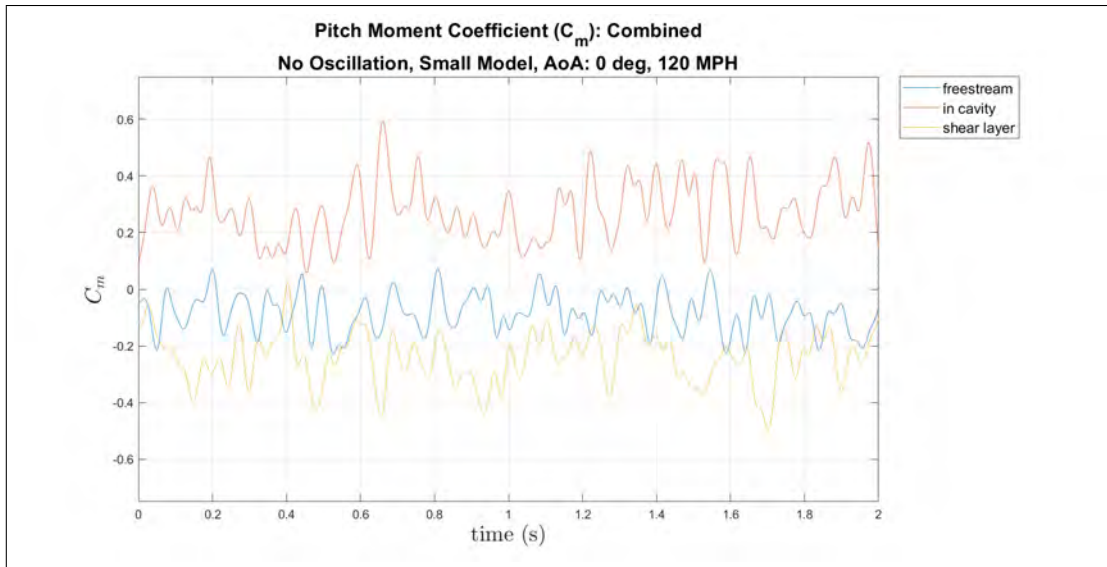


(a) Pitch Moment Coefficient, cavity apparatus, small model, 0° AoA, 100 MPH

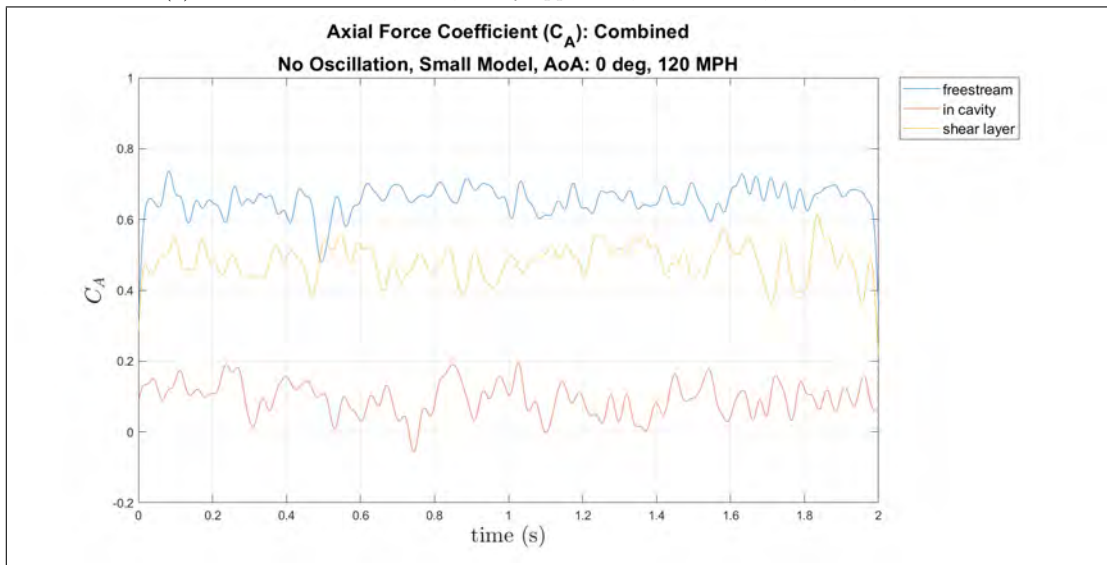


(b) Axial Force Coefficient, cavity apparatus, small model, 0° AoA, 100 MPH

Figure 91: Small model at 0° AoA of the pitch moment and axial force coefficients for the cavity apparatus, 100 MPH

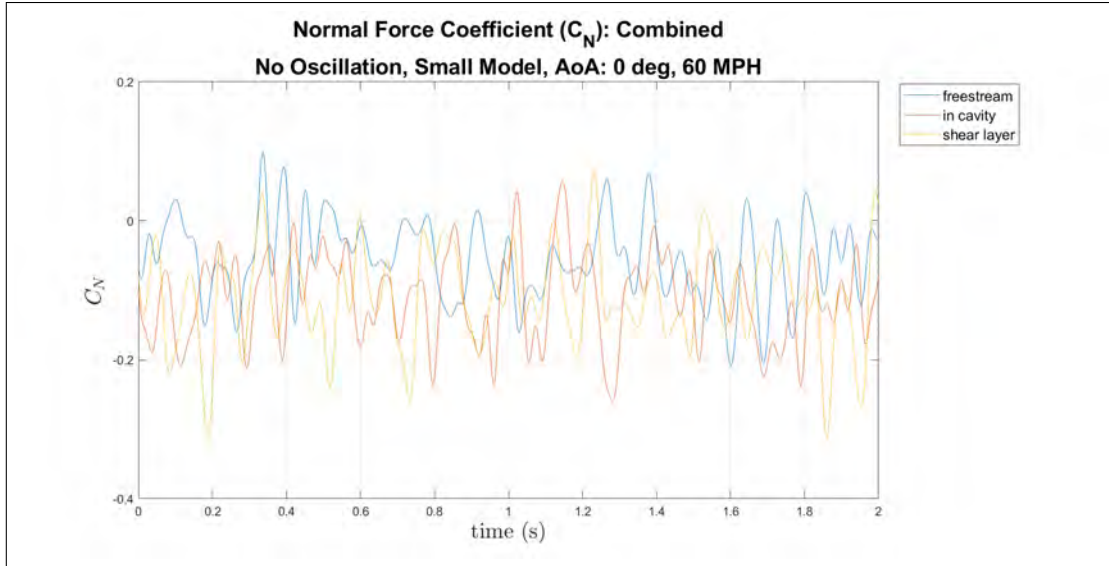


(a) Pitch Moment Coefficient, cavity apparatus, small model, 0° AoA, 120 MPH

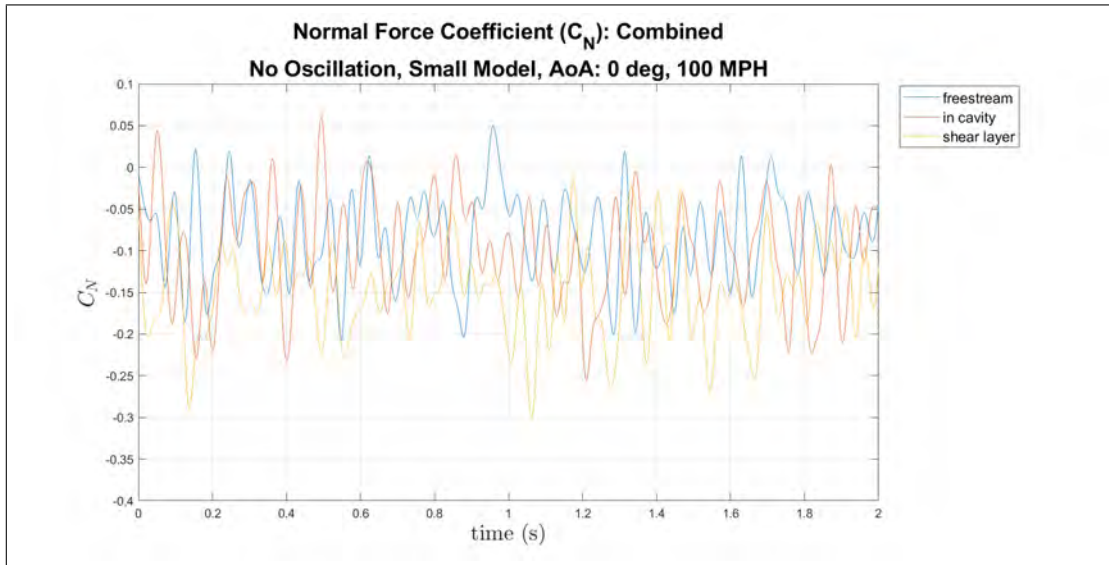


(b) Axial Force Coefficient, cavity apparatus, small model, 0° AoA, 120 MPH

Figure 92: Small model at 0° AoA of the pitch moment and axial force coefficients for the cavity apparatus, 120 MPH



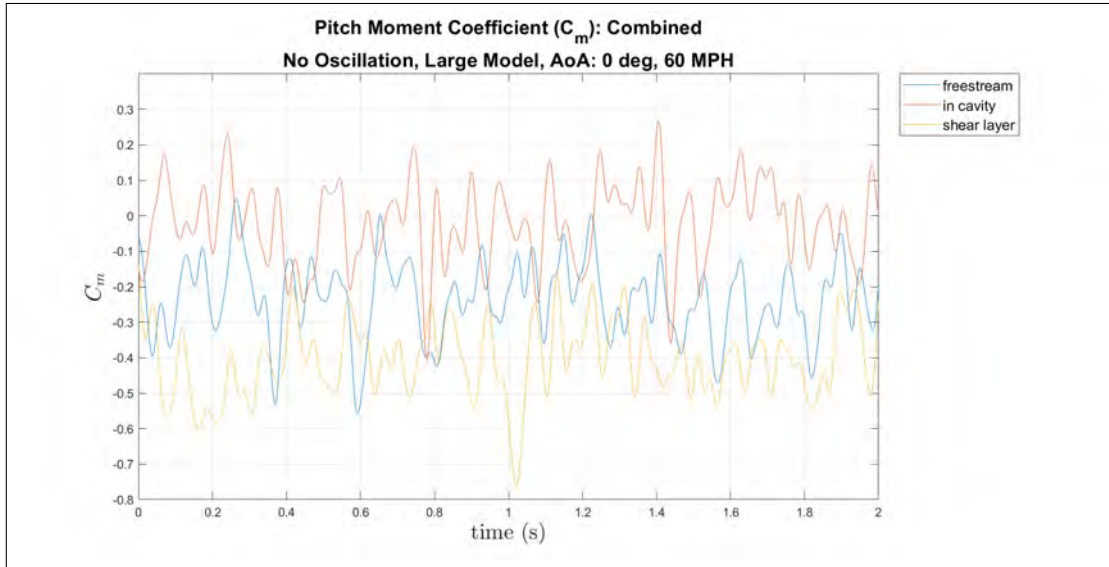
(a) Normal Force Coefficient, cavity apparatus, small model, 0° AoA, 60 MPH



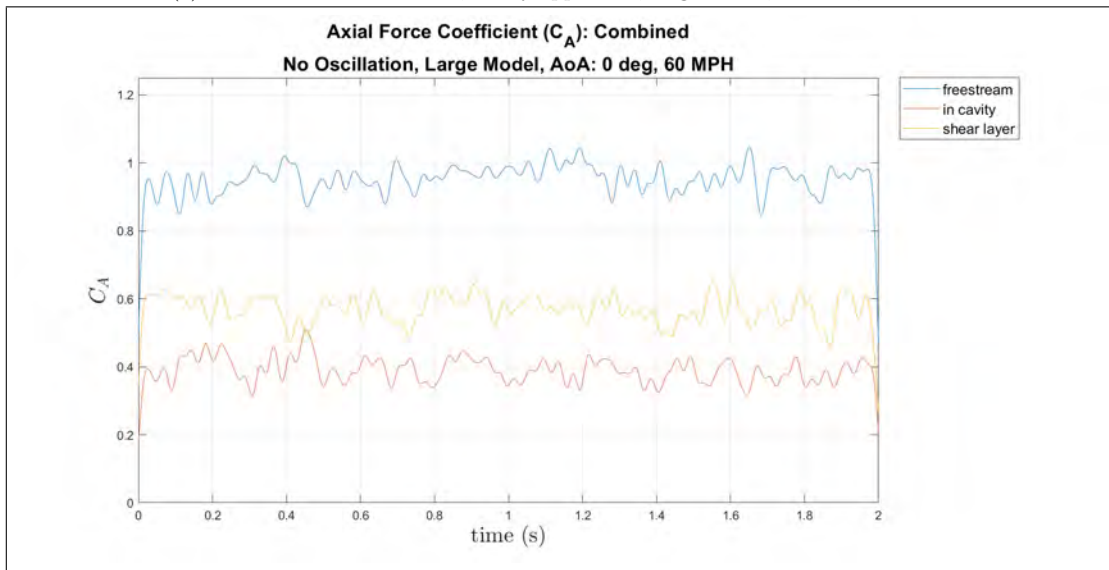
(b) Normal Force Coefficient, cavity apparatus, small model, 0° AoA, 100 MPH

Figure 93: Small model at 0° AoA of the normal force coefficients for the cavity apparatus, 60 MPH and 100 MPH

Large Model, 0° AoA

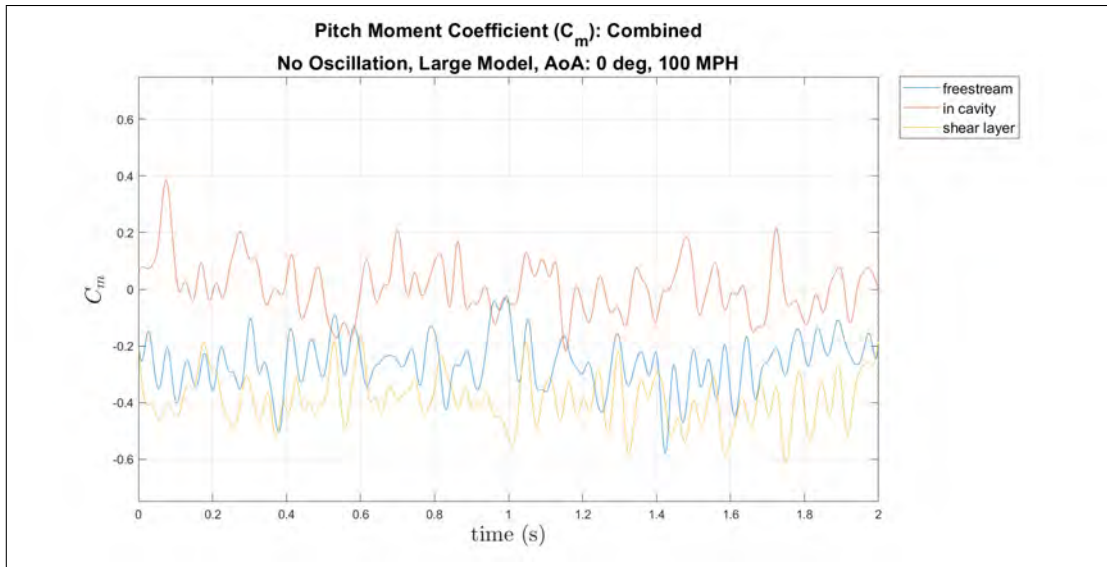


(a) Pitch Moment Coefficient, cavity apparatus, large model, 0° AoA, 60 MPH

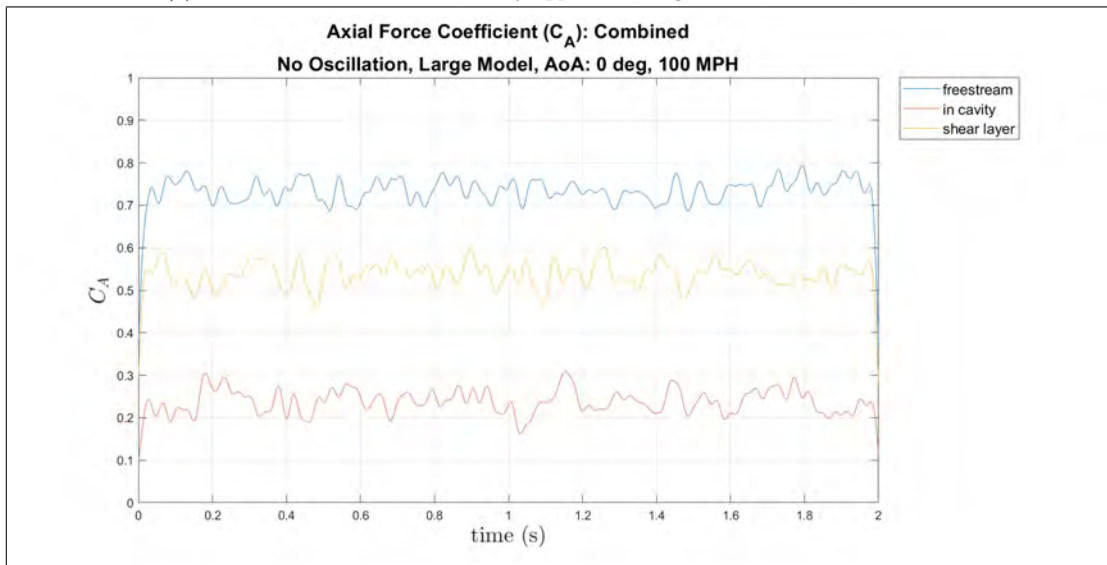


(b) Axial Force Coefficient, cavity apparatus, large model, 0° AoA, 60 MPH

Figure 94: Large model at 0° AoA of the pitch moment and axial force coefficients for the cavity apparatus, 60 MPH

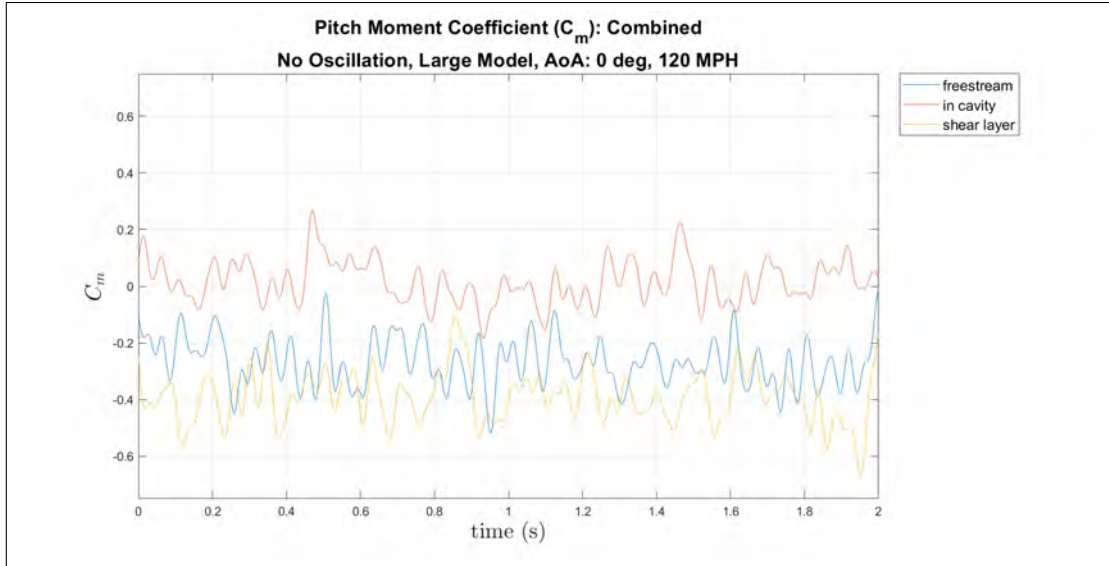


(a) Pitch Moment Coefficient, cavity apparatus, large model, 0° AoA, 100 MPH

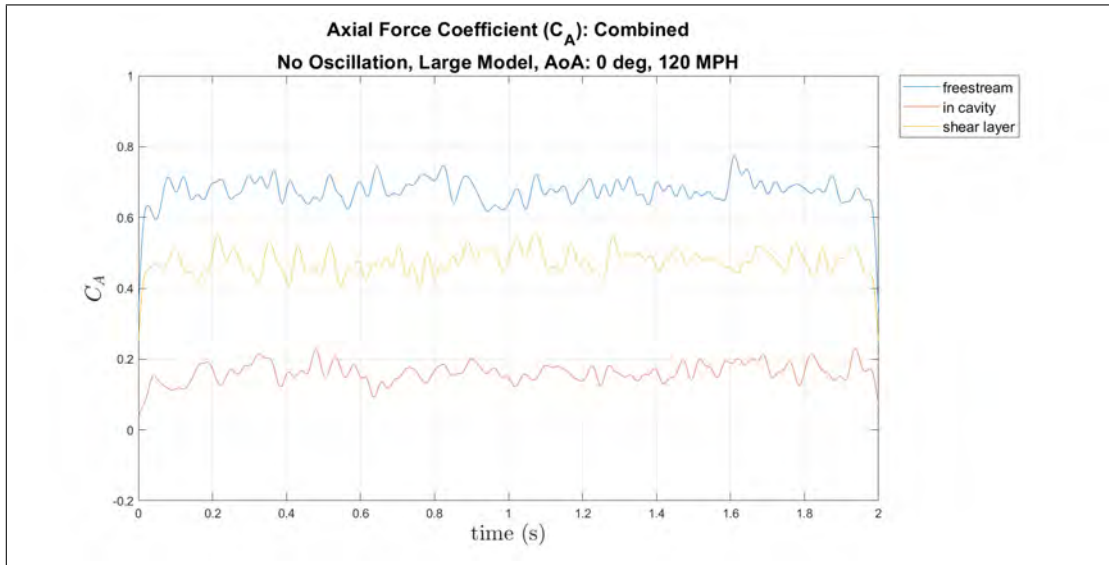


(b) Axial Force Coefficient, cavity apparatus, large model, 0° AoA, 100 MPH

Figure 95: Large model at 0° AoA of the pitch moment and axial force coefficients for the cavity apparatus, 100 MPH

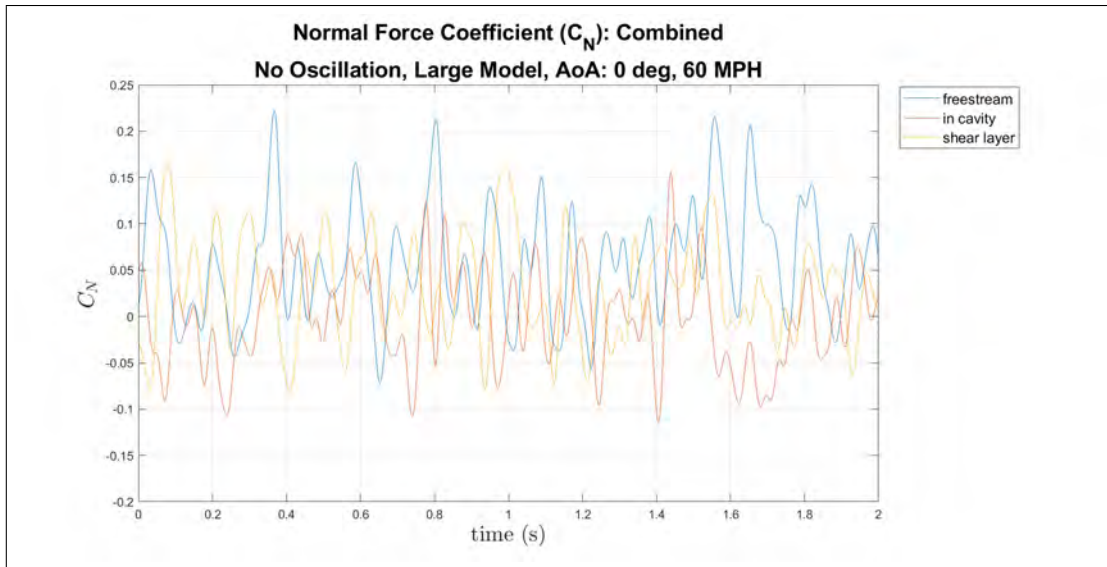


(a) Pitch Moment Coefficient, cavity apparatus, large model, 0° AoA, 120 MPH

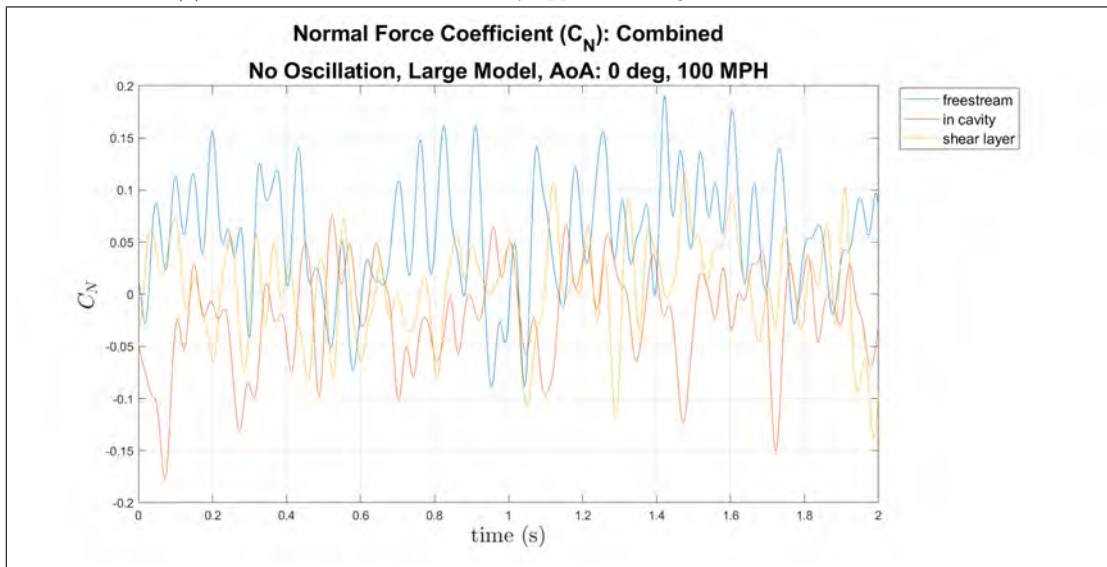


(b) Axial Force Coefficient, cavity apparatus, large model, 0° AoA, 120 MPH

Figure 96: Large model at 0° AoA of the pitch moment and axial force coefficients for the cavity apparatus, 120 MPH



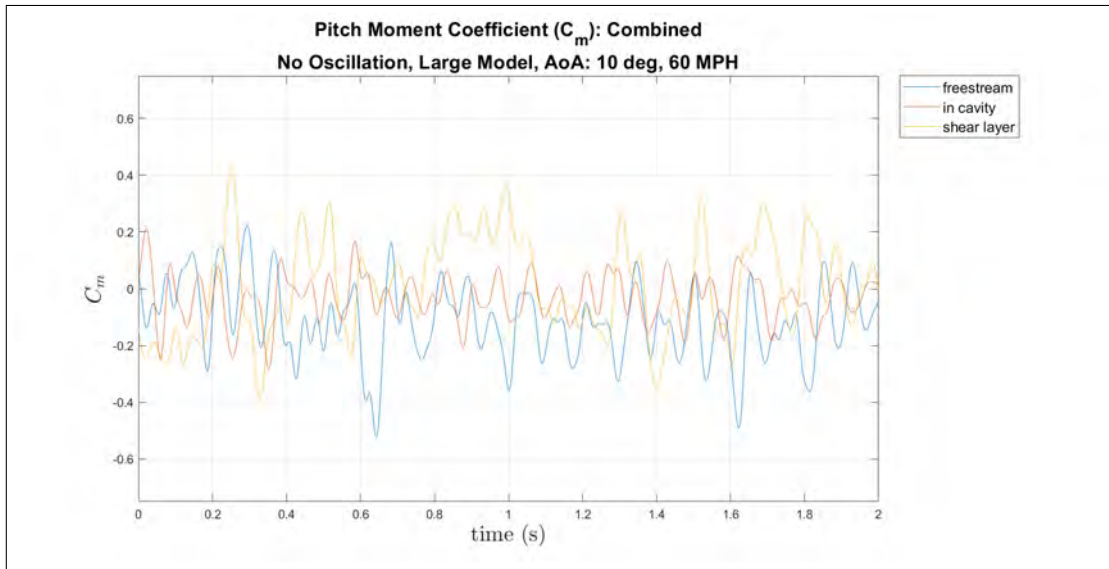
(a) Normal Force Coefficient, cavity apparatus, large model, 0° AoA, 60 MPH



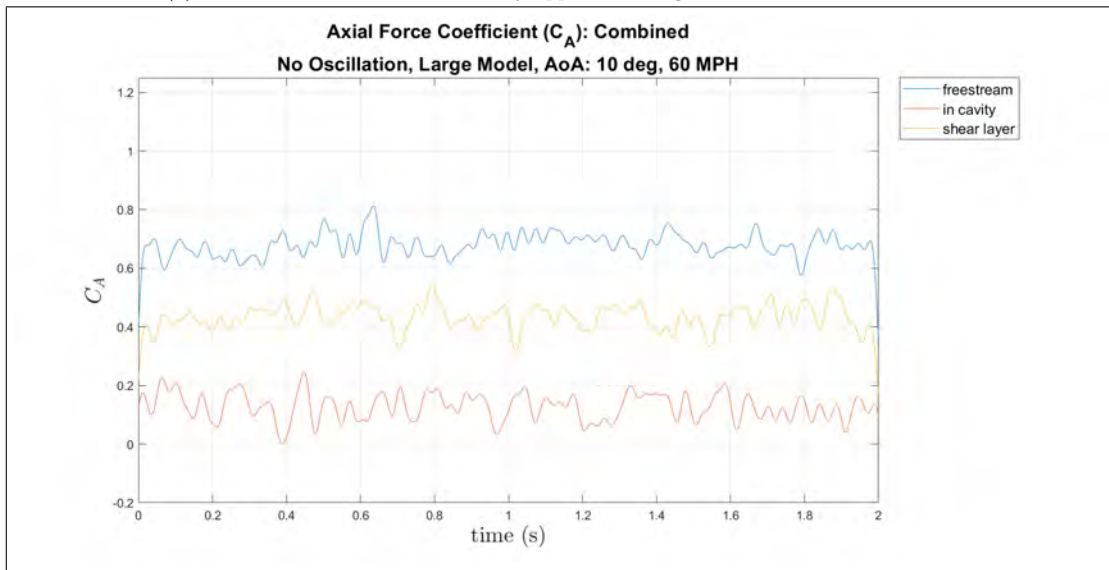
(b) Normal Force Coefficient, cavity apparatus, large model, 0° AoA, 100 MPH

Figure 97: Large model at 0° AoA of the normal force coefficients for the cavity apparatus, 60 MPH and 100 MPH

Small Model, 10° AoA

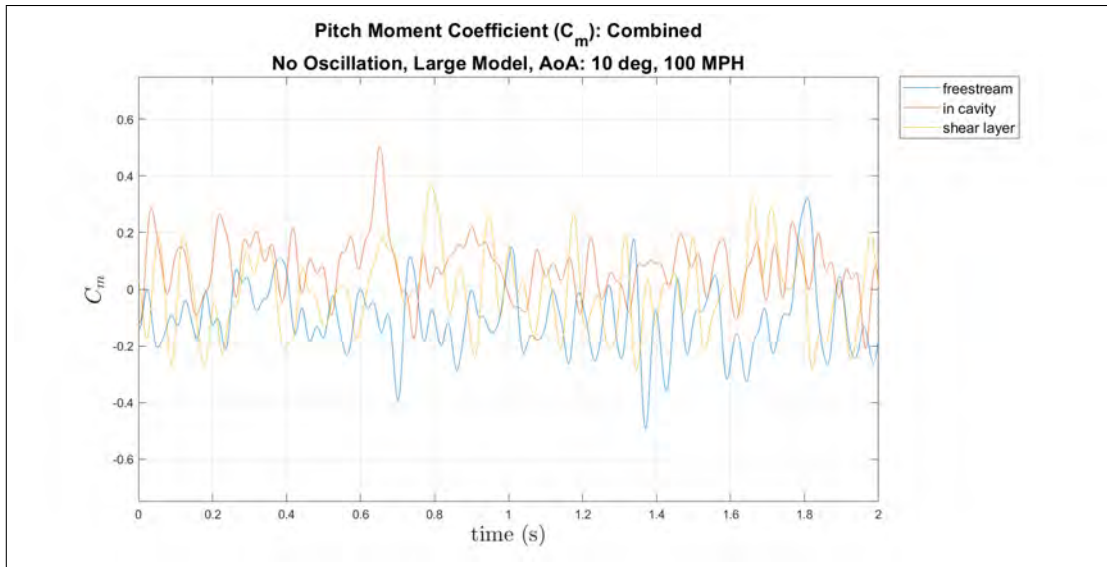


(a) Pitch Moment Coefficient, cavity apparatus, large model, 10° AoA, 60 MPH

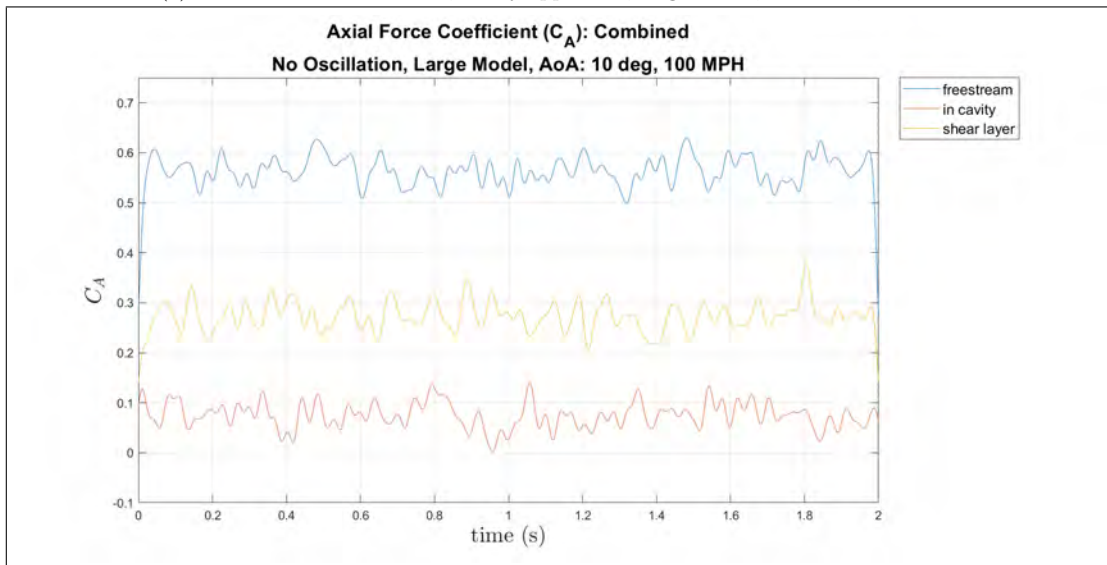


(b) Axial Force Coefficient, cavity apparatus, large model, 10° AoA, 60 MPH

Figure 98: Large model at 10° AoA of the pitch moment and axial force coefficients for the cavity apparatus, 60 MPH

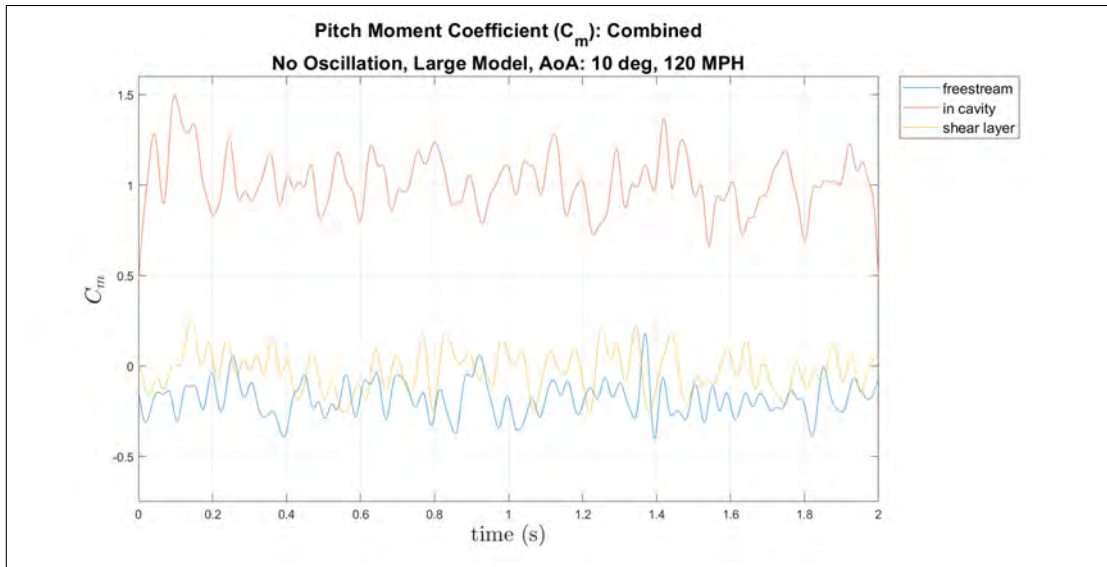


(a) Pitch Moment Coefficient, cavity apparatus, large model, 10° AoA, 100 MPH

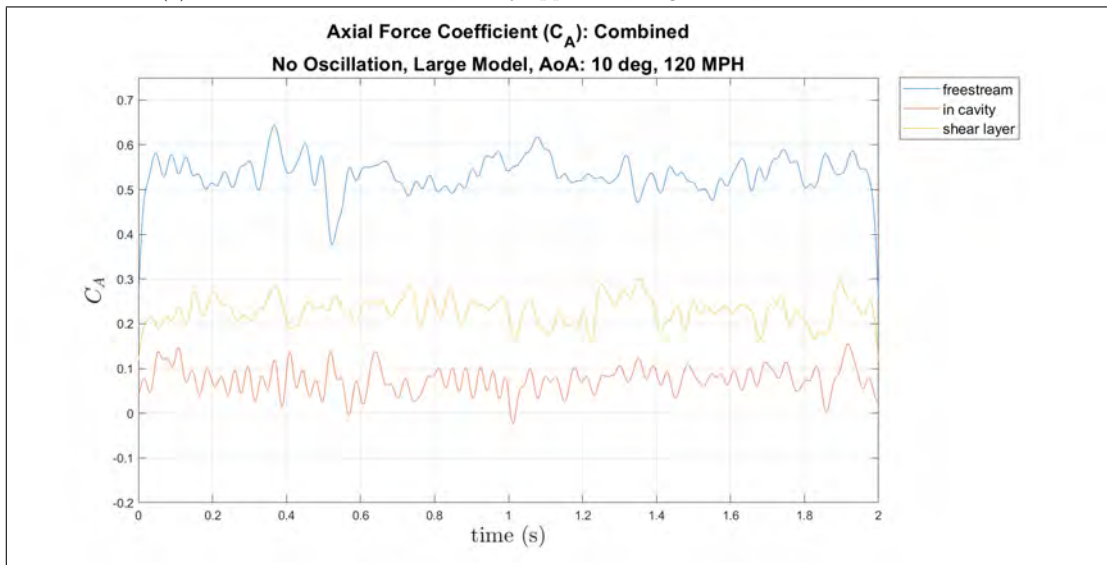


(b) Axial Force Coefficient, cavity apparatus, large model, 10° AoA, 100 MPH

Figure 99: Large model at 10° AoA of the pitch moment and axial force coefficients for the cavity apparatus, 100 MPH

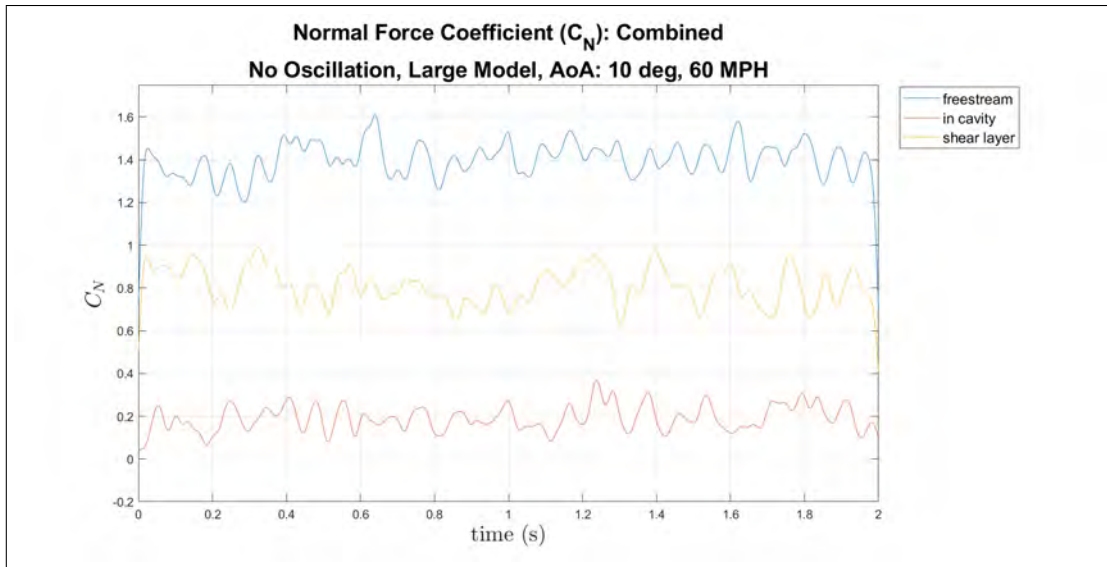


(a) Pitch Moment Coefficient, cavity apparatus, large model, 10° AoA, 120 MPH

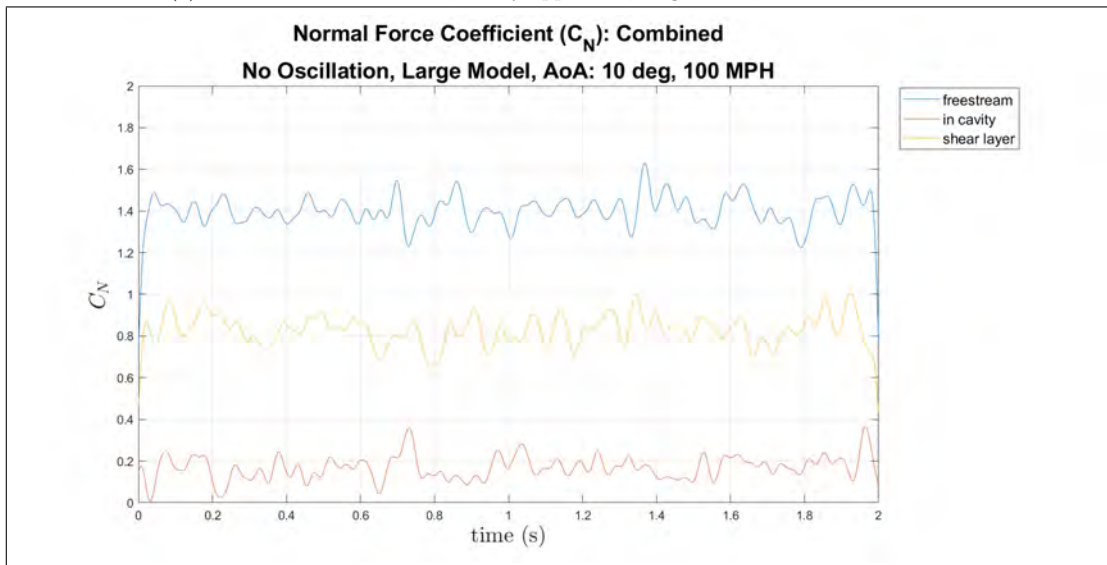


(b) Axial Force Coefficient, cavity apparatus, large model, 10° AoA, 120 MPH

Figure 100: Large model at 10° AoA of the pitch moment and axial force coefficients for the cavity apparatus, 120 MPH



(a) Normal Force Coefficient, cavity apparatus, large model, 10° AoA, 60 MPH



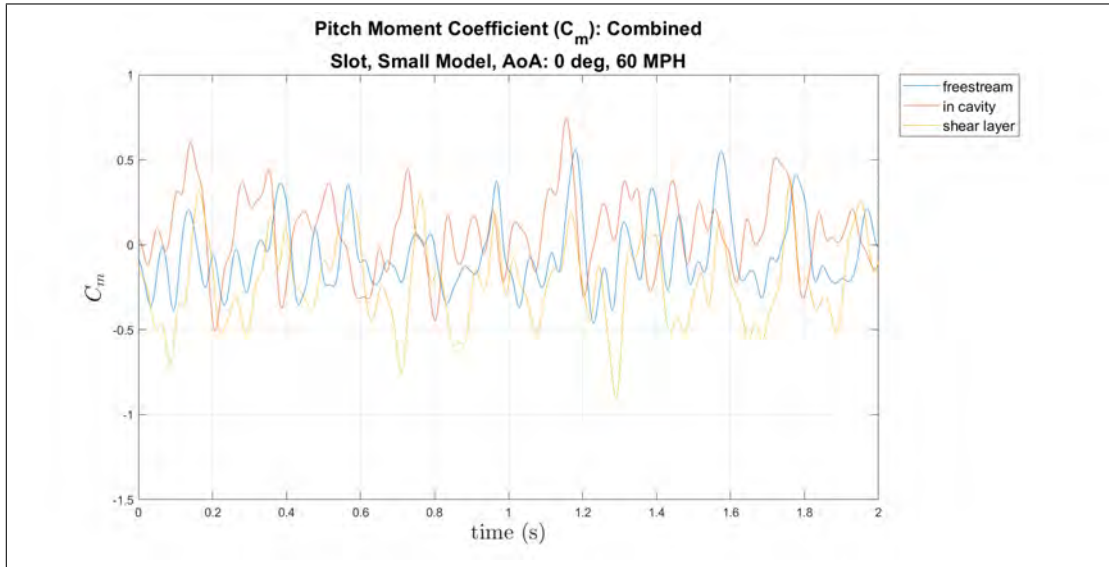
(b) Normal Force Coefficient, cavity apparatus, large model, 10° AoA, 100 MPH

Figure 101: Large model at 10° AoA of the normal force coefficients for the cavity apparatus, 60 MPH and 100 MPH

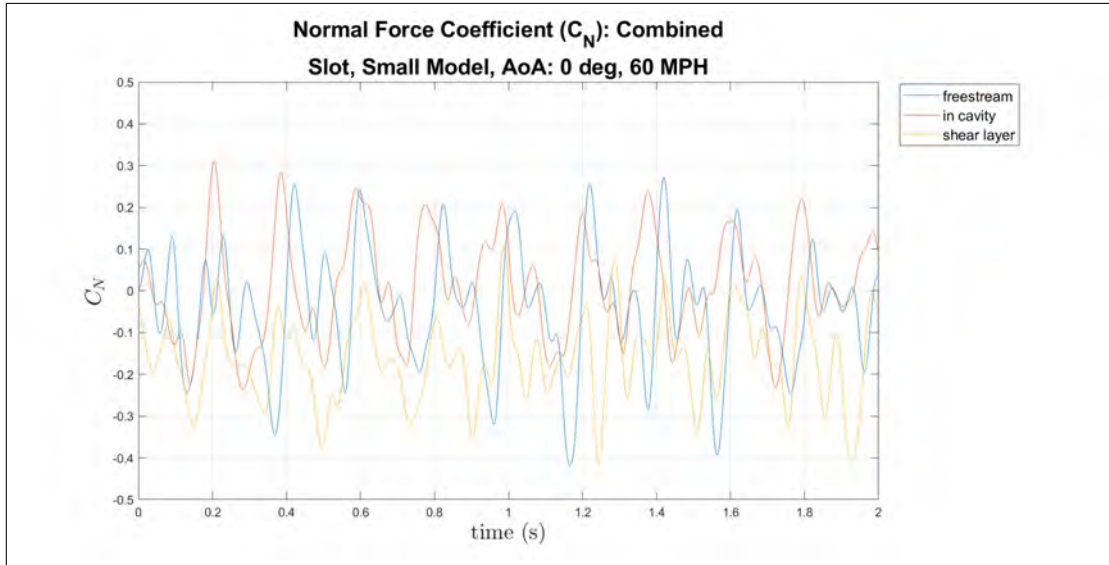
Phase I: Cavity Apparatus with Flow Control

Normal Force, Pitch Moment, and Axial Force Coefficients

Small Model, Slot, 0° AoA

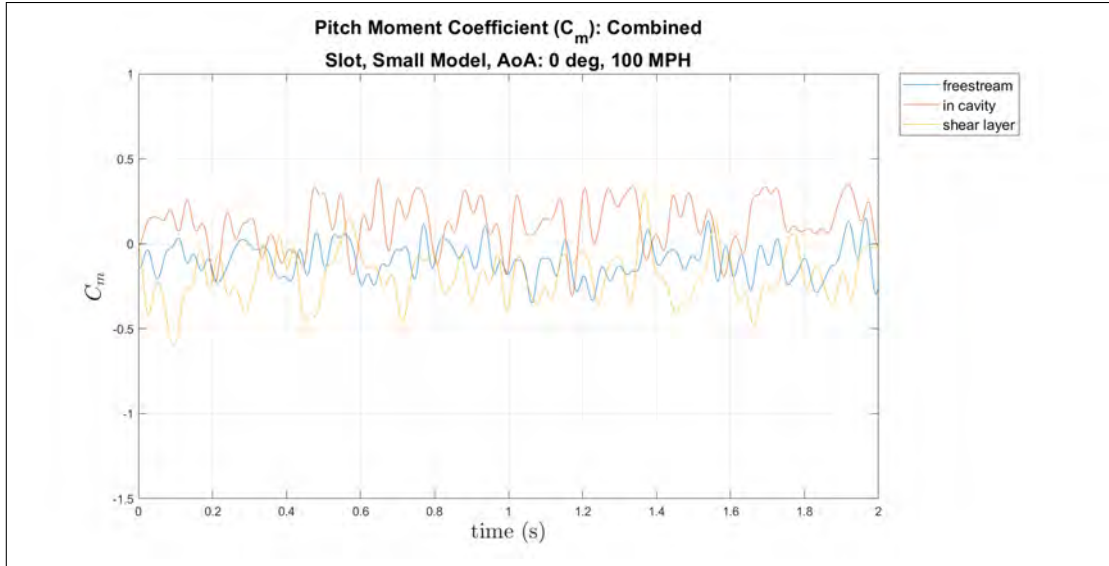


(a) Pitch Moment Coefficient, all positions, flow control, small model, 0° AoA, slot, 60 MPH

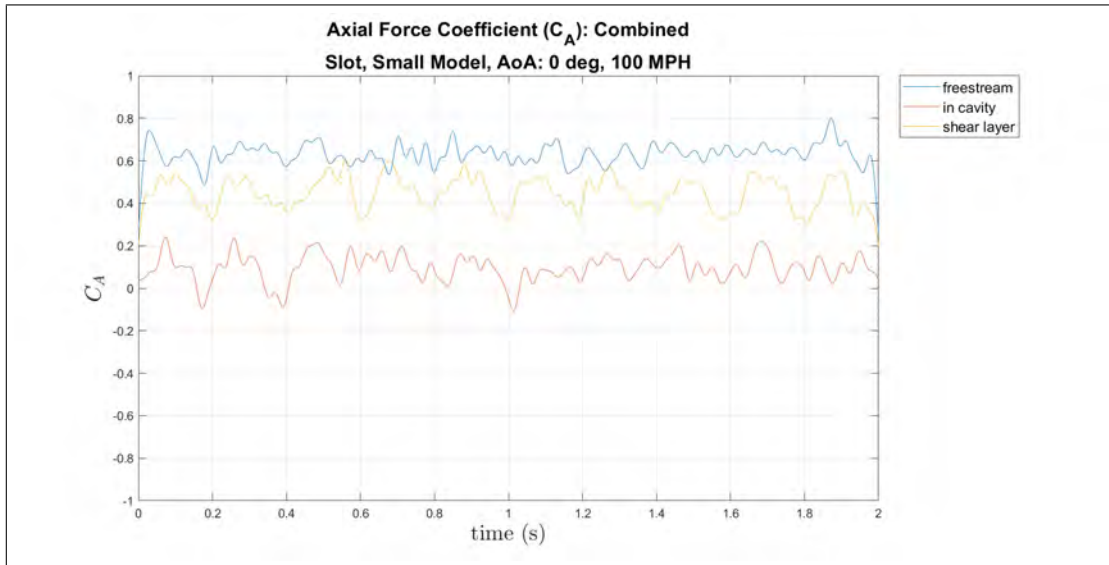


(b) Normal Force Coefficient, all positions, flow control, small model, 0° AoA, slot, 60 MPH

Figure 102: Small model at 0° AoA of the pitch moment and normal force coefficients for various positions, slot, 60 MPH

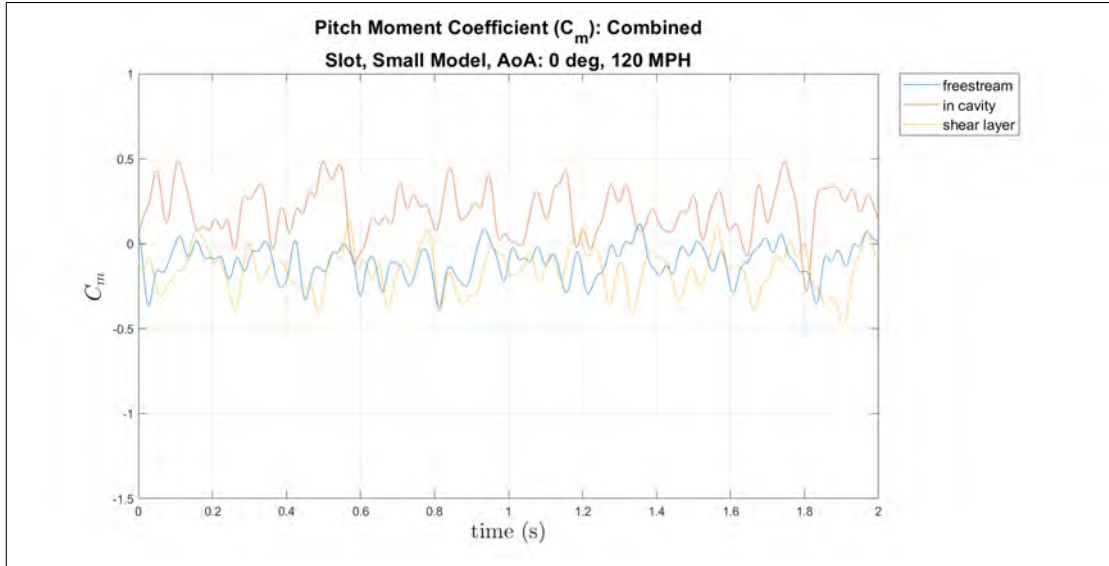


(a) Pitch Moment Coefficient, all positions, flow control, small model, 0° AoA, slot, 100 MPH

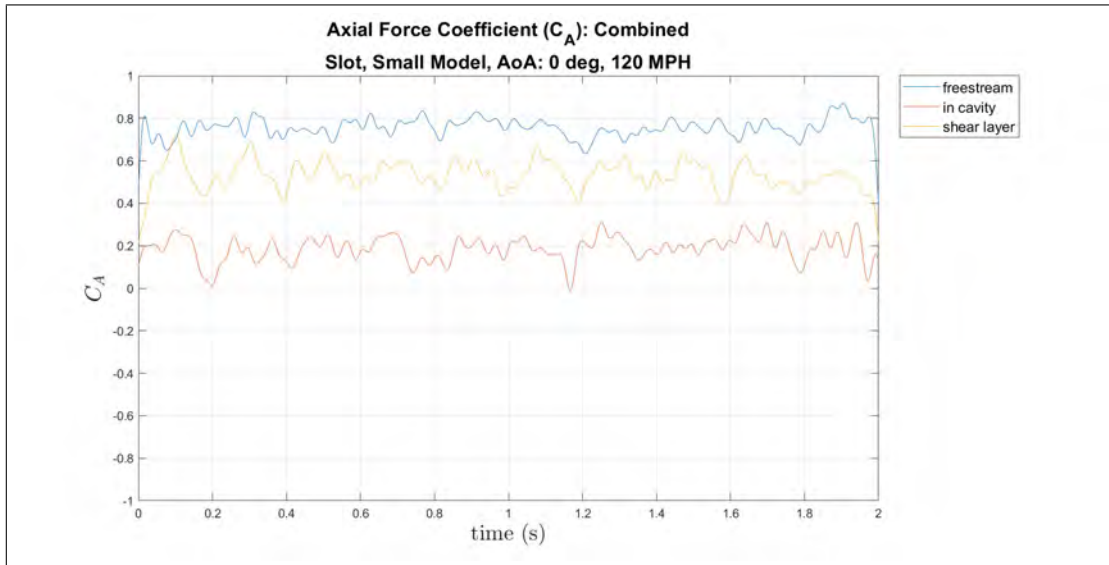


(b) Axial Force Coefficient, all positions, flow control, small model, 0° AoA, slot, 100 MPH

Figure 103: Small model at 0° AoA of the pitch moment and axial force coefficients for various positions, flow control, slot, 100 MPH

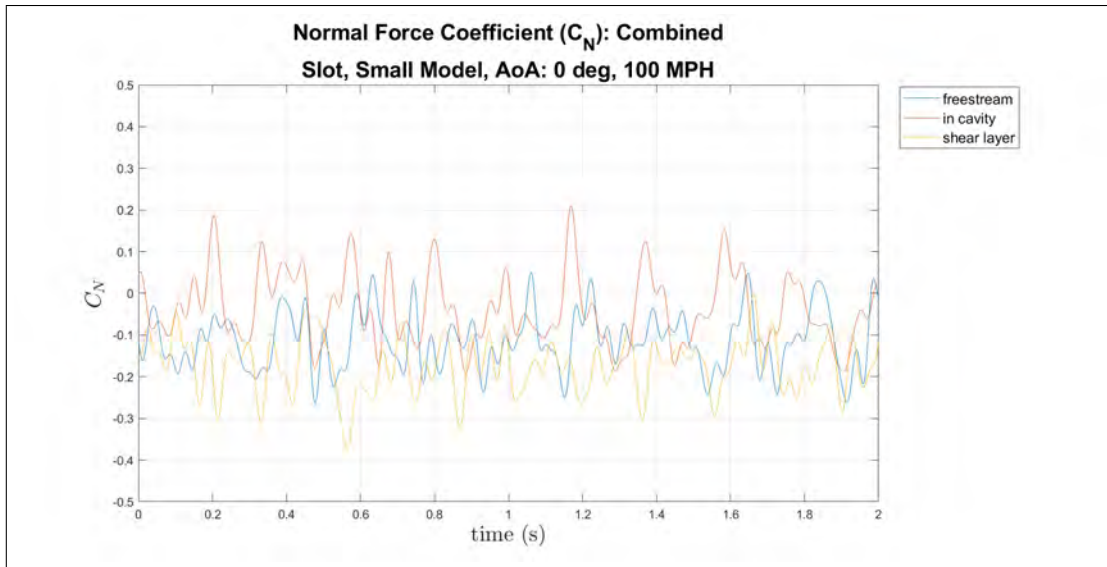


(a) Pitch Moment Coefficient, all positions, flow control, small model, 0° AoA, slot, 120 MPH

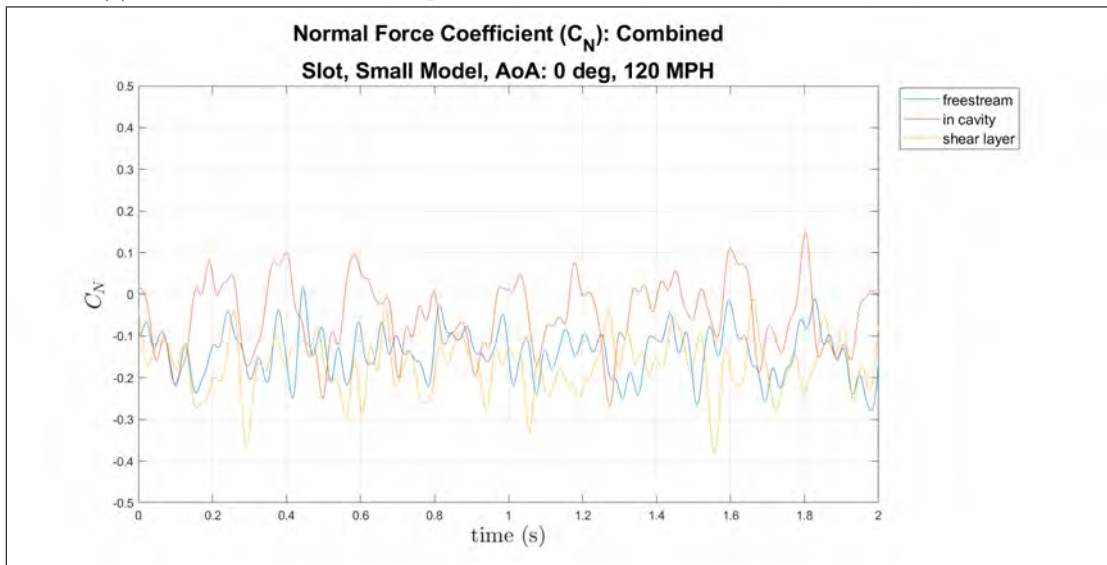


(b) Axial Force Coefficient, all positions, flow control, small model, 0° AoA, slot, 120 MPH

Figure 104: Small model at 0° AoA of the pitch moment and axial force coefficients for various positions, flow control, slot, 120 MPH



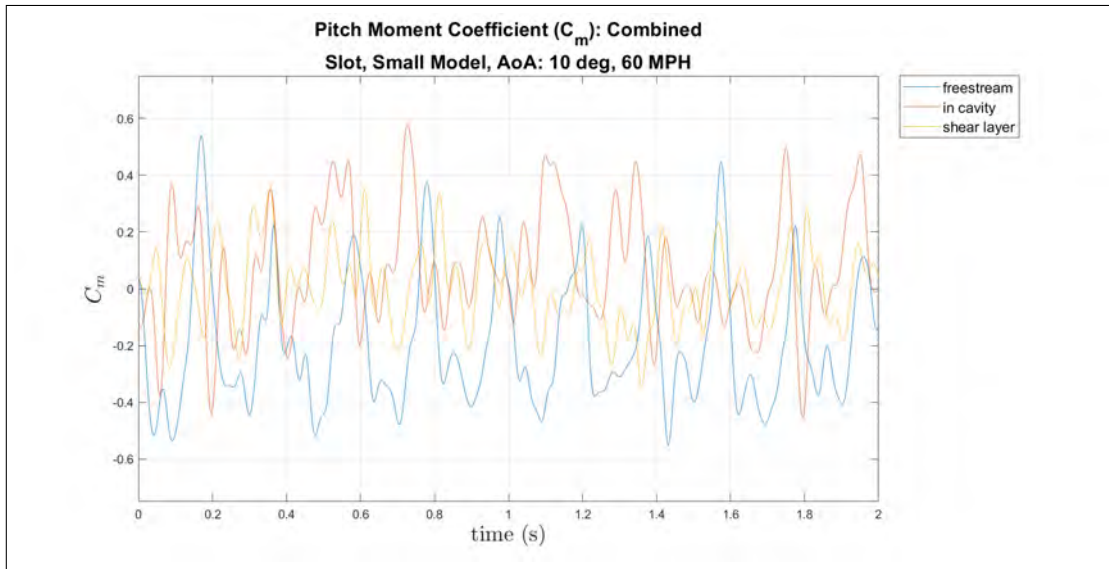
(a) Normal Force Coefficient, all positions, flow control, small model, 0° AoA, slot, 100 MPH



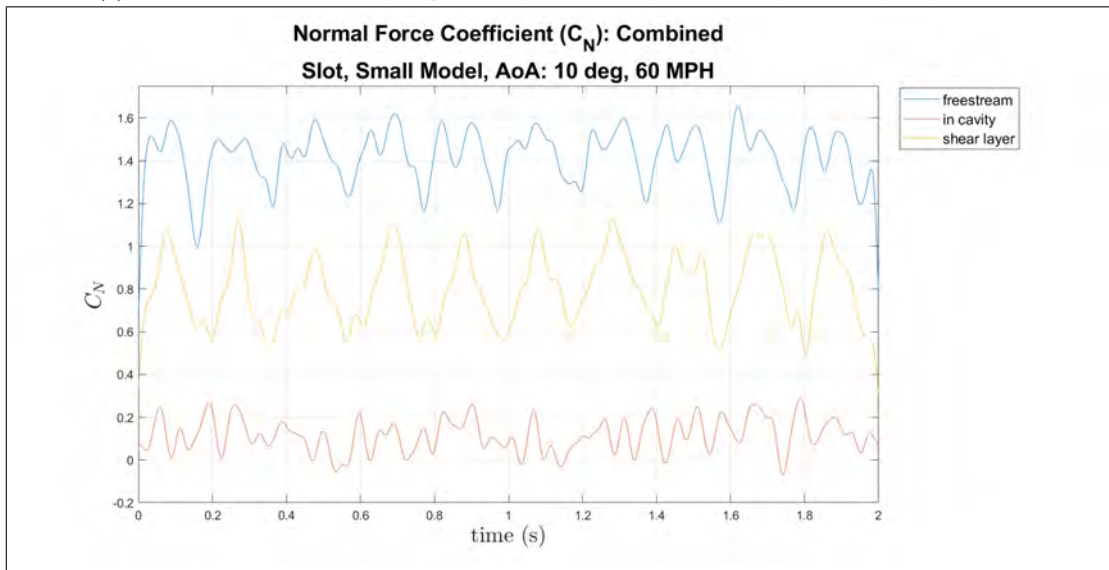
(b) Normal Force Coefficient, all positions, flow control, small model, 0° AoA, slot, 120 MPH

Figure 105: Small model at 0° AoA of the normal force coefficient for various positions, flow control, slot, 100 MPH and 120 MPH

Small Model, Slot, 10° AoA

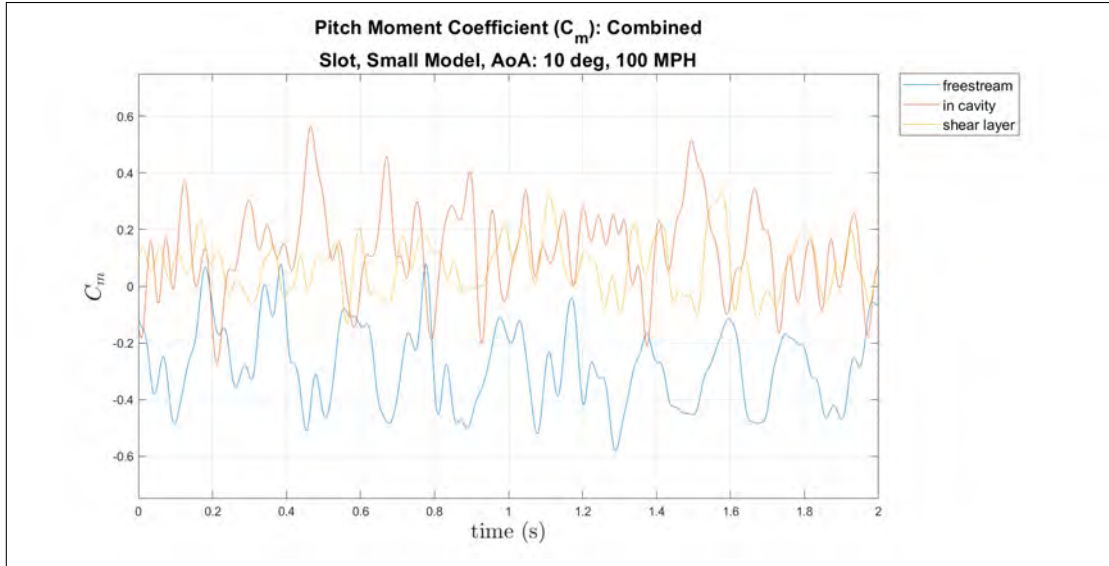


(a) Pitch Moment Coefficient, all positions, flow control, small model, 10° AoA, slot, 60 MPH

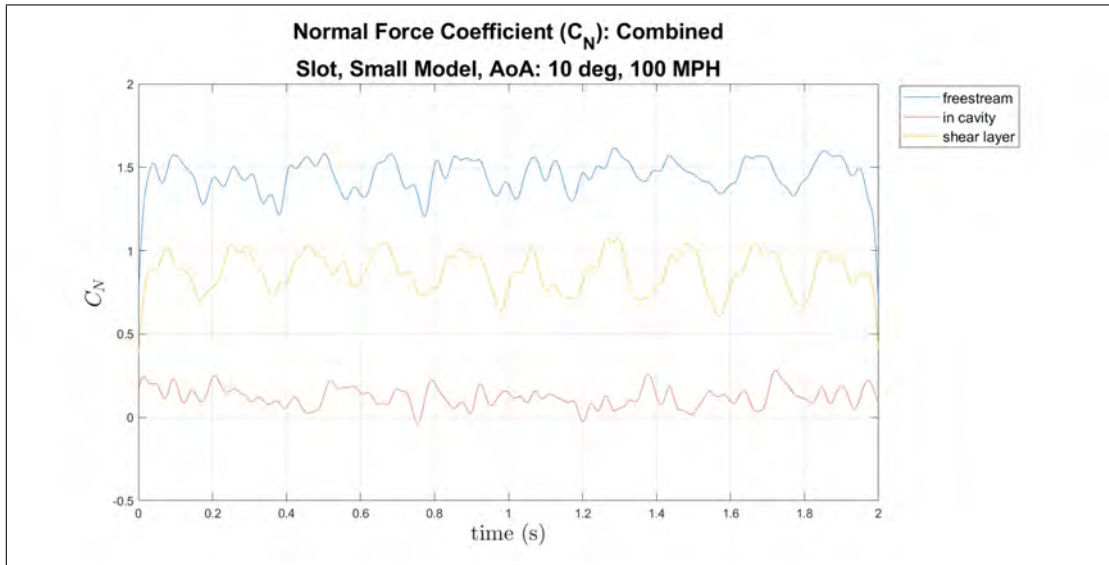


(b) Normal Force Coefficient, all positions, flow control, small model, 10° AoA, slot, 60 MPH

Figure 106: Small model at 10° AoA of the pitch moment and normal force coefficients for various positions, flow control, slot, 60 MPH

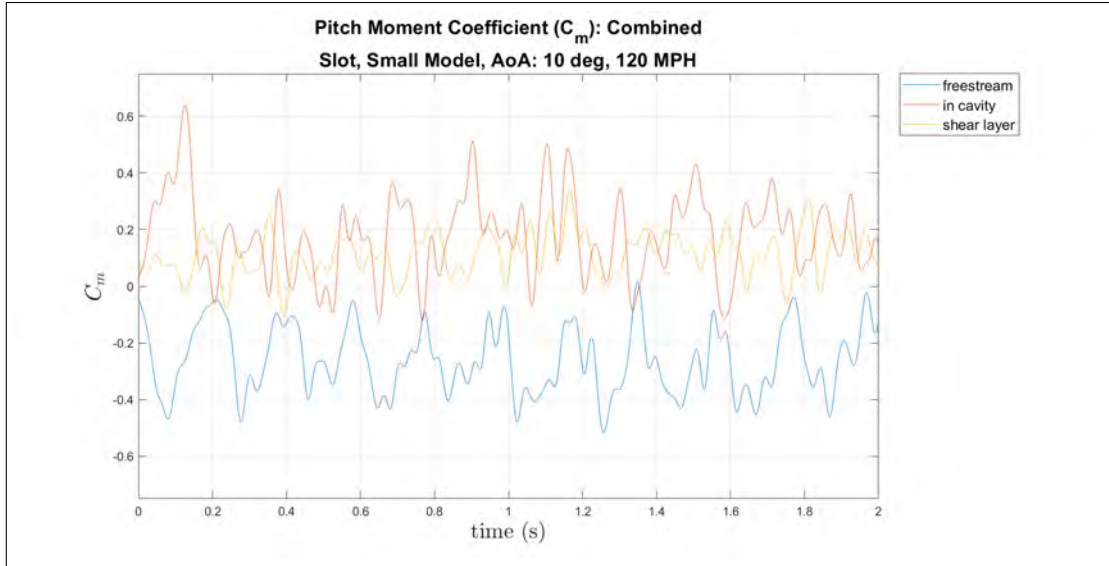


(a) Pitch Moment Coefficient, all positions, flow control, small model, 10° AoA, slot, 100 MPH

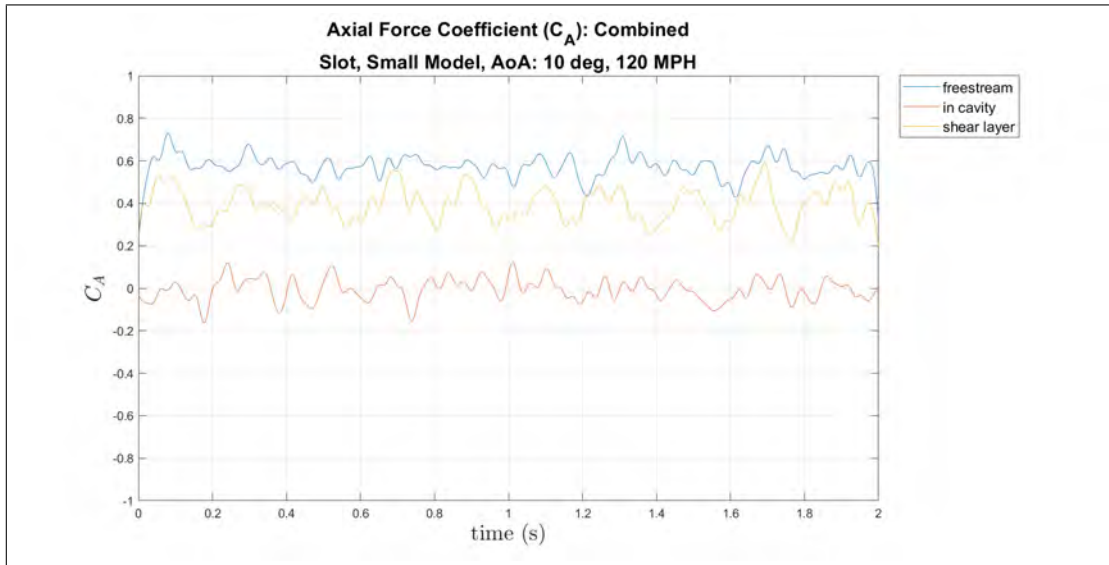


(b) Normal Force Coefficient, all positions, flow control, small model, 10° AoA, slot, 100 MPH

Figure 107: Small model at 10° AoA of the pitch moment and normal force coefficients for various positions, flow control, slot, 100 MPH



(a) Pitch Moment Coefficient, all positions, flow control, small model, 10° AoA, slot, 120 MPH



(b) Axial Force Coefficient, all positions, flow control, small model, 10° AoA, slot, 120 MPH

Figure 108: Small model at 10° AoA of the pitch moment and axial force coefficients for various positions, flow control, slot, 120 MPH

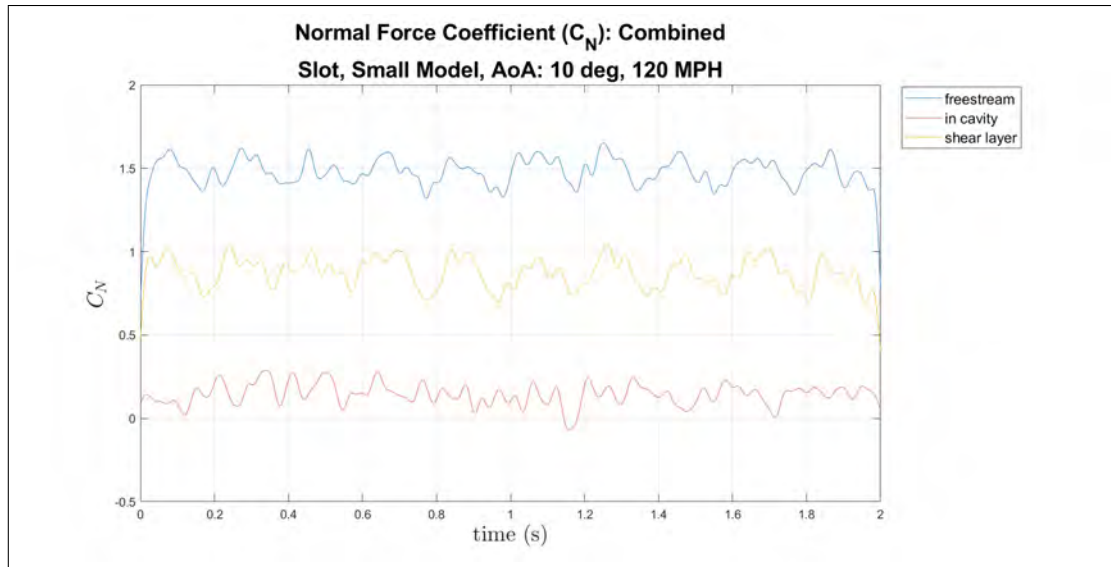
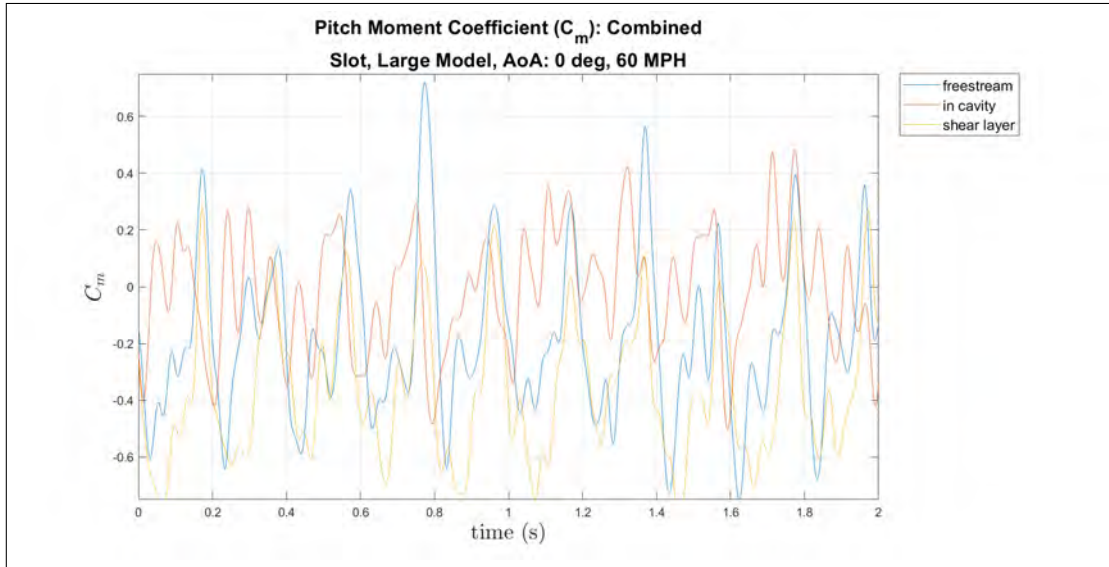
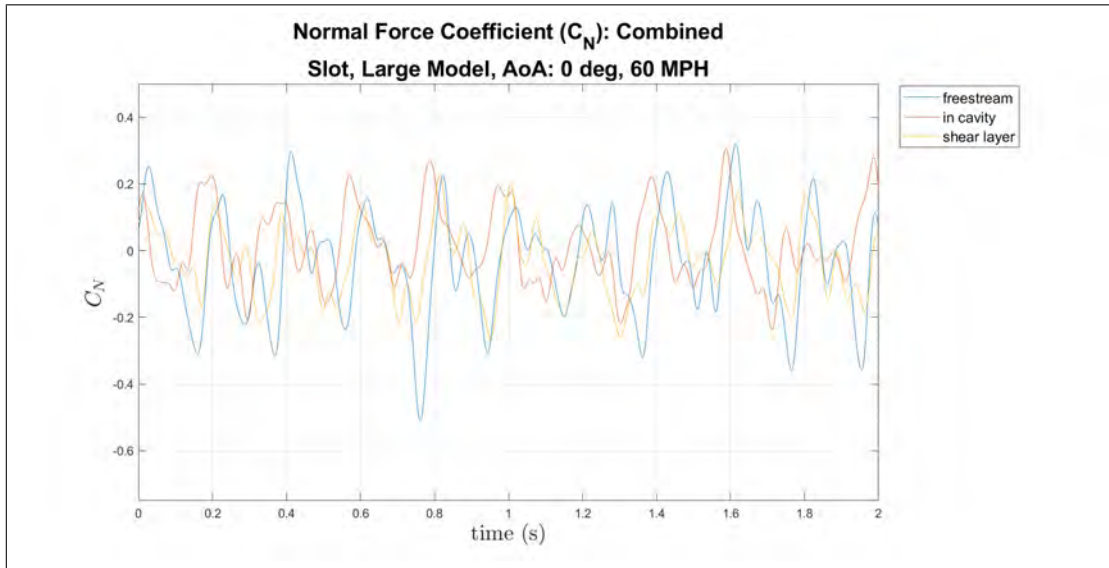


Figure 109: Normal Force Coefficient, all positions, flow control, small model, 10° AoA, slot, 120 MPH

Large Model, Slot, 0° AoA

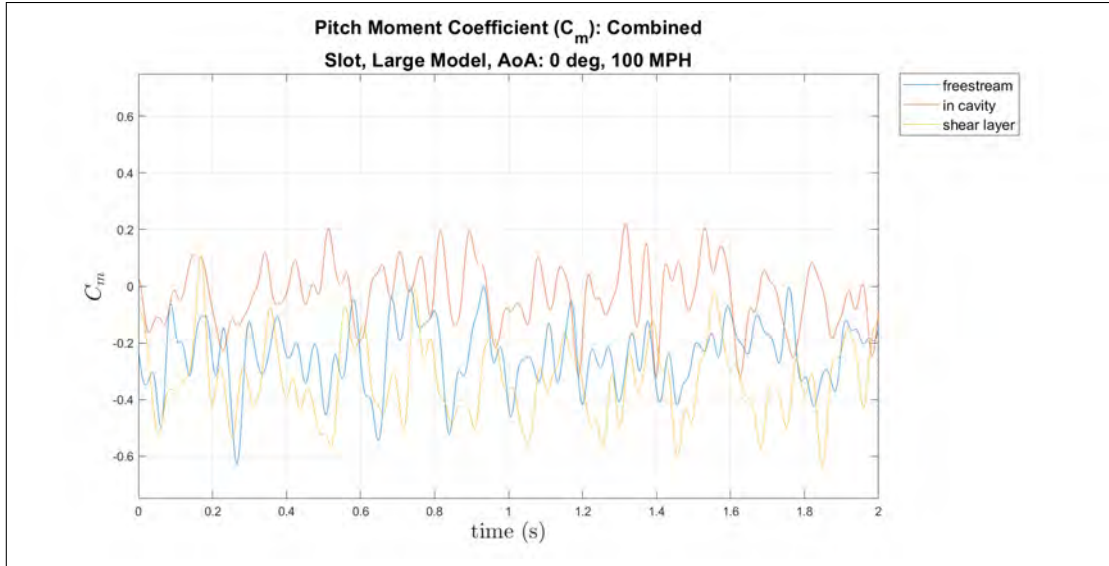


(a) Pitch Moment Coefficient, all positions, flow control, large model, 0° AoA, slot, 60 MPH

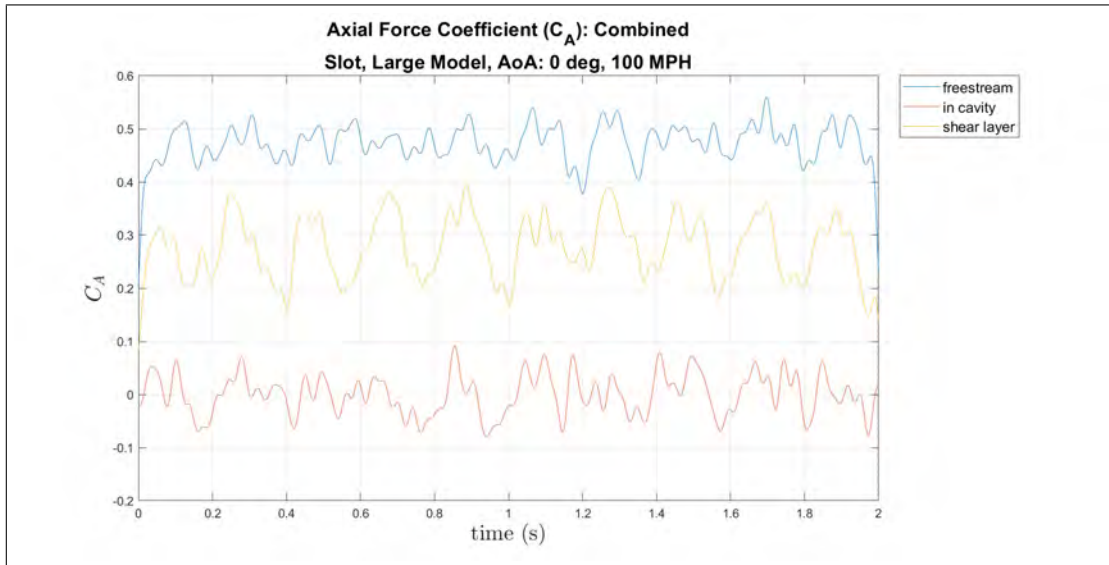


(b) Normal Force Coefficient, all positions, flow control, large model, 0° AoA, slot, 60 MPH

Figure 110: Large model at 0° AoA of the pitch moment and normal force coefficients for various positions, flow control, slot, 60 MPH

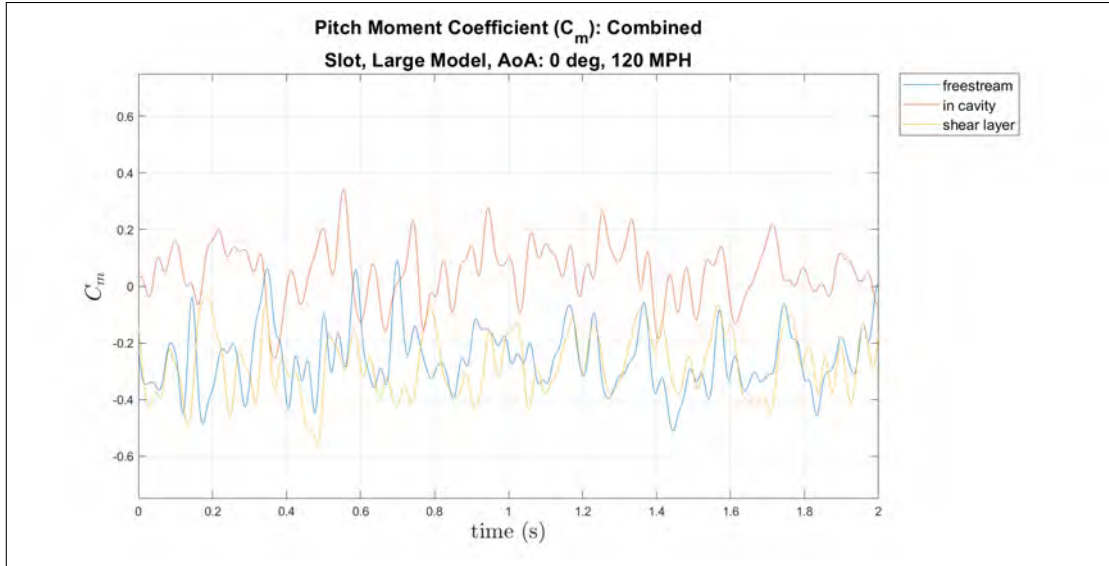


(a) Pitch Moment Coefficient, all positions, flow control, large model, 0° AoA, slot, 100 MPH

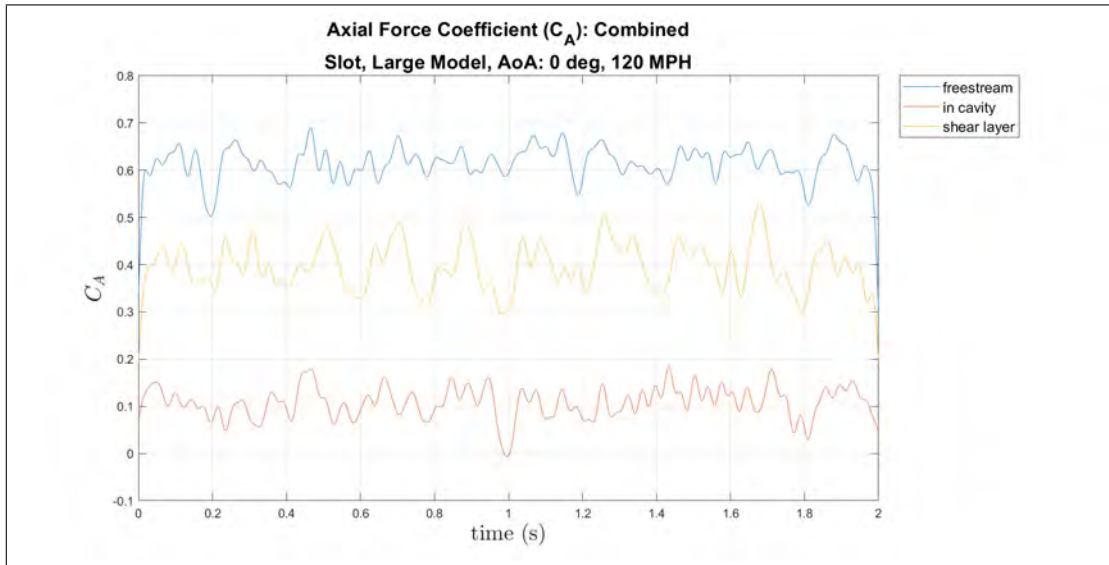


(b) Axial Force Coefficient, all positions, flow control, large model, 0° AoA, slot, 100 MPH

Figure 111: Large model at 0° AoA of the pitch moment and axial force coefficients for various positions, flow control, slot, 100 MPH

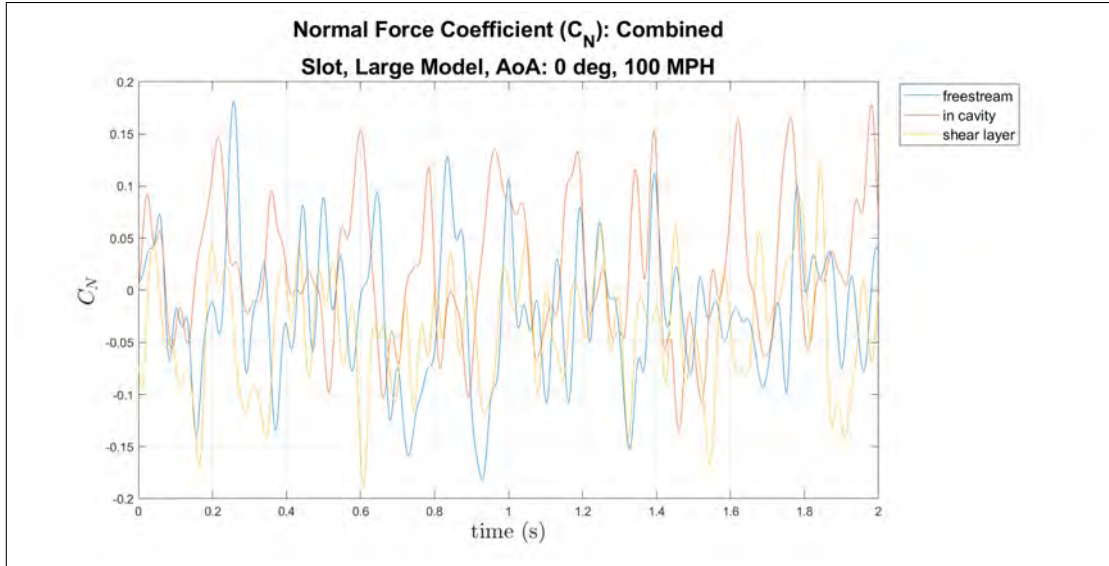


(a) Pitch Moment Coefficient, all positions, flow control, large model, 0° AoA, slot, 120 MPH

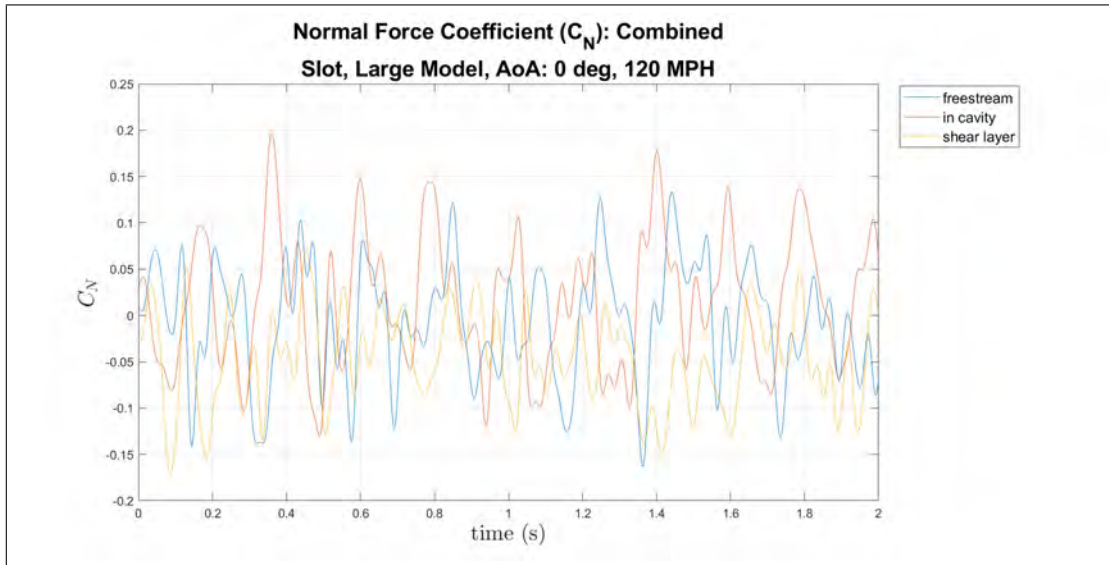


(b) Axial Force Coefficient, all positions, flow control, large model, 0° AoA, slot, 120 MPH

Figure 112: Large model at 0° AoA of the pitch moment and axial force coefficients for various positions, flow control, slot, 120 MPH



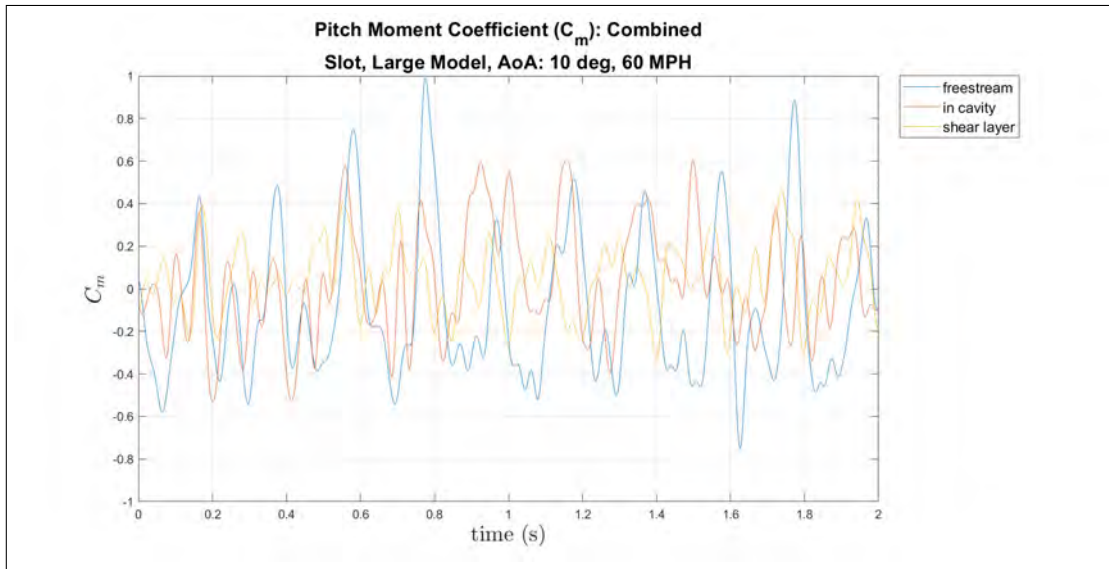
(a) Normal Force Coefficient, all positions, flow control, large model, 0° AoA, slot, 100 MPH



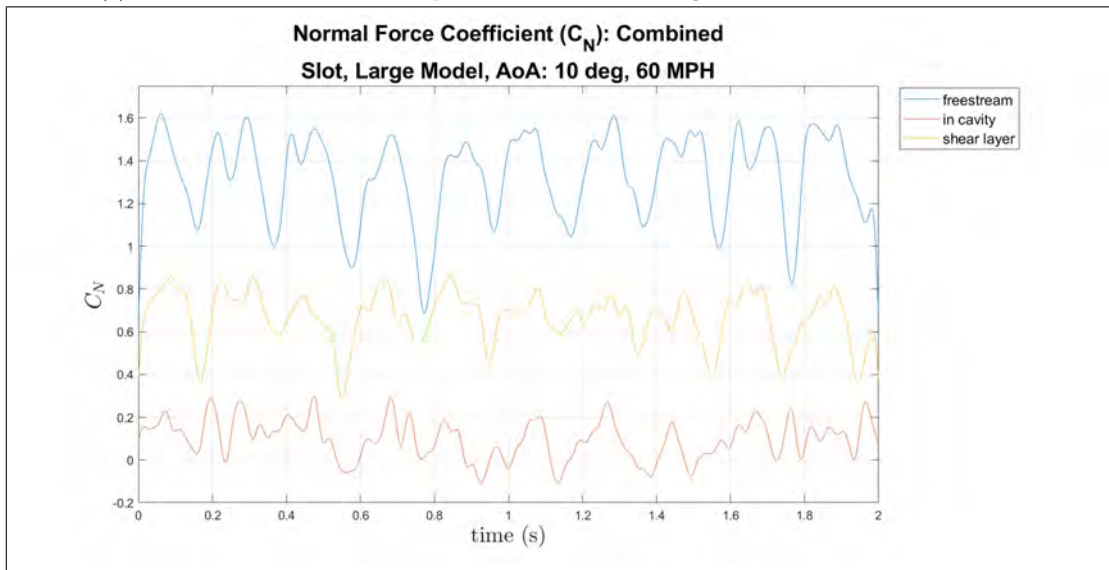
(b) Normal Force Coefficient, all positions, flow control, large model, 0° AoA, slot, 120 MPH

Figure 113: Large model at 0° AoA of the normal force coefficient for various positions, flow control, slot, 100 MPH and 120 MPH

Large Model, Slot, 10° AoA

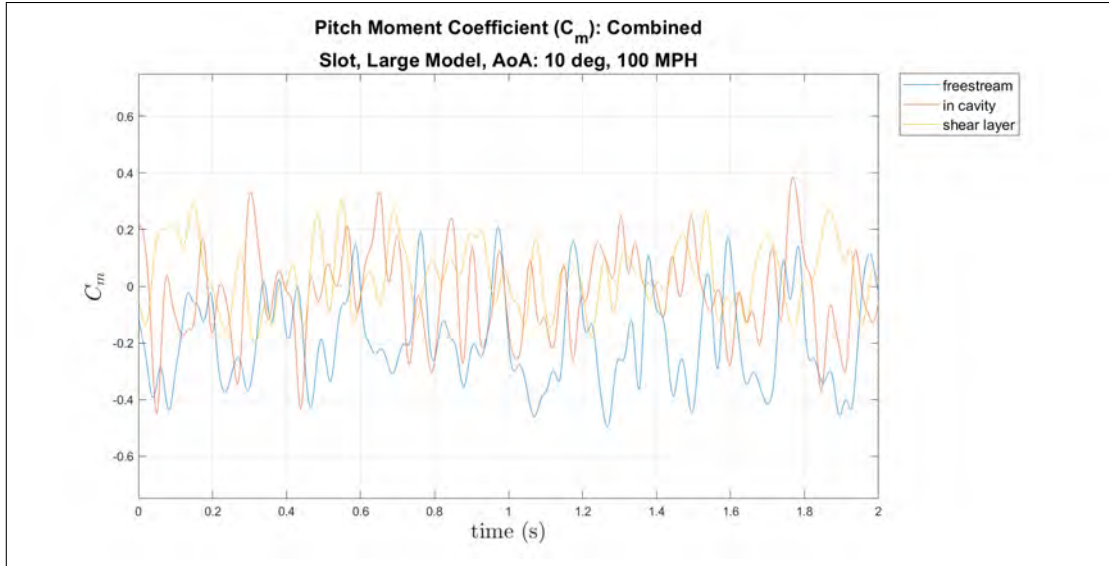


(a) Pitch Moment Coefficient, all positions, flow control, large model, 10° AoA, slot, 60 MPH

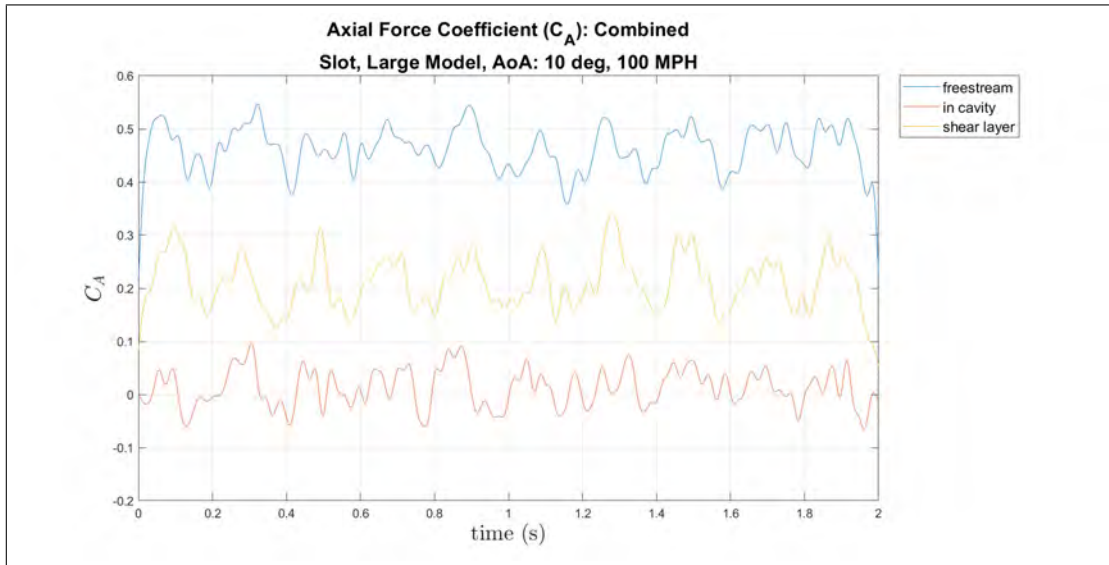


(b) Normal Force Coefficient, all positions, flow control, large model, 10° AoA, slot, 60 MPH

Figure 114: Large model at 10° AoA of the pitch moment and normal force coefficients for various positions, flow control, slot, 60 MPH

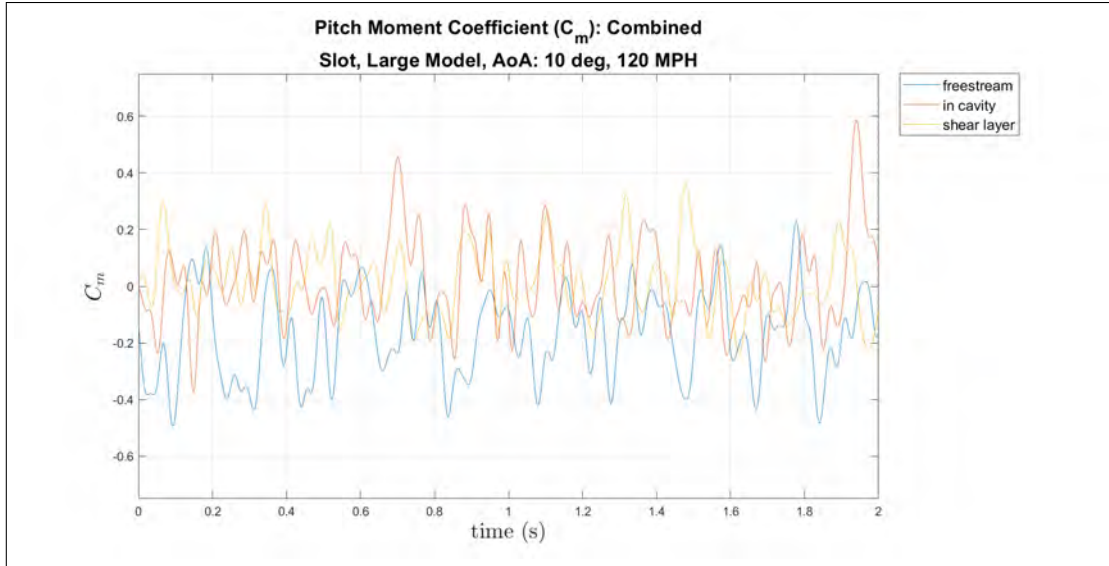


(a) Pitch Moment Coefficient, all positions, flow control, large model, 10° AoA, slot, 100 MPH

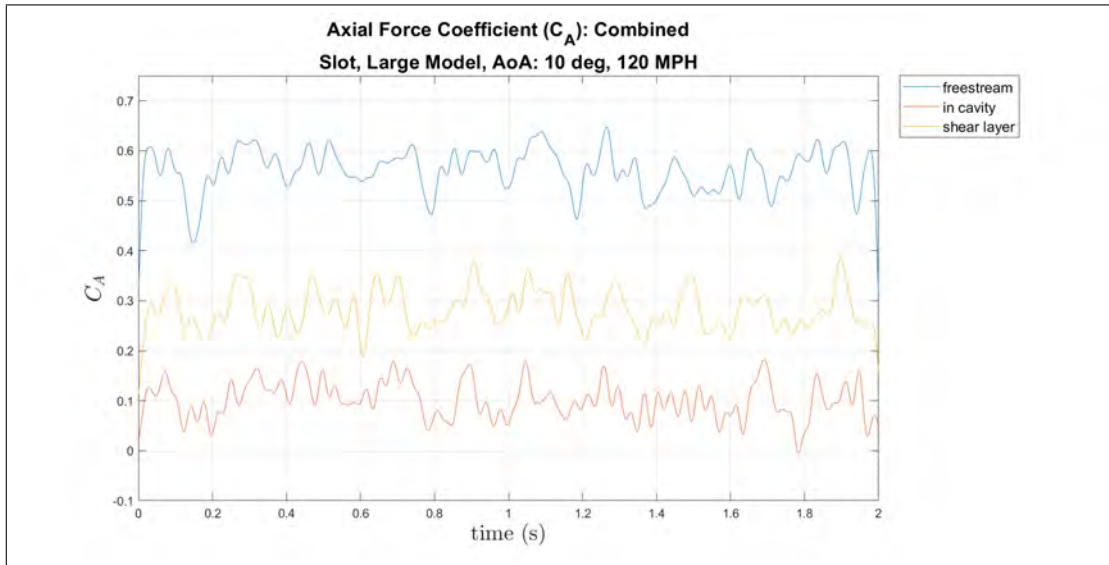


(b) Axial Force Coefficient, all positions, flow control, large model, 10° AoA, slot, 100 MPH

Figure 115: Large model at 10° AoA of the pitch moment and axial force coefficients for various positions, flow control, slot, 100 MPH

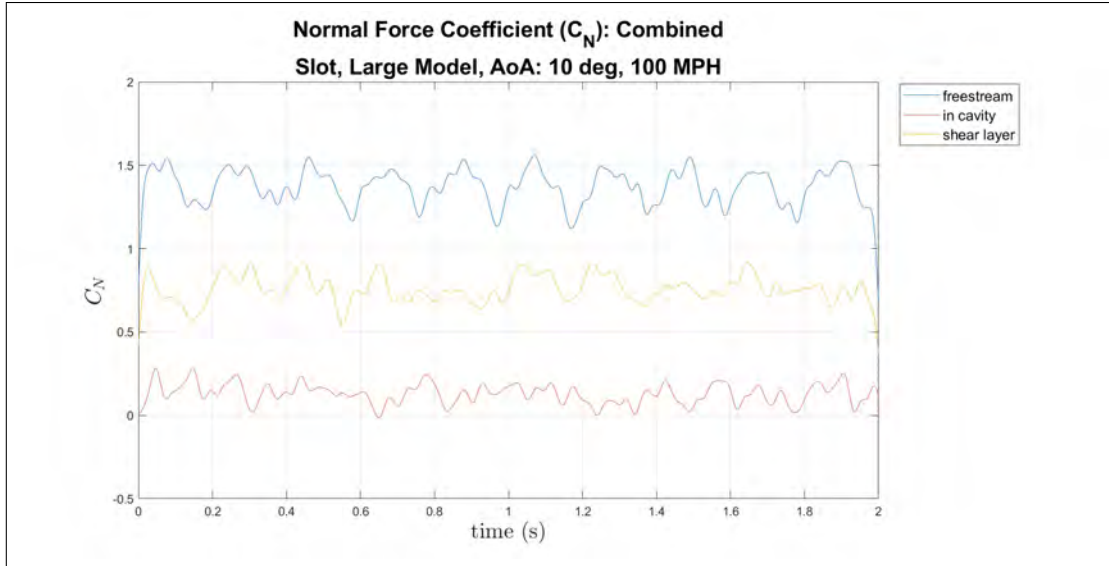


(a) Pitch Moment Coefficient, all positions, flow control, large model, 10° AoA, slot, 120 MPH

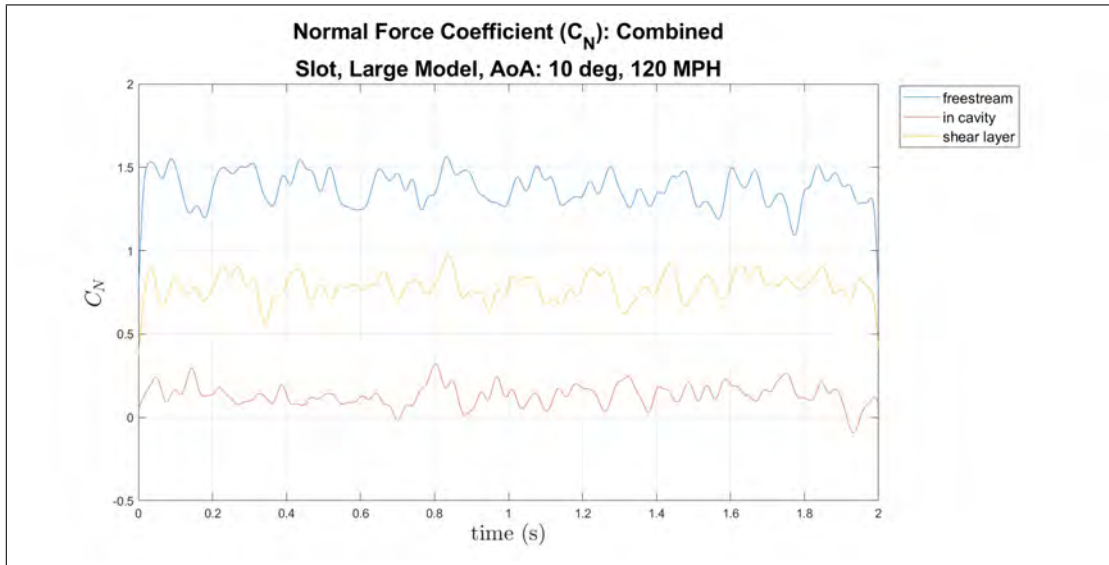


(b) Axial Force Coefficient, all positions, flow control, large model, 10° AoA, slot, 120 MPH

Figure 116: Large model at 10° AoA of the pitch moment and axial force coefficients for various positions, flow control, slot, 120 MPH



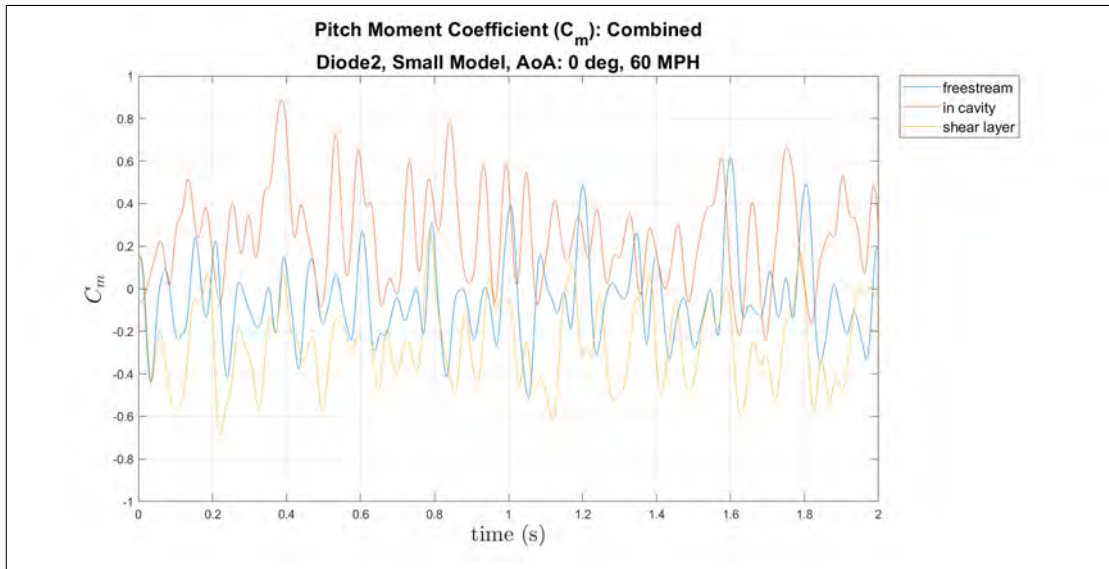
(a) Normal Force Coefficient, all positions, flow control, large model, 10° AoA, slot, 100 MPH



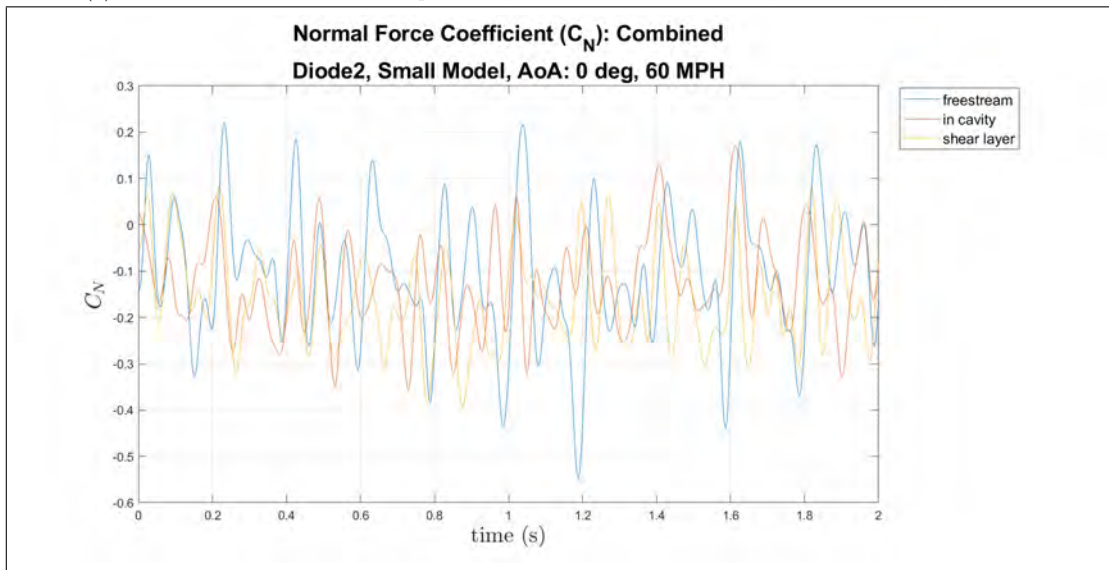
(b) Normal Force Coefficient, all positions, flow control, large model, 10° AoA, slot, 120 MPH

Figure 117: Large model at 10° AoA of the normal force coefficients for various positions, flow control, slot, 100 MPH and 120 MPH

Small Model, Diode 2, 0° AoA

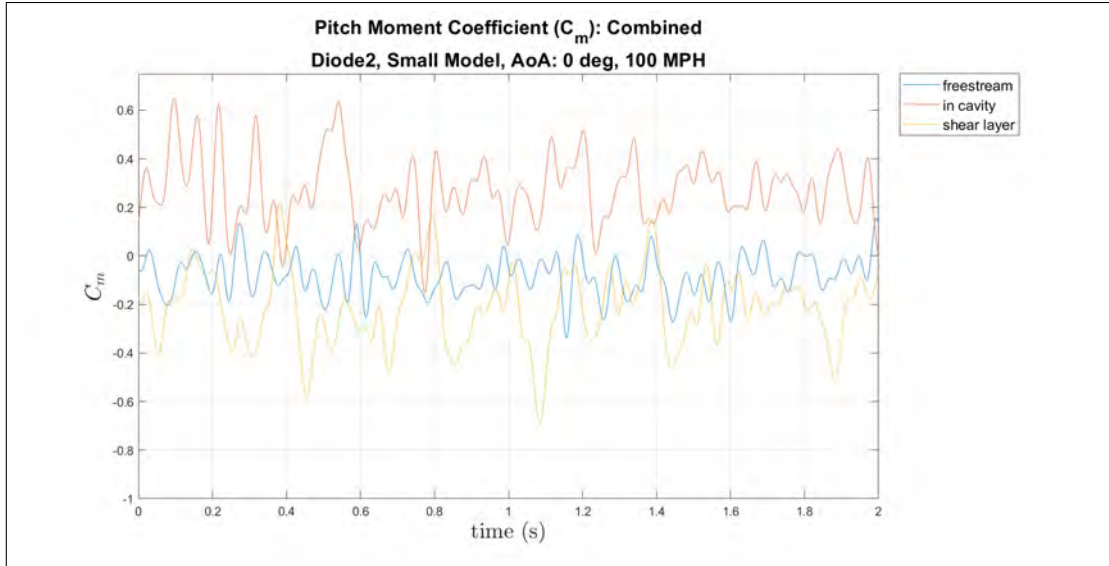


(a) Pitch Moment Coefficient, all positions, flow control, small model, 0° AoA, diode 2, 60 MPH

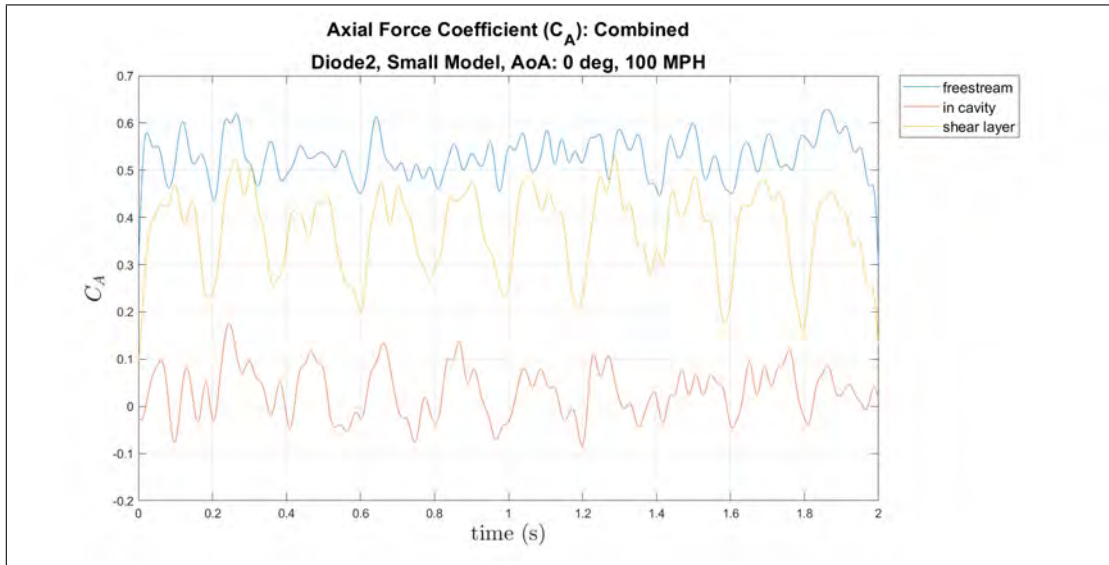


(b) Normal Force Coefficient, all positions, flow control, small model, 0° AoA, diode 2, 60 MPH

Figure 118: Small model at 0° AoA of the pitch moment and normal force coefficients for various positions, flow control, diode 2, 60 MPH

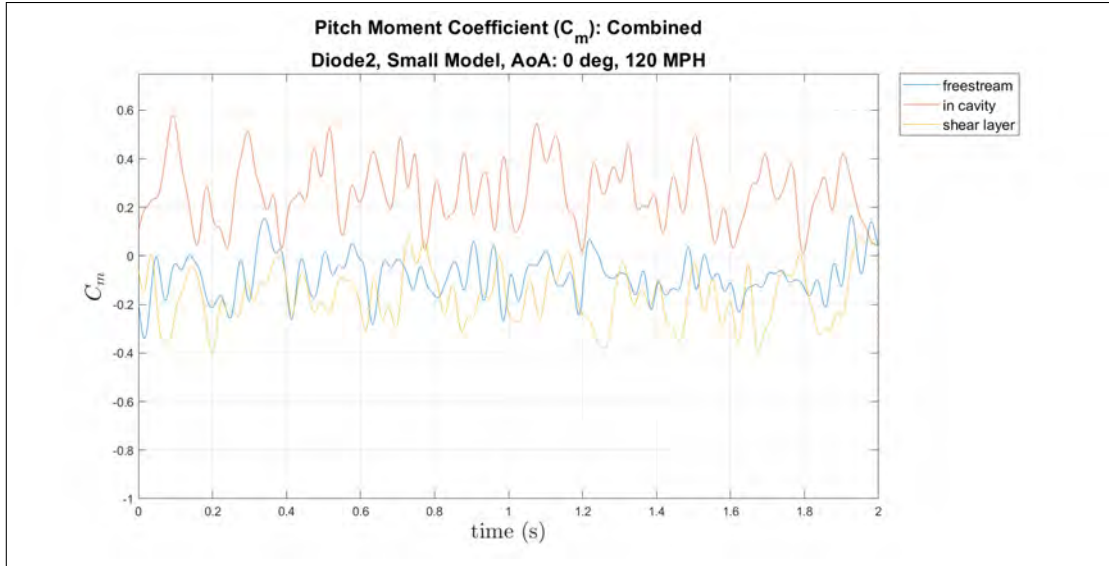


(a) Pitch Moment Coefficient, all positions, flow control, small model, 0° AoA, diode 2, 100 MPH

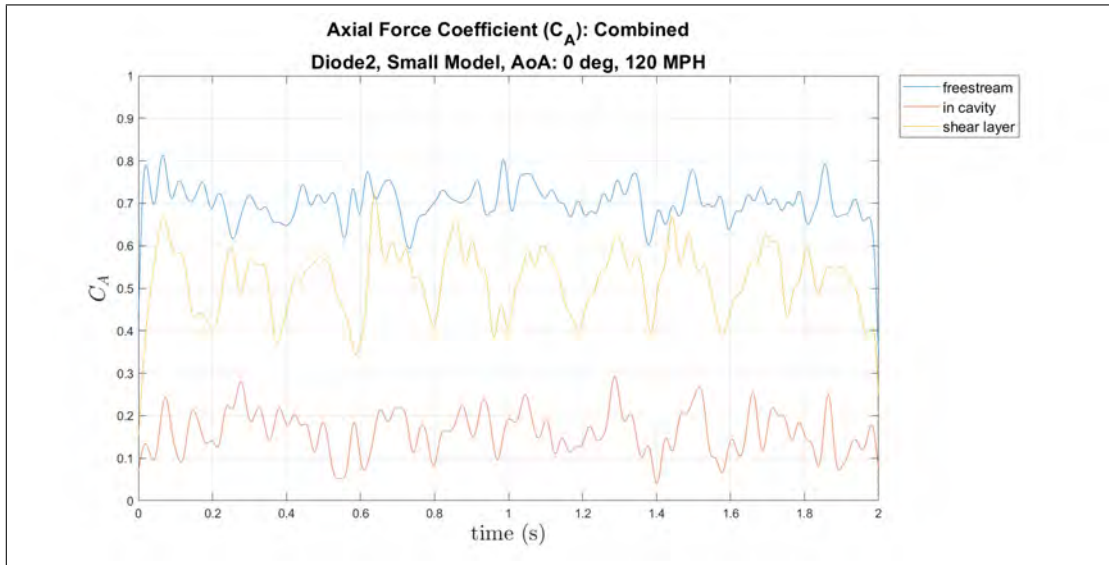


(b) Axial Force Coefficient, all positions, flow control, small model, 0° AoA, diode 2, 100 MPH

Figure 119: Small model at 0° AoA of the pitch moment and axial force coefficients for various positions, flow control, diode 2, 100 MPH

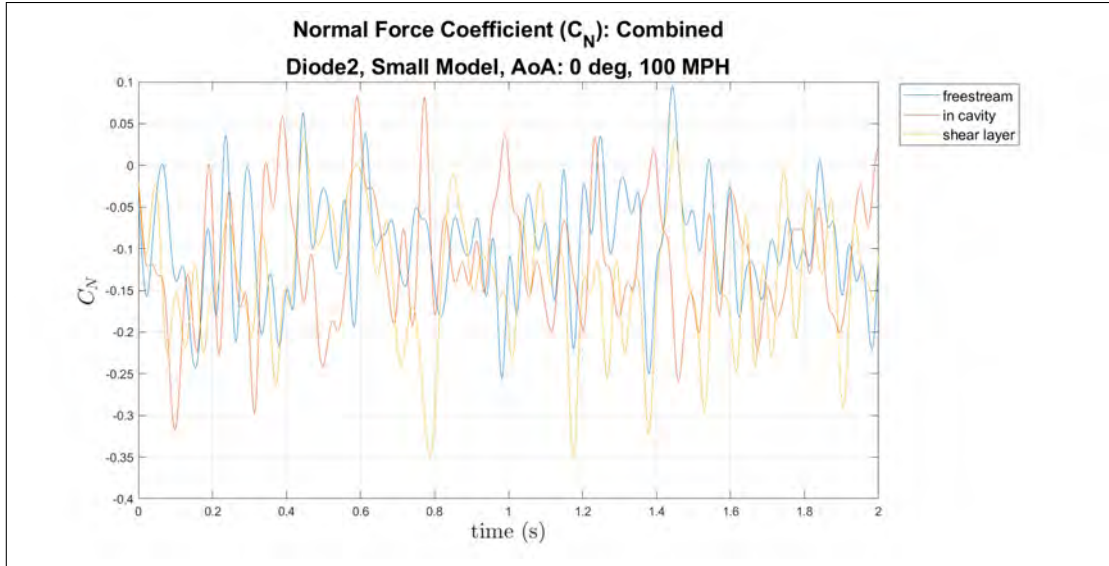


(a) Pitch Moment Coefficient, all positions, flow control, small model, 0° AoA, diode 2, 120 MPH

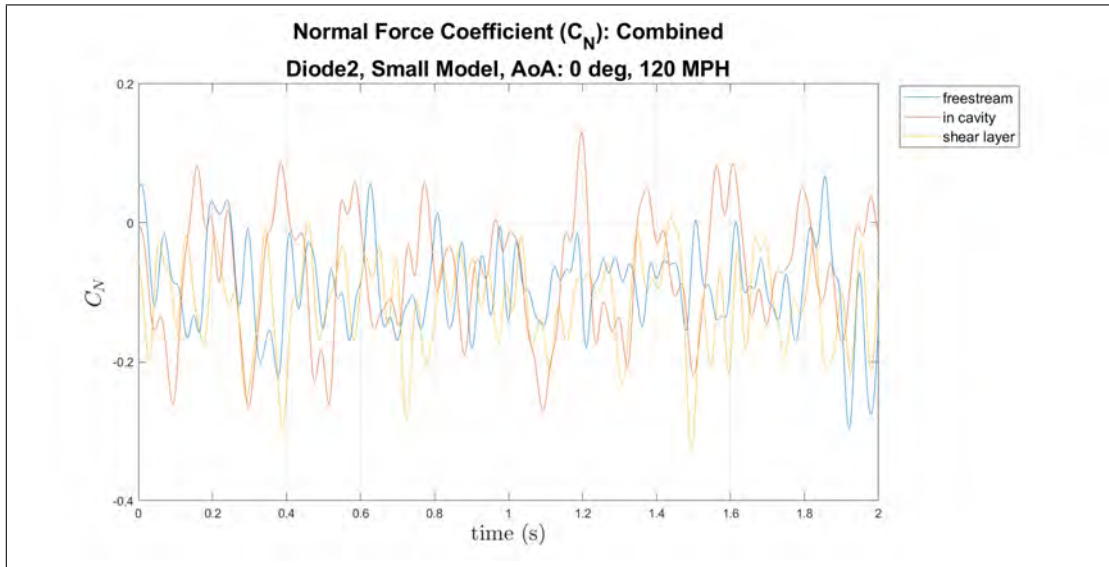


(b) Axial Force Coefficient, all positions, flow control, small model, 0° AoA, diode 2, 120 MPH

Figure 120: Small model at 0° AoA of the pitch moment and axial force coefficients for various positions, flow control, diode 2, 120 MPH



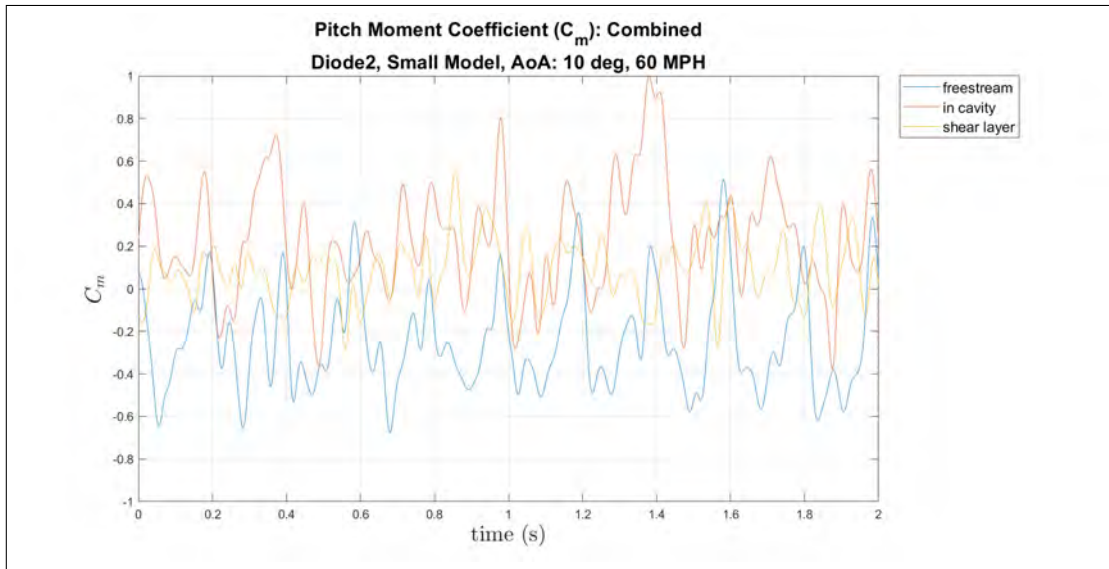
(a) Normal Force Coefficient, all positions, flow control, small model, 0° AoA, diode 2, 100 MPH



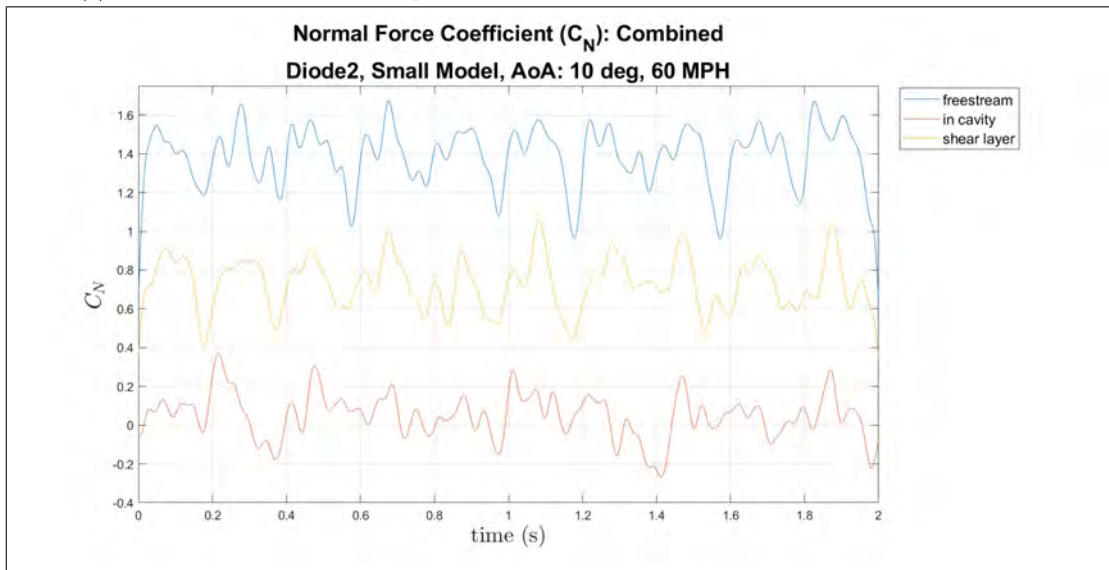
(b) Normal Force Coefficient, all positions, flow control, small model, 0° AoA, diode 2, 120 MPH

Figure 121: Small model at 0° AoA of the normal force coefficient for various positions, flow control, diode 2, 100 MPH and 120 MPH

Small Model, Diode 2, 10° AoA

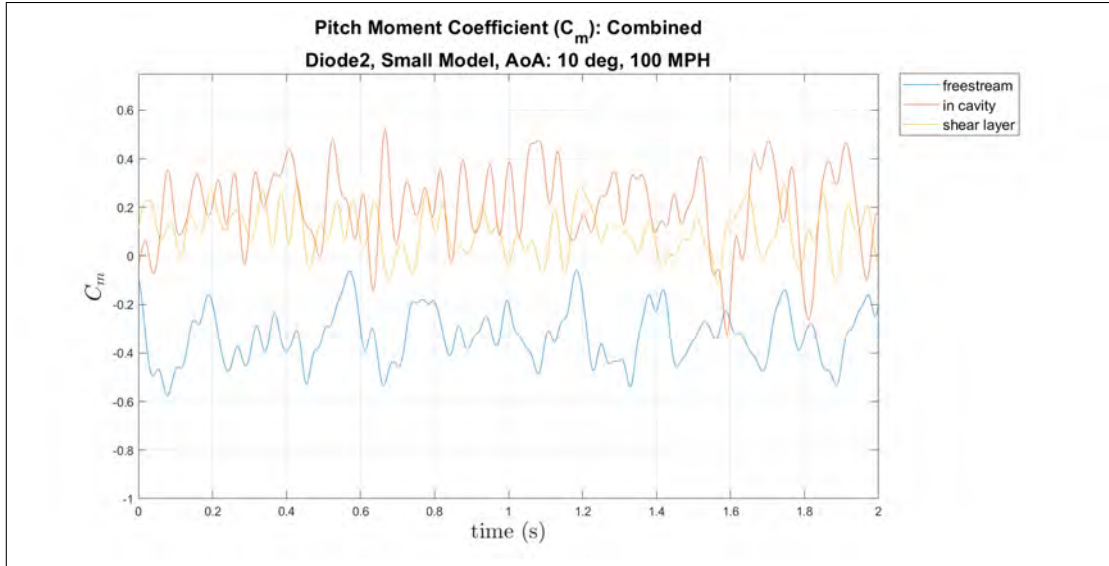


(a) Pitch Moment Coefficient, all positions, flow control, small model, 10° AoA, diode 2, 60 MPH

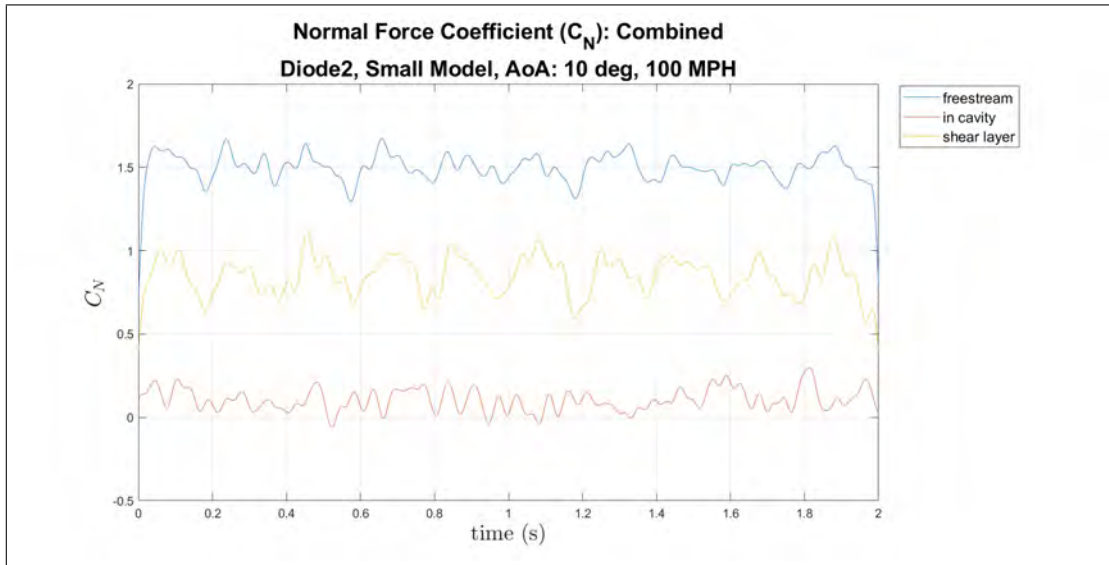


(b) Normal Force Coefficient, all positions, flow control, small model, 10° AoA, diode 2, 60 MPH

Figure 122: Small model at 10° AoA of the pitch moment and normal force coefficients for various positions, flow control, diode 2, 60 MPH

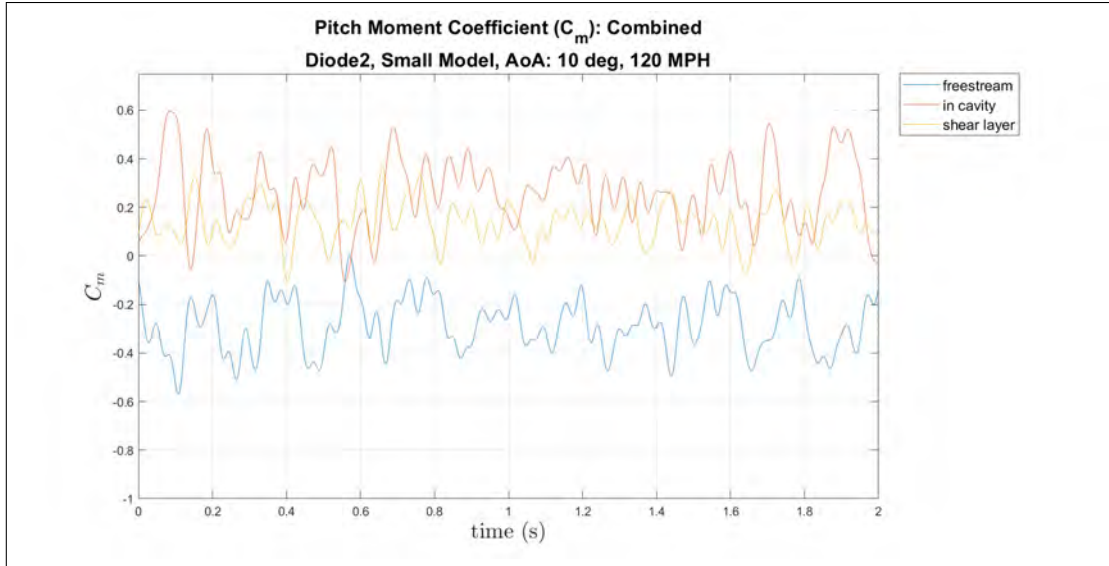


(a) Pitch Moment Coefficient, all positions, flow control, small model, 10° AoA, diode 2, 100 MPH

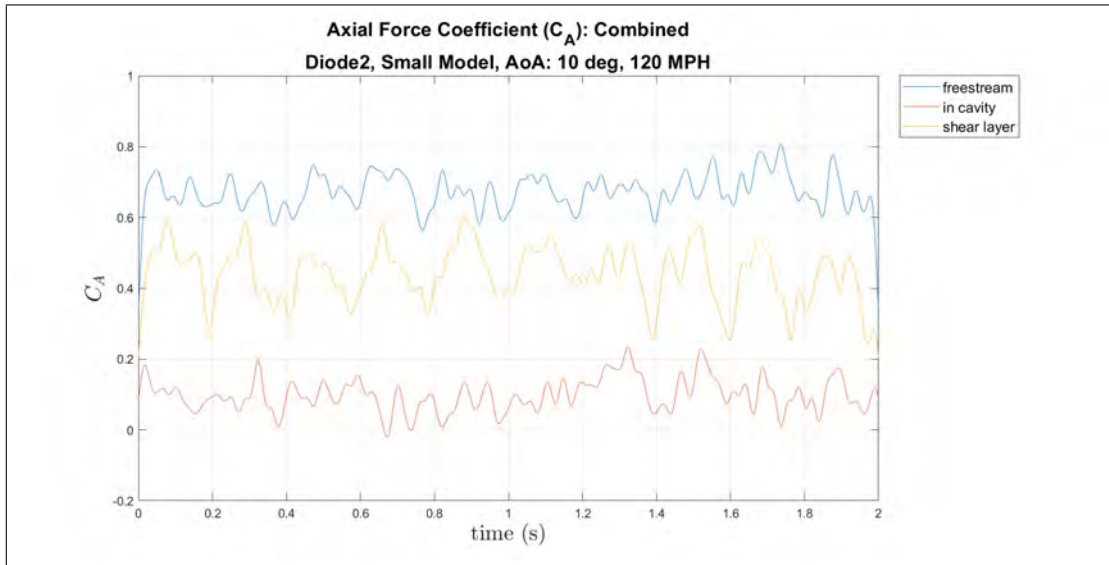


(b) Normal Force Coefficient, all positions, flow control, small model, 10° AoA, diode 2, 100 MPH

Figure 123: Small model at 10° AoA of the pitch moment and normal force coefficients for various positions, flow control, diode 2, 100 MPH



(a) Pitch Moment Coefficient, all positions, flow control, small model, 10° AoA, diode 2, 120 MPH



(b) Axial Force Coefficient, all positions, flow control, small model, 10° AoA, diode 2, 120 MPH

Figure 124: Small model at 10° AoA of the pitch moment and axial force coefficients for various positions, flow control, diode 2, 120 MPH

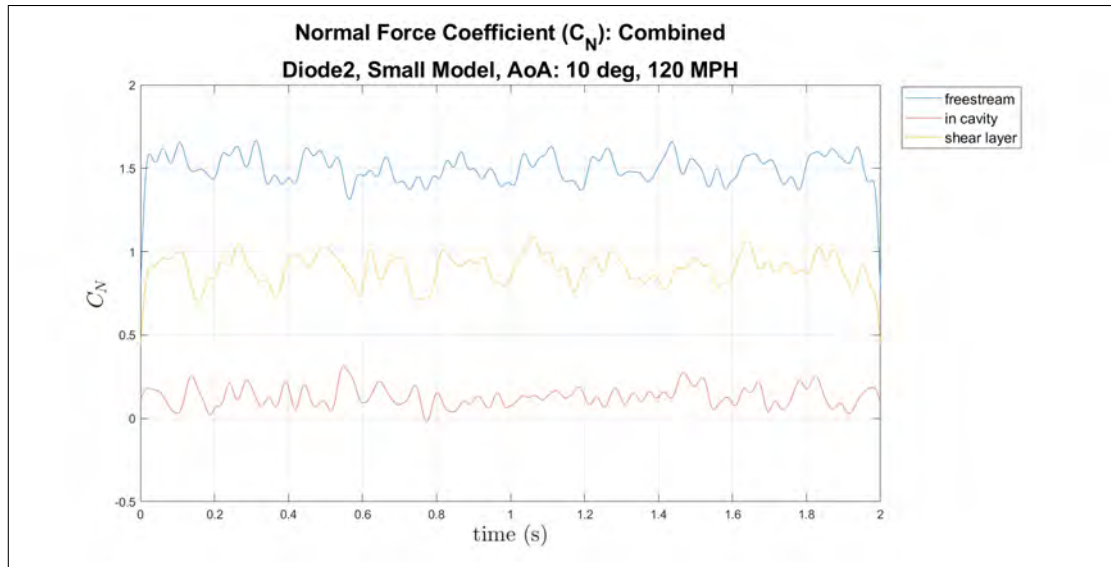
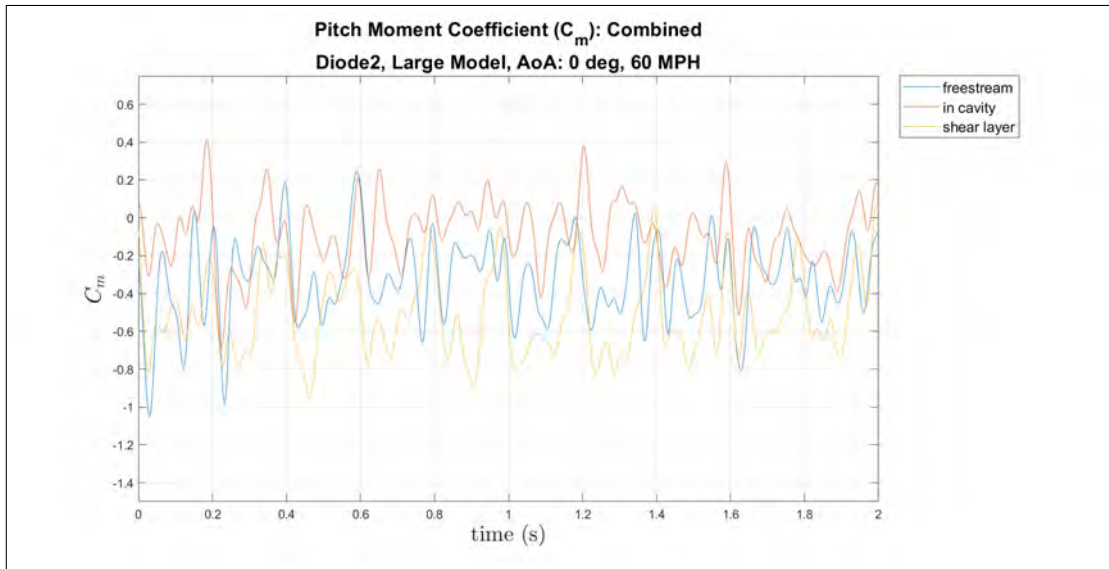
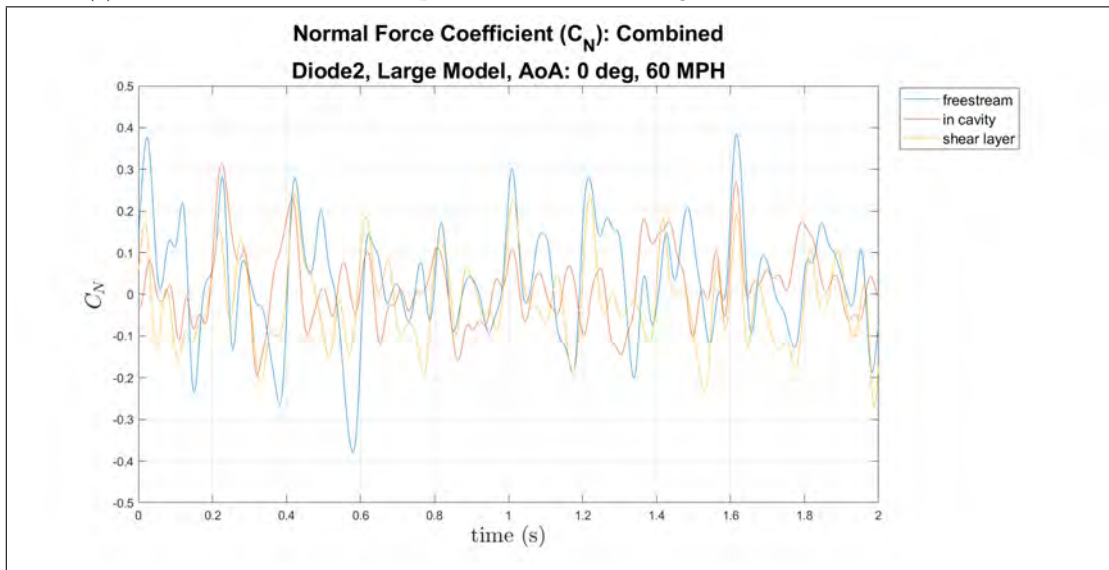


Figure 125: Normal Force Coefficient, all positions, flow control, small model, 10° AoA, diode 2, 120 MPH

Large Model, Diode 2, 0° AoA

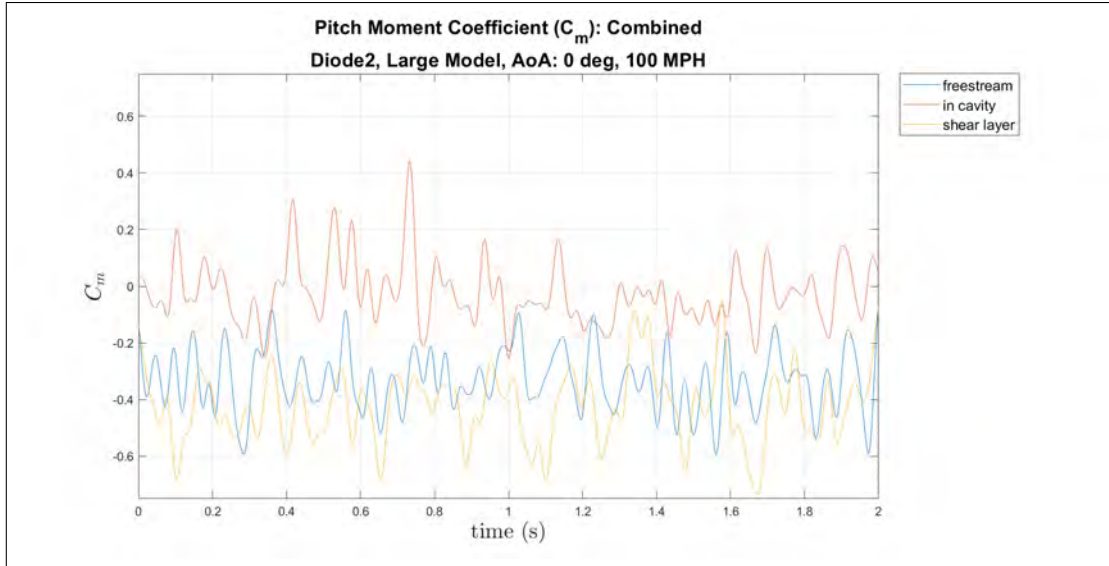


(a) Pitch Moment Coefficient, all positions, flow control, large model, 0° AoA, diode 2, 60 MPH

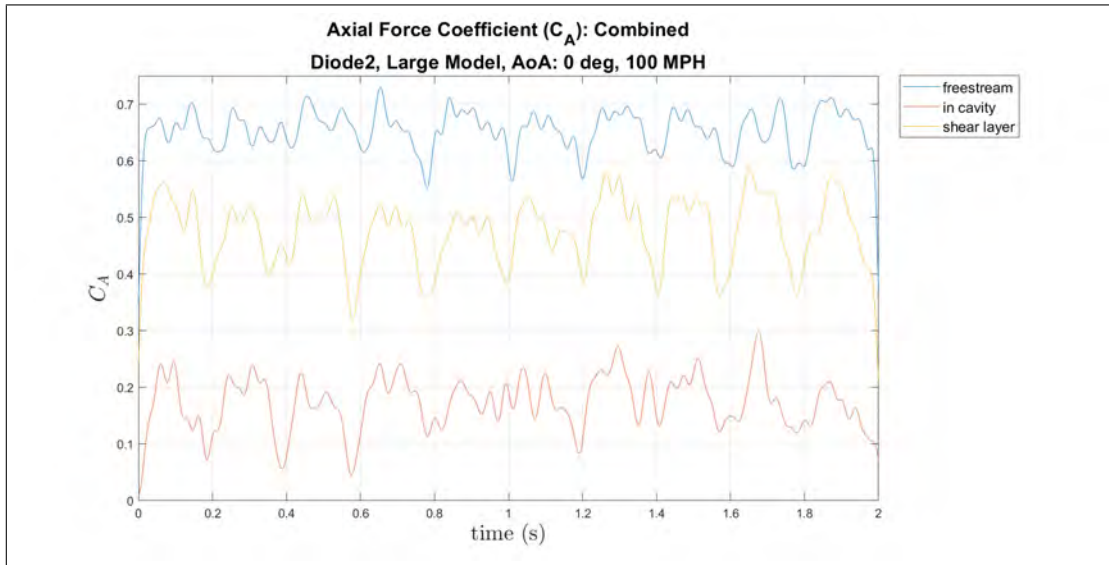


(b) Normal Force Coefficient, all positions, flow control, large model, 0° AoA, diode 2, 60 MPH

Figure 126: Large model at 0° AoA of the pitch moment and normal force coefficients for various positions, flow control, diode 2, 60 MPH

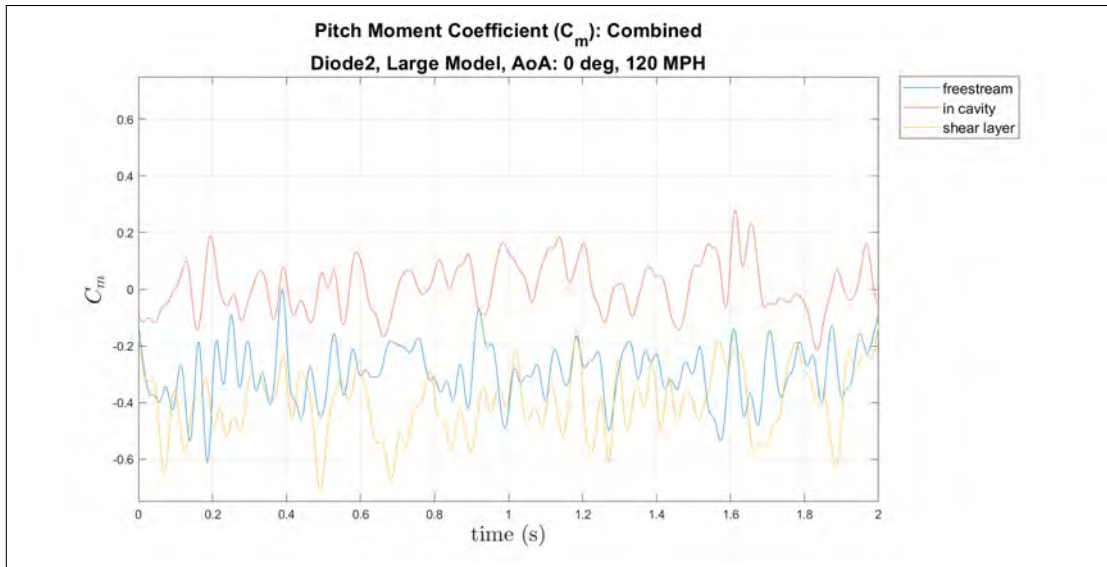


(a) Pitch Moment Coefficient, all positions, flow control, large model, 0° AoA, diode 2, 100 MPH

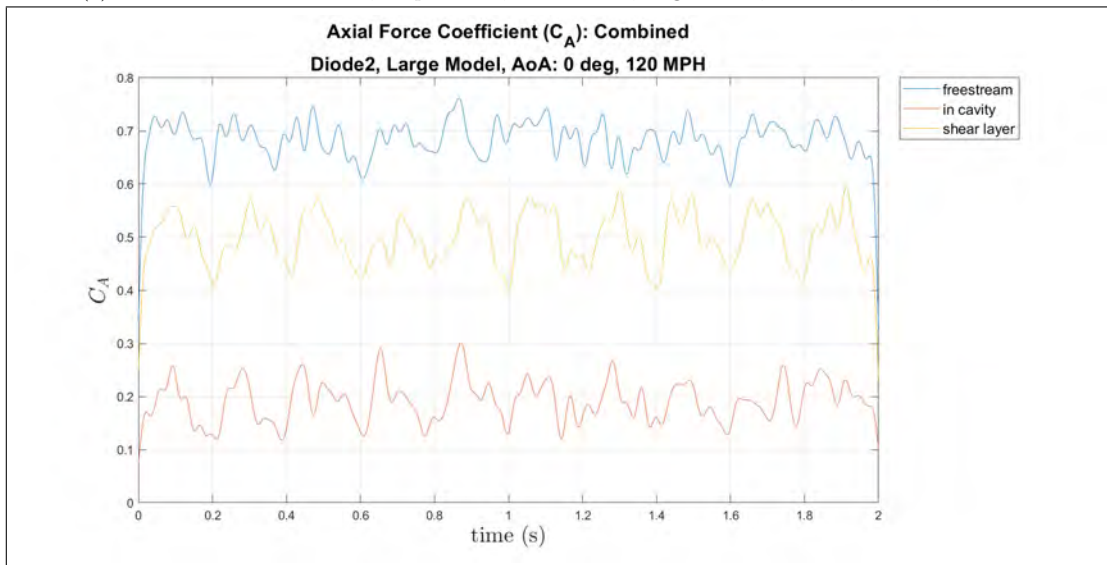


(b) Axial Force Coefficient, all positions, flow control, large model, 0° AoA, diode 2, 100 MPH

Figure 127: Large model at 0° AoA of the pitch moment and axial force coefficients for various positions, flow control, diode 2, 100 MPH

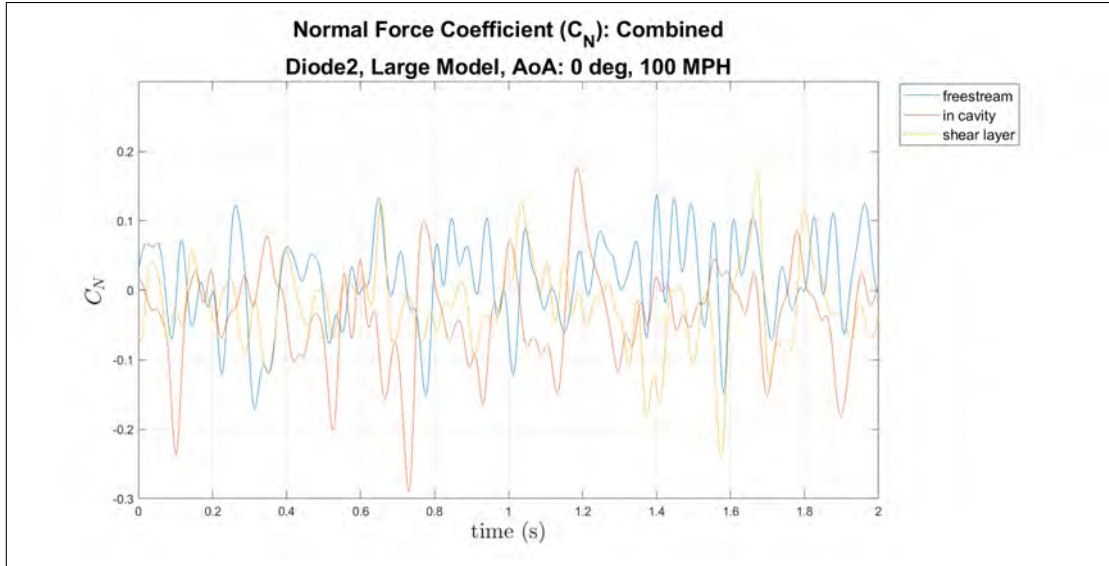


(a) Pitch Moment Coefficient, all positions, flow control, large model, 0° AoA, diode 2, 120 MPH

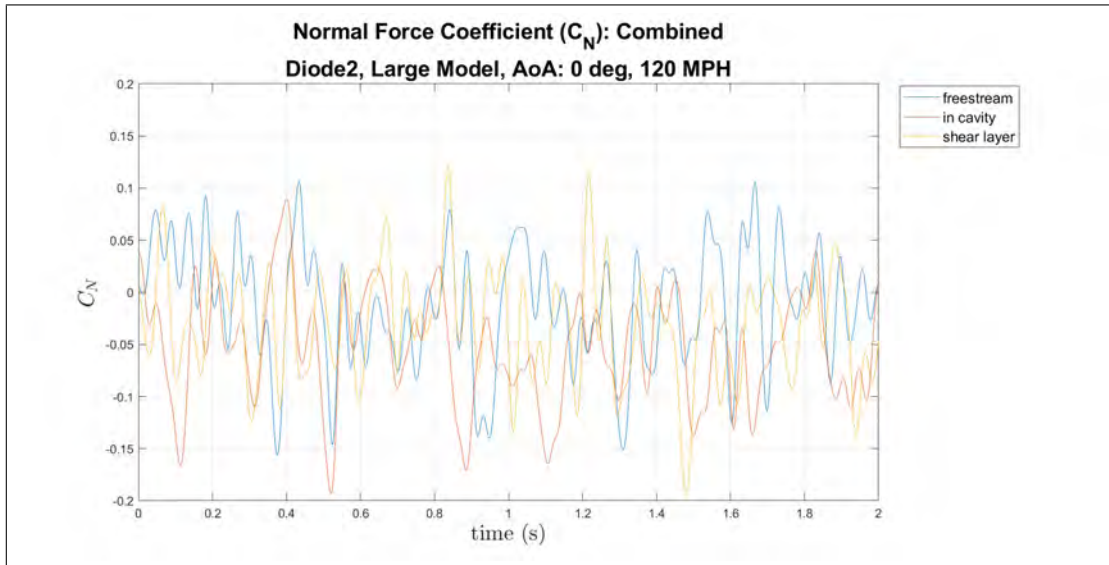


(b) Axial Force Coefficient, all positions, flow control, large model, 0° AoA, diode 2, 120 MPH

Figure 128: Large model at 0° AoA of the pitch moment and axial force coefficients for various positions, flow control, diode 2, 120 MPH



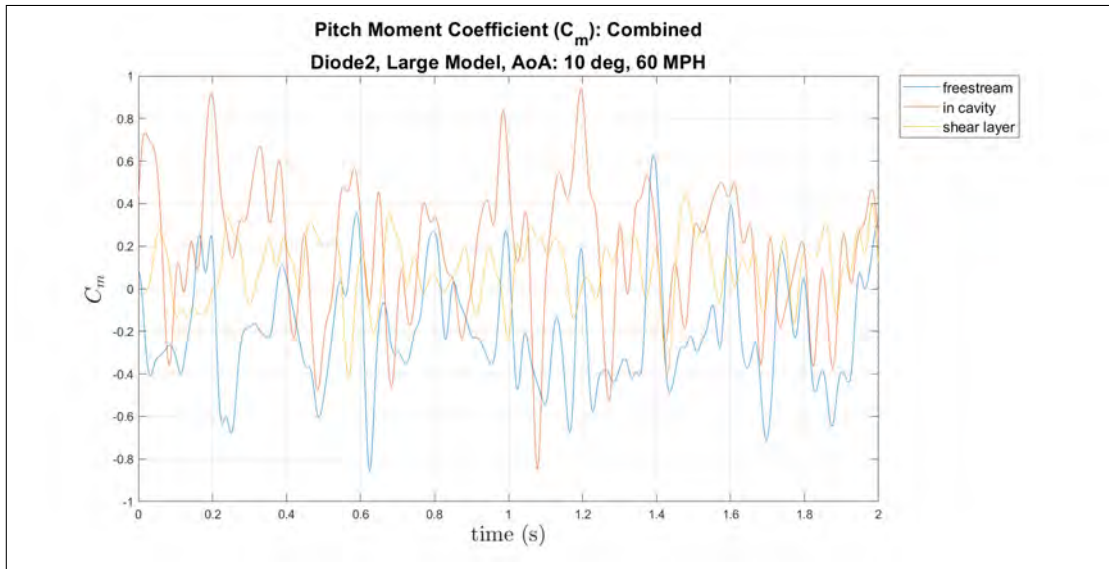
(a) Normal Force Coefficient, all positions, flow control, large model, 0° AoA, diode 2, 100 MPH



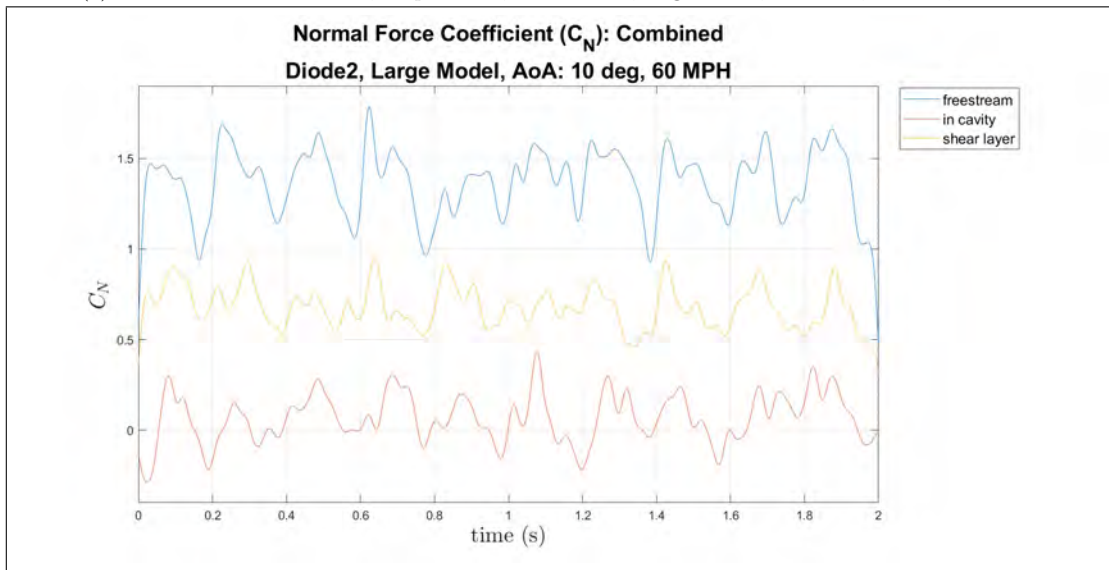
(b) Normal Force Coefficient, all positions, flow control, large model, 0° AoA, diode 2, 120 MPH

Figure 129: Large model at 0° AoA of the normal force coefficient for various positions, flow control, diode 2, 100 MPH and 120 MPH

Large Model, Diode 2, 10° AoA

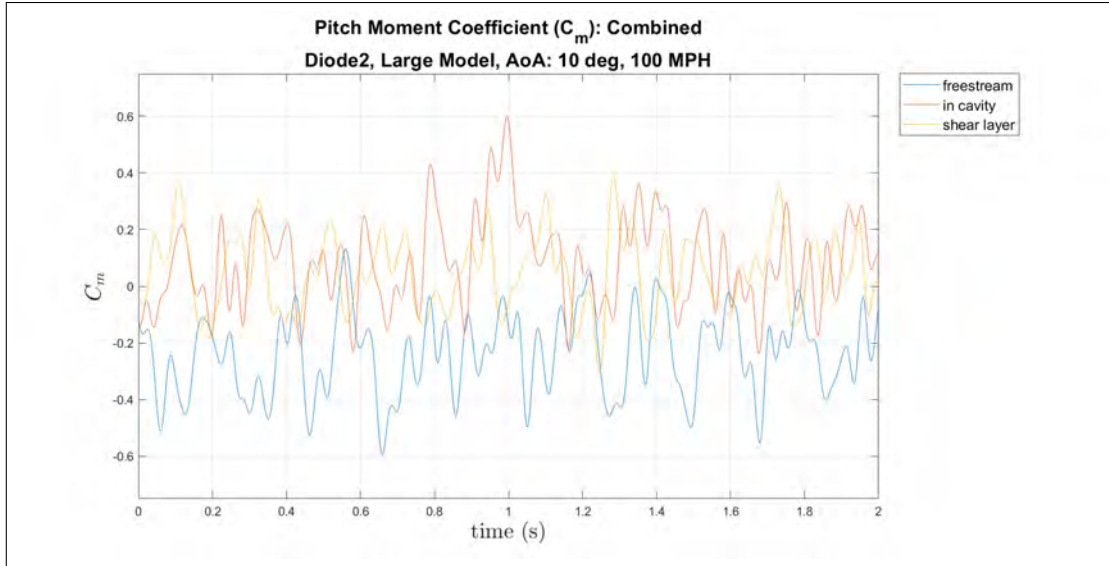


(a) Pitch Moment Coefficient, all positions, flow control, large model, 10° AoA, diode 2, 60 MPH

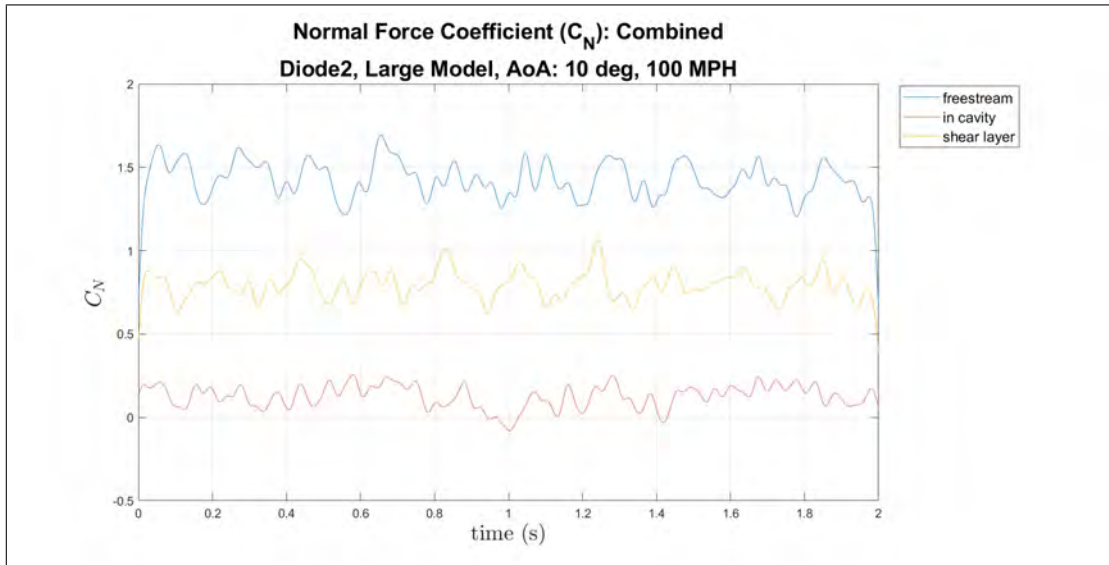


(b) Normal Force Coefficient, all positions, flow control, large model, 10° AoA, diode 2, 60 MPH

Figure 130: Large model at 10° AoA of the pitch moment and normal force coefficients for various positions, flow control, diode 2, 60 MPH

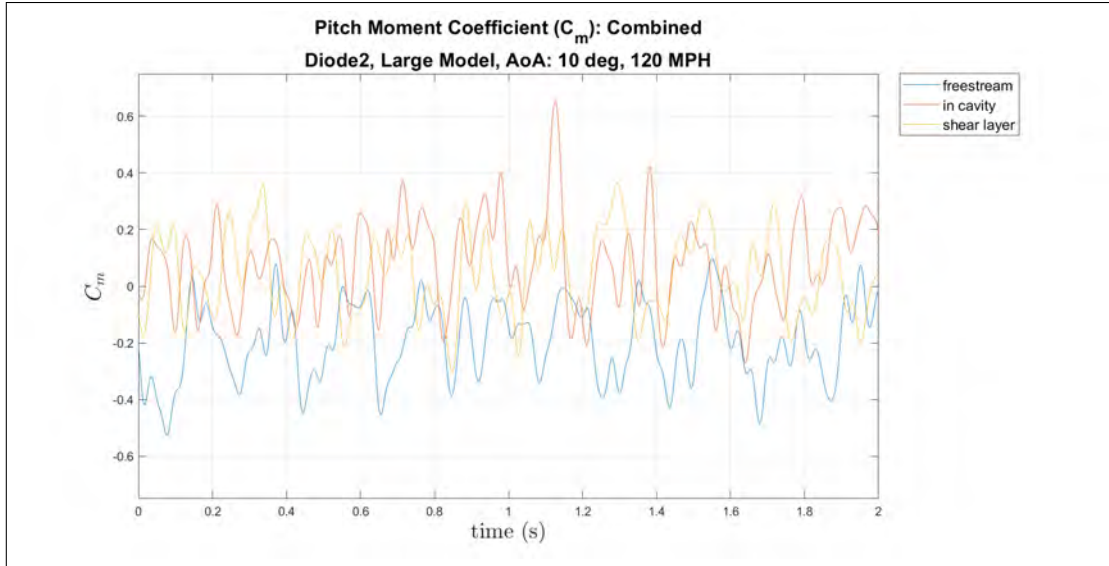


(a) Pitch Moment Coefficient, all positions, flow control, large model, 10° AoA, diode 2, 100 MPH

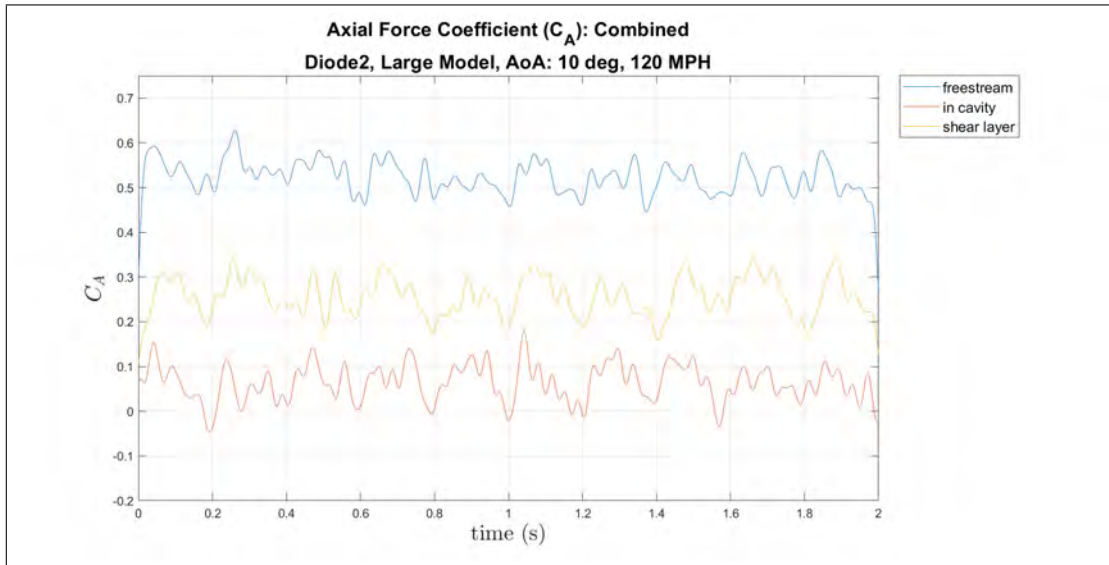


(b) Normal Force Coefficient, all positions, flow control, large model, 10° AoA, diode 2, 100 MPH

Figure 131: Large model at 10° AoA of the pitch moment and normal force coefficients for various positions, flow control, diode 2, 100 MPH



(a) Pitch Moment Coefficient, all positions, flow control, large model, 10° AoA, diode 2, 120 MPH



(b) Axial Force Coefficient, all positions, flow control, large model, 10° AoA, diode 2, 120 MPH

Figure 132: Large model at 10° AoA of the pitch moment and axial force coefficients for various positions, flow control, diode 2, 120 MPH

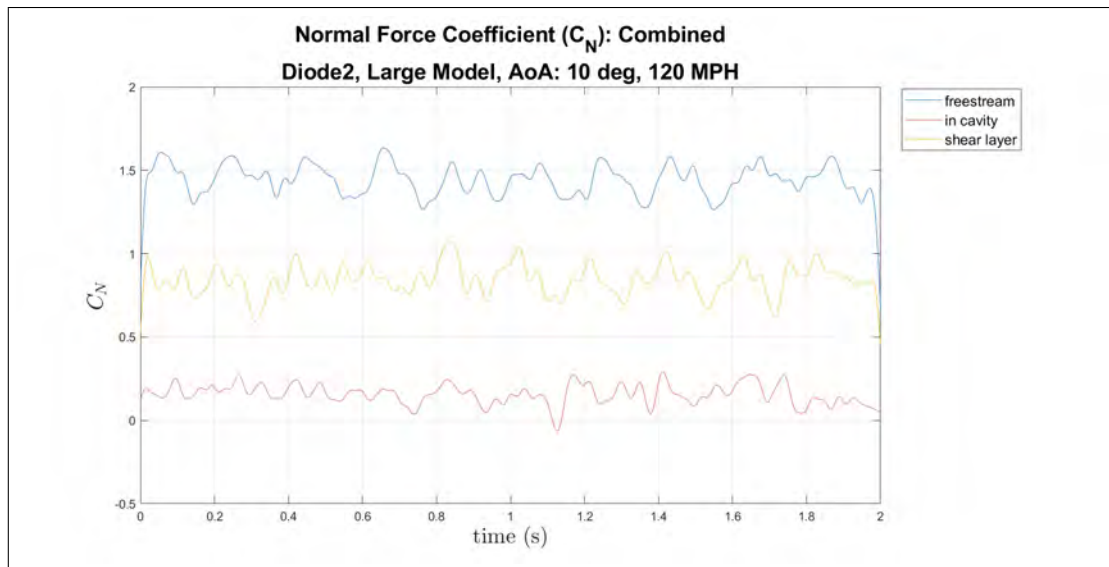
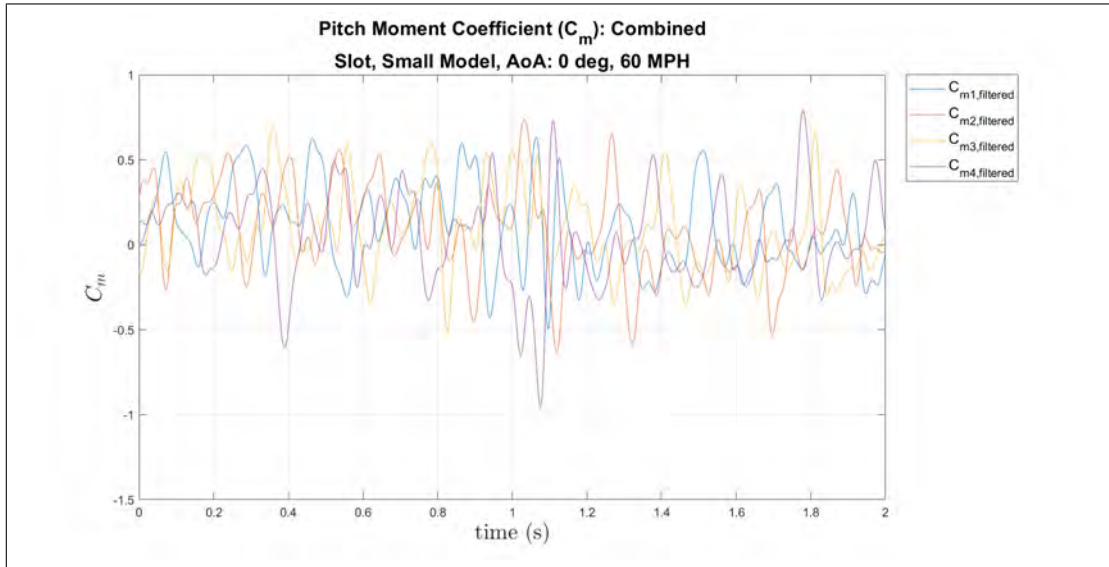


Figure 133: Normal Force Coefficient, all positions, flow control, large model, 10° AoA, diode 2, 120 MPH

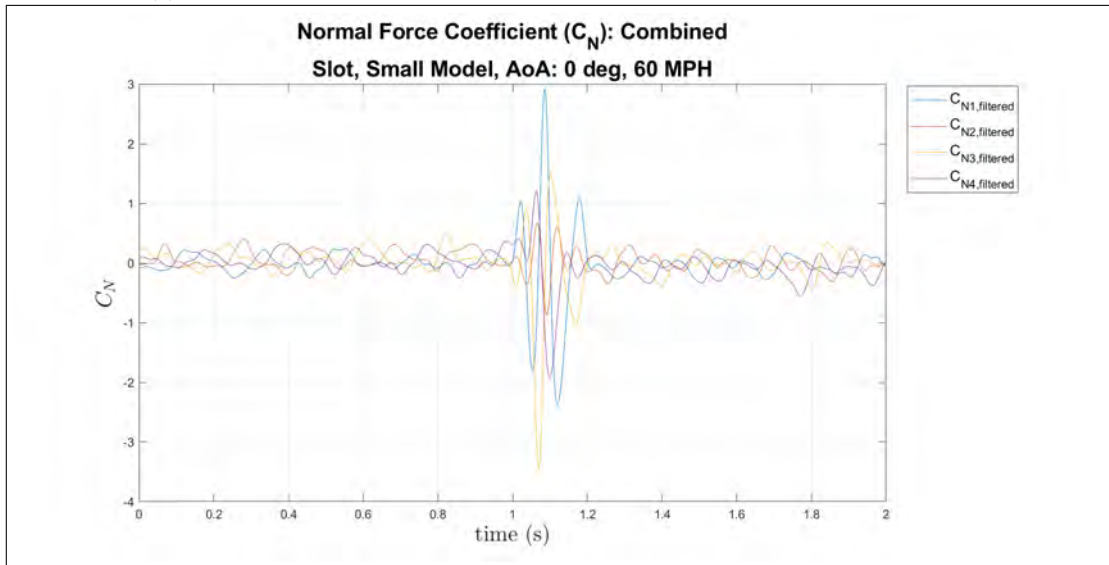
Phase II: Dynamic Store Release

Normal Force, Pitch Moment, and Axial Force Coefficients

Small Model, Slot, 0° AoA

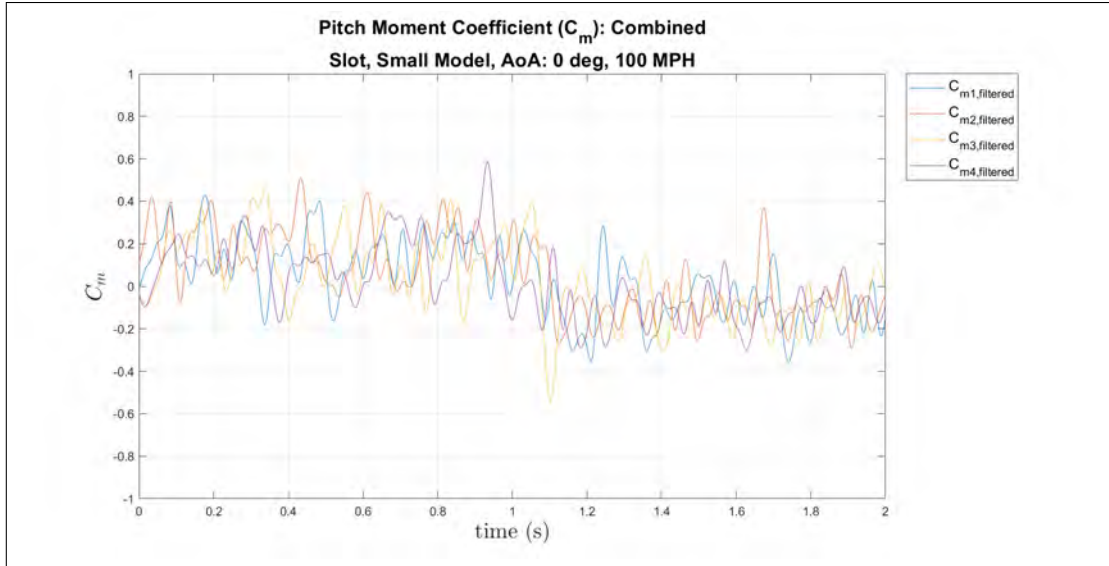


(a) Pitch Moment Coefficient, dynamic release, small model, 0° AoA, slot, 60 MPH

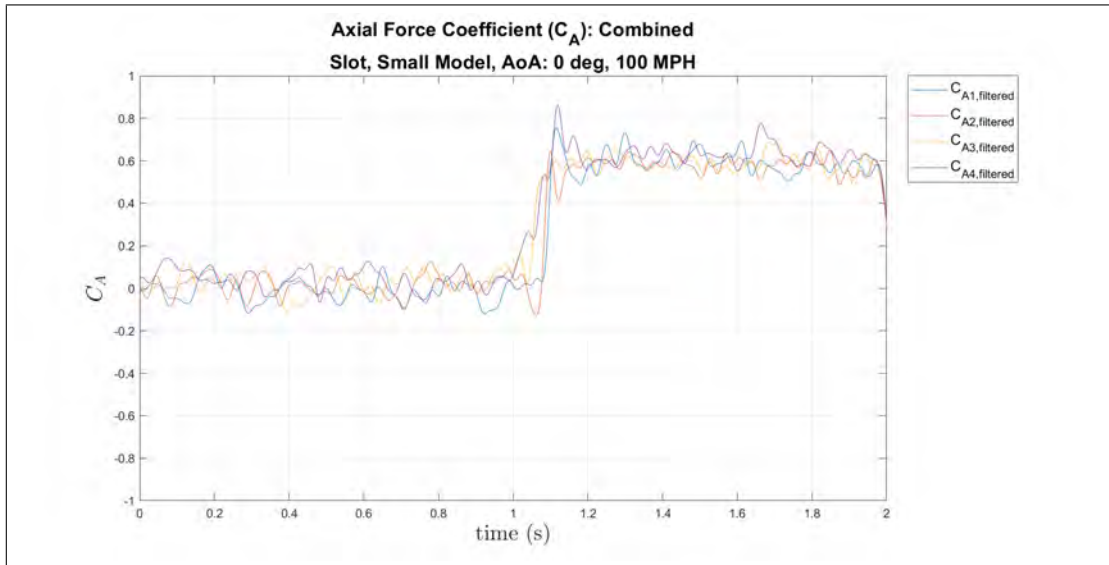


(b) Normal Force Coefficient, dynamic release, small model, 0° AoA, slot, 60 MPH

Figure 134: Small model at 0° AoA of the pitch moment and normal force coefficients, dynamic release, slot, 60 MPH



(a) Pitch Moment Coefficient, dynamic release, small model, 0° AoA, slot, 100 MPH



(b) Axial Force Coefficient, dynamic release, small model, 0° AoA, slot, 100 MPH

Figure 135: Small model at 0° AoA of the pitch moment and axial force coefficients, dynamic release, slot, 100 MPH

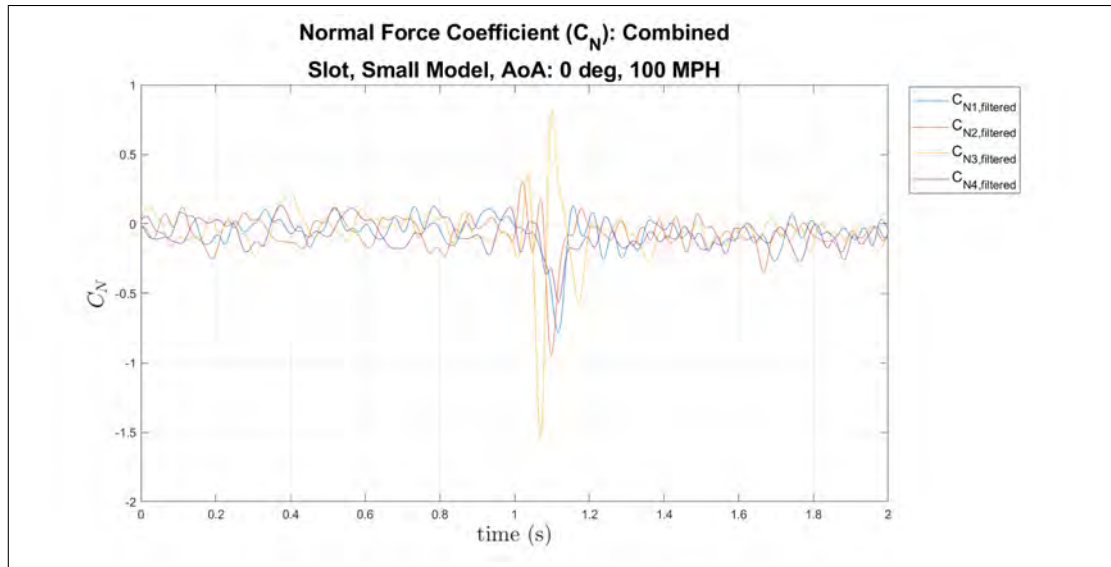
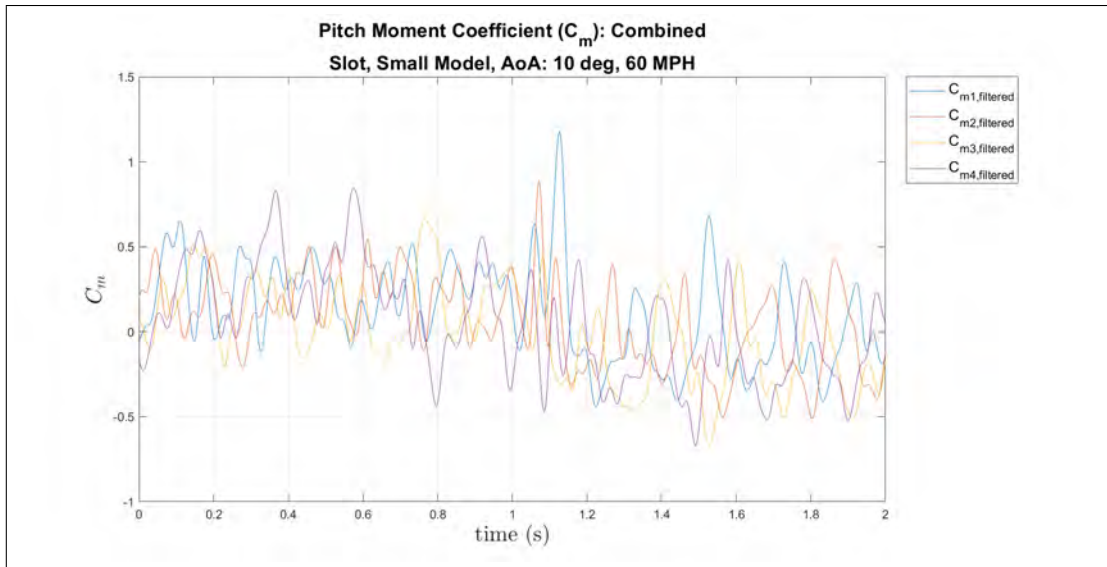
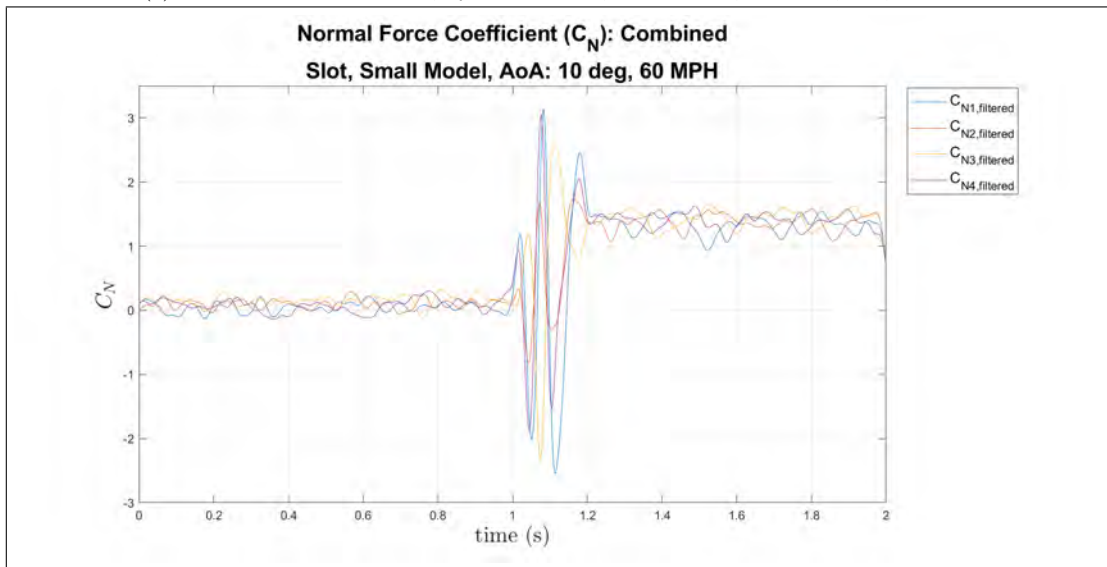


Figure 136: Normal Force Coefficient, dynamic release, small model, 0° AoA, slot, 100 MPH

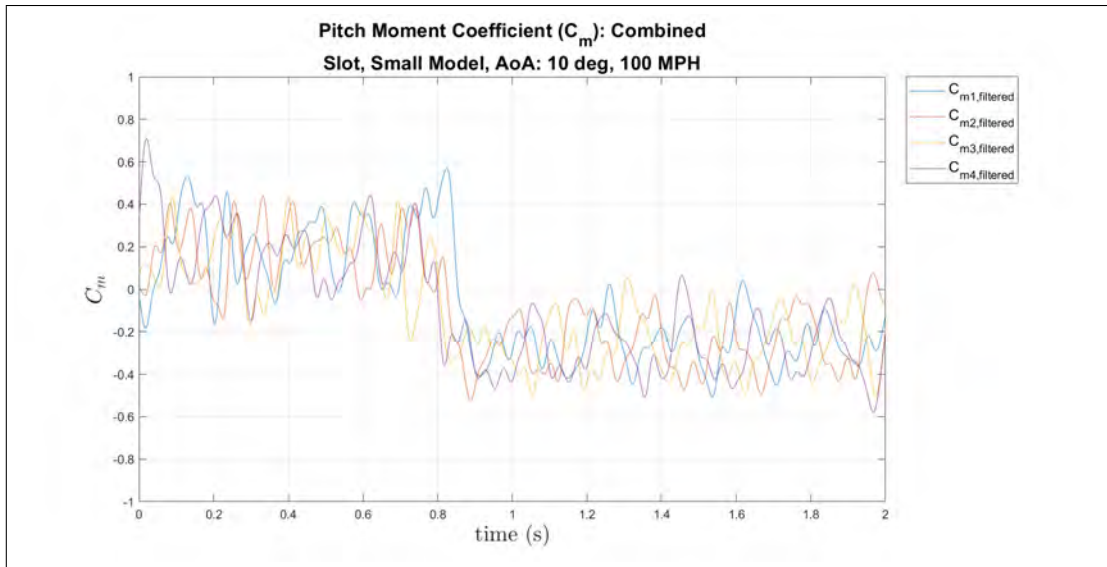


(a) Pitch Moment Coefficient, dynamic release, small model, 10° AoA, slot, 60 MPH

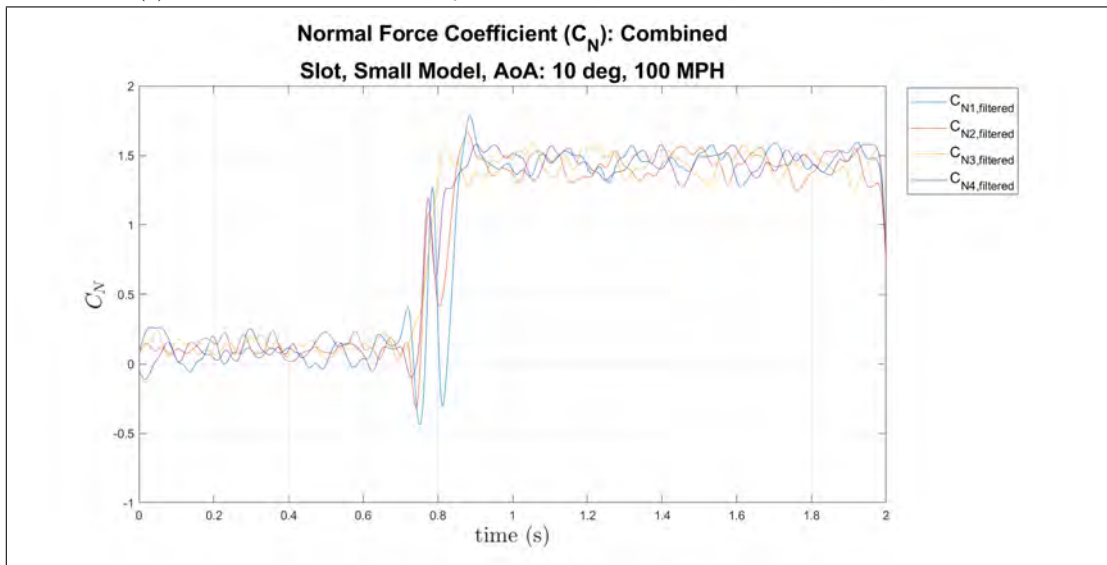


(b) Normal Force Coefficient, dynamic release, small model, 10° AoA, slot, 60 MPH

Figure 137: Small model at 10° AoA of the pitch moment and normal force coefficients, dynamic release, slot, 60 MPH



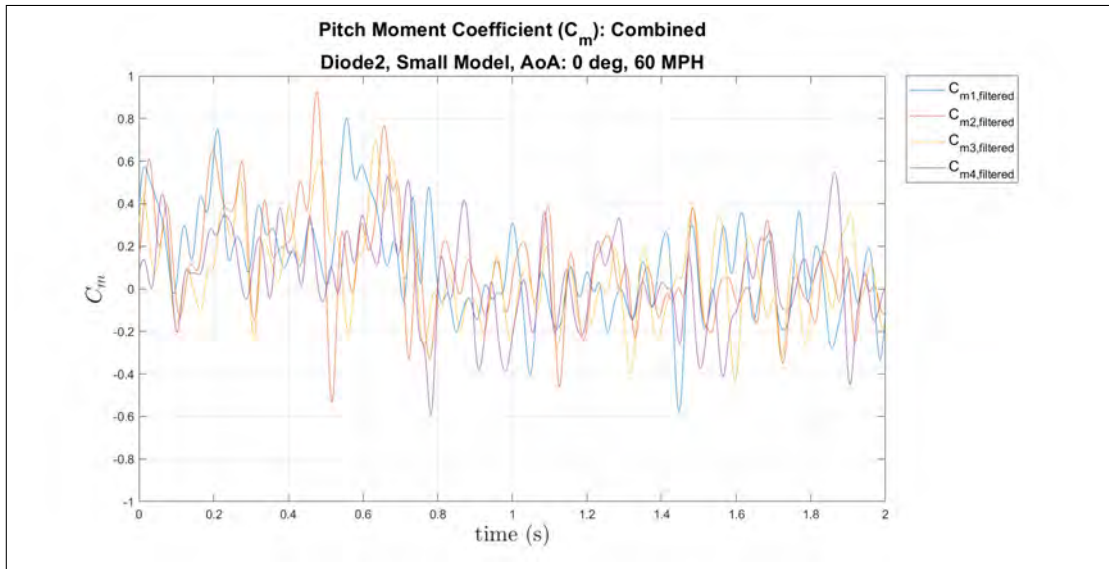
(a) Pitch Moment Coefficient, dynamic release, small model, 10° AoA, slot, 100 MPH



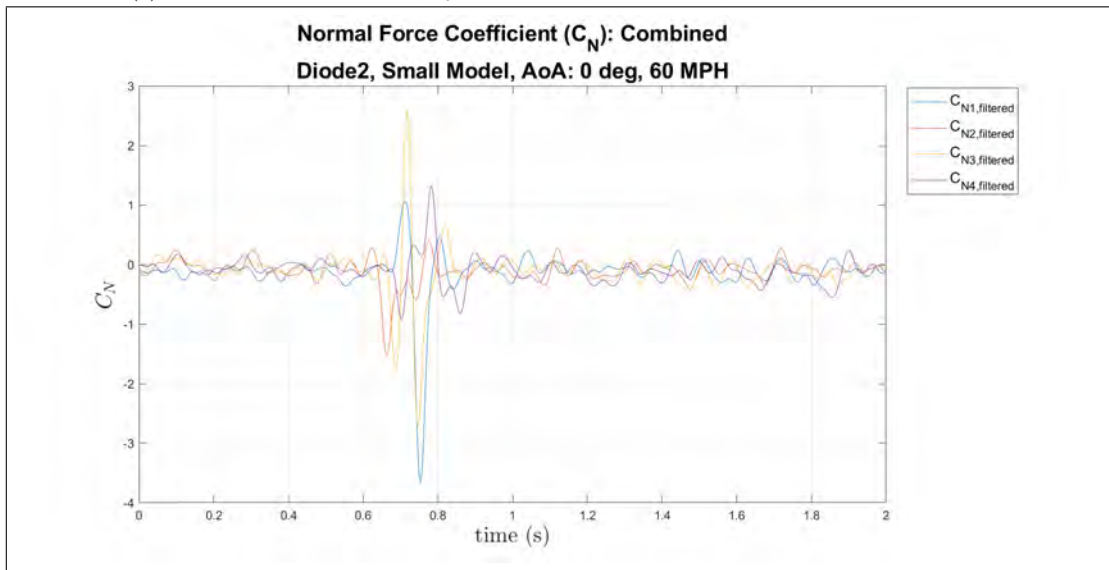
(b) Normal Force Coefficient, dynamic release, small model, 10° AoA, slot, 100 MPH

Figure 138: Small model at 10° AoA of the pitch moment and normal force coefficients, dynamic release, slot, 100 MPH

Small Model, Diode 2, 0° AoA

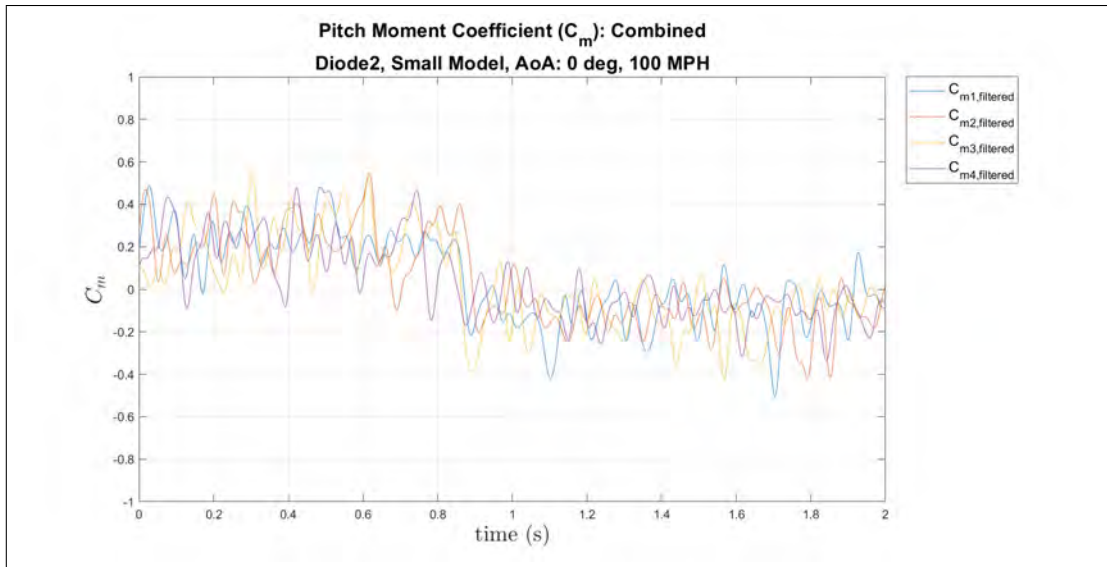


(a) Pitch Moment Coefficient, dynamic release, small model, 0° AoA, diode 2, 60 MPH

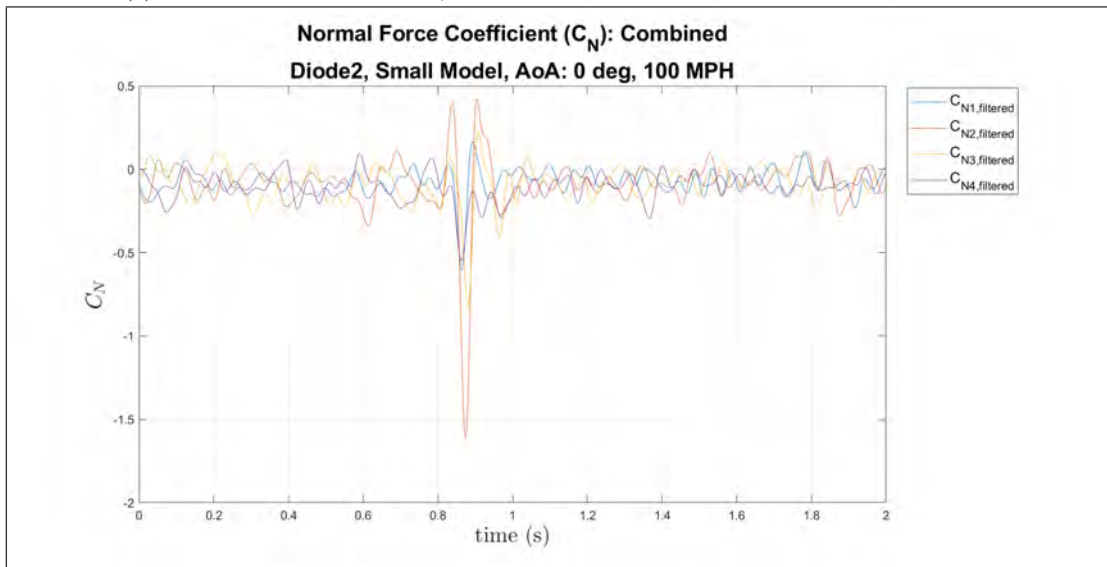


(b) Normal Force Coefficient, dynamic release, small model, 0° AoA, diode 2, 60 MPH

Figure 139: Small model at 0° AoA of the pitch moment and normal force coefficients, dynamic release, diode 2, 60 MPH

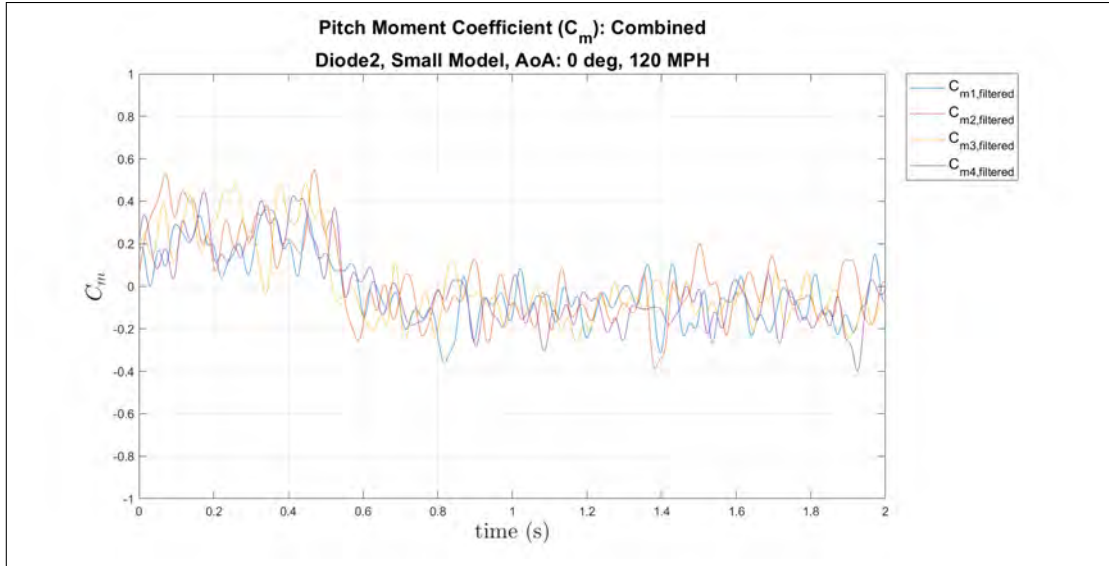


(a) Pitch Moment Coefficient, dynamic release, small model, 0° AoA, diode 2, 100 MPH

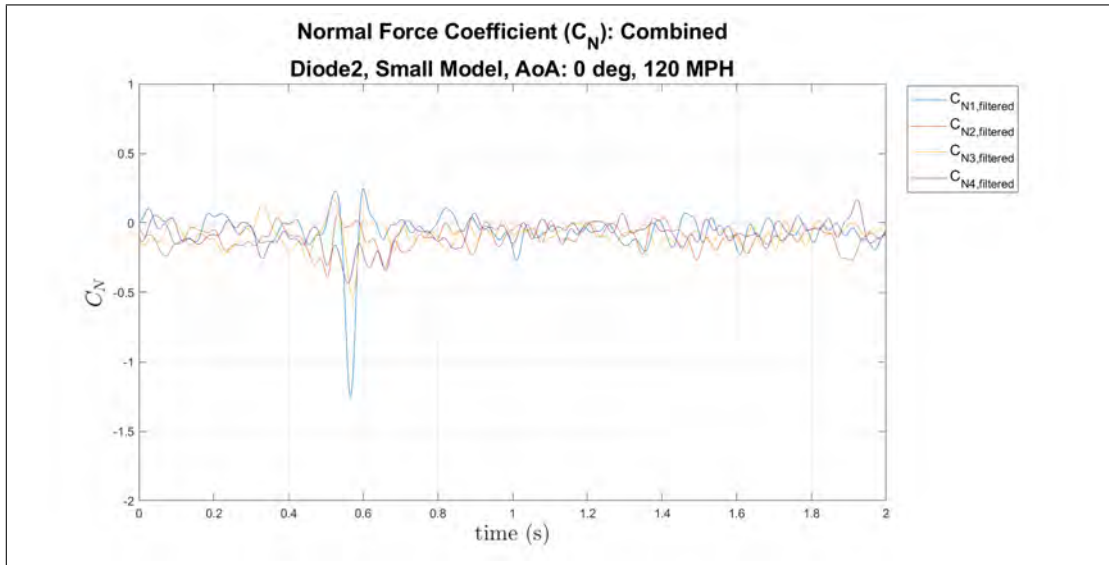


(b) Normal Force Coefficient, dynamic release, small model, 0° AoA, diode 2, 100 MPH

Figure 140: Small model at 0° AoA of the pitch moment and normal force coefficients, dynamic release, diode 2, 100 MPH



(a) Pitch Moment Coefficient, dynamic release, small model, 0° AoA, diode 2, 120 MPH



(b) Normal Force Coefficient, dynamic release, small model, 0° AoA, diode 2, 120 MPH

Figure 141: Small model at 0° AoA of the pitch moment and normal force coefficients, dynamic release, diode 2, 120 MPH

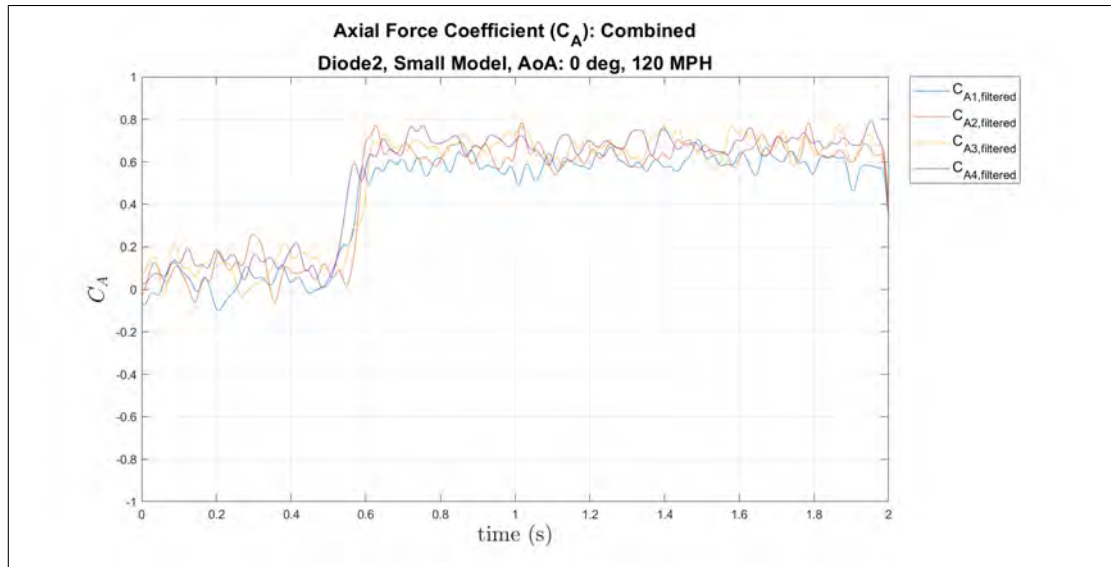
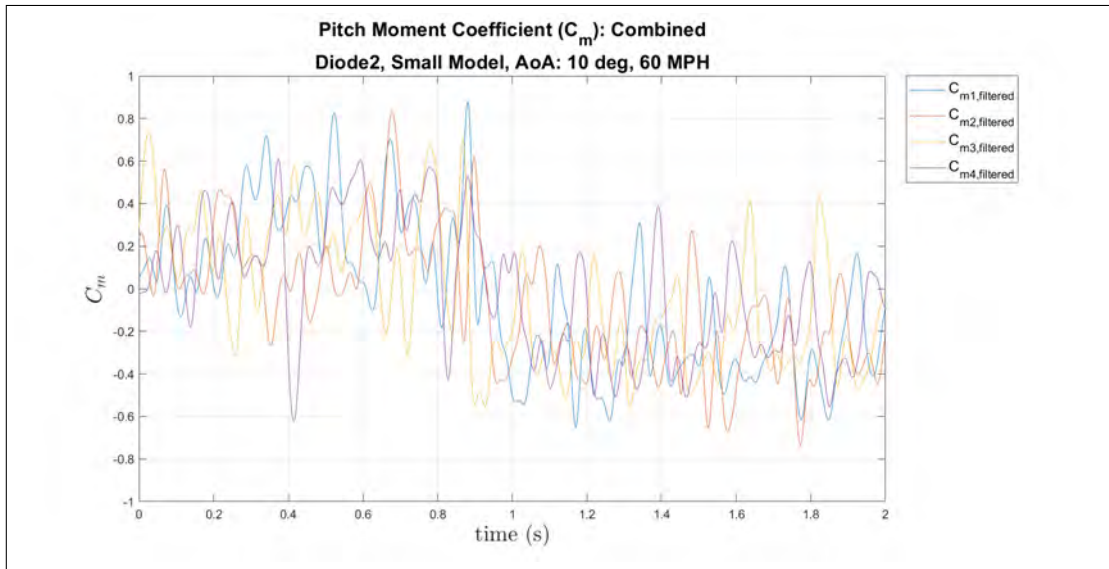
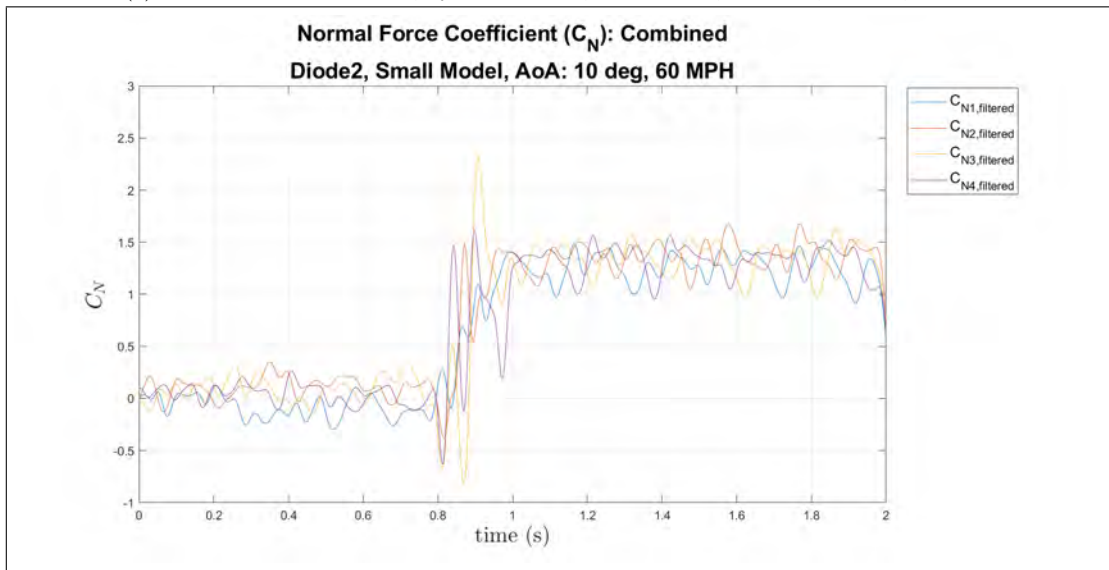


Figure 142: Normal Force Coefficient, dynamic release, small model, 0° AoA, diode 2, 100 MPH

Small Model, Diode 2, 10° AoA

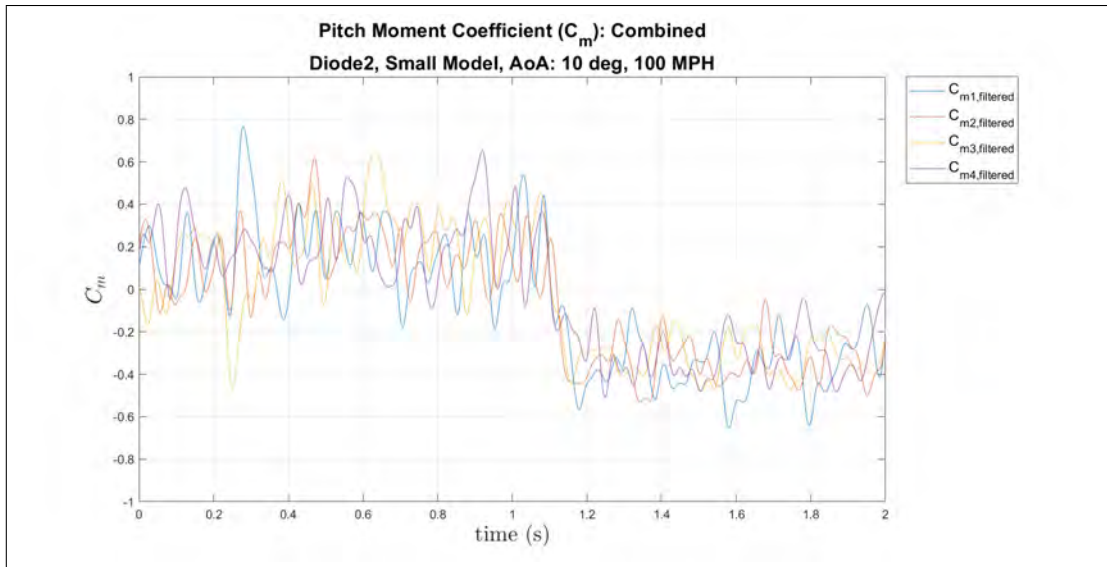


(a) Pitch Moment Coefficient, dynamic release, small model, 10° AoA, diode 2, 60 MPH

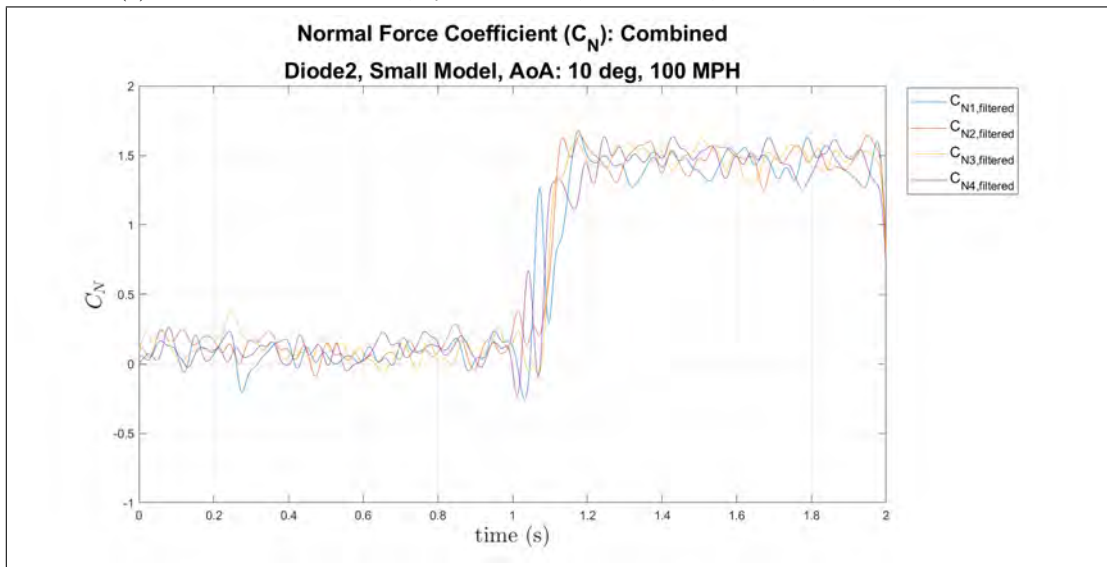


(b) Normal Force Coefficient, dynamic release, small model, 10° AoA, diode 2, 60 MPH

Figure 143: Small model at 10° AoA of the pitch moment and normal force coefficients, dynamic release, diode 2, 60 MPH

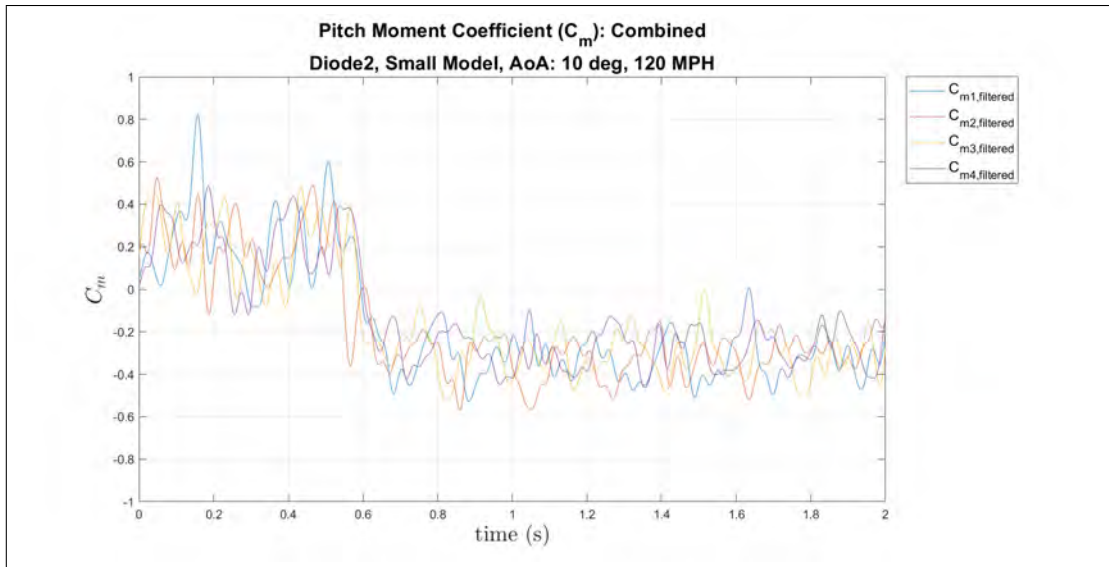


(a) Pitch Moment Coefficient, dynamic release, small model, 10° AoA, diode 2, 100 MPH

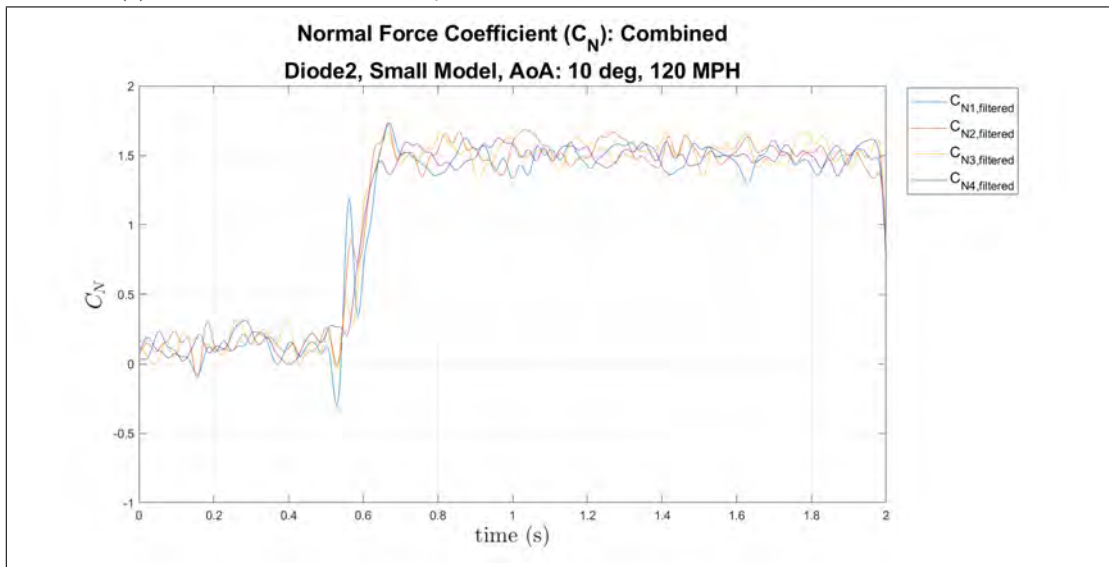


(b) Normal Force Coefficient, dynamic release, small model, 10° AoA, diode 2, 100 MPH

Figure 144: Small model at 10° AoA of the pitch moment and normal force coefficients, dynamic release, diode 2, 100 MPH



(a) Pitch Moment Coefficient, dynamic release, small model, 10° AoA, diode 2, 120 MPH



(b) Normal Force Coefficient, dynamic release, small model, 10° AoA, diode 2, 120 MPH

Figure 145: Small model at 10° AoA of the pitch moment and normal force coefficients, dynamic release, diode 2, 120 MPH

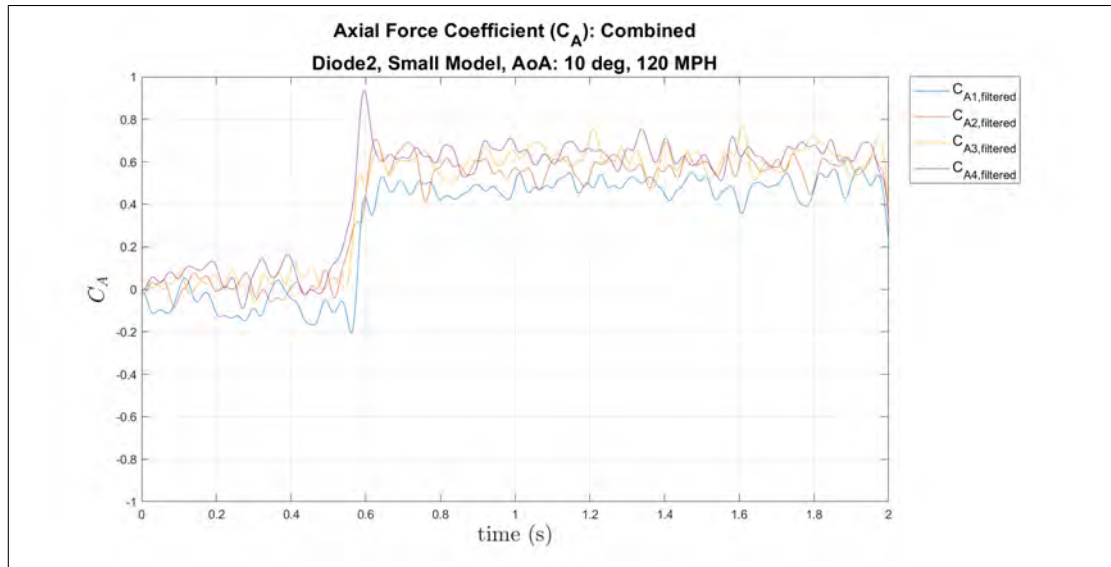
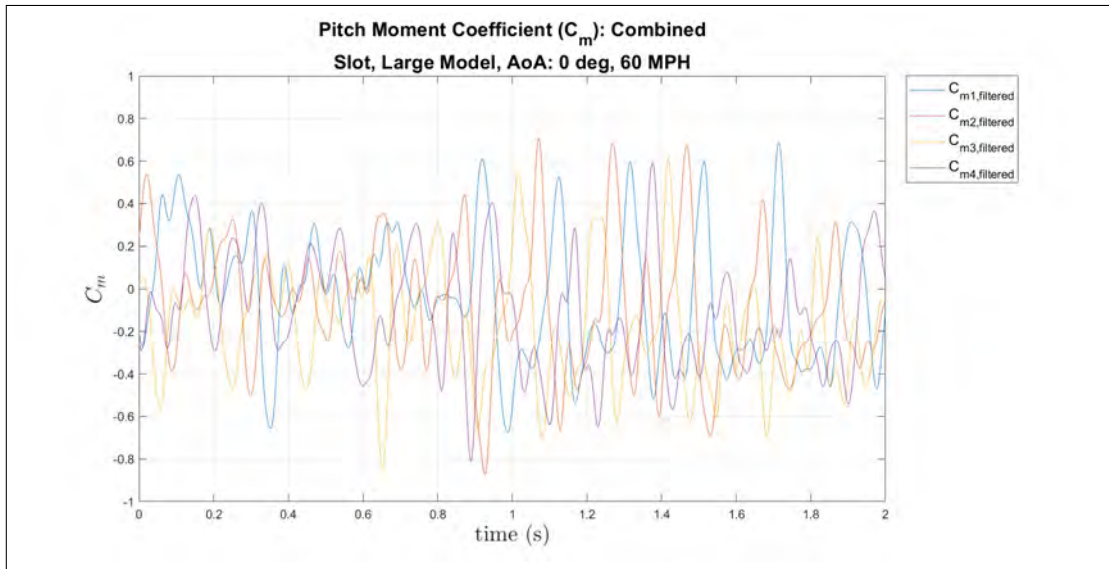
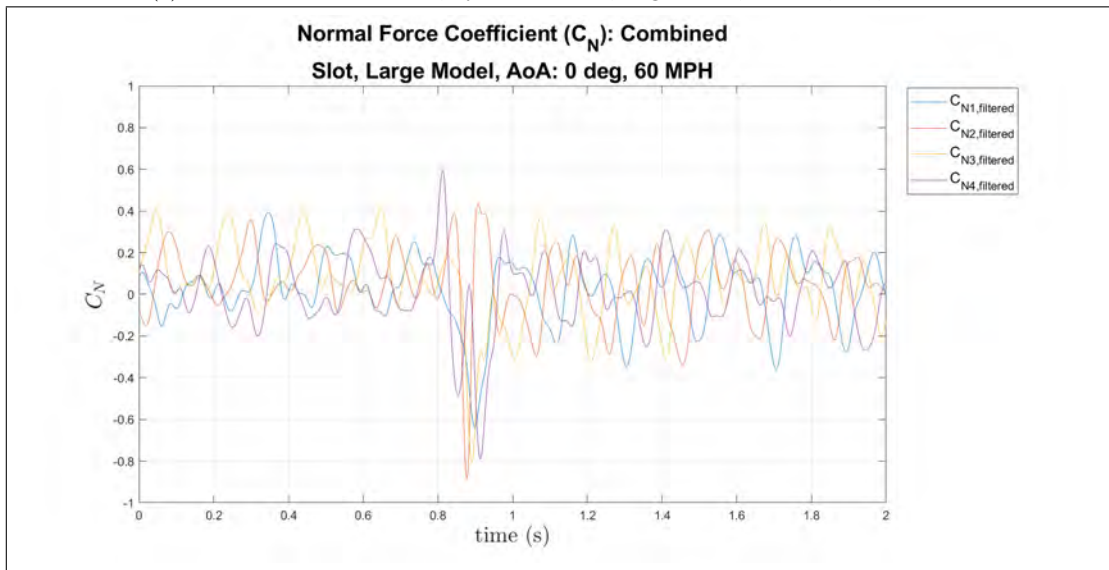


Figure 146: Normal Force Coefficient, dynamic release, small model, 10° AoA, diode 2, 100 MPH

Large Model, Slot

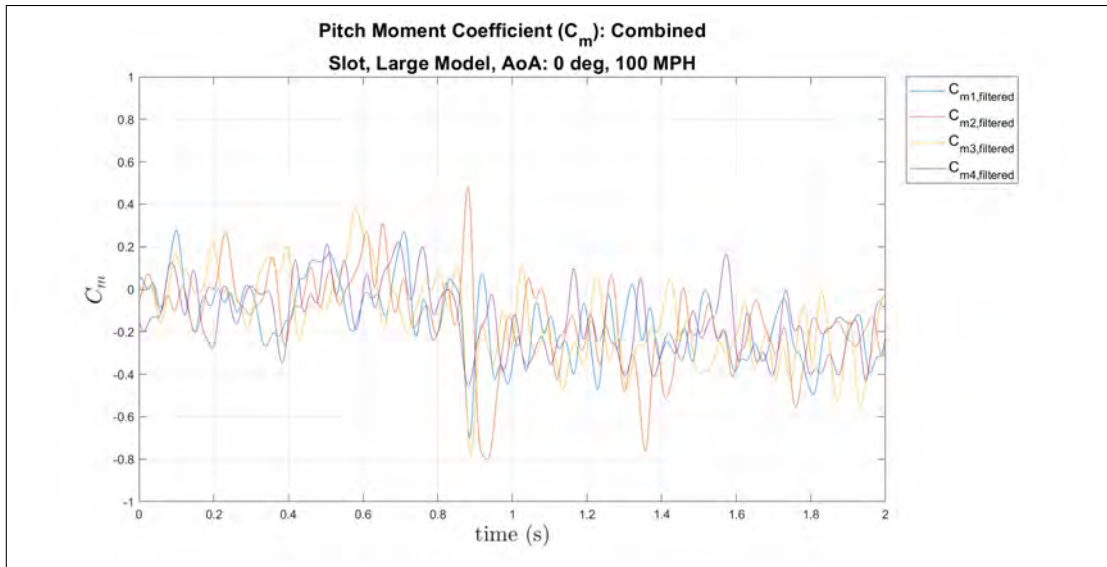


(a) Pitch Moment Coefficient, dynamic release, large model, 0° AoA, slot, 60 MPH

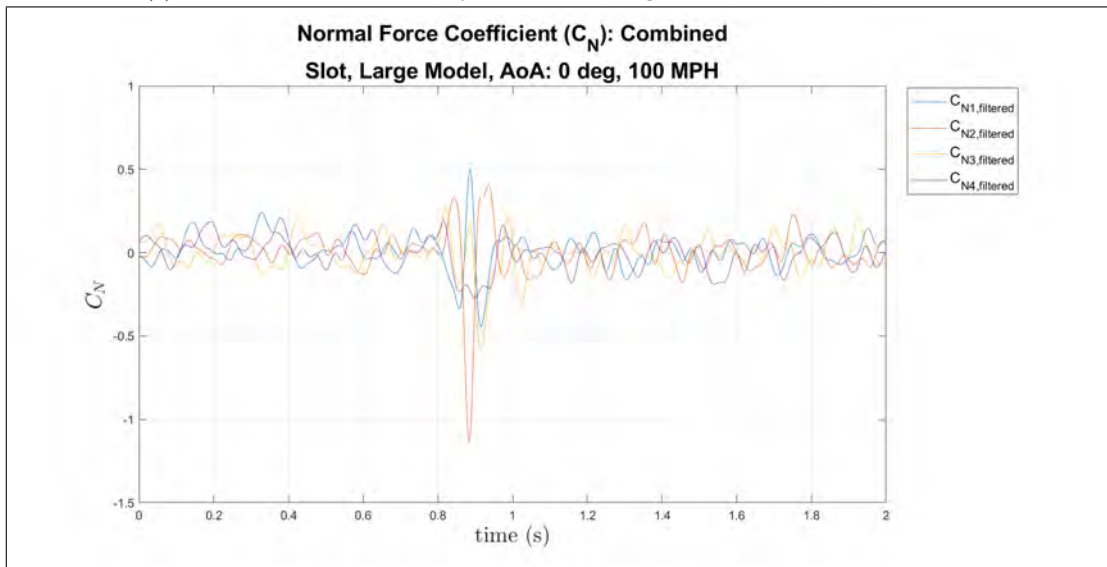


(b) Normal Force Coefficient, dynamic release, large model, 0° AoA, slot, 60 MPH

Figure 147: Large model at 0° AoA of the pitch moment and normal force coefficients, dynamic release, slot, 60 MPH



(a) Pitch Moment Coefficient, dynamic release, large model, 0° AoA, slot, 100 MPH



(b) Normal Force Coefficient, dynamic release, large model, 0° AoA, slot, 100 MPH

Figure 148: Large model at 0° AoA of the pitch moment and normal force coefficients, dynamic release, slot, 100 MPH

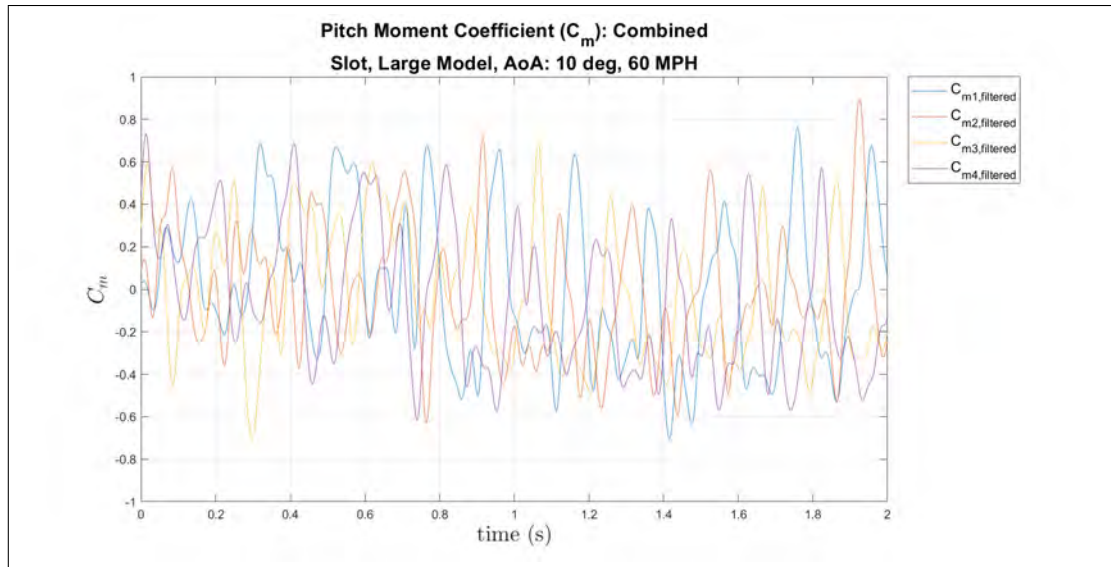
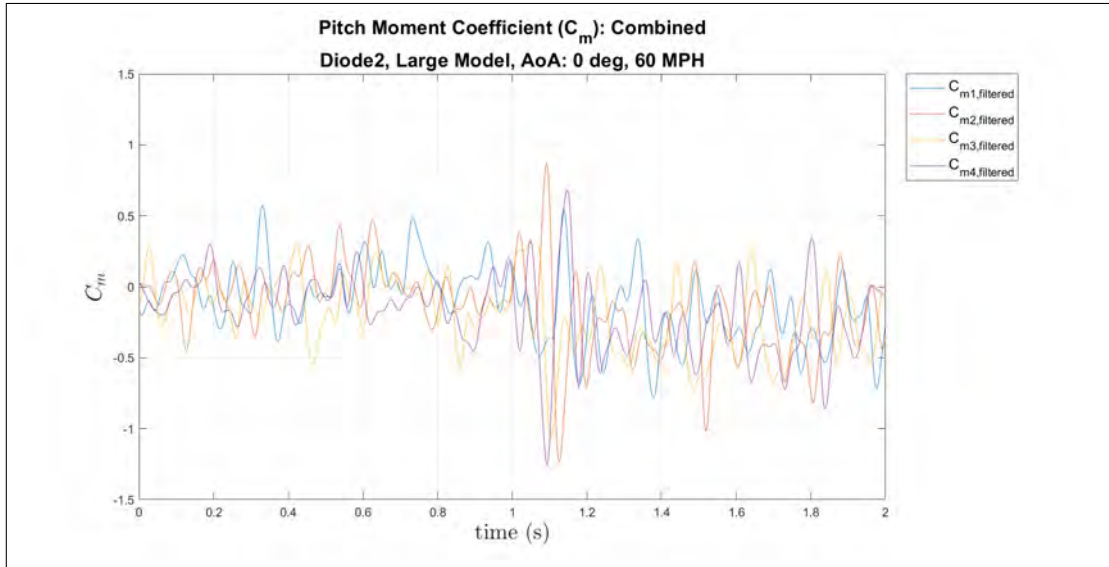
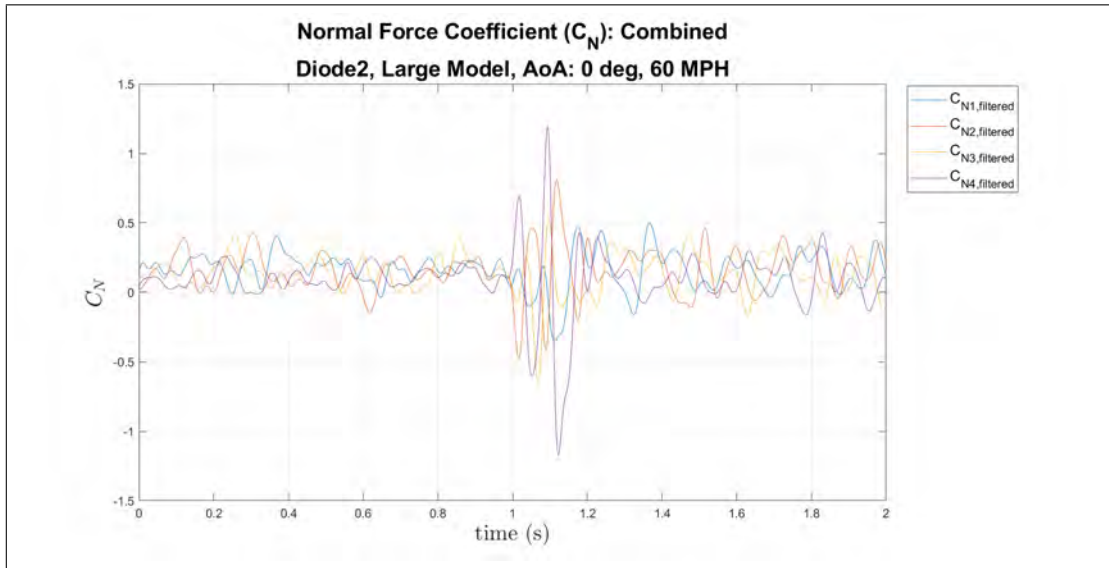


Figure 149: Pitch Moment Coefficient, dynamic release, large model, 10° AoA, slot, 60 MPH

Large Model, Diode2, 0° AoA

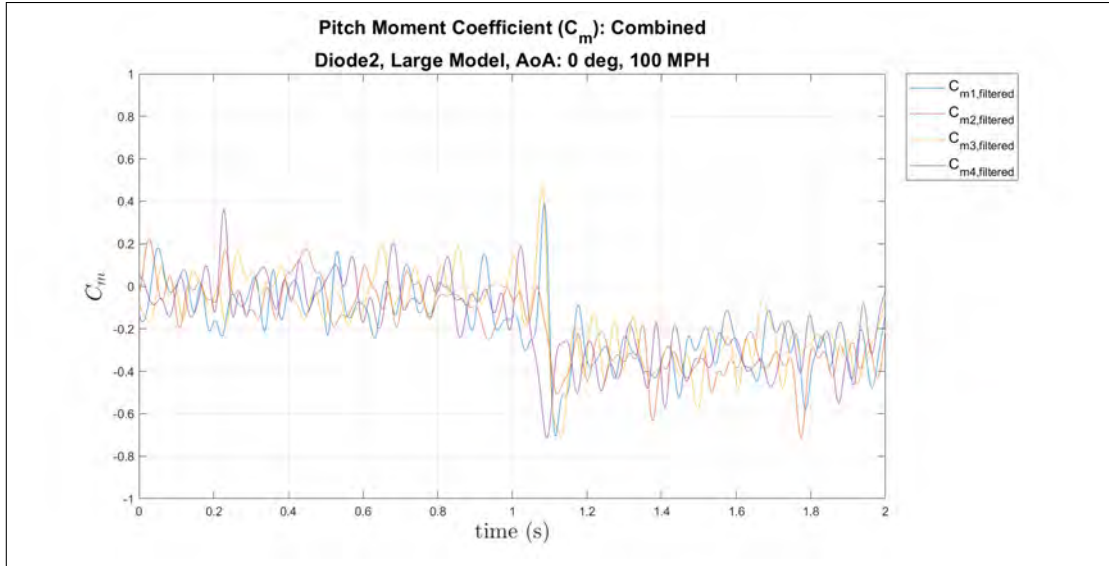


(a) Pitch Moment Coefficient, dynamic release, large model, 0° AoA, diode 2, 60 MPH

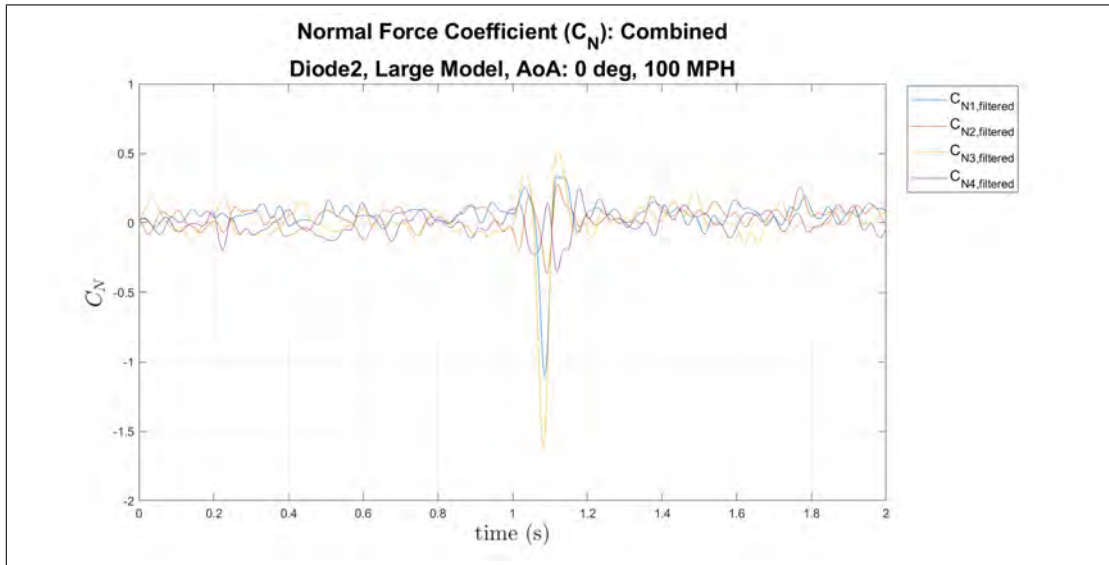


(b) Normal Force Coefficient, dynamic release, large model, 0° AoA, diode 2, 60 MPH

Figure 150: Large model at 0° AoA of the pitch moment and normal force coefficients, dynamic release, diode 2, 60 MPH

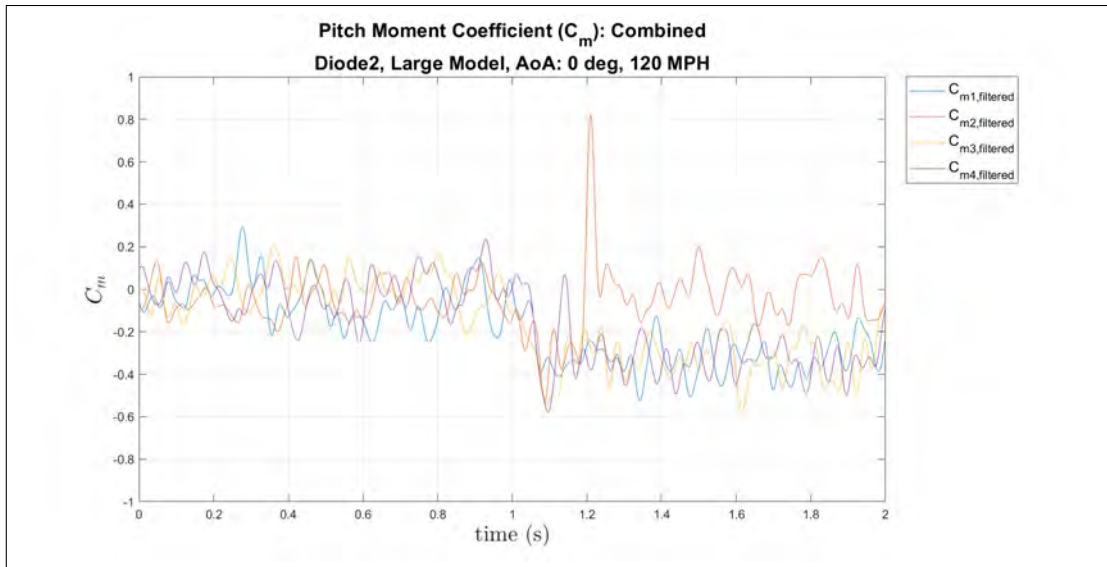


(a) Pitch Moment Coefficient, dynamic release, large model, 0° AoA, diode 2, 100 MPH

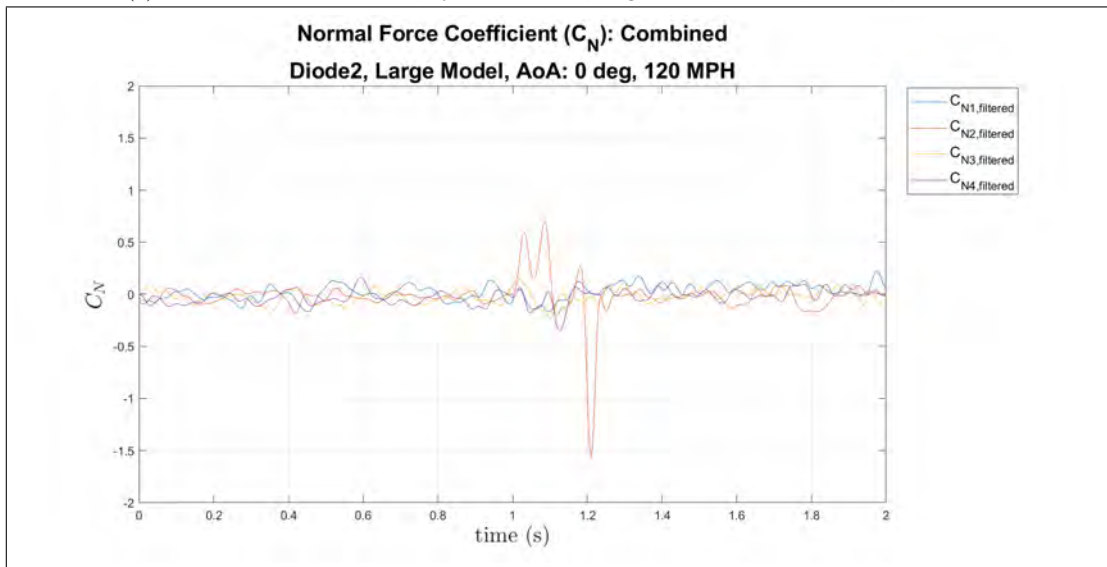


(b) Normal Force Coefficient, dynamic release, large model, 0° AoA, diode 2, 100 MPH

Figure 151: Large model at 0° AoA of the pitch moment and normal force coefficients, dynamic release, diode 2, 100 MPH



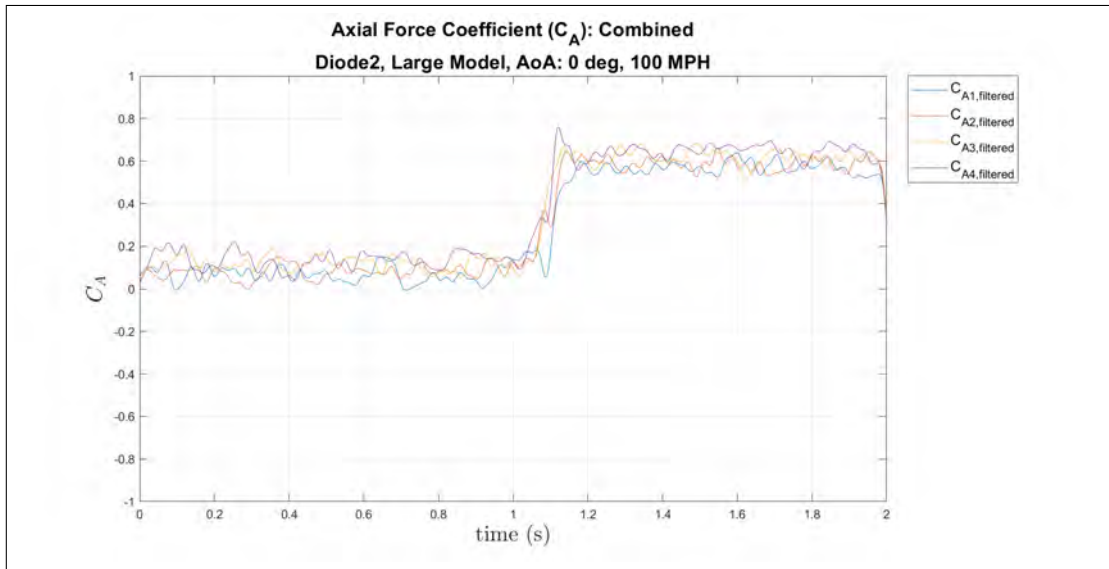
(a) Pitch Moment Coefficient, dynamic release, large model, 0° AoA, diode 2, 120 MPH



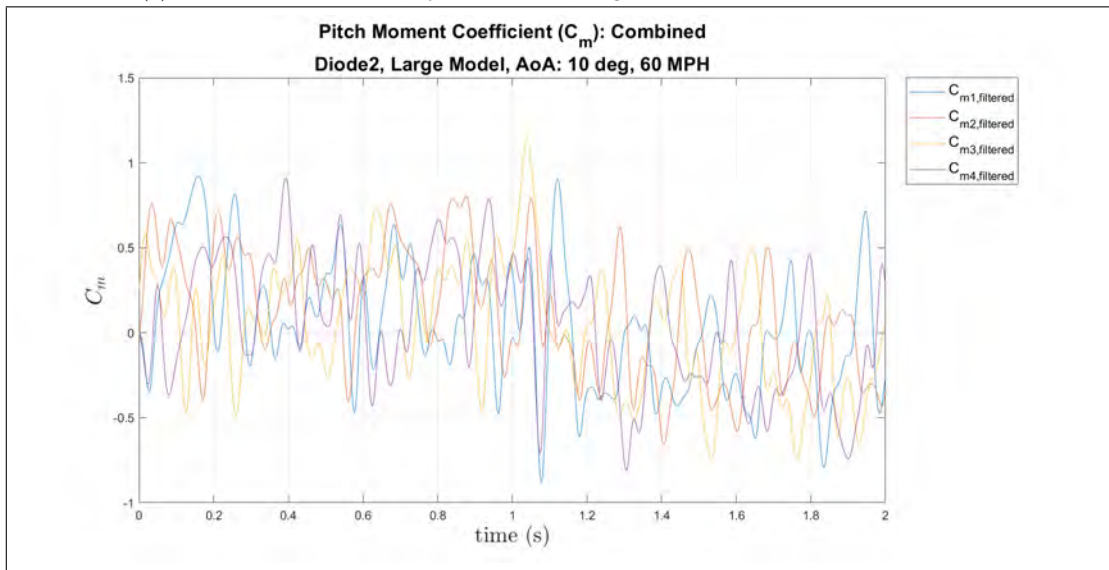
(b) Normal Force Coefficient, dynamic release, large model, 0° AoA, diode 2, 120 MPH

Figure 152: Large model at 0° AoA of the pitch moment and normal force coefficients, dynamic release, diode 2, 120 MPH

Large Model, Diode2, 10° AoA

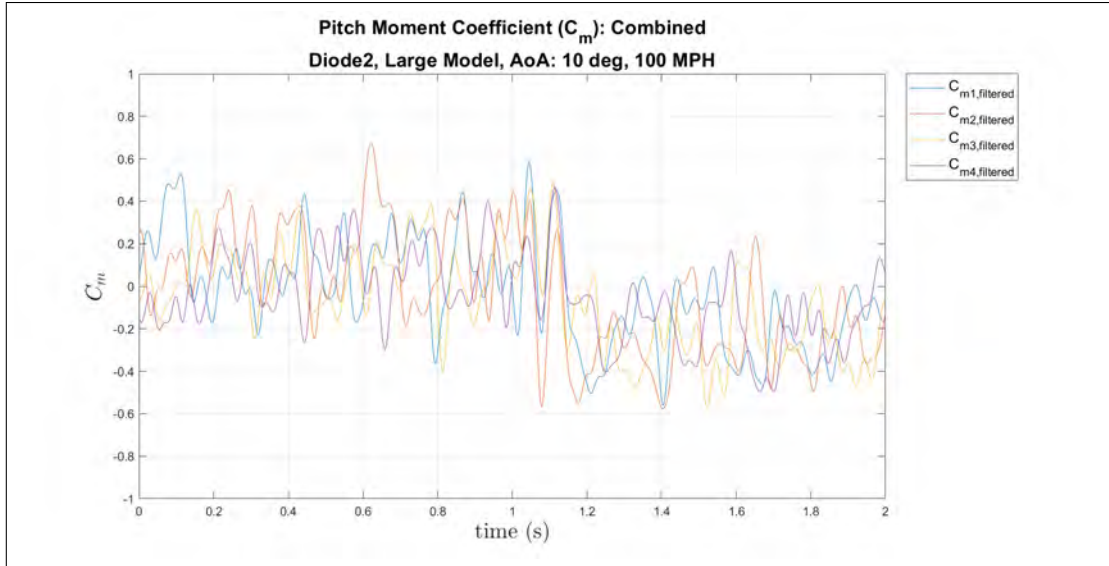


(a) Axial Force Coefficient, dynamic release, large model, 0° AoA, diode 2, 100 MPH

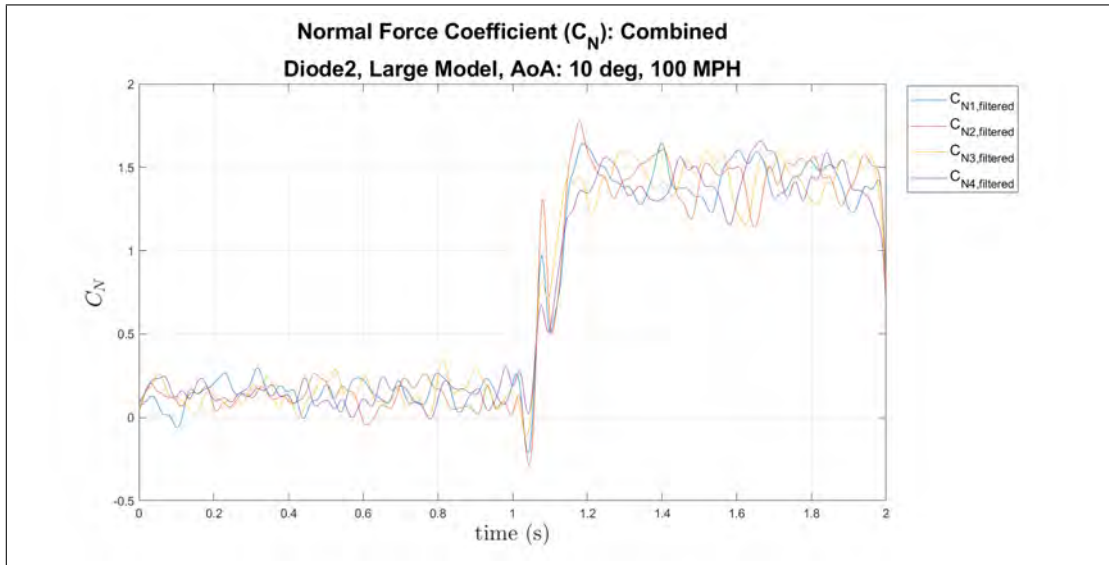


(b) Pitch Moment Coefficient, dynamic release, large model, 10° AoA, diode 2, 60 MPH

Figure 153: Large model at 0° AoA of the pitch moment and normal force coefficients, dynamic release, diode 2, 120 MPH

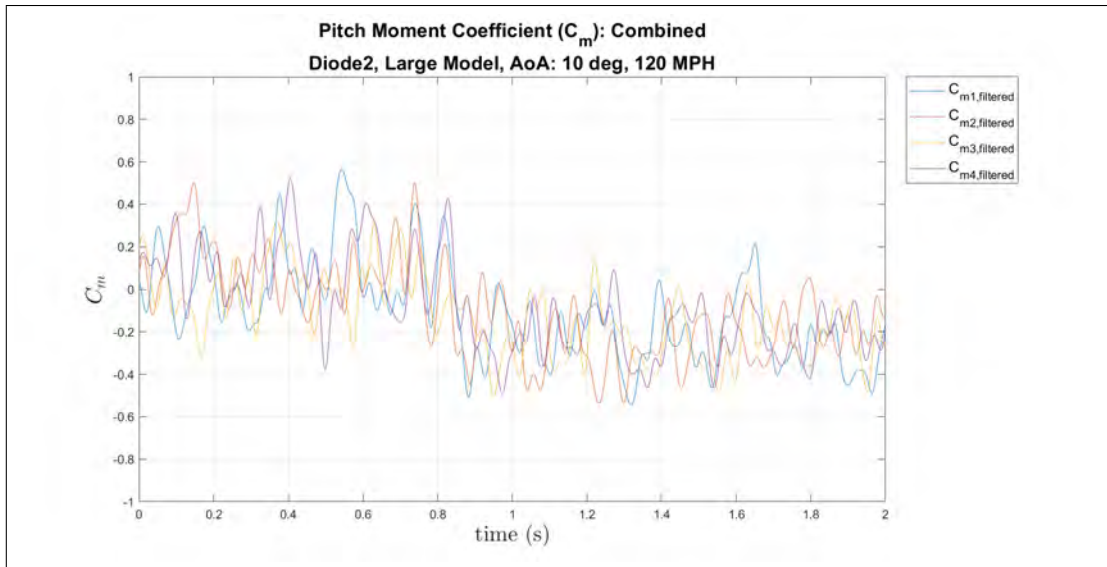


(a) Pitch Moment Coefficient, dynamic release, large model, 10° AoA, diode 2, 100 MPH

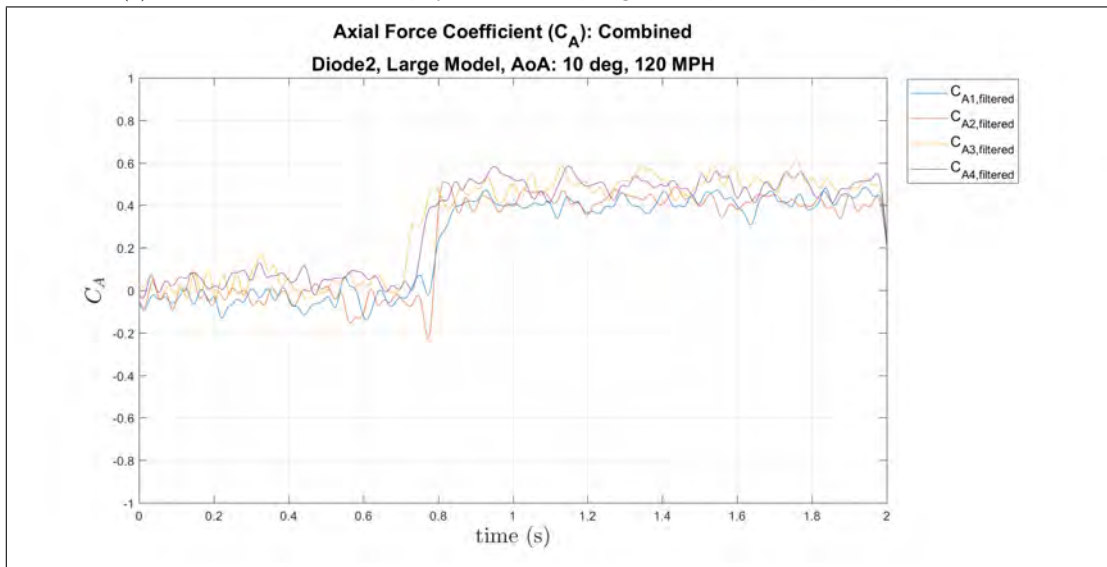


(b) Normal Force Coefficient, dynamic release, large model, 10° AoA, diode 2, 100 MPH

Figure 154: Large model at 10° AoA of the pitch moment and normal force coefficients, dynamic release, diode 2, 100 MPH



(a) Pitch Moment Coefficient, dynamic release, large model, 10° AoA, diode 2, 120 MPH

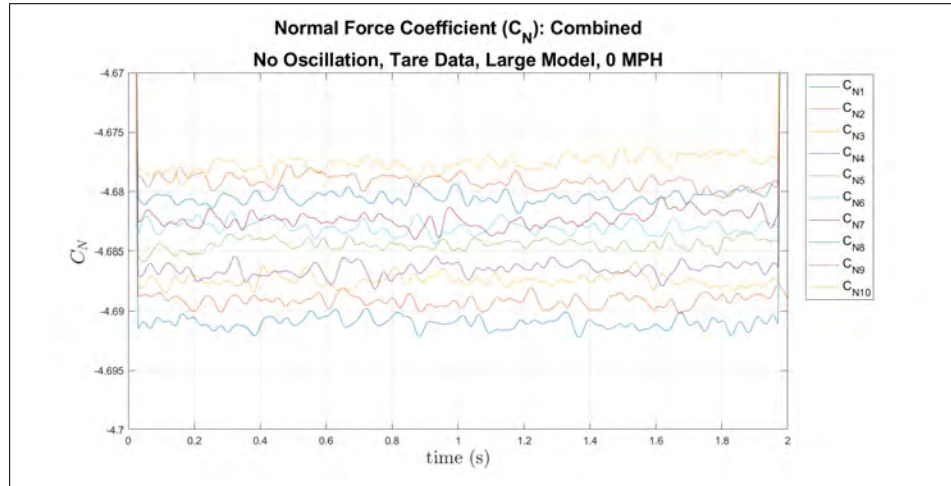


(b) Axial Force Coefficient, dynamic release, large model, 10° AoA, diode 2, 120 MPH

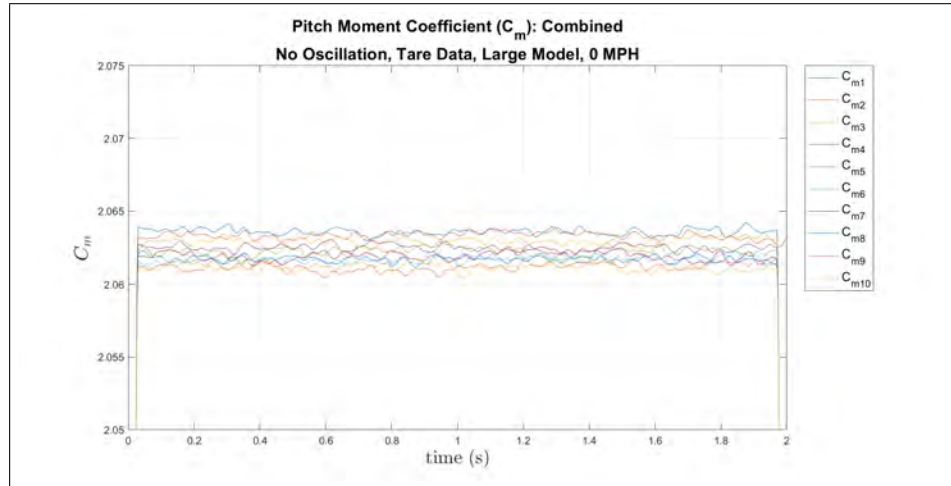
Figure 155: Large model at 10° AoA of the pitch moment and normal force coefficients, dynamic release, diode 2, 120 MPH

Repeatability Trials

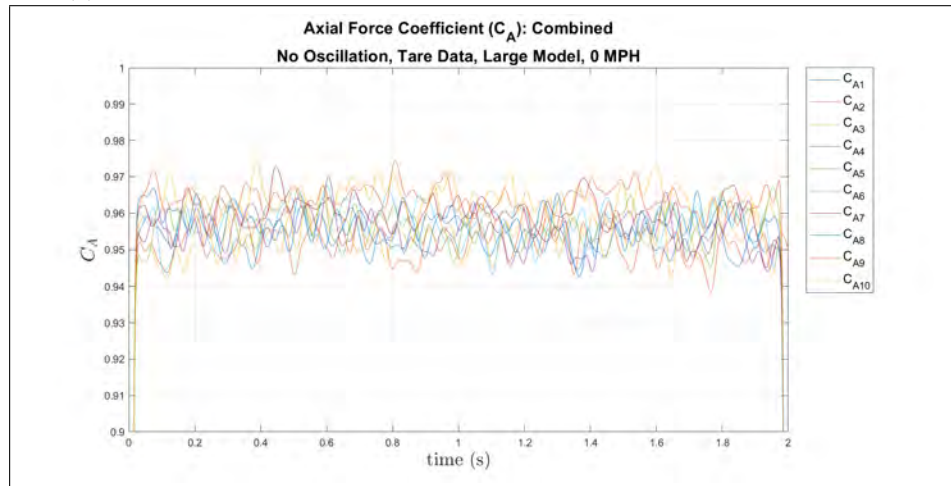
Normal Force, Pitch Moment, and Axial Force Coefficients



(a) Static normal force coefficient, large model, 10° AoA, diode 2, 0 MPH, 10 trials

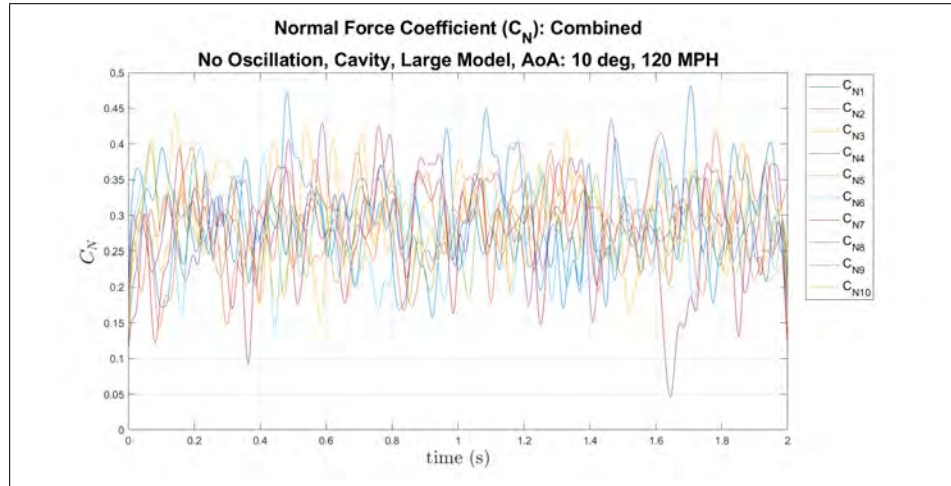


(b) Static pitch moment coefficient, large model, 10° AoA, diode 2, 0 MPH, 10 trials

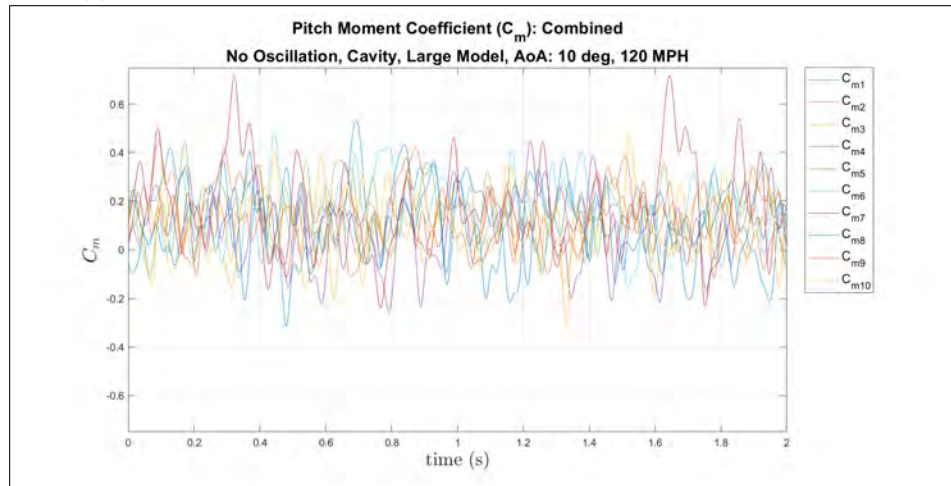


(c) Static axial force coefficient, large model, 10° AoA, diode 2, 0 MPH, 10 trials

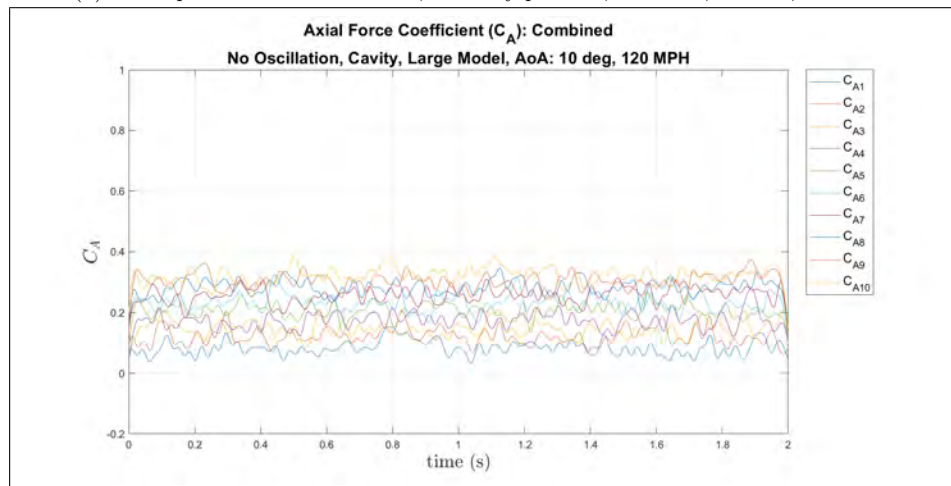
Figure 156: Repeatability of static coefficients, large model, 10° AoA, diode 2, 0 MPH, 10 trials



(a) Static normal force coefficient, in cavity position, 10° AoA, diode 2, 120 MPH

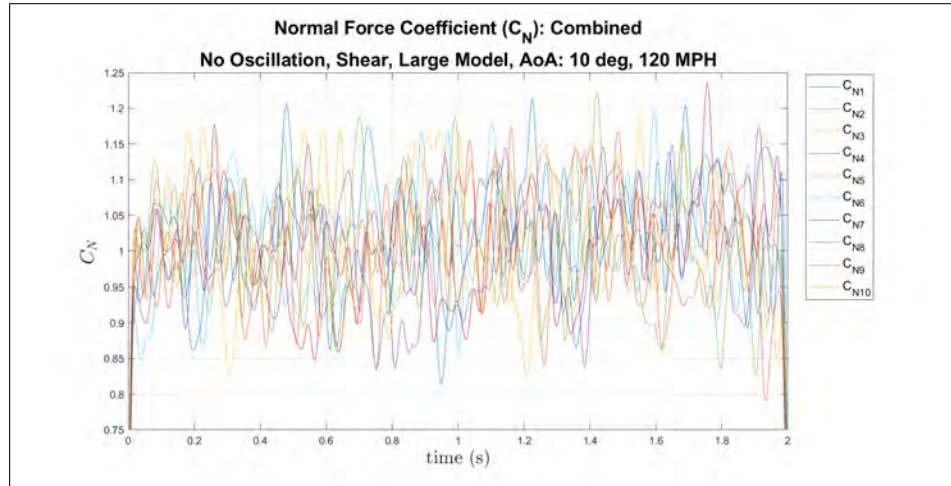


(b) Static pitch moment coefficient, in cavity position, 10° AoA, diode 2, 120 MPH

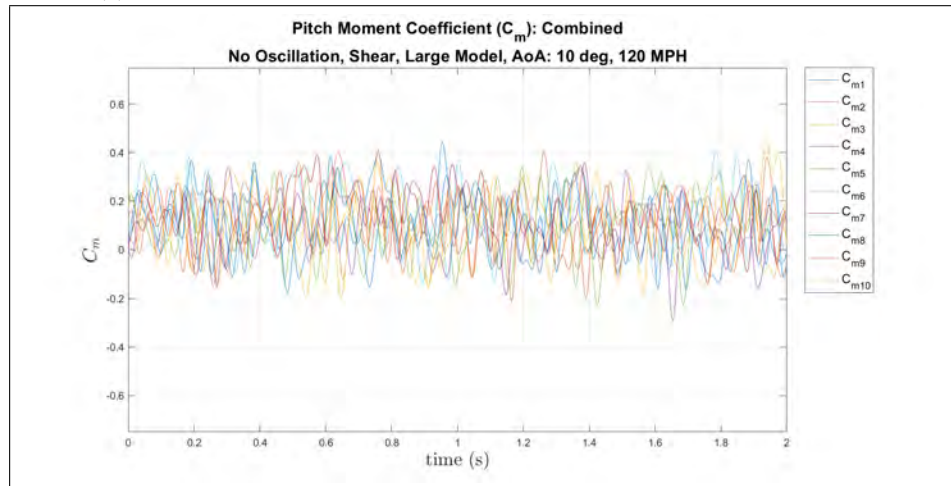


(c) Static axial force coefficient, in cavity position, 10° AoA, diode 2, 120 MPH

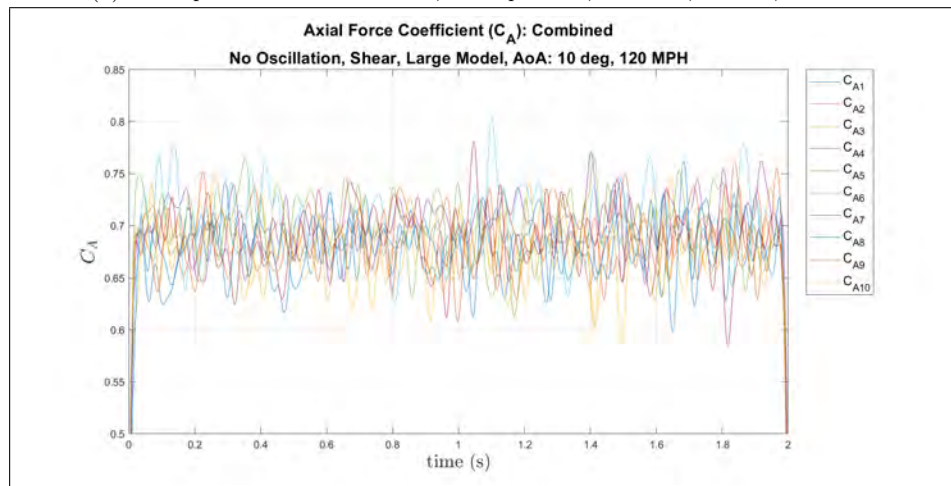
Figure 157: Repeatability of static coefficients, in cavity position, 10° AoA, diode 2, 120 MPH



(a) Static normal force coefficient, shear position, 10° AoA, diode 2, 120 MPH

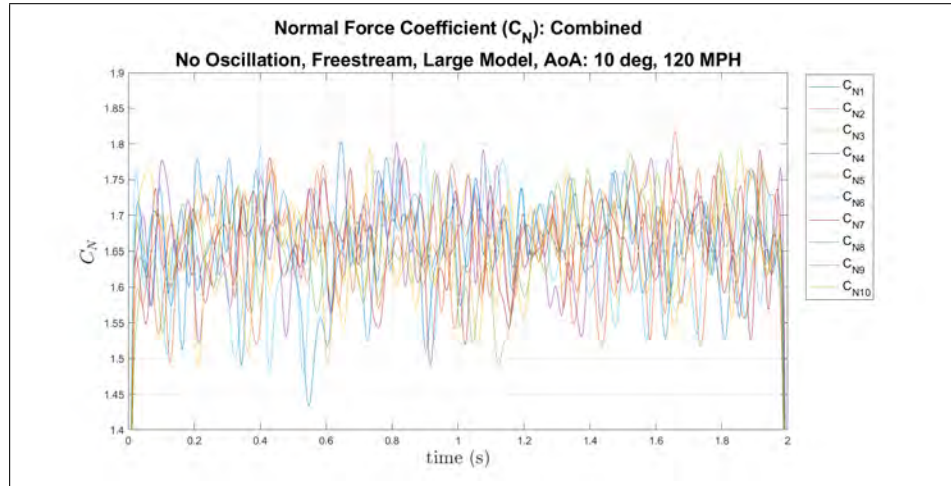


(b) Static pitch moment coefficient, shear position, 10° AoA, diode 2, 120 MPH

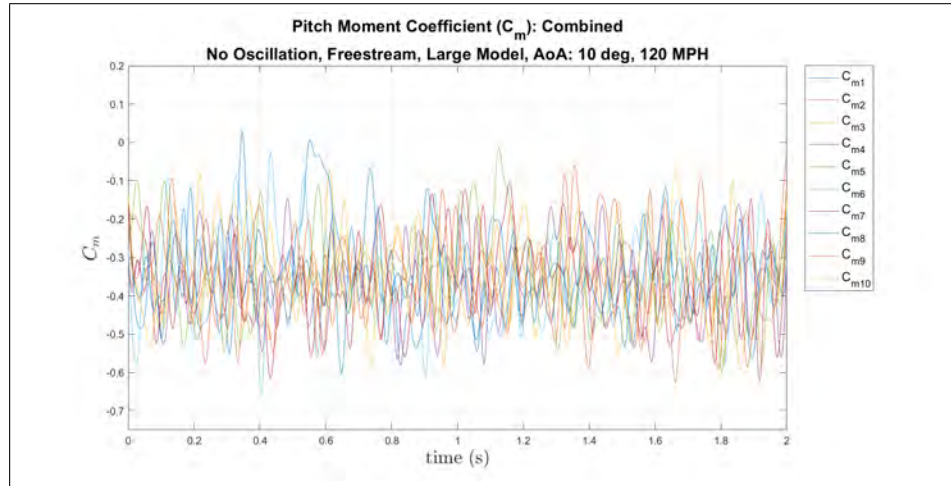


(c) Static axial force coefficient, shear position, 10° AoA, diode 2, 120 MPH

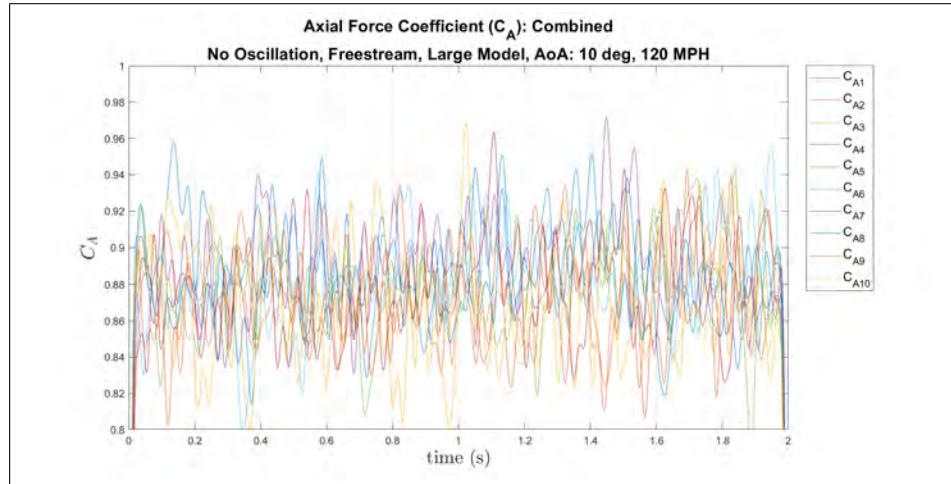
Figure 158: Repeatability of static coefficients, shear position, 10° AoA, diode 2, 120 MPH



(a) Static normal force coefficient, out of cavity position, 10° AoA, diode 2, 120 MPH

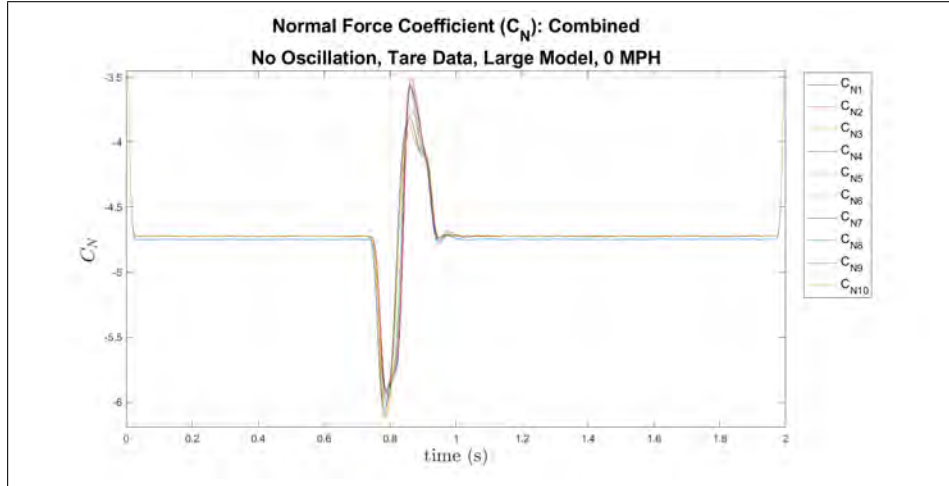


(b) Static pitch moment coefficient, out of cavity position, 10° AoA, diode 2, 120 MPH

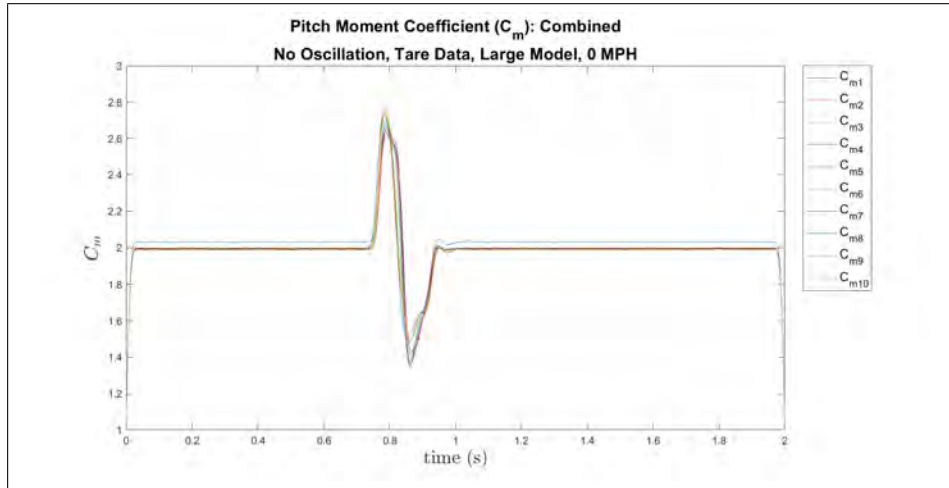


(c) Static axial force coefficient, out of cavity position, 10° AoA, diode 2, 120 MPH

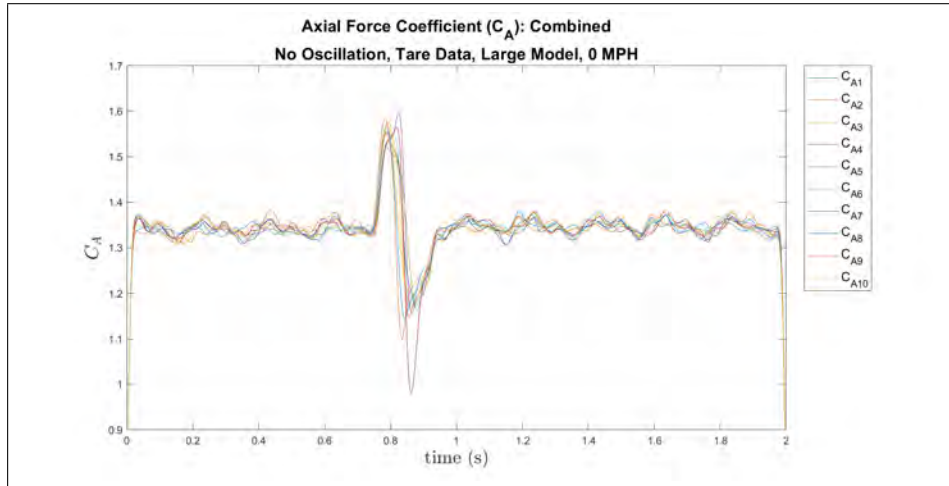
Figure 159: Repeatability of static coefficients, out of cavity position, 10° AoA, diode 2, 120 MPH



(a) Dynamic normal force coefficient, large model, 10° AoA, diode 2, 0 MPH, 10 trials

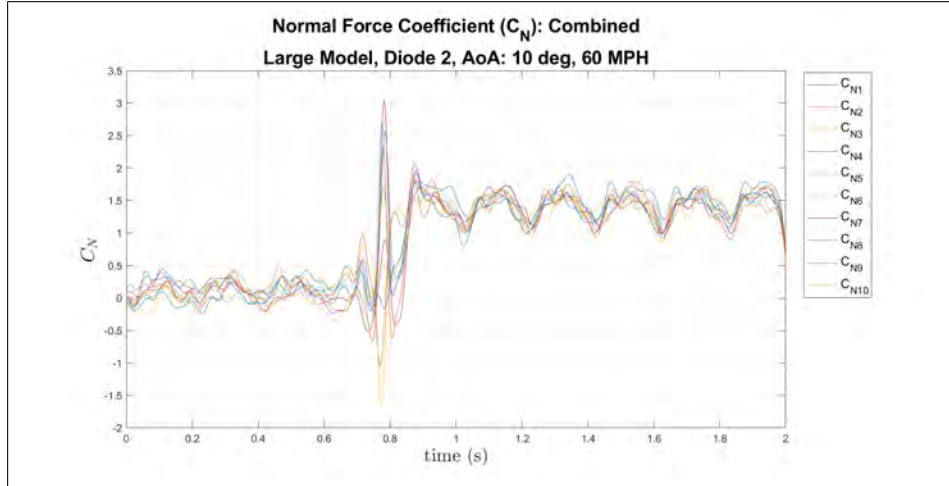


(b) Dynamic pitch moment coefficient, large model, 10° AoA, diode 2, 0 MPH, 10 trials

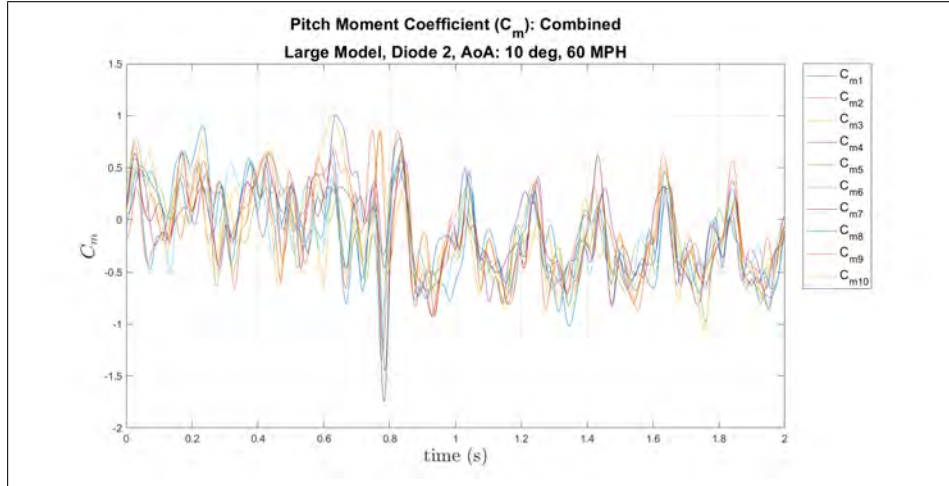


(c) Dynamic axial force coefficient, large model, 10° AoA, diode 2, 0 MPH, 10 trials

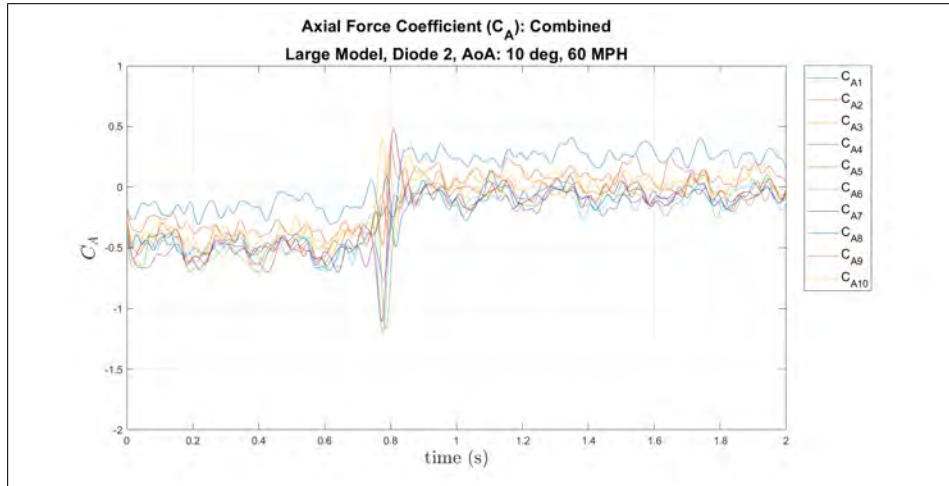
Figure 160: Repeatability of dynamic coefficients, large model, 10° AoA, diode 2, 0 MPH, 10 trials



(a) Dynamic normal force coefficient, large model, 10° AoA, diode 2, 60 MPH, 10 trials

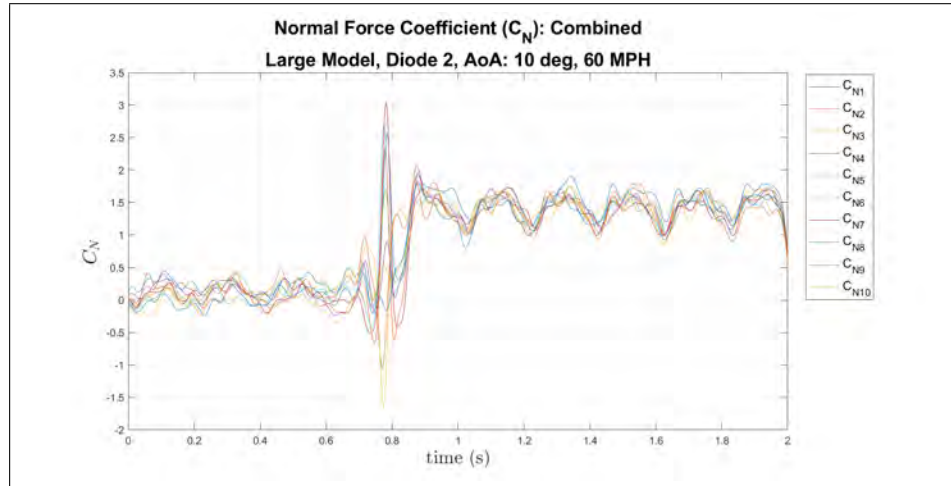


(b) Dynamic pitch moment coefficient, large model, 10° AoA, diode 2, 60 MPH, 10 trials

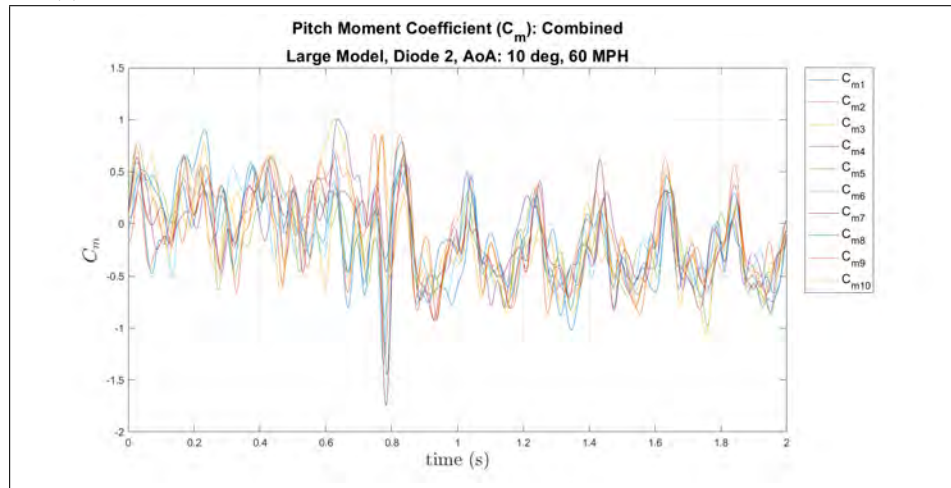


(c) Dynamic axial force coefficient, large model, 10° AoA, diode 2, 60 MPH, 10 trials

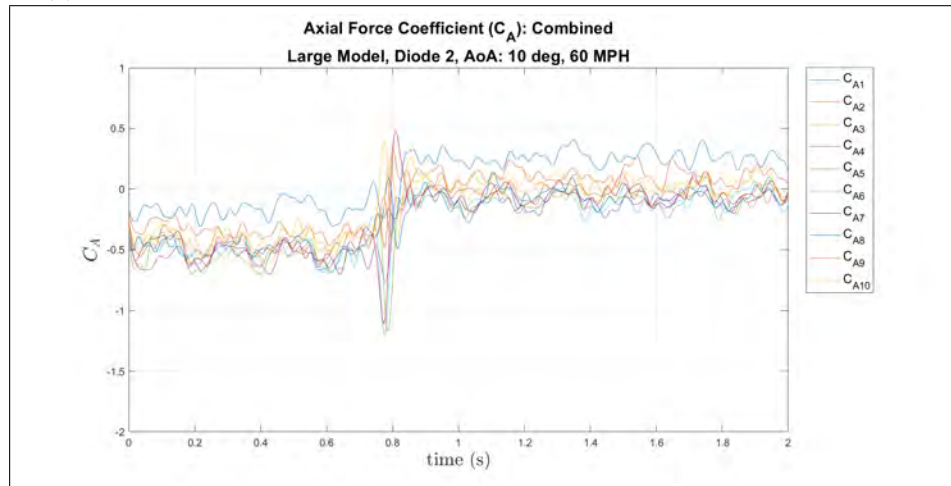
Figure 161: Repeatability of dynamic coefficients, large model, 10° AoA, diode 2, 60 MPH, 10 trials



(a) Dynamic normal force coefficient, large model, 10° AoA, diode 2, 60 MPH, 10 trials

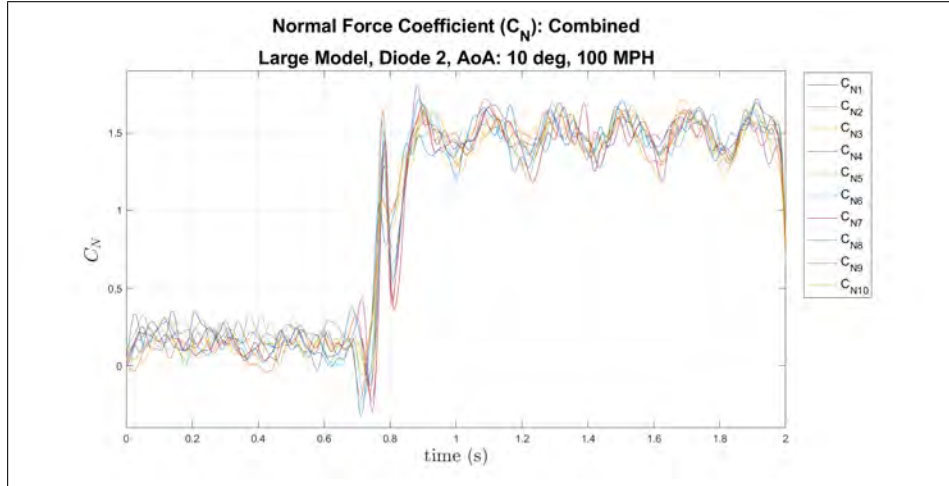


(b) Dynamic pitch moment coefficient, large model, 10° AoA, diode 2, 60 MPH, 10 trials

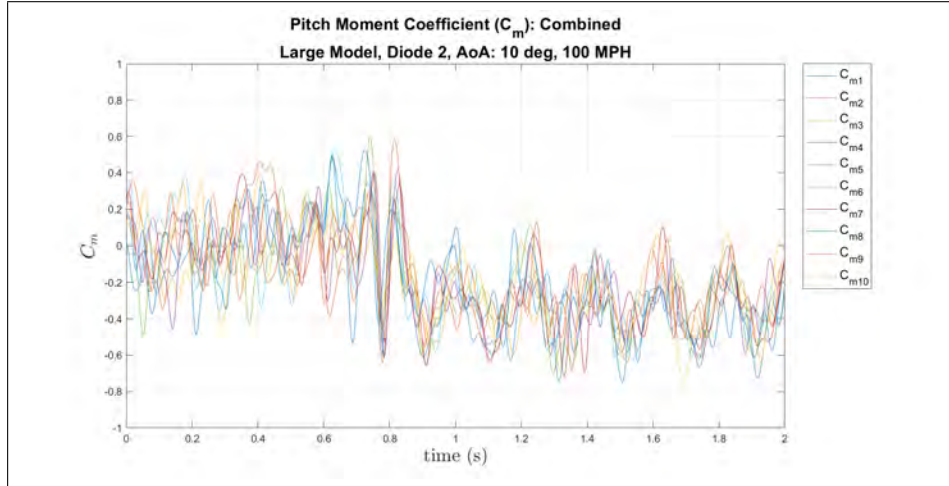


(c) Dynamic axial force coefficient, large model, 10° AoA, diode 2, 60 MPH, 10 trials

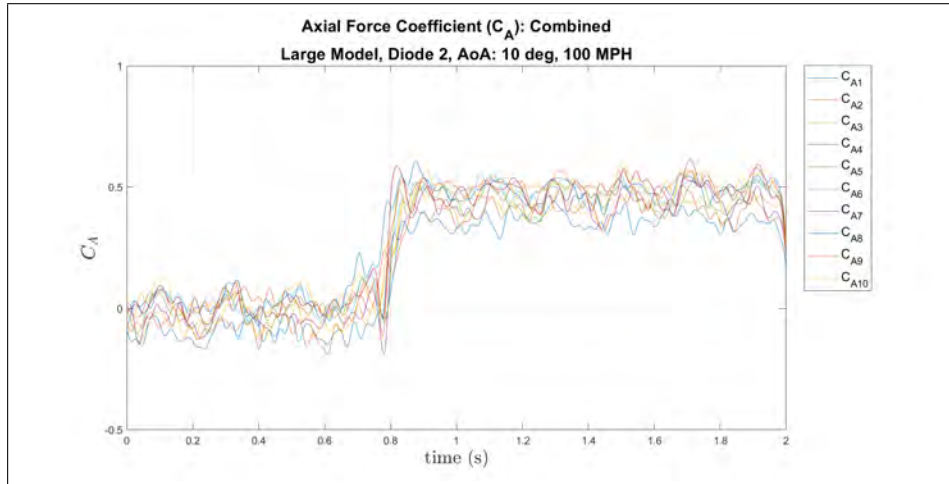
Figure 162: Repeatability of dynamic coefficients, large model, 10° AoA, diode 2, 60 MPH, 10 trials



(a) Dynamic normal force coefficient, large model, 10° AoA, diode 2, 100 MPH, 10 trials

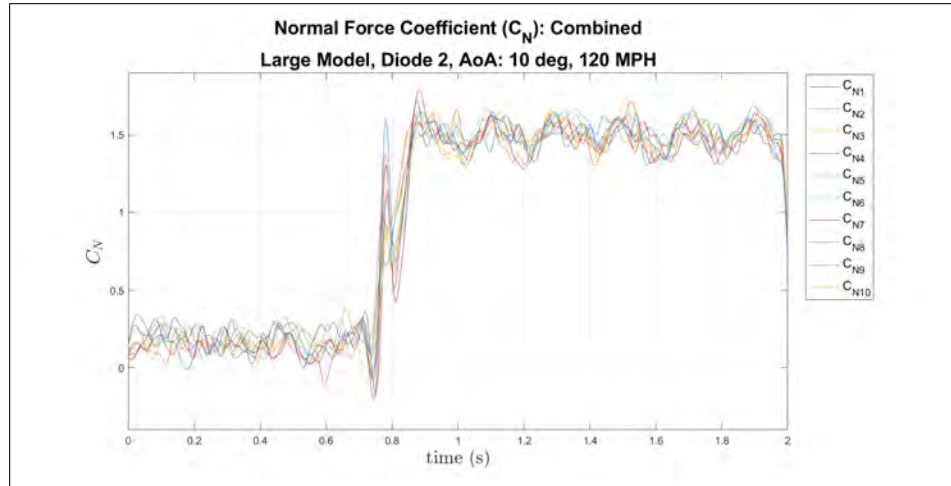


(b) Dynamic pitch moment coefficient, large model, 10° AoA, diode 2, 100 MPH, 10 trials

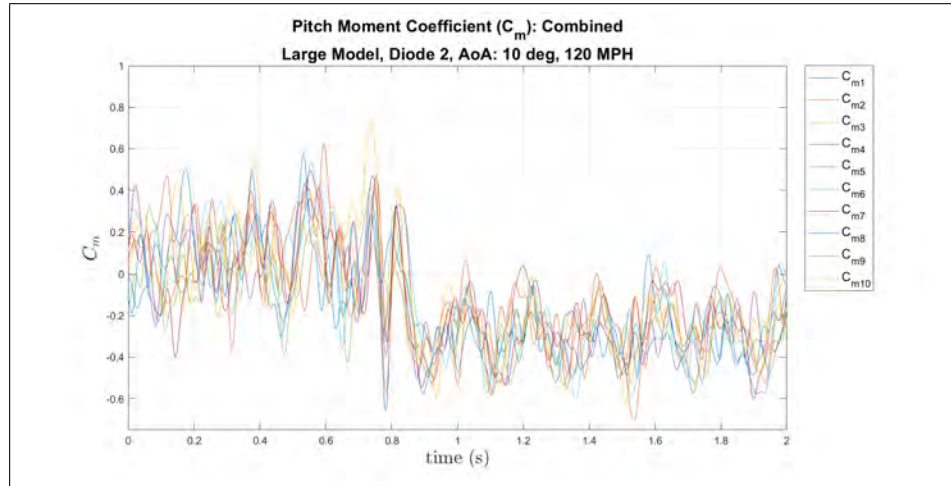


(c) Dynamic axial force coefficient, large model, 10° AoA, diode 2, 100 MPH, 10 trials

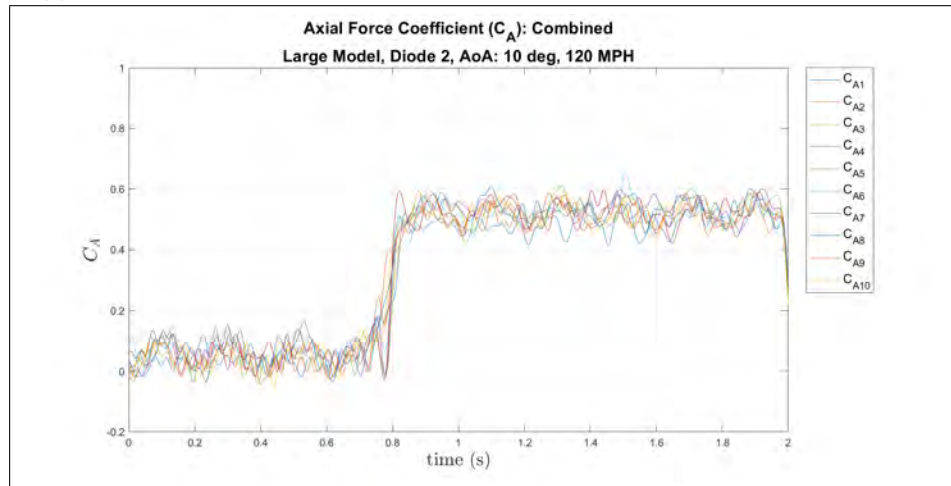
Figure 163: Repeatability of dynamic coefficients, large model, 10° AoA, diode 2, 100 MPH, 10 trials



(a) Dynamic normal force coefficient, large model, 10° AoA, diode 2, 120 MPH, 10 trials



(b) Dynamic pitch moment coefficient, large model, 10° AoA, diode 2, 120 MPH, 10 trials



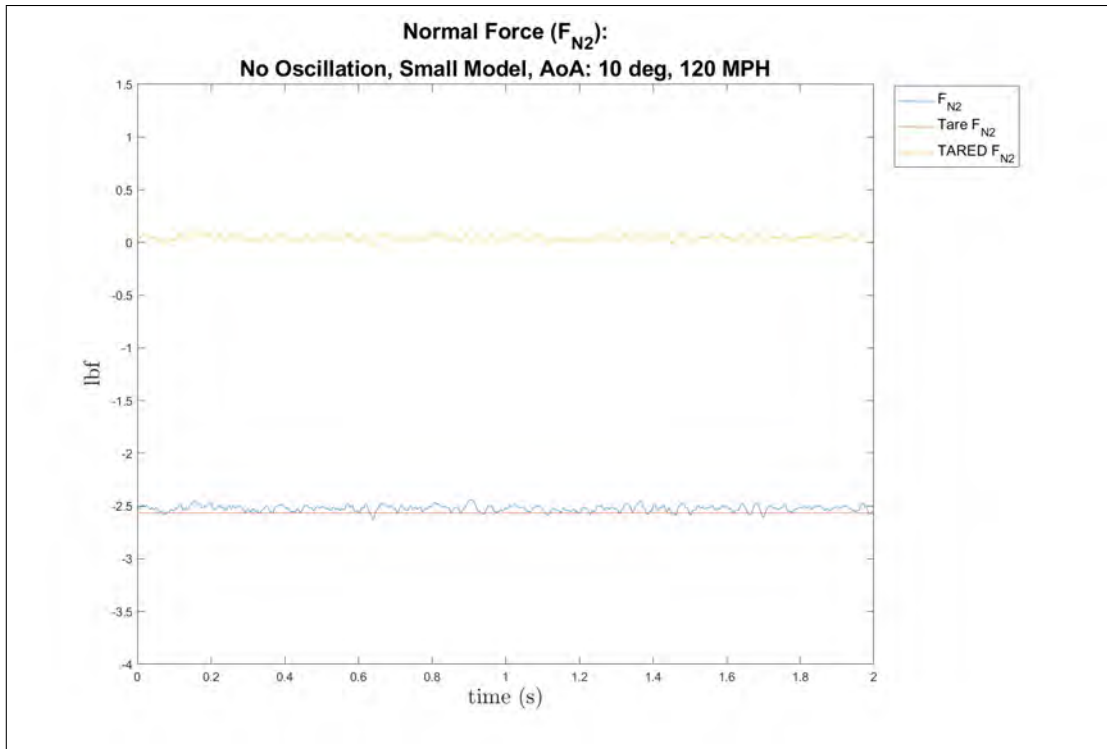
(c) Dynamic axial force coefficient, large model, 10° AoA, diode 2, 120 MPH, 10 trials

Figure 164: Repeatability of dynamic coefficients, large model, 10° AoA, diode 2, 120 MPH, 10 trials

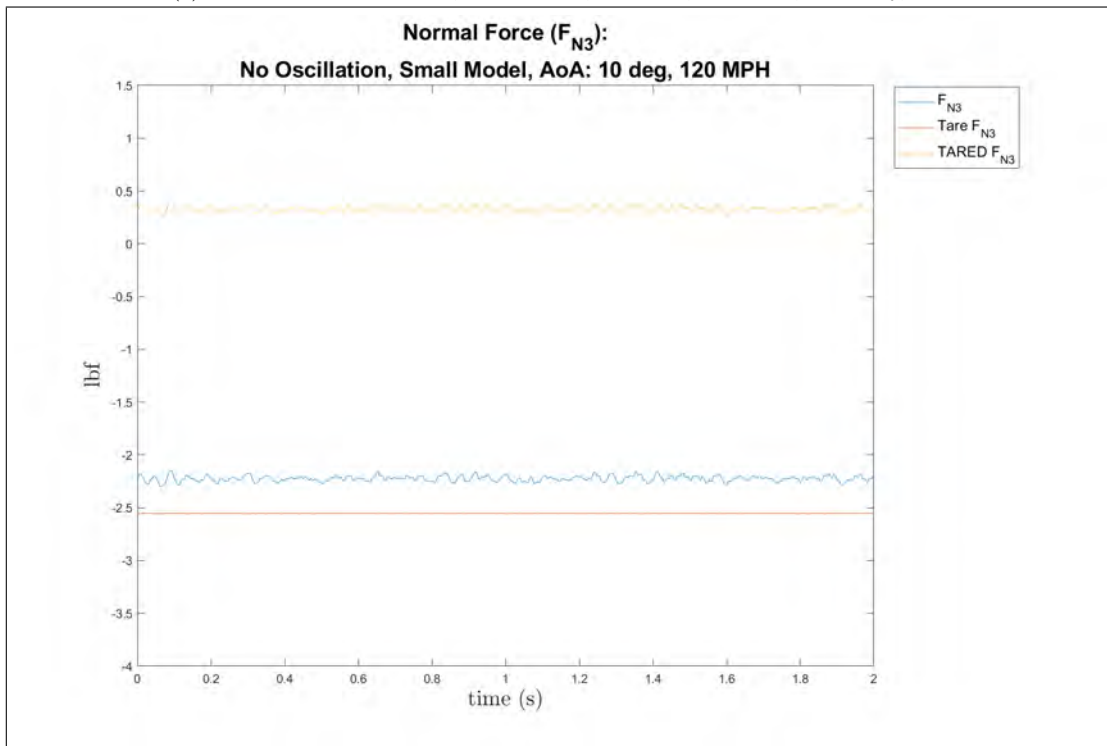
Tare Examples 10 Degrees

Normal Force, Pitch Moment, and Axial Force Coefficients

Small Model, Cavity Apparatus, 10° AoA, 120 MPH

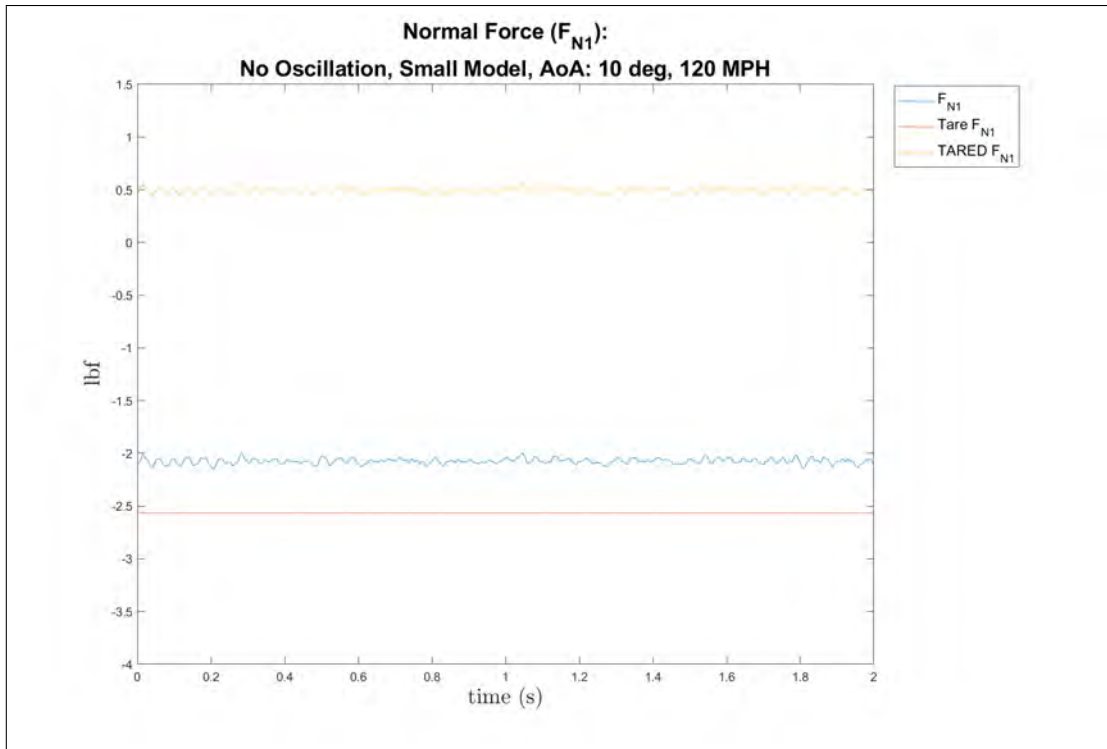


(a) Normal Force Coefficient, small model, 10° AoA, 120 MPH, In Cavity, tare

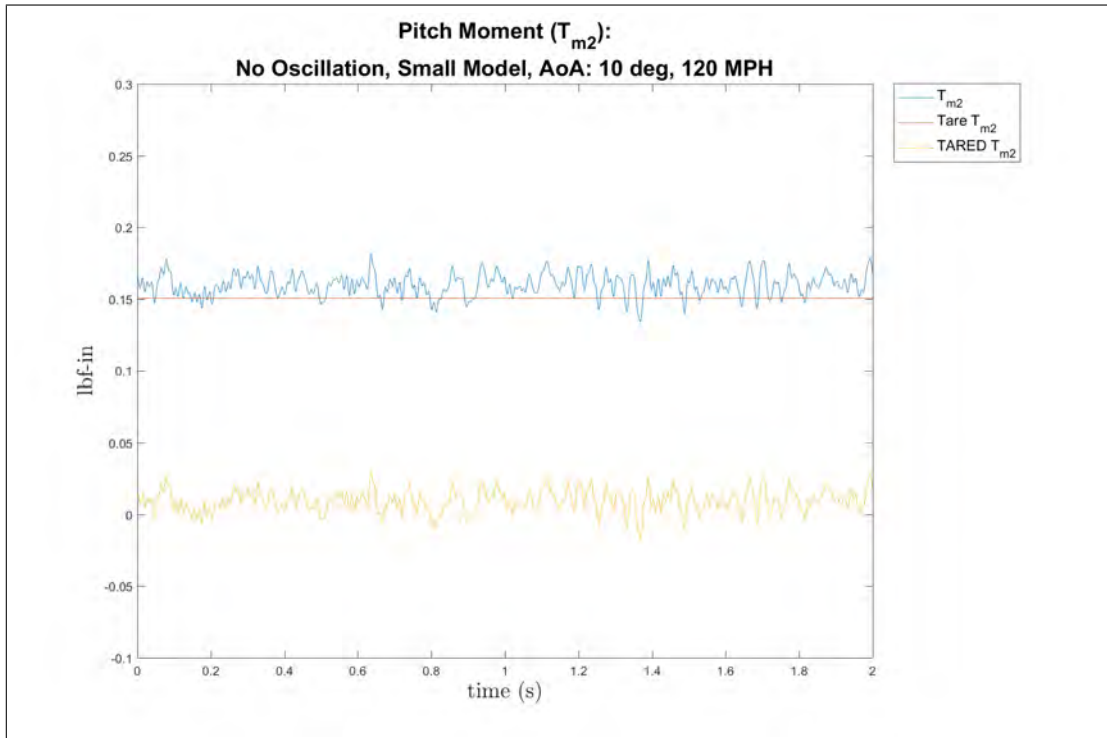


(b) Normal Force Coefficient, small model, 10° AoA, 120 MPH, Shear Layer, tare

Figure 165: Small model at 10° AoA of the normal force coefficient, 120 MPH, tare

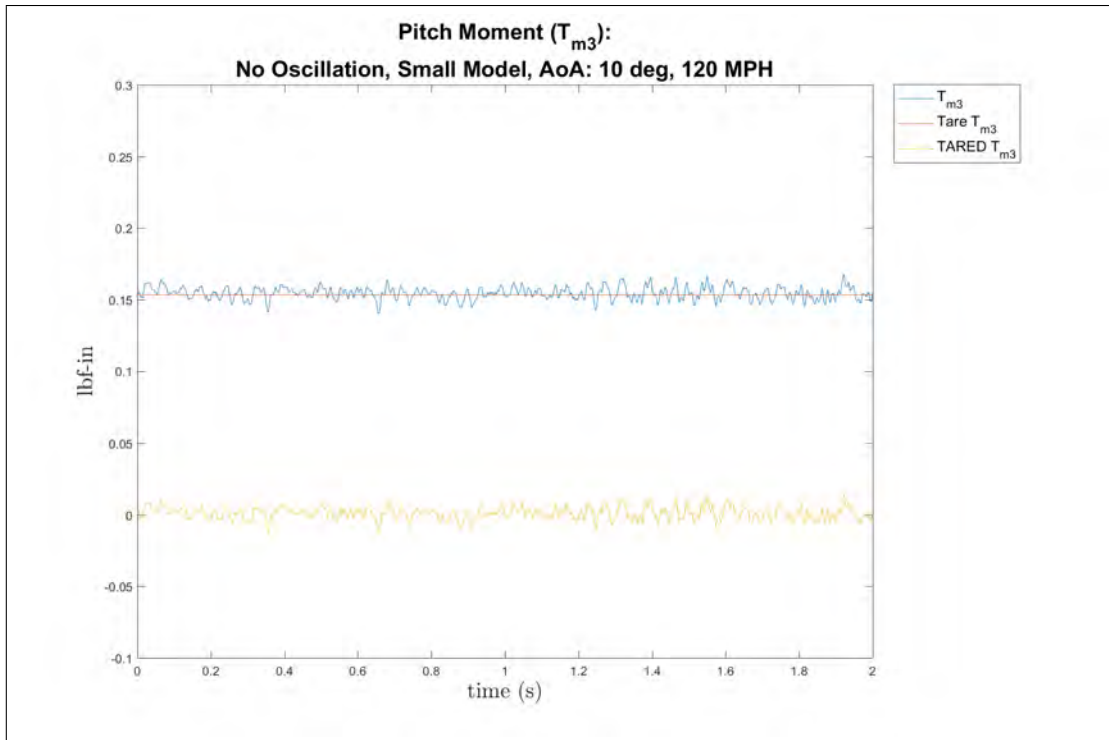


(a) Normal Force Coefficient, small model, 10° AoA, 120 MPH, Out Cavity, tare

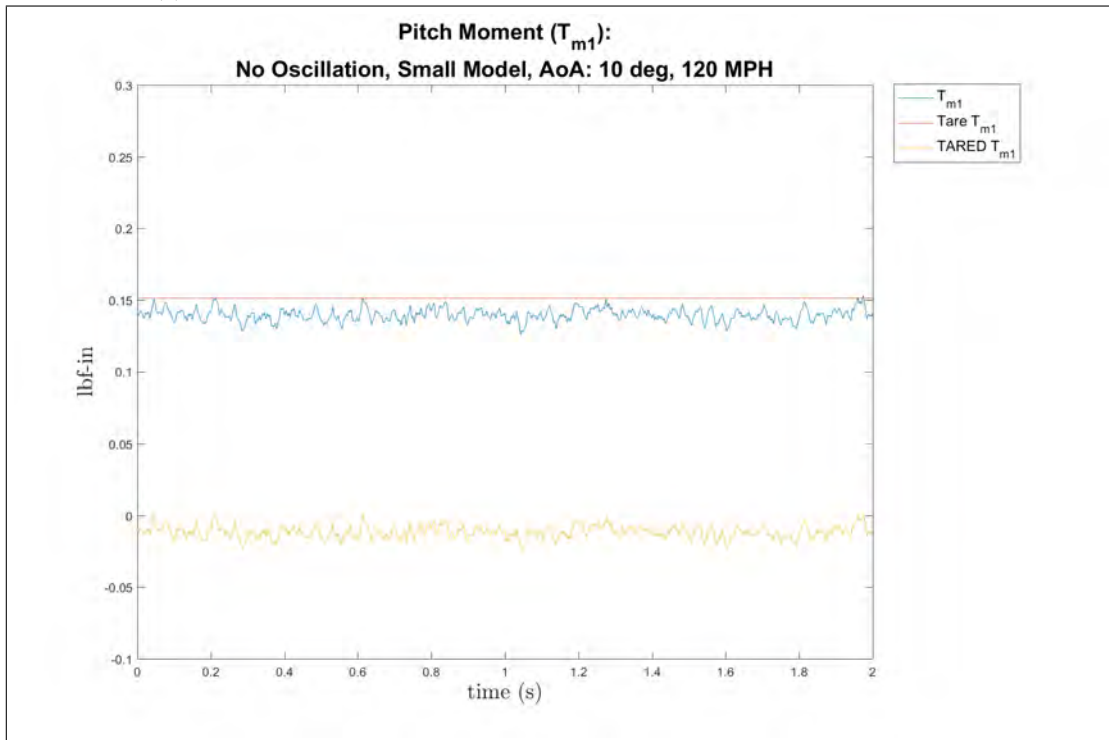


(b) Pitch Moment Coefficient, small model, 10° AoA, 120 MPH, In Cavity, tare

Figure 166: Small model at 10° AoA of the pitch moment and normal force coefficients, 120 MPH, tare

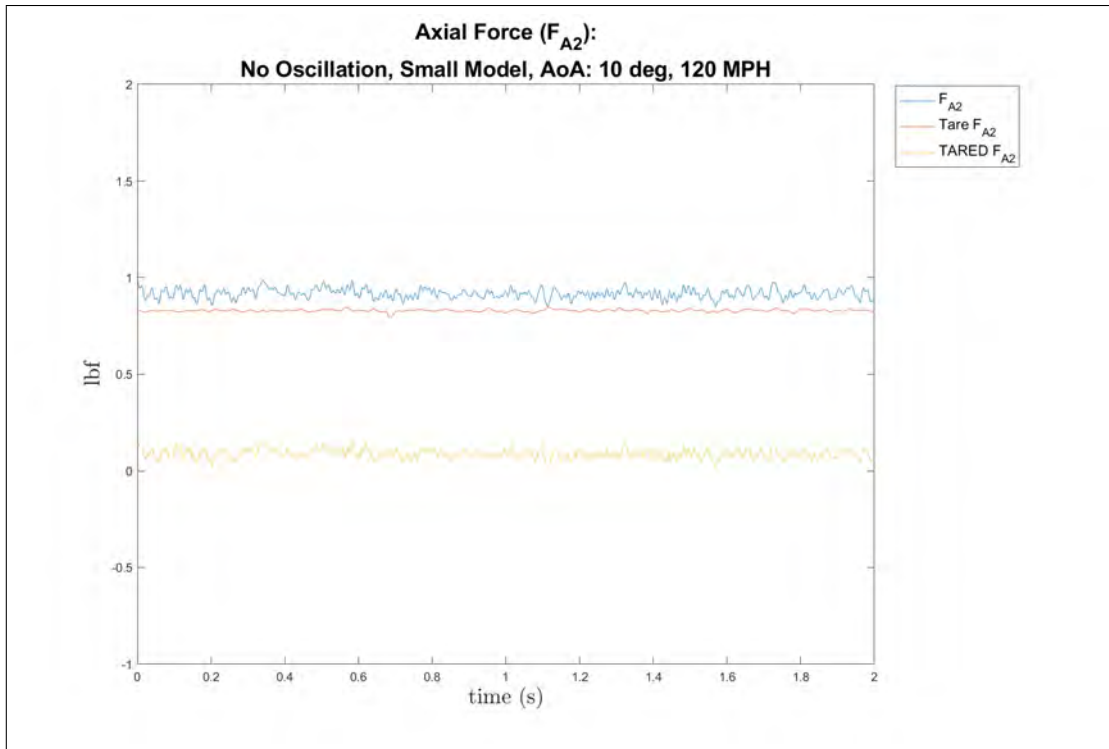


(a) Pitch Moment Coefficient, small model, 10° AoA, 120 MPH, Shear Layer, tare

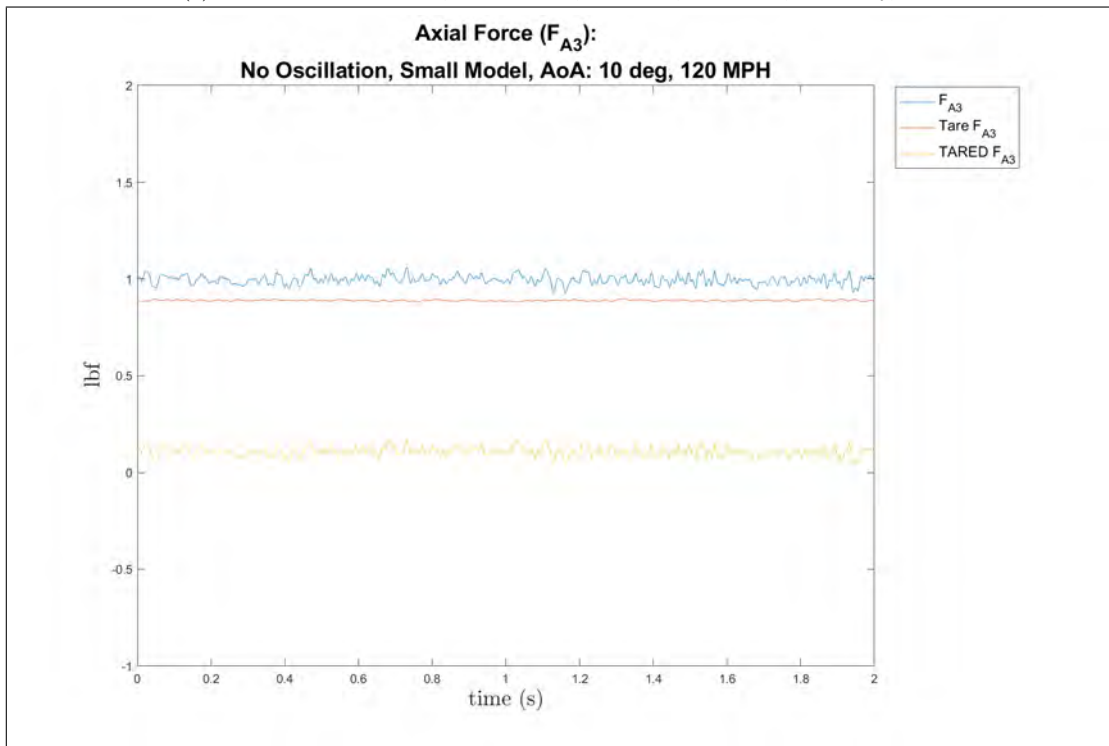


(b) Pitch Moment Coefficient, small model, 10° AoA, 120 MPH, Out Cavity, tare

Figure 167: Small model at 10° AoA of the pitch moment coefficient, 120 MPH, tare

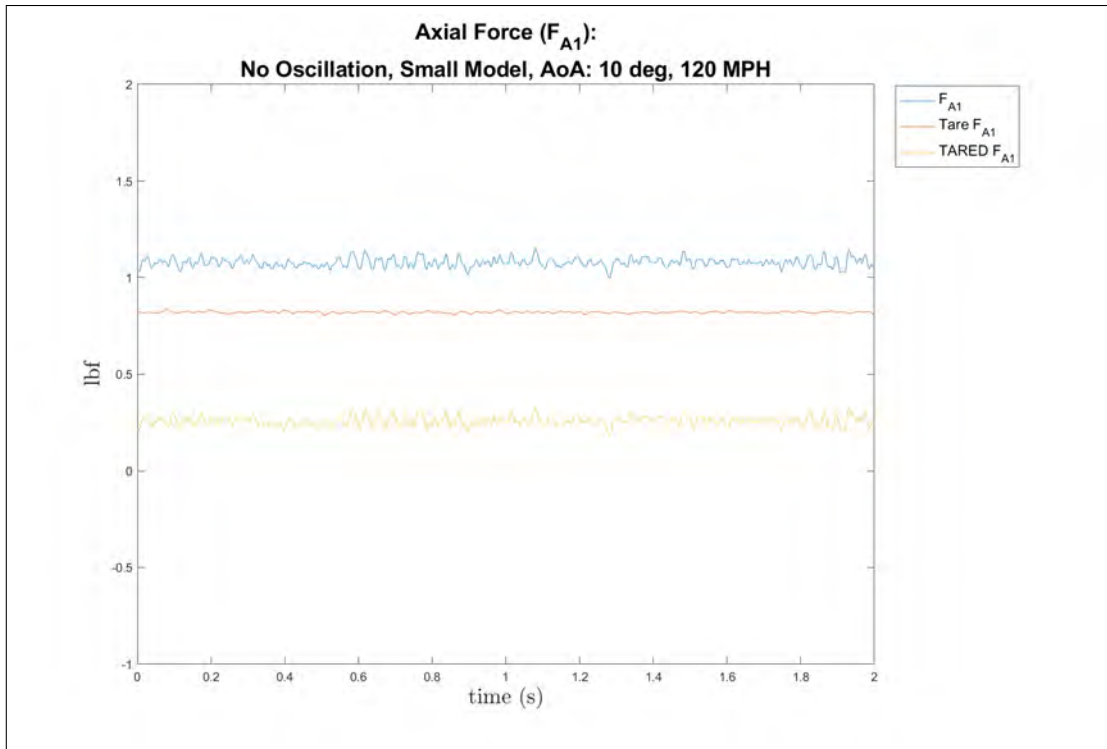


(a) Axial Force Coefficient, small model, 10° AoA, 120 MPH, In Cavity, tare

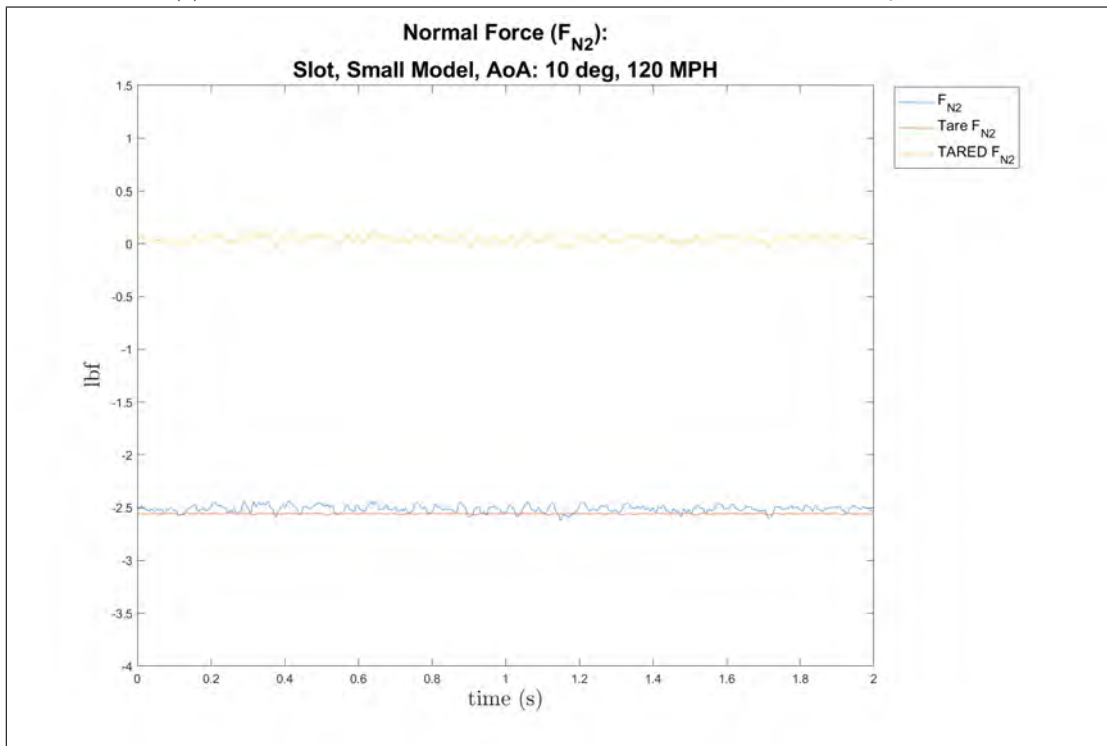


(b) Axial Force Coefficient, small model, 10° AoA, 120 MPH, Shear Layer, tare

Figure 168: Small model at 10° AoA of the Axial Force coefficient, 120 MPH, tare

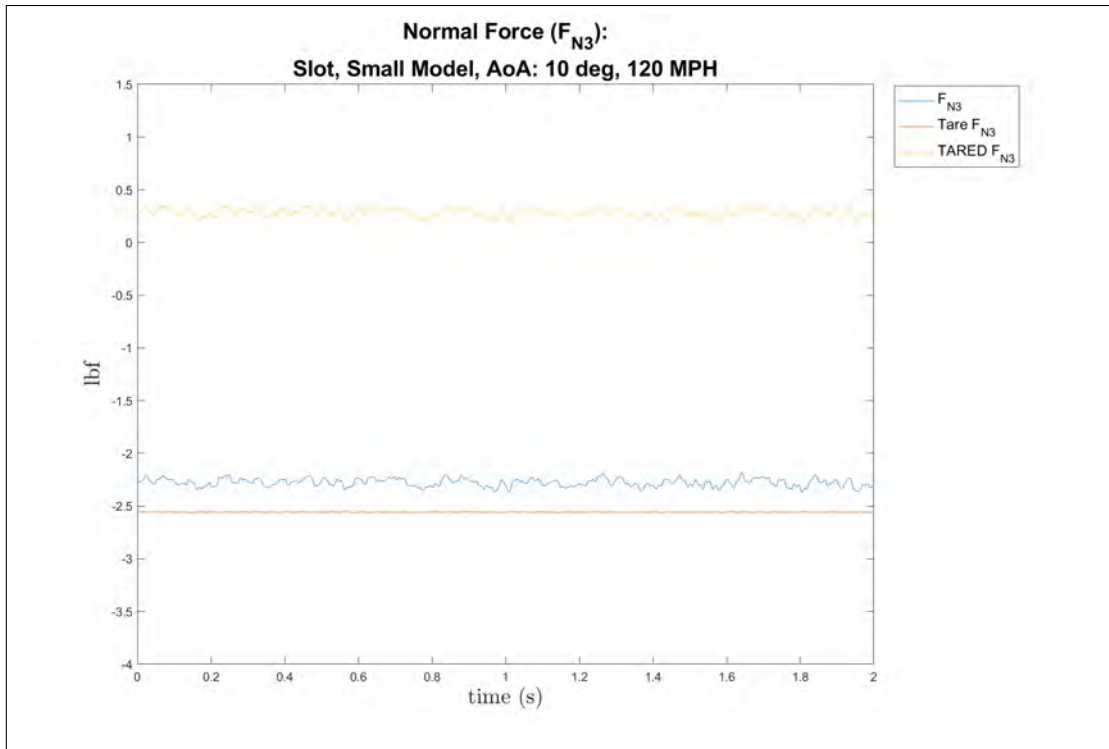


(a) Axial Force Coefficient, small model, 10° AoA, 120 MPH, Out Cavity, tare

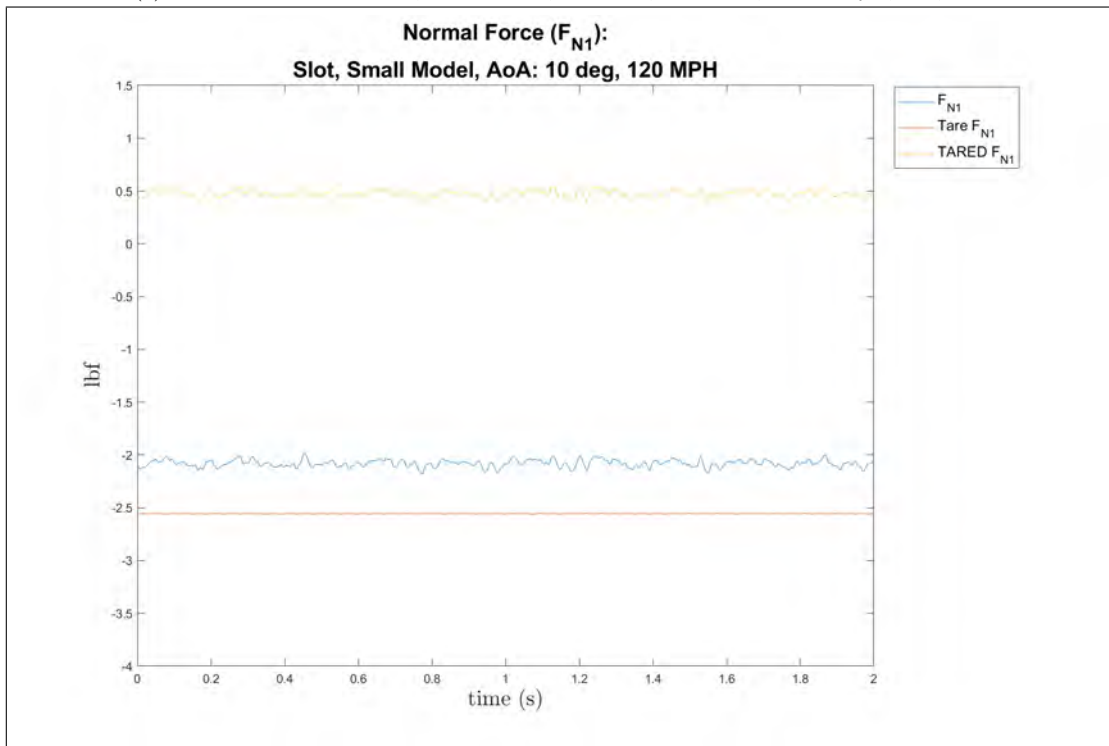


(b) Noormal Force Coefficient, small model, 10° AoA, 120 MPH, In Cavity, slot, tare

Figure 169: Small model at 10° AoA of the axial force and normal force coefficients, 120 MPH, tare

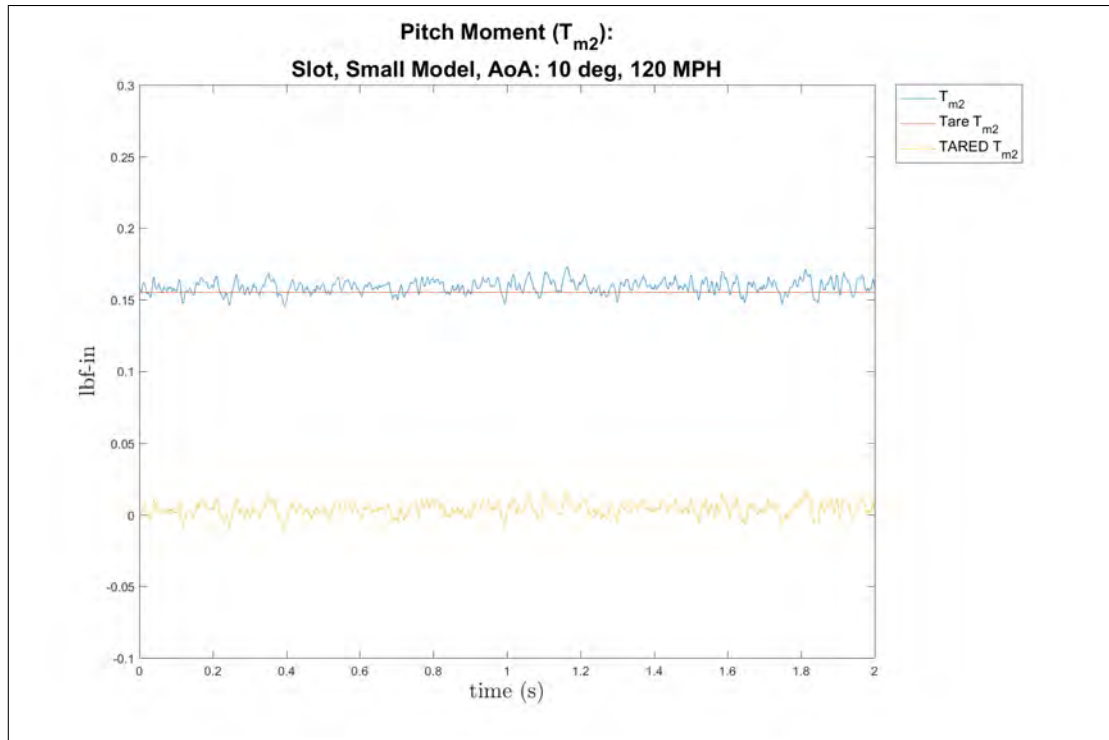


(a) Normal Force Coefficient, small model, 10° AoA, 120 MPH, Shear Layer, slot, tare

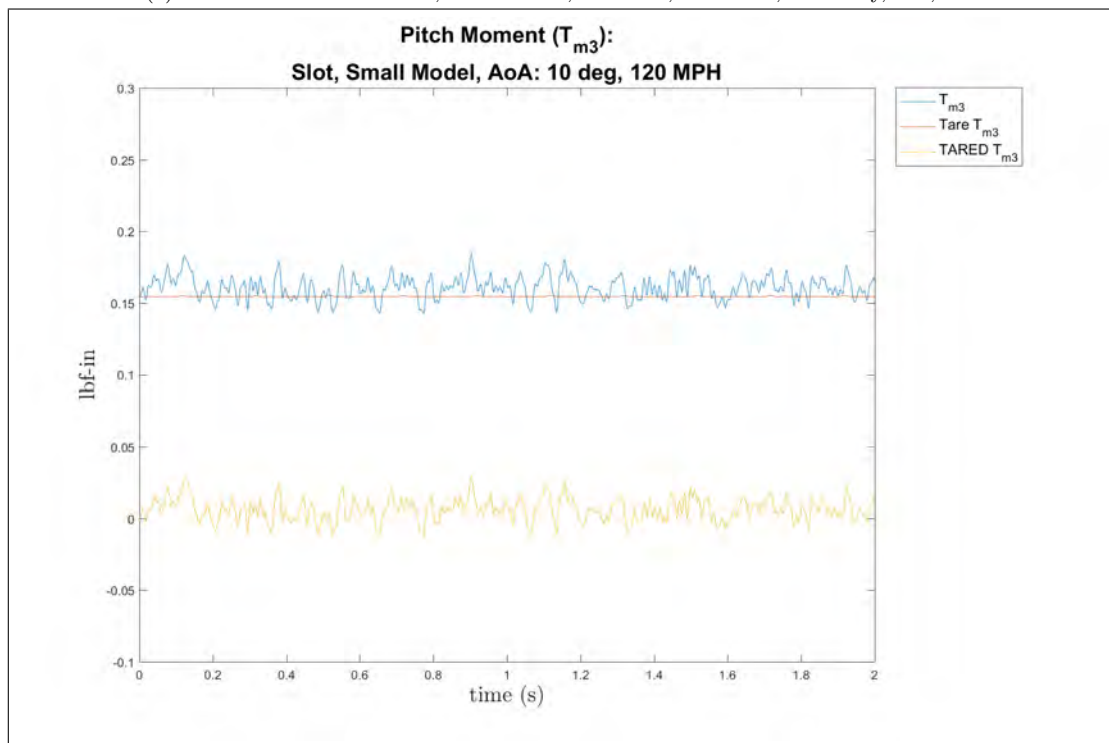


(b) Normal Force Coefficient, small model, 10° AoA, 120 MPH, Out Cavity, slot, tare

Figure 170: Small model at 10° AoA of the normal force coefficient, 120 MPH, slot, tare

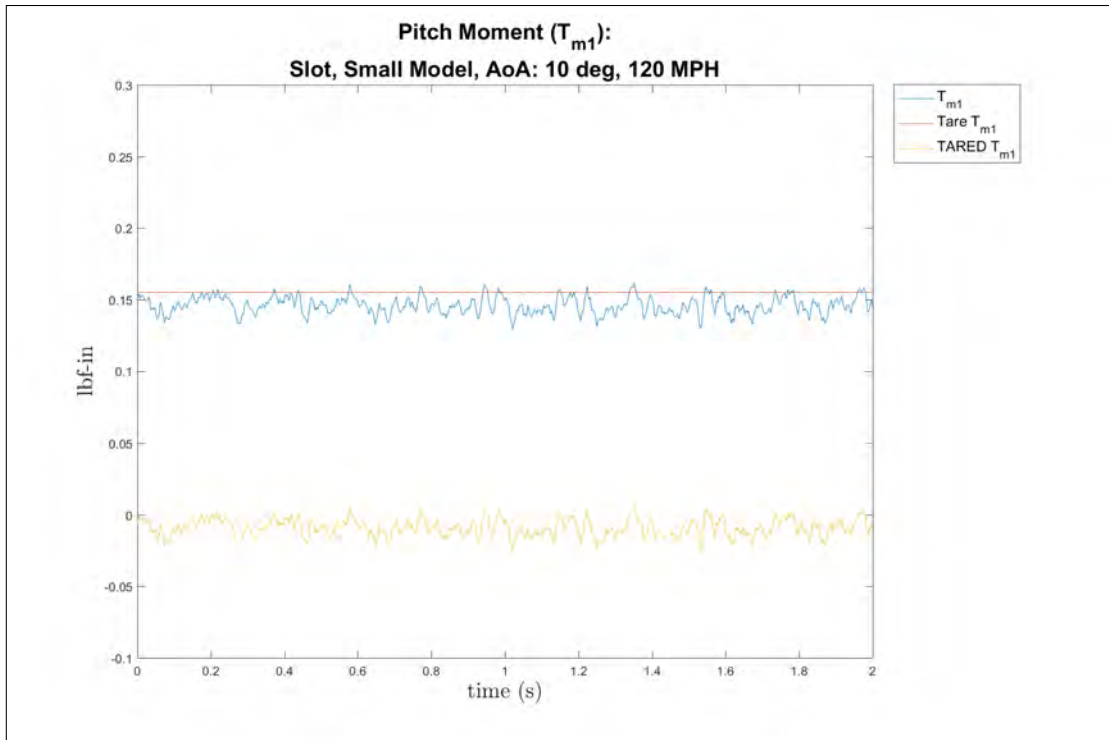


(a) Pitch Moment Coefficient, small model, 10° AoA, 120 MPH, In Cavity, slot, tare

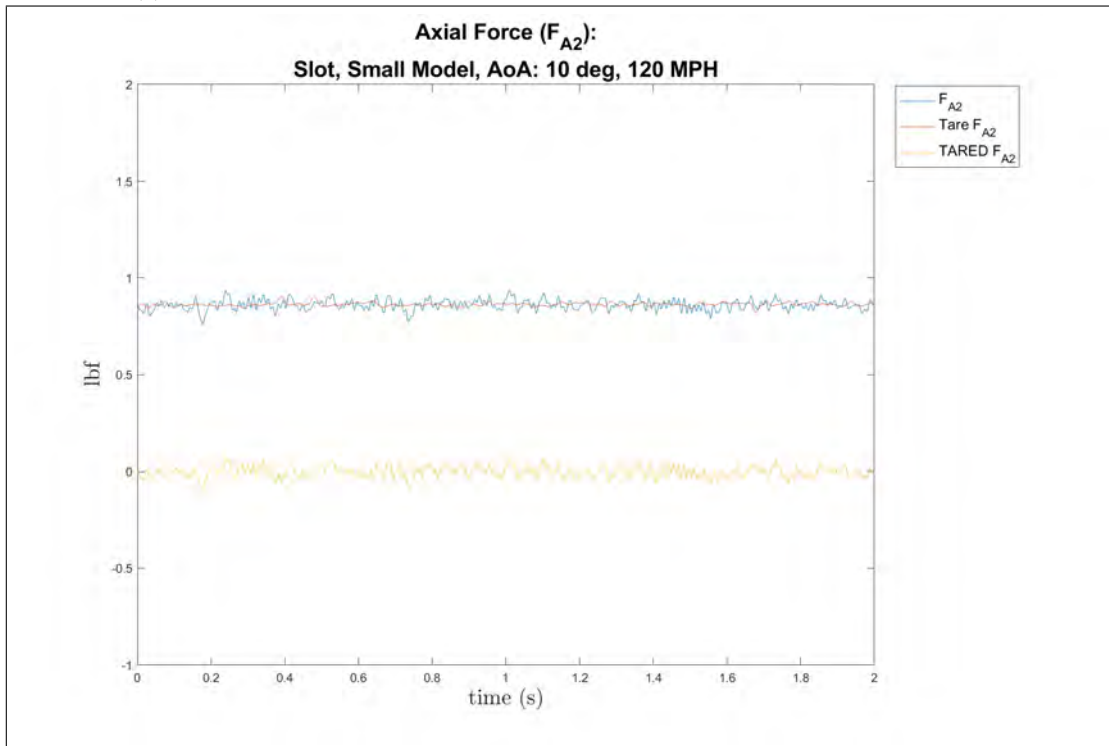


(b) Pitch Moment Coefficient, small model, 10° AoA, 120 MPH, Shear Layer, slot, tare

Figure 171: Small model at 10° AoA of the pitch moment coefficient, 120 MPH, slot, tare

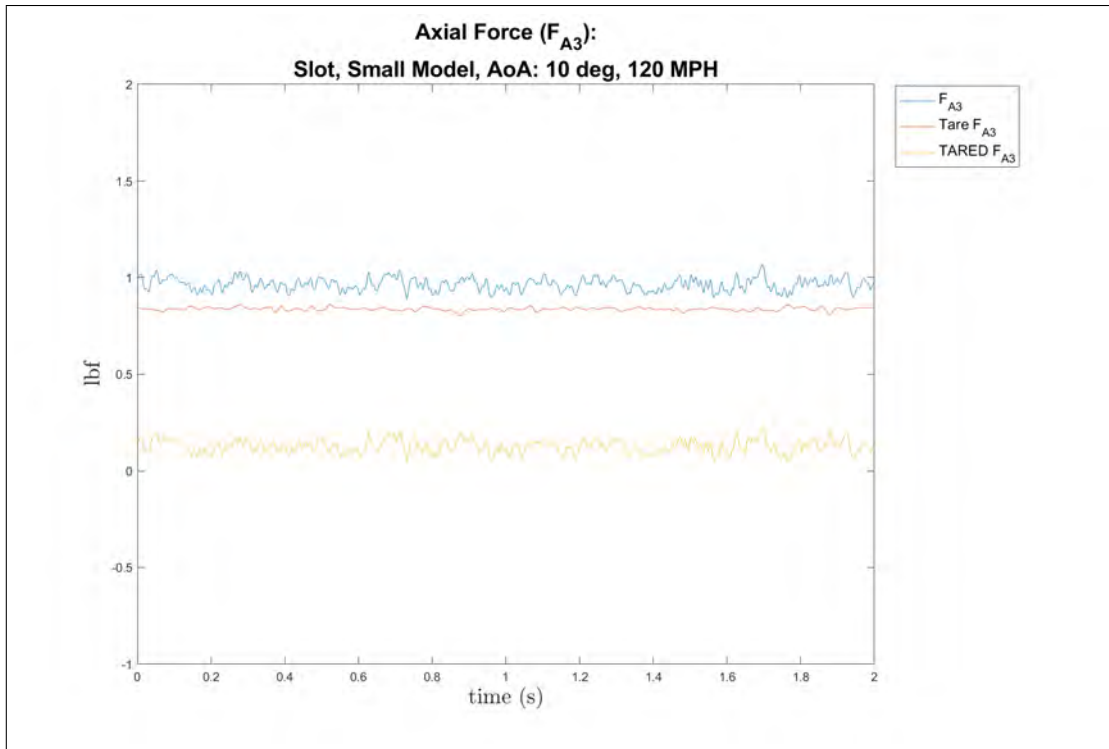


(a) Pitch Moment Coefficient, small model, 10° AoA, 120 MPH, Out Cavity, slot, tare

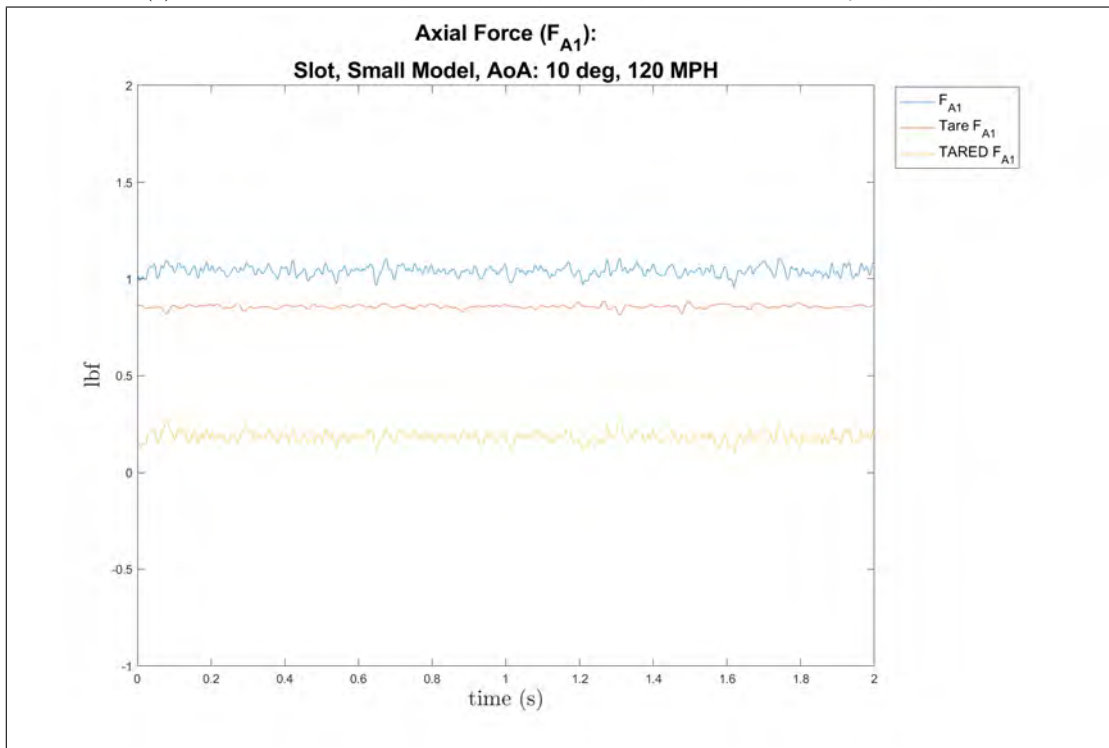


(b) Axial Force Coefficient, small model, 10° AoA, 120 MPH, In Cavity, slot, tare

Figure 172: Small model at 10° AoA of the pitch moment and axial force coefficients, 120 MPH, slot, tare



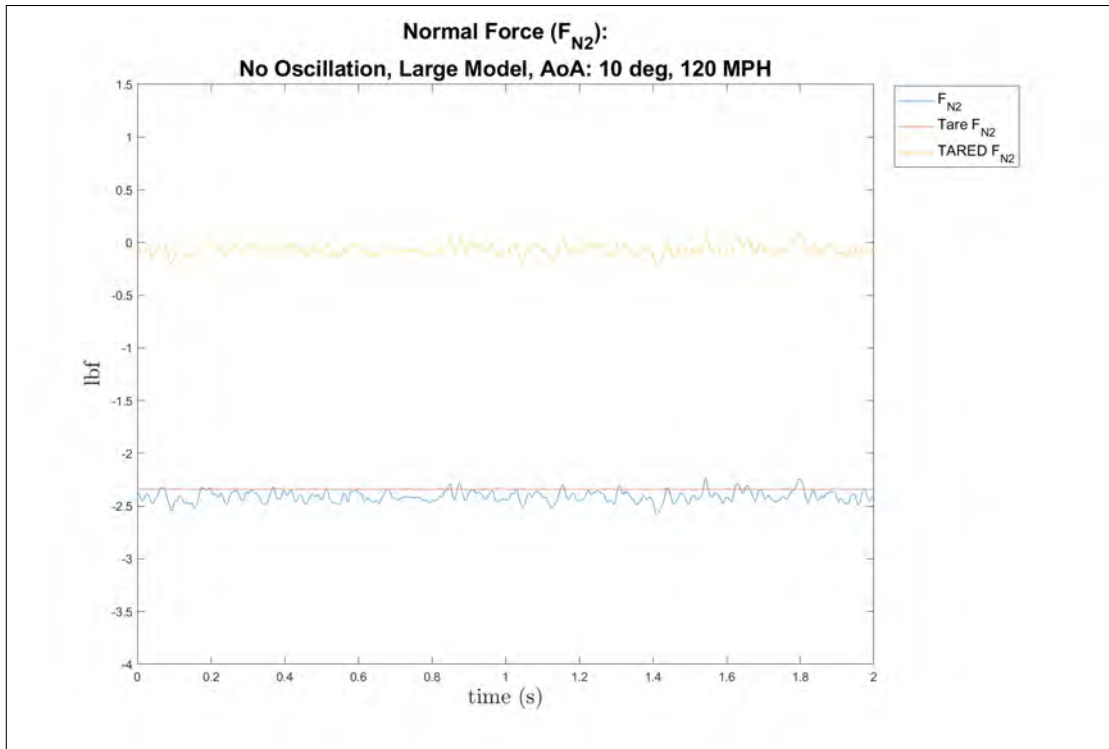
(a) Axial Force Coefficient, small model, 10° AoA, 120 MPH, Shear Layer, slot, tare



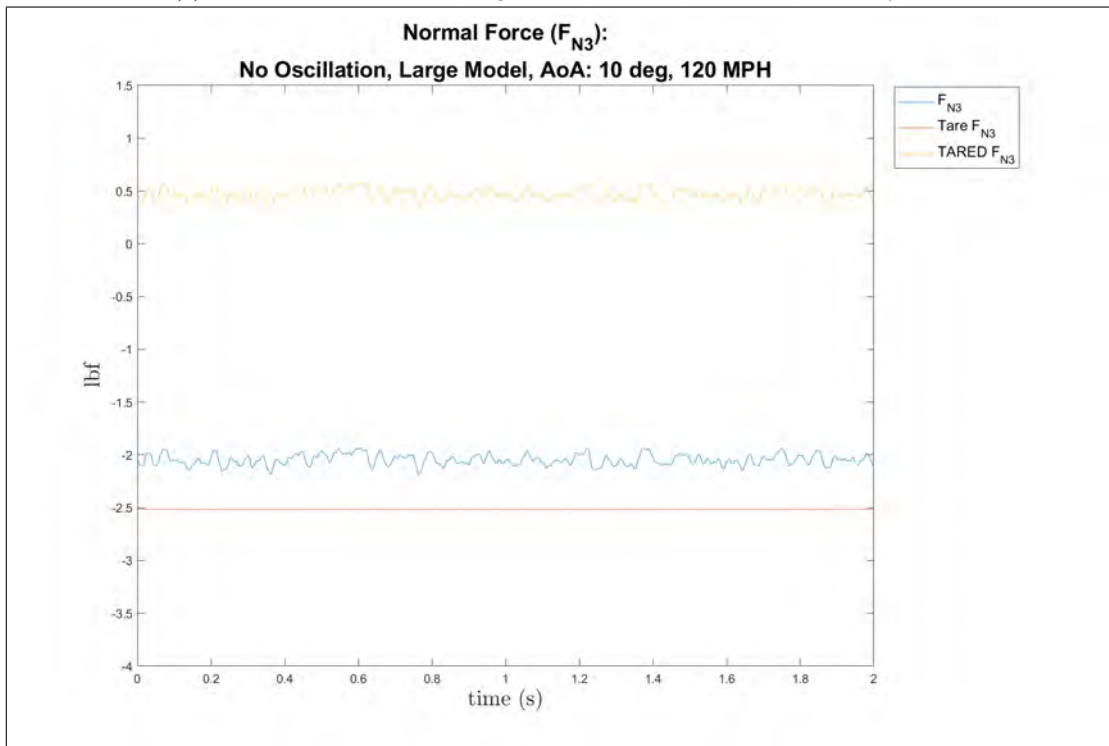
(b) Axial Force Coefficient, small model, 10° AoA, 120 MPH, Out Cavity, slot, tare

Figure 173: Small model at 10° AoA of the axial force coefficient, 120 MPH, slot, tare

Large Model, Cavity Apparatus, 10° AoA, 120 MPH

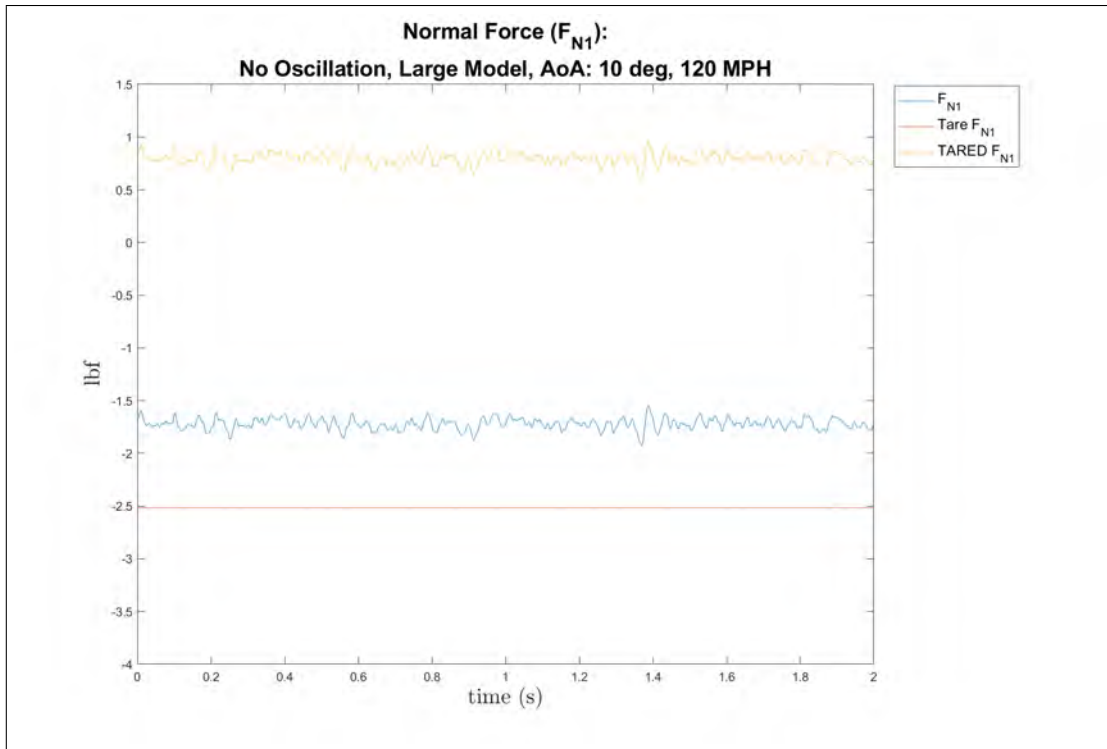


(a) Normal Force Coefficient, large model, 10° AoA, 120 MPH, In Cavity, tare

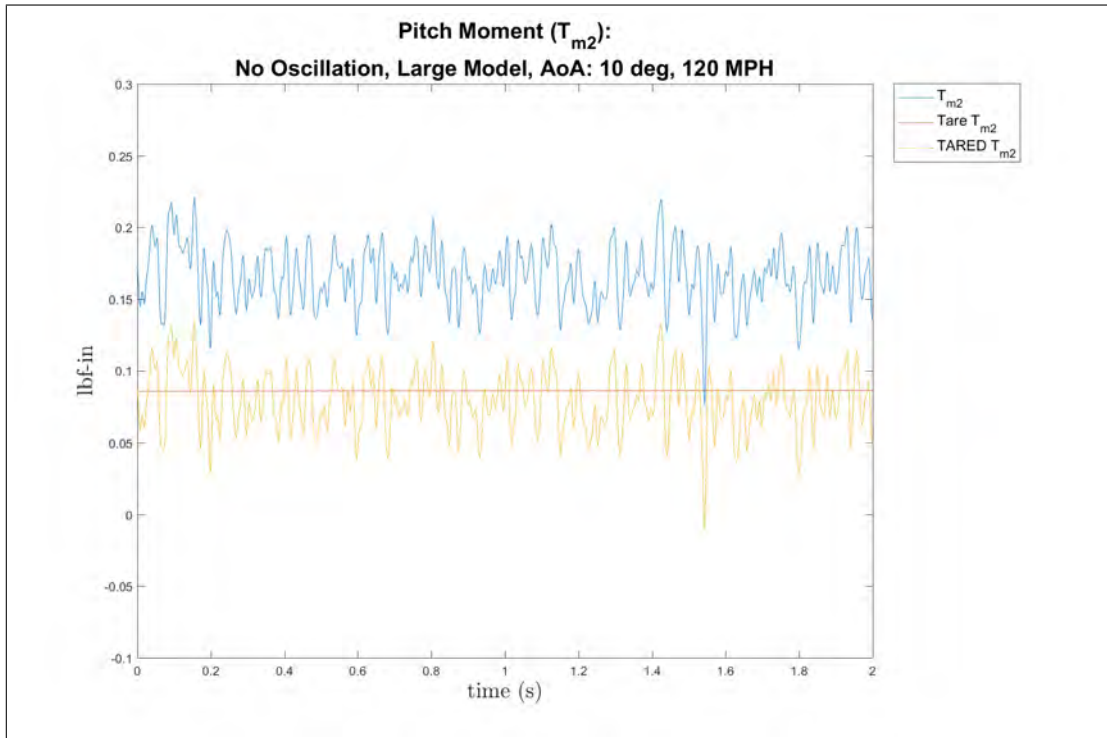


(b) Normal Force Coefficient, large model, 10° AoA, 120 MPH, Shear Layer, tare

Figure 174: Large model at 10° AoA of the normal force coefficient, 120 MPH, tare

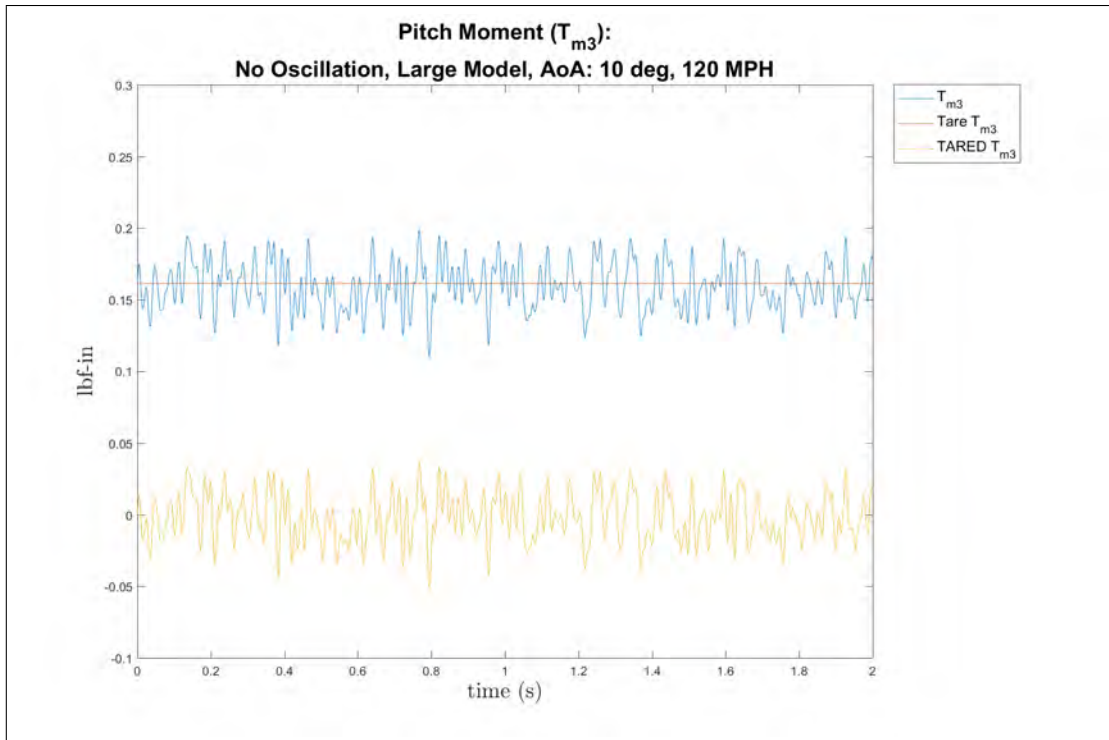


(a) Normal Force Coefficient, large model, 10° AoA, 120 MPH, Out Cavity, tare

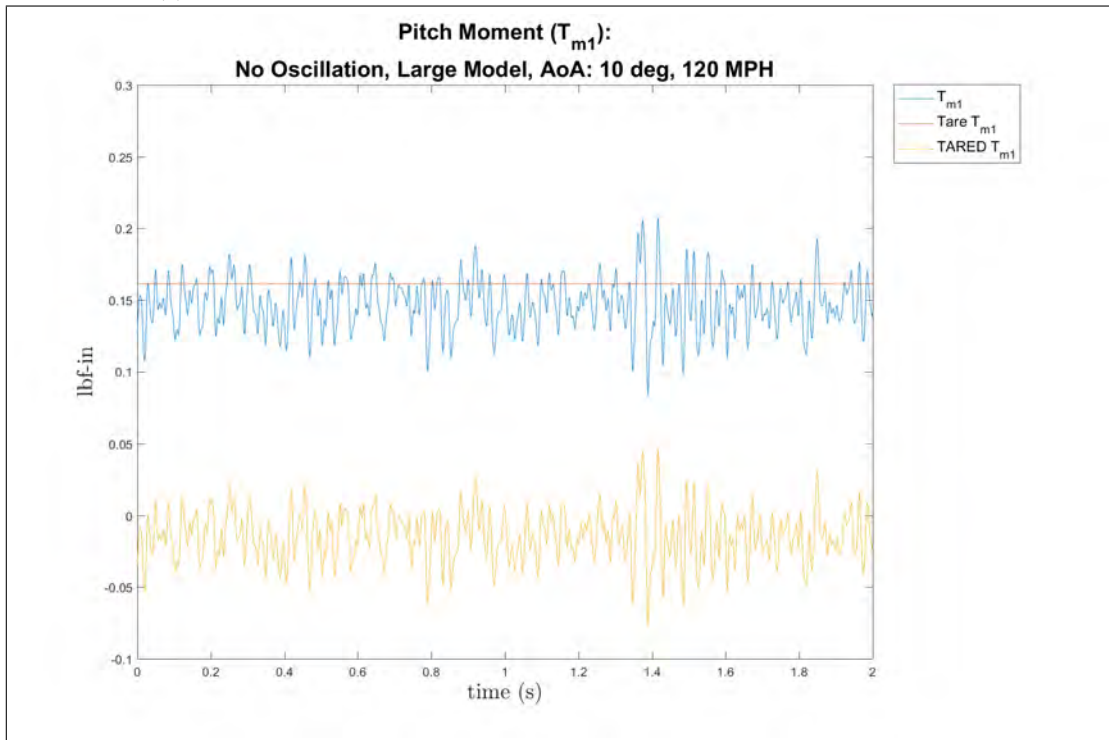


(b) Pitch Moment Coefficient, large model, 10° AoA, 120 MPH, In Cavity, tare

Figure 175: Large model at 10° AoA of the pitch moment and normal force coefficients, 120 MPH, tare

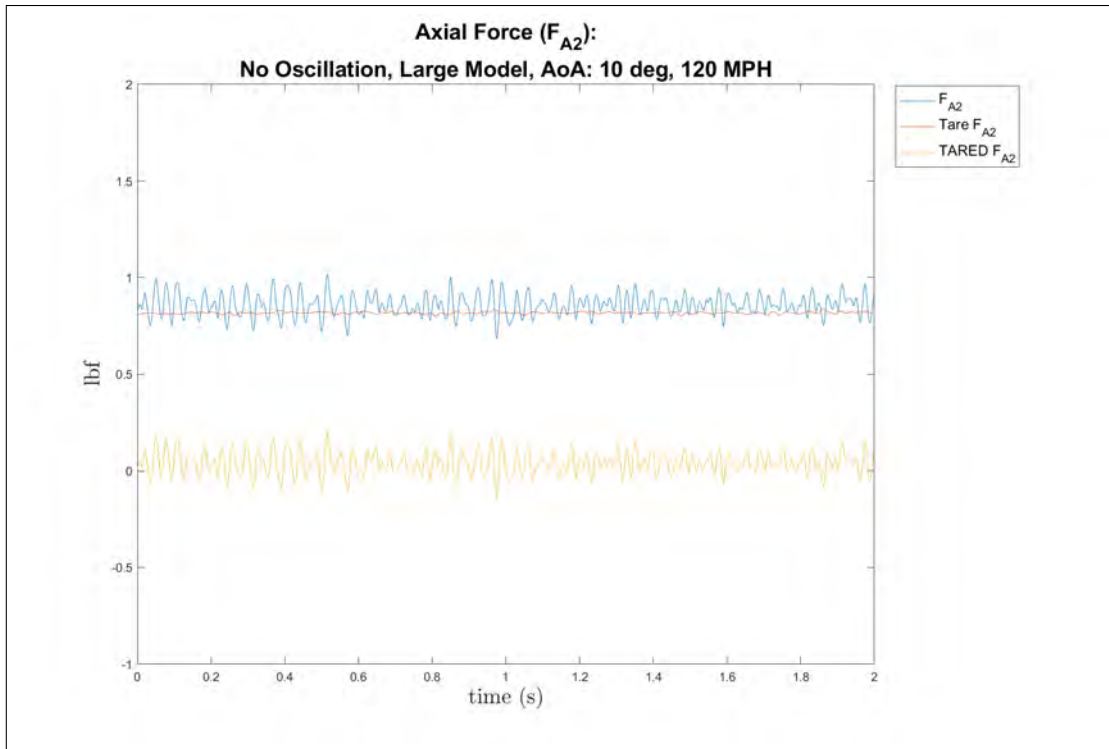


(a) Pitch Moment Coefficient, large model, 10° AoA, 120 MPH, Shear Layer, tare

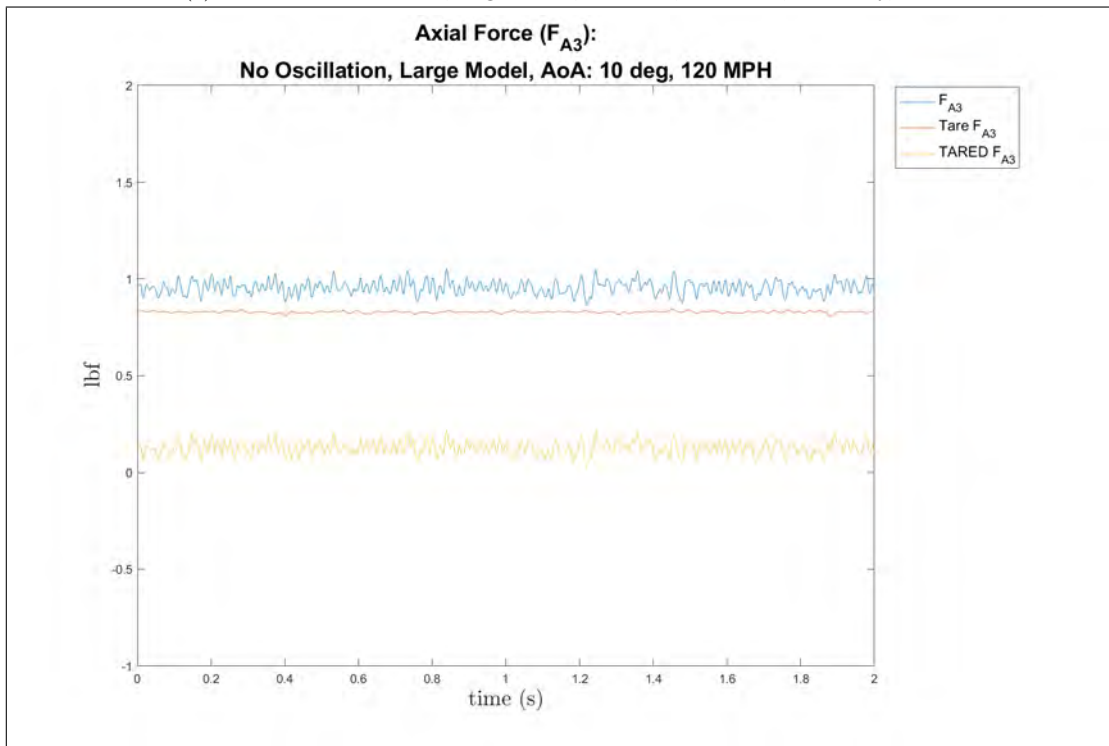


(b) Pitch Moment Coefficient, large model, 10° AoA, 120 MPH, Out Cavity, tare

Figure 176: Large model at 10° AoA of the pitch moment coefficient, 120 MPH, tare

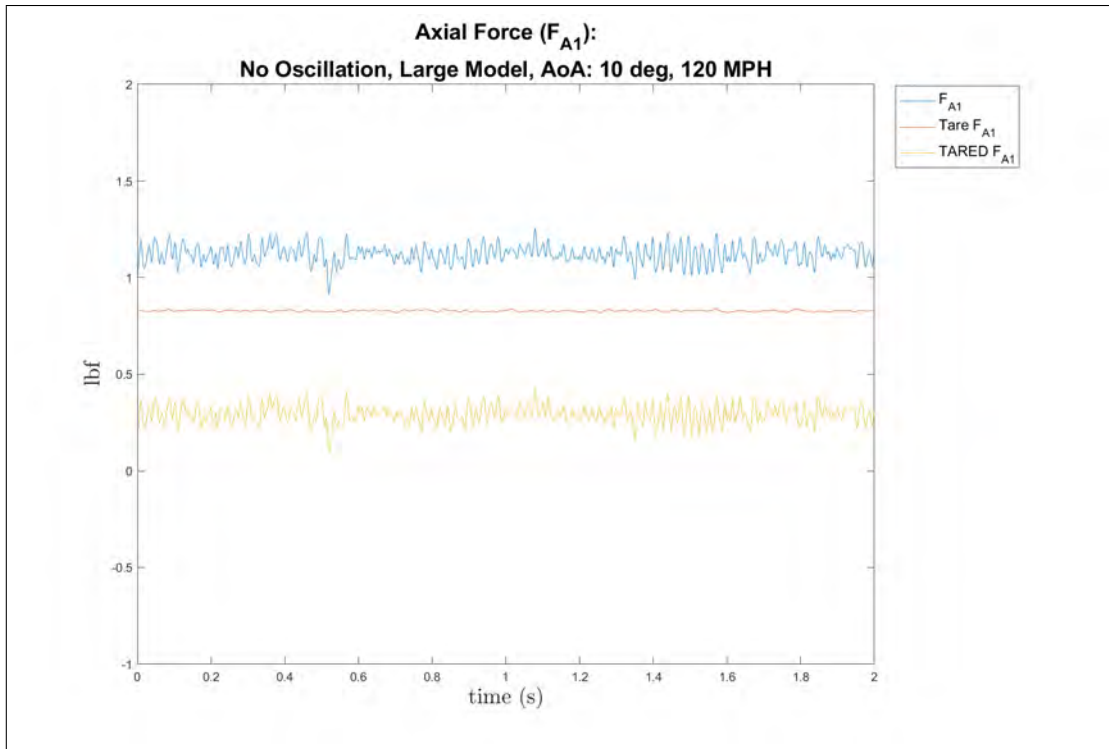


(a) Axial Force Coefficient, large model, 10° AoA, 120 MPH, In Cavity, tare

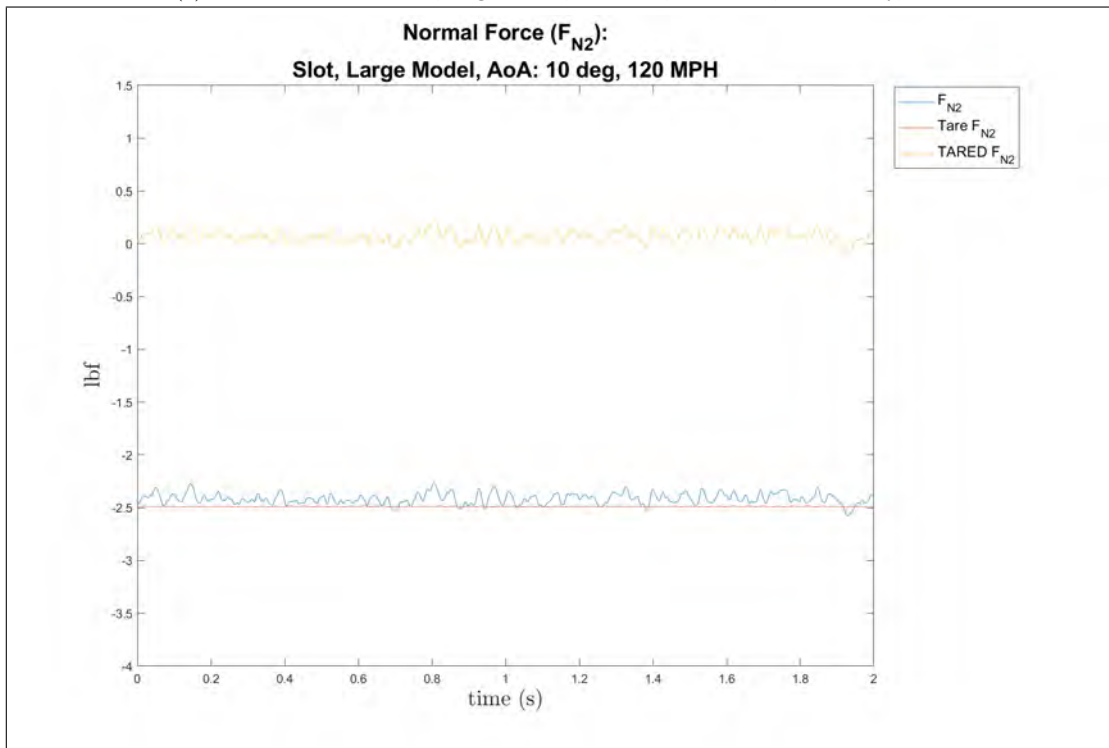


(b) Axial Force Coefficient, large model, 10° AoA, 120 MPH, Shear Layer, tare

Figure 177: Large model at 10° AoA of the Axial Force coefficient, 120 MPH, tare

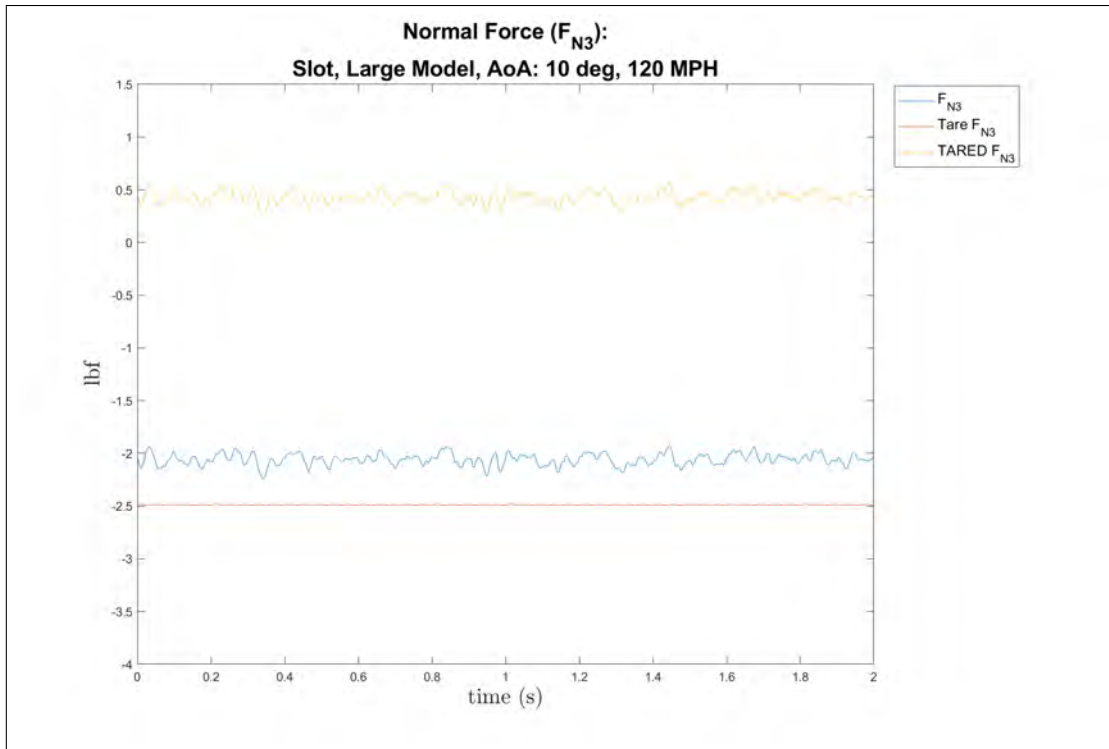


(a) Axial Force Coefficient, large model, 10° AoA, 120 MPH, Out Cavity, tare

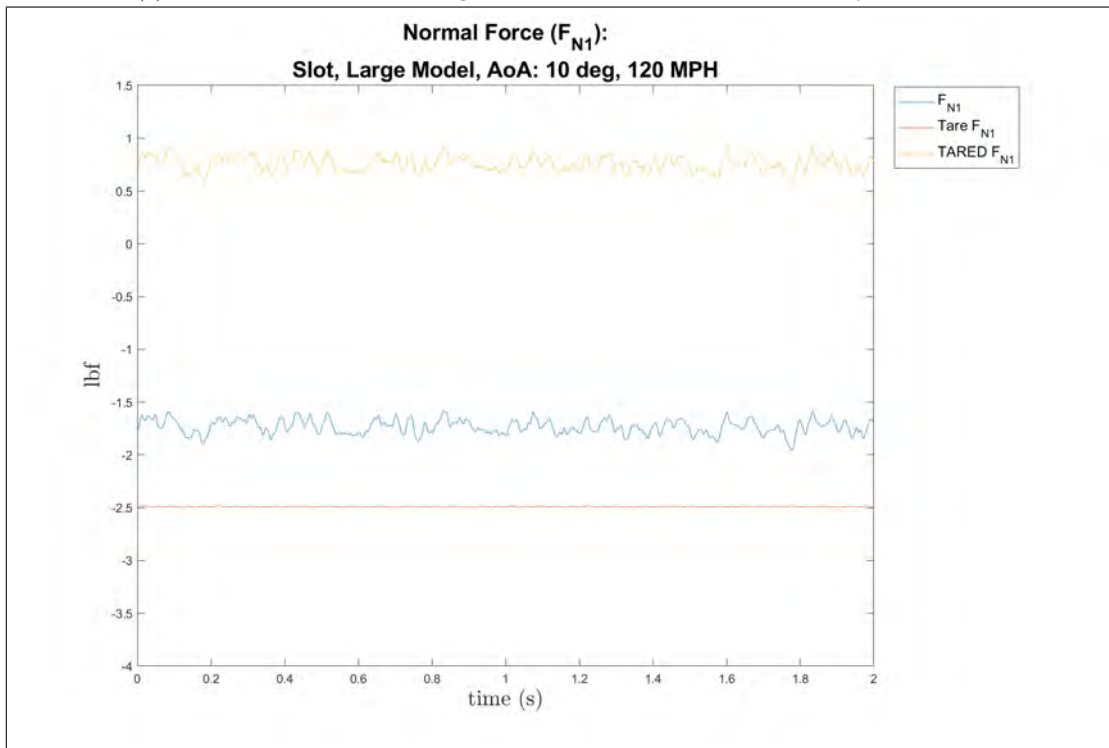


(b) Noormal Force Coefficient, large model, 10° AoA, 120 MPH, In Cavity, slot, tare

Figure 178: Large model at 10° AoA of the axial force and normal force coefficients, 120 MPH, tare

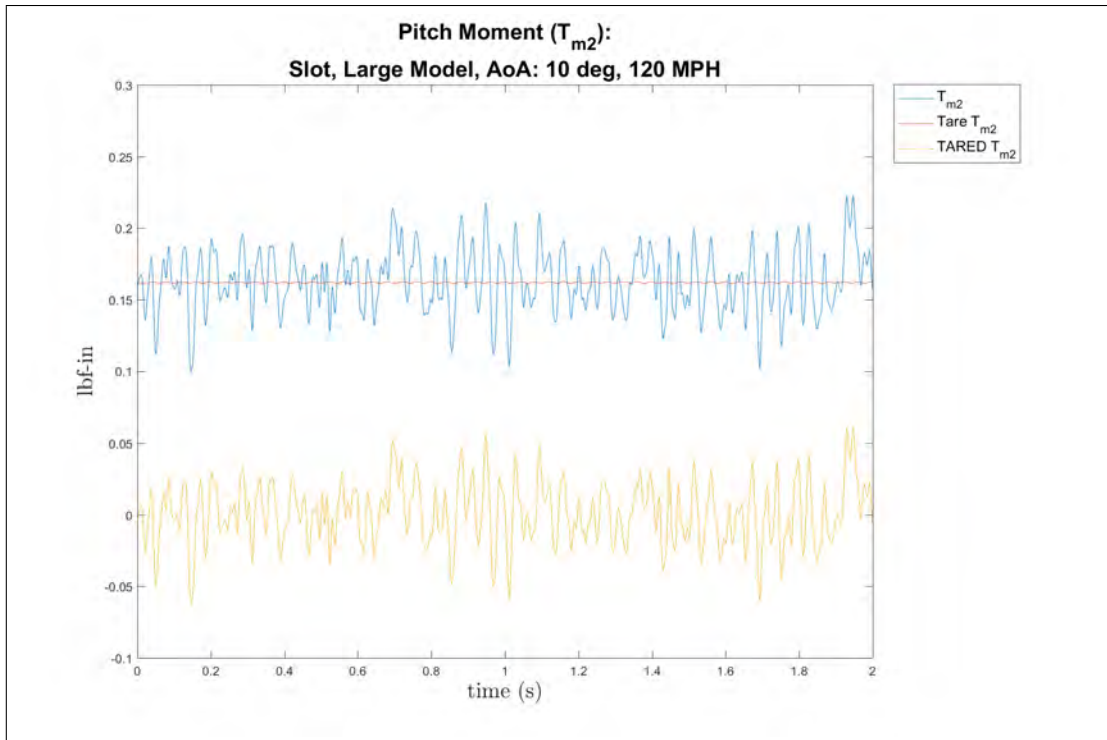


(a) Normal Force Coefficient, large model, 10° AoA, 120 MPH, Shear Layer, slot, tare

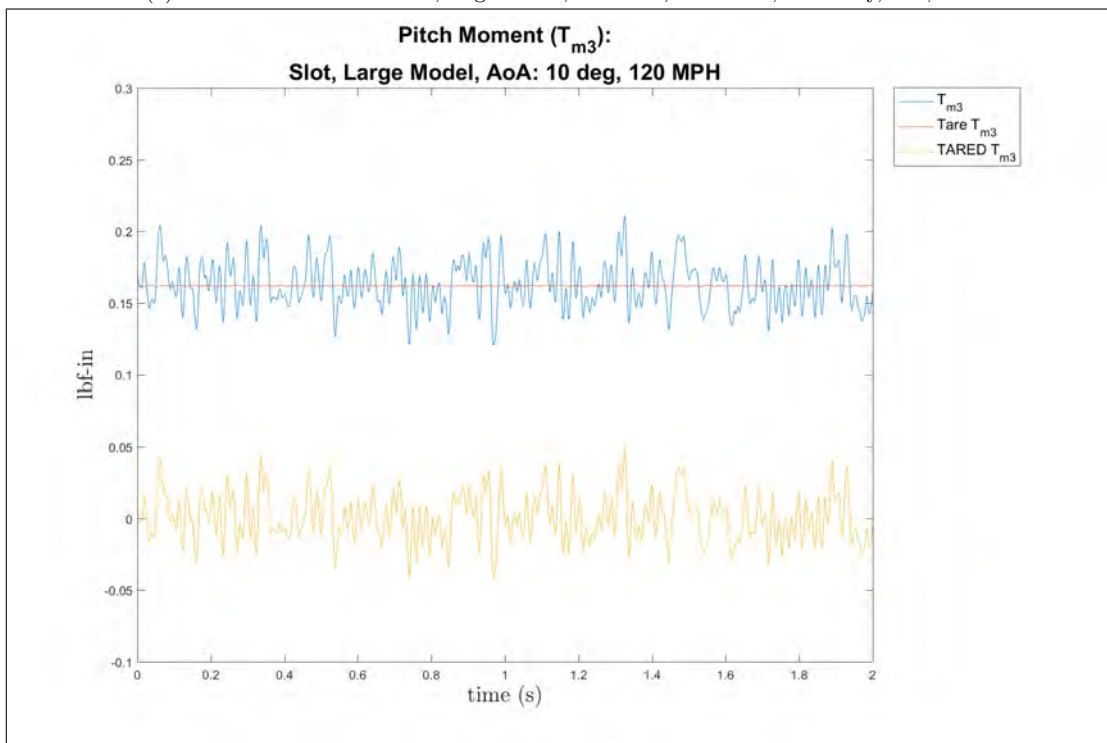


(b) Normal Force Coefficient, large model, 10° AoA, 120 MPH, Out Cavity, slot, tare

Figure 179: Large model at 10° AoA of the normal force coefficient, 120 MPH, slot, tare

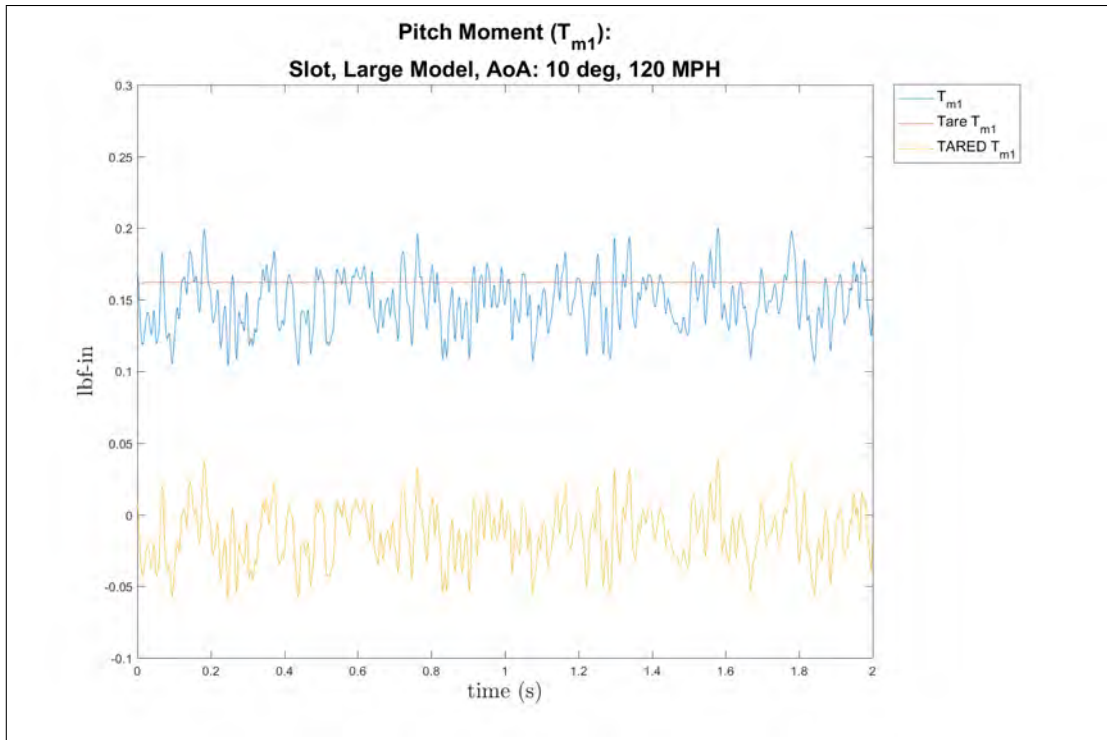


(a) Pitch Moment Coefficient, large model, 10° AoA, 120 MPH, In Cavity, slot, tare

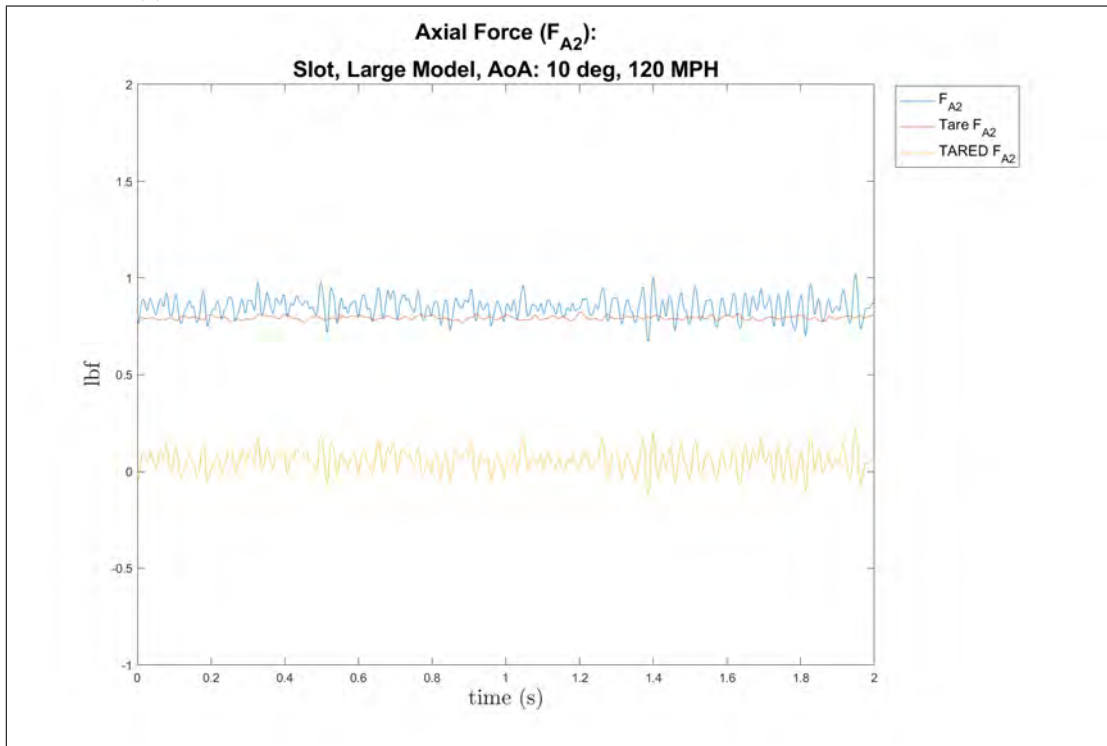


(b) Pitch Moment Coefficient, large model, 10° AoA, 120 MPH, Shear Layer, slot, tare

Figure 180: Large model at 10° AoA of the pitch moment coefficient, 120 MPH, slot, tare

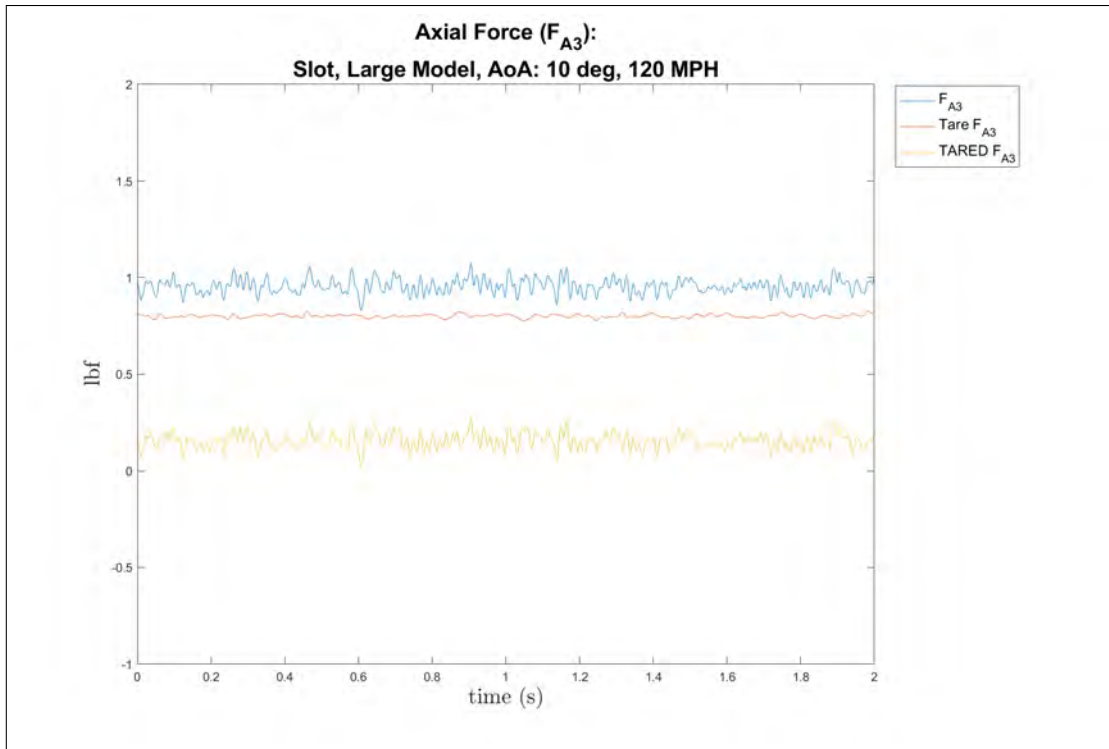


(a) Pitch Moment Coefficient, large model, 10° AoA, 120 MPH, Out Cavity, slot, tare

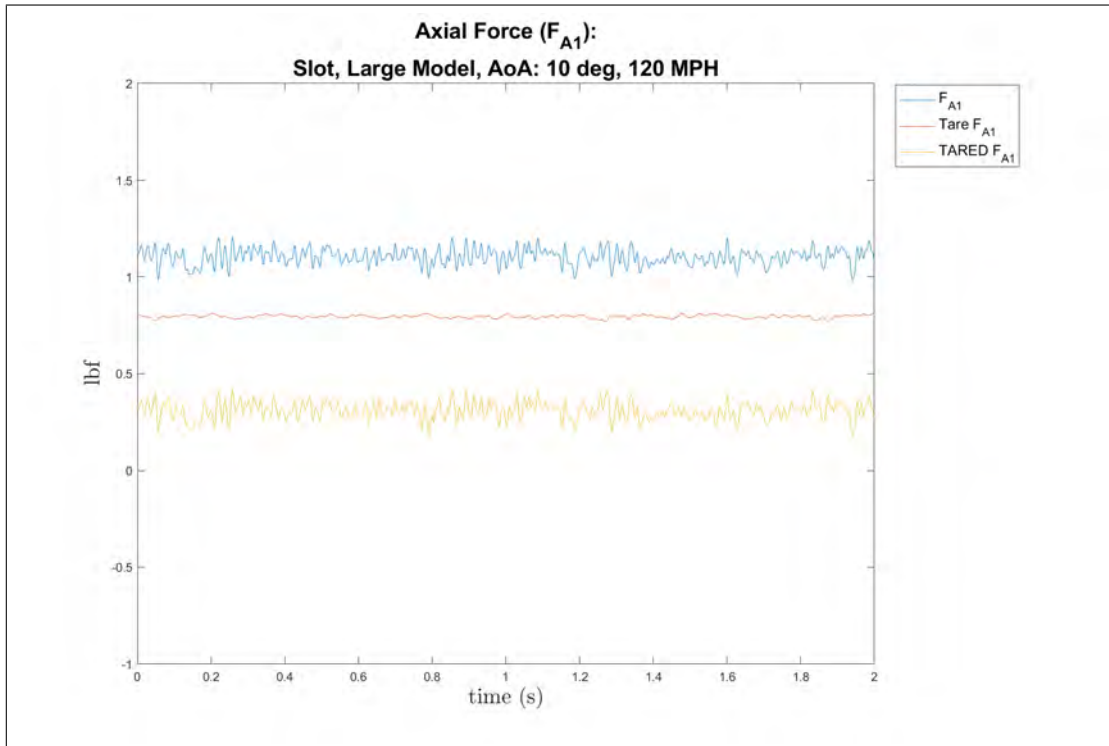


(b) Axial Force Coefficient, large model, 10° AoA, 120 MPH, In Cavity, slot, tare

Figure 181: Large model at 10° AoA of the pitch moment and axial force coefficients, 120 MPH, slot, tare



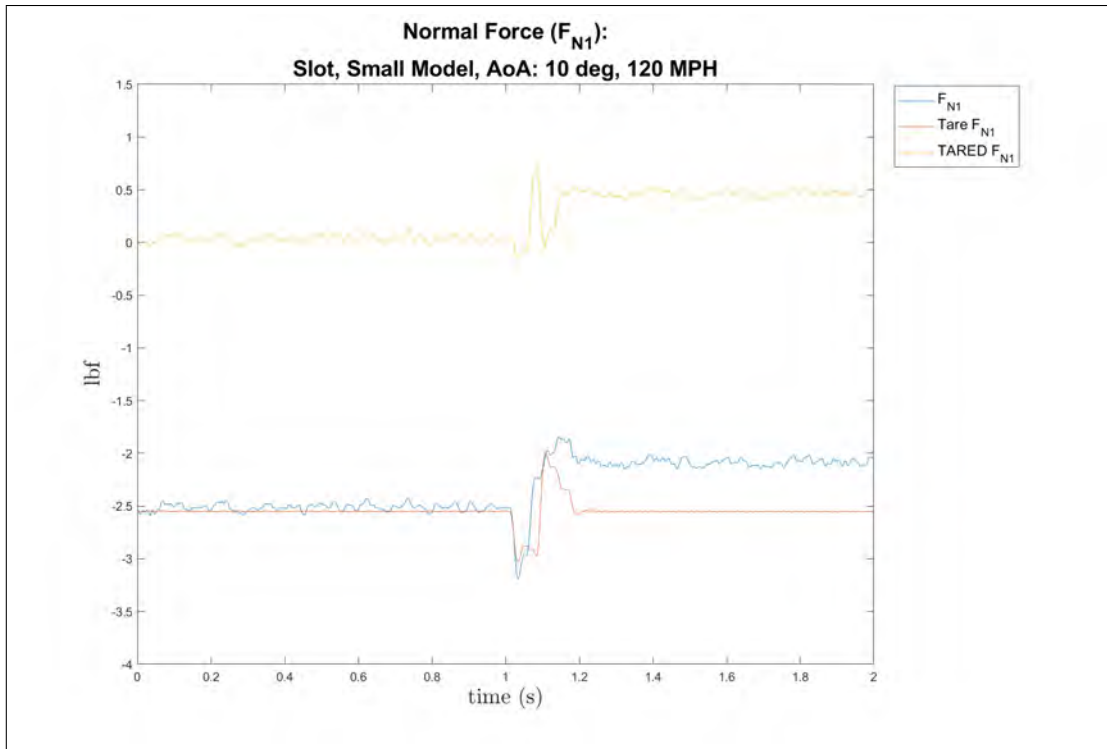
(a) Axial Force Coefficient, large model, 10° AoA, 120 MPH, Shear Layer, slot, tare



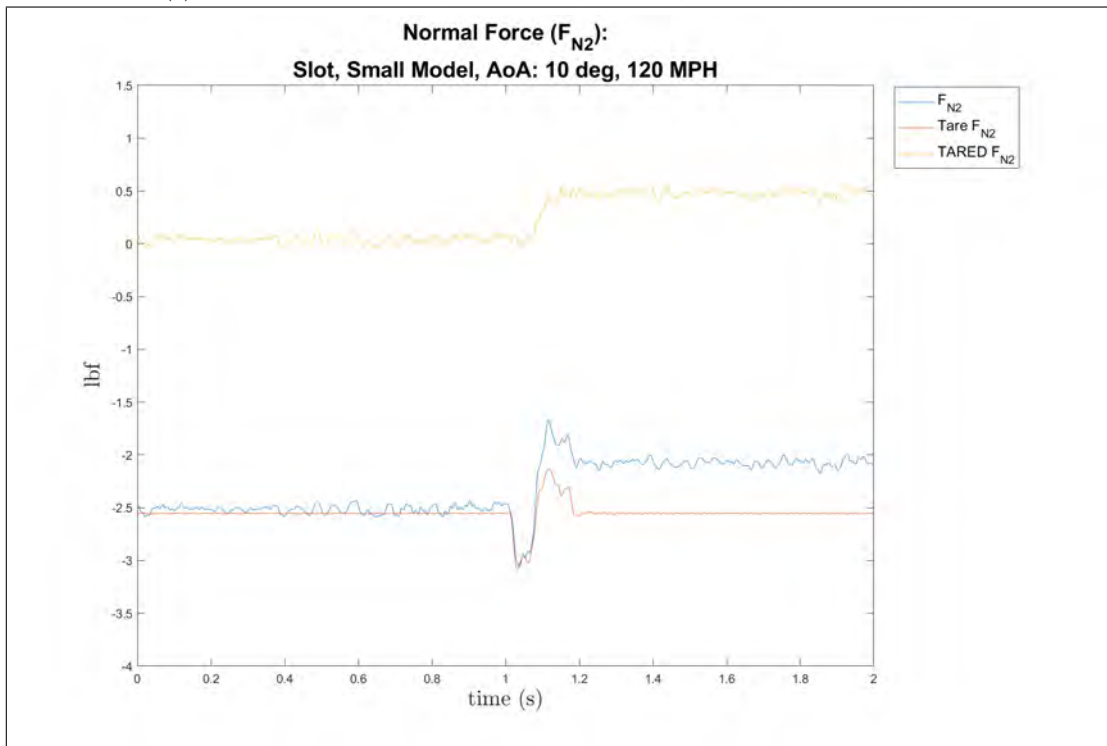
(b) Axial Force Coefficient, large model, 10° AoA, 120 MPH, Out Cavity, slot, tare

Figure 182: Large model at 10° AoA of the axial force coefficient, 120 MPH, slot, tare

Small Model, Dynamic Release, 10° AoA, 120 MPH

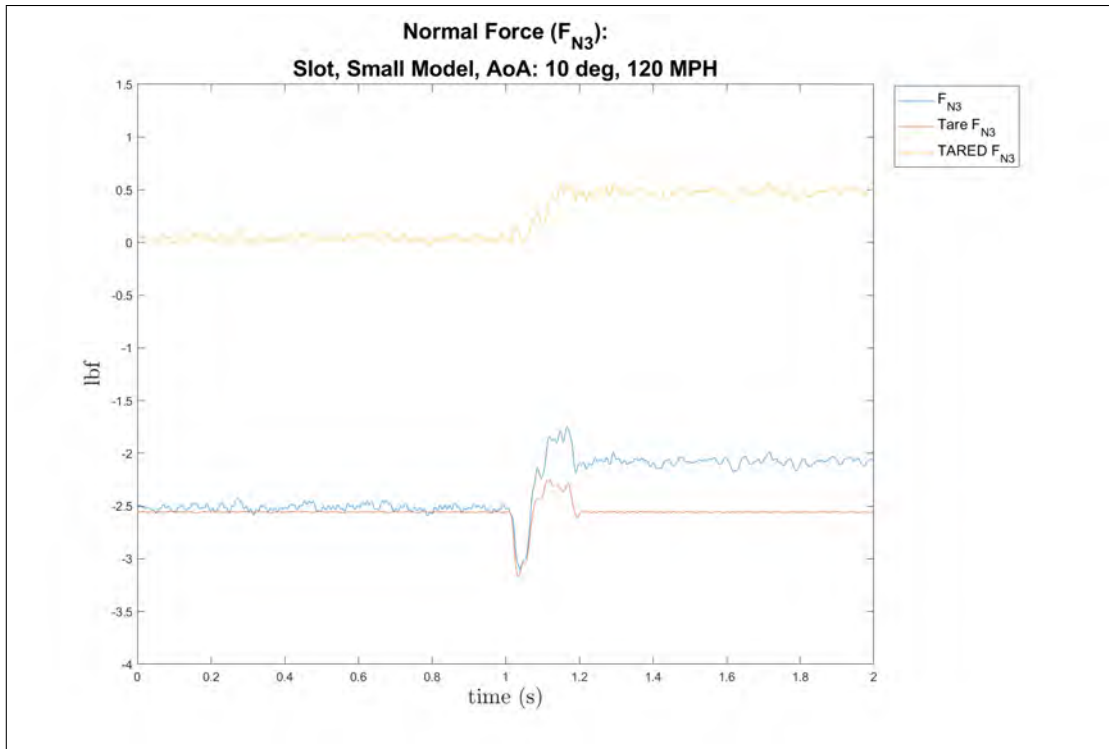


(a) Normal Force Coefficient, small model, 10° AoA, 120 MPH, release one, tare

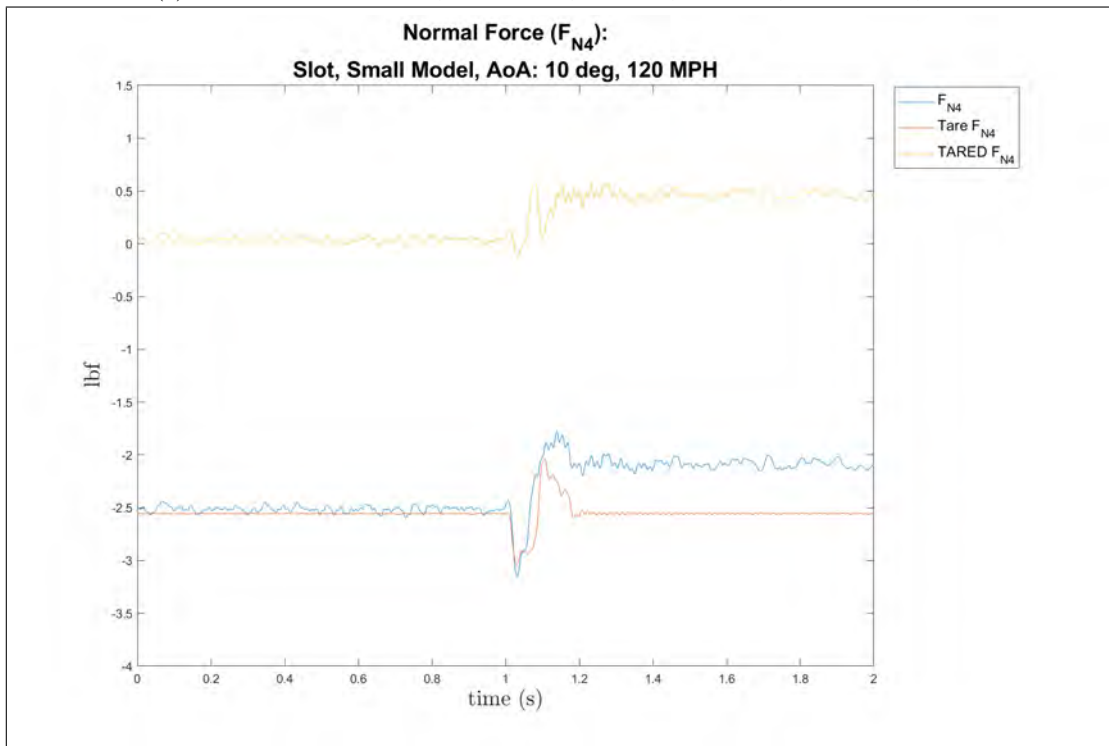


(b) Normal Force Coefficient, small model, 10° AoA, 120 MPH, release two, tare

Figure 183: Small model at 10° AoA of the normal force coefficient, release times one and two, 120 MPH, tare

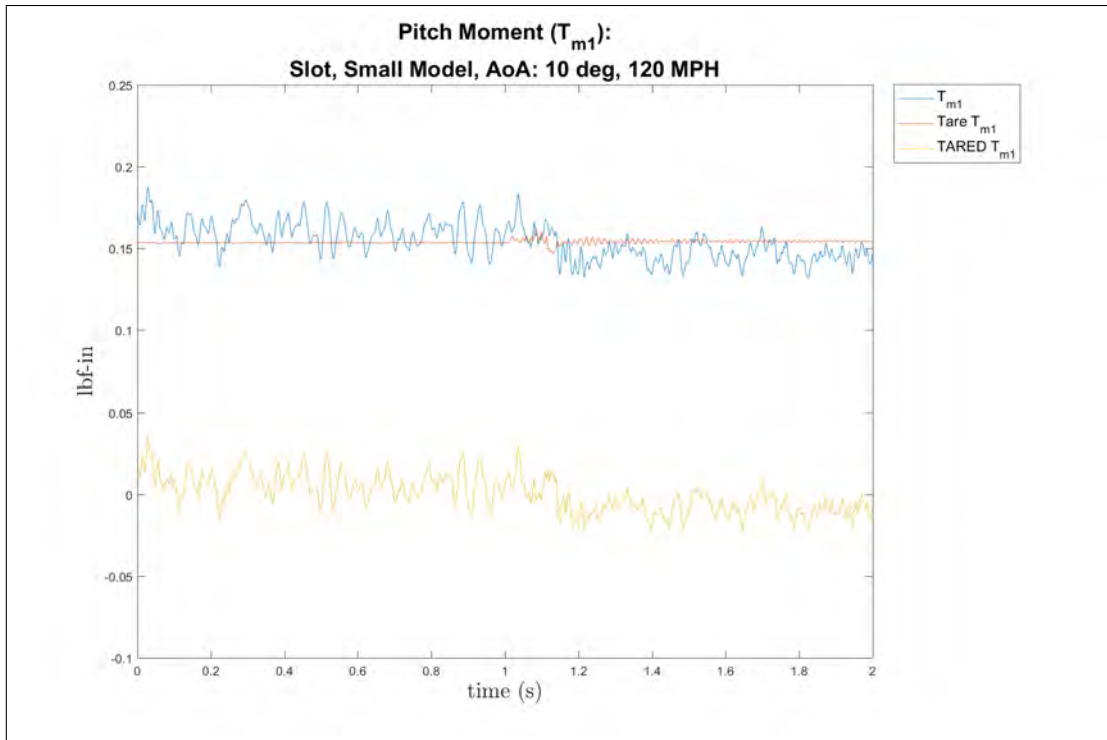


(a) Normal Force Coefficient, small model, 10° AoA, 120 MPH, release three, tare

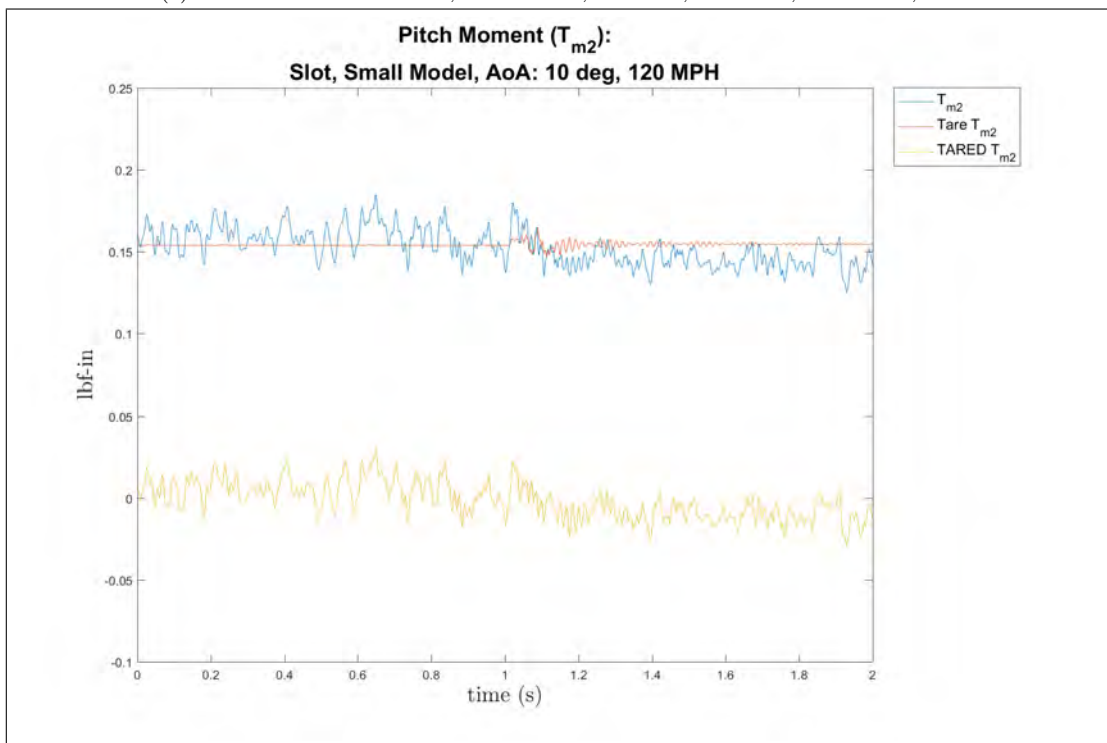


(b) Normal Force Coefficient, small model, 10° AoA, 120 MPH, release four, tare

Figure 184: Small model at 10° AoA of the normal force coefficient, release times three and four, 120 MPH, tare

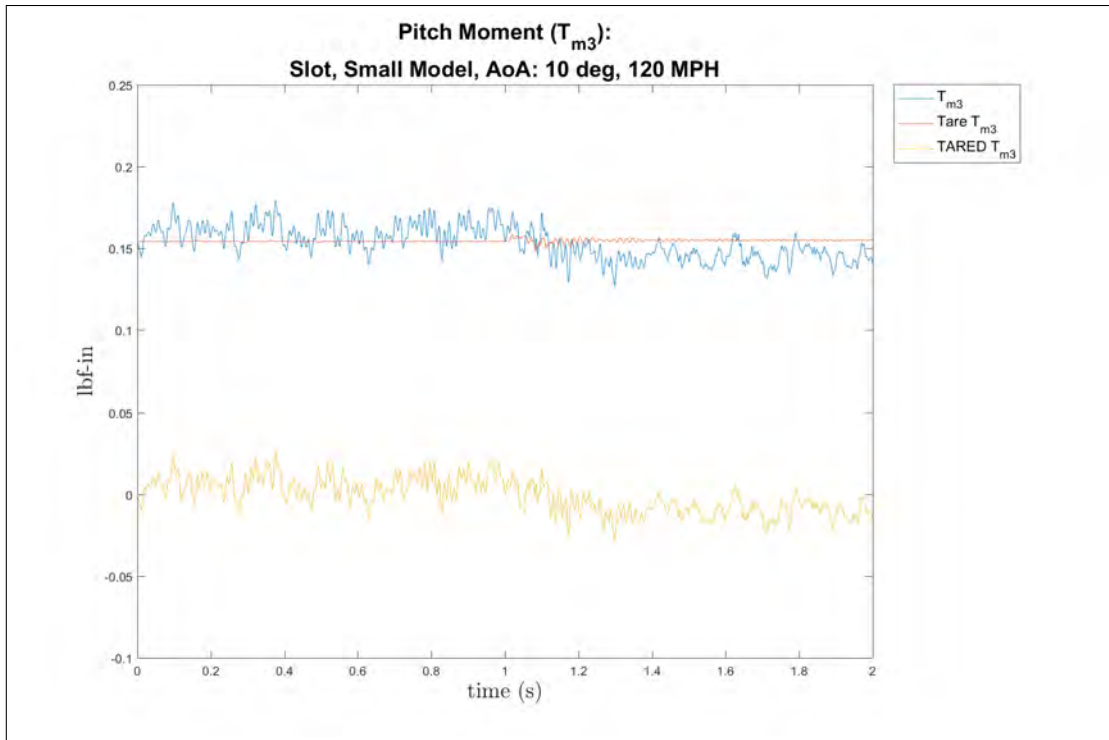


(a) Pitch Moment Coefficient, small model, 10° AoA, 120 MPH, release one, tare

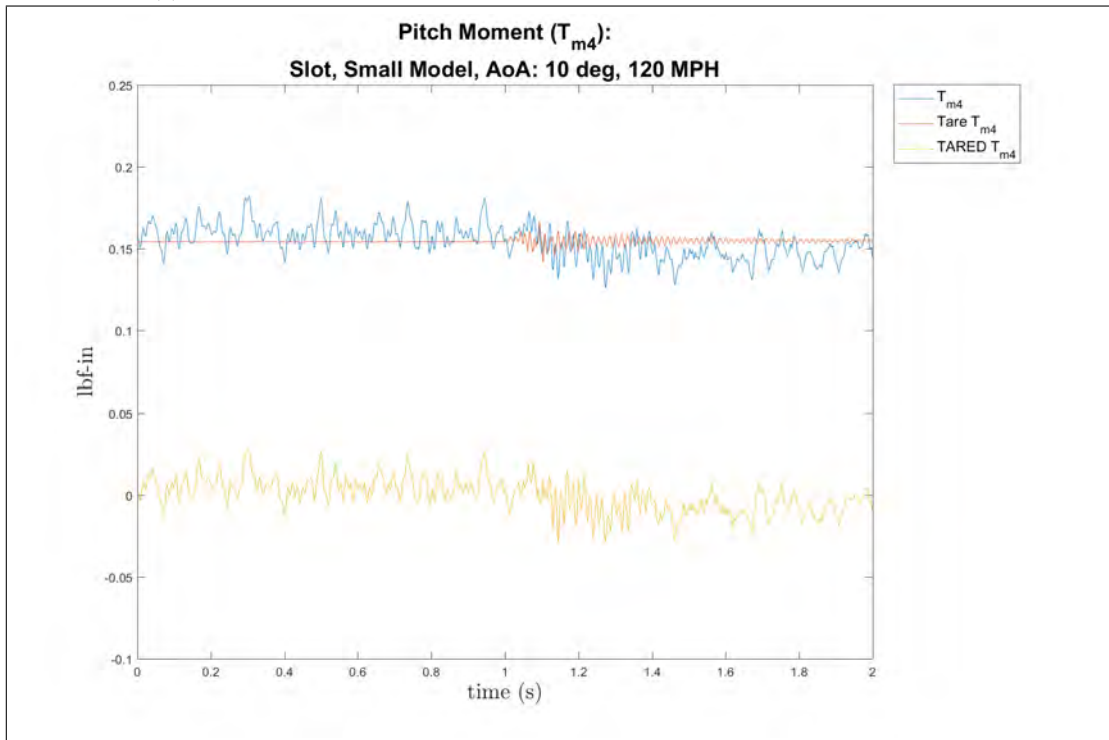


(b) Pitch Moment Coefficient, small model, 10° AoA, 120 MPH, release two, tare

Figure 185: Small model at 10° AoA of the pitch moment coefficient, release times one and two, 120 MPH, tare

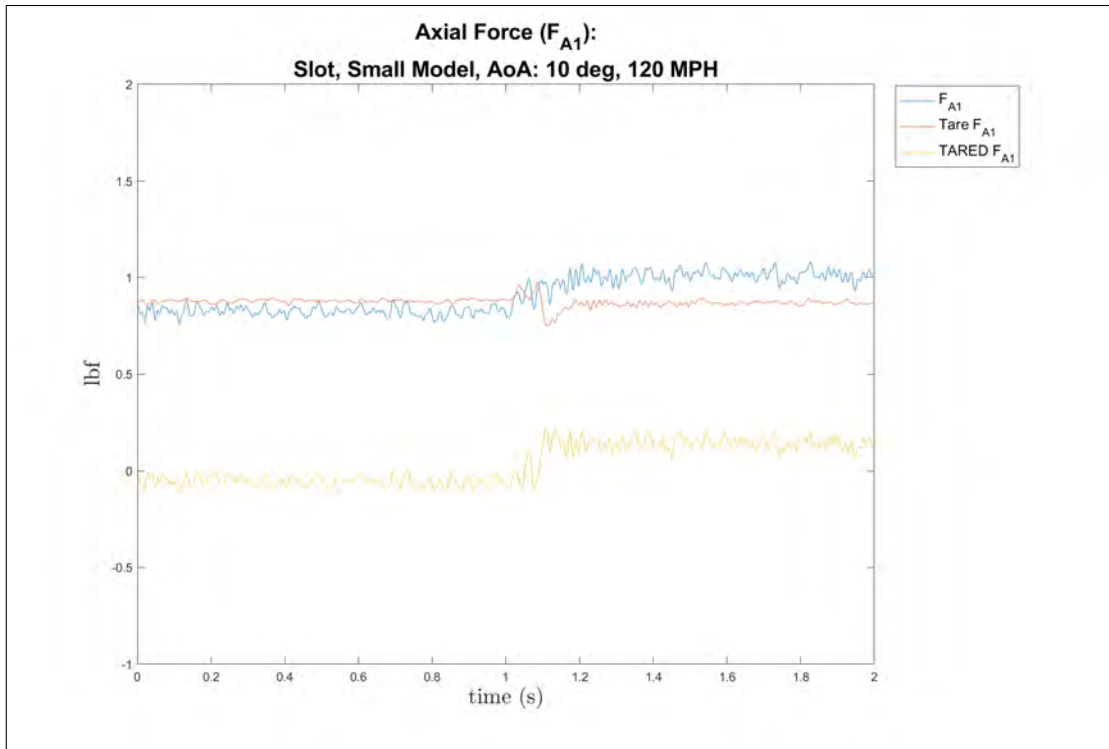


(a) Pitch Moment Coefficient, small model, 10° AoA, 120 MPH, release three, tare

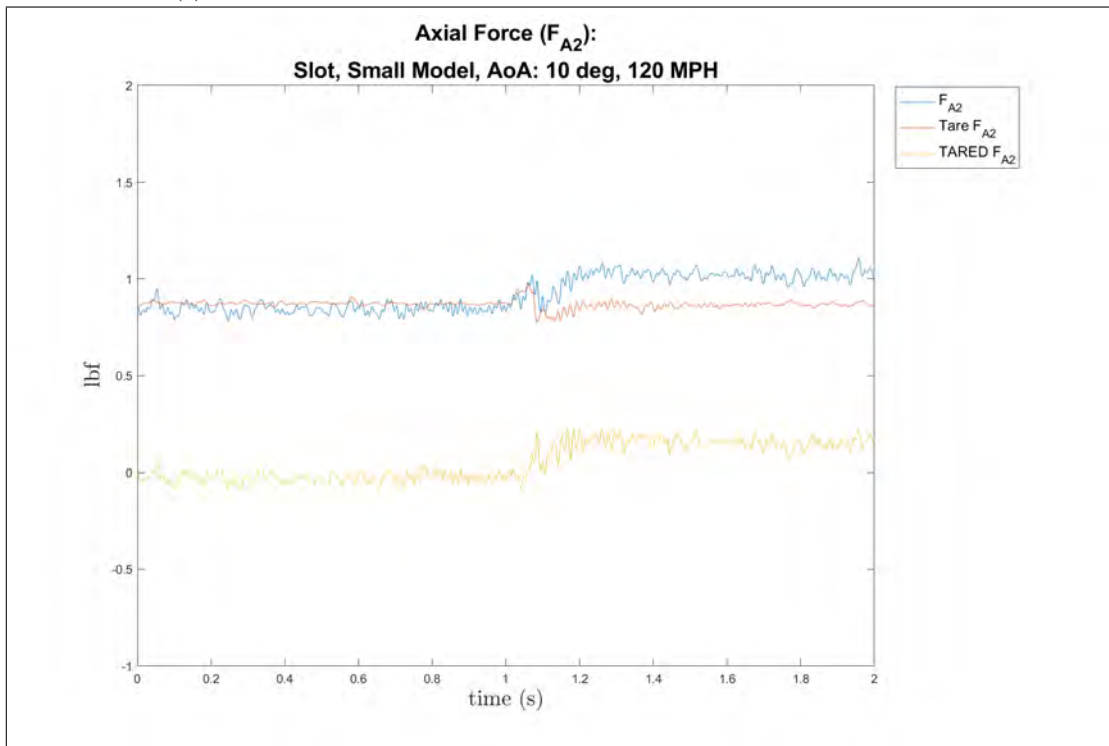


(b) Pitch Moment Coefficient, small model, 10° AoA, 120 MPH, release four, tare

Figure 186: Small model at 10° AoA of the pitch moment coefficient, release times three and four, 120 MPH, tare

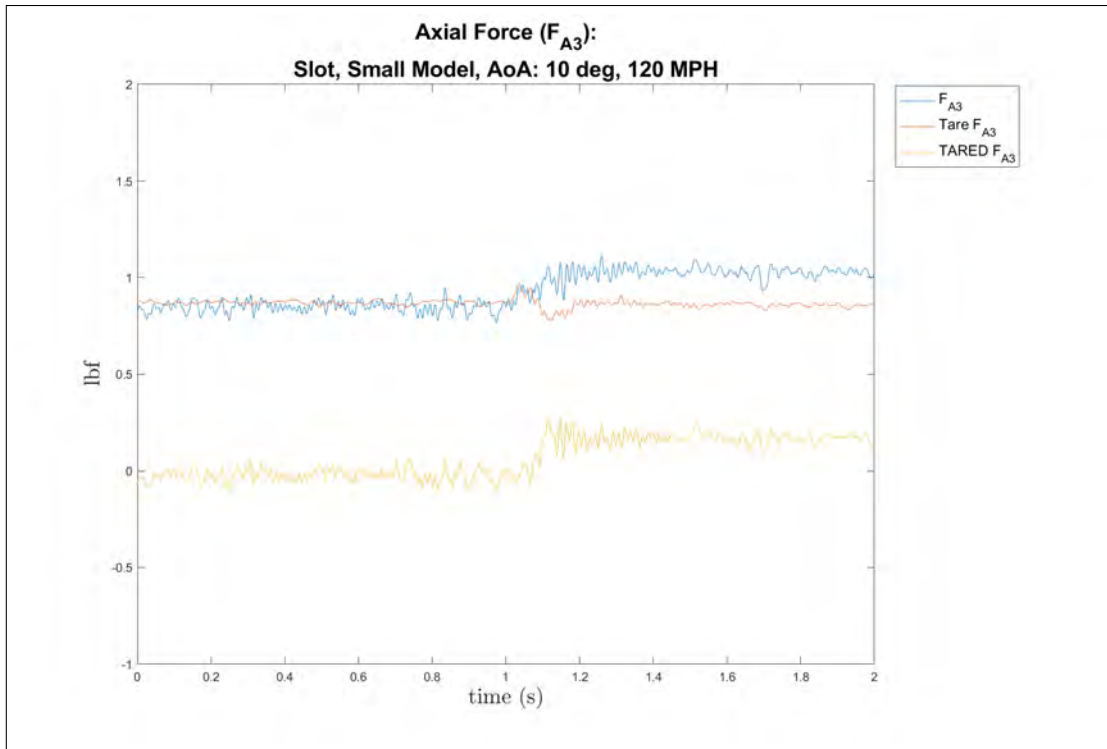


(a) Axial Force Coefficient, small model, 10° AoA, 120 MPH, release one, tare

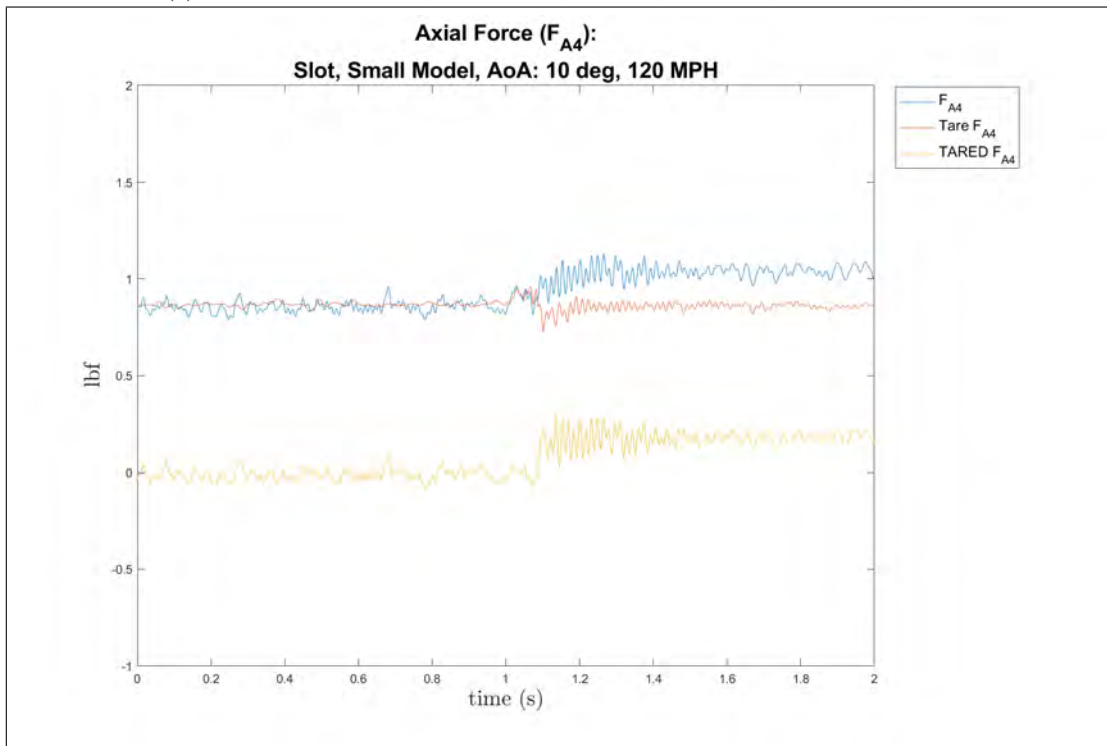


(b) Axial Force Coefficient, small model, 10° AoA, 120 MPH, release two, tare

Figure 187: Small model at 10° AoA of the axial force coefficient, release times one and two, 120 MPH, tare



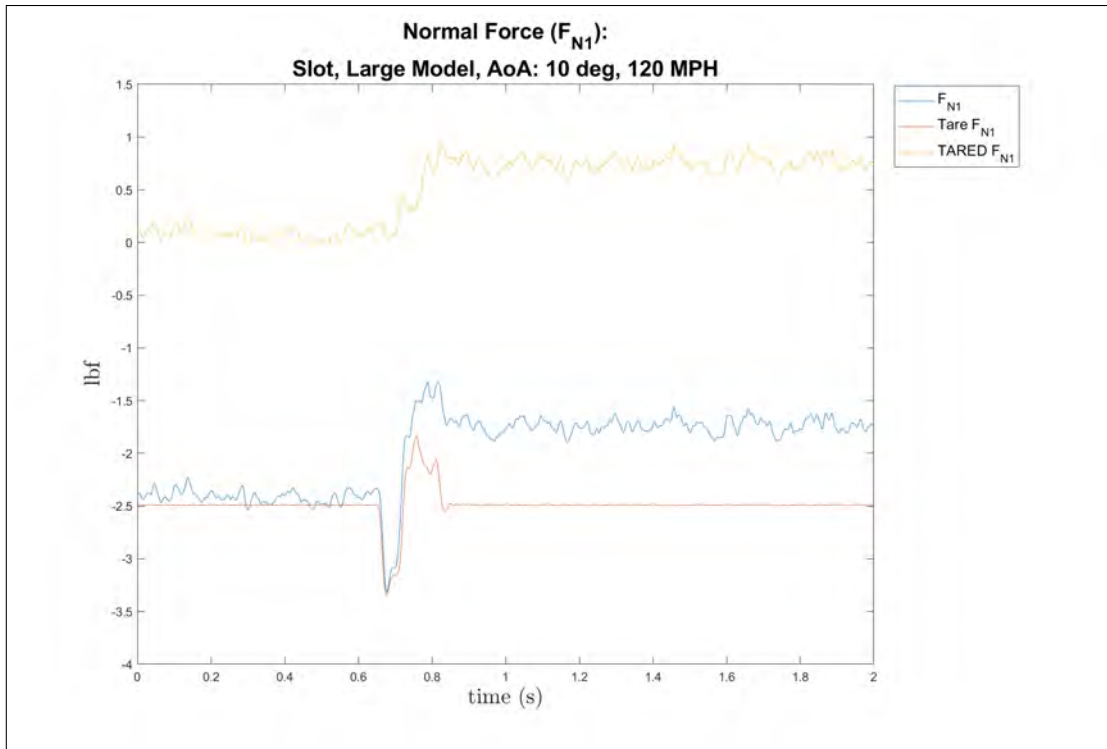
(a) Axial Force Coefficient, small model, 10° AoA, 120 MPH, release three, tare



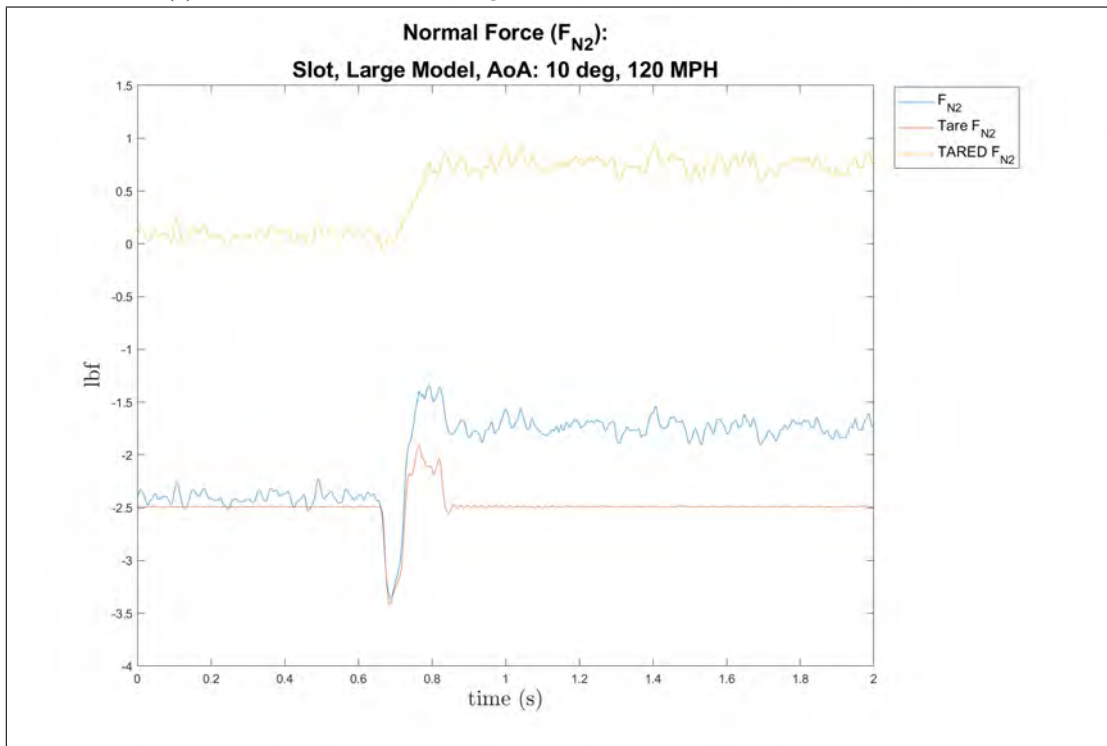
(b) Axial Force Coefficient, small model, 10° AoA, 120 MPH, release four, tare

Figure 188: Small model at 10° AoA of the axial force coefficient, release times three and four, 120 MPH, tare

Large Model, Dynamic Release, 10° AoA, 120 MPH

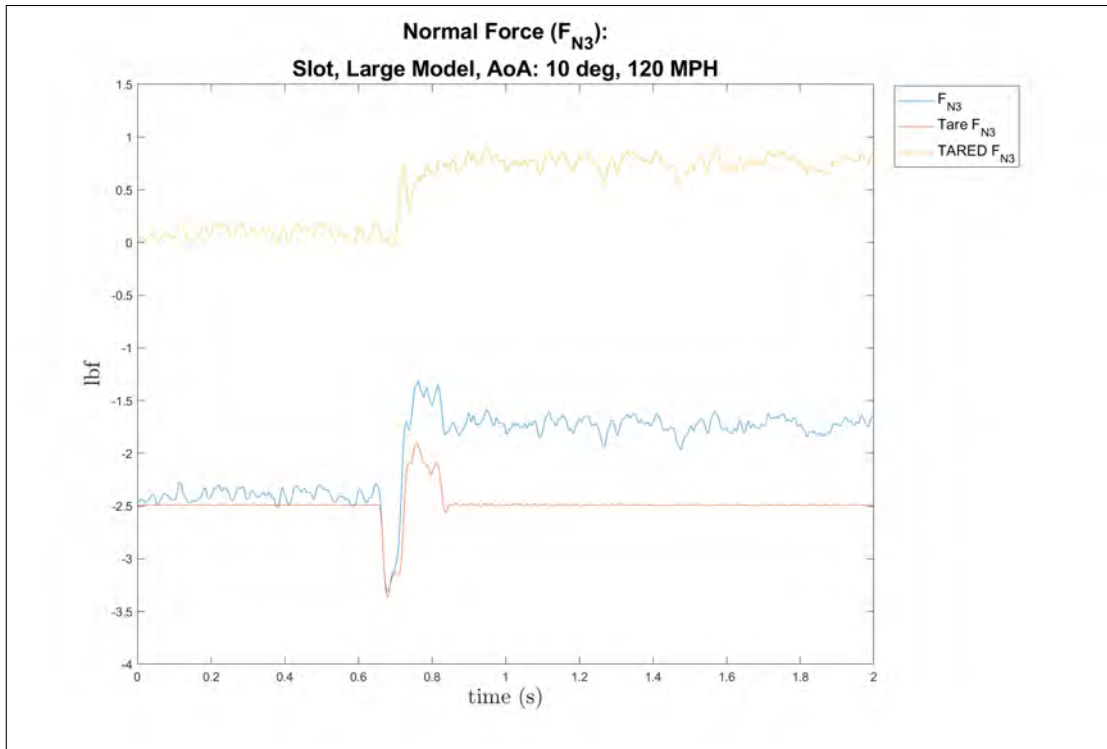


(a) Normal Force Coefficient, large model, 10° AoA, 120 MPH, release one, tare

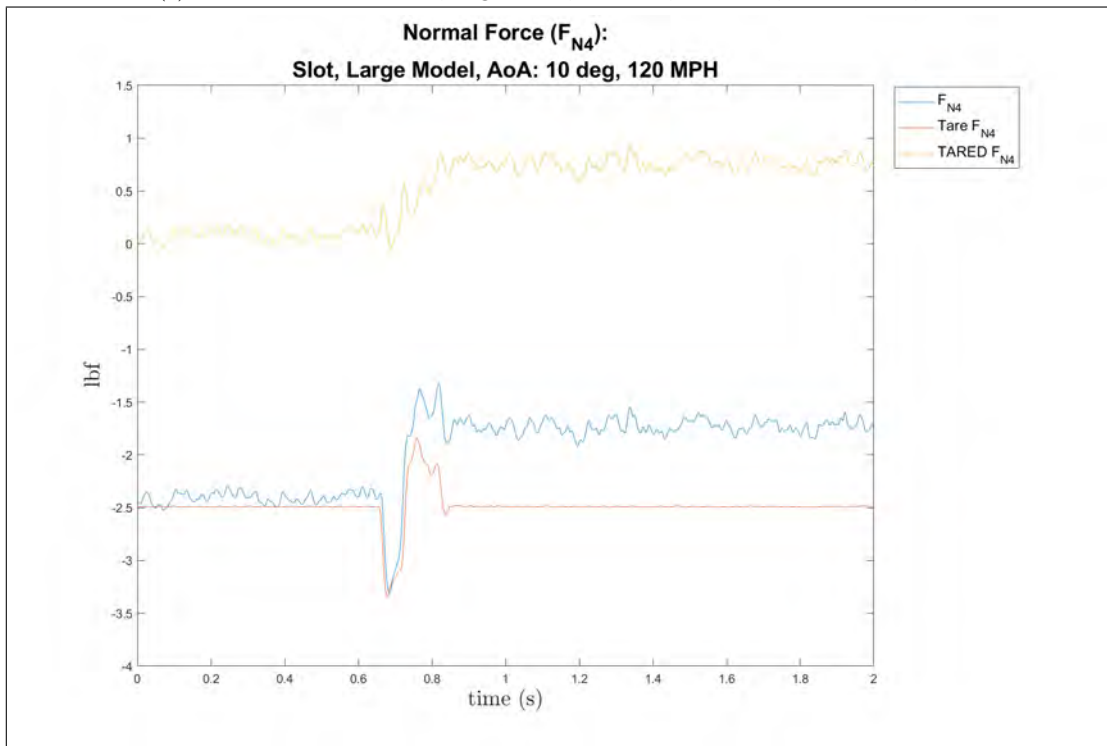


(b) Normal Force Coefficient, large model, 10° AoA, 120 MPH, release two, tare

Figure 189: Large model at 10° AoA of the normal force coefficient, release times one and two, 120 MPH, tare

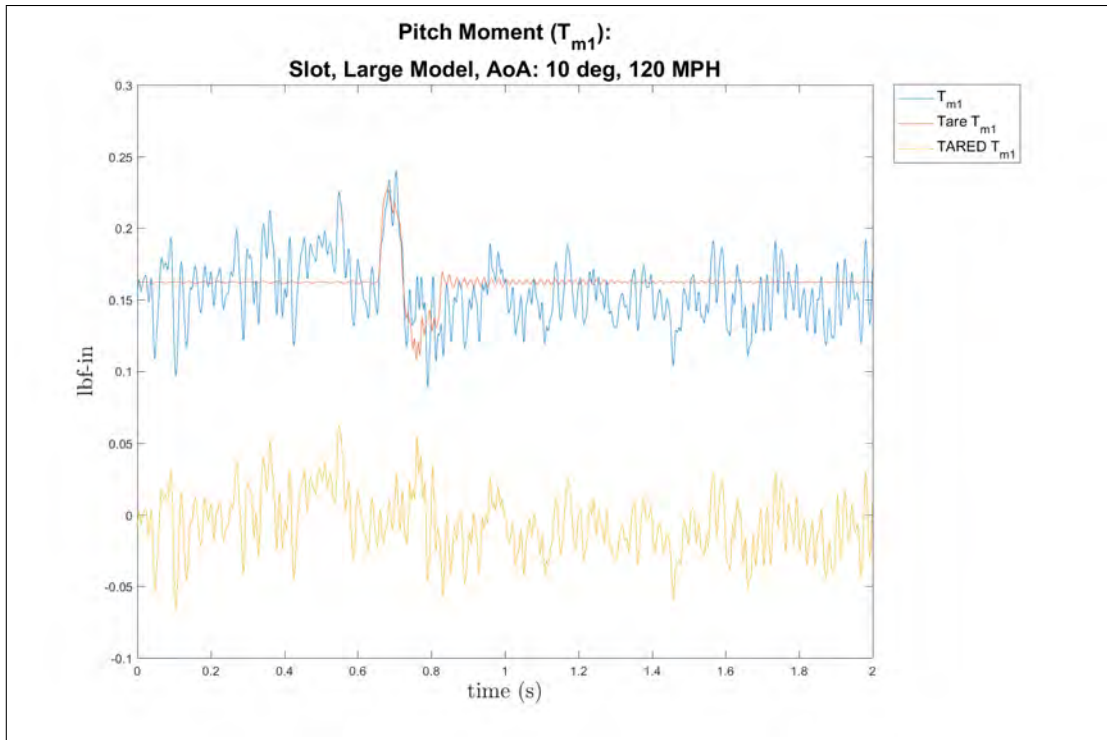


(a) Normal Force Coefficient, large model, 10° AoA, 120 MPH, release three, tare

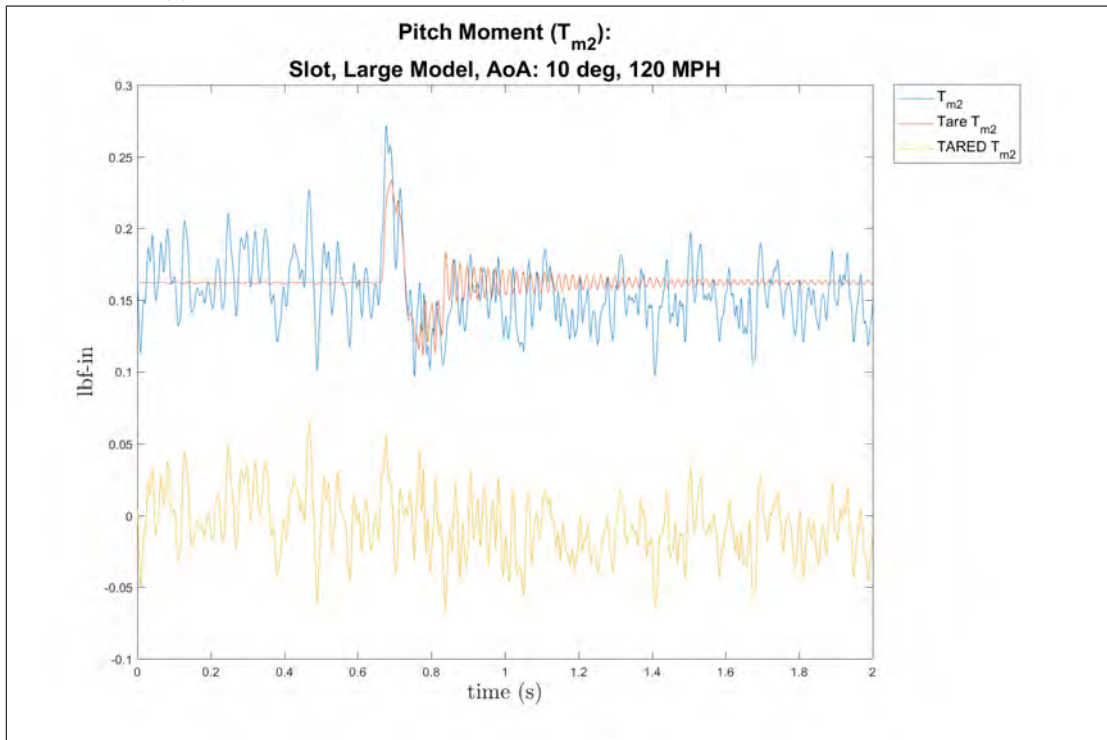


(b) Normal Force Coefficient, large model, 10° AoA, 120 MPH, release four, tare

Figure 190: Large model at 10° AoA of the normal force coefficient, release times three and four, 120 MPH, tare

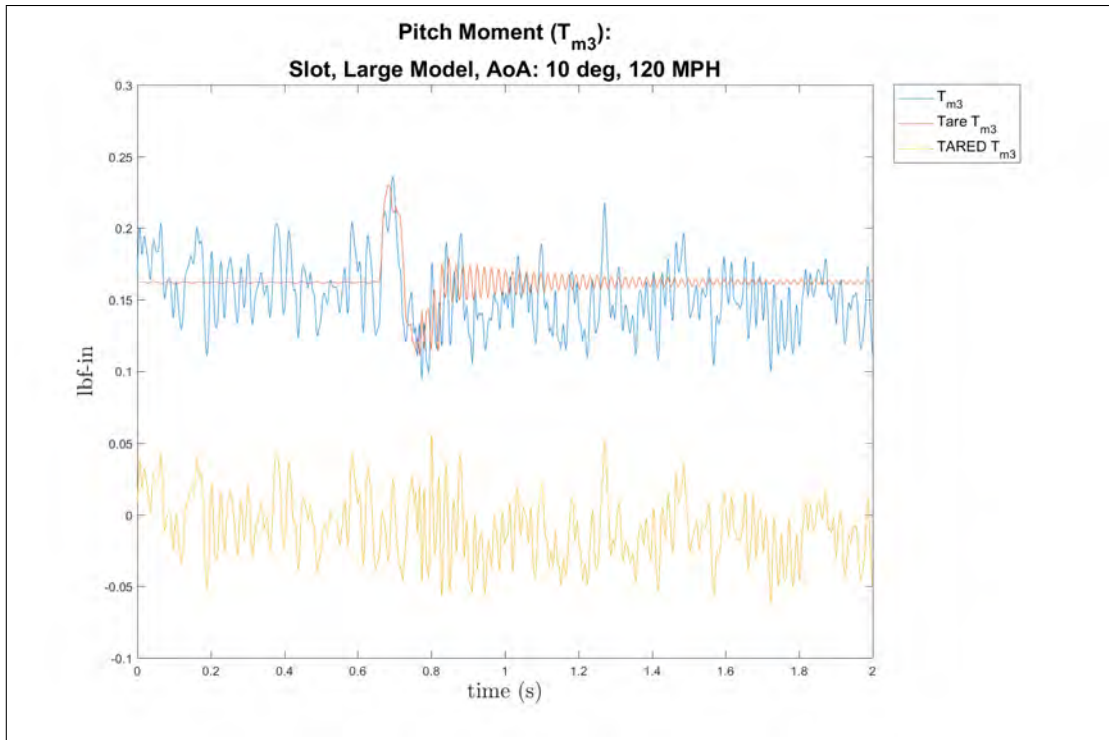


(a) Pitch Moment Coefficient, large model, 10° AoA, 120 MPH, release one, tare

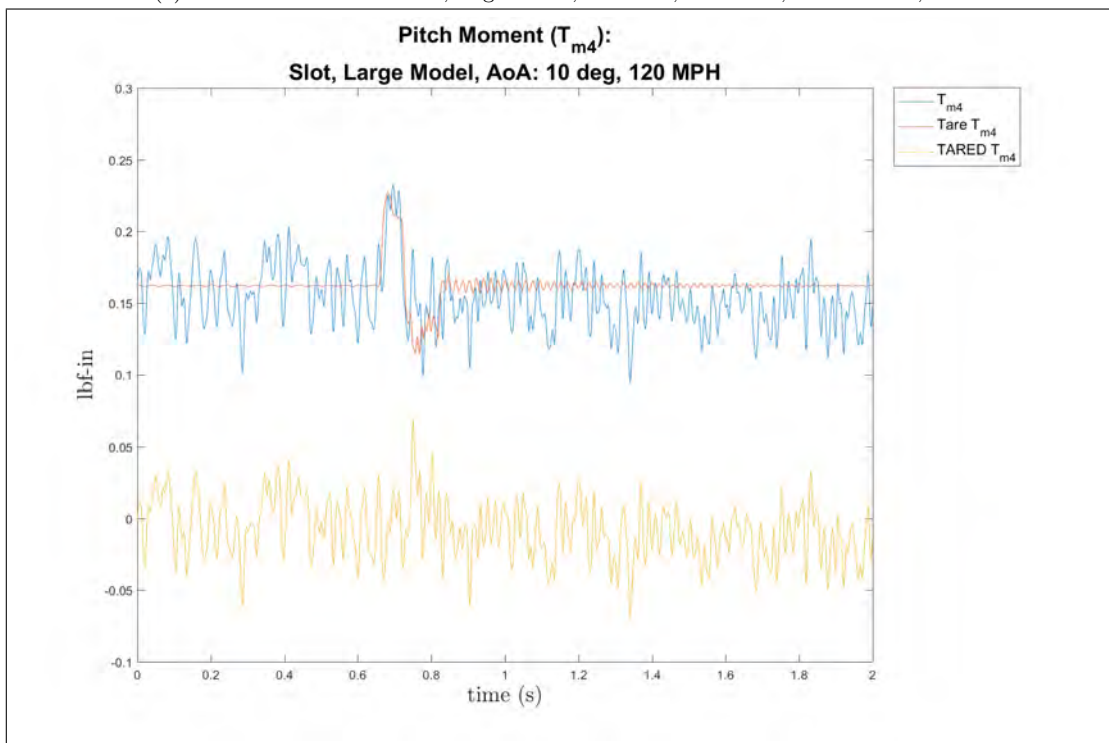


(b) Pitch Moment Coefficient, large model, 10° AoA, 120 MPH, release two, tare

Figure 191: Large model at 10° AoA of the pitch moment coefficient, release times one and two, 120 MPH, tare

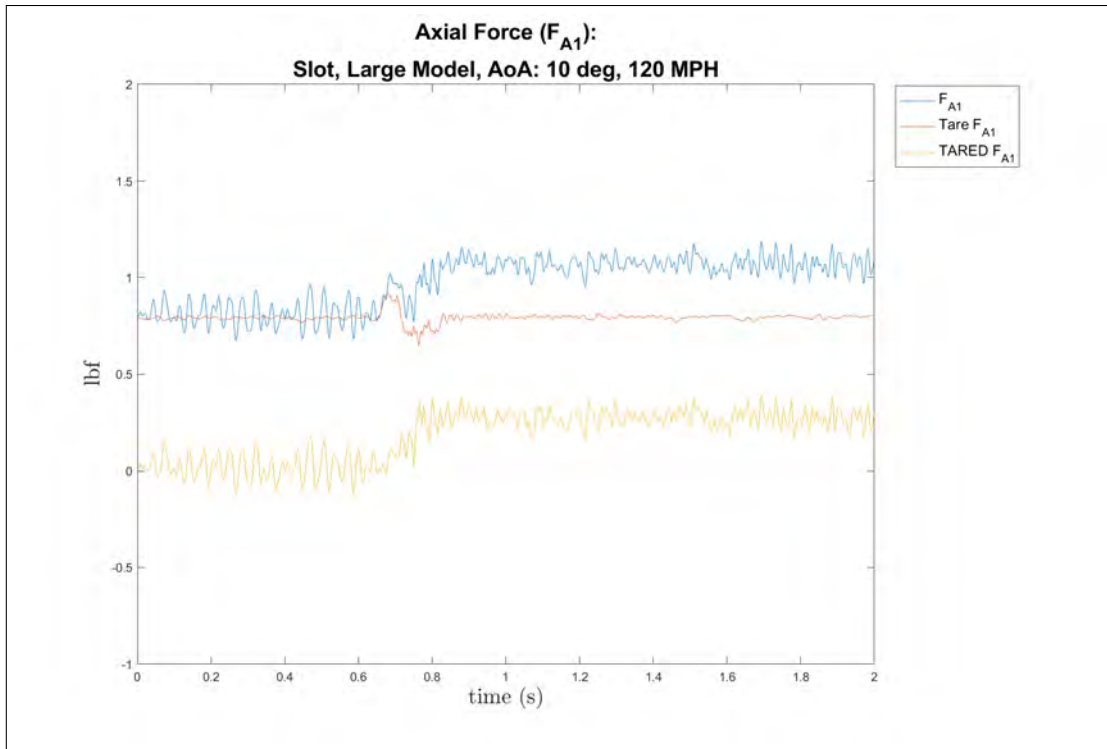


(a) Pitch Moment Coefficient, large model, 10° AoA, 120 MPH, release three, tare

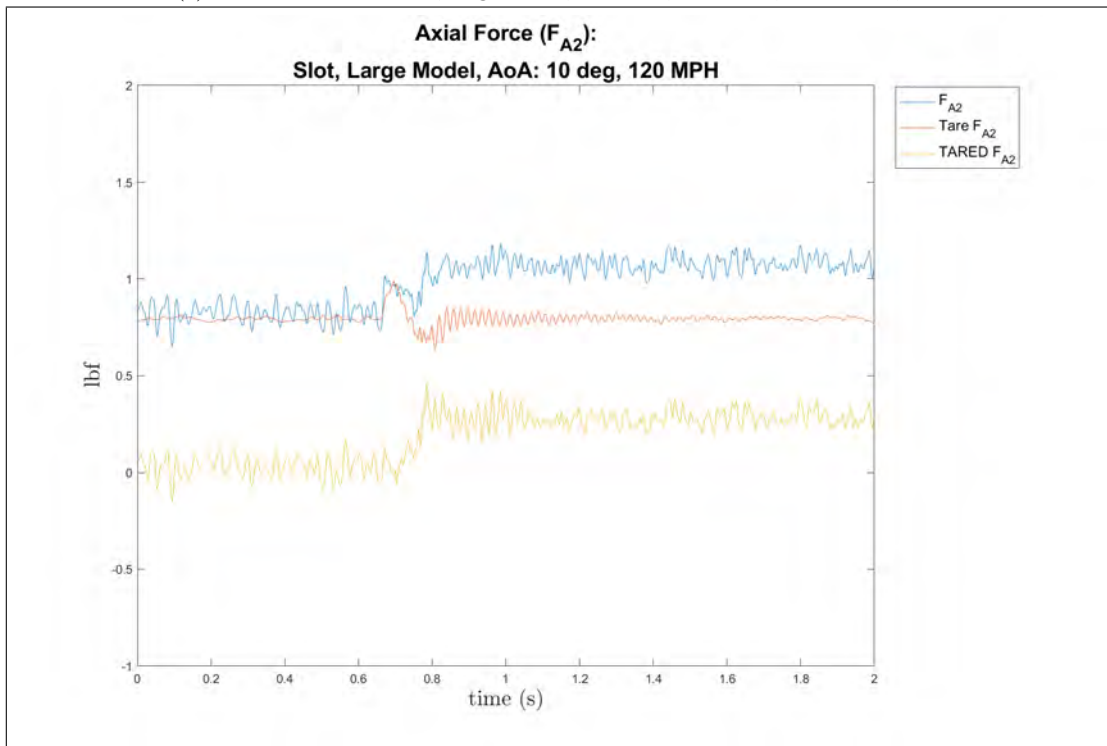


(b) Pitch Moment Coefficient, large model, 10° AoA, 120 MPH, release four, tare

Figure 192: Large model at 10° AoA of the pitch moment coefficient, release times three and four, 120 MPH, tare

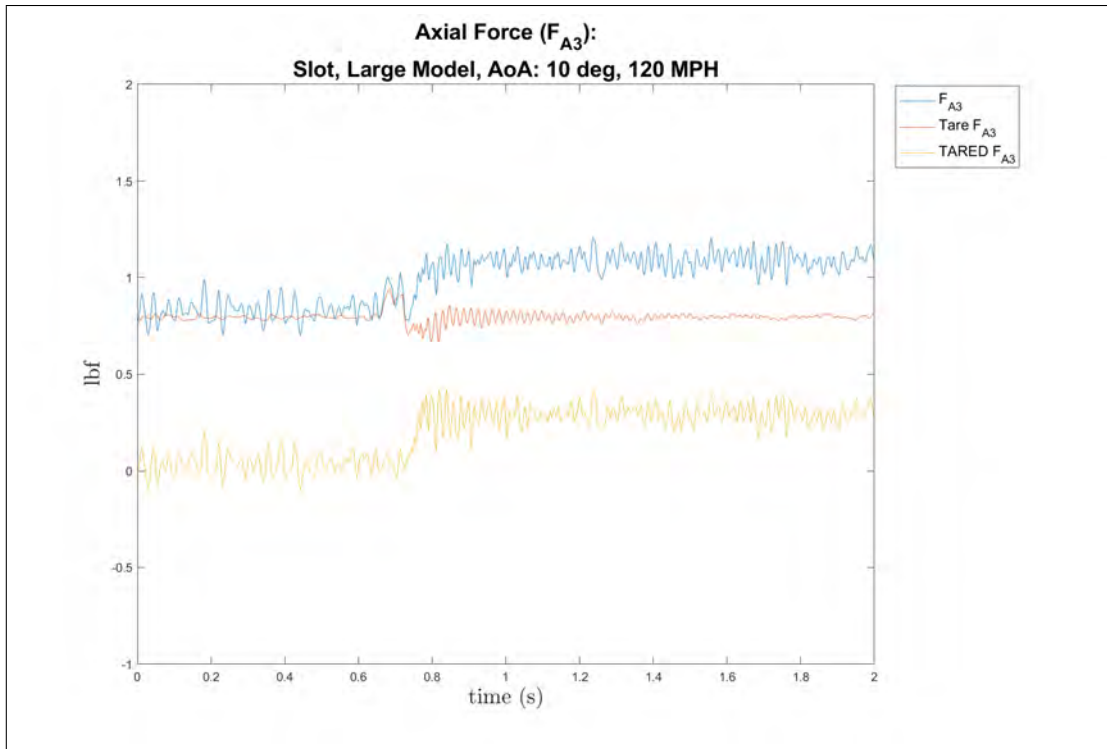


(a) Axial Force Coefficient, large model, 10° AoA, 120 MPH, release one, tare

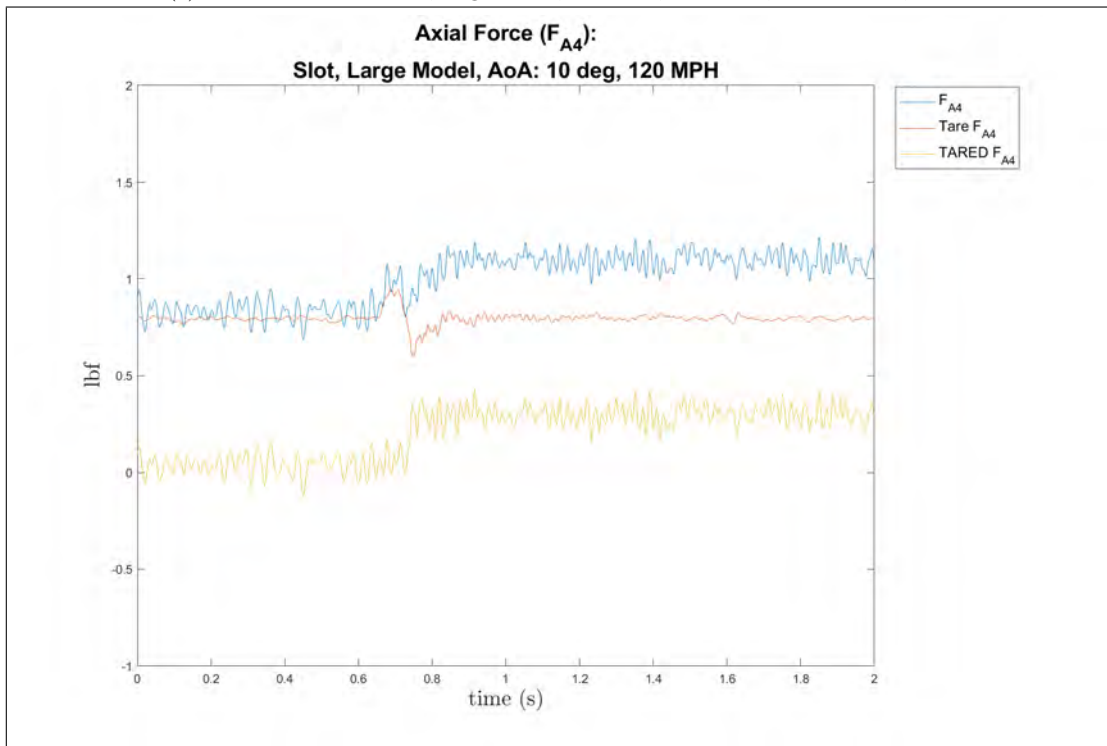


(b) Axial Force Coefficient, large model, 10° AoA, 120 MPH, release two, tare

Figure 193: Large model at 10° AoA of the axial force coefficient, release times one and two, 120 MPH, tare



(a) Axial Force Coefficient, large model, 10° AoA, 120 MPH, release three, tare



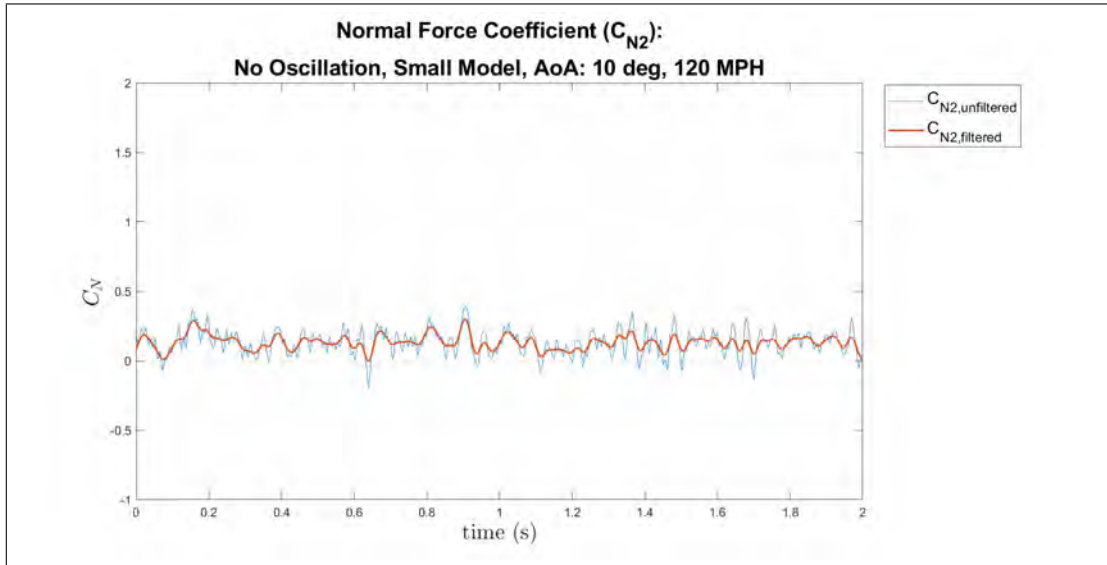
(b) Axial Force Coefficient, large model, 10° AoA, 120 MPH, release four, tare

Figure 194: Large model at 10° AoA of the axial force coefficient, release times three and four, 120 MPH, tare

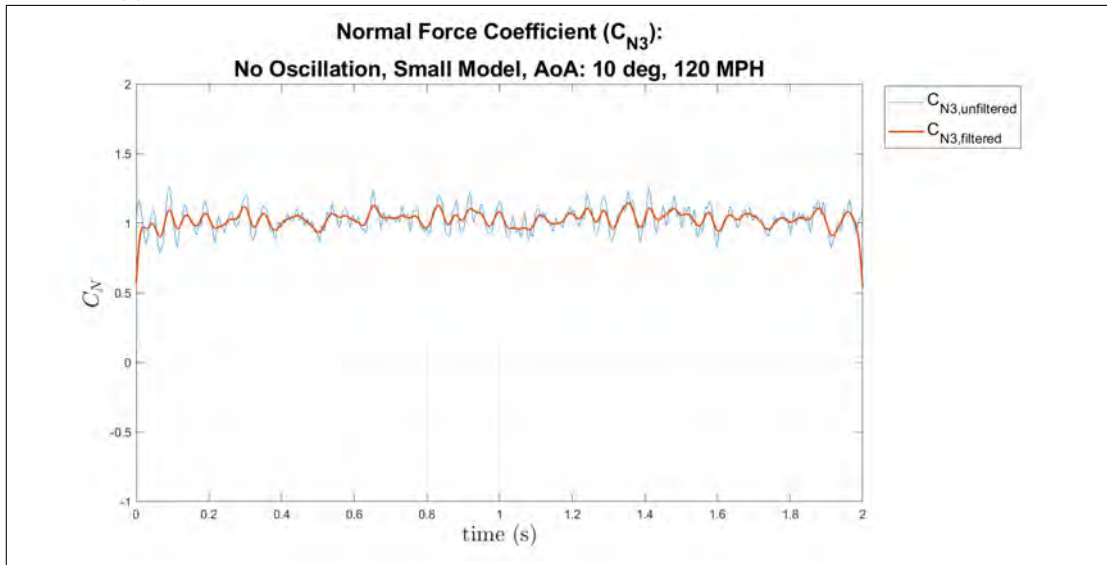
Individual Examples 10 Degrees

Normal Force, Pitch Moment, and Axial Force Coefficients

Small Model, Cavity Apparatus, 10° AoA, 120 MPH

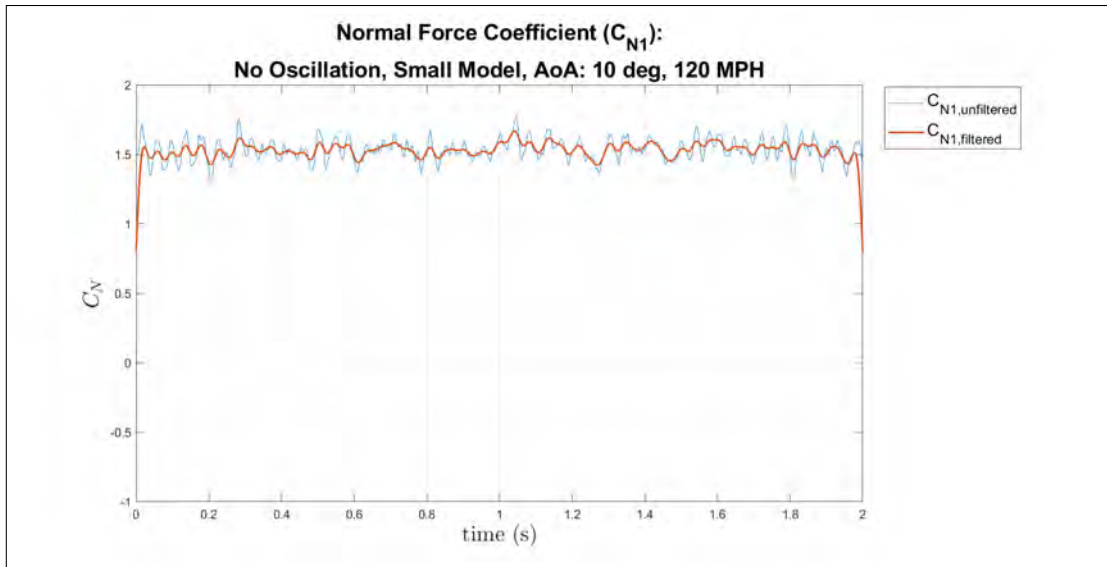


(a) Normal Force Coefficient, small model, 10° AoA, 120 MPH, In Cavity, individual trial

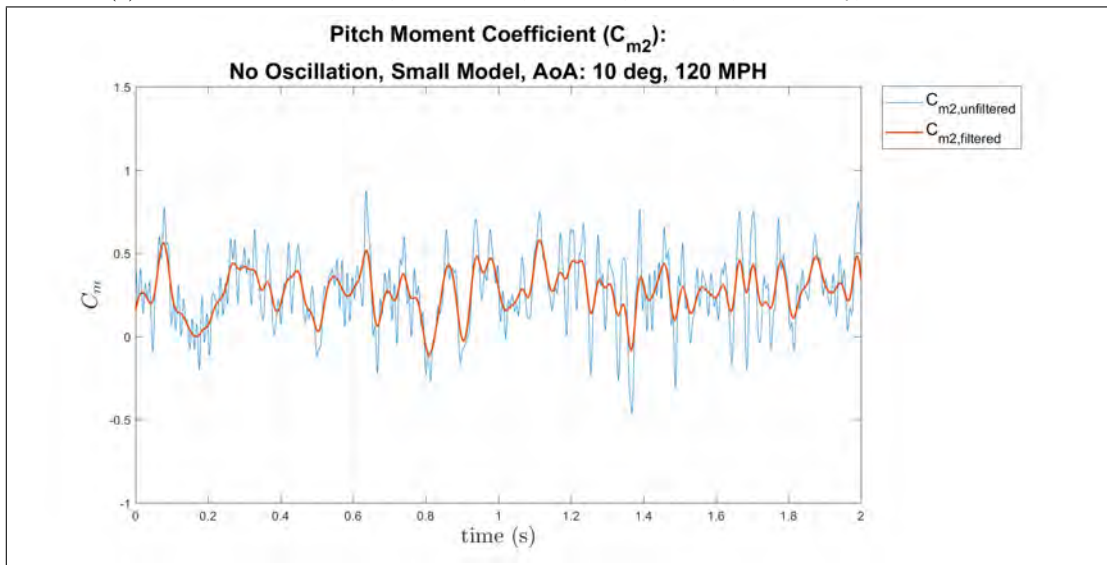


(b) Normal Force Coefficient, small model, 10° AoA, 120 MPH, Shear Layer, individual trial

Figure 195: Small model at 10° AoA of the normal force coefficient, 120 MPH, individual trial

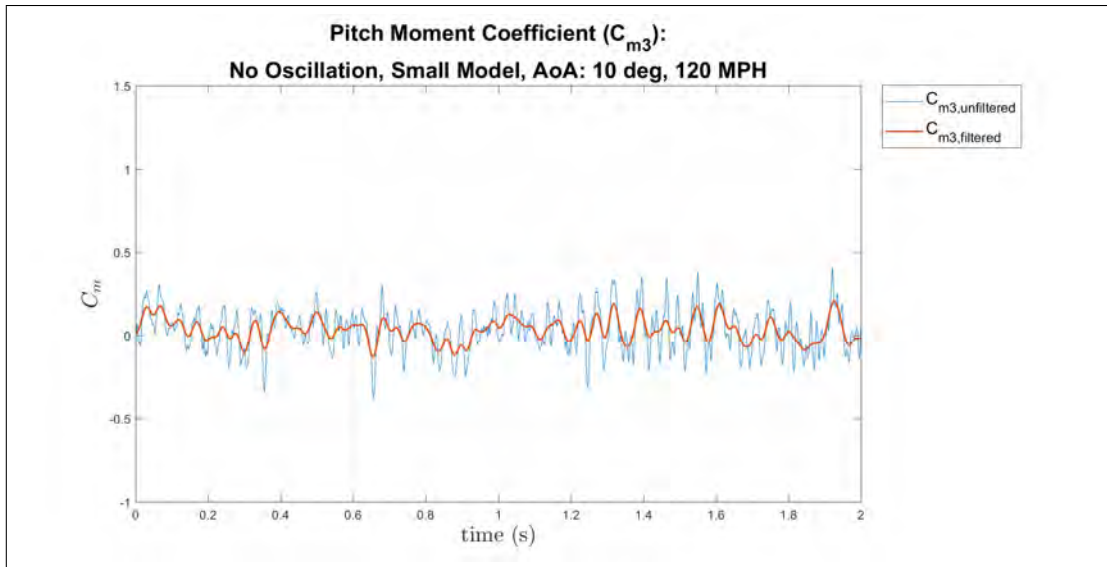


(a) Normal Force Coefficient, small model, 10° AoA, 120 MPH, Out Cavity, individual trial

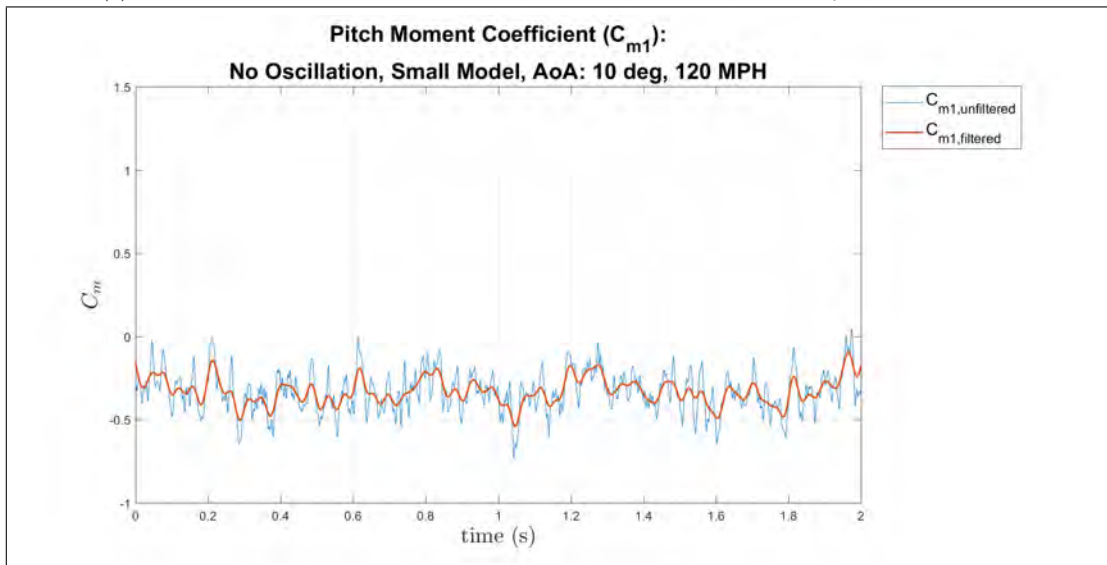


(b) Pitch Moment Coefficient, small model, 10° AoA, 120 MPH, In Cavity, individual trial

Figure 196: Small model at 10° AoA of the pitch moment and normal force coefficients, 120 MPH, individual trial

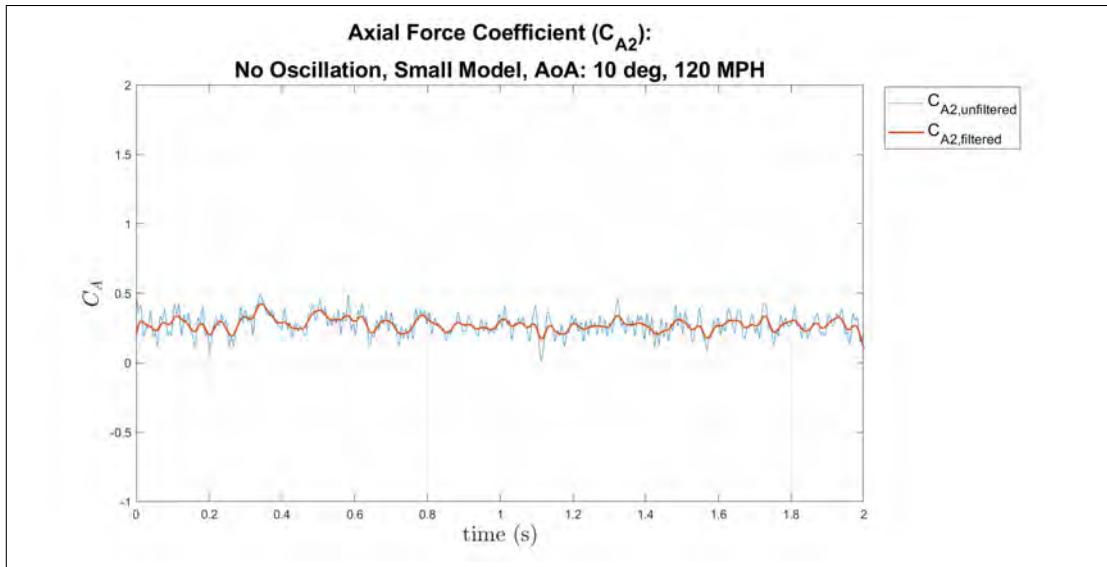


(a) Pitch Moment Coefficient, small model, 10° AoA, 120 MPH, Shear Layer, individual trial

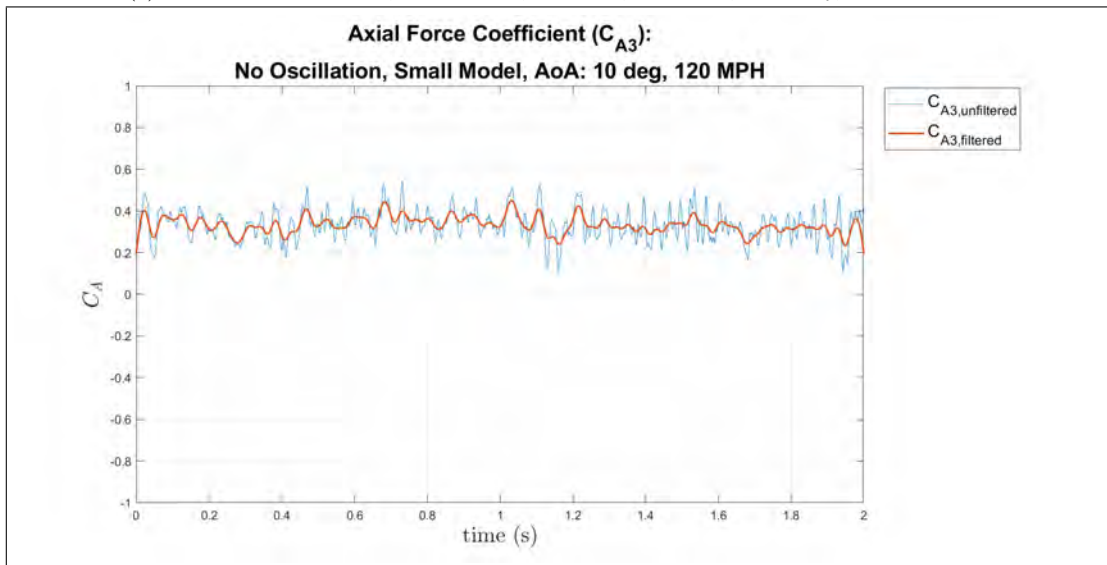


(b) Pitch Moment Coefficient, small model, 10° AoA, 120 MPH, Out Cavity, individual trial

Figure 197: Small model at 10° AoA of the pitch moment coefficient, 120 MPH, individual trial

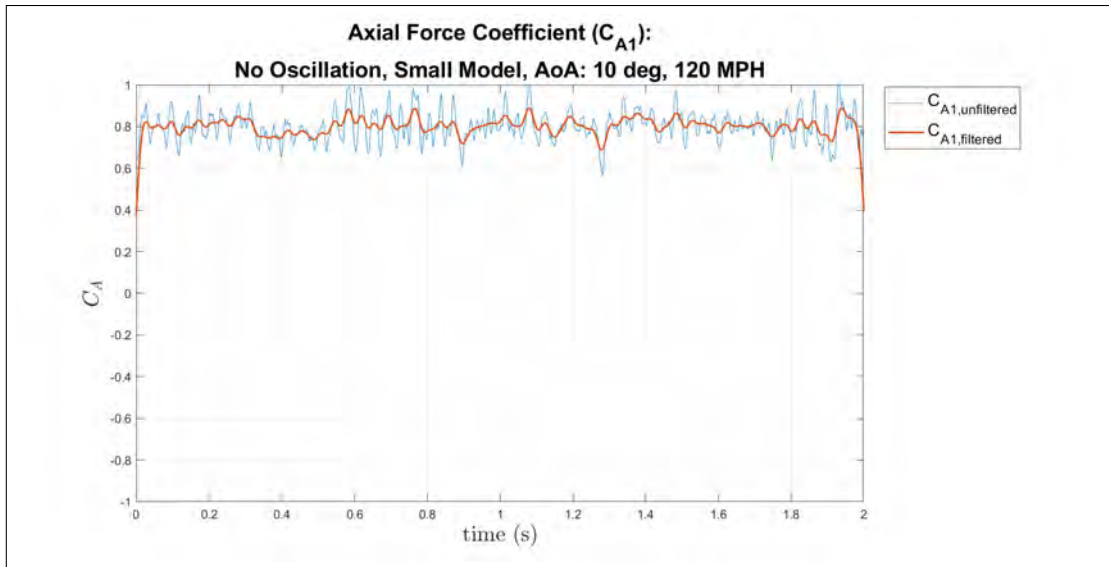


(a) Axial Force Coefficient, small model, 10° AoA, 120 MPH, In Cavity, individual trial

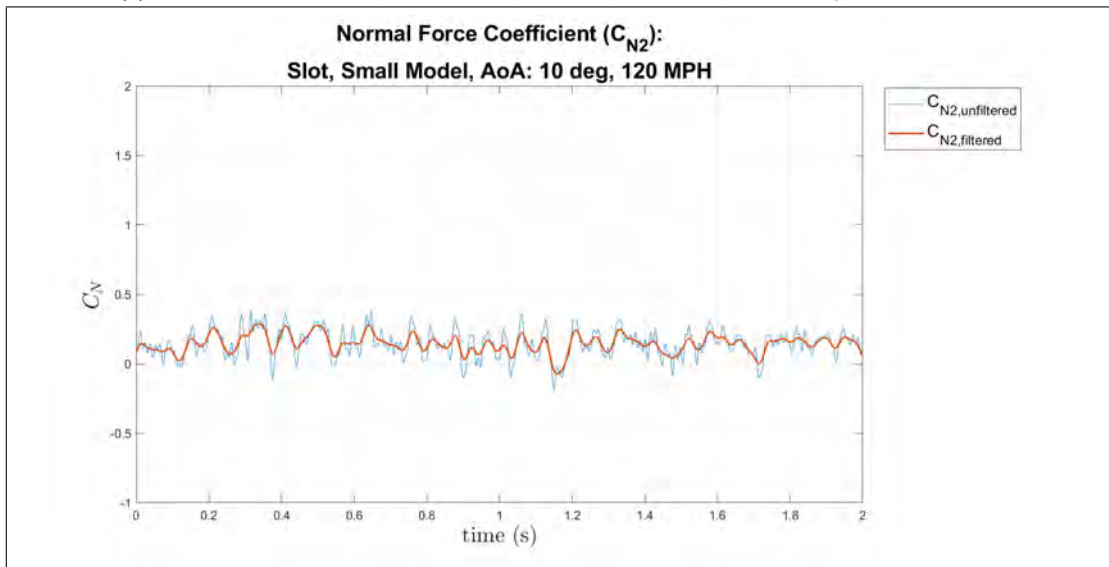


(b) Axial Force Coefficient, small model, 10° AoA, 120 MPH, Shear Layer, individual trial

Figure 198: Small model at 10° AoA of the Axial Force coefficient, 120 MPH, individual trial

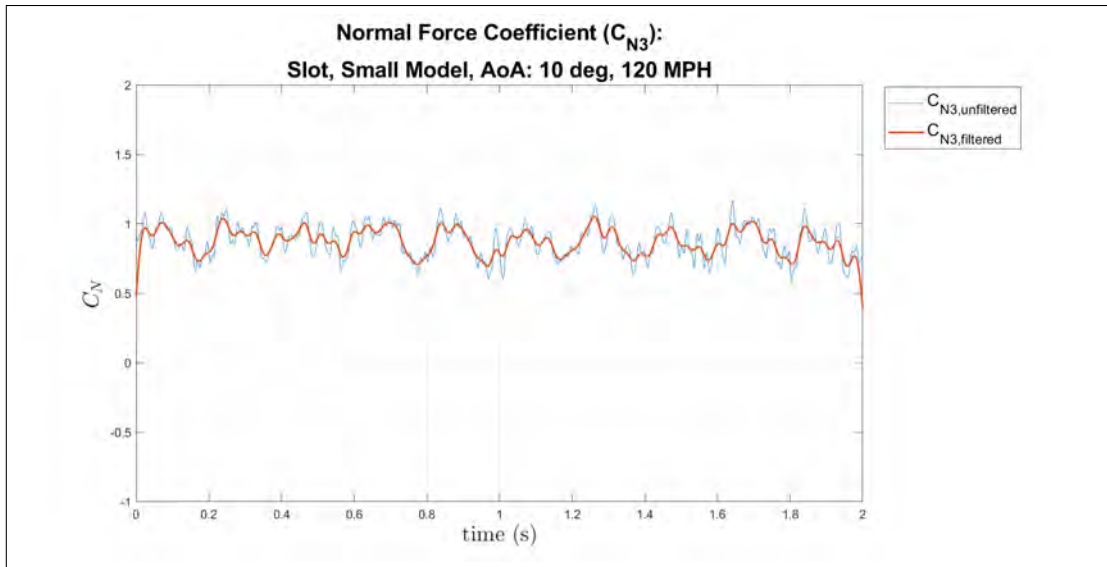


(a) Axial Force Coefficient, small model, 10° AoA, 120 MPH, Out Cavity, individual trial

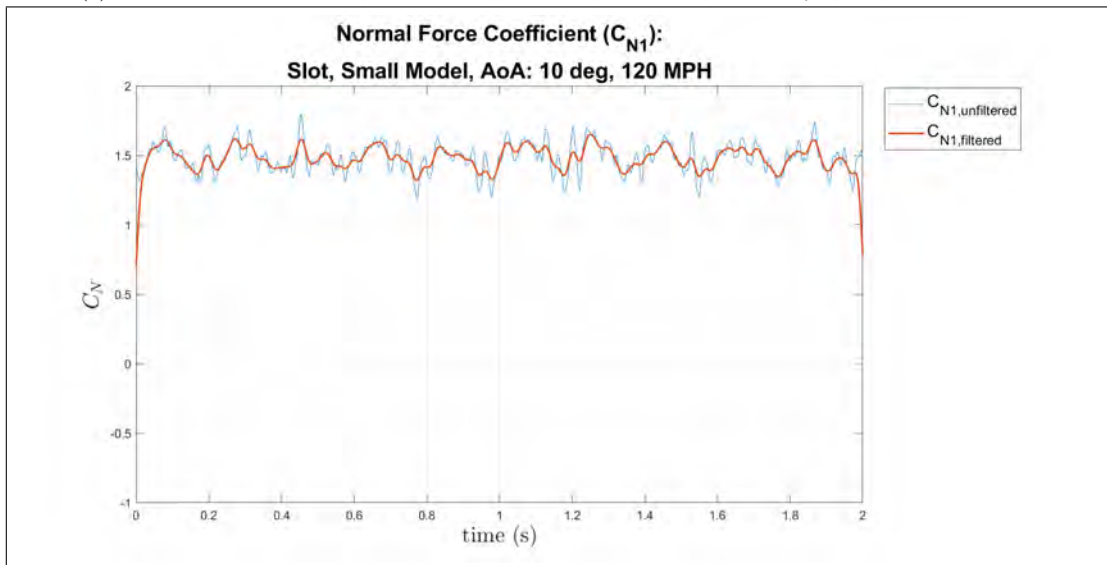


(b) Normal Force Coefficient, small model, 10° AoA, 120 MPH, In Cavity, slot, individual trial

Figure 199: Small model at 10° AoA of the axial force and normal force coefficients, 120 MPH, individual trial

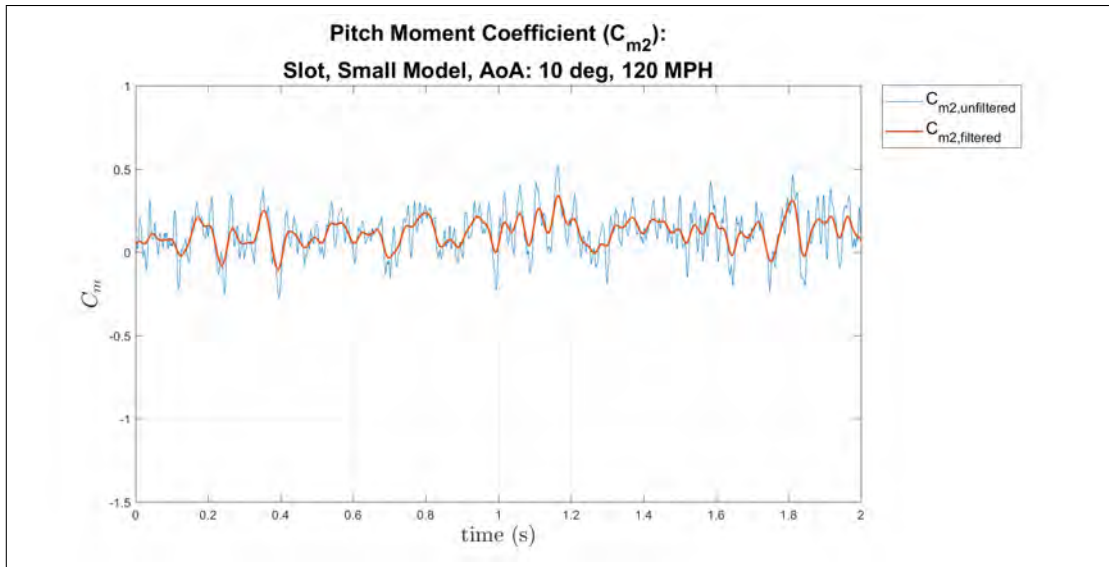


(a) Normal Force Coefficient, small model, 10° AoA, 120 MPH, Shear Layer, slot, individual trial

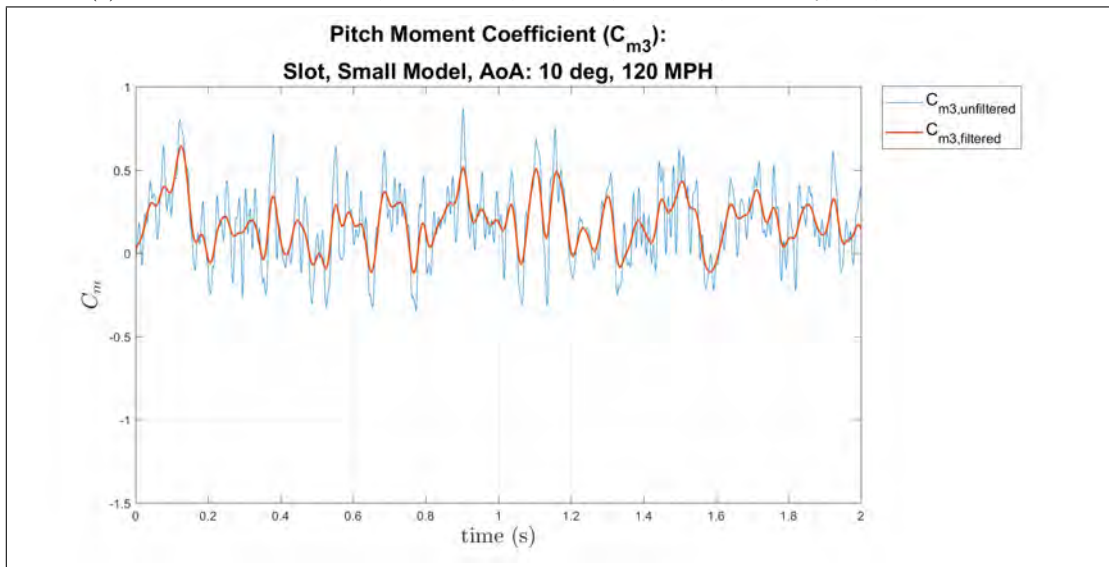


(b) Normal Force Coefficient, small model, 10° AoA, 120 MPH, Out Cavity, slot, individual trial

Figure 200: Small model at 10° AoA of the normal force coefficient, 120 MPH, slot, individual trial

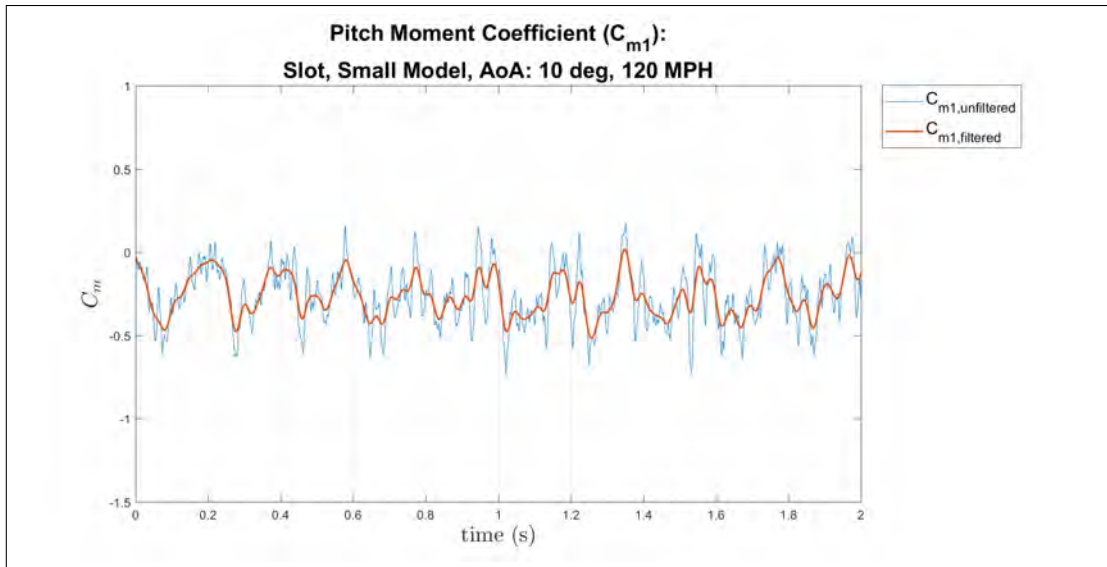


(a) Pitch Moment Coefficient, small model, 10° AoA, 120 MPH, In Cavity, slot, individual trial

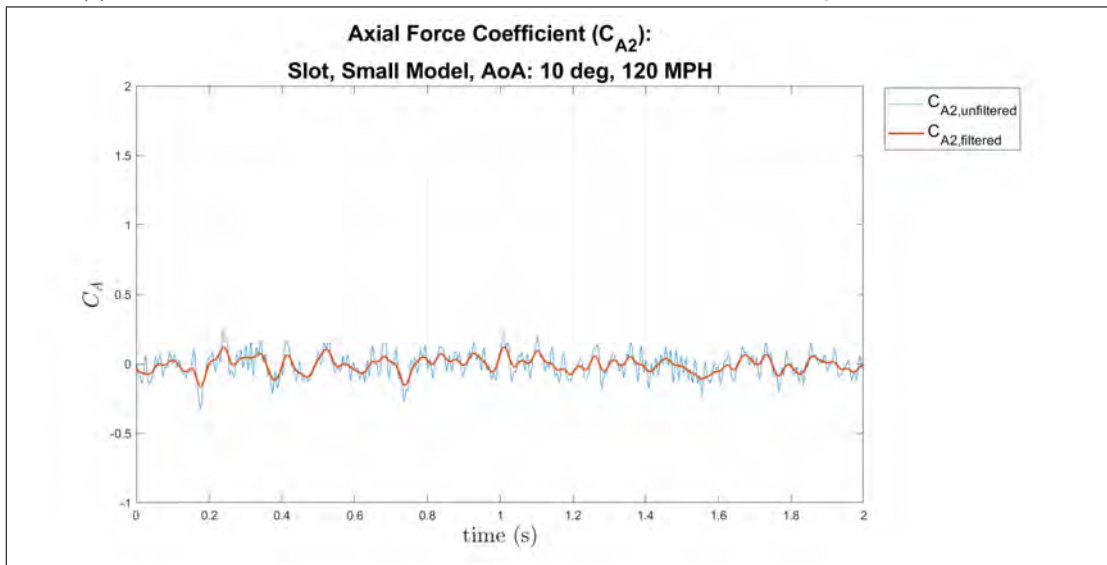


(b) Pitch Moment Coefficient, small model, 10° AoA, 120 MPH, Shear Layer, slot, individual trial

Figure 201: Small model at 10° AoA of the pitch moment coefficient, 120 MPH, slot, individual trial

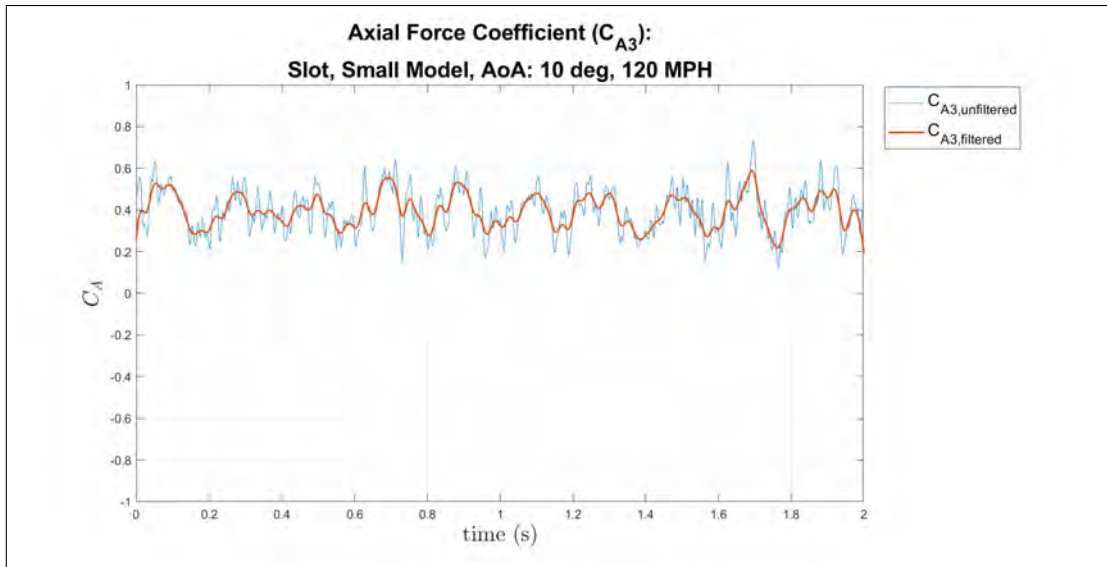


(a) Pitch Moment Coefficient, small model, 10° AoA, 120 MPH, Out Cavity, slot, individual trial

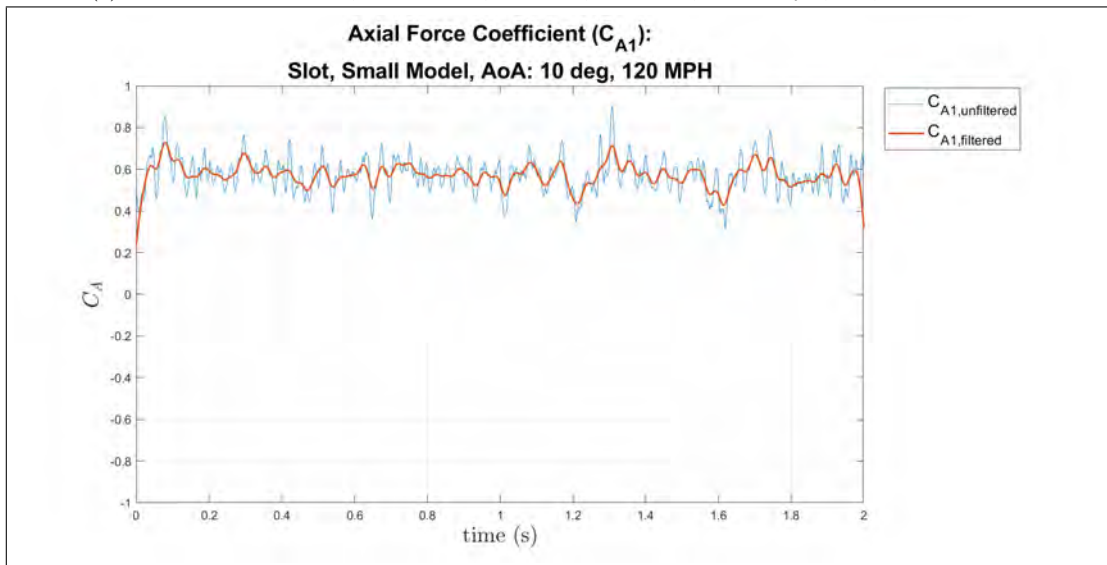


(b) Axial Force Coefficient, small model, 10° AoA, 120 MPH, In Cavity, slot, individual trial

Figure 202: Small model at 10° AoA of the pitch moment and axial force coefficients, 120 MPH, slot, individual trial



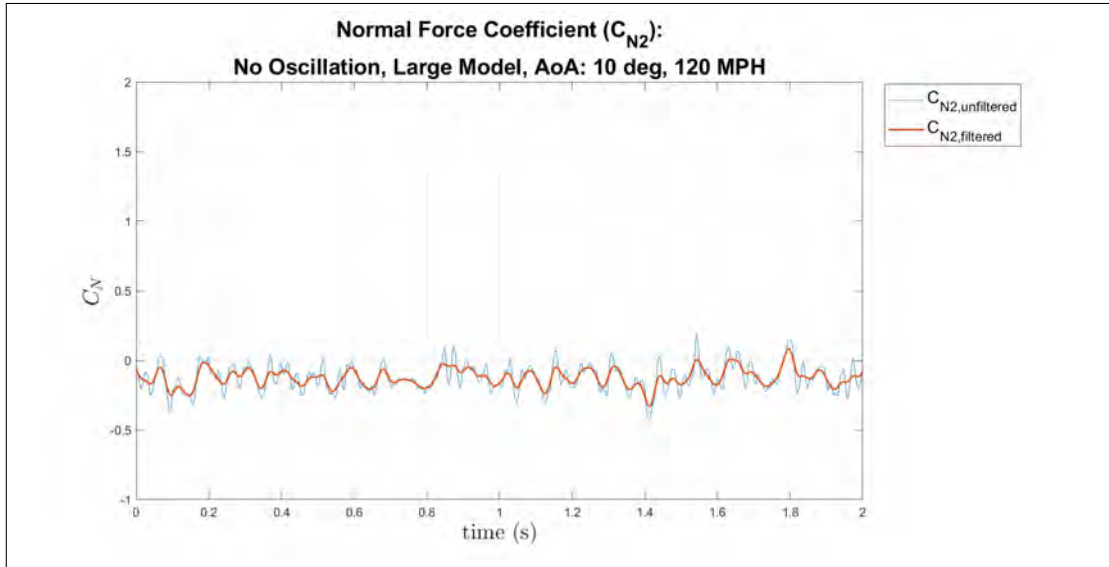
(a) Axial Force Coefficient, small model, 10° AoA, 120 MPH, Shear Layer, slot, individual trial



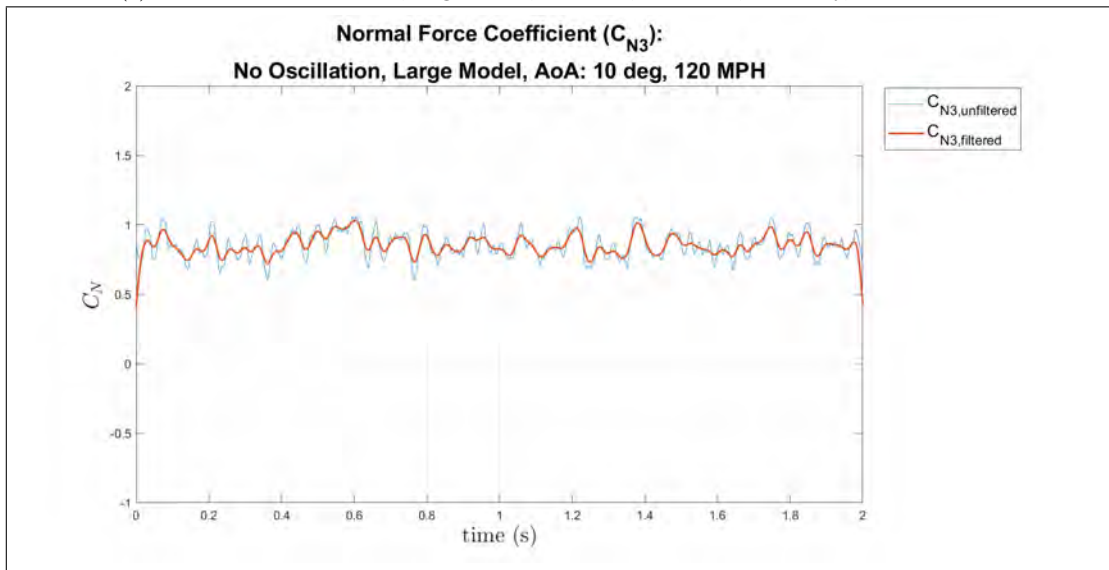
(b) Axial Force Coefficient, small model, 10° AoA, 120 MPH, Out Cavity, slot, individual trial

Figure 203: Small model at 10° AoA of the axial force coefficient, 120 MPH, slot, individual trial

Large Model, Cavity Apparatus, 10° AoA, 120 MPH

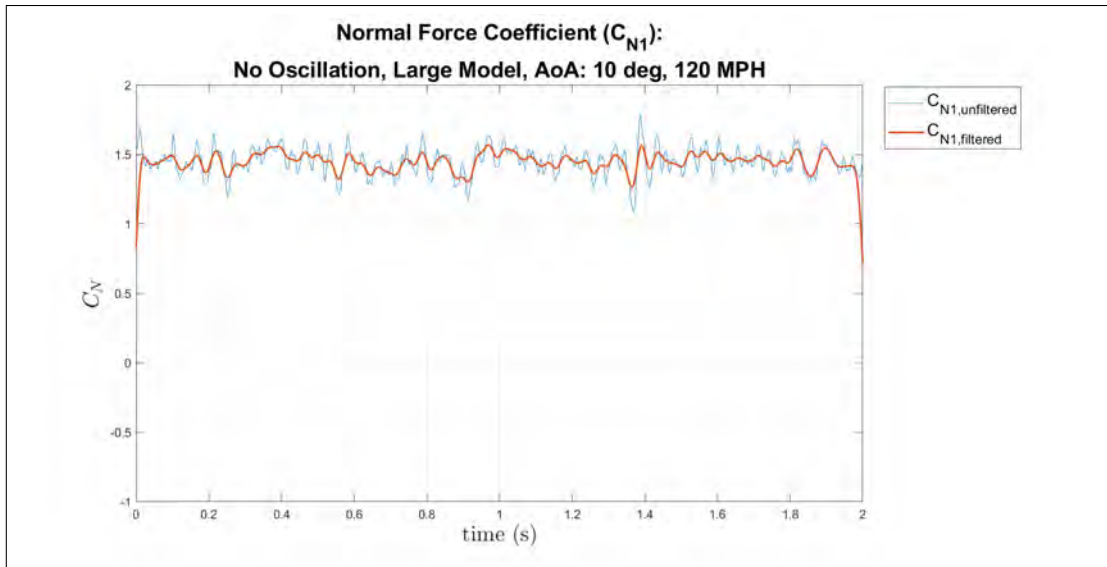


(a) Normal Force Coefficient, large model, 10° AoA, 120 MPH, In Cavity, individual trial

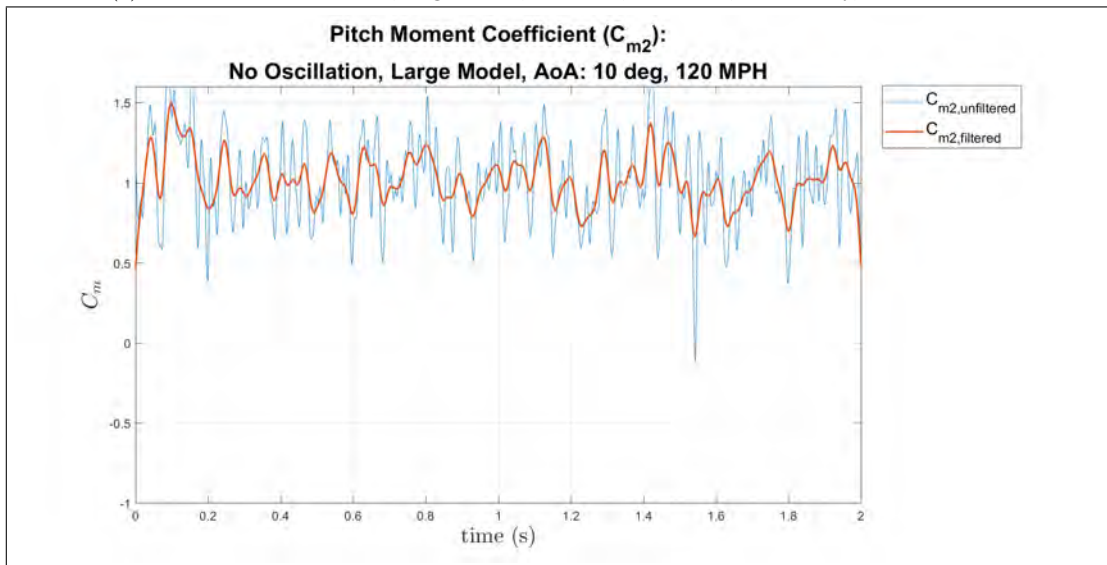


(b) Normal Force Coefficient, large model, 10° AoA, 120 MPH, Shear Layer, individual trial

Figure 204: Large model at 10° AoA of the normal force coefficient, 120 MPH, individual trial

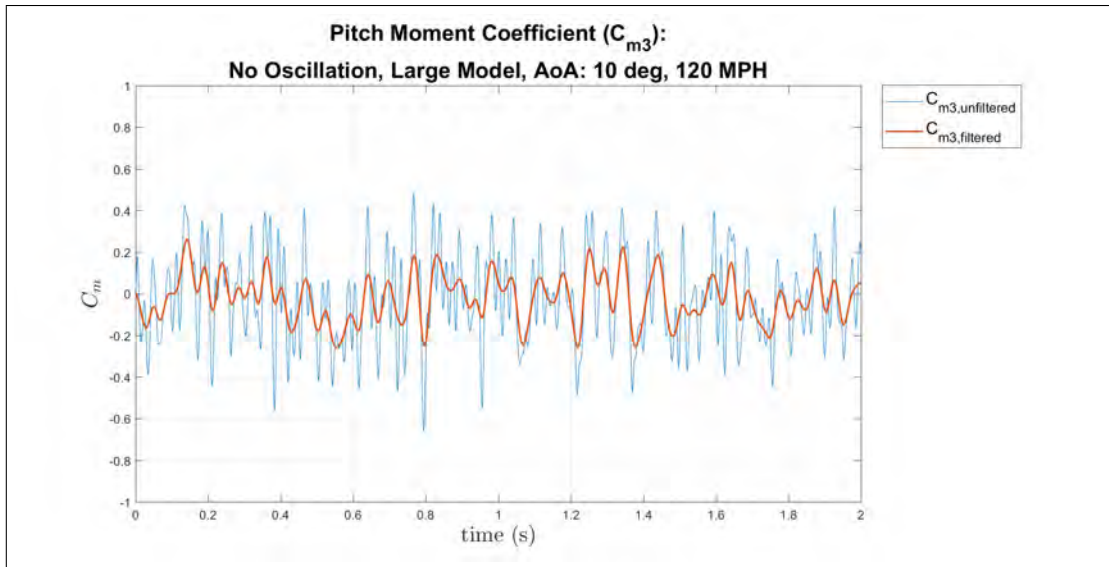


(a) Normal Force Coefficient, large model, 10° AoA, 120 MPH, Out Cavity, individual trial

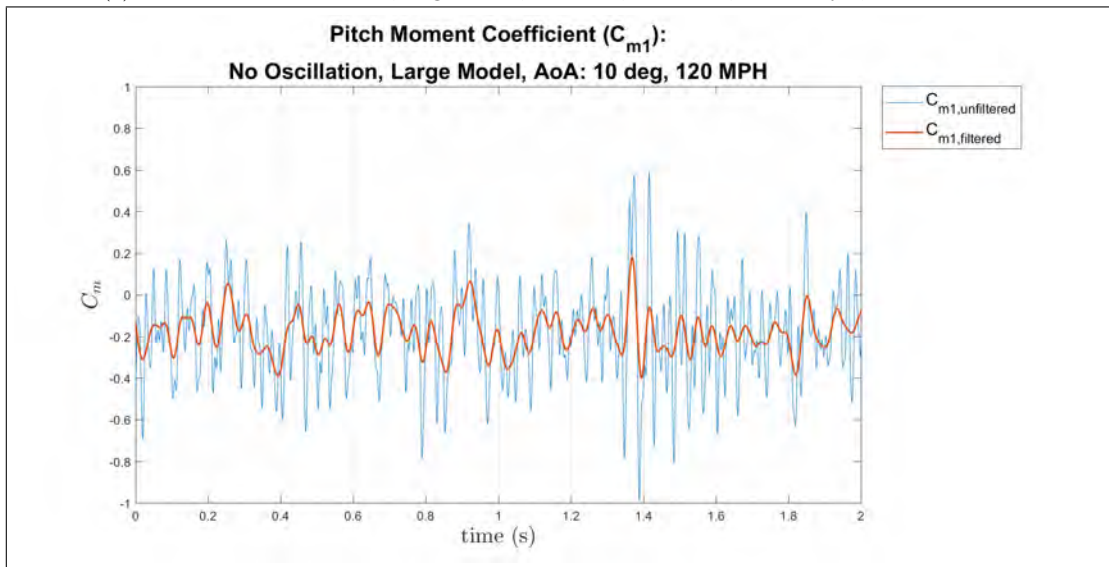


(b) Pitch Moment Coefficient, large model, 10° AoA, 120 MPH, In Cavity, individual trial

Figure 205: Large model at 10° AoA of the pitch moment and normal force coefficients, 120 MPH, individual trial

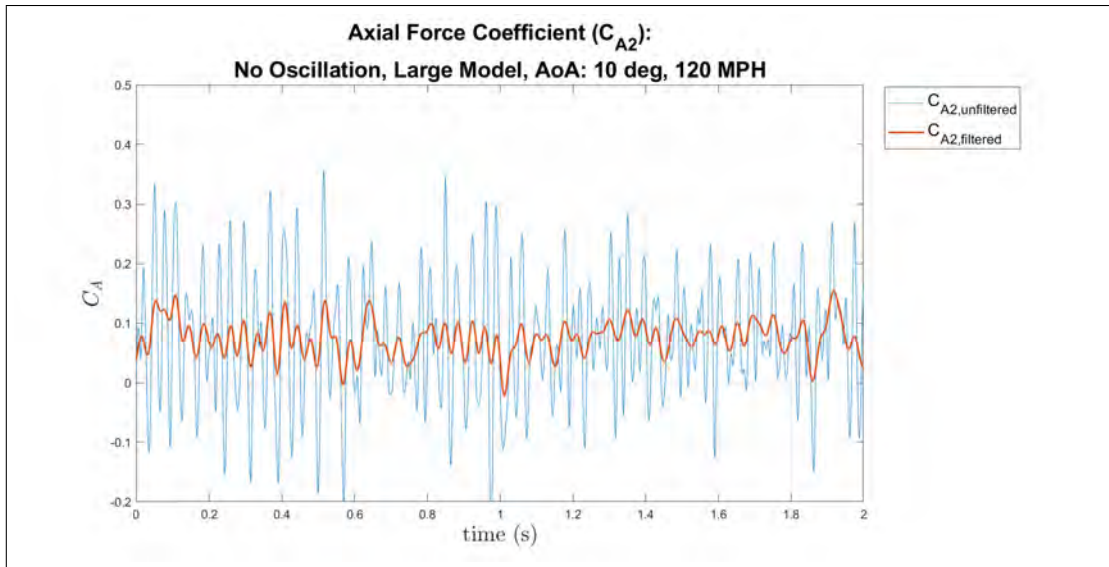


(a) Pitch Moment Coefficient, large model, 10° AoA, 120 MPH, Shear Layer, individual trial

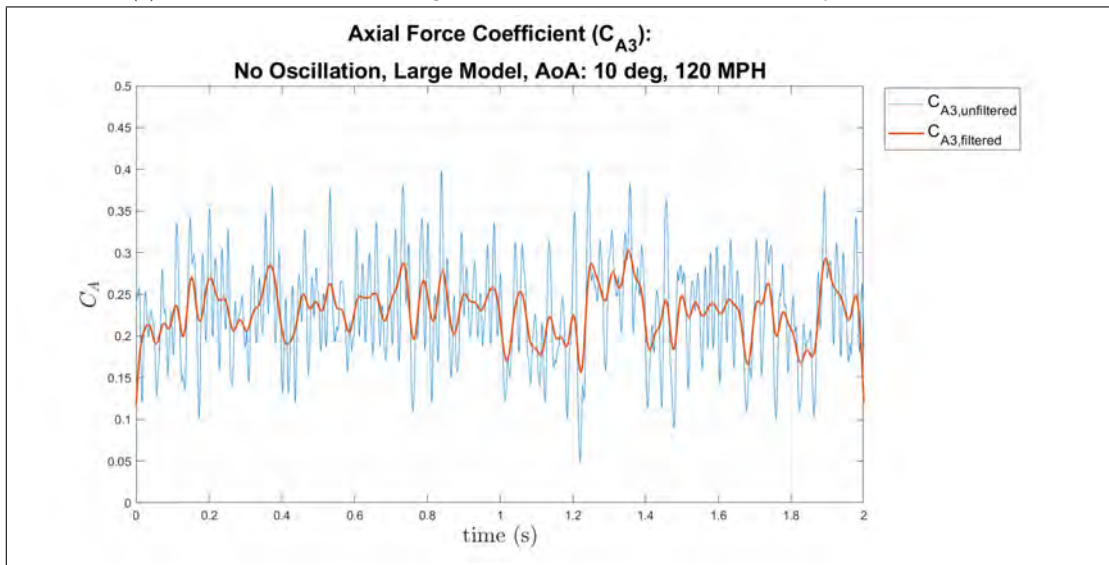


(b) Pitch Moment Coefficient, large model, 10° AoA, 120 MPH, Out Cavity, individual trial

Figure 206: Large model at 10° AoA of the pitch moment coefficient, 120 MPH, individual trial

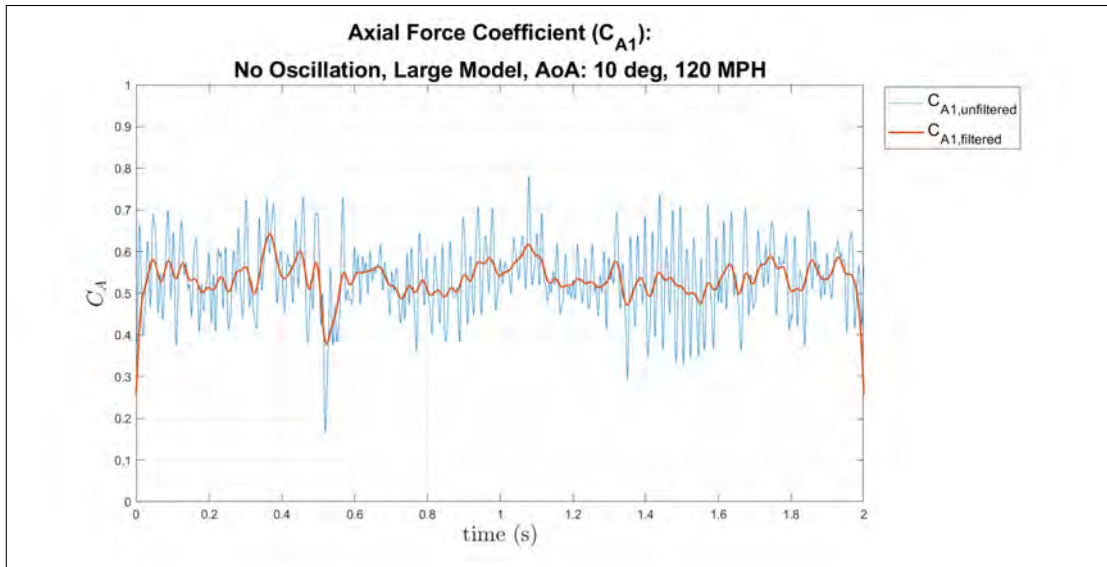


(a) Axial Force Coefficient, large model, 10° AoA, 120 MPH, In Cavity, individual trial

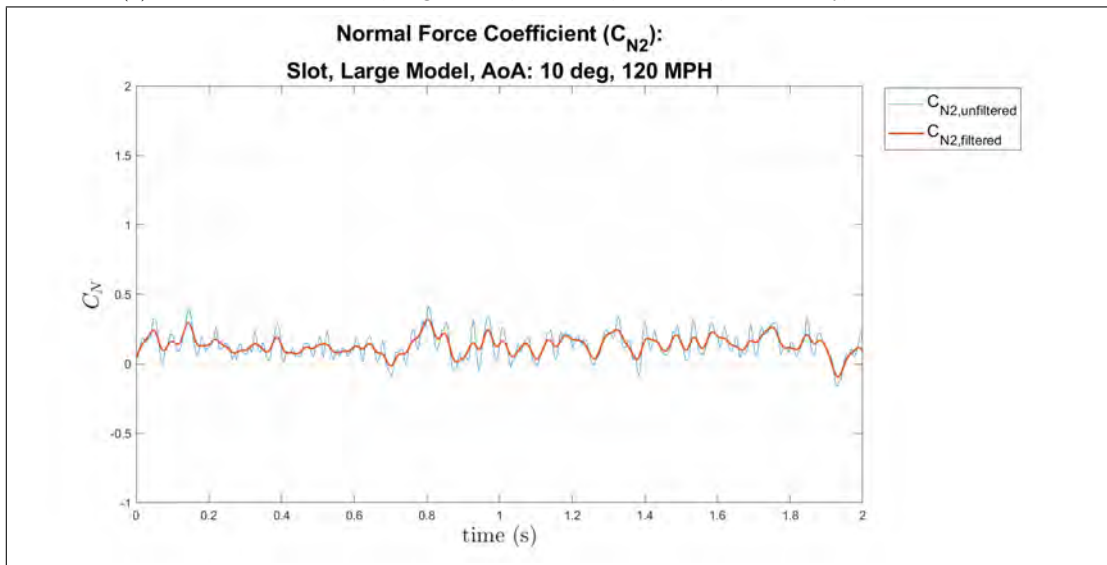


(b) Axial Force Coefficient, large model, 10° AoA, 120 MPH, Shear Layer, individual trial

Figure 207: Large model at 10° AoA of the Axial Force coefficient, 120 MPH, individual trial

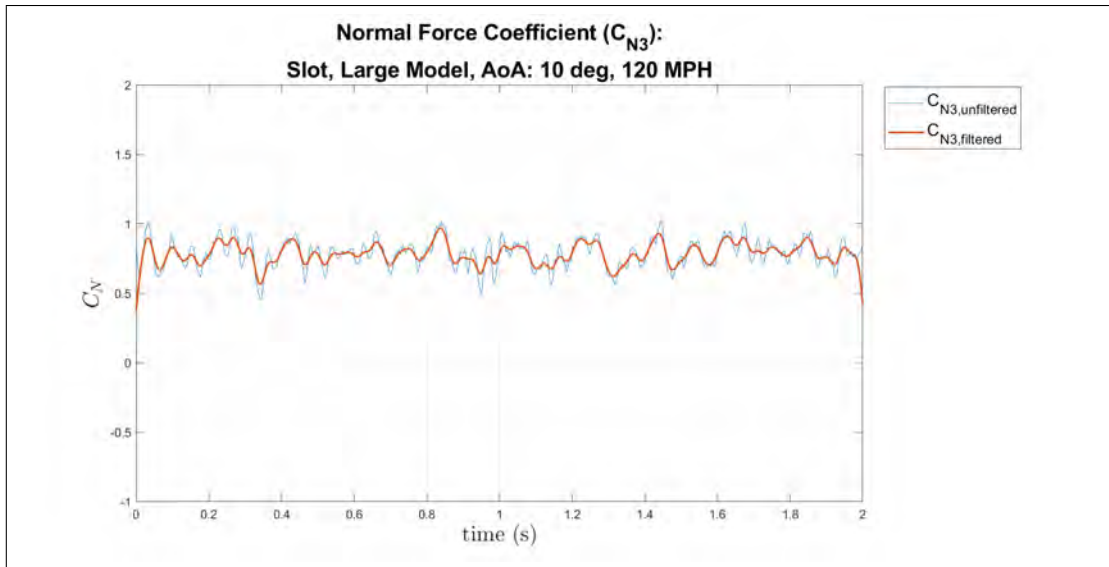


(a) Axial Force Coefficient, large model, 10° AoA, 120 MPH, Out Cavity, individual trial

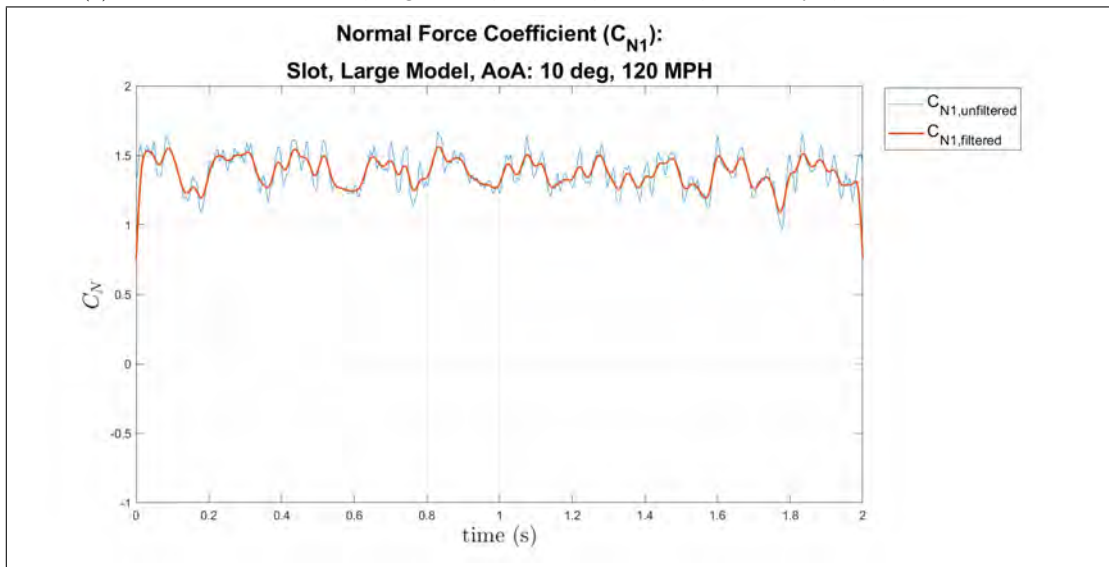


(b) Normal Force Coefficient, large model, 10° AoA, 120 MPH, In Cavity, slot, individual trial

Figure 208: Large model at 10° AoA of the axial force and normal force coefficients, 120 MPH, individual trial

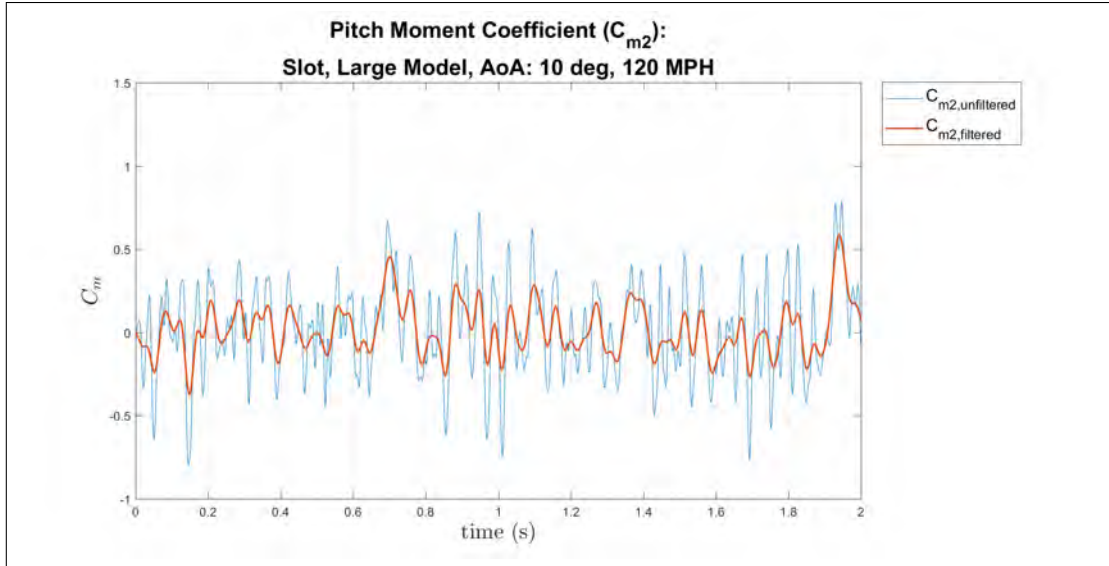


(a) Normal Force Coefficient, large model, 10° AoA, 120 MPH, Shear Layer, slot, individual trial

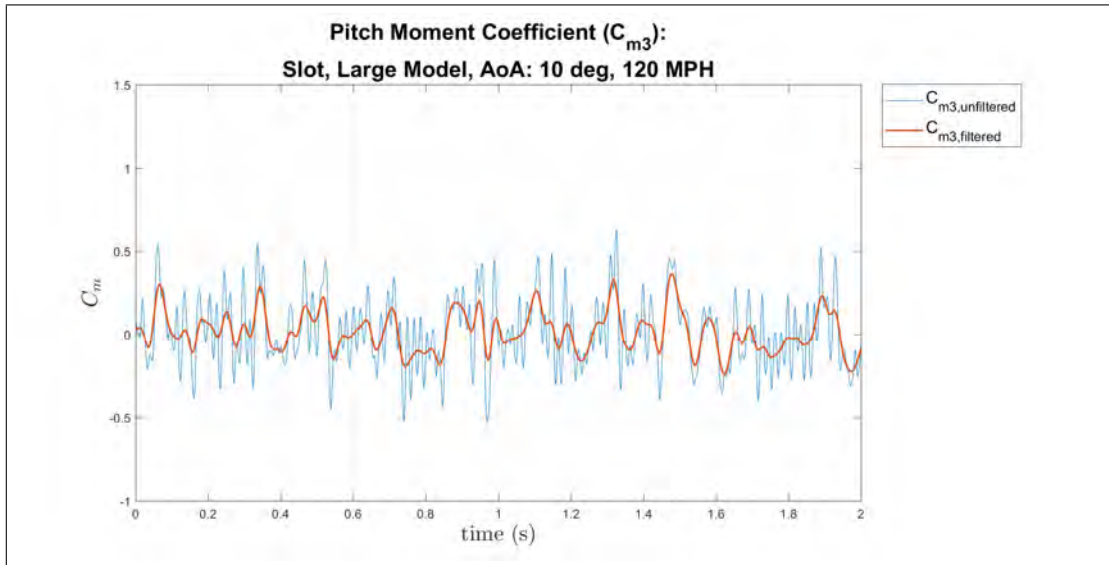


(b) Normal Force Coefficient, large model, 10° AoA, 120 MPH, Out Cavity, slot, individual trial

Figure 209: Large model at 10° AoA of the normal force coefficient, 120 MPH, slot, individual trial

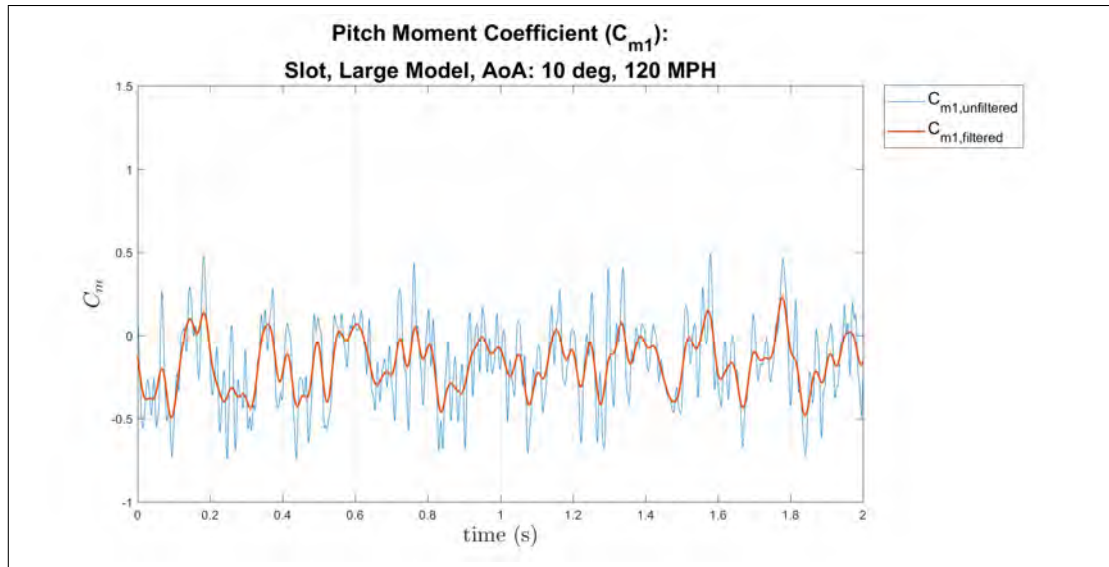


(a) Pitch Moment Coefficient, large model, 10° AoA, 120 MPH, In Cavity, slot, individual trial

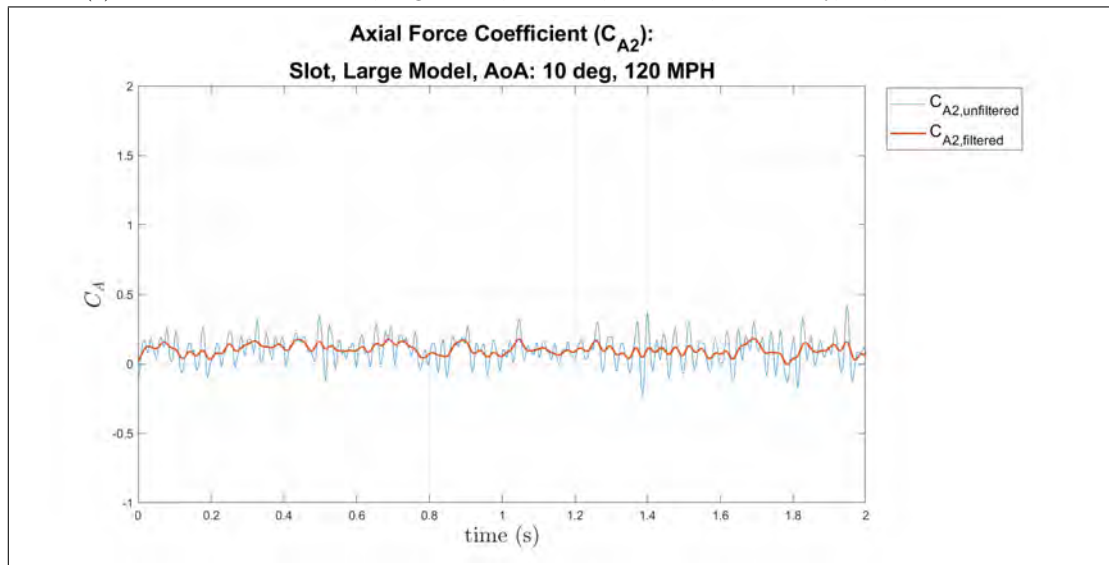


(b) Pitch Moment Coefficient, large model, 10° AoA, 120 MPH, Shear Layer, slot, individual trial

Figure 210: Large model at 10° AoA of the pitch moment coefficient, 120 MPH, slot, individual trial

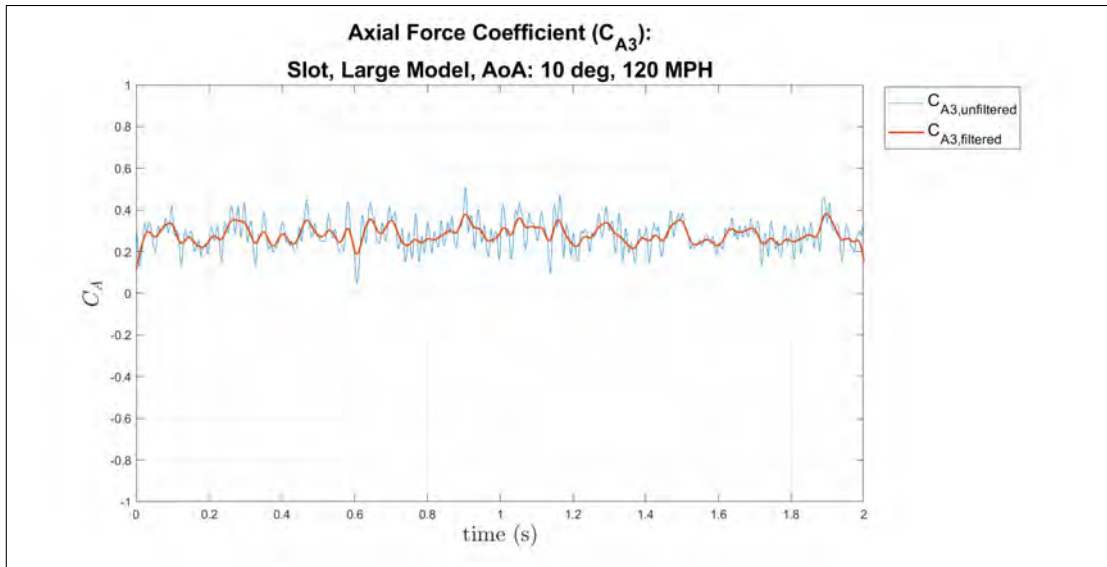


(a) Pitch Moment Coefficient, large model, 10° AoA, 120 MPH, Out Cavity, slot, individual trial

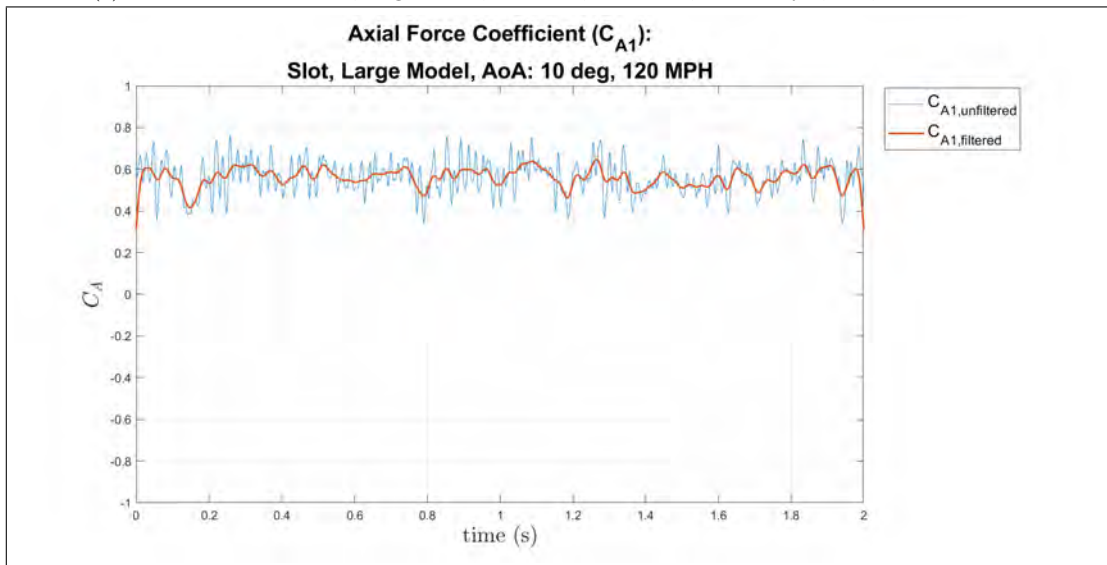


(b) Axial Force Coefficient, large model, 10° AoA, 120 MPH, In Cavity, slot, individual trial

Figure 211: Large model at 10° AoA of the pitch moment and axial force coefficients, 120 MPH, slot, individual trial



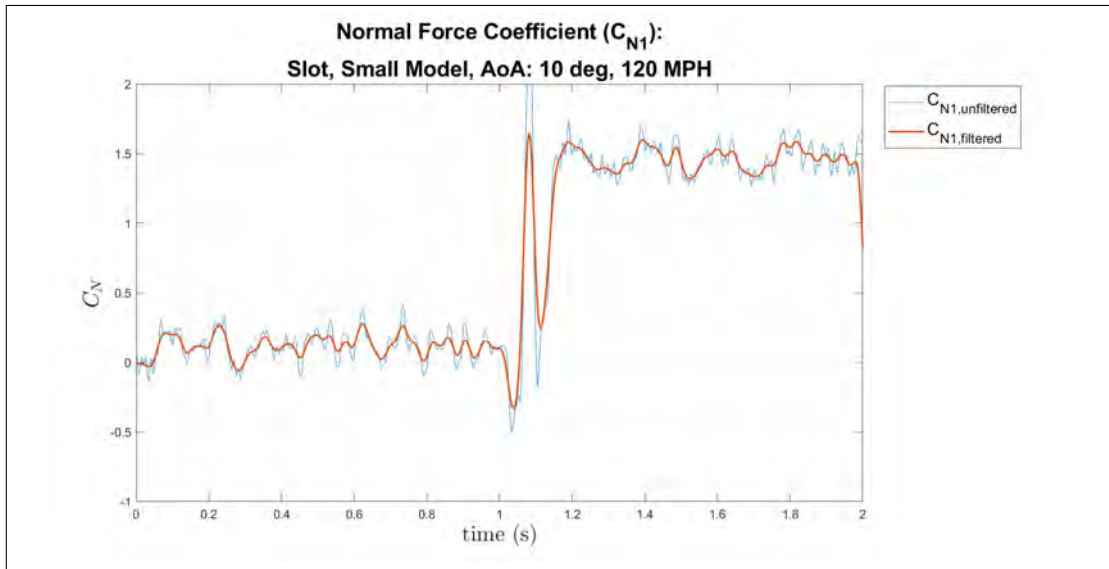
(a) Axial Force Coefficient, large model, 10° AoA, 120 MPH, Shear Layer, slot, individual trial



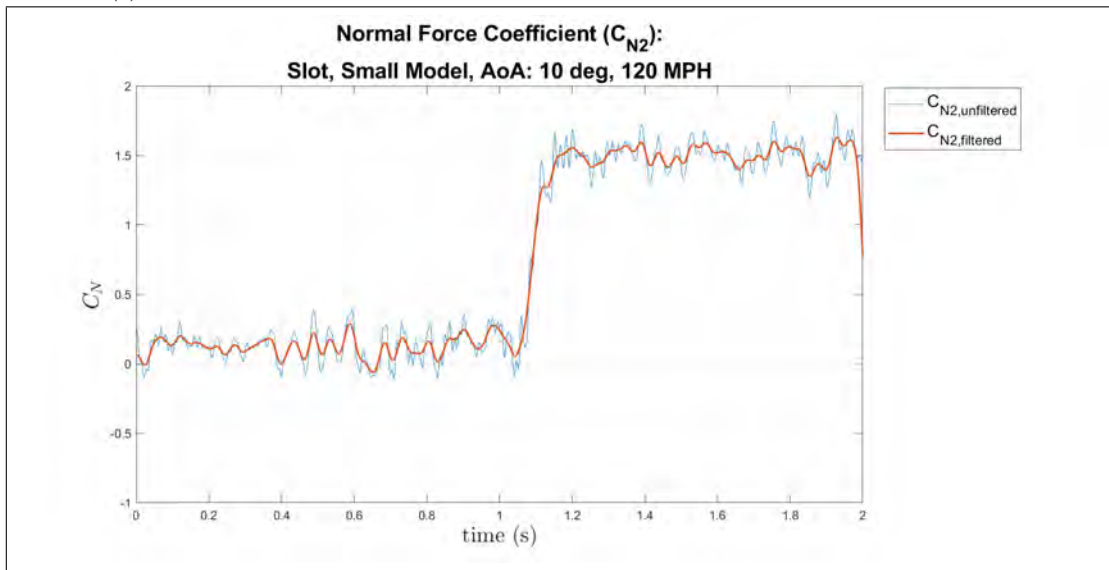
(b) Axial Force Coefficient, large model, 10° AoA, 120 MPH, Out Cavity, slot, individual trial

Figure 212: Large model at 10° AoA of the axial force coefficient, 120 MPH, slot, individual trial

Small Model, Dynamic Release, 10° AoA, 120 MPH

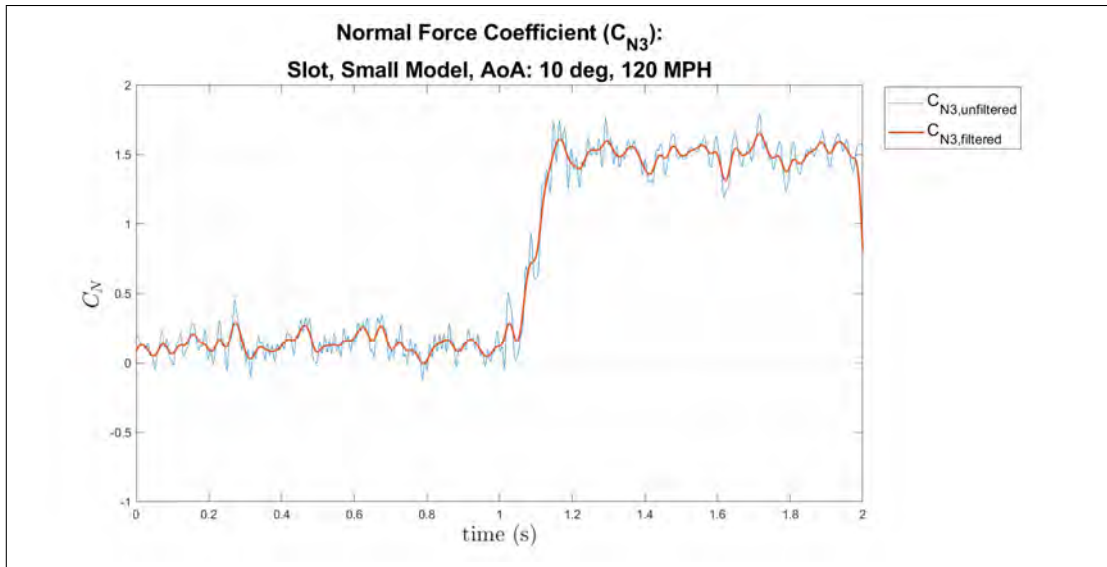


(a) Normal Force Coefficient, small model, 10° AoA, 120 MPH, release one, individual trial

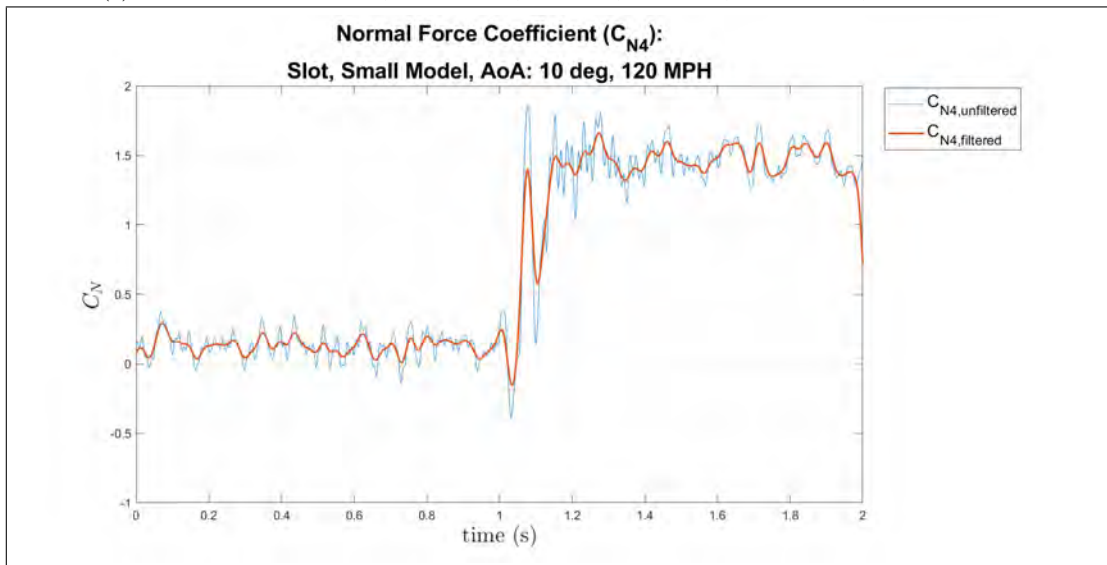


(b) Normal Force Coefficient, small model, 10° AoA, 120 MPH, release two, individual trial

Figure 213: Small model at 10° AoA of the normal force coefficient, release times one and two, 120 MPH, individual trial

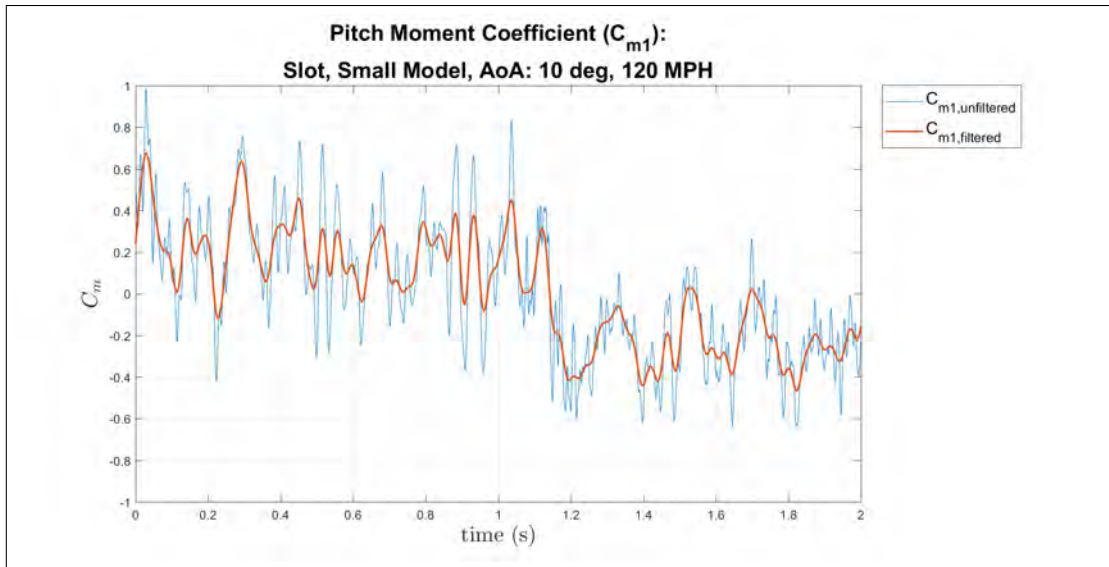


(a) Normal Force Coefficient, small model, 10° AoA, 120 MPH, release three, individual trial

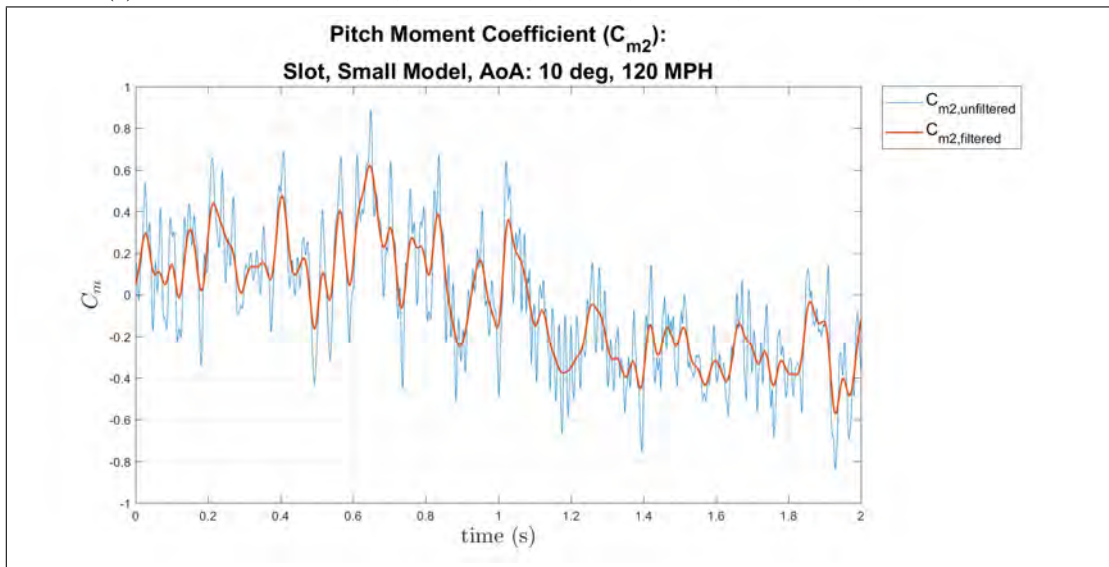


(b) Normal Force Coefficient, small model, 10° AoA, 120 MPH, release four, individual trial

Figure 214: Small model at 10° AoA of the normal force coefficient, release times three and four, 120 MPH, individual trial

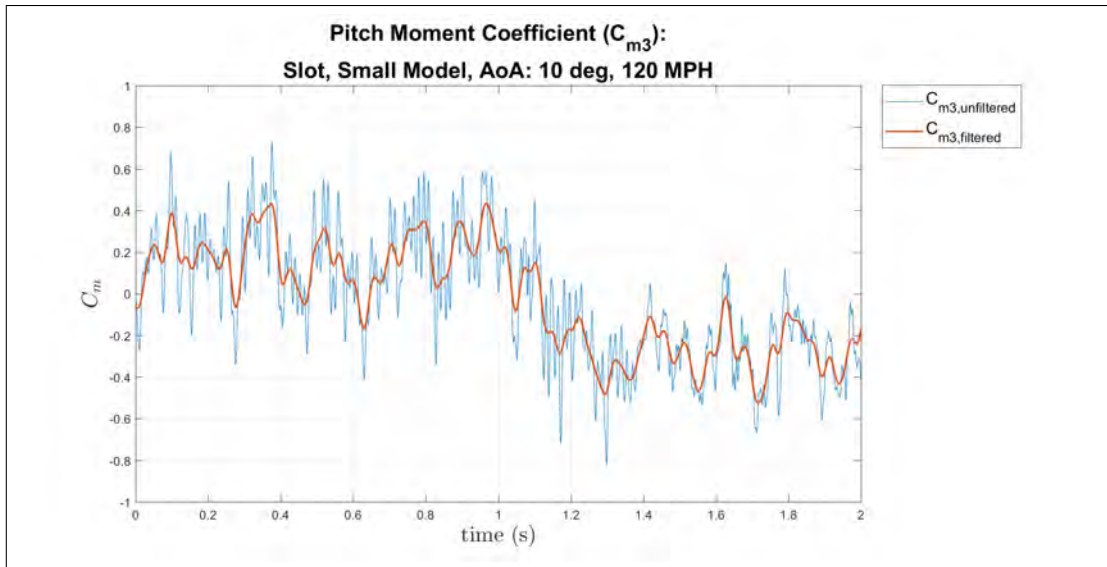


(a) Pitch Moment Coefficient, small model, 10° AoA, 120 MPH, release one, individual trial

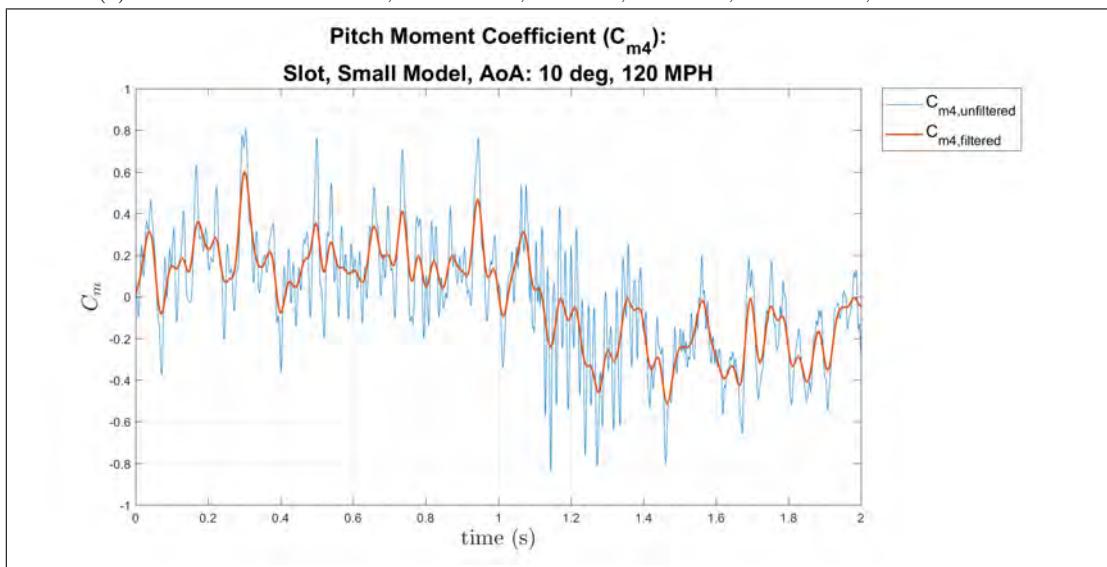


(b) Pitch Moment Coefficient, small model, 10° AoA, 120 MPH, release two, individual trial

Figure 215: Small model at 10° AoA of the pitch moment coefficient, release times one and two, 120 MPH, individual trial

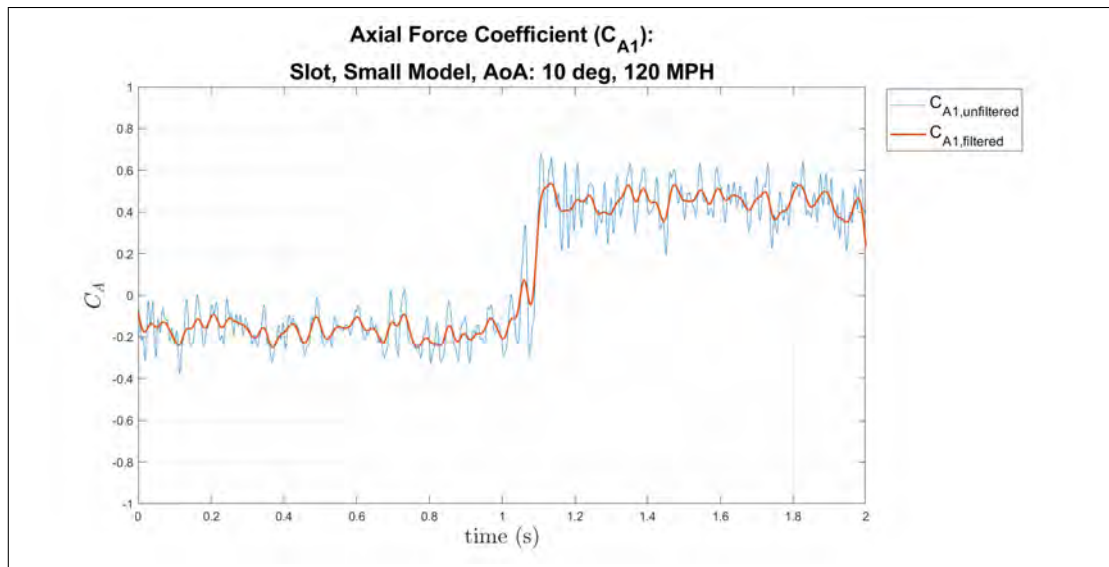


(a) Pitch Moment Coefficient, small model, 10° AoA, 120 MPH, release three, individual trial

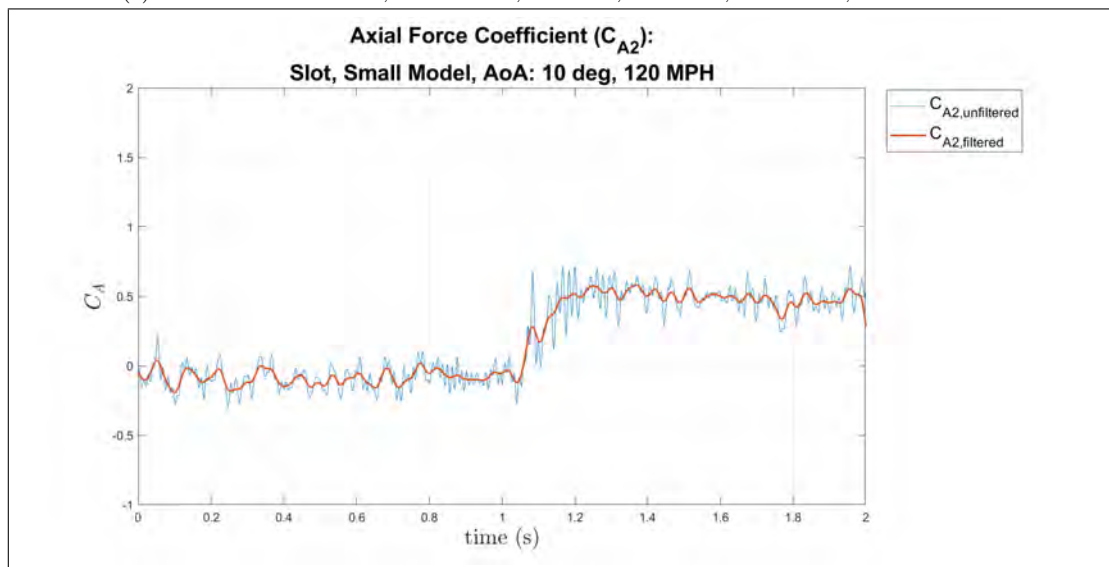


(b) Pitch Moment Coefficient, small model, 10° AoA, 120 MPH, release four, individual trial

Figure 216: Small model at 10° AoA of the pitch moment coefficient, release times three and four, 120 MPH, individual trial

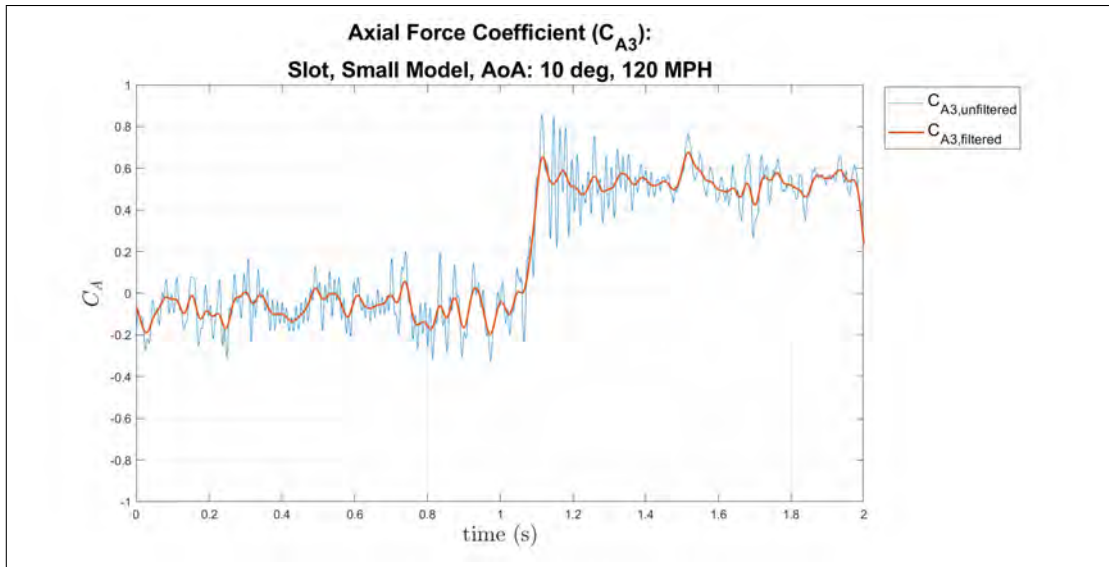


(a) Axial Force Coefficient, small model, 10° AoA, 120 MPH, release one, individual trial

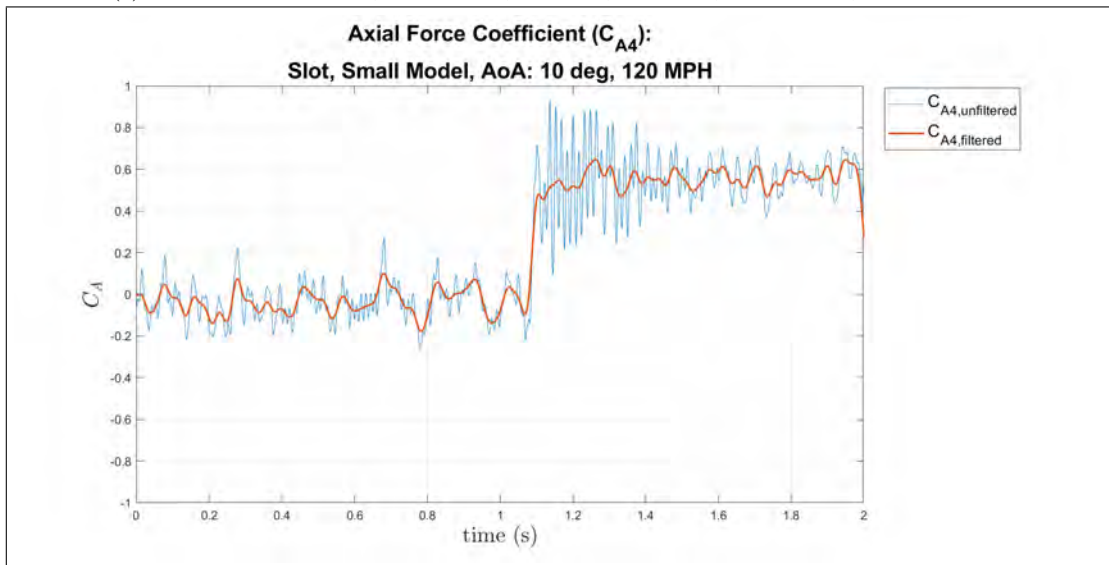


(b) Axial Force Coefficient, small model, 10° AoA, 120 MPH, release two, individual trial

Figure 217: Small model at 10° AoA of the axial force coefficient, release times one and two, 120 MPH, individual trial



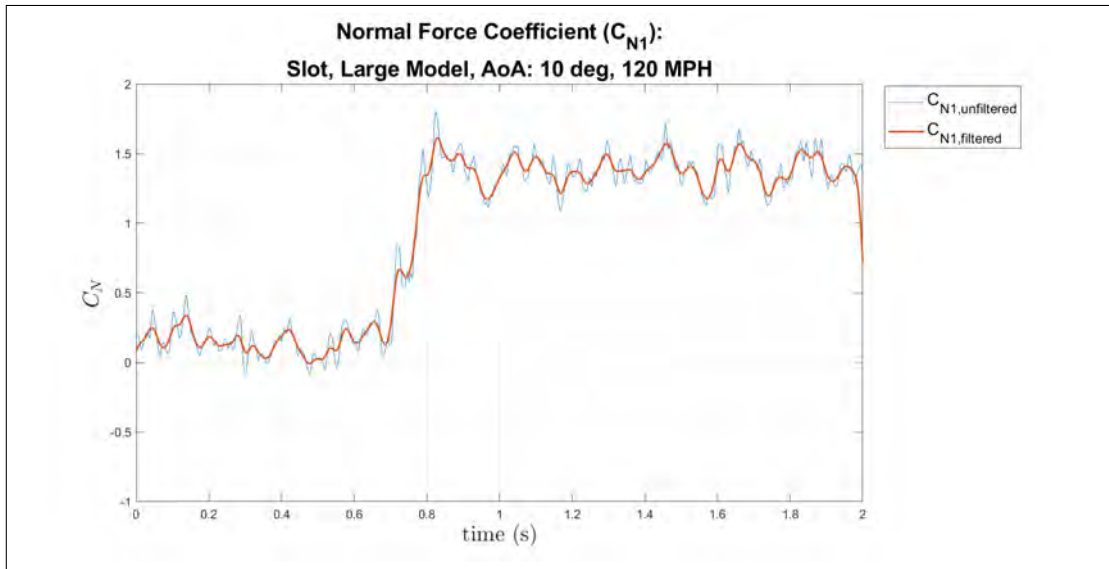
(a) Axial Force Coefficient, small model, 10° AoA, 120 MPH, release three, individual trial



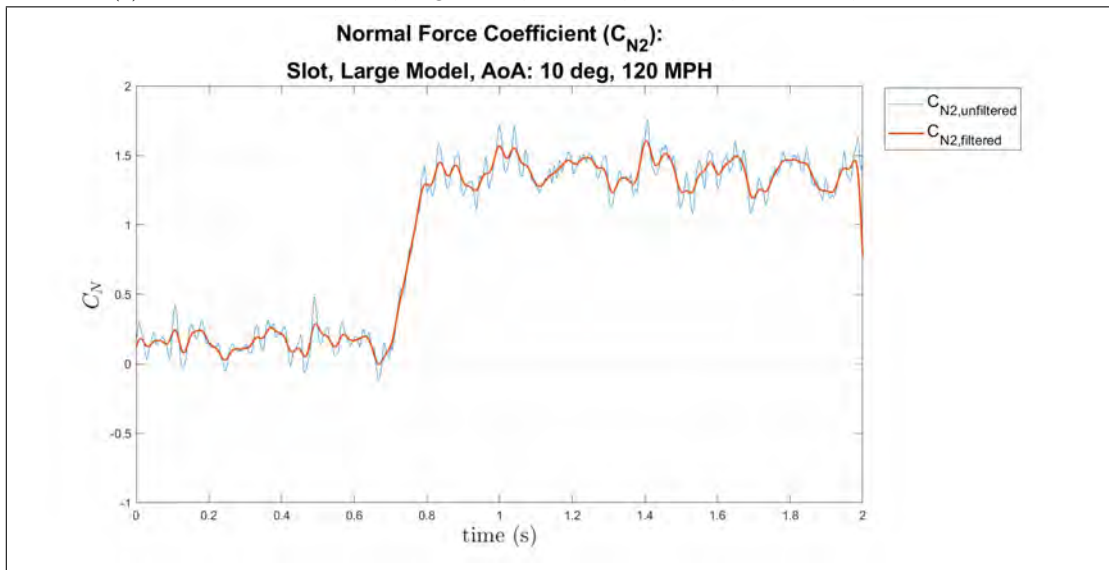
(b) Axial Force Coefficient, small model, 10° AoA, 120 MPH, release four, individual trial

Figure 218: Small model at 10° AoA of the axial force coefficient, release times three and four, 120 MPH, individual trial

Large Model, Dynamic Release, 10° AoA, 120 MPH

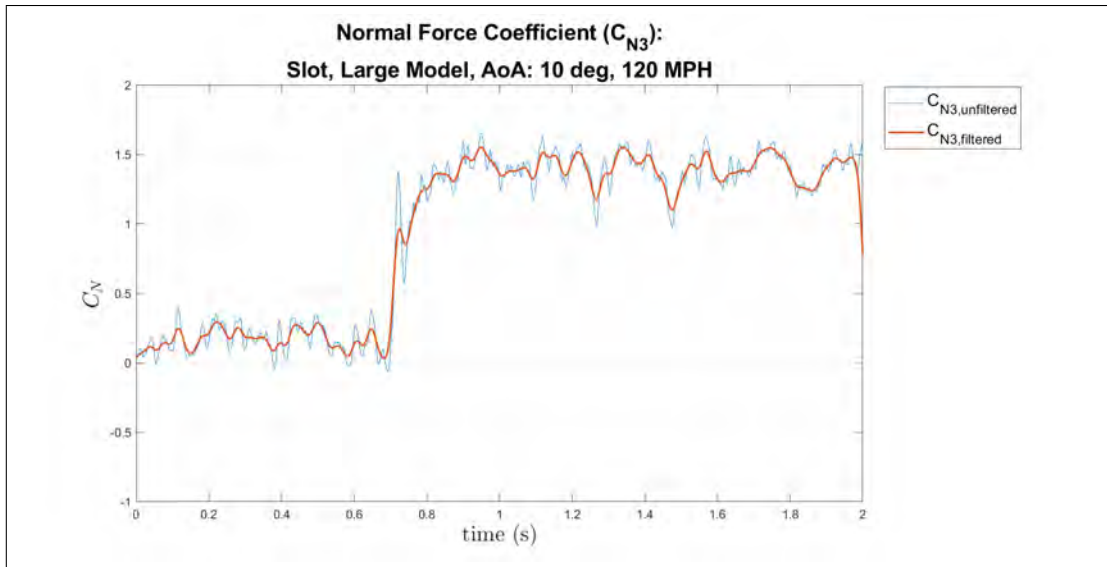


(a) Normal Force Coefficient, large model, 10° AoA, 120 MPH, release one, individual trial

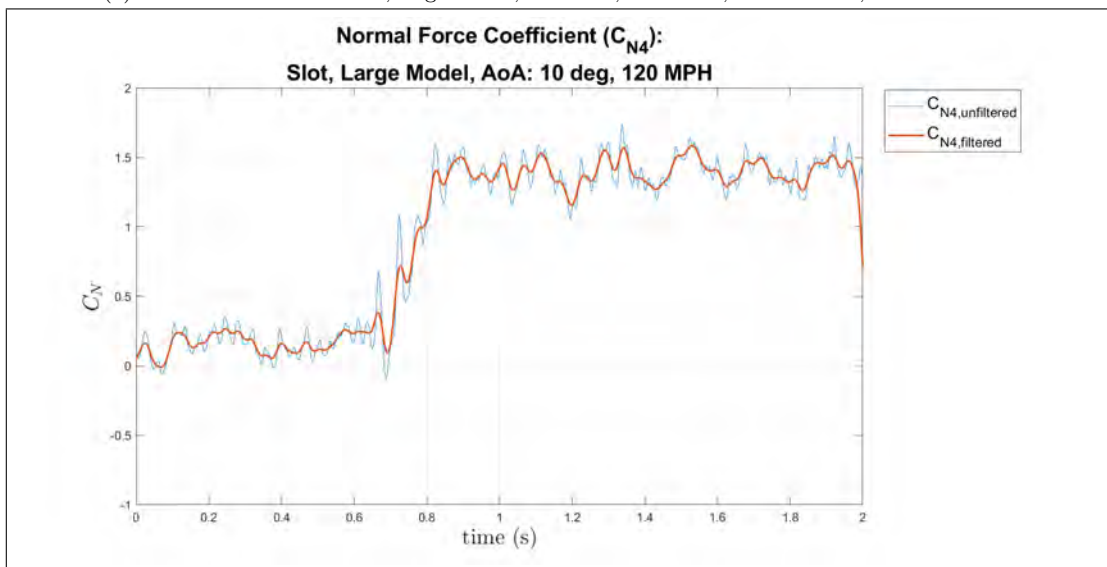


(b) Normal Force Coefficient, large model, 10° AoA, 120 MPH, release two, individual trial

Figure 219: Large model at 10° AoA of the normal force coefficient, release times one and two, 120 MPH, individual trial

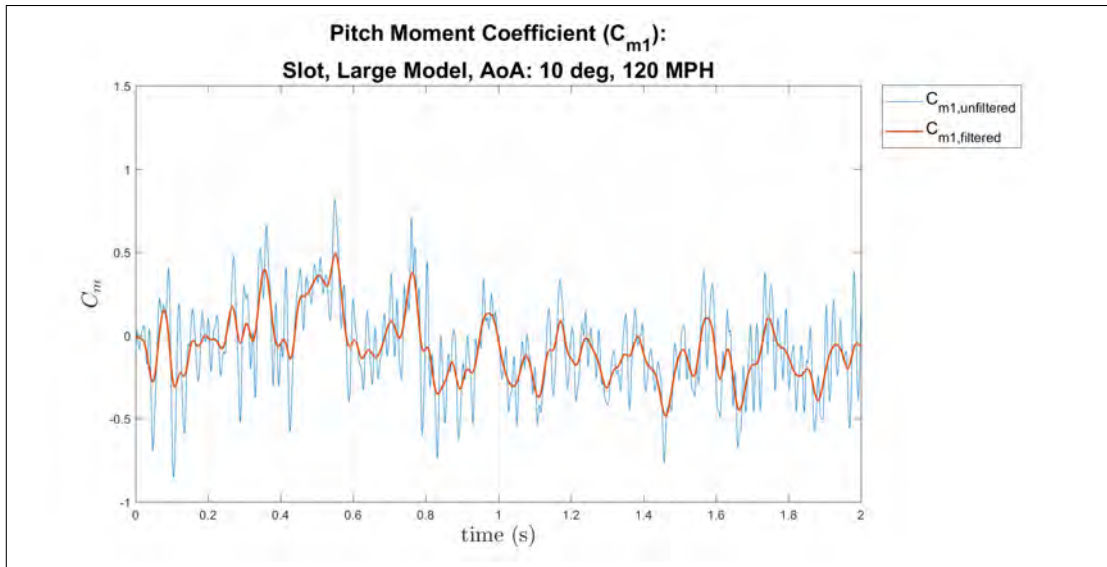


(a) Normal Force Coefficient, large model, 10° AoA, 120 MPH, release three, individual trial

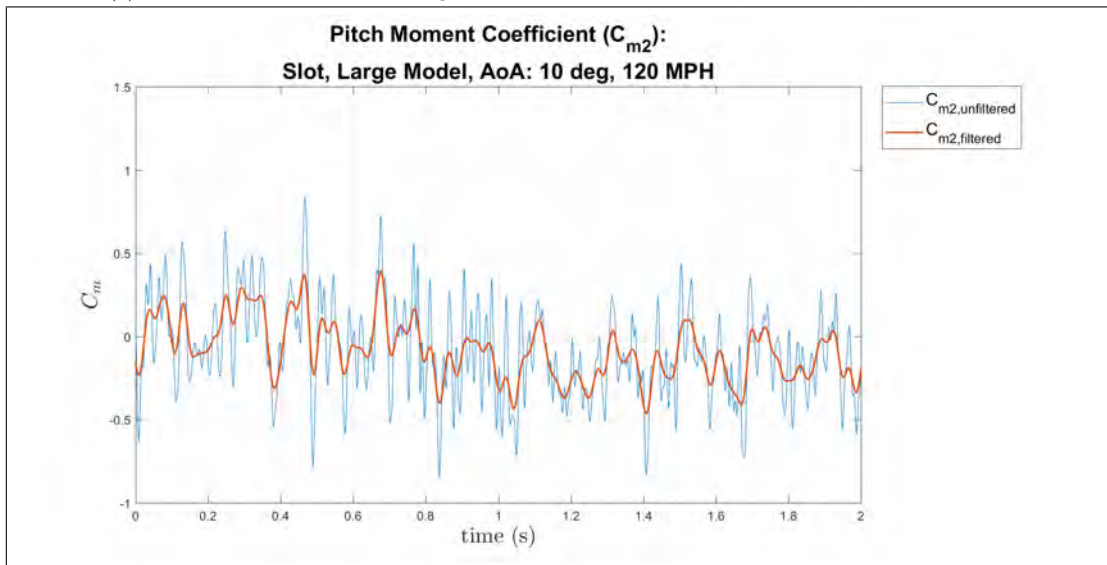


(b) Normal Force Coefficient, large model, 10° AoA, 120 MPH, release four, individual trial

Figure 220: Large model at 10° AoA of the normal force coefficient, release times three and four, 120 MPH, individual trial

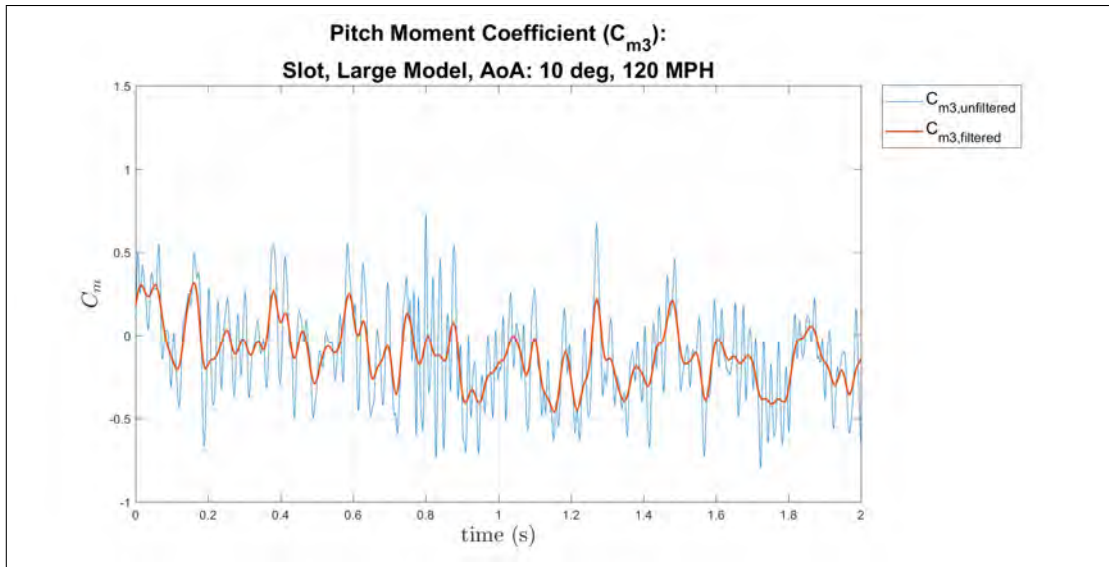


(a) Pitch Moment Coefficient, large model, 10° AoA, 120 MPH, release one, individual trial

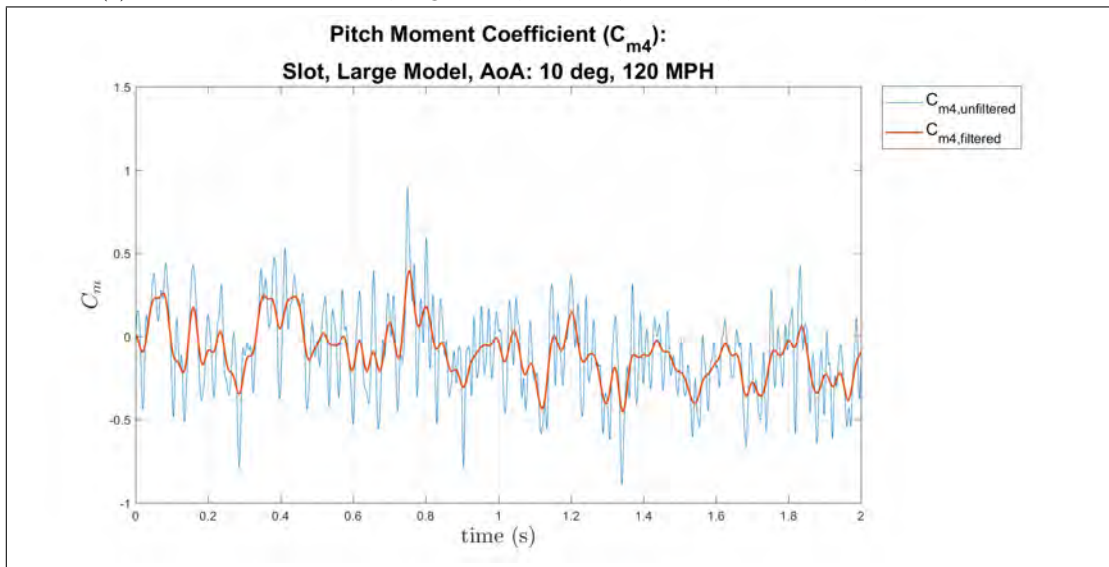


(b) Pitch Moment Coefficient, large model, 10° AoA, 120 MPH, release two, individual trial

Figure 221: Large model at 10° AoA of the pitch moment coefficient, release times one and two, 120 MPH, individual trial

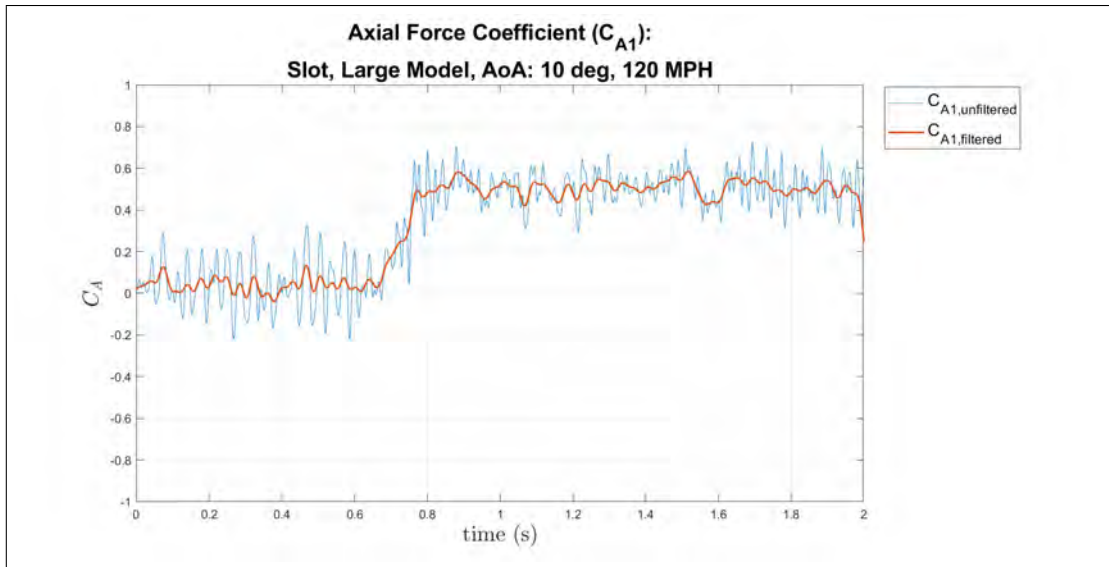


(a) Pitch Moment Coefficient, large model, 10° AoA, 120 MPH, release three, individual trial

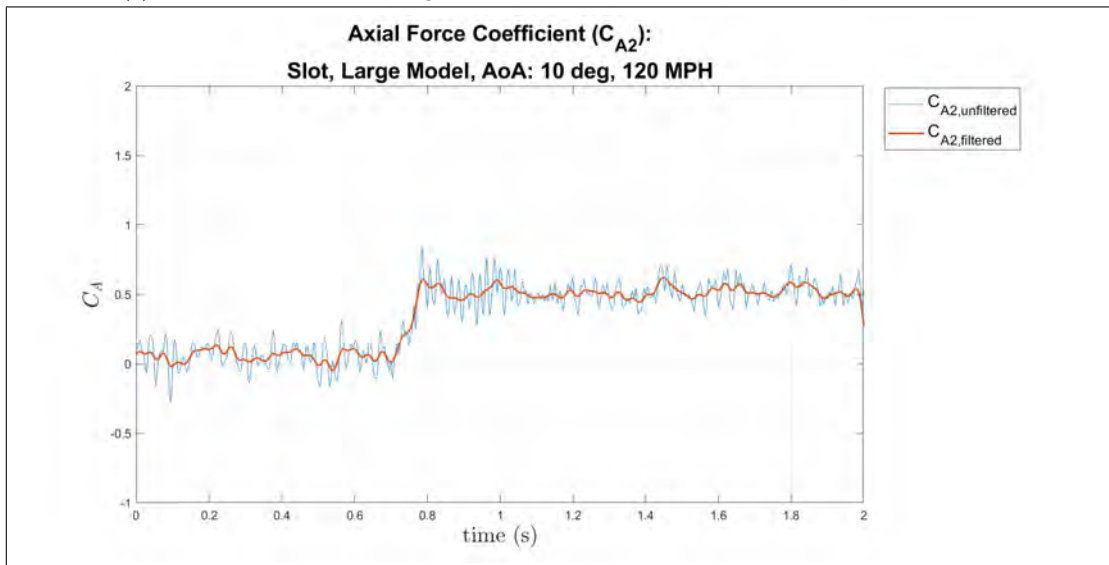


(b) Pitch Moment Coefficient, large model, 10° AoA, 120 MPH, release four, individual trial

Figure 222: Large model at 10° AoA of the pitch moment coefficient, release times three and four, 120 MPH, individual trial

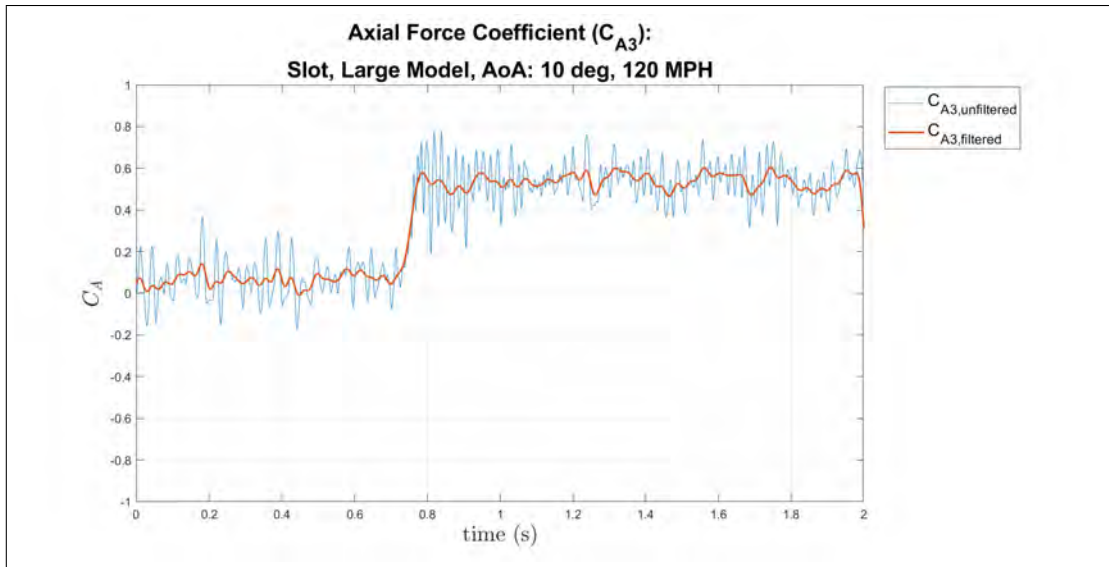


(a) Axial Force Coefficient, large model, 10° AoA, 120 MPH, release one, individual trial

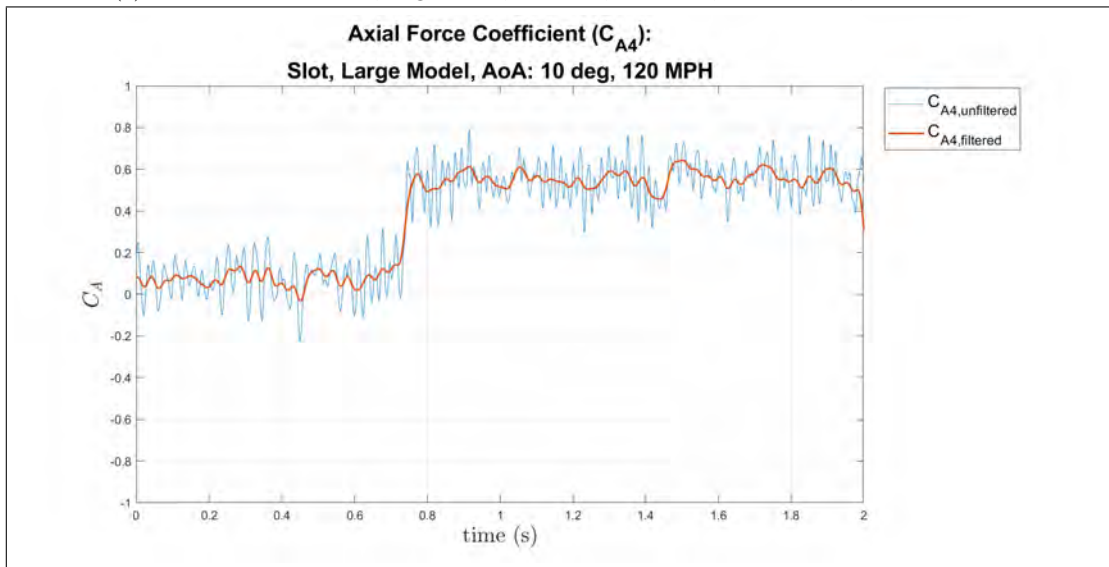


(b) Axial Force Coefficient, large model, 10° AoA, 120 MPH, release two, individual trial

Figure 223: Large model at 10° AoA of the axial force coefficient, release times one and two, 120 MPH, individual trial



(a) Axial Force Coefficient, large model, 10° AoA, 120 MPH, release three, individual trial

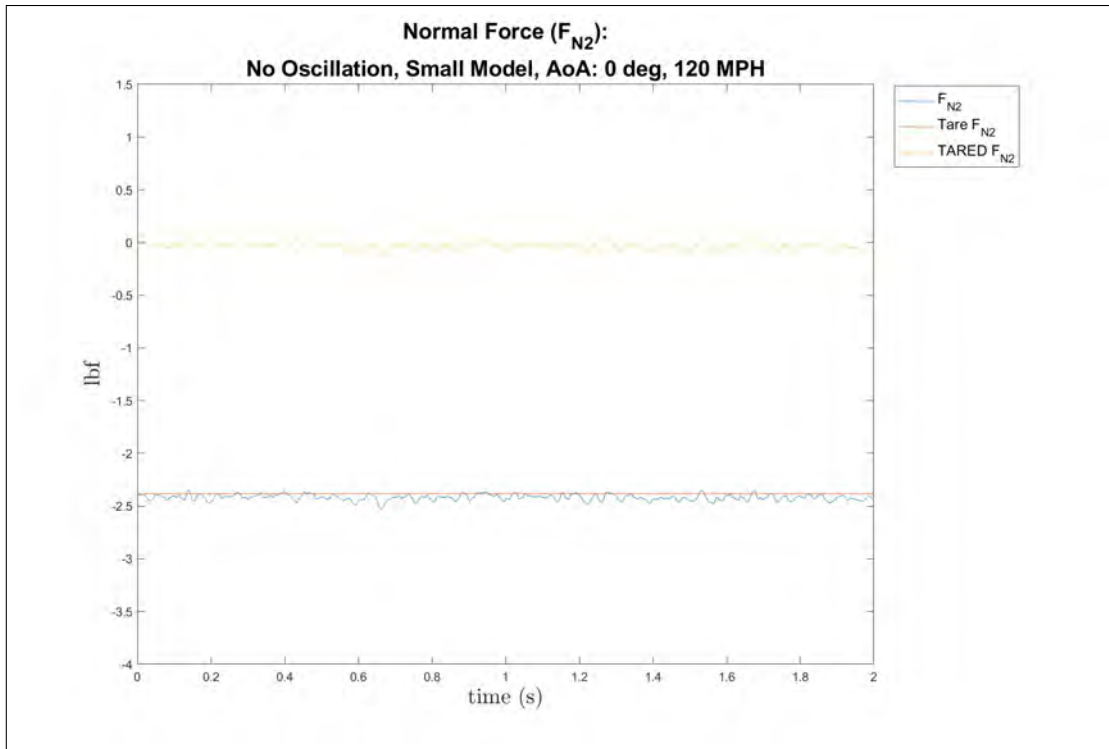


(b) Axial Force Coefficient, large model, 10° AoA, 120 MPH, release four, individual trial

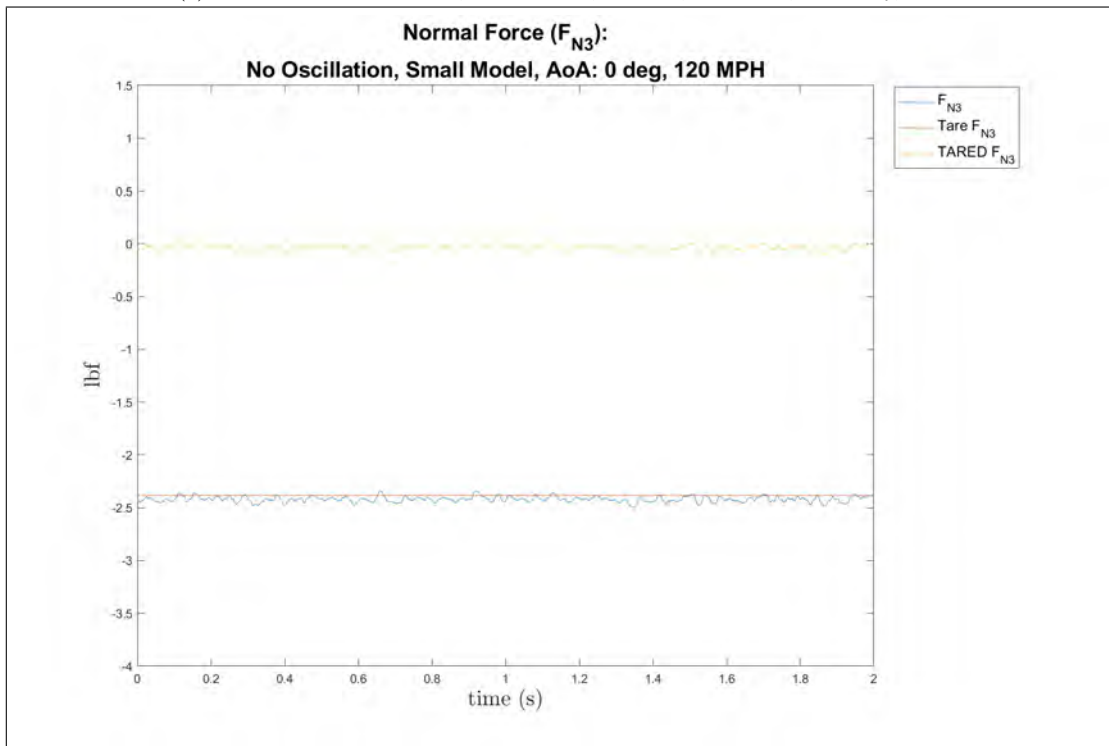
Figure 224: Large model at 10° AoA of the axial force coefficient, release times three and four, 120 MPH, individual trial

Tare Examples 0 Degrees

Small Model, Cavity Apparatus, 0° AoA, 120 MPH

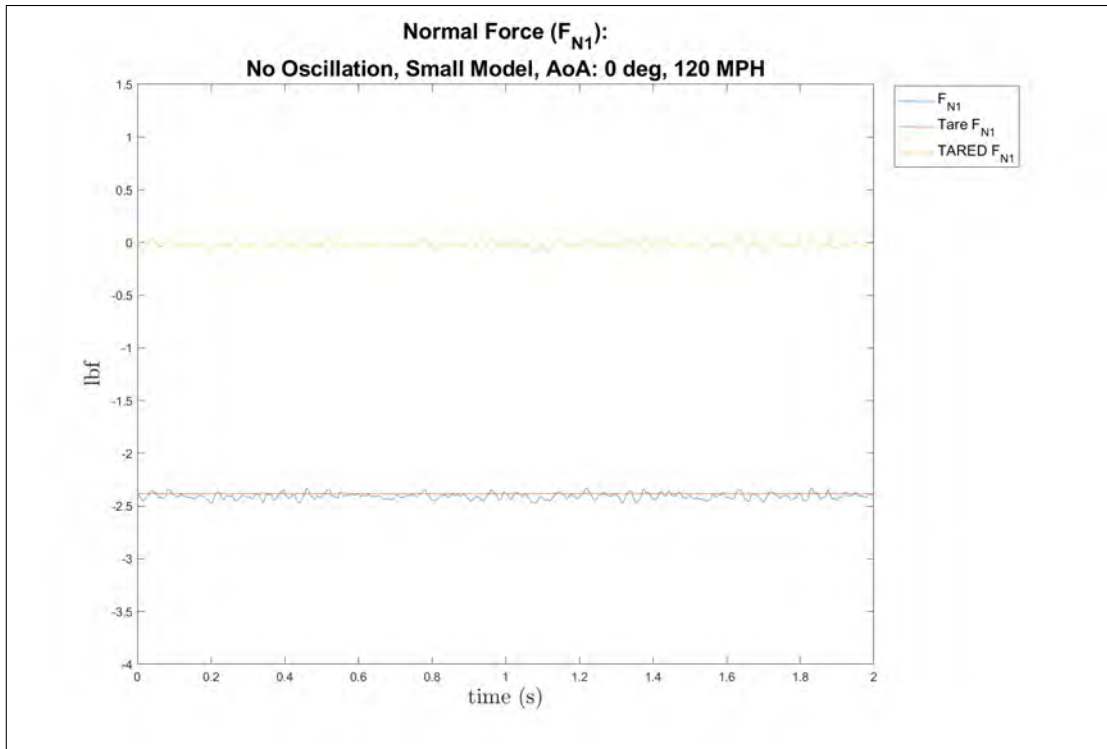


(a) Normal Force Coefficient, small model, 0° AoA, 120 MPH, In Cavity, tare

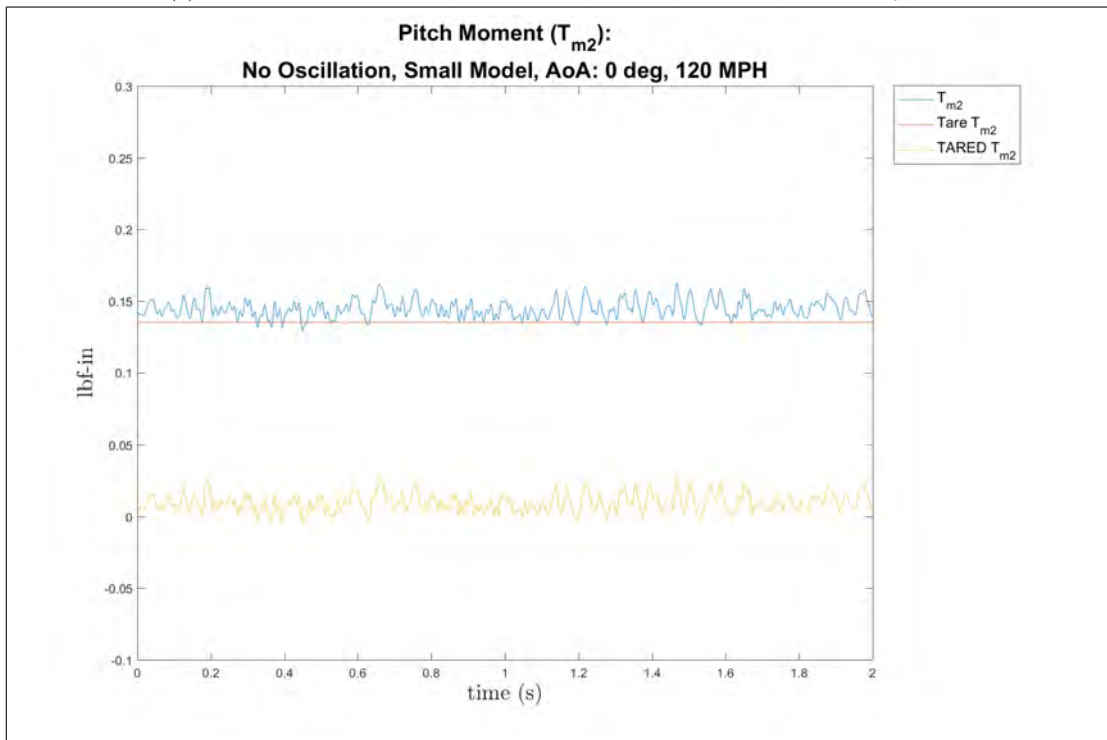


(b) Normal Force Coefficient, small model, 0° AoA, 120 MPH, Shear Layer, tare

Figure 225: Small model at 0° AoA of the normal force coefficient, 120 MPH, tare

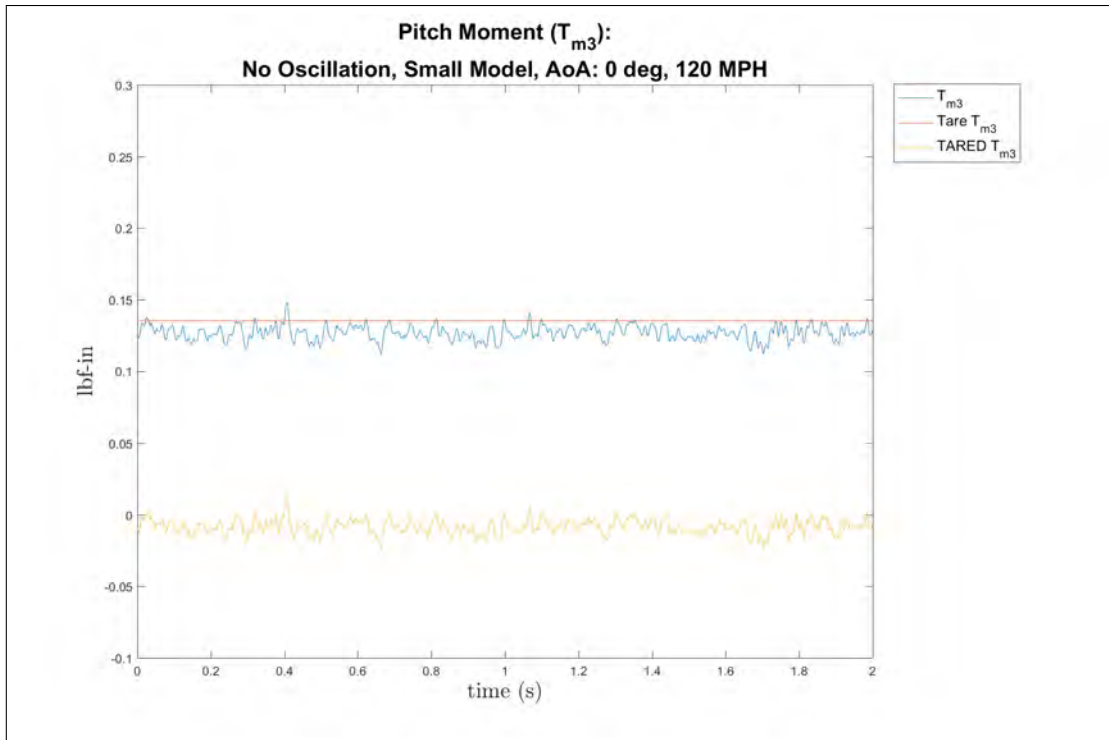


(a) Normal Force Coefficient, small model, 0° AoA, 120 MPH, Out Cavity, tare

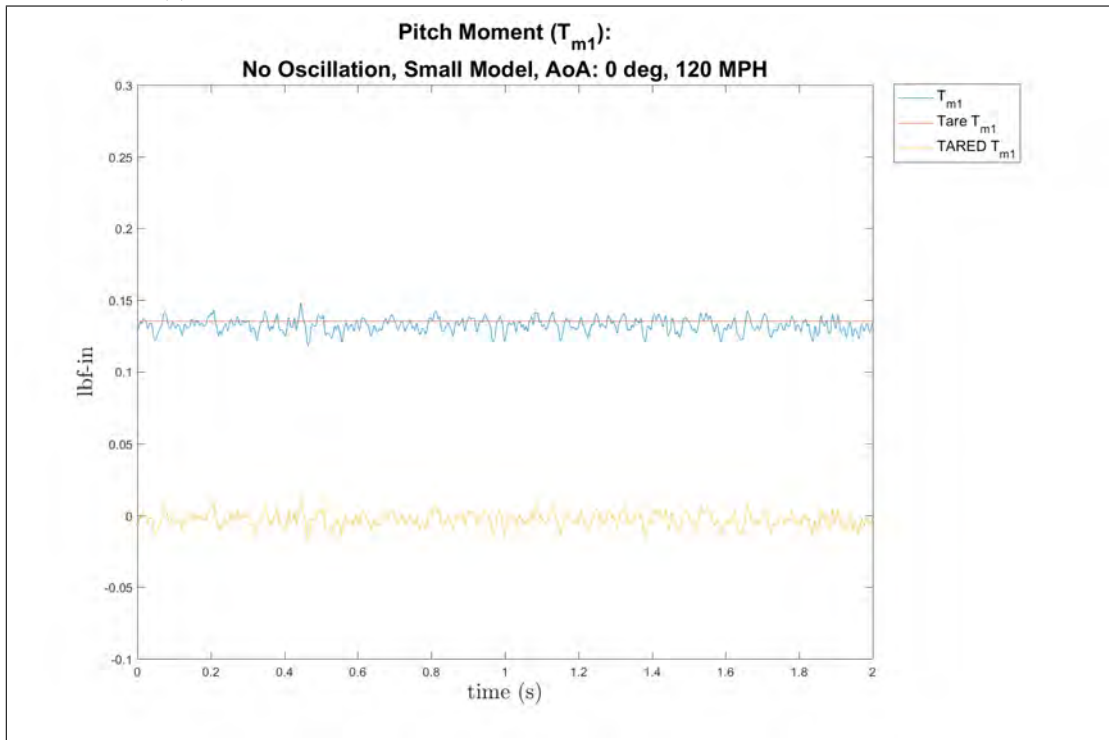


(b) Pitch Moment Coefficient, small model, 0° AoA, 120 MPH, In Cavity, tare

Figure 226: Small model at 0° AoA of the pitch moment and normal force coefficients, 120 MPH, tare

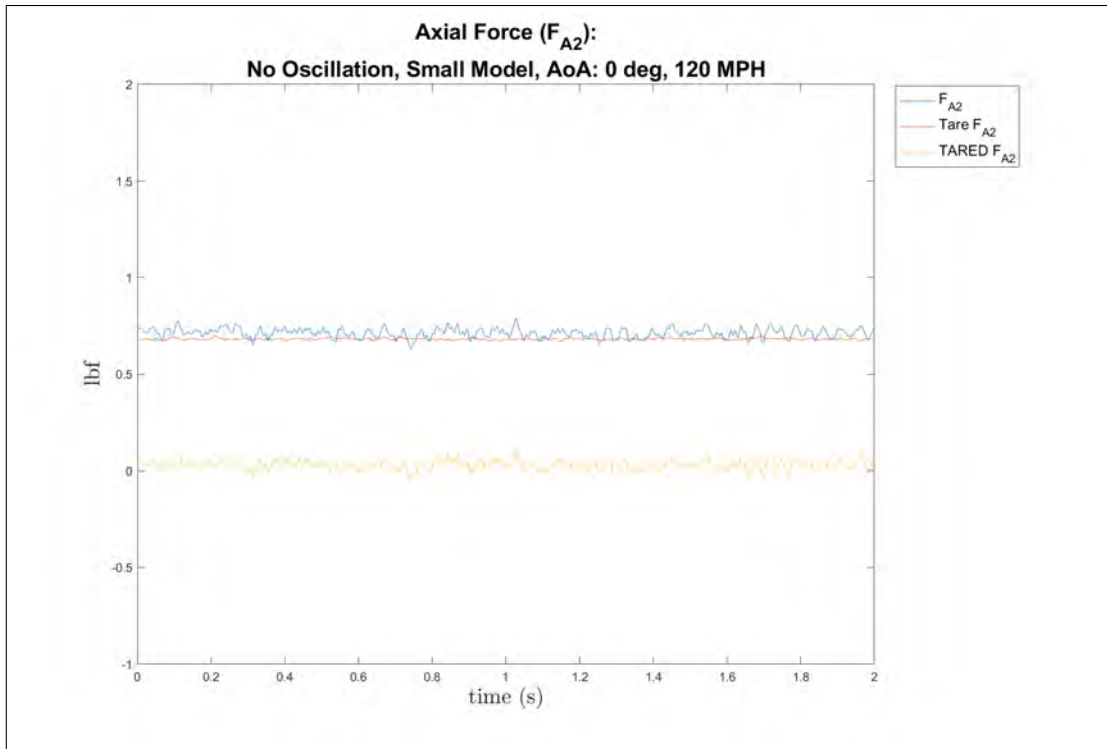


(a) Pitch Moment Coefficient, small model, 0° AoA, 120 MPH, Shear Layer, tare

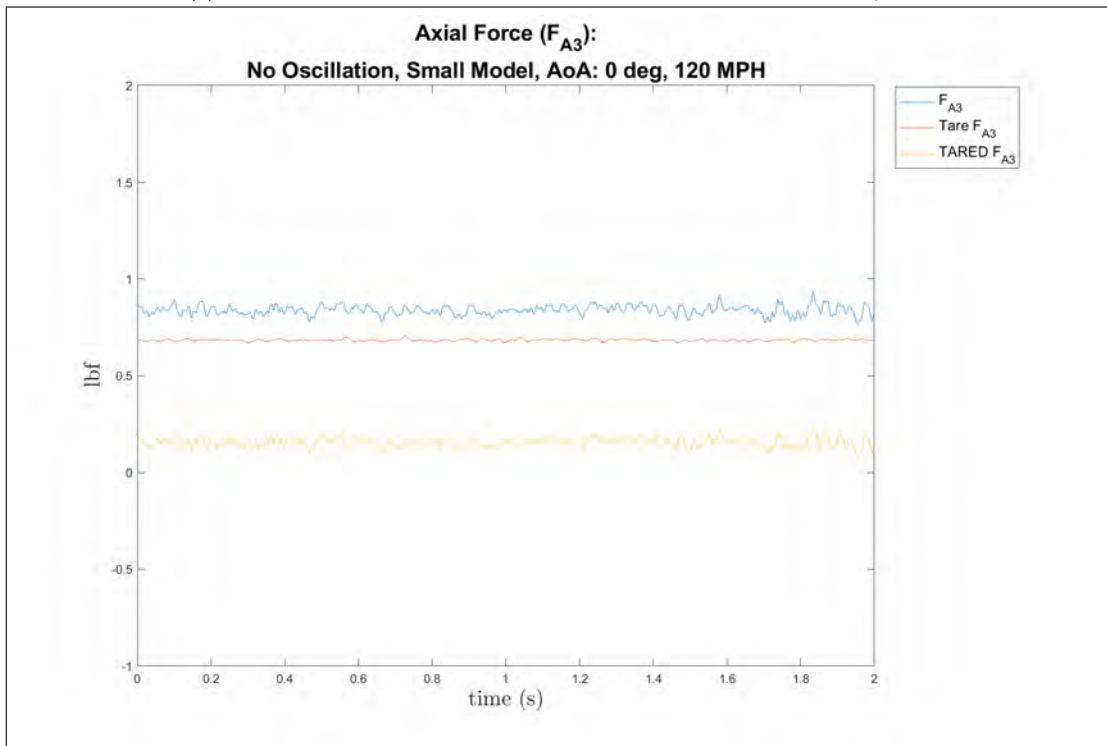


(b) Pitch Moment Coefficient, small model, 0° AoA, 120 MPH, Out Cavity, tare

Figure 227: Small model at 0° AoA of the pitch moment coefficient, 120 MPH, tare

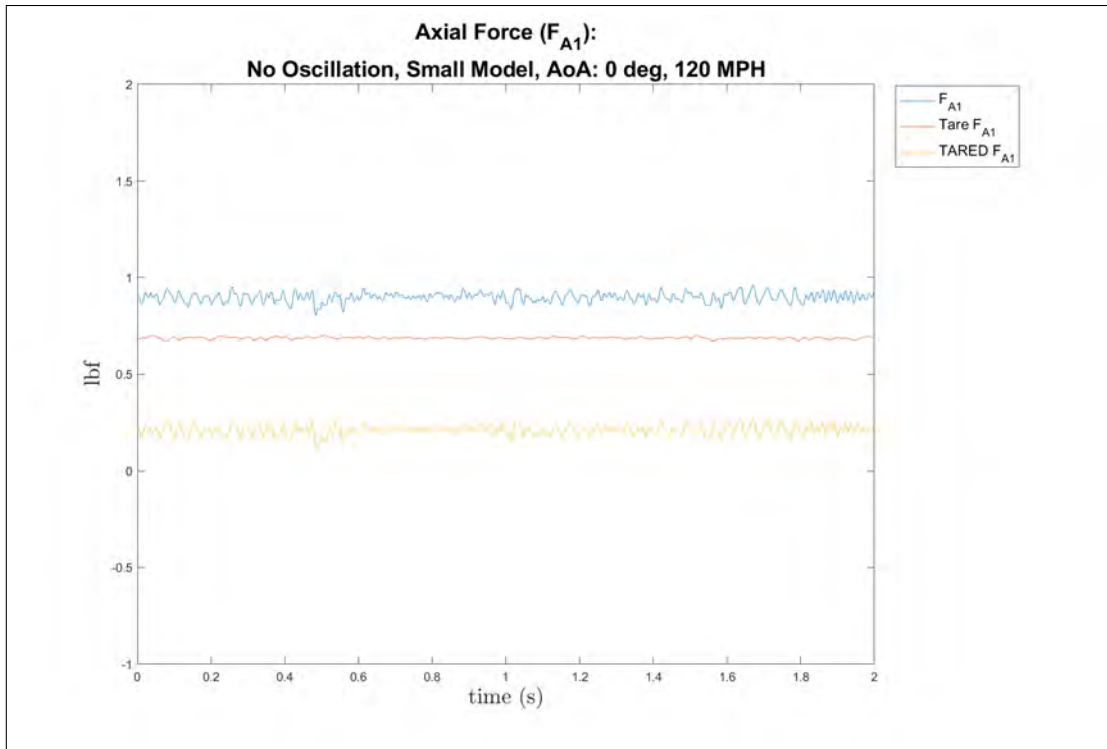


(a) Axial Force Coefficient, small model, 0° AoA, 120 MPH, In Cavity, tare

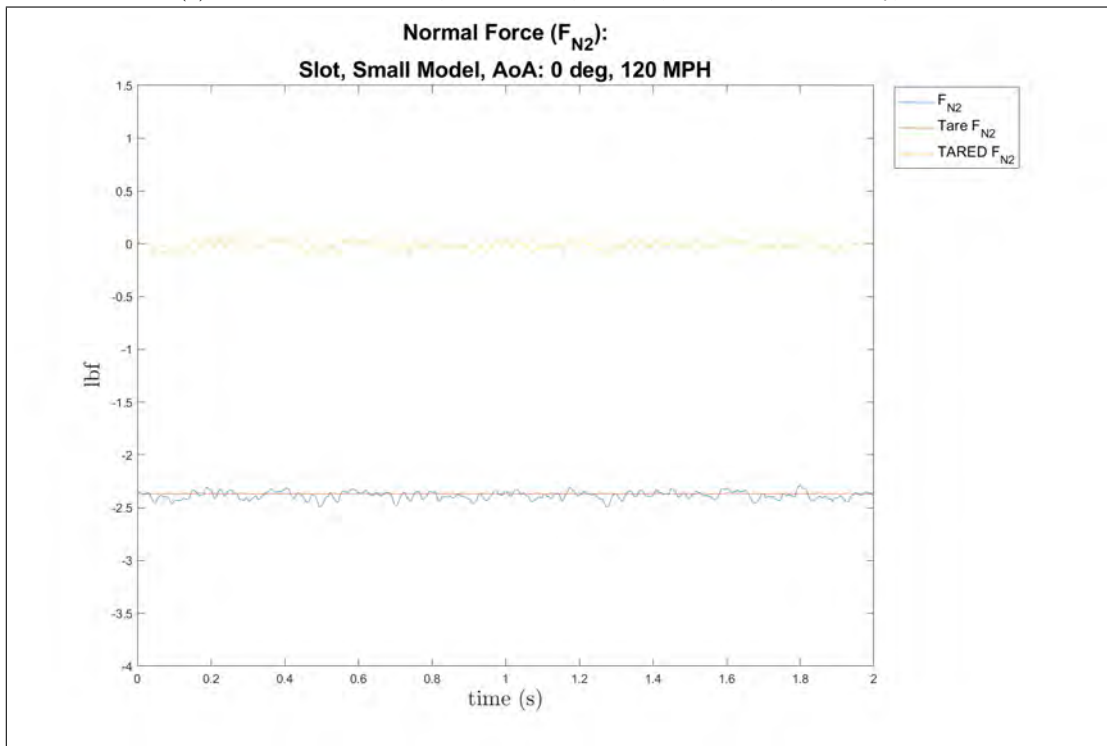


(b) Axial Force Coefficient, small model, 0° AoA, 120 MPH, Shear Layer, tare

Figure 228: Small model at 0° AoA of the Axial Force coefficient, 120 MPH, tare

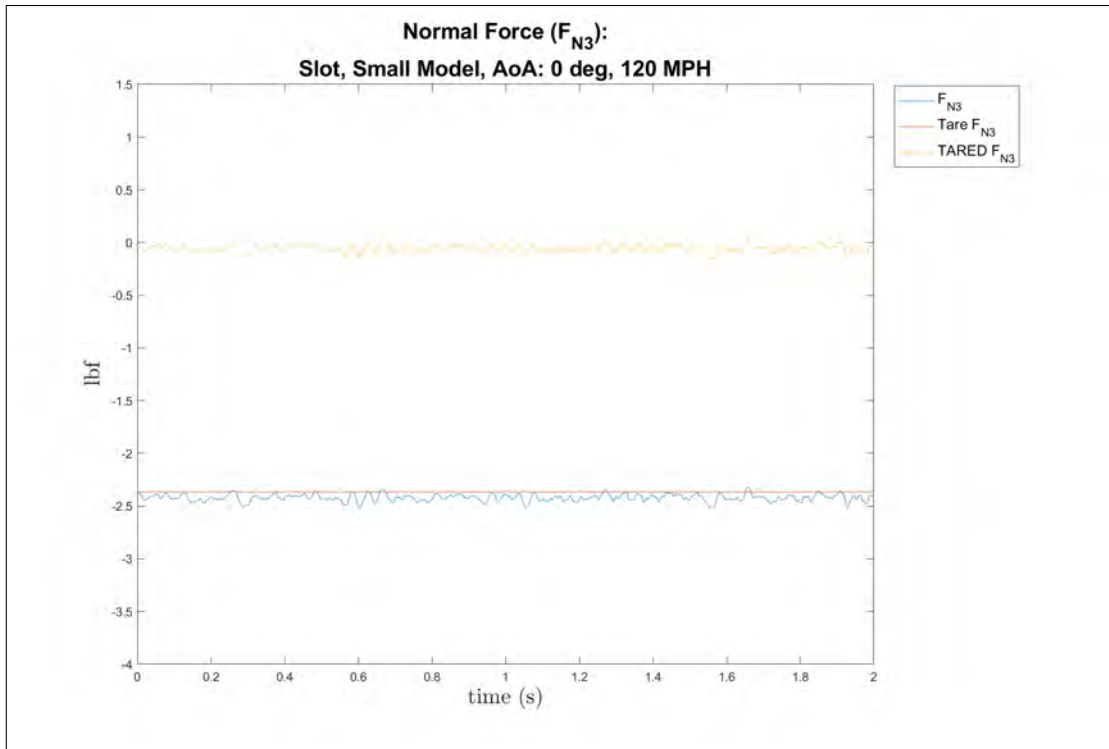


(a) Axial Force Coefficient, small model, 0° AoA, 120 MPH, Out Cavity, tare

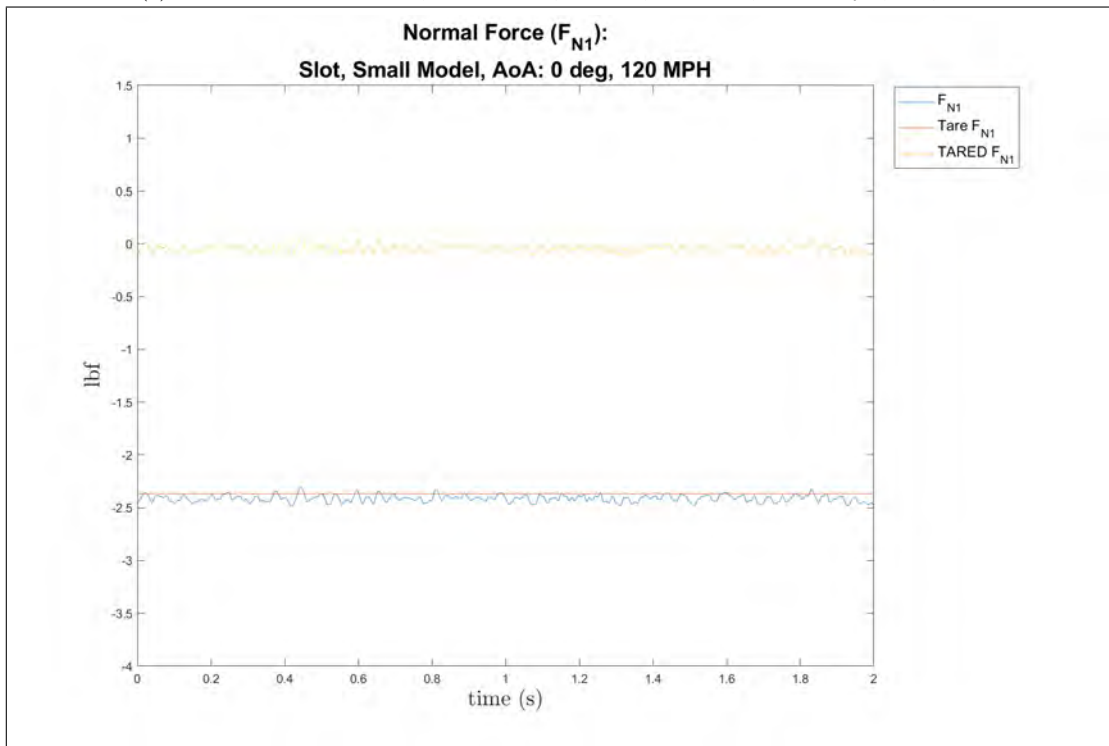


(b) Noormal Force Coefficient, small model, 0° AoA, 120 MPH, In Cavity, slot, tare

Figure 229: Small model at 0° AoA of the axial force and normal force coefficients, 120 MPH, tare

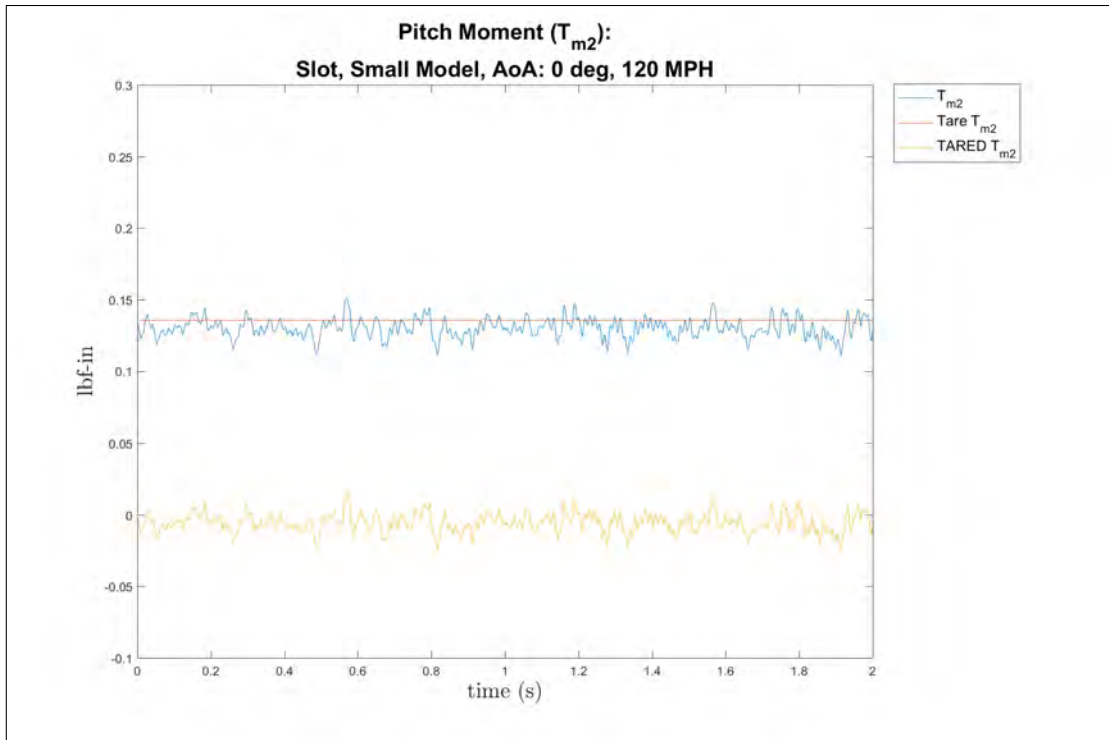


(a) Normal Force Coefficient, small model, 0° AoA, 120 MPH, Shear Layer, slot, tare

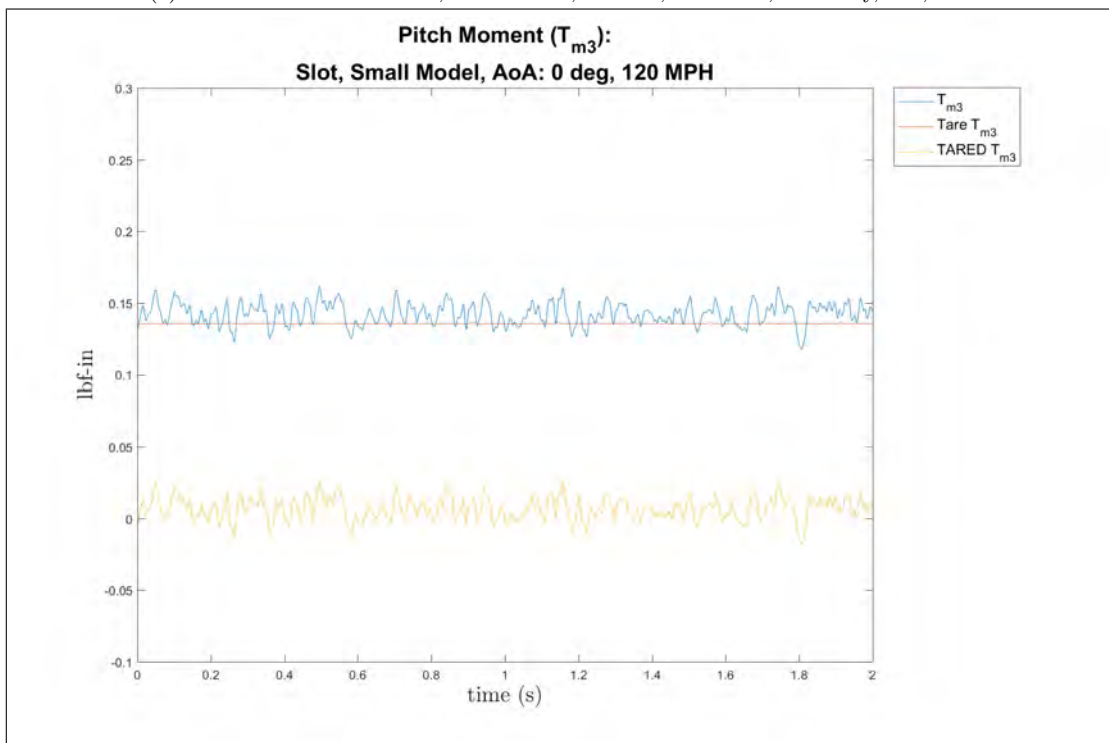


(b) Normal Force Coefficient, small model, 0° AoA, 120 MPH, Out Cavity, slot, tare

Figure 230: Small model at 0° AoA of the normal force coefficient, 120 MPH, slot, tare

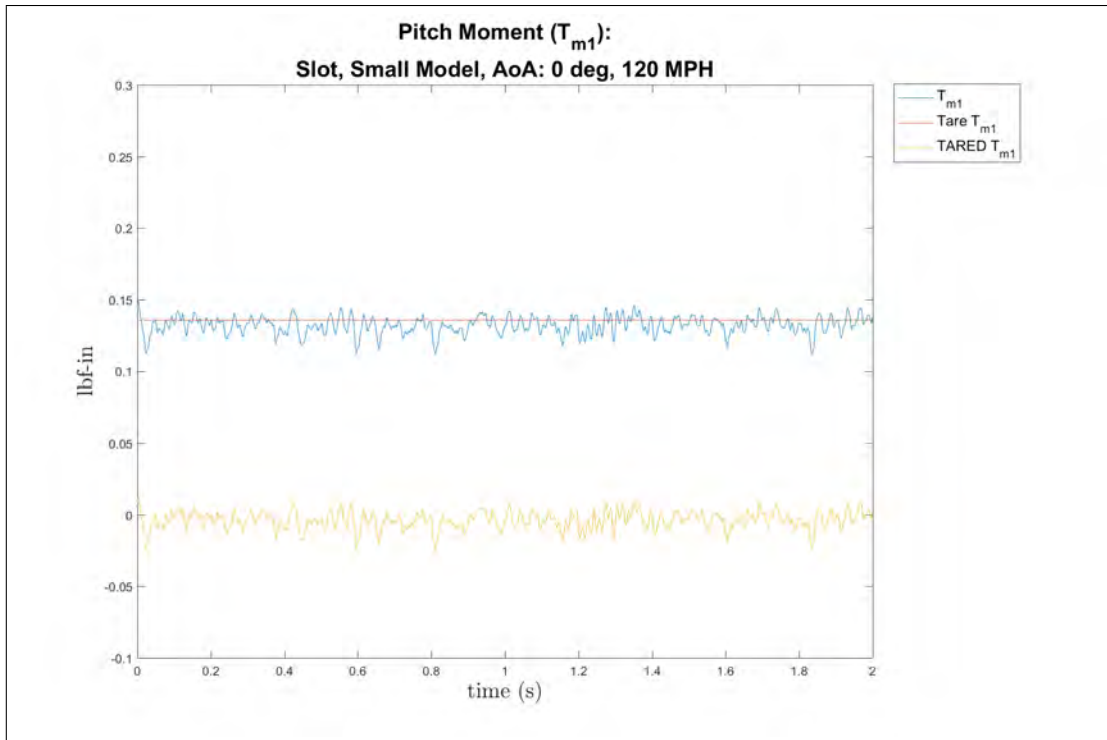


(a) Pitch Moment Coefficient, small model, 0° AoA, 120 MPH, In Cavity, slot, tare

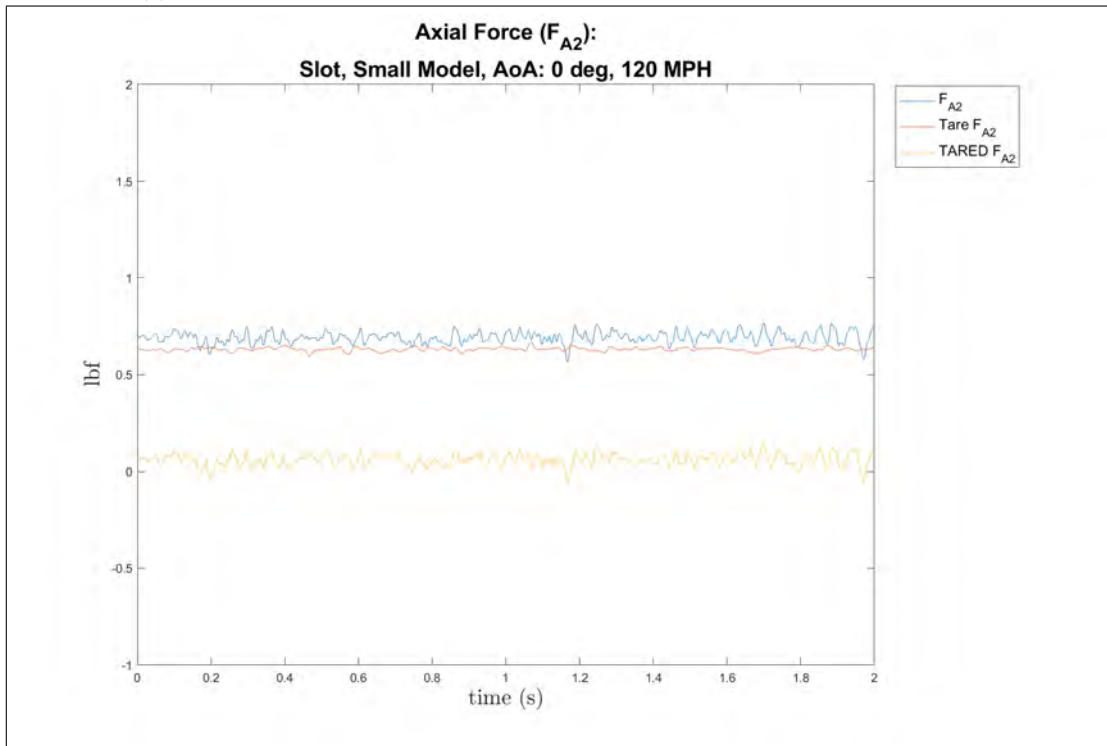


(b) Pitch Moment Coefficient, small model, 0° AoA, 120 MPH, Shear Layer, slot, tare

Figure 231: Small model at 0° AoA of the pitch moment coefficient, 120 MPH, slot, tare

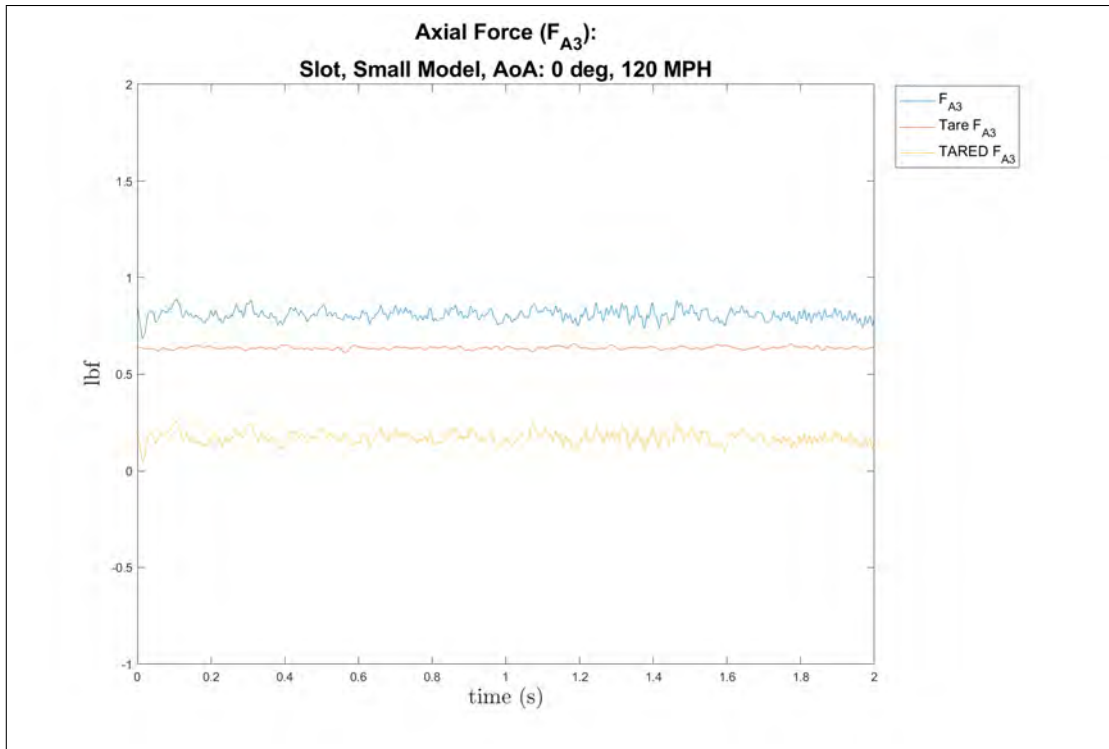


(a) Pitch Moment Coefficient, small model, 0° AoA, 120 MPH, Out Cavity, slot, tare

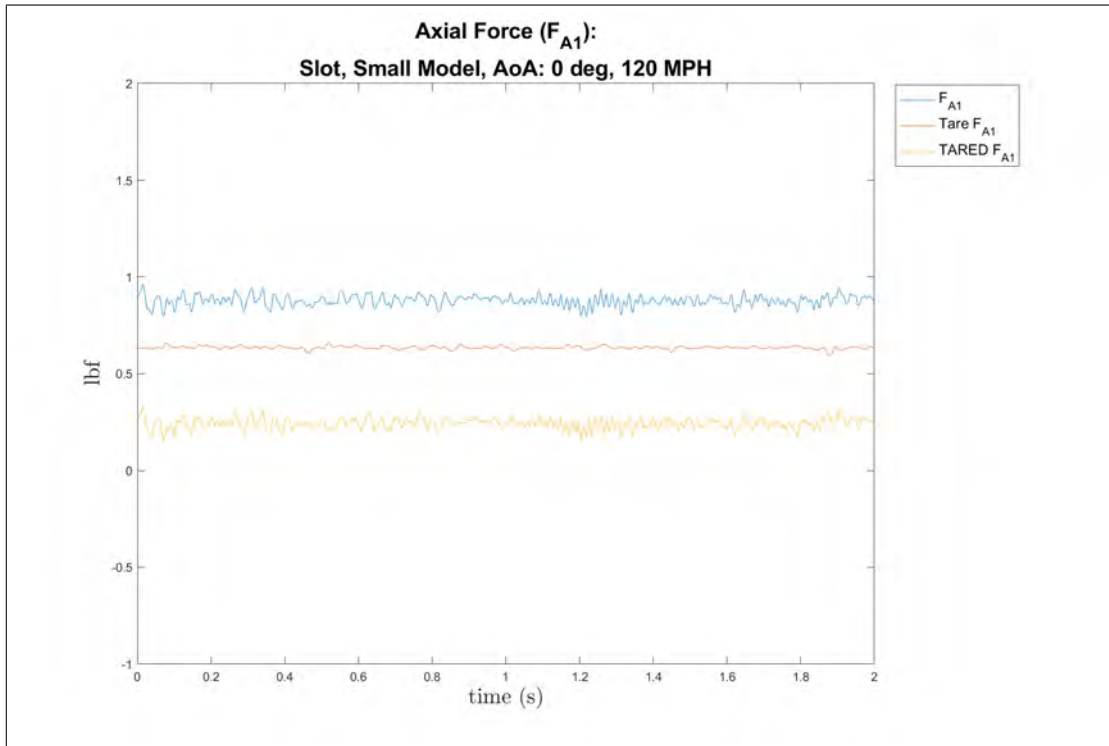


(b) Axial Force Coefficient, small model, 0° AoA, 120 MPH, In Cavity, slot, tare

Figure 232: Small model at 0° AoA of the pitch moment and axial force coefficients, 120 MPH, slot, tare



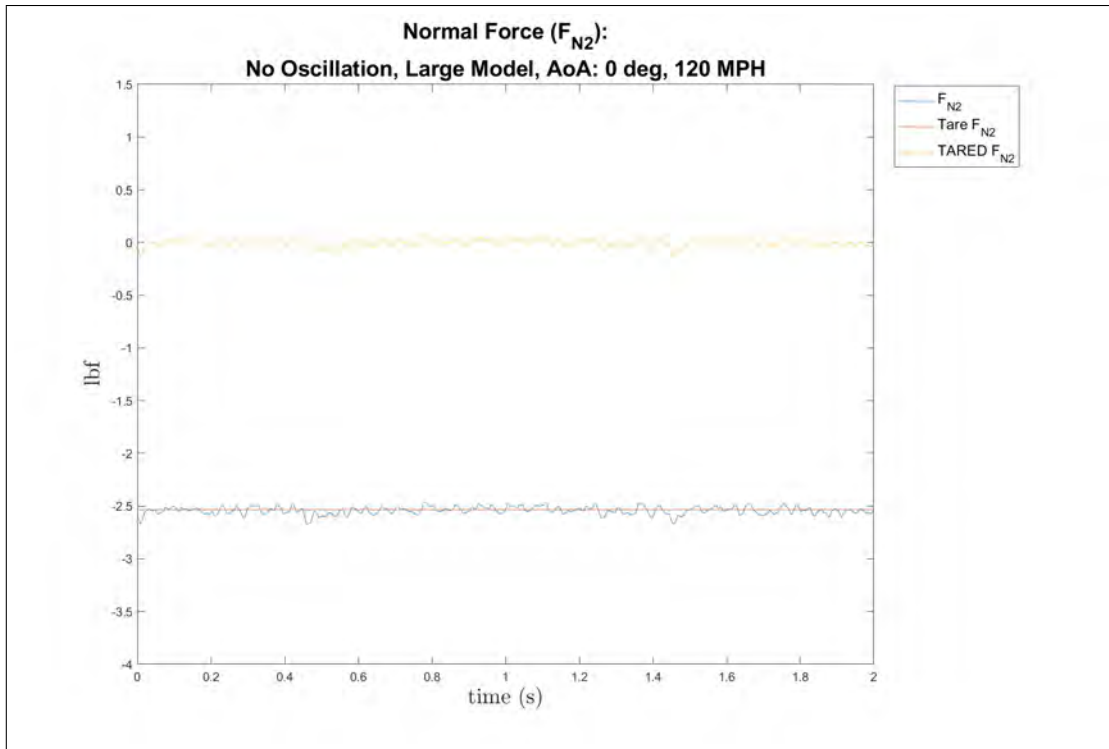
(a) Axial Force Coefficient, small model, 0° AoA, 120 MPH, Shear Layer, slot, tare



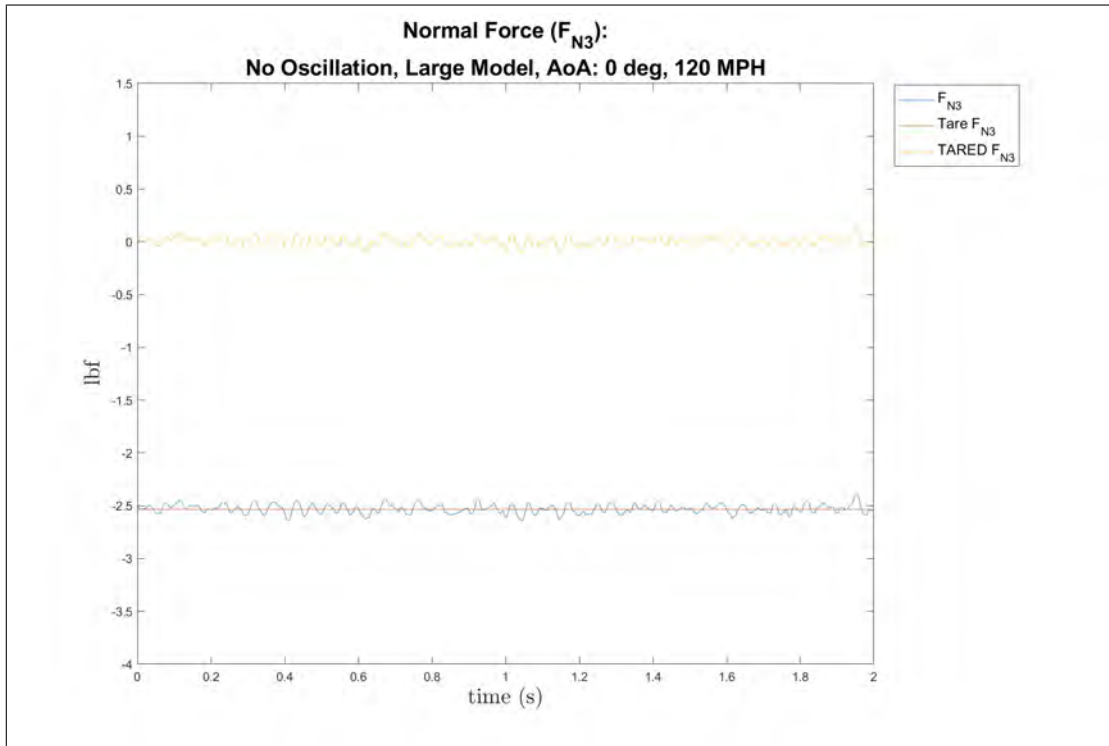
(b) Axial Force Coefficient, small model, 0° AoA, 120 MPH, Out Cavity, slot, tare

Figure 233: Small model at 0° AoA of the axial force coefficient, 120 MPH, slot, tare

Large Model, Cavity Apparatus, 0° AoA, 120 MPH

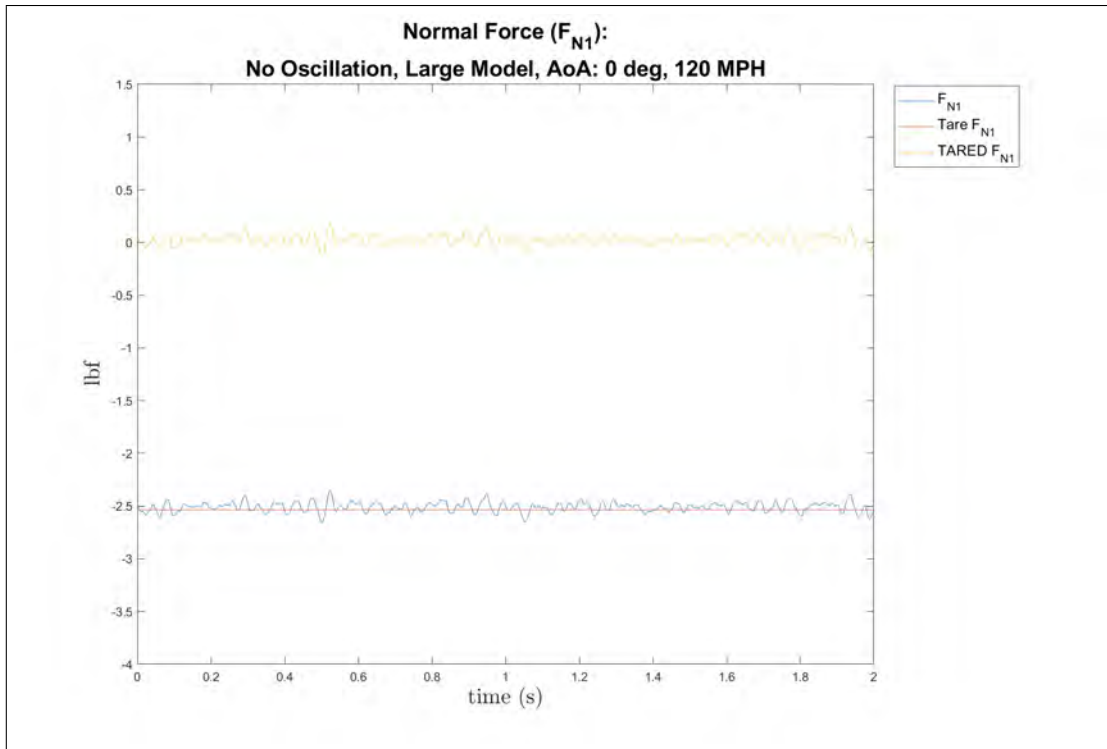


(a) Normal Force Coefficient, large model, 0° AoA, 120 MPH, In Cavity, tare

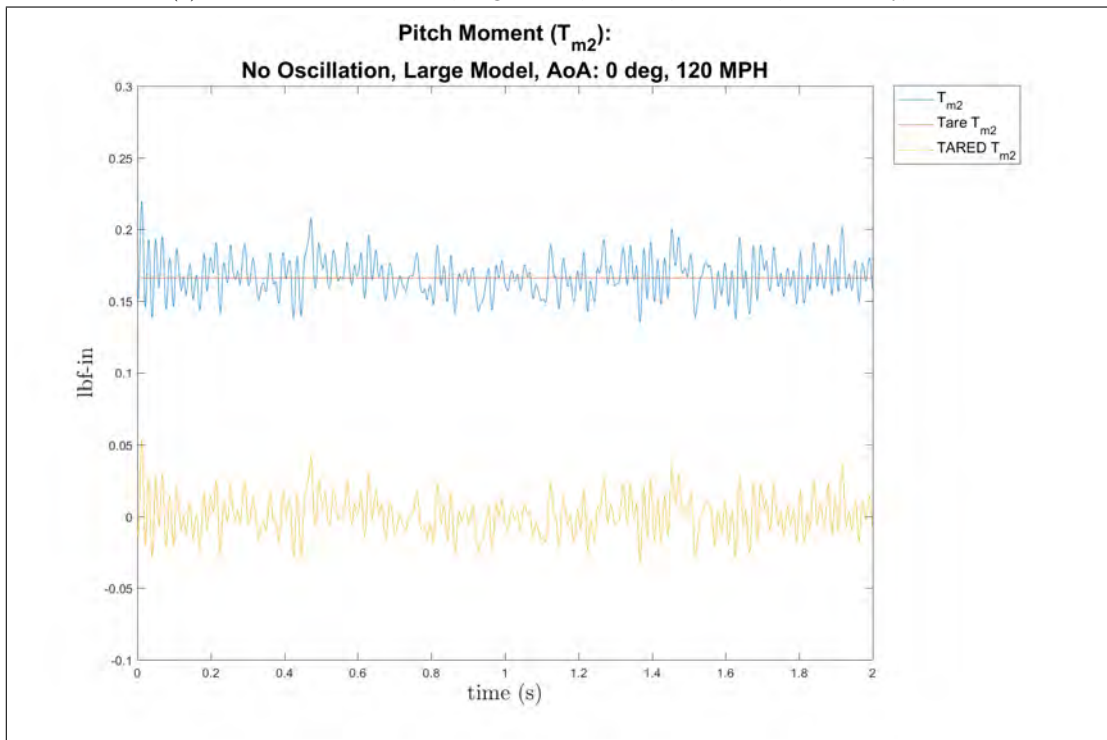


(b) Normal Force Coefficient, large model, 0° AoA, 120 MPH, Shear Layer, tare

Figure 234: Large model at 0° AoA of the normal force coefficient, 120 MPH, tare

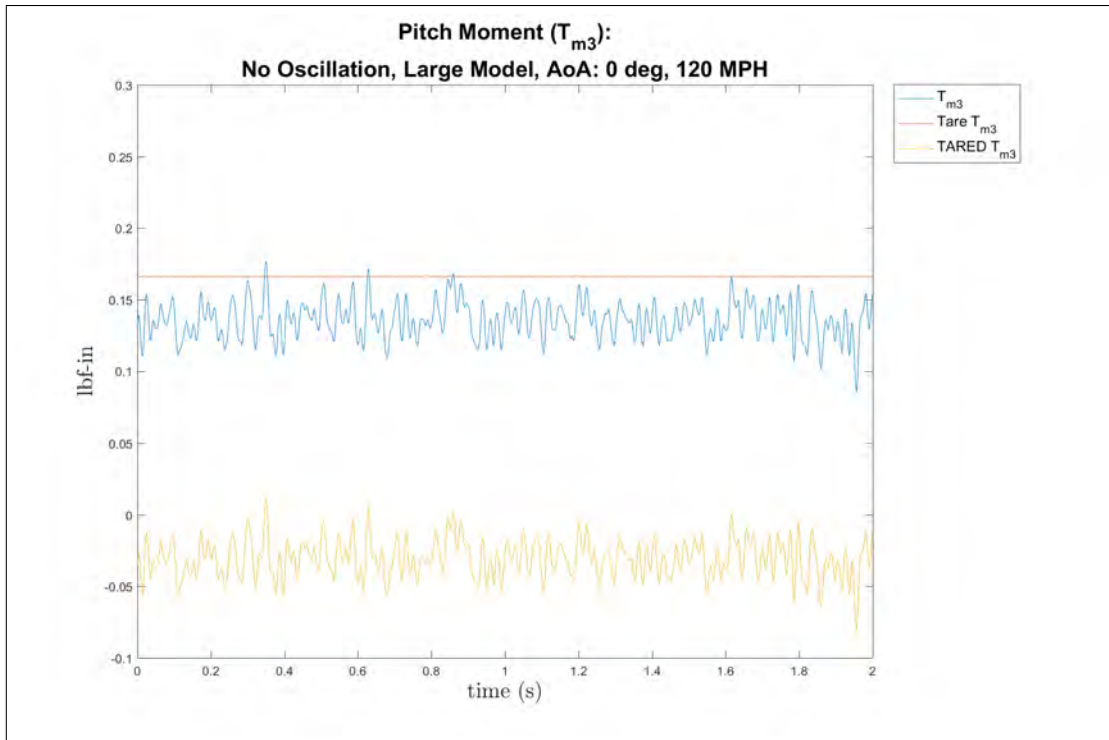


(a) Normal Force Coefficient, large model, 0° AoA, 120 MPH, Out Cavity, tare

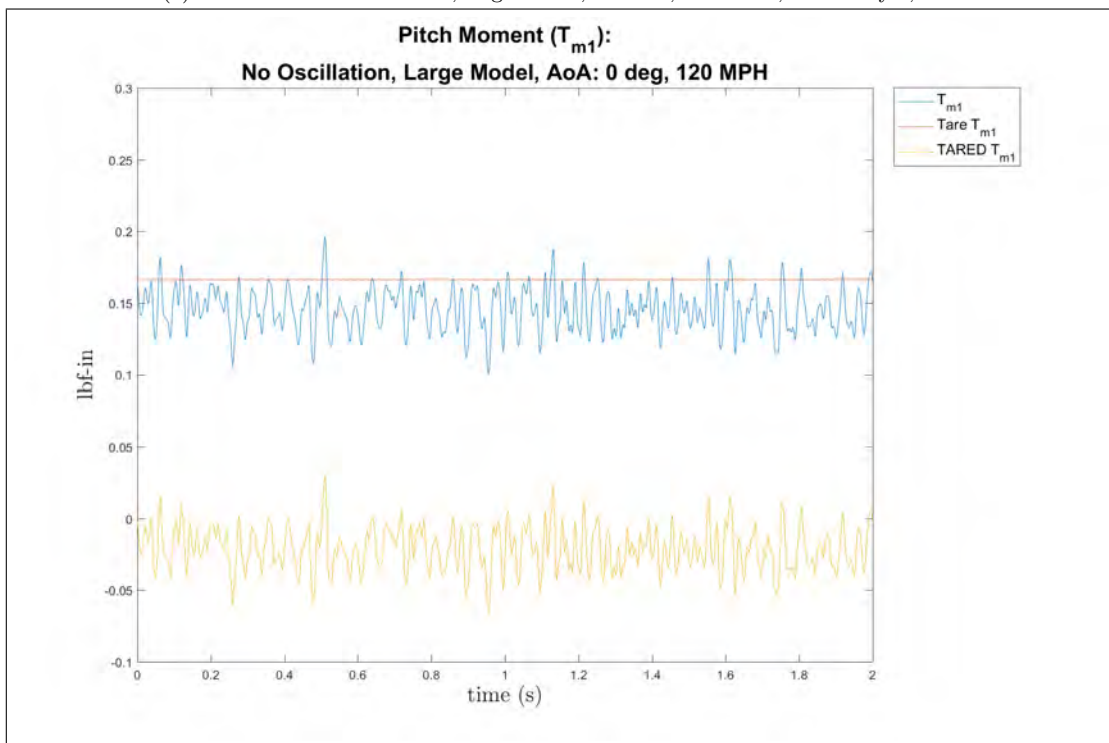


(b) Pitch Moment Coefficient, large model, 0° AoA, 120 MPH, In Cavity, tare

Figure 235: Large model at 0° AoA of the pitch moment and normal force coefficients, 120 MPH, tare

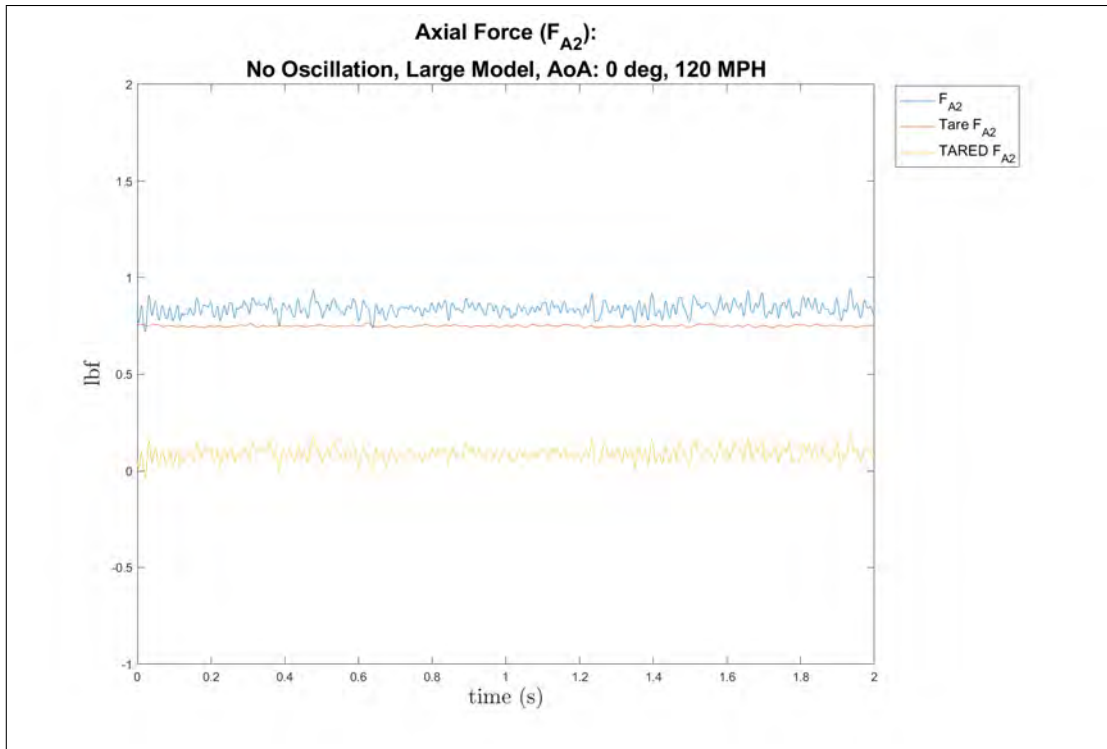


(a) Pitch Moment Coefficient, large model, 0° AoA, 120 MPH, Shear Layer, tare

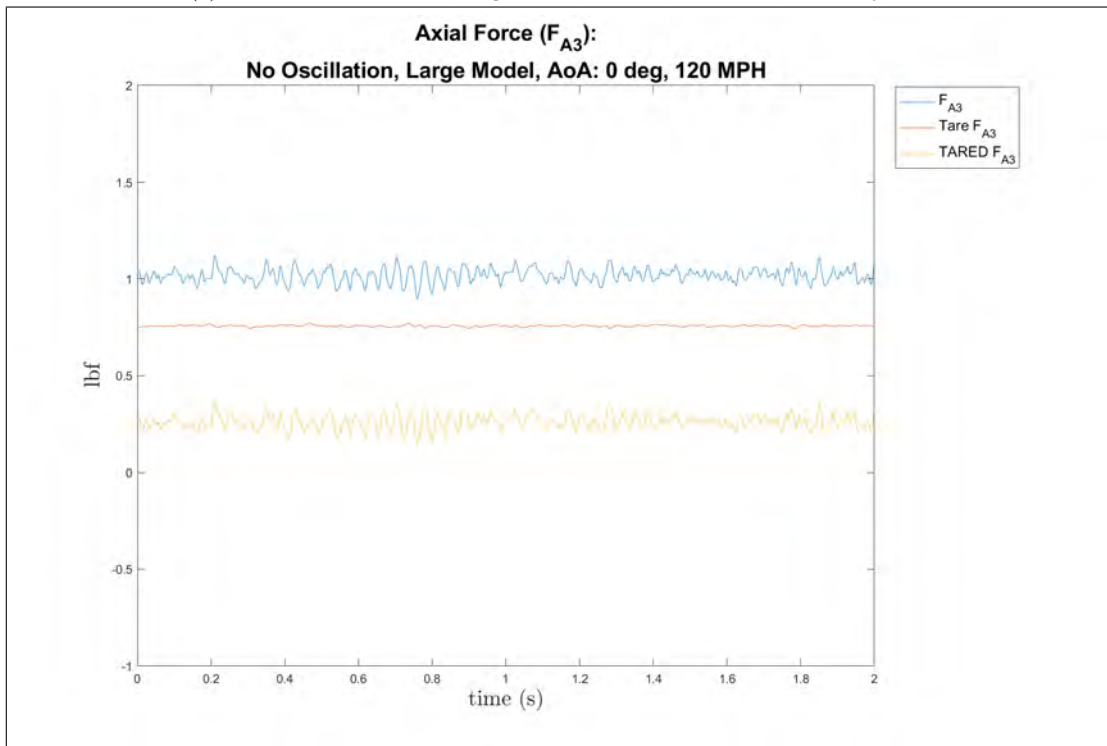


(b) Pitch Moment Coefficient, large model, 0° AoA, 120 MPH, Out Cavity, tare

Figure 236: Large model at 0° AoA of the pitch moment coefficient, 120 MPH, tare

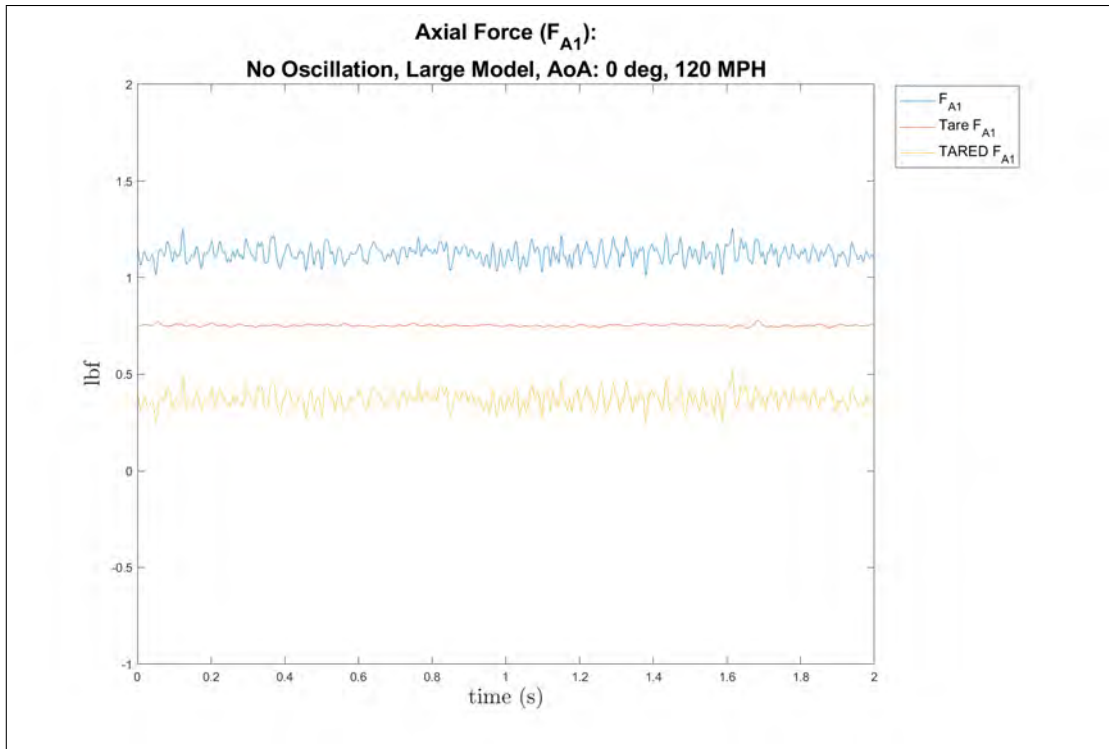


(a) Axial Force Coefficient, large model, 0° AoA, 120 MPH, In Cavity, tare

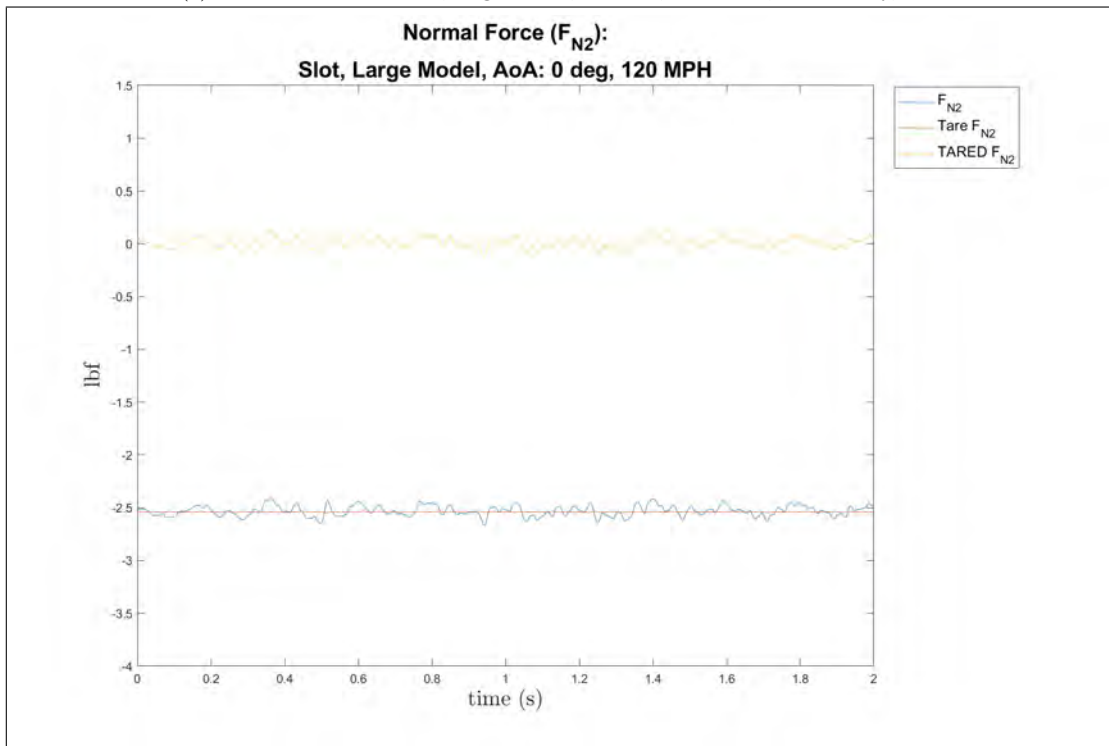


(b) Axial Force Coefficient, large model, 0° AoA, 120 MPH, Shear Layer, tare

Figure 237: Large model at 0° AoA of the Axial Force coefficient, 120 MPH, tare

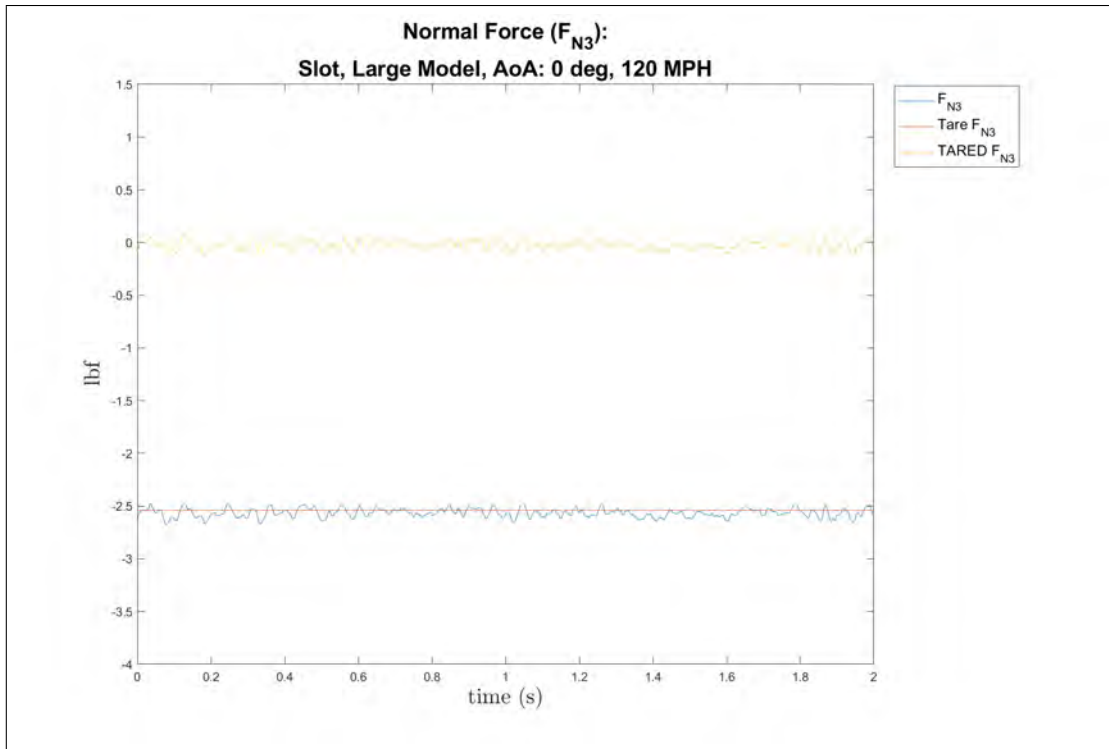


(a) Axial Force Coefficient, large model, 0° AoA, 120 MPH, Out Cavity, tare

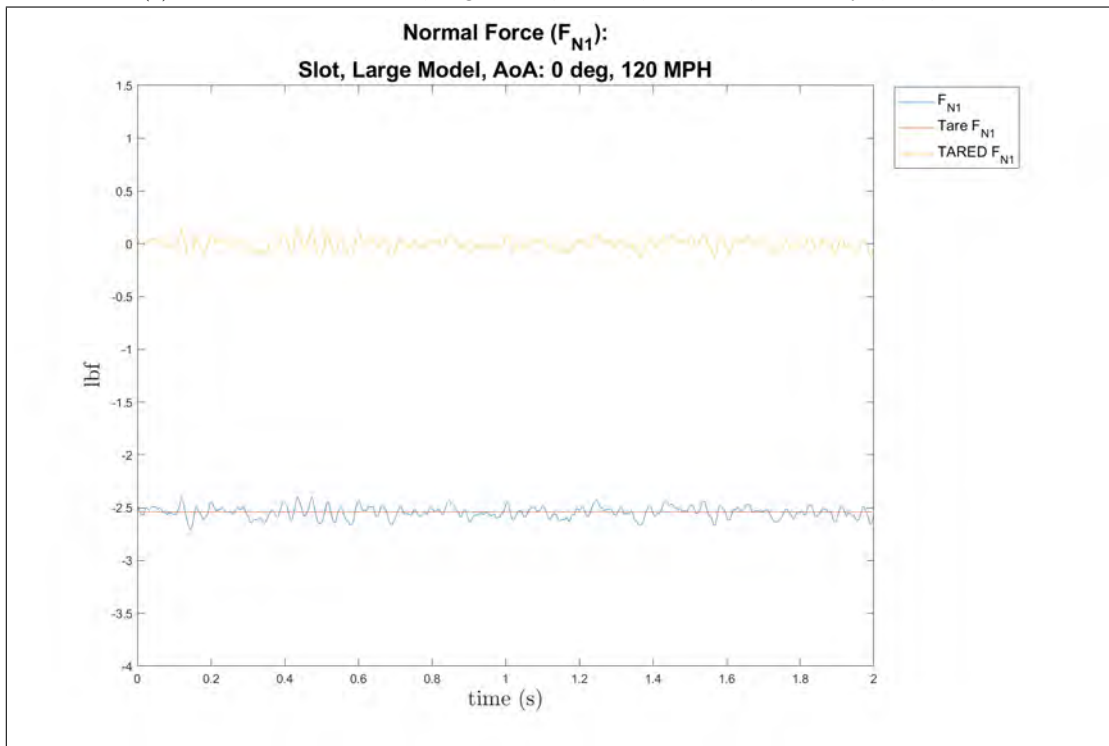


(b) Noormal Force Coefficient, large model, 0° AoA, 120 MPH, In Cavity, slot, tare

Figure 238: Large model at 0° AoA of the axial force and normal force coefficients, 120 MPH, tare

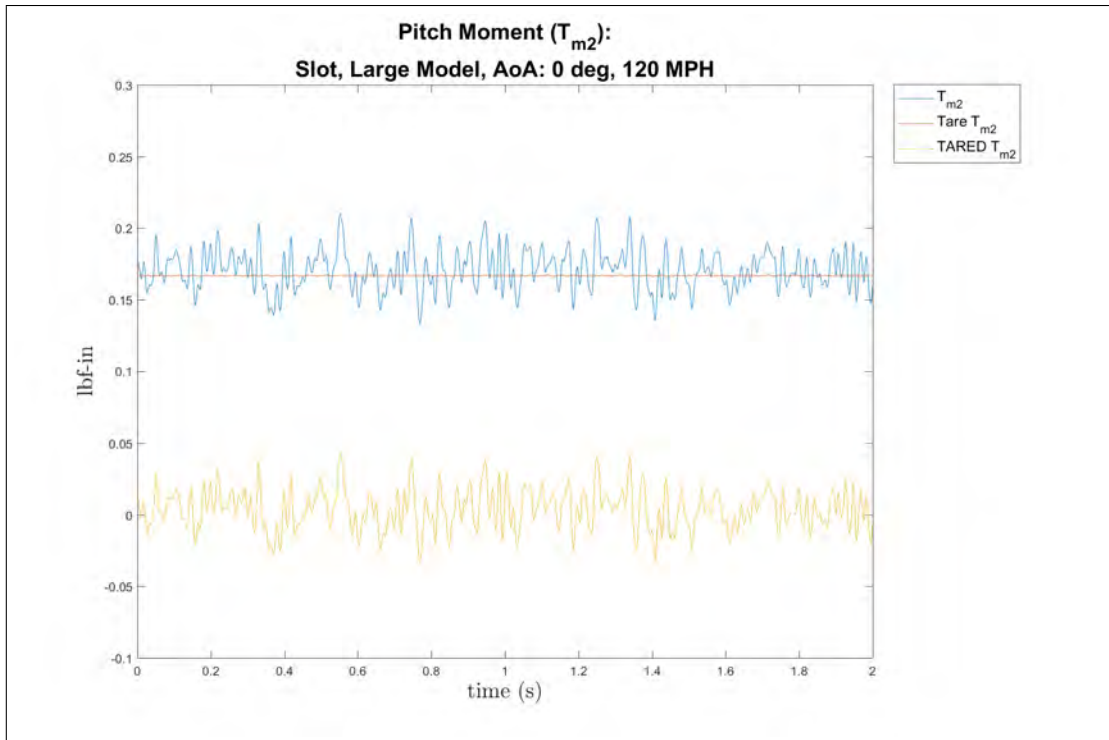


(a) Normal Force Coefficient, large model, 0° AoA, 120 MPH, Shear Layer, slot, tare

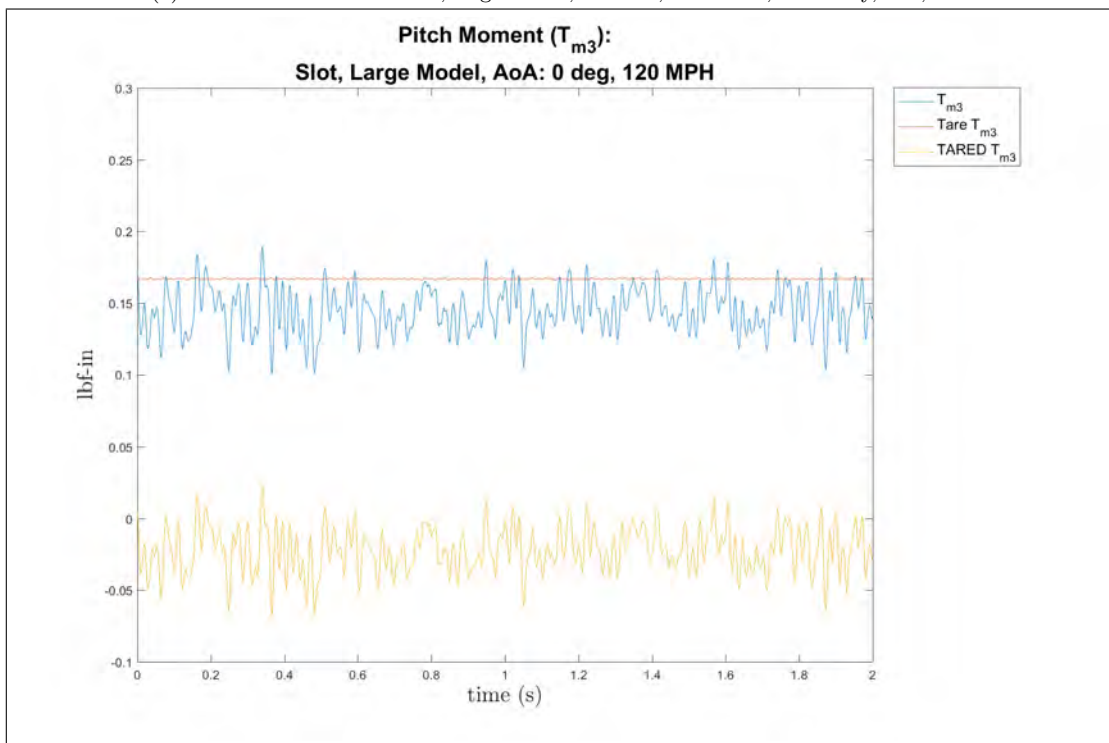


(b) Normal Force Coefficient, large model, 0° AoA, 120 MPH, Out Cavity, slot, tare

Figure 239: Large model at 0° AoA of the normal force coefficient, 120 MPH, slot, tare

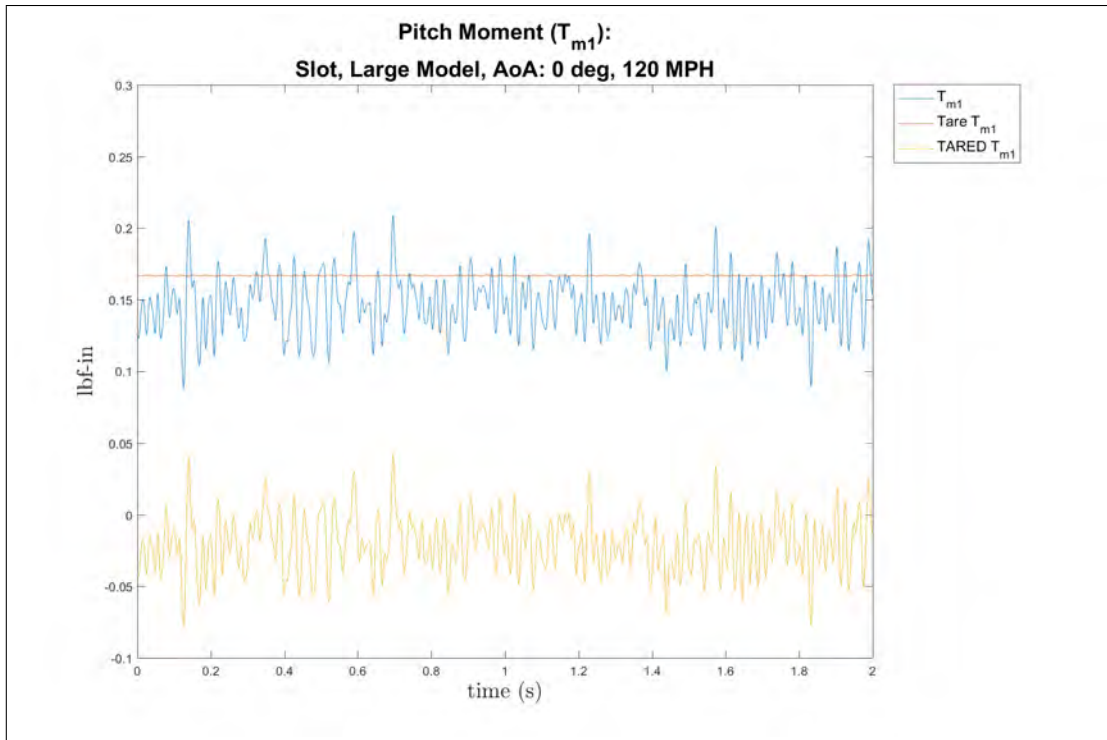


(a) Pitch Moment Coefficient, large model, 0° AoA, 120 MPH, In Cavity, slot, tare

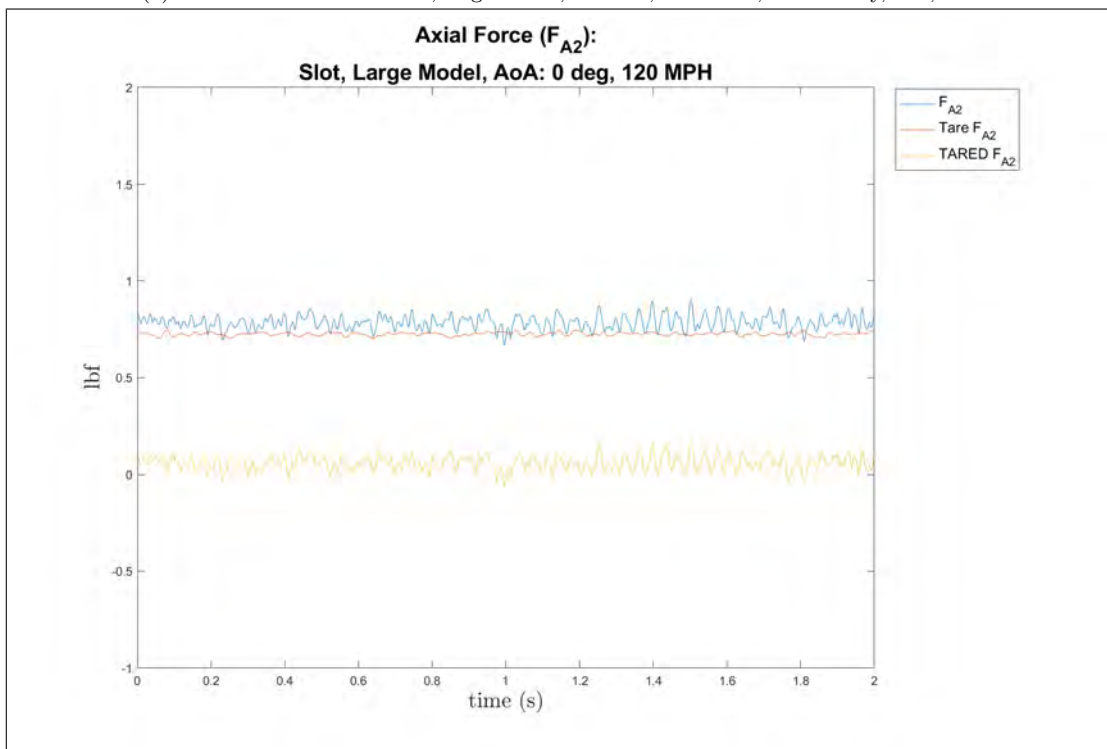


(b) Pitch Moment Coefficient, large model, 0° AoA, 120 MPH, Shear Layer, slot, tare

Figure 240: Large model at 0° AoA of the pitch moment coefficient, 120 MPH, slot, tare

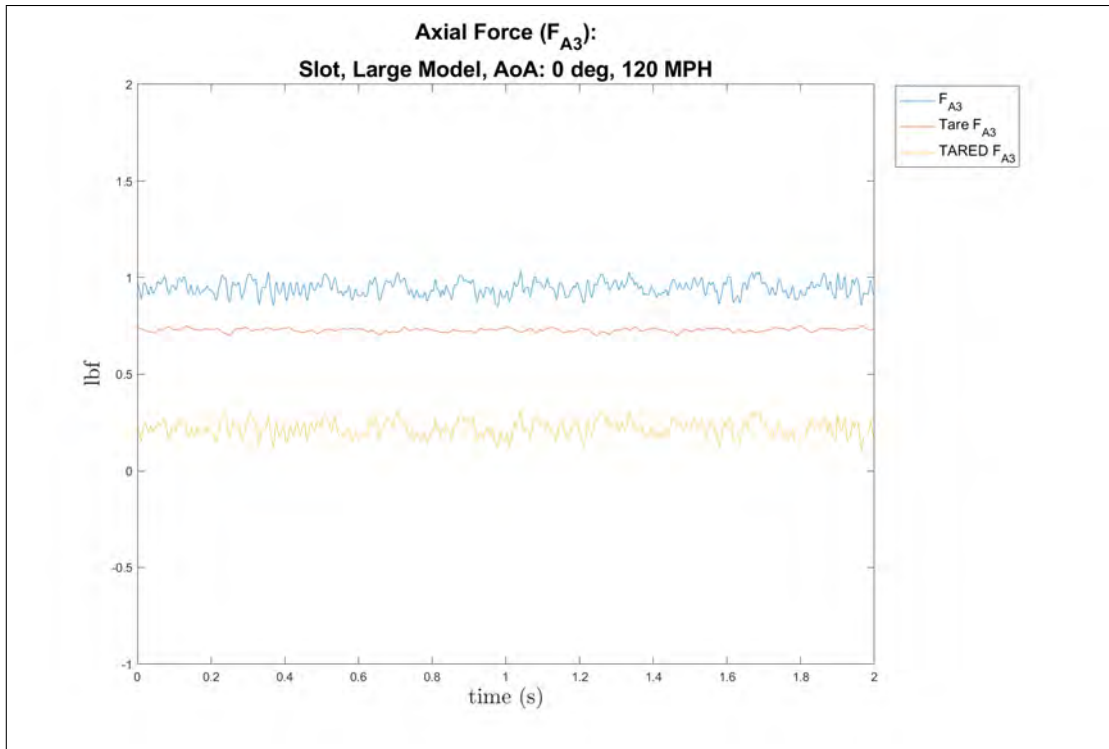


(a) Pitch Moment Coefficient, large model, 0° AoA, 120 MPH, Out Cavity, slot, tare

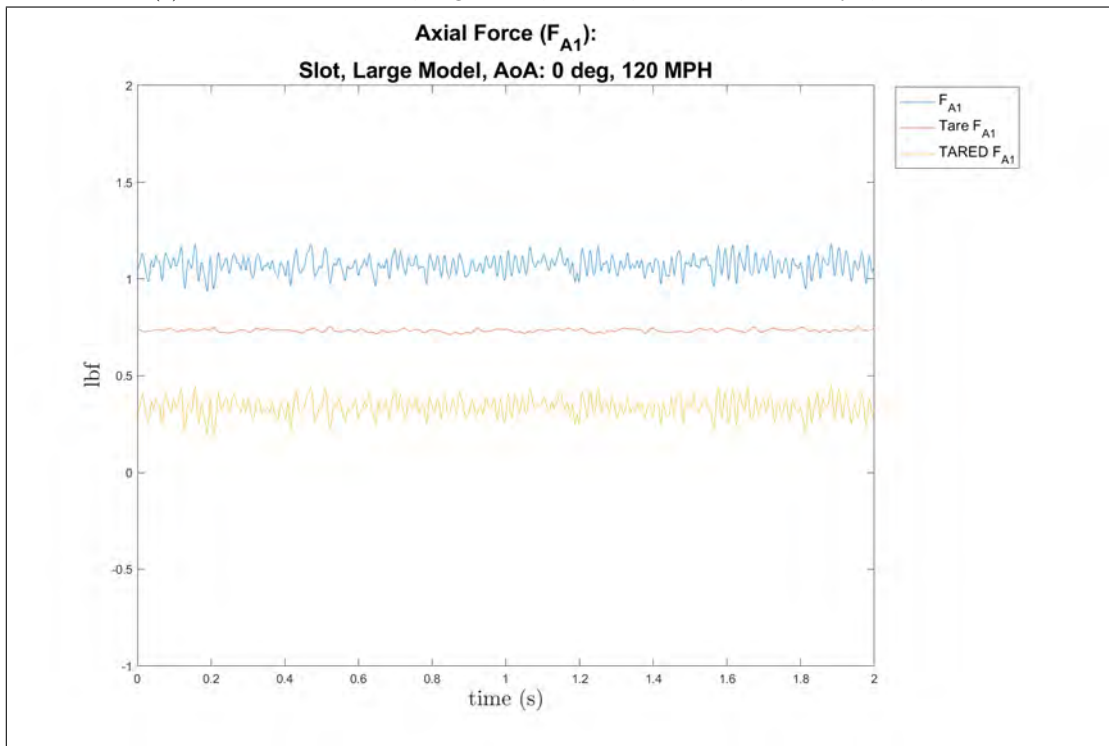


(b) Axial Force Coefficient, large model, 0° AoA, 120 MPH, In Cavity, slot, tare

Figure 241: Large model at 0° AoA of the pitch moment and axial force coefficients, 120 MPH, slot, tare



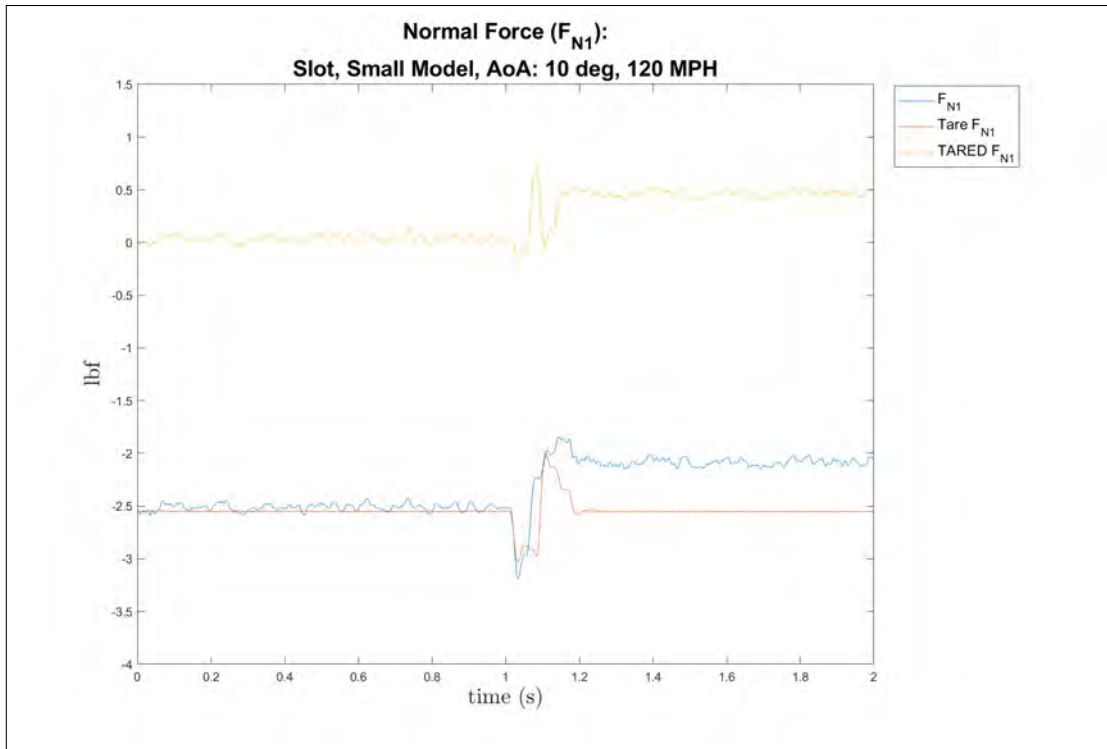
(a) Axial Force Coefficient, large model, 0° AoA, 120 MPH, Shear Layer, slot, tare



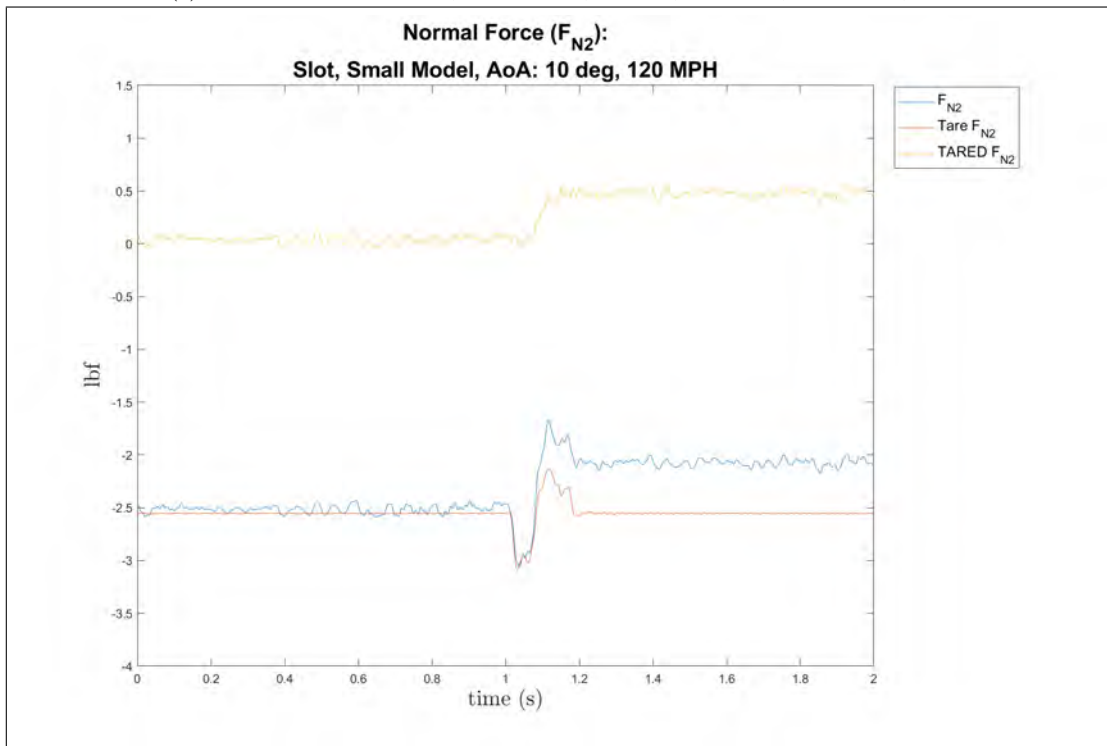
(b) Axial Force Coefficient, large model, 0° AoA, 120 MPH, Out Cavity, slot, tare

Figure 242: Large model at 0° AoA of the axial force coefficient, 120 MPH, slot, tare

Small Model, Dynamic Release, 0° AoA, 120 MPH

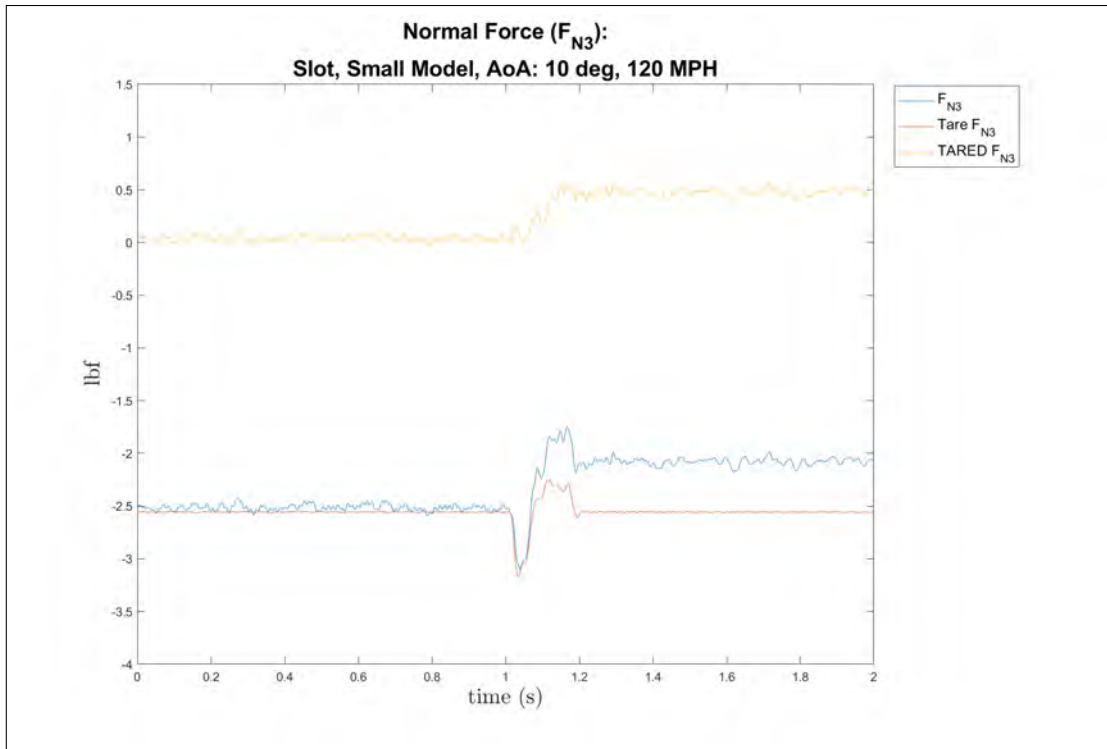


(a) Normal Force Coefficient, small model, 0° AoA, 120 MPH, release one, tare

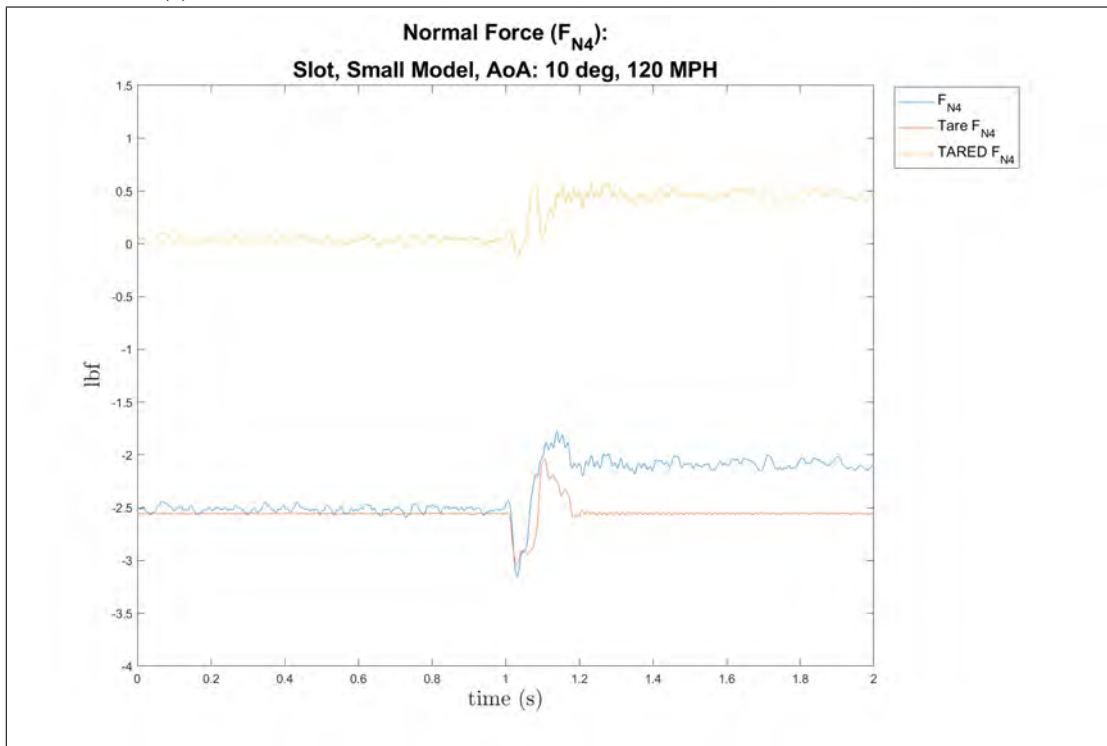


(b) Normal Force Coefficient, small model, 0° AoA, 120 MPH, release two, tare

Figure 243: Small model at 0° AoA of the normal force coefficient, release times one and two, 120 MPH, tare

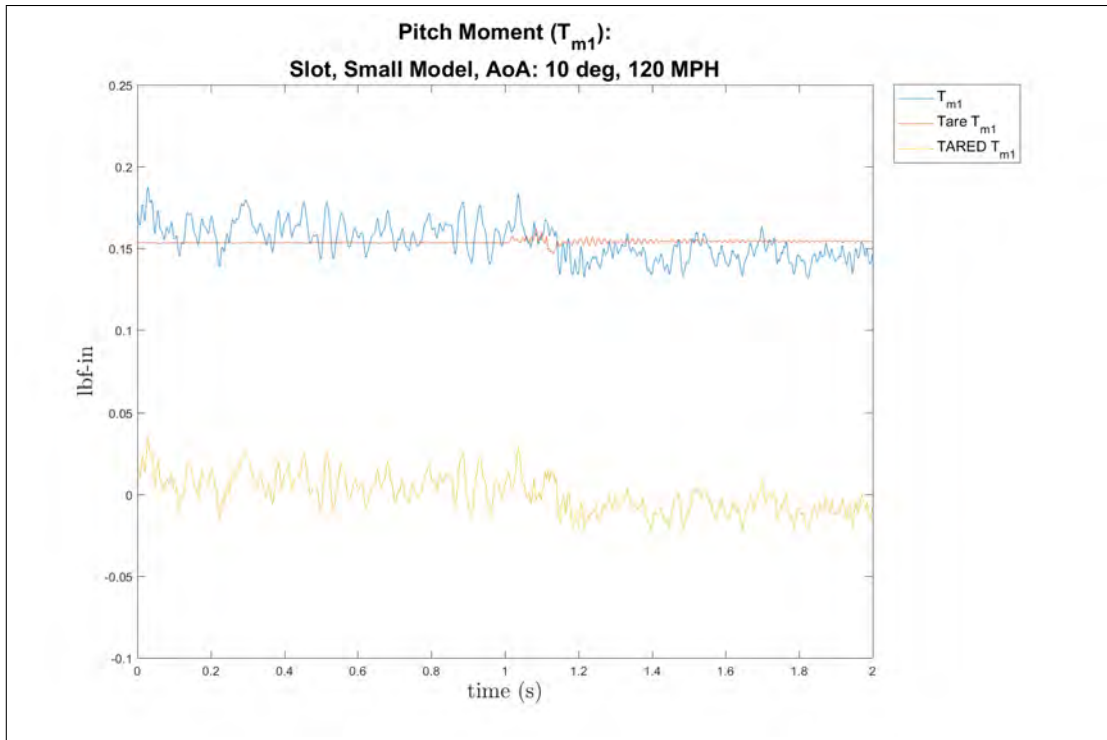


(a) Normal Force Coefficient, small model, 0° AoA, 120 MPH, release three, tare

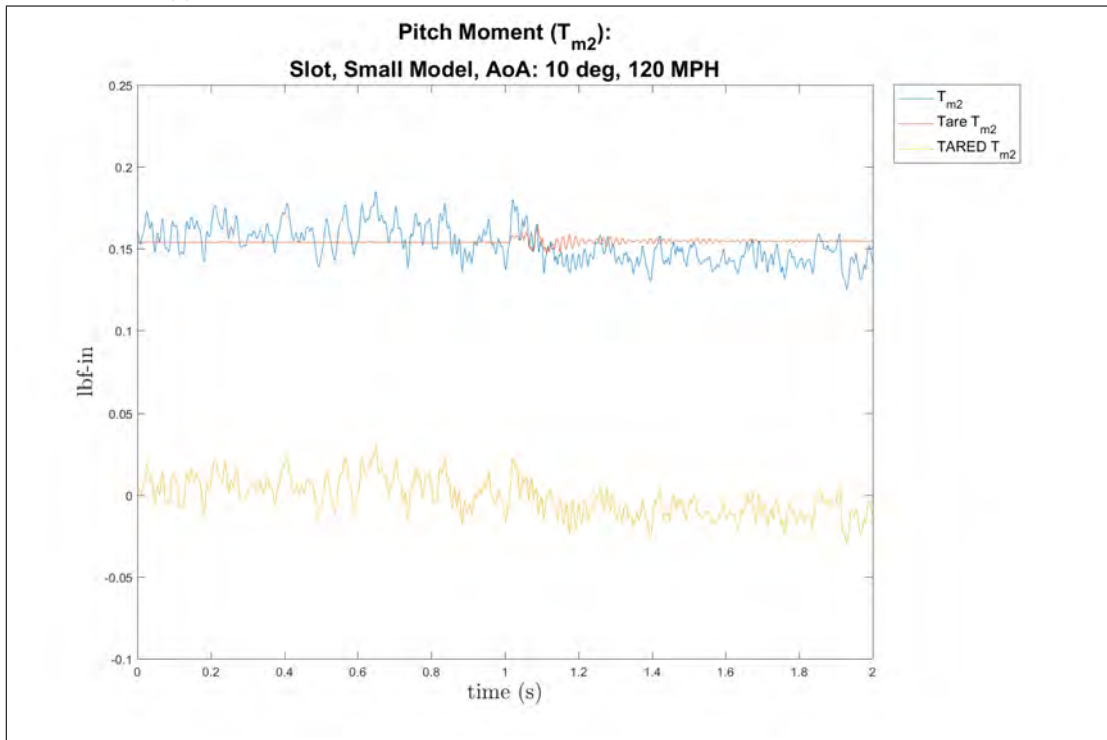


(b) Normal Force Coefficient, small model, 0° AoA, 120 MPH, release four, tare

Figure 244: Small model at 0° AoA of the normal force coefficient, release times three and four, 120 MPH, tare

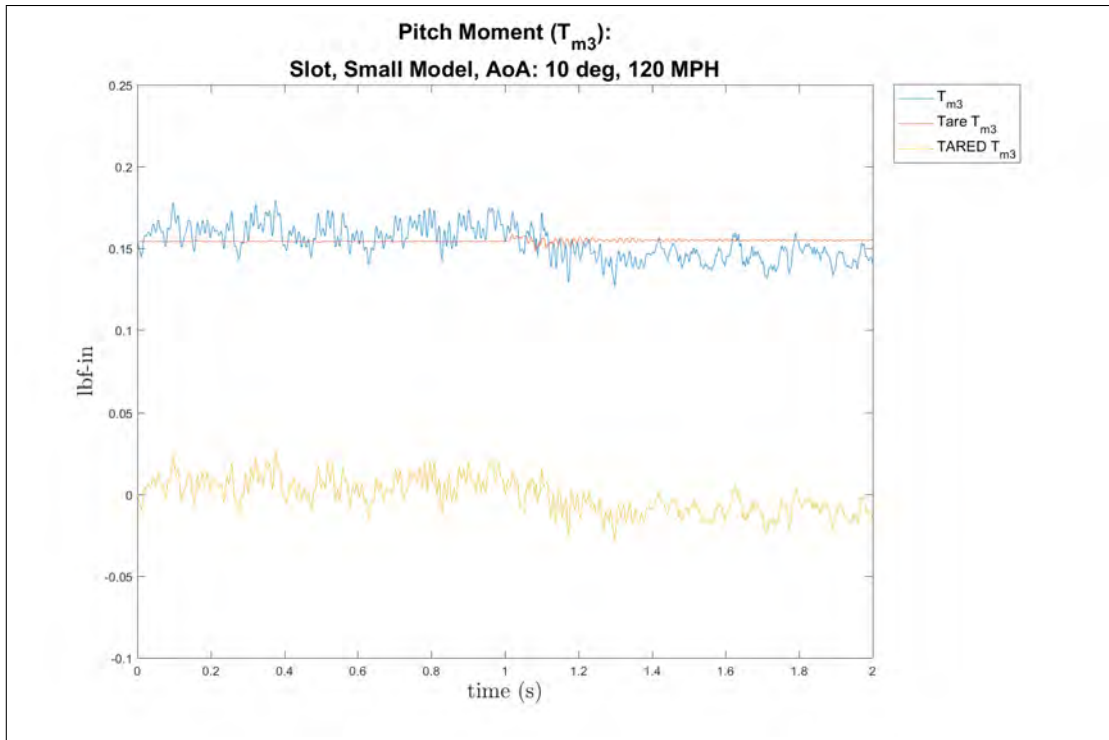


(a) Pitch Moment Coefficient, small model, 0° AoA, 120 MPH, release one, tare

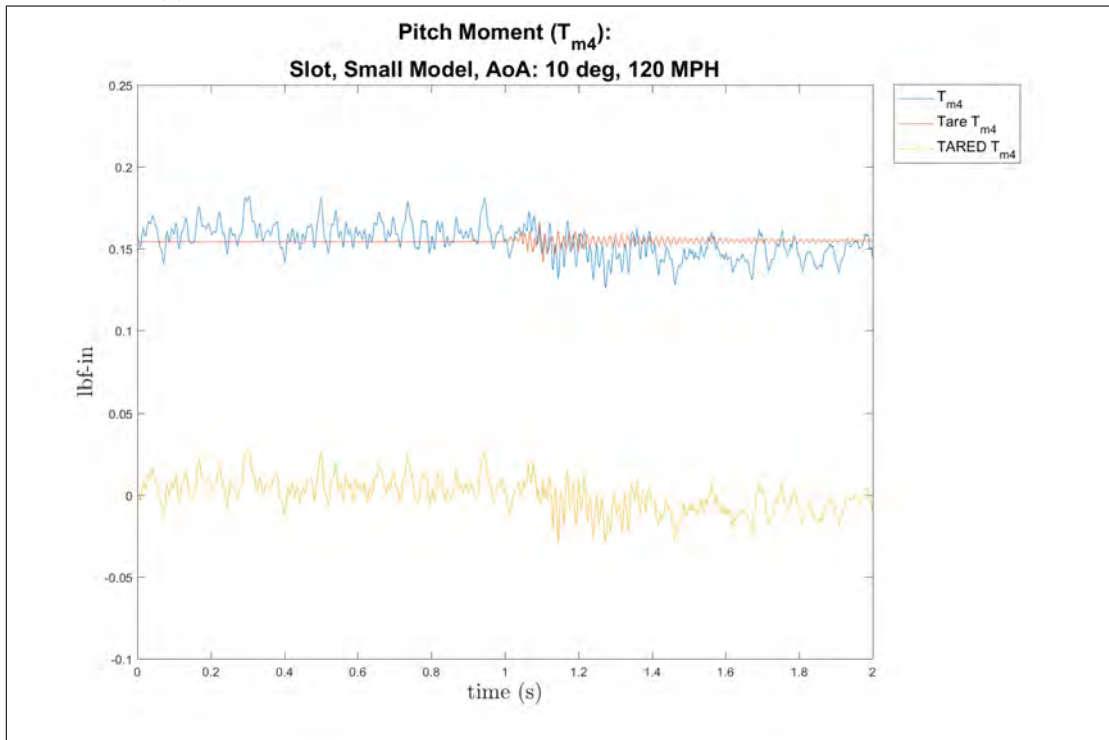


(b) Pitch Moment Coefficient, small model, 0° AoA, 120 MPH, release two, tare

Figure 245: Small model at 0° AoA of the pitch moment coefficient, release times one and two, 120 MPH, tare

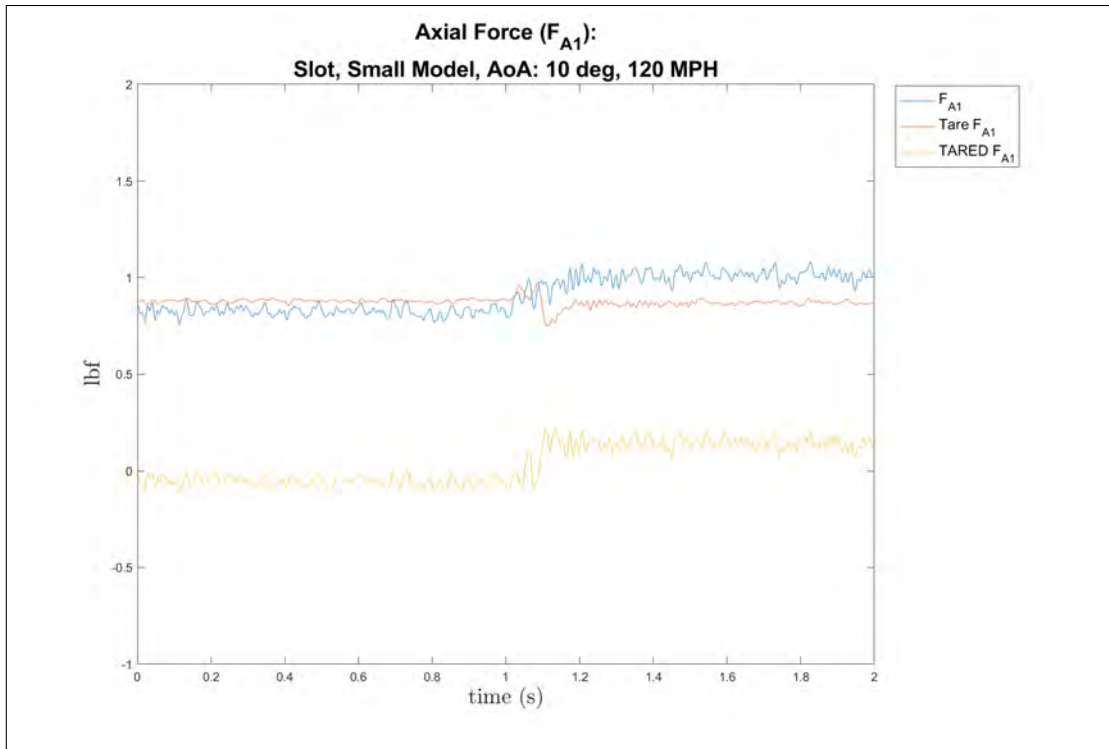


(a) Pitch Moment Coefficient, small model, 0° AoA, 120 MPH, release three, tare

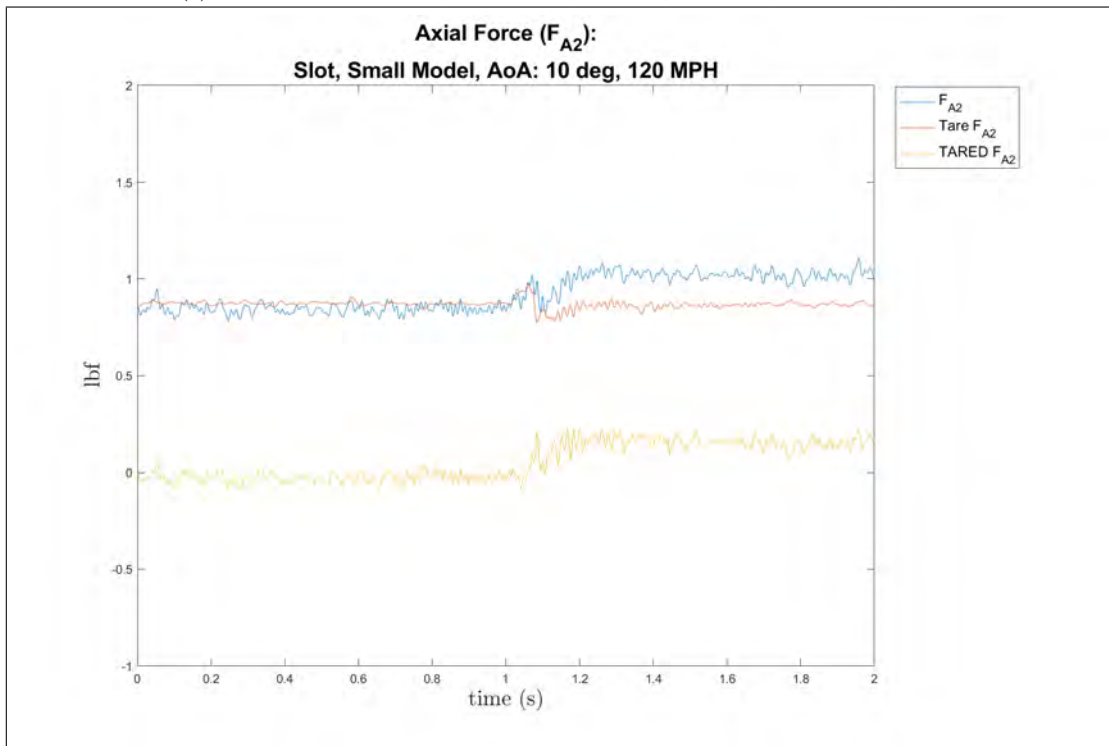


(b) Pitch Moment Coefficient, small model, 0° AoA, 120 MPH, release four, tare

Figure 246: Small model at 0° AoA of the pitch moment coefficient, release times three and four, 120 MPH, tare

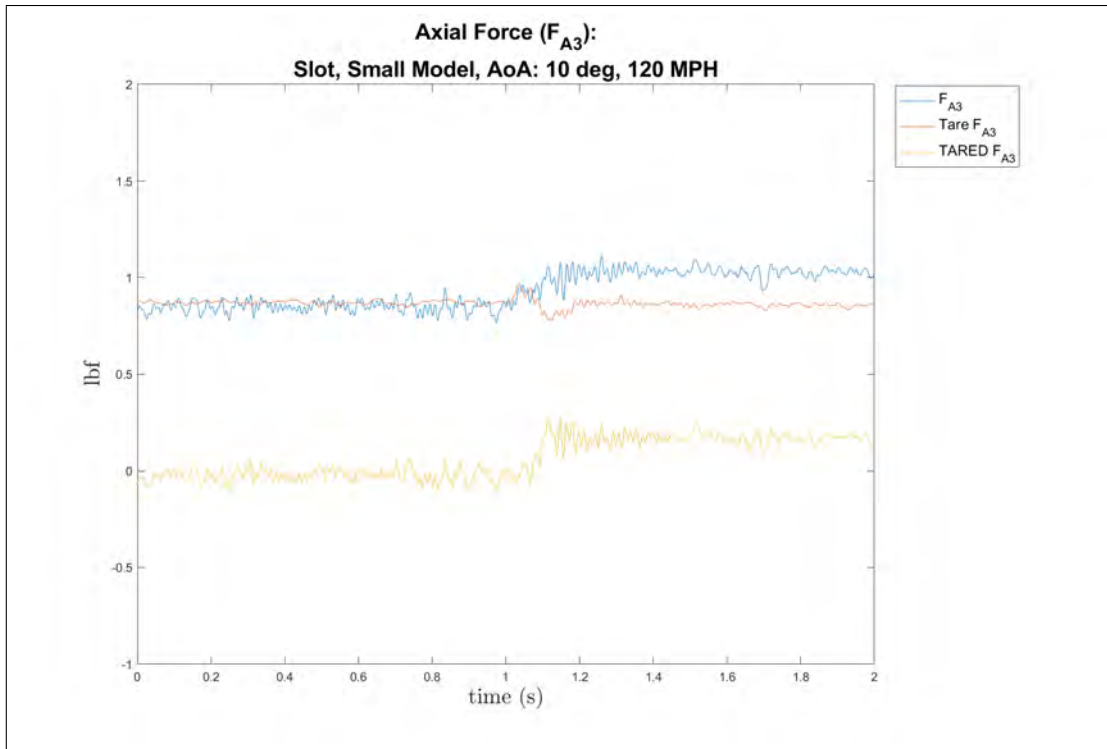


(a) Axial Force Coefficient, small model, 0° AoA, 120 MPH, release one, tare

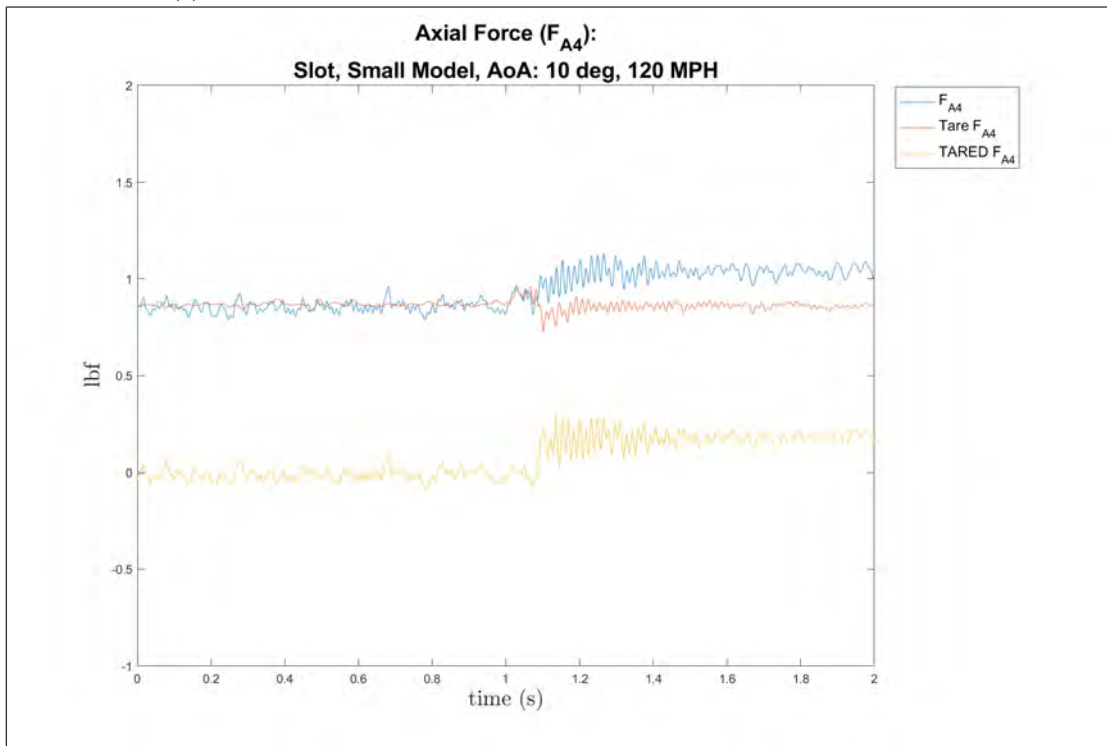


(b) Axial Force Coefficient, small model, 0° AoA, 120 MPH, release two, tare

Figure 247: Small model at 0° AoA of the axial force coefficient, release times one and two, 120 MPH, tare



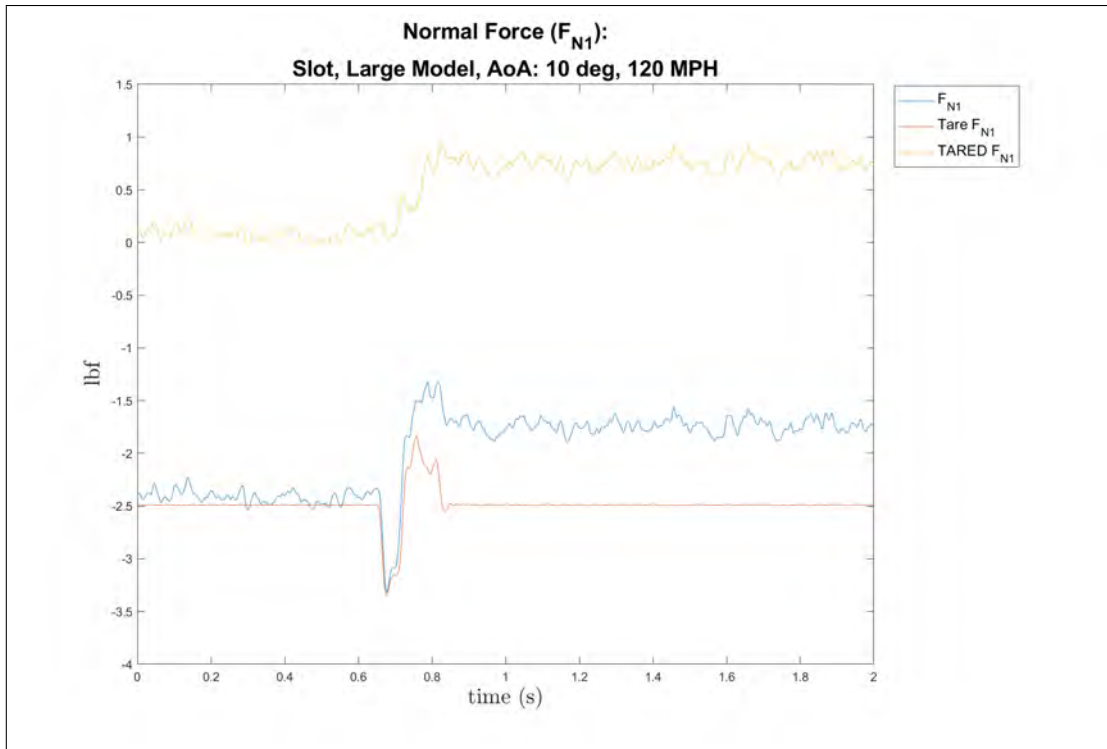
(a) Axial Force Coefficient, small model, 0° AoA, 120 MPH, release three, tare



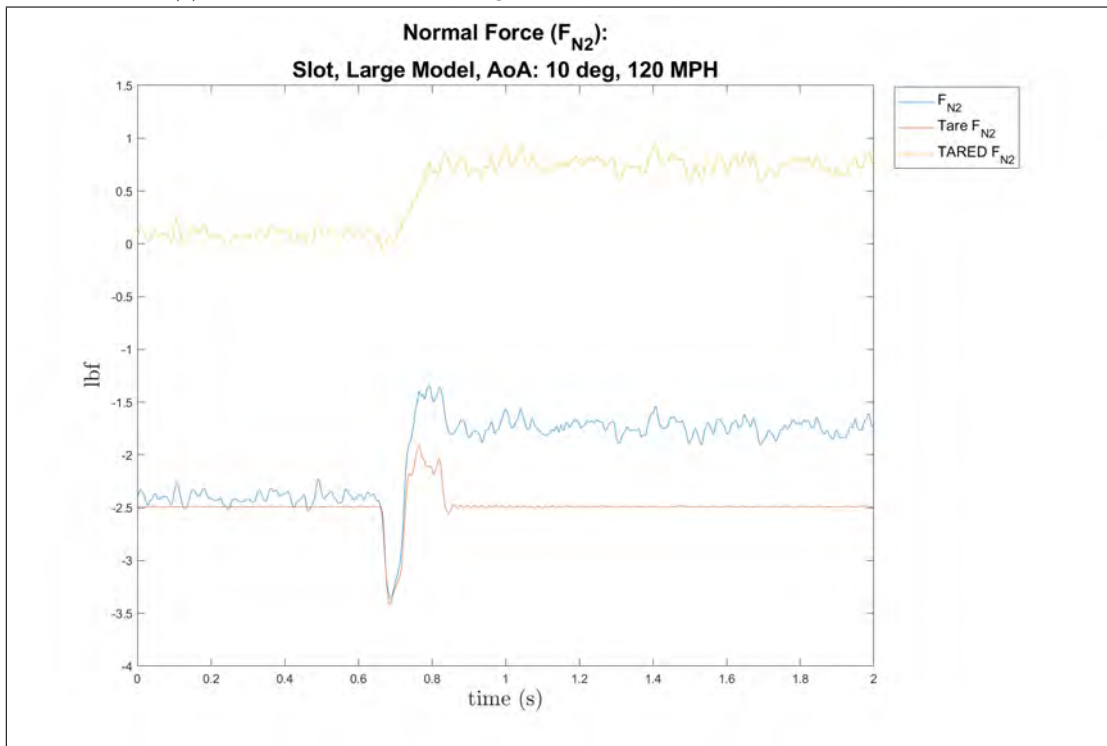
(b) Axial Force Coefficient, small model, 0° AoA, 120 MPH, release four, tare

Figure 248: Small model at 0° AoA of the axial force coefficient, release times three and four, 120 MPH, tare

Large Model, Dynamic Release, 0° AoA, 120 MPH

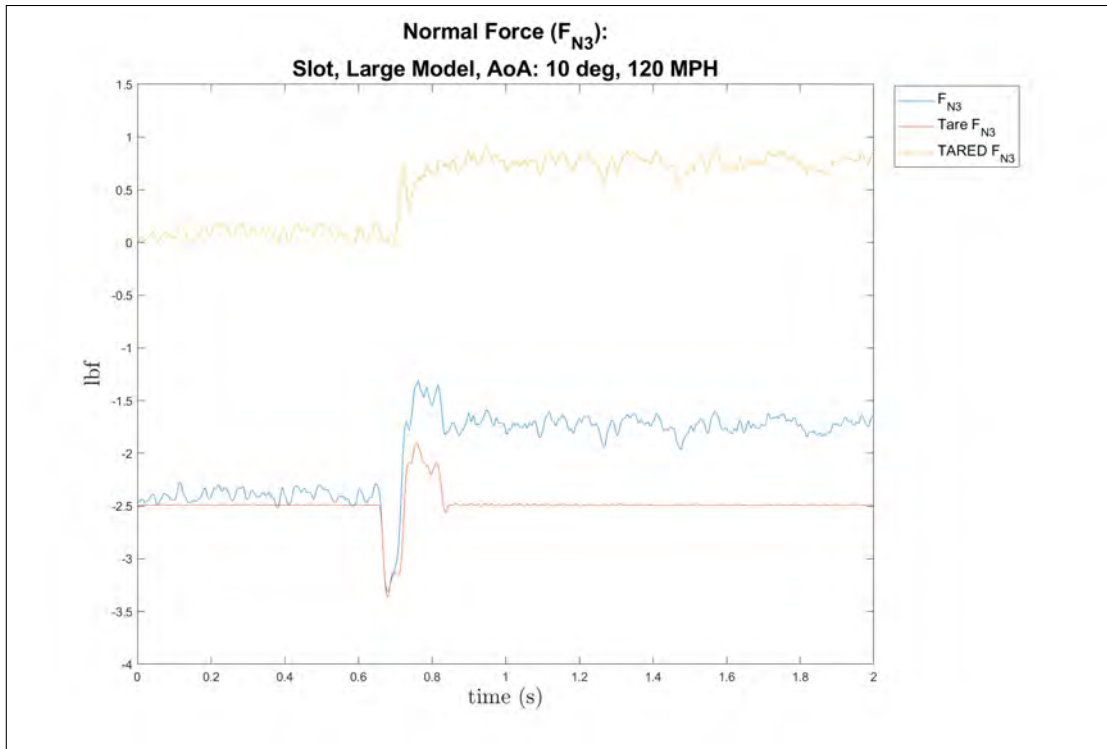


(a) Normal Force Coefficient, large model, 0° AoA, 120 MPH, release one, tare

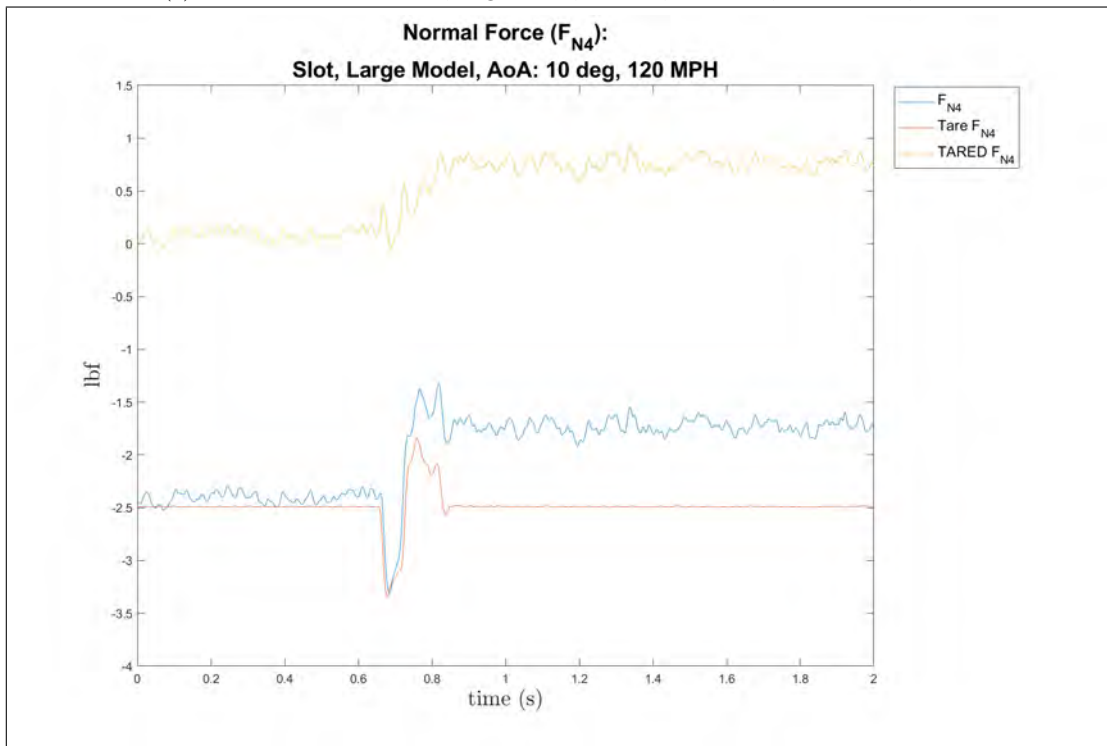


(b) Normal Force Coefficient, large model, 0° AoA, 120 MPH, release two, tare

Figure 249: Large model at 0° AoA of the normal force coefficient, release times one and two, 120 MPH, tare

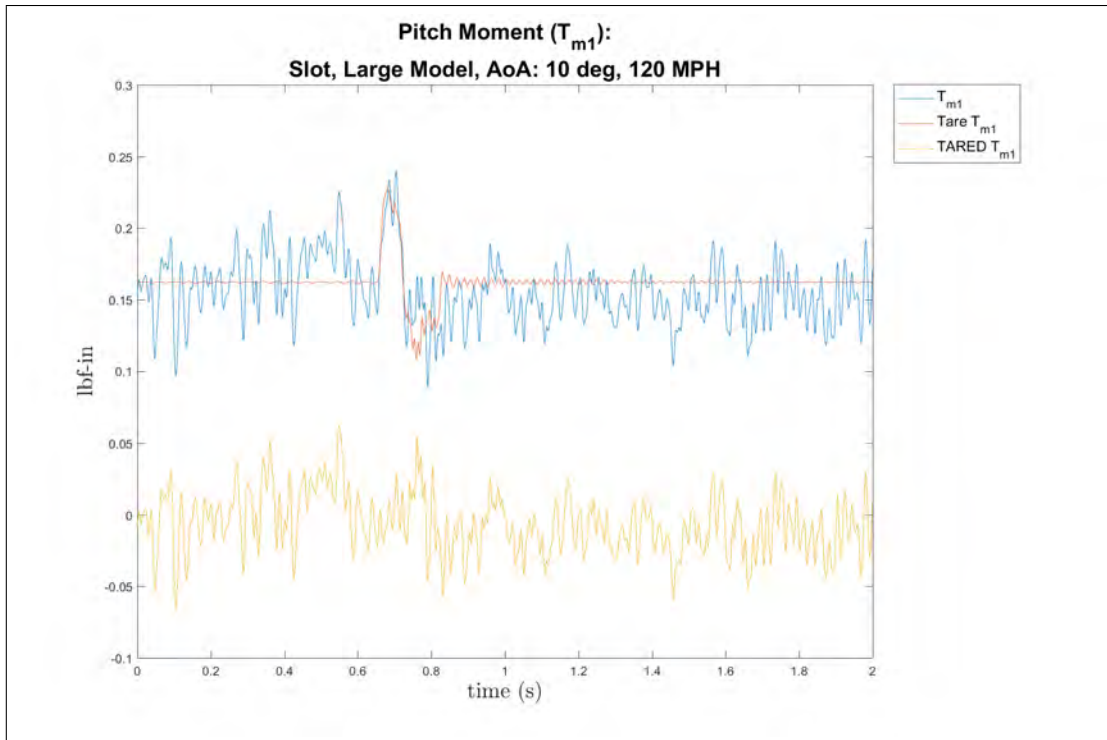


(a) Normal Force Coefficient, large model, 0° AoA, 120 MPH, release three, tare

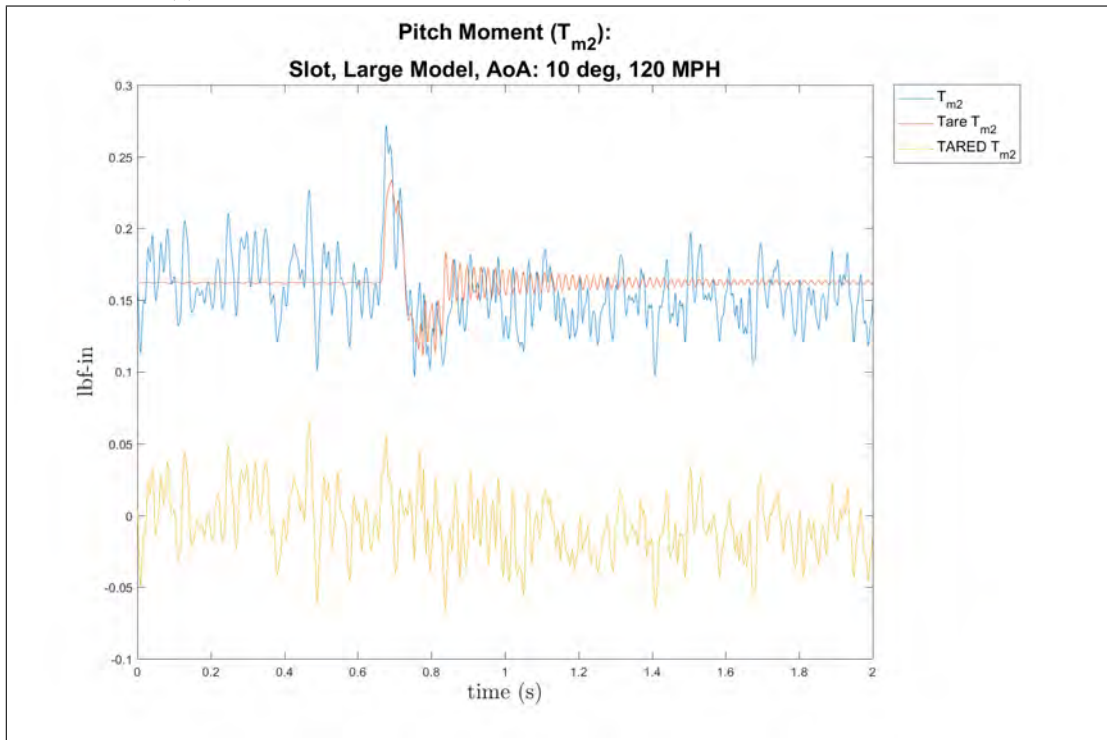


(b) Normal Force Coefficient, large model, 0° AoA, 120 MPH, release four, tare

Figure 250: Large model at 0° AoA of the normal force coefficient, release times three and four, 120 MPH, tare

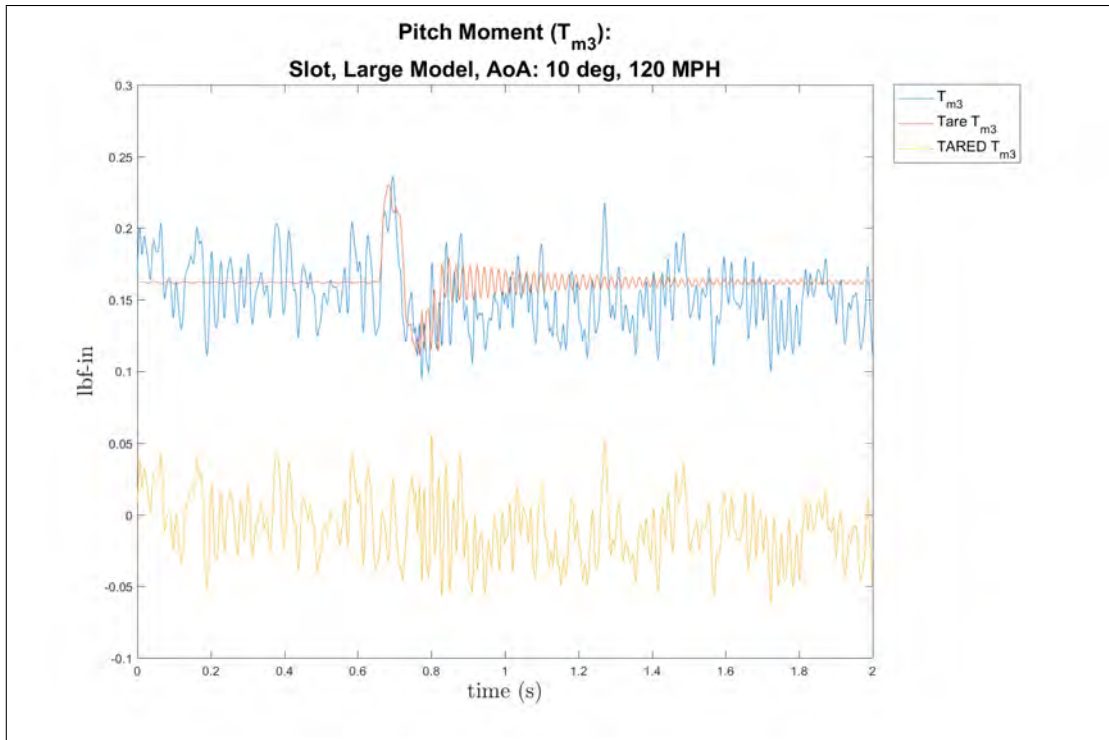


(a) Pitch Moment Coefficient, large model, 0° AoA, 120 MPH, release one, tare

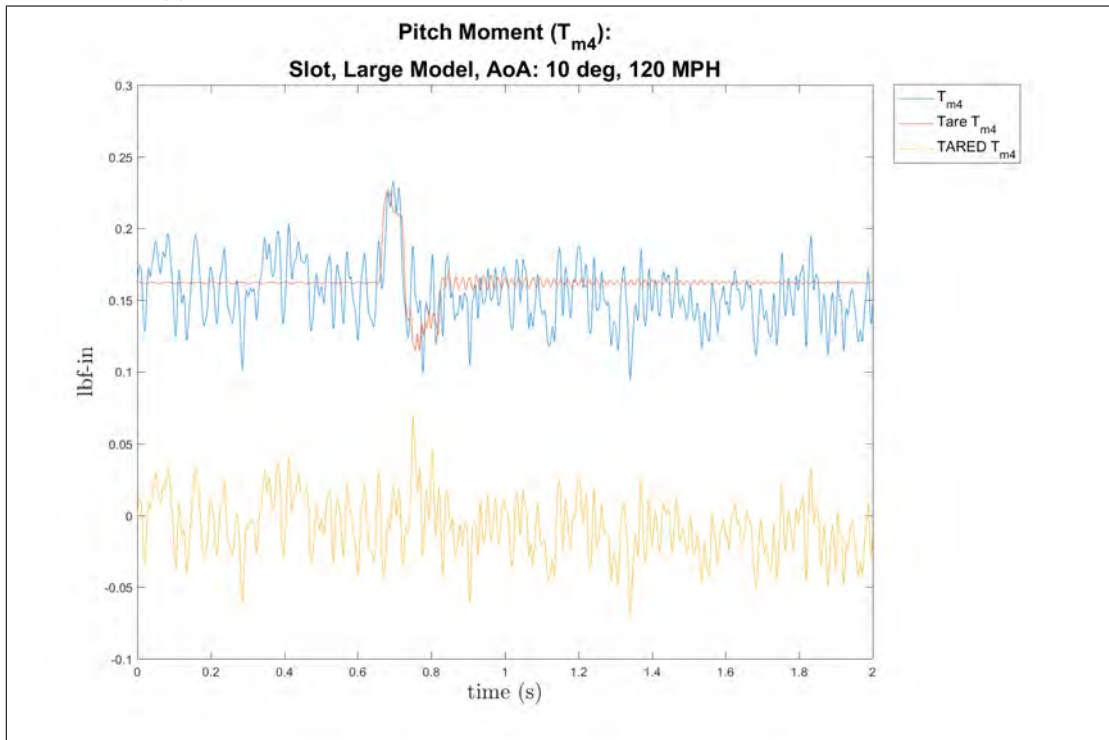


(b) Pitch Moment Coefficient, large model, 0° AoA, 120 MPH, release two, tare

Figure 251: Large model at 0° AoA of the pitch moment coefficient, release times one and two, 120 MPH, tare

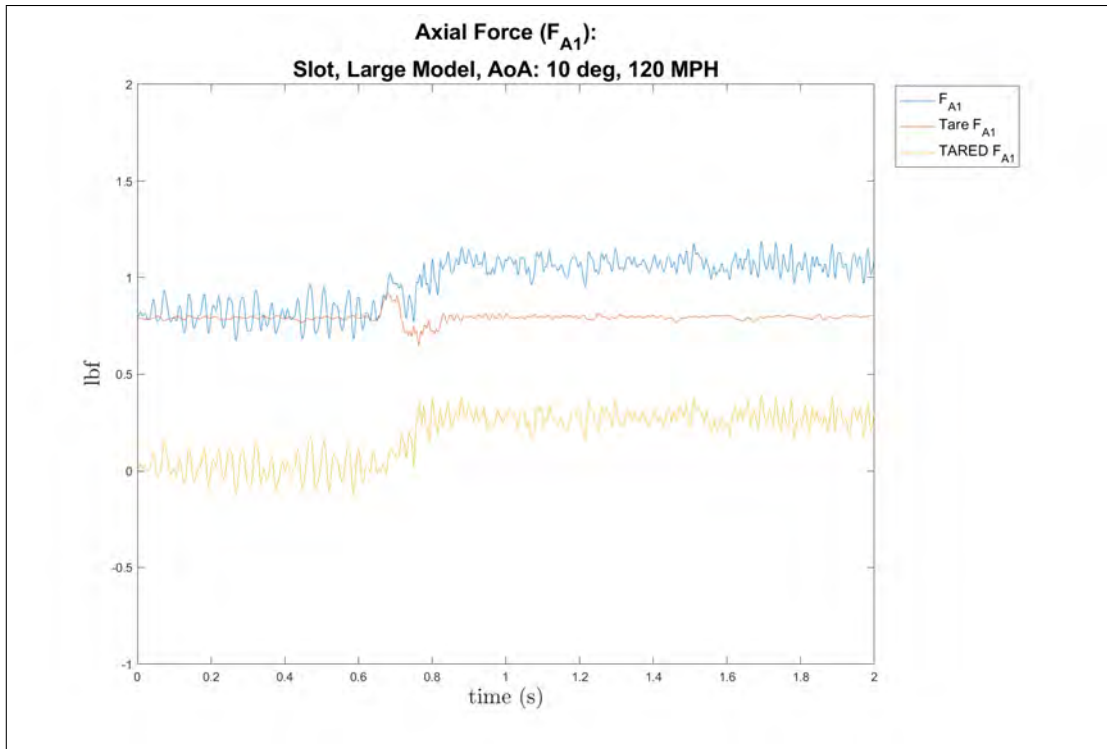


(a) Pitch Moment Coefficient, large model, 0° AoA, 120 MPH, release three, tare

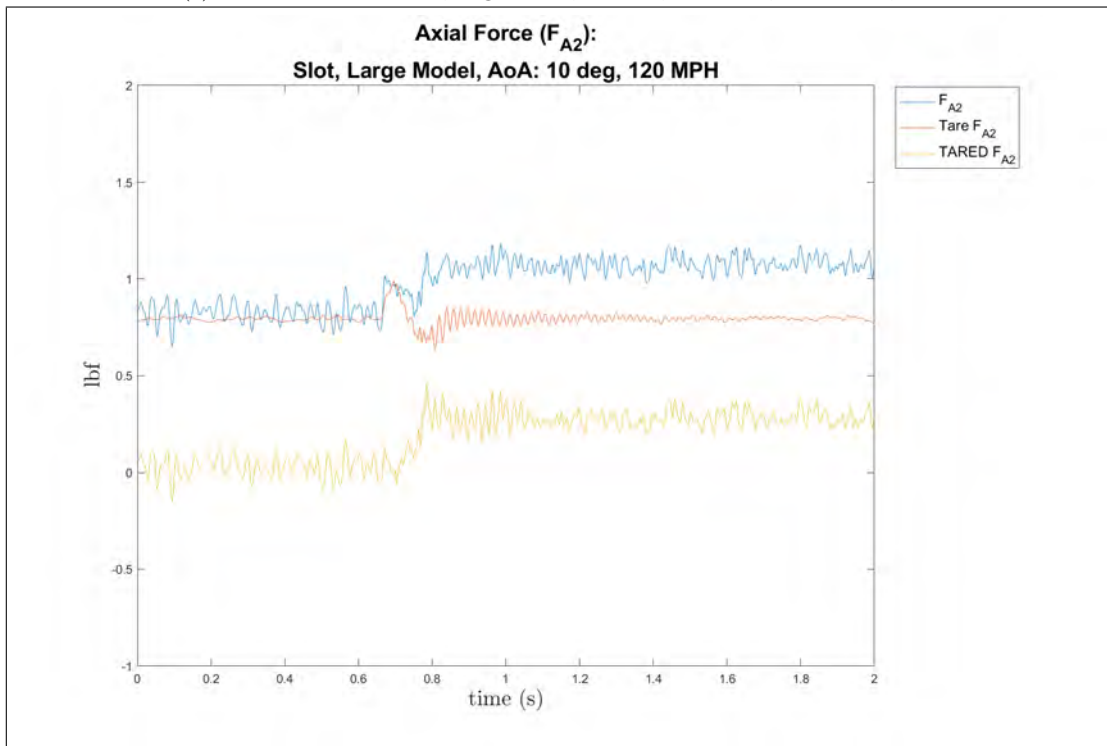


(b) Pitch Moment Coefficient, large model, 0° AoA, 120 MPH, release four, tare

Figure 252: Large model at 0° AoA of the pitch moment coefficient, release times three and four, 120 MPH, tare

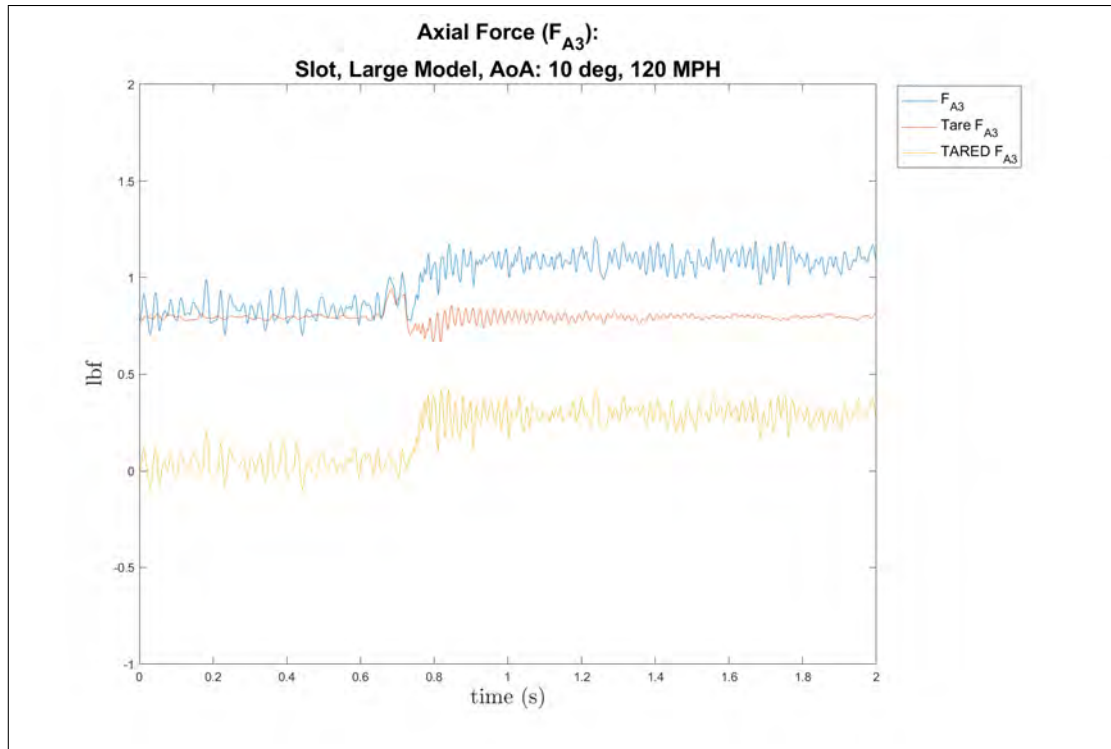


(a) Axial Force Coefficient, large model, 0° AoA, 120 MPH, release one, tare

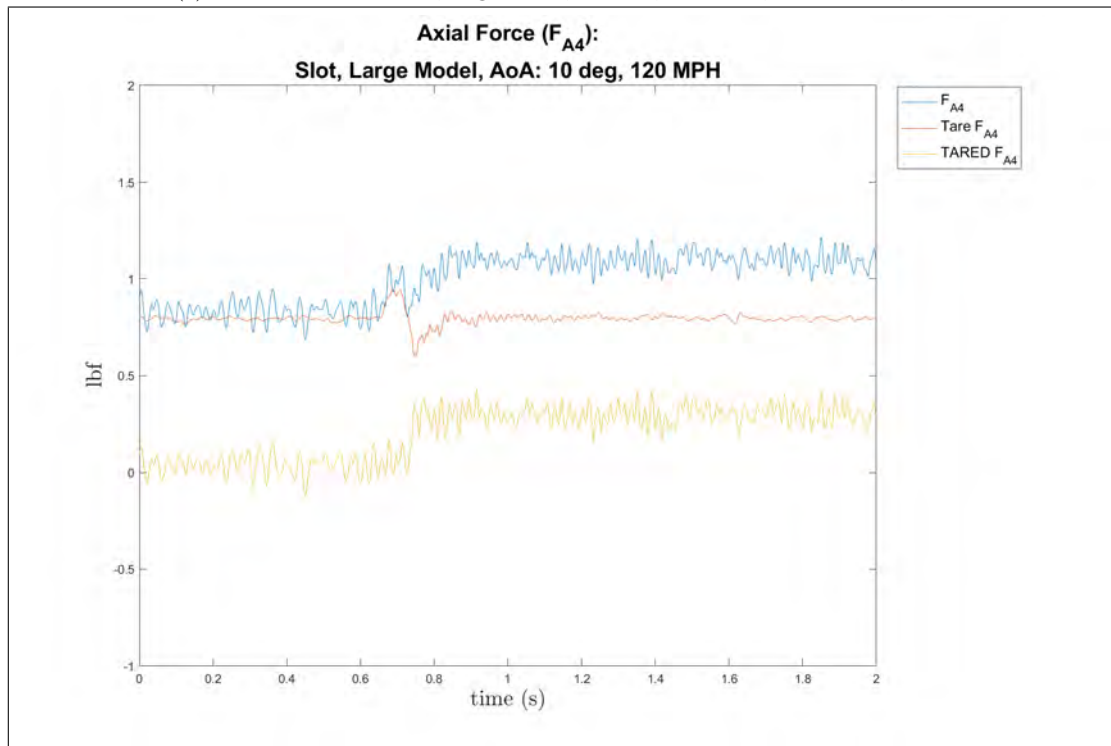


(b) Axial Force Coefficient, large model, 0° AoA, 120 MPH, release two, tare

Figure 253: Large model at 0° AoA of the axial force coefficient, release times one and two, 120 MPH, tare



(a) Axial Force Coefficient, large model, 0° AoA, 120 MPH, release three, tare



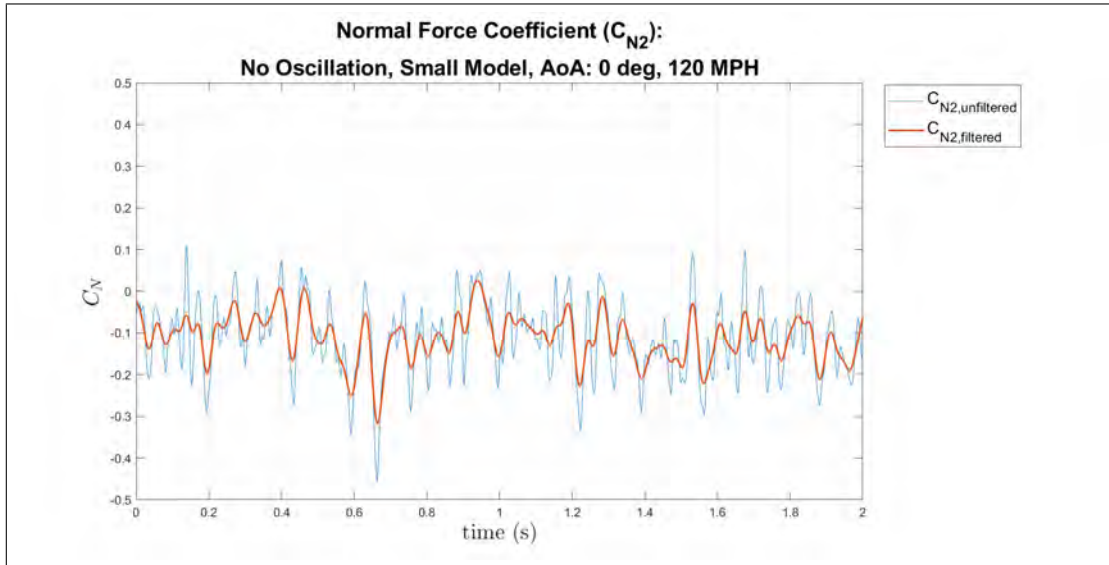
(b) Axial Force Coefficient, large model, 0° AoA, 120 MPH, release four, tare

Figure 254: Large model at 0° AoA of the axial force coefficient, release times three and four, 120 MPH, tare

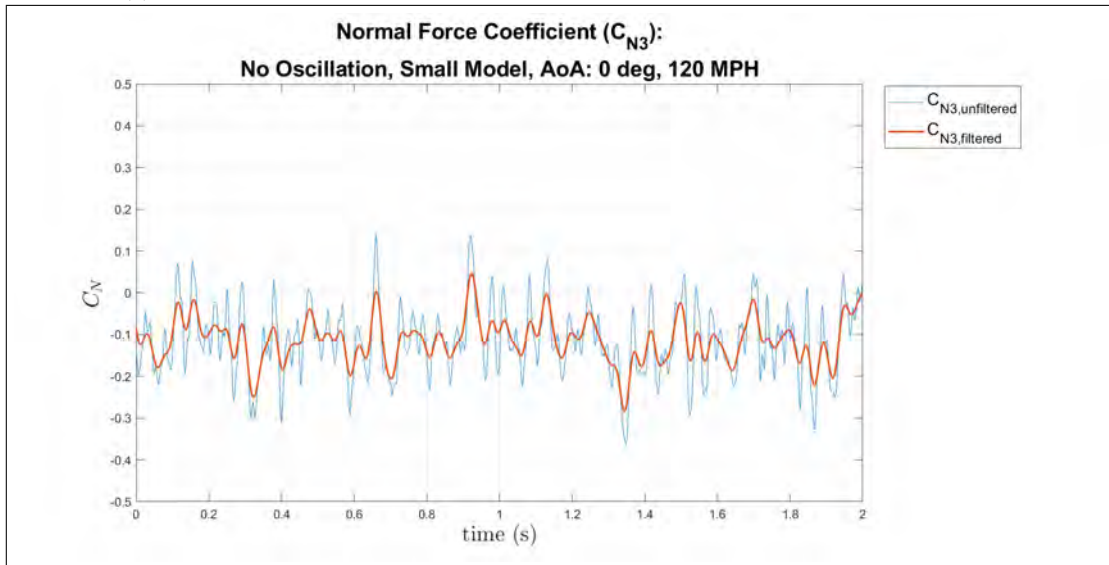
Individual Examples 0 Degrees

Normal Force, Pitch Moment, and Axial Force Coefficients

Small Model, Cavity Apparatus, 0° AoA, 120 MPH

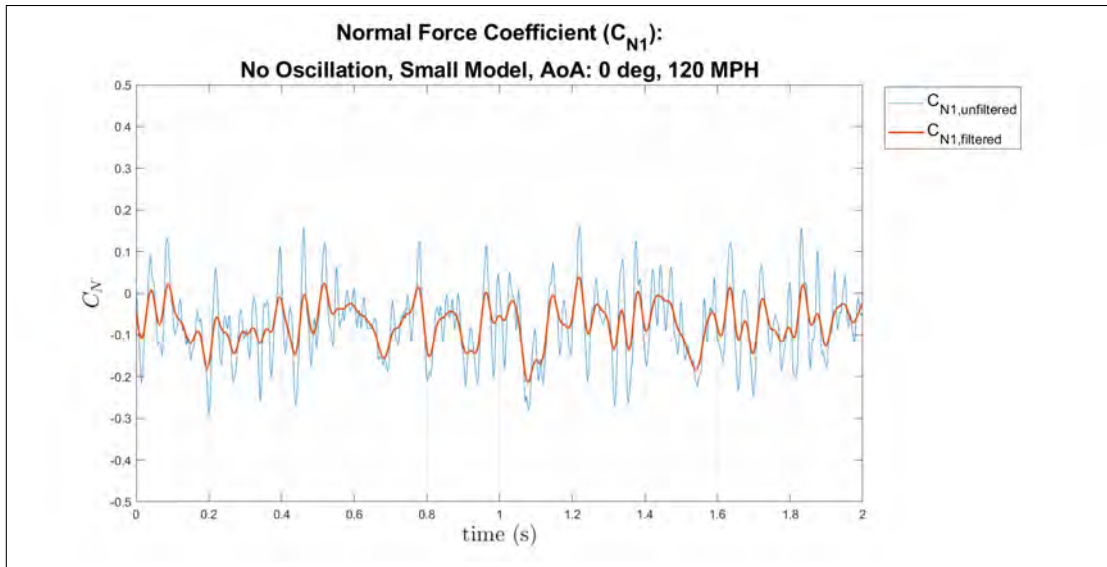


(a) Normal Force Coefficient, small model, 0° AoA, 120 MPH, In Cavity, individual trial

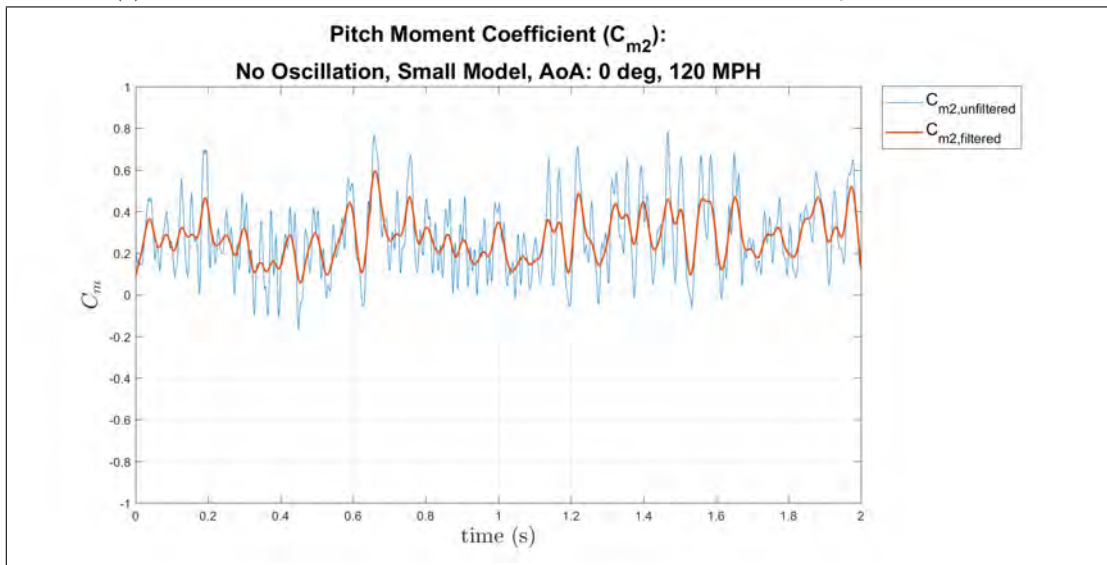


(b) Normal Force Coefficient, small model, 0° AoA, 120 MPH, Shear Layer, individual trial

Figure 255: Small model at 0° AoA of the normal force coefficient, 120 MPH, individual trial

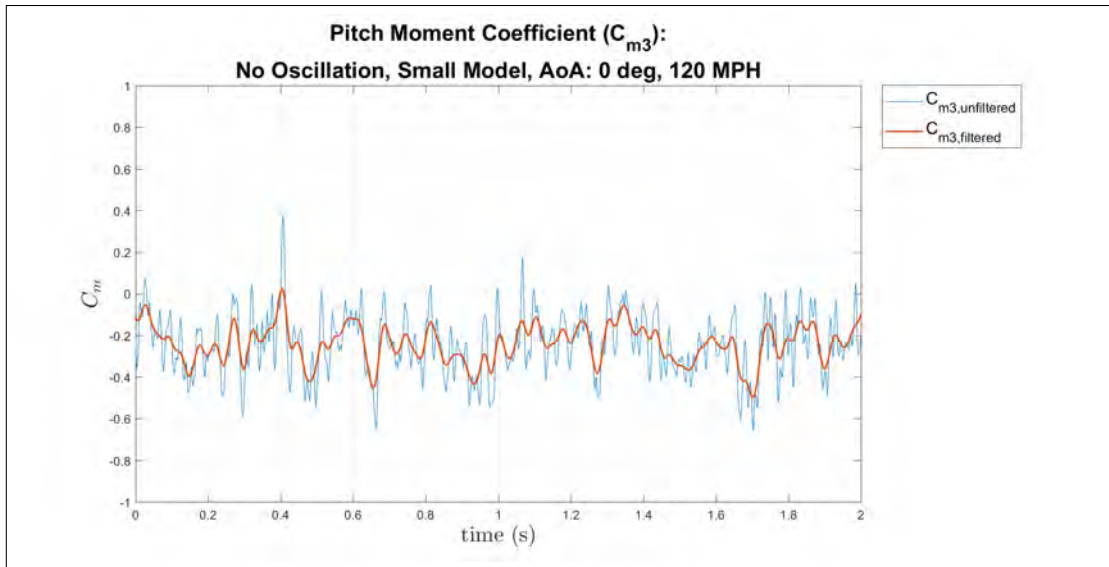


(a) Normal Force Coefficient, small model, 0° AoA, 120 MPH, Out Cavity, individual trial

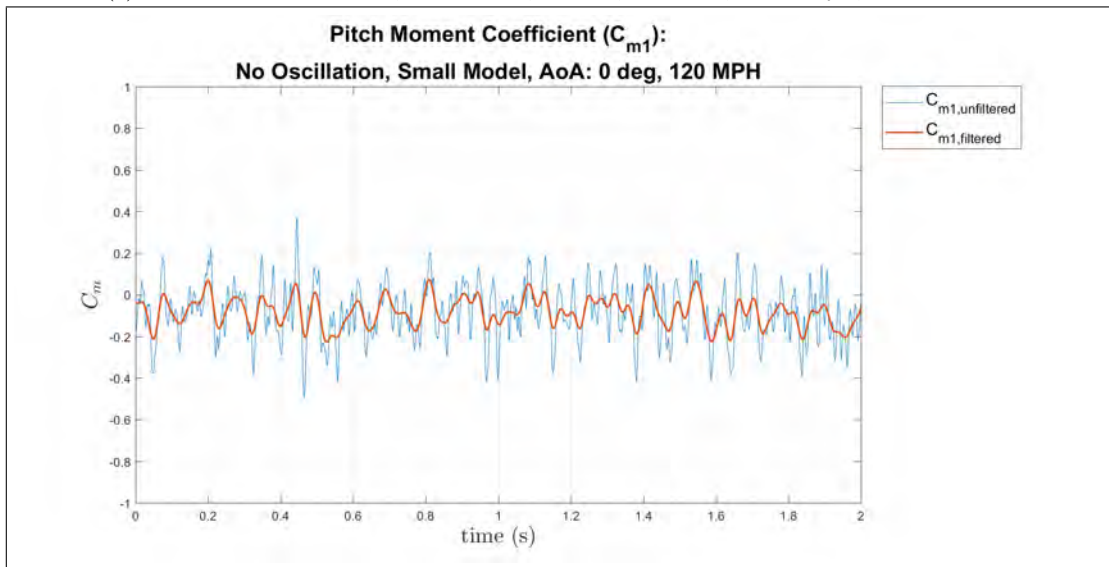


(b) Pitch Moment Coefficient, small model, 0° AoA, 120 MPH, In Cavity, individual trial

Figure 256: Small model at 0° AoA of the pitch moment and normal force coefficients, 120 MPH, individual trial

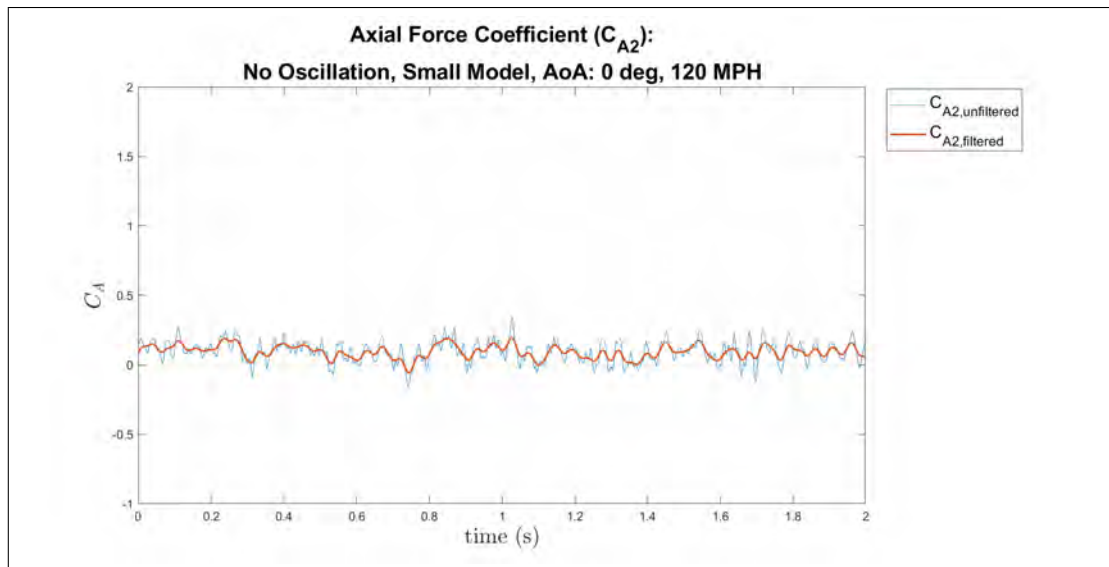


(a) Pitch Moment Coefficient, small model, 0° AoA, 120 MPH, Shear Layer, individual trial

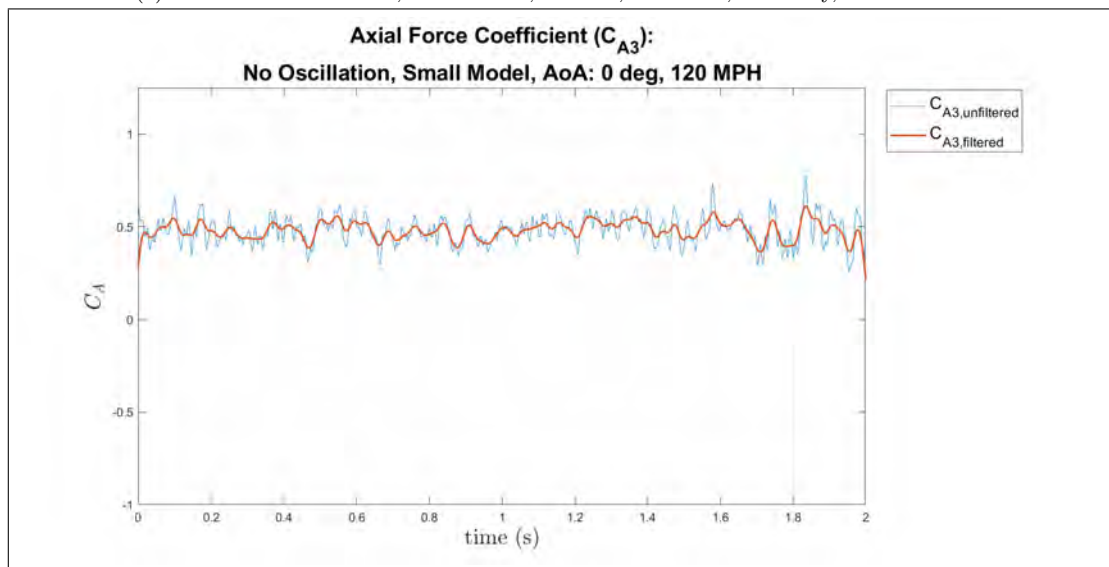


(b) Pitch Moment Coefficient, small model, 0° AoA, 120 MPH, Out Cavity, individual trial

Figure 257: Small model at 0° AoA of the pitch moment coefficient, 120 MPH, individual trial

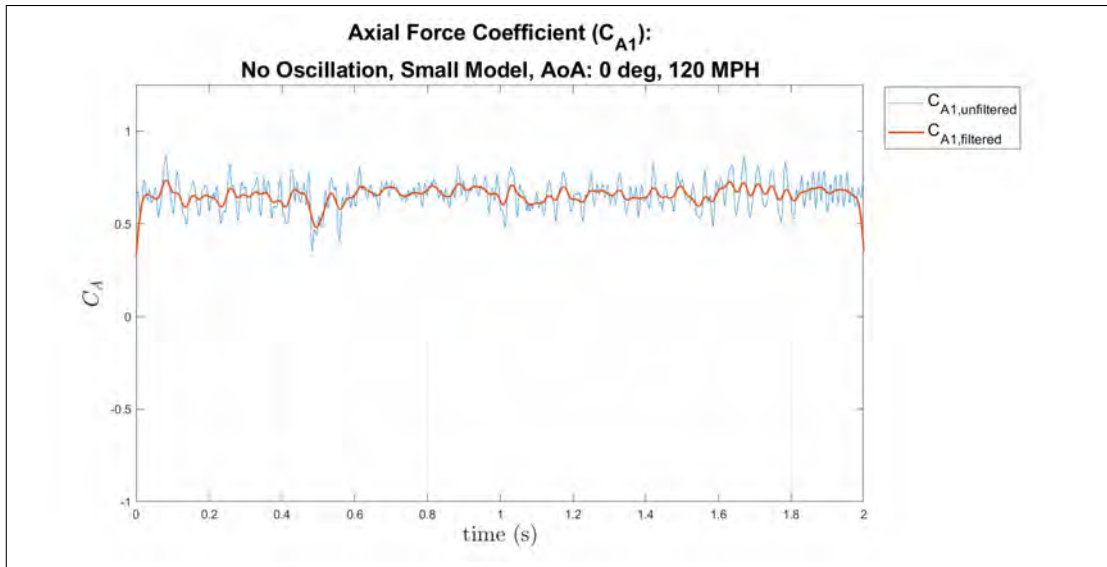


(a) Axial Force Coefficient, small model, 0° AoA, 120 MPH, In Cavity, individual trial

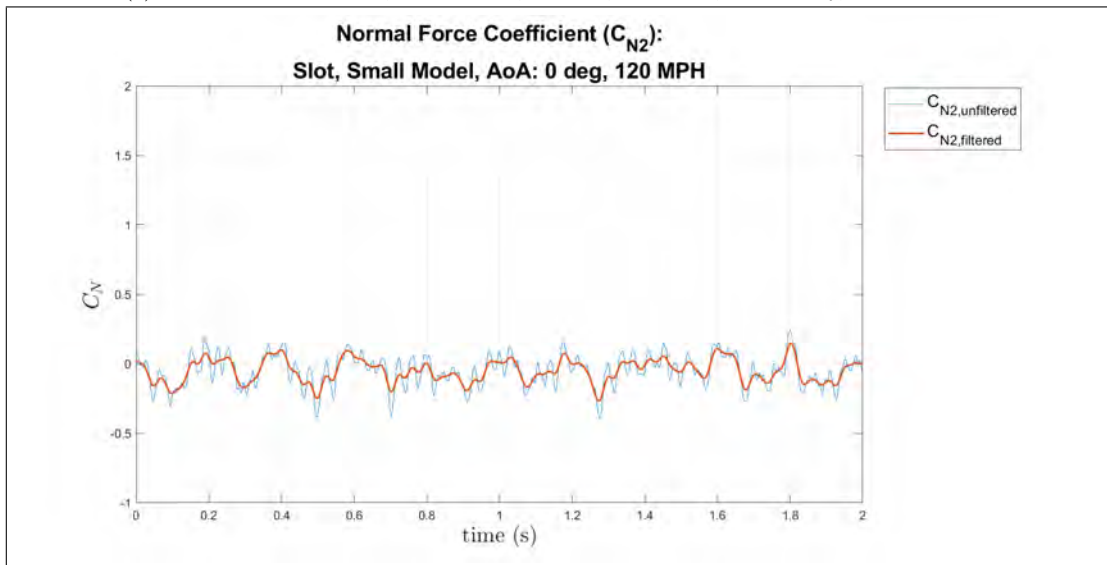


(b) Axial Force Coefficient, small model, 0° AoA, 120 MPH, Shear Layer, individual trial

Figure 258: Small model at 0° AoA of the Axial Force coefficient, 120 MPH, individual trial

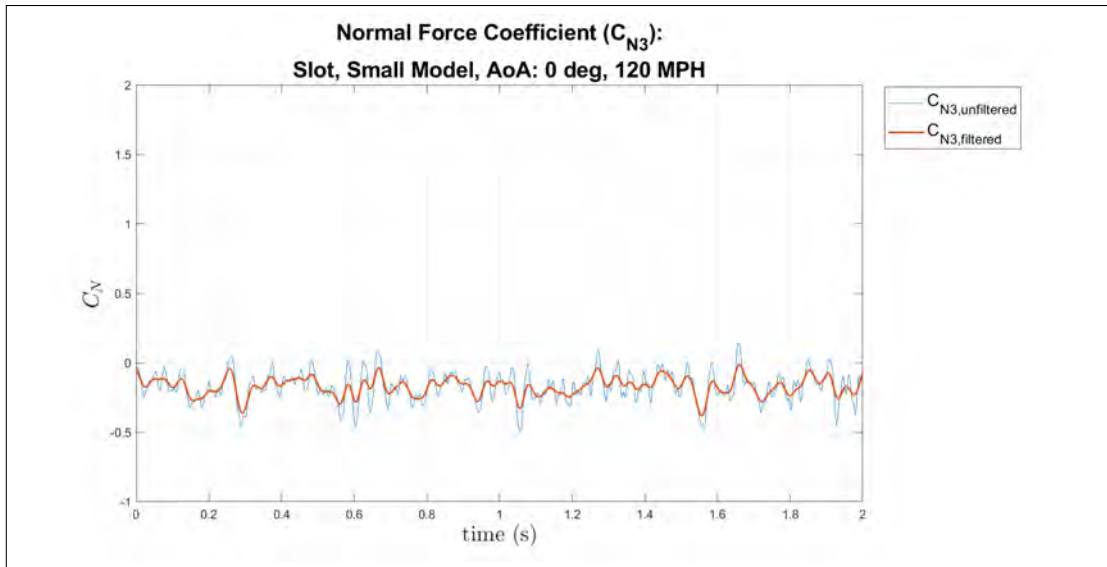


(a) Axial Force Coefficient, small model, 0° AoA, 120 MPH, Out Cavity, individual trial

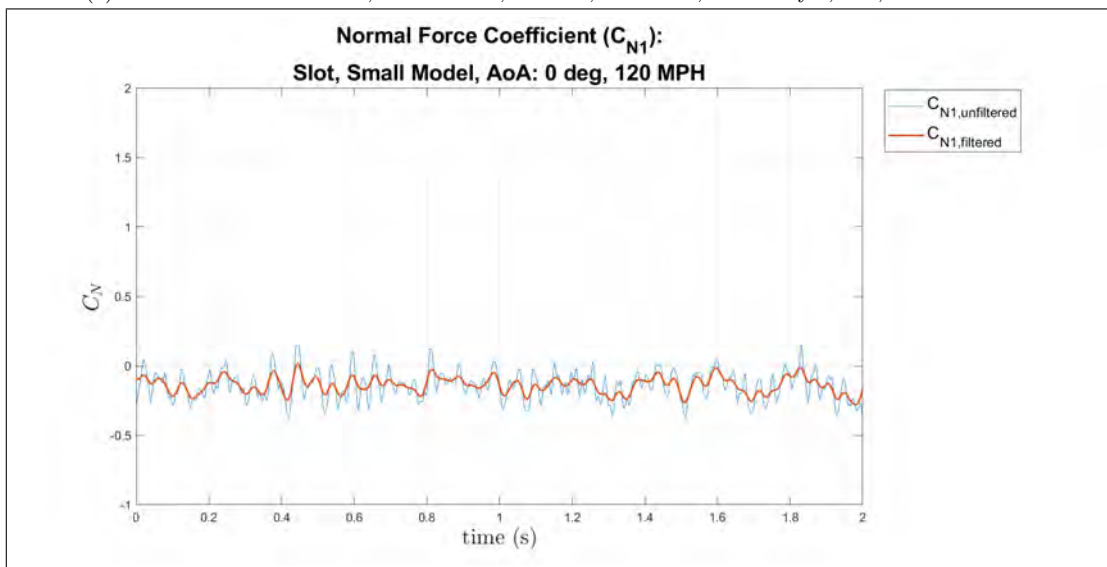


(b) Normal Force Coefficient, small model, 0° AoA, 120 MPH, In Cavity, slot, individual trial

Figure 259: Small model at 0° AoA of the axial force and normal force coefficients, 120 MPH, individual trial

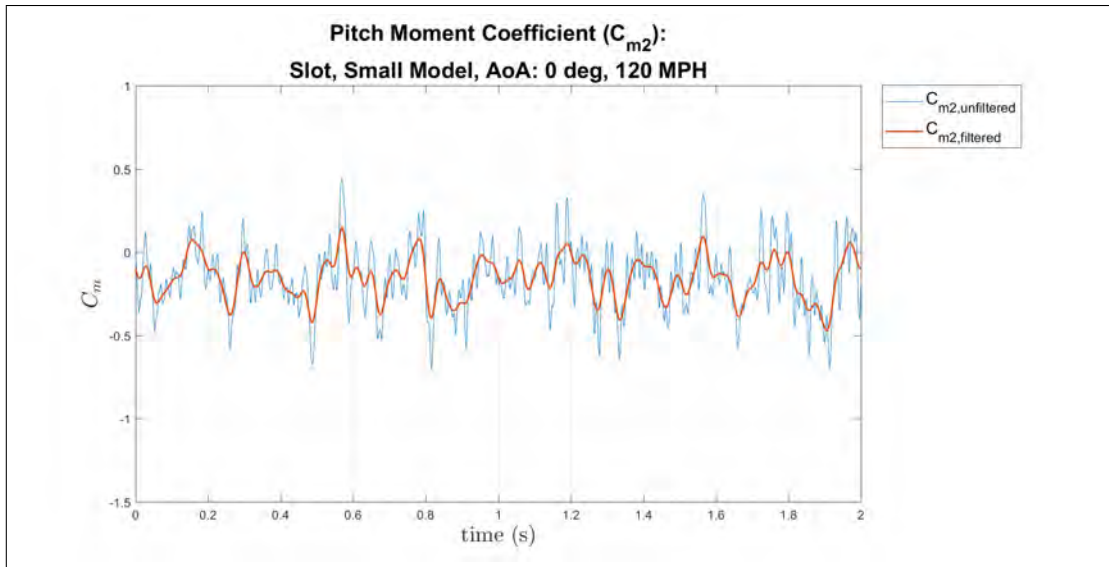


(a) Normal Force Coefficient, small model, 0° AoA, 120 MPH, Shear Layer, slot, individual trial

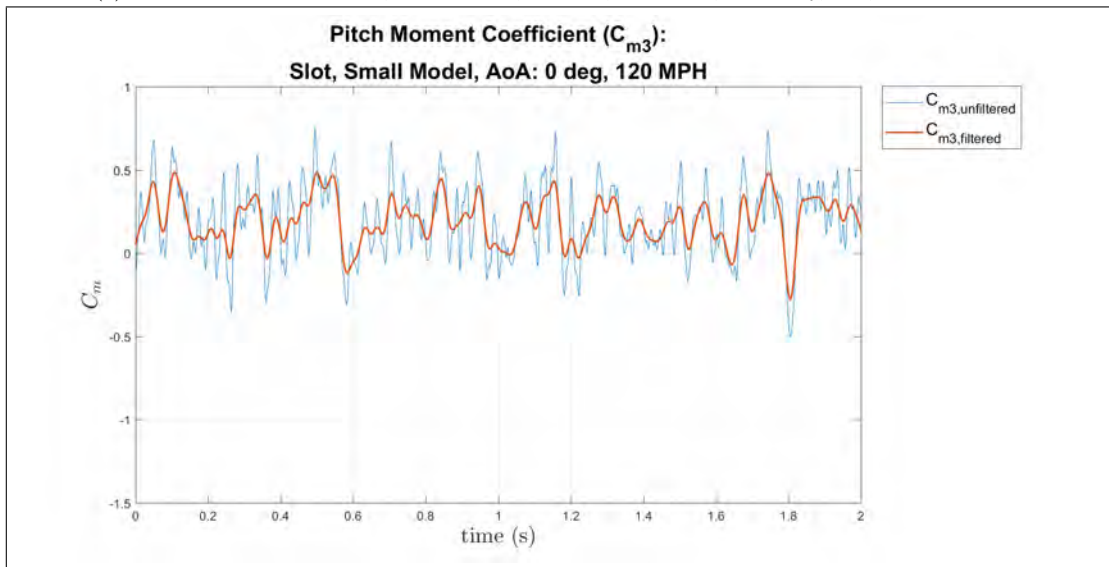


(b) Normal Force Coefficient, small model, 0° AoA, 120 MPH, Out Cavity, slot, individual trial

Figure 260: Small model at 0° AoA of the normal force coefficient, 120 MPH, slot, individual trial

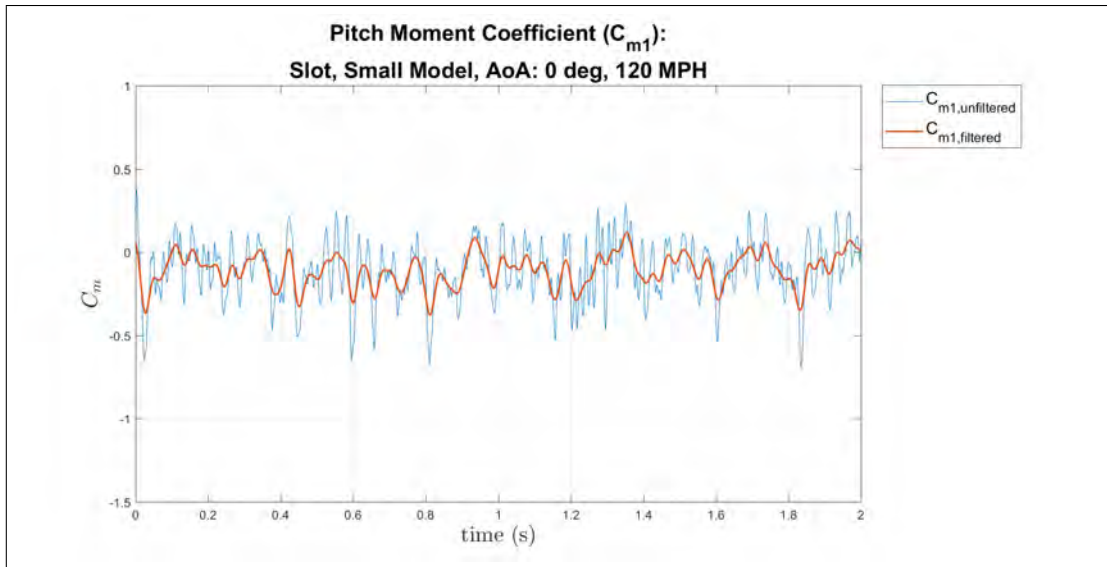


(a) Pitch Moment Coefficient, small model, 0° AoA, 120 MPH, In Cavity, slot, individual trial

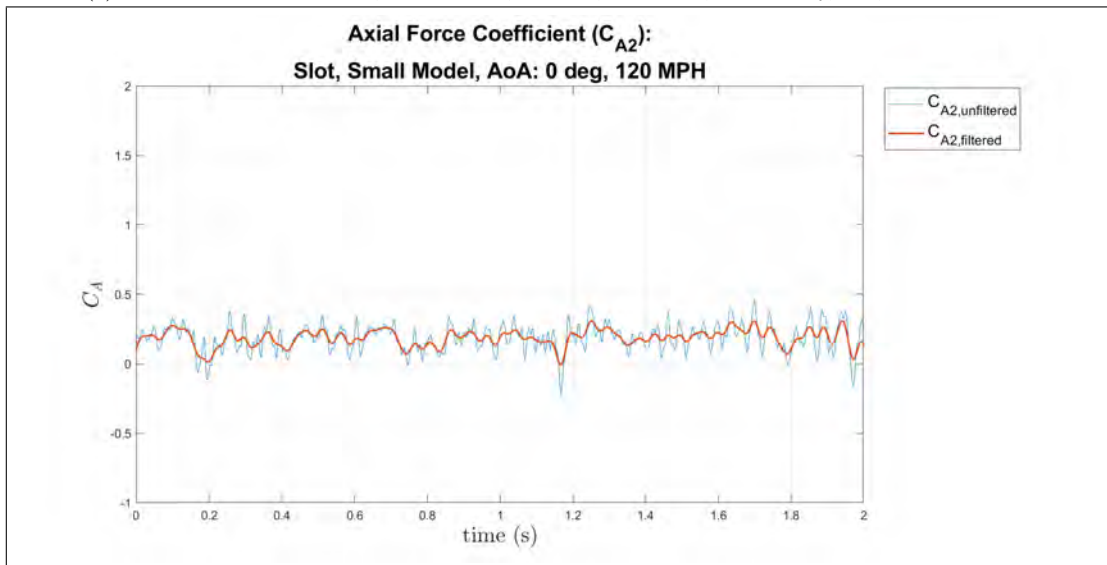


(b) Pitch Moment Coefficient, small model, 0° AoA, 120 MPH, Shear Layer, slot, individual trial

Figure 261: Small model at 0° AoA of the pitch moment coefficient, 120 MPH, slot, individual trial

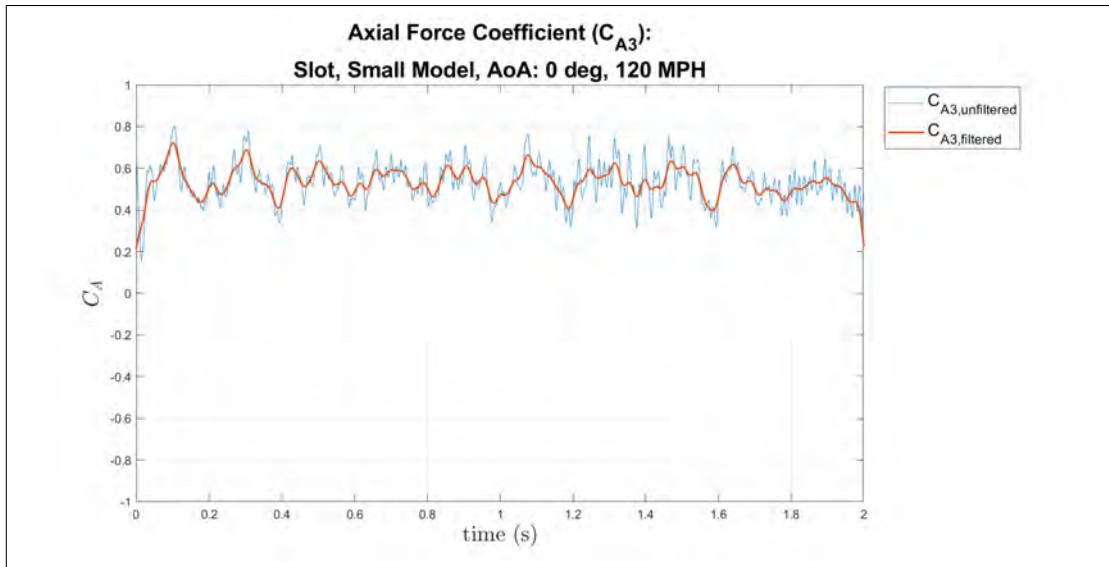


(a) Pitch Moment Coefficient, small model, 0° AoA, 120 MPH, Out Cavity, slot, individual trial

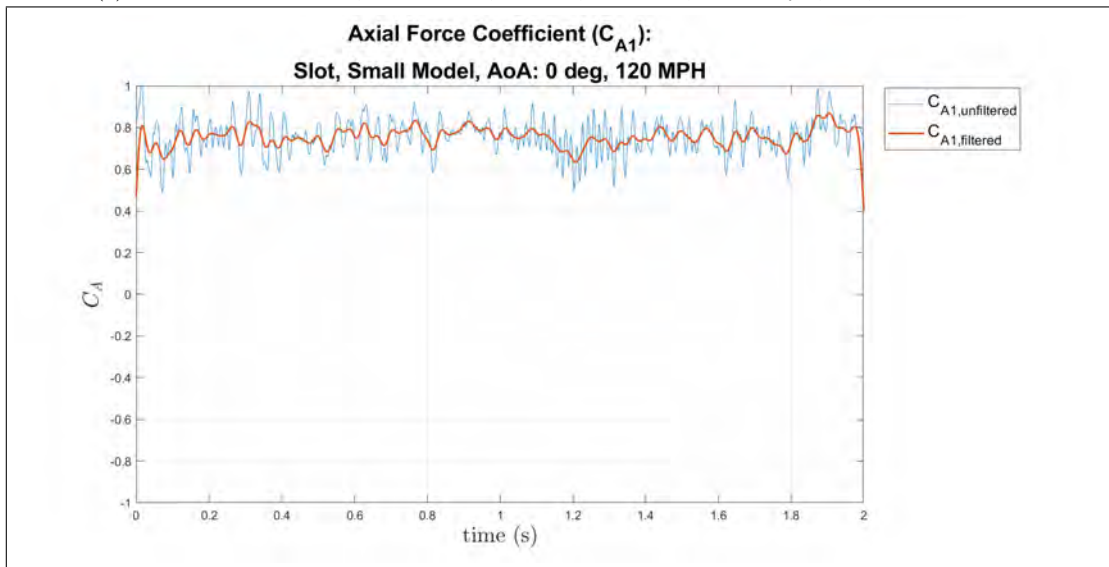


(b) Axial Force Coefficient, small model, 0° AoA, 120 MPH, In Cavity, slot, individual trial

Figure 262: Small model at 0° AoA of the pitch moment and axial force coefficients, 120 MPH, slot, individual trial



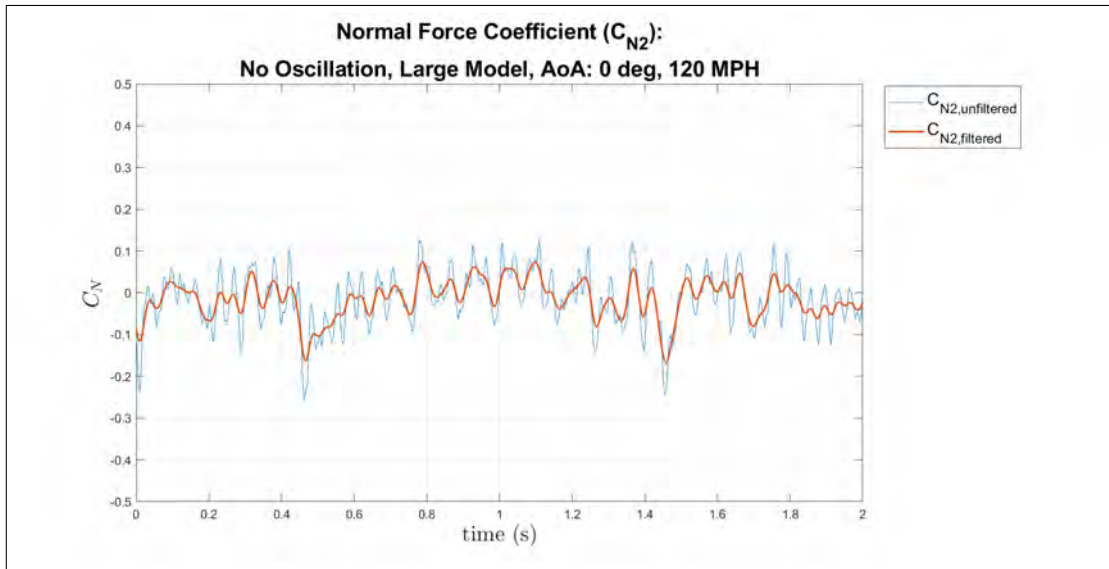
(a) Axial Force Coefficient, small model, 0° AoA, 120 MPH, Shear Layer, slot, individual trial



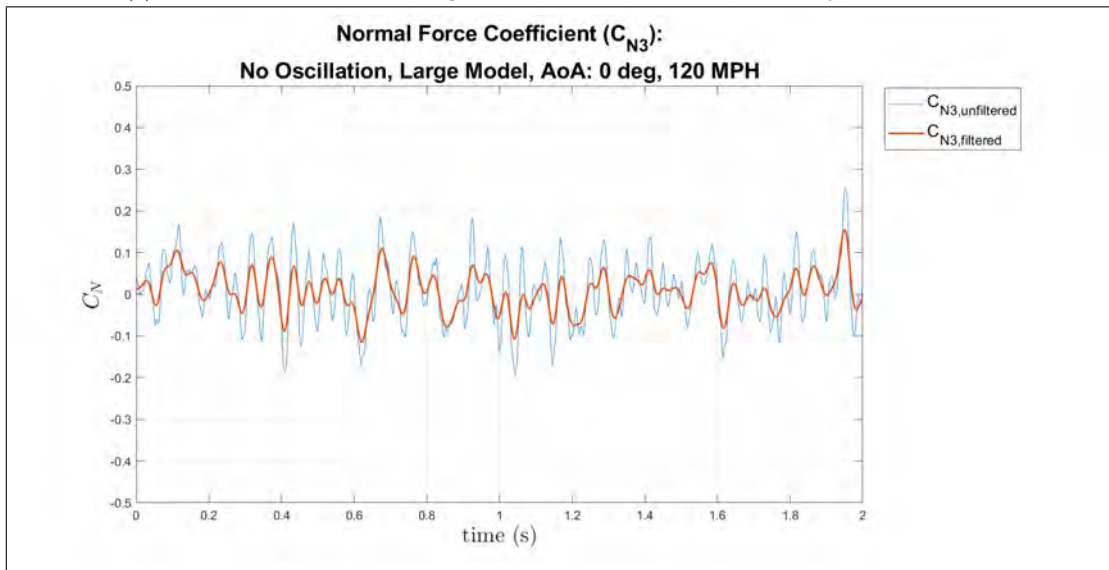
(b) Axial Force Coefficient, small model, 0° AoA, 120 MPH, Out Cavity, slot, individual trial

Figure 263: Small model at 0° AoA of the axial force coefficient, 120 MPH, slot, individual trial

Large Model, Cavity Apparatus, 0° AoA, 120 MPH

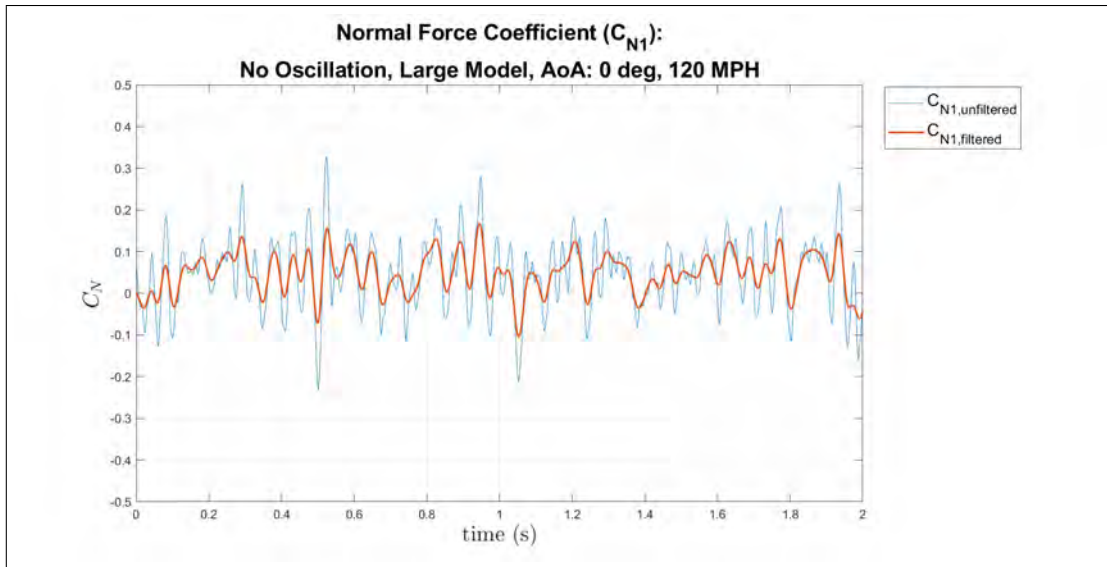


(a) Normal Force Coefficient, large model, 0° AoA, 120 MPH, In Cavity, individual trial

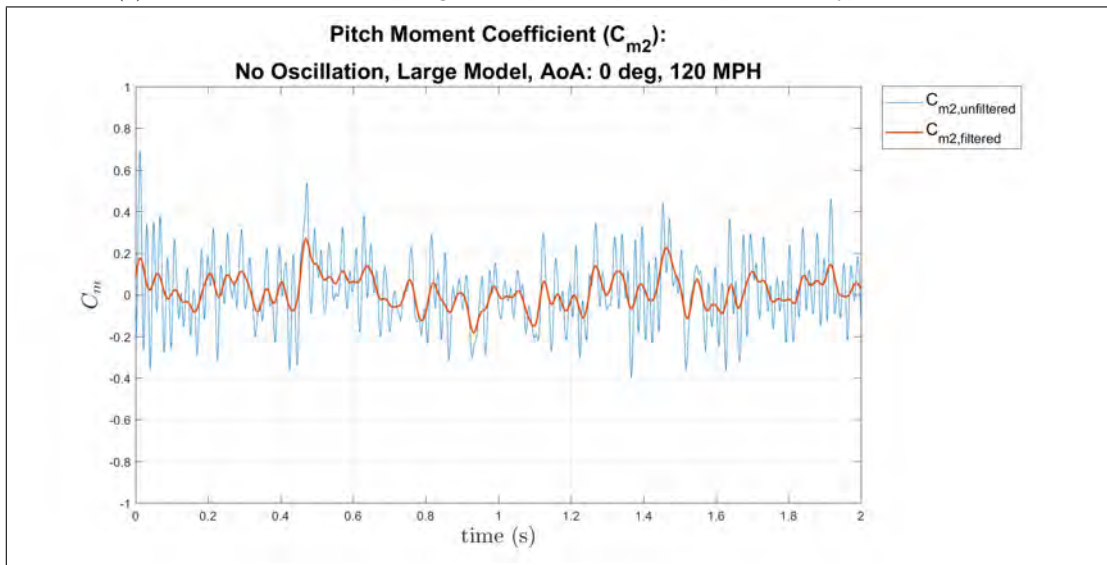


(b) Normal Force Coefficient, large model, 0° AoA, 120 MPH, Shear Layer, individual trial

Figure 264: Large model at 0° AoA of the normal force coefficient, 120 MPH, individual trial

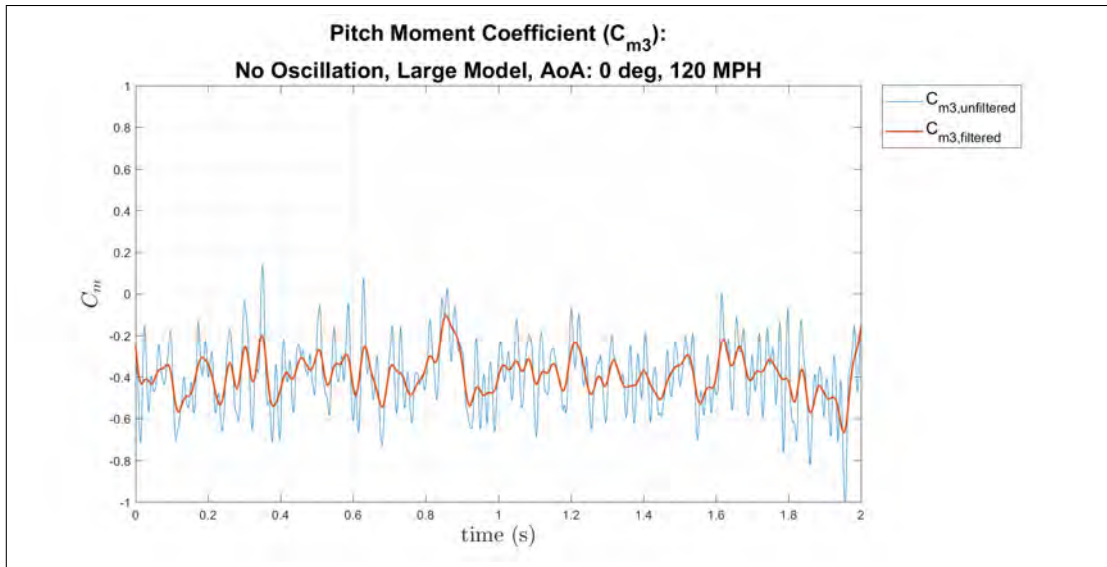


(a) Normal Force Coefficient, large model, 0° AoA, 120 MPH, Out Cavity, individual trial

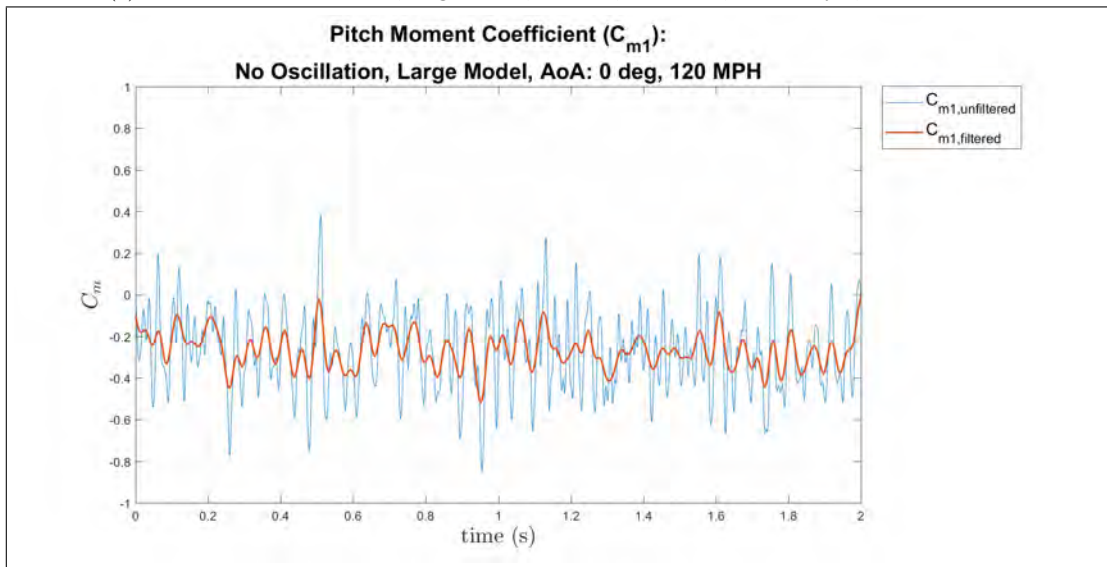


(b) Pitch Moment Coefficient, large model, 0° AoA, 120 MPH, In Cavity, individual trial

Figure 265: Large model at 0° AoA of the pitch moment and normal force coefficients, 120 MPH, individual trial

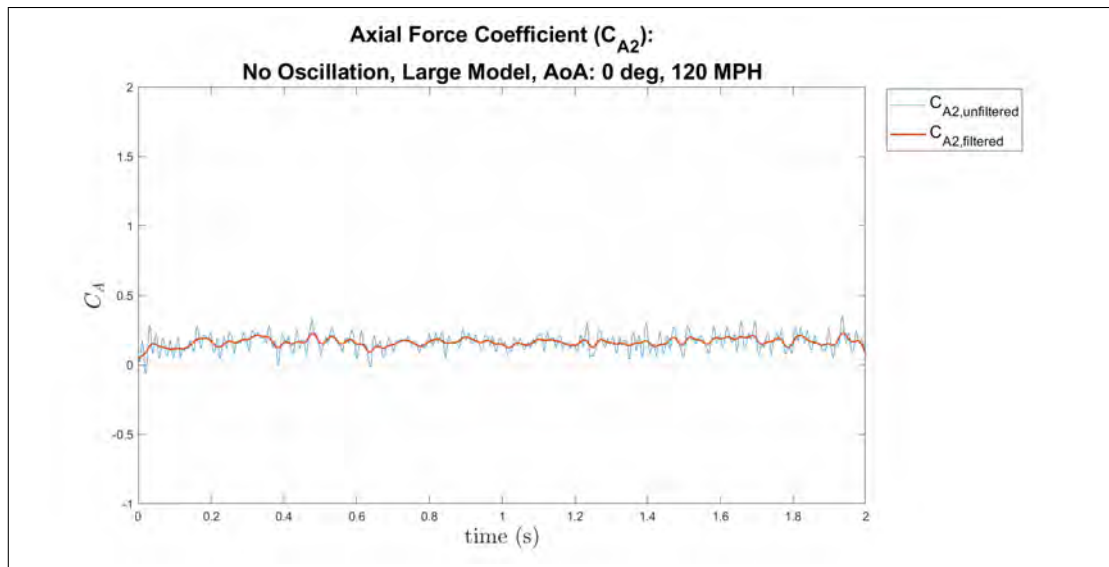


(a) Pitch Moment Coefficient, large model, 0° AoA, 120 MPH, Shear Layer, individual trial

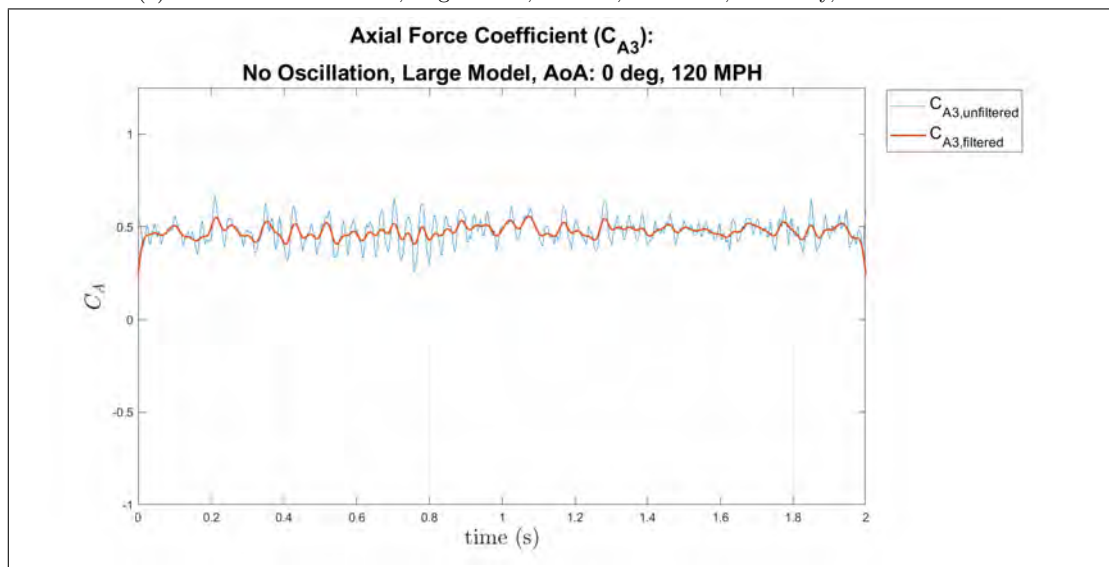


(b) Pitch Moment Coefficient, large model, 0° AoA, 120 MPH, Out Cavity, individual trial

Figure 266: Large model at 0° AoA of the pitch moment coefficient, 120 MPH, individual trial

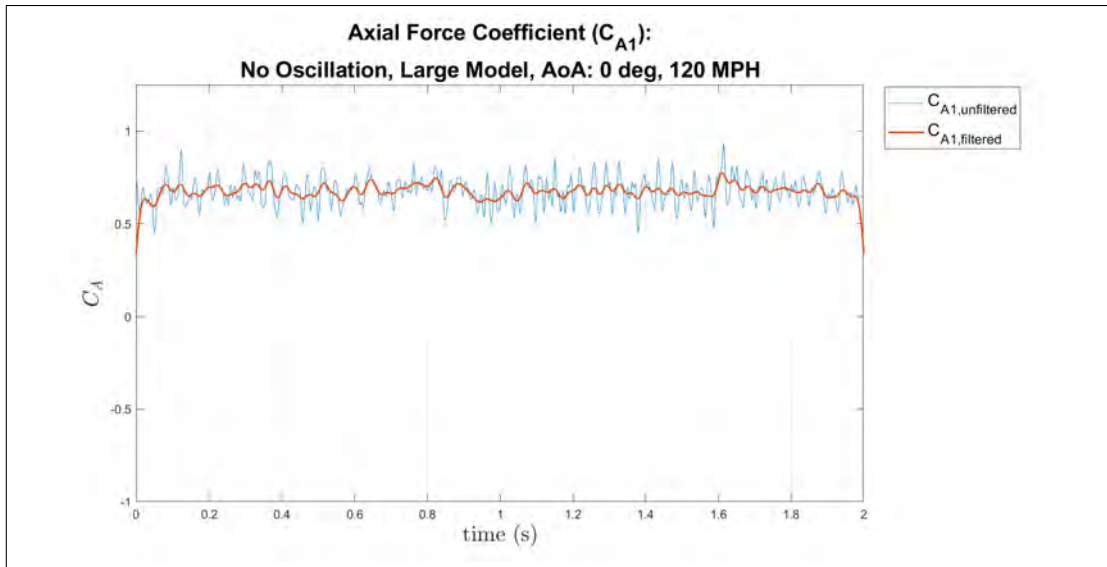


(a) Axial Force Coefficient, large model, 0° AoA, 120 MPH, In Cavity, individual trial

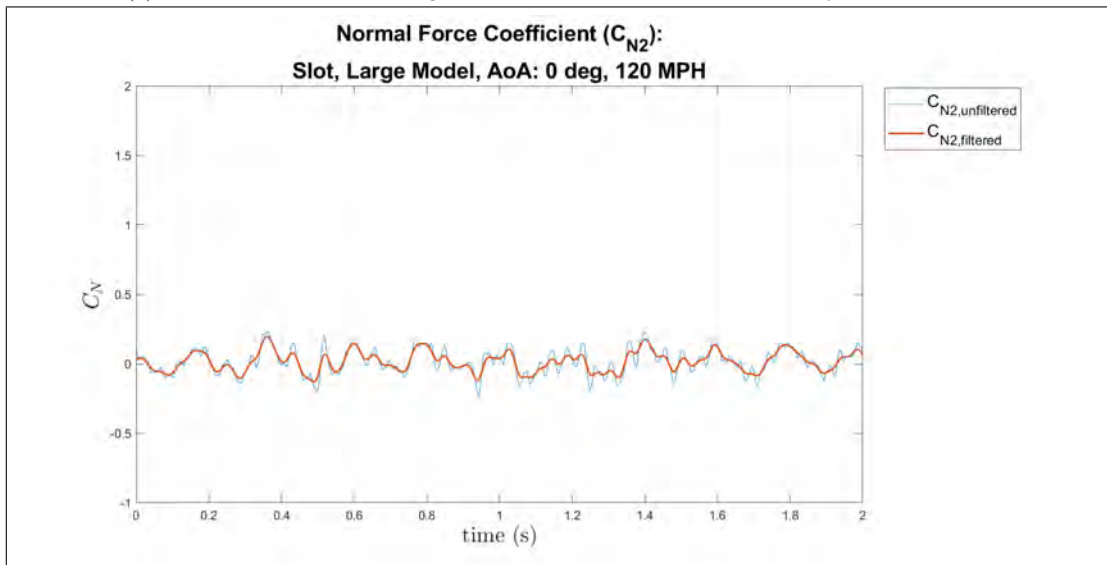


(b) Axial Force Coefficient, large model, 0° AoA, 120 MPH, Shear Layer, individual trial

Figure 267: Large model at 0° AoA of the Axial Force coefficient, 120 MPH, individual trial

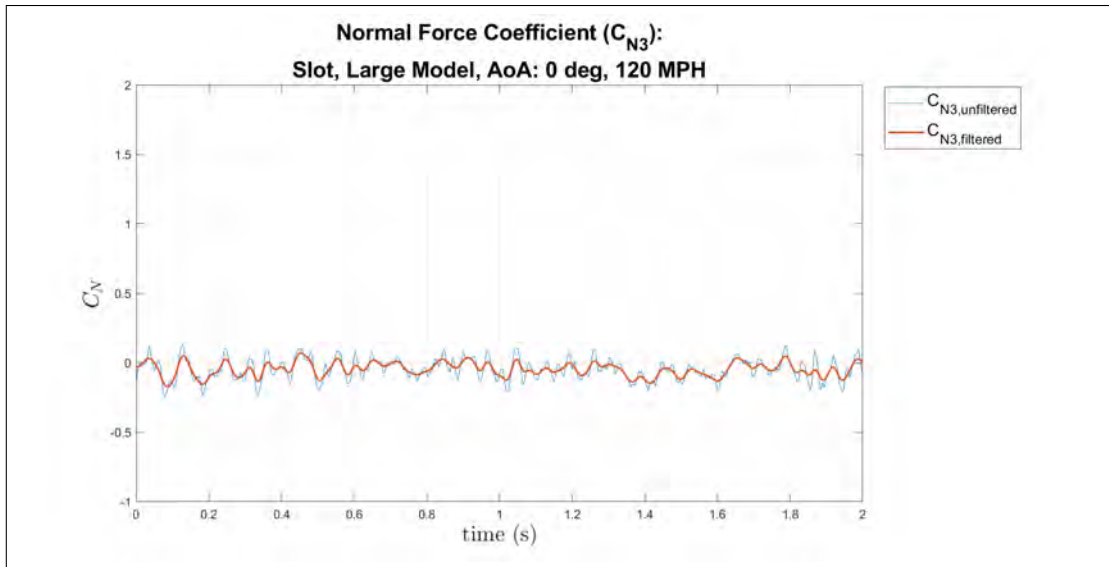


(a) Axial Force Coefficient, large model, 0° AoA, 120 MPH, Out Cavity, individual trial

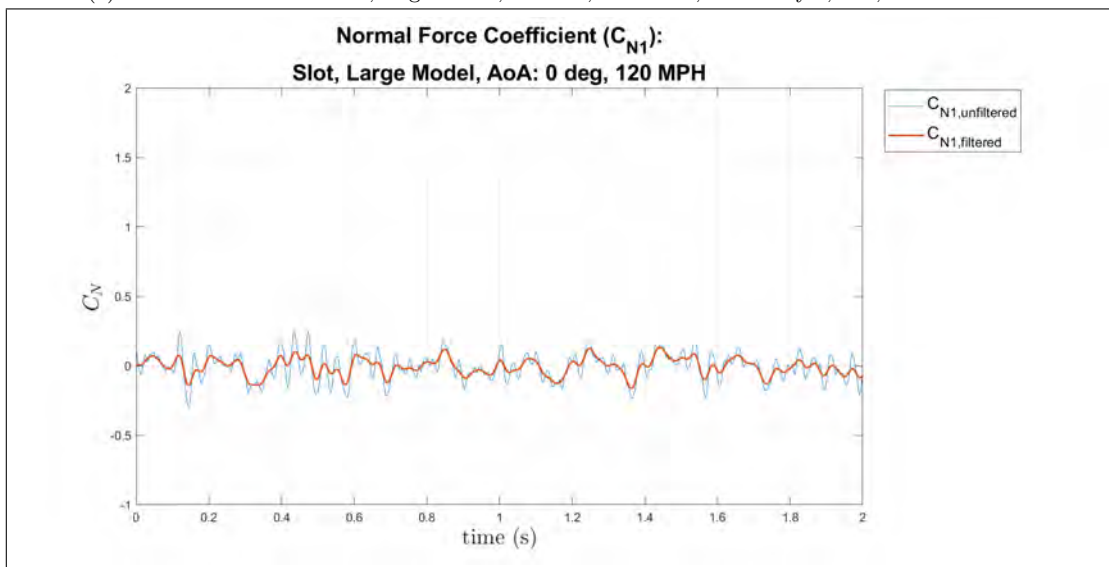


(b) Normal Force Coefficient, large model, 0° AoA, 120 MPH, In Cavity, slot, individual trial

Figure 268: Large model at 0° AoA of the axial force and normal force coefficients, 120 MPH, individual trial

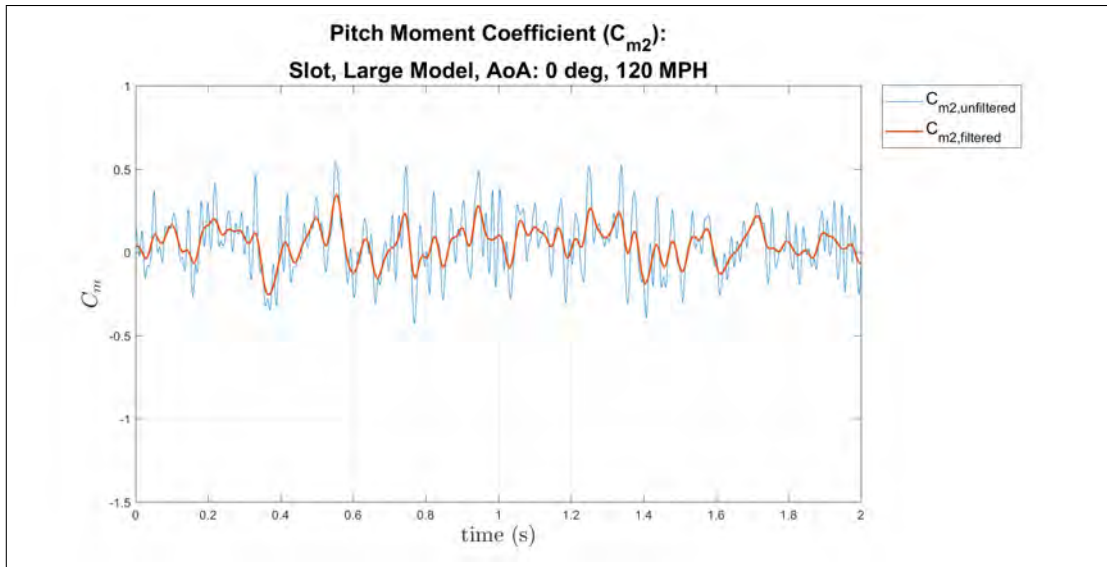


(a) Normal Force Coefficient, large model, 0° AoA, 120 MPH, Shear Layer, slot, individual trial

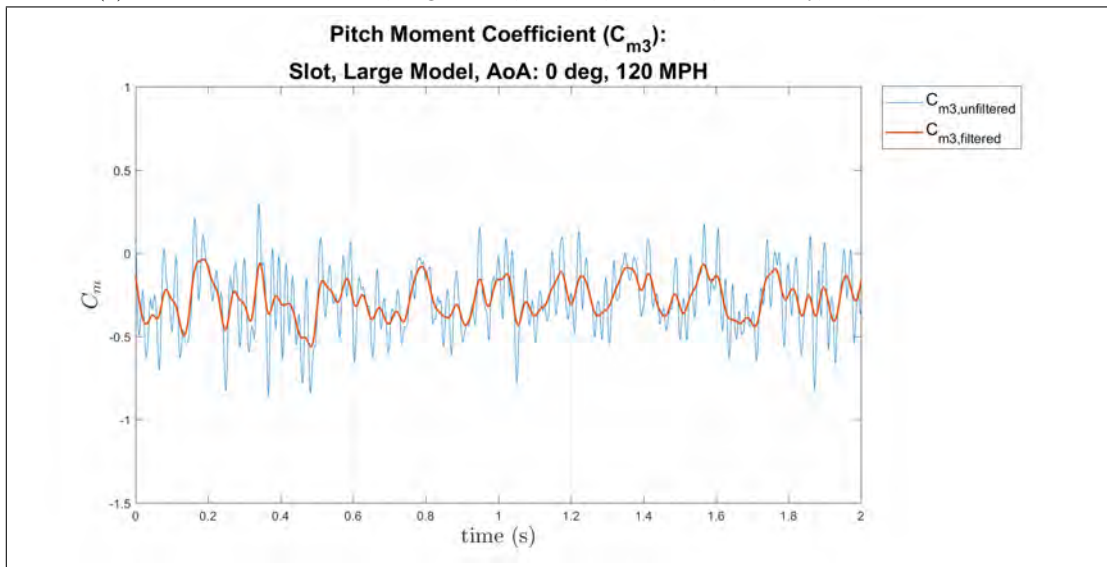


(b) Normal Force Coefficient, large model, 0° AoA, 120 MPH, Out Cavity, slot, individual trial

Figure 269: Large model at 0° AoA of the normal force coefficient, 120 MPH, slot, individual trial

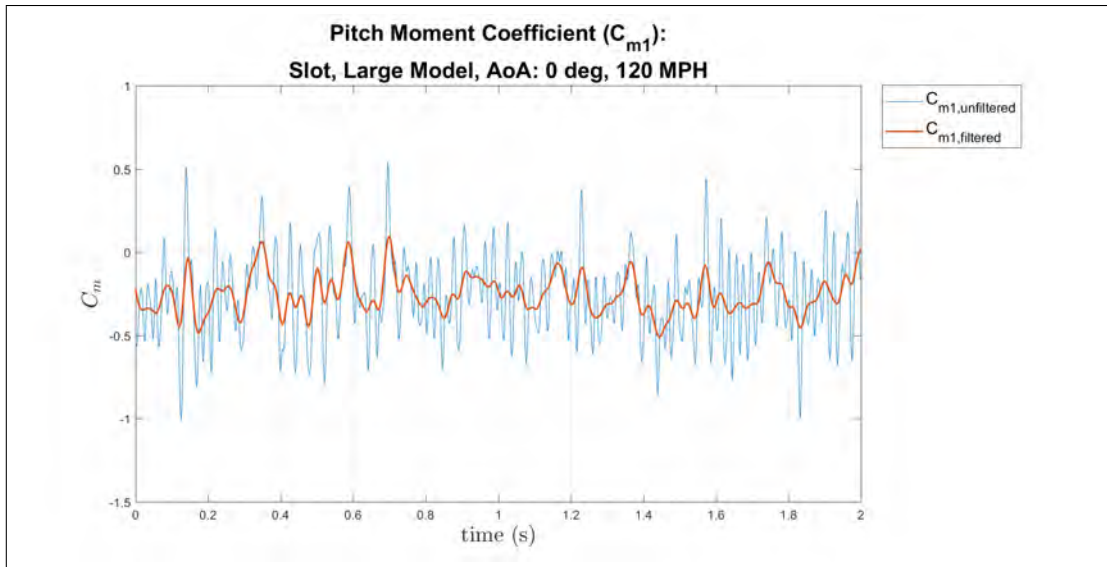


(a) Pitch Moment Coefficient, large model, 0° AoA, 120 MPH, In Cavity, slot, individual trial

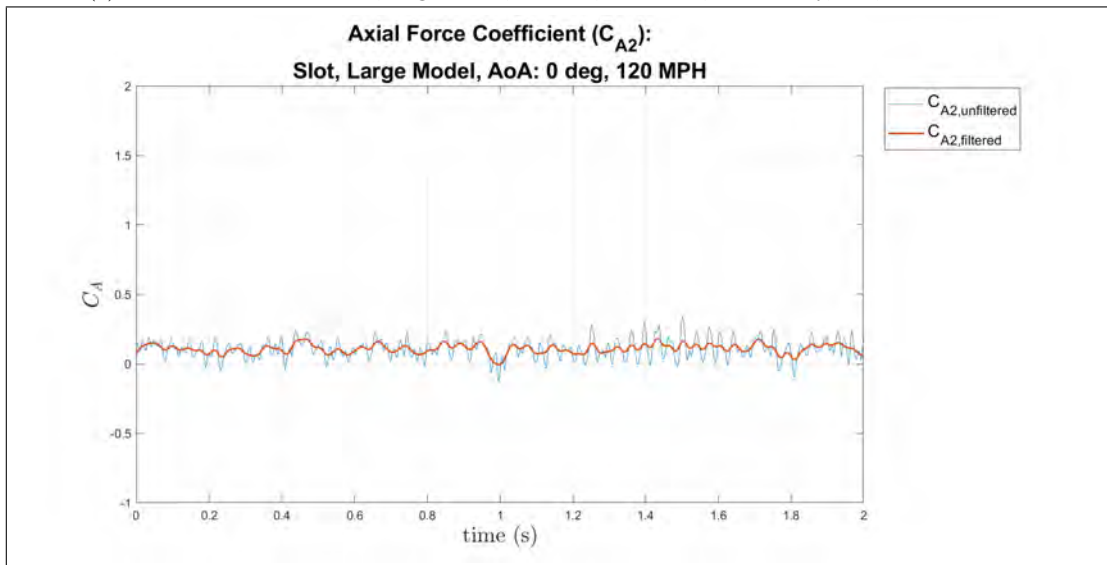


(b) Pitch Moment Coefficient, large model, 0° AoA, 120 MPH, Shear Layer, slot, individual trial

Figure 270: Large model at 0° AoA of the pitch moment coefficient, 120 MPH, slot, individual trial

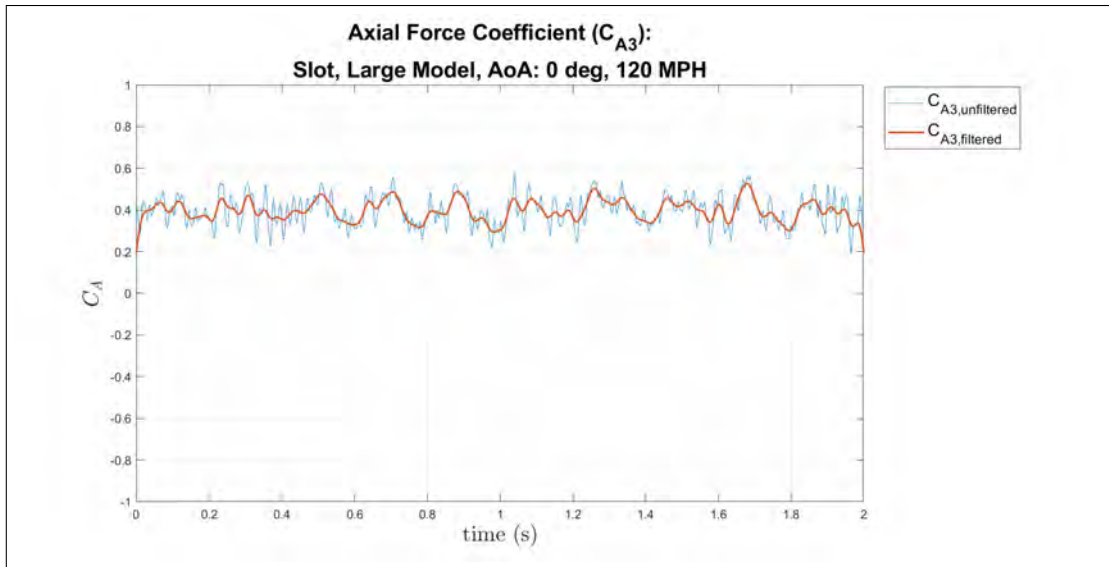


(a) Pitch Moment Coefficient, large model, 0° AoA, 120 MPH, Out Cavity, slot, individual trial

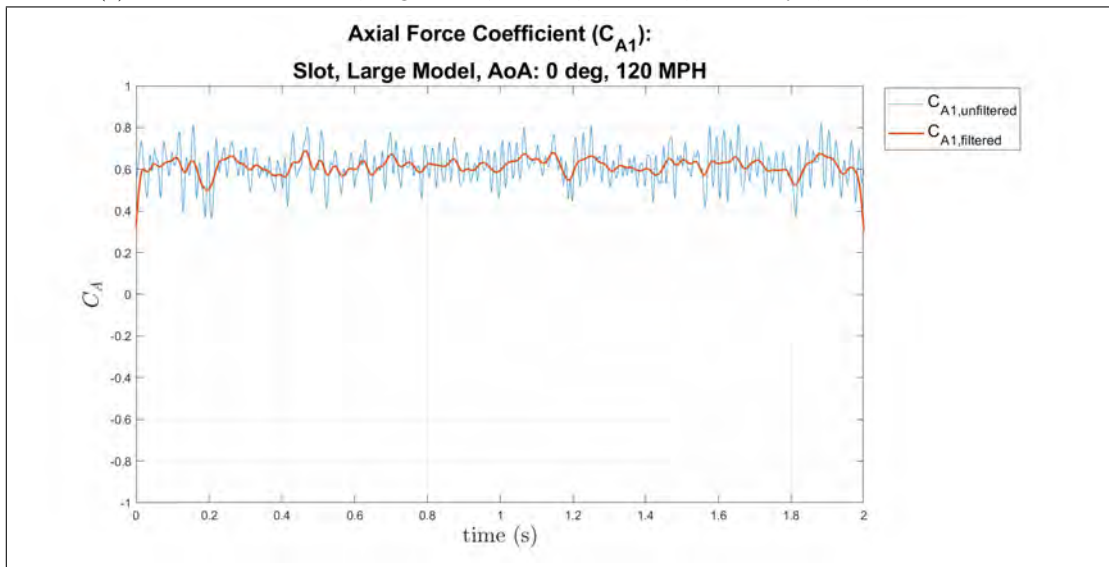


(b) Axial Force Coefficient, large model, 0° AoA, 120 MPH, In Cavity, slot, individual trial

Figure 271: Large model at 0° AoA of the pitch moment and axial force coefficients, 120 MPH, slot, individual trial



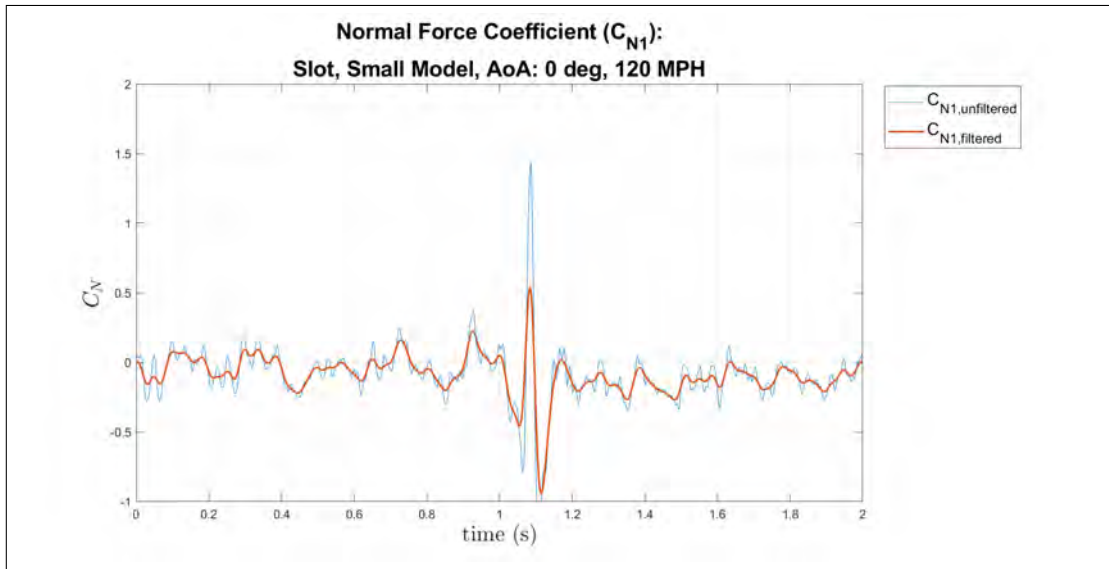
(a) Axial Force Coefficient, large model, 0° AoA, 120 MPH, Shear Layer, slot, individual trial



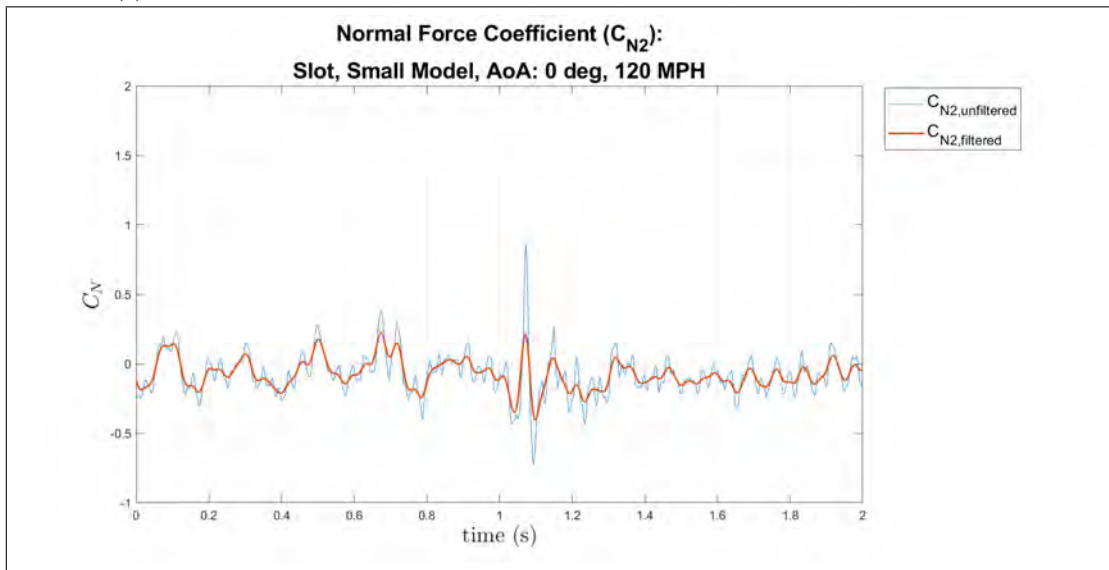
(b) Axial Force Coefficient, large model, 0° AoA, 120 MPH, Out Cavity, slot, individual trial

Figure 272: Large model at 0° AoA of the axial force coefficient, 120 MPH, slot, individual trial

Small Model, Dynamic Release, 0° AoA, 120 MPH

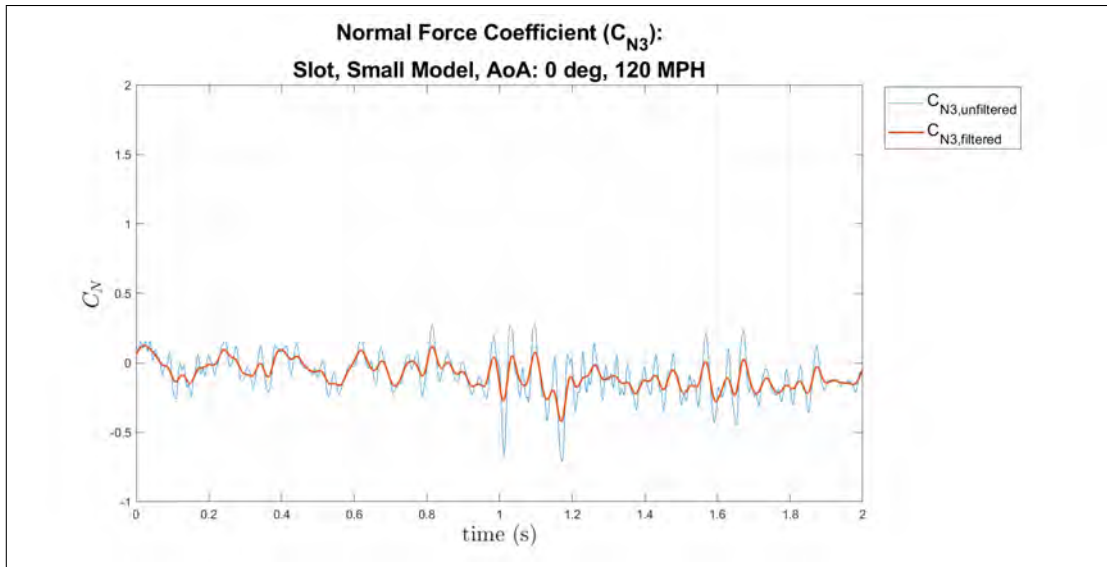


(a) Normal Force Coefficient, small model, 0° AoA, 120 MPH, release one, individual trial

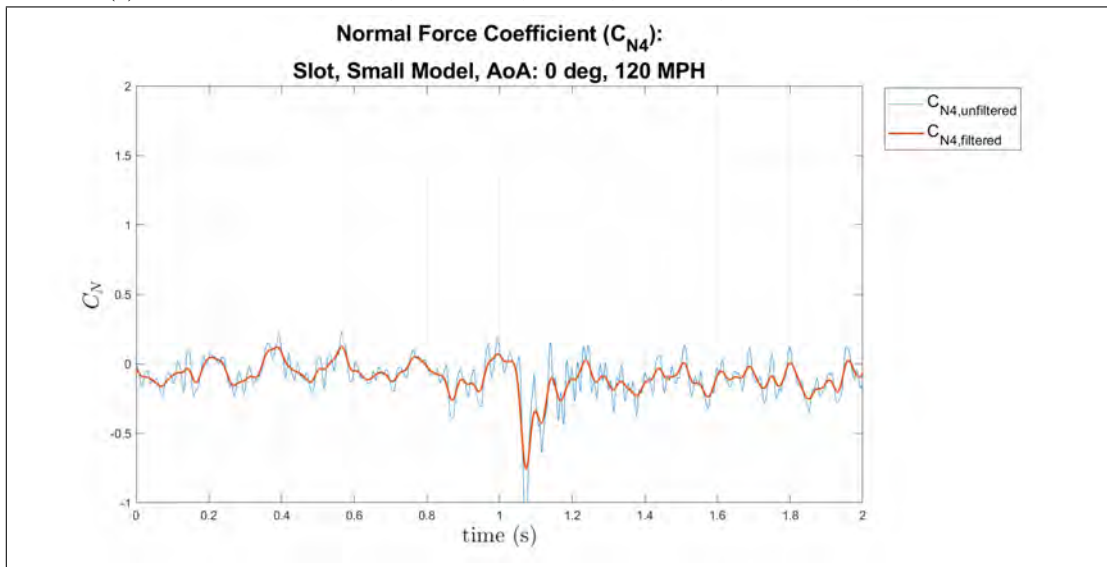


(b) Normal Force Coefficient, small model, 0° AoA, 120 MPH, release two, individual trial

Figure 273: Small model at 0° AoA of the normal force coefficient, release times one and two, 120 MPH, individual trial

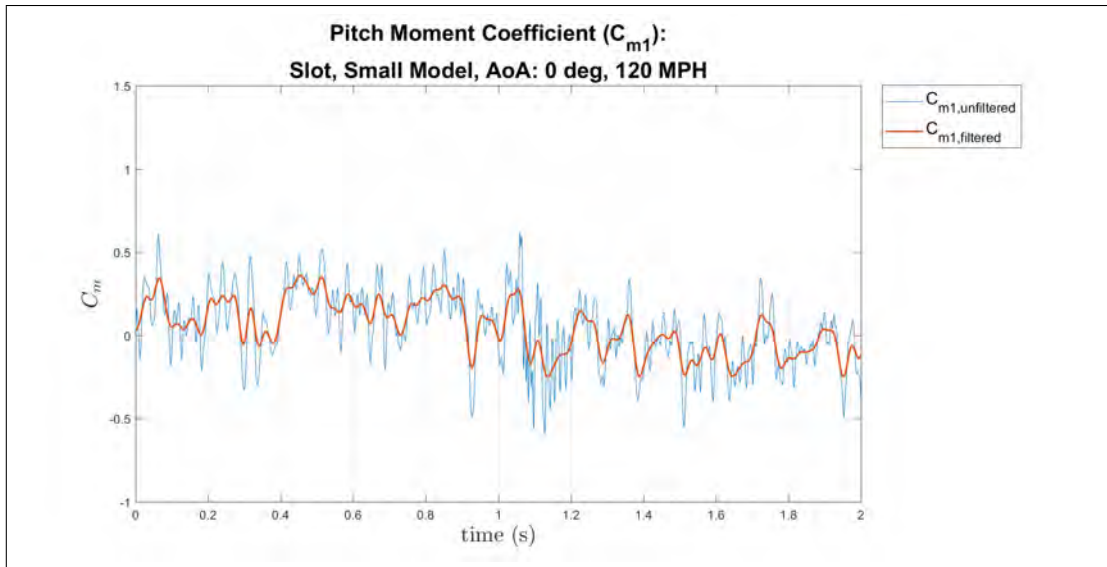


(a) Normal Force Coefficient, small model, 0° AoA, 120 MPH, release three, individual trial

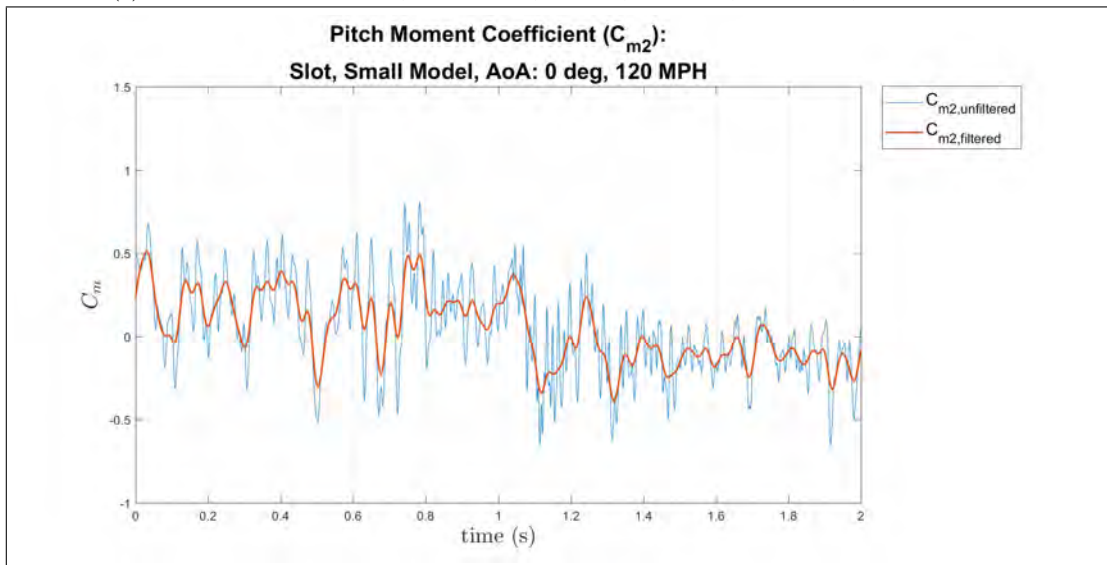


(b) Normal Force Coefficient, small model, 0° AoA, 120 MPH, release four, individual trial

Figure 274: Small model at 0° AoA of the normal force coefficient, release times three and four, 120 MPH, individual trial

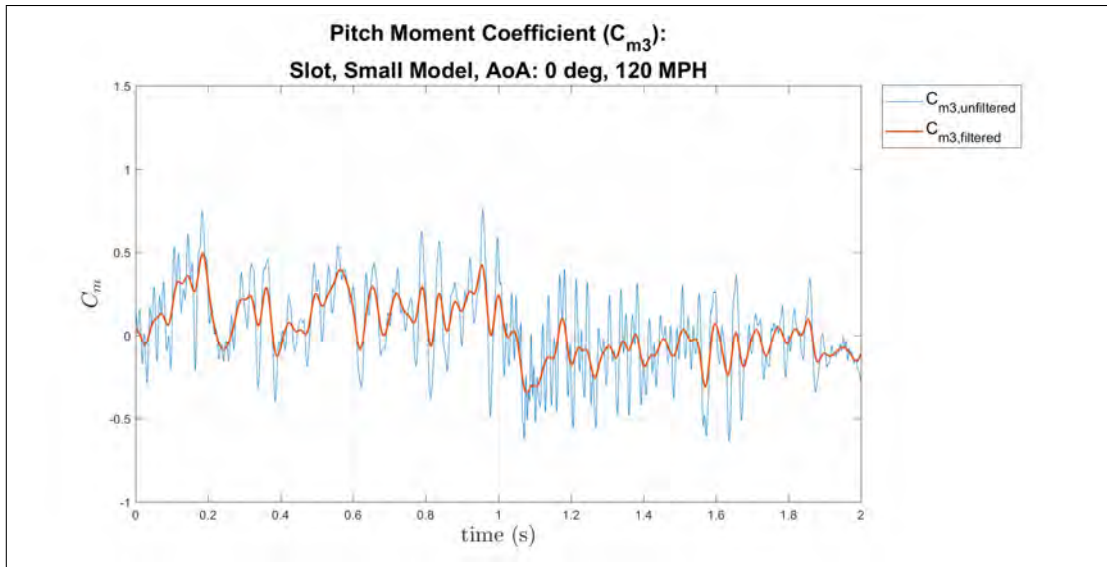


(a) Pitch Moment Coefficient, small model, 0° AoA, 120 MPH, release one, individual trial

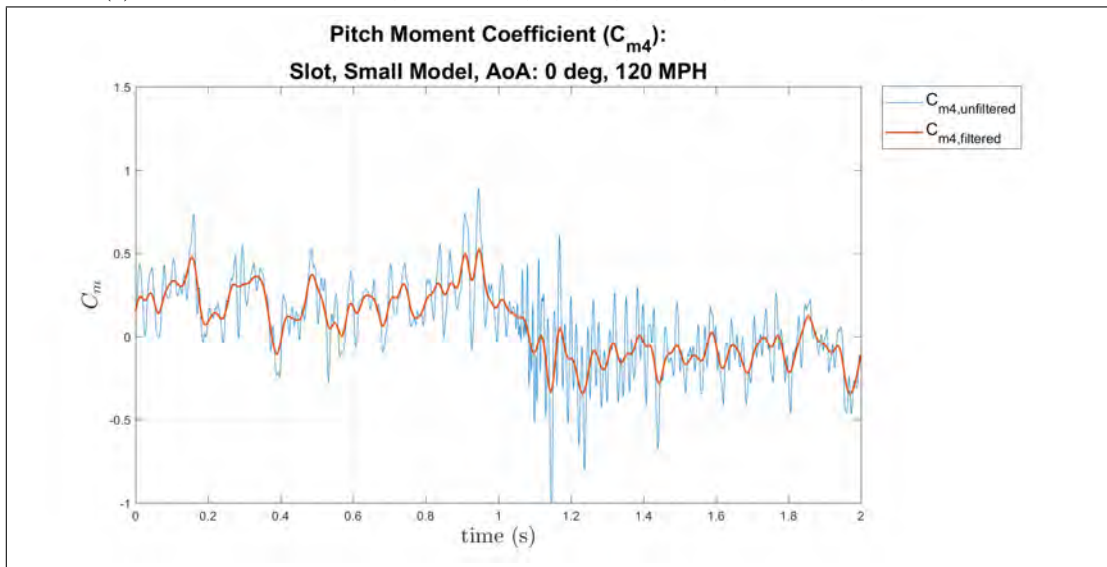


(b) Pitch Moment Coefficient, small model, 0° AoA, 120 MPH, release two, individual trial

Figure 275: Small model at 0° AoA of the pitch moment coefficient, release times one and two, 120 MPH, individual trial

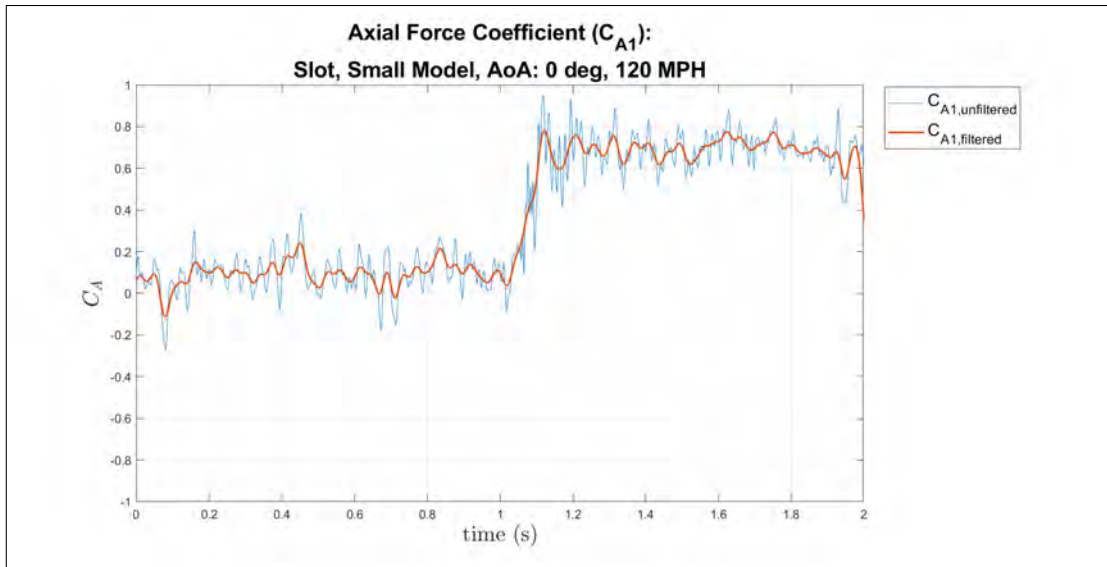


(a) Pitch Moment Coefficient, small model, 0° AoA, 120 MPH, release three, individual trial

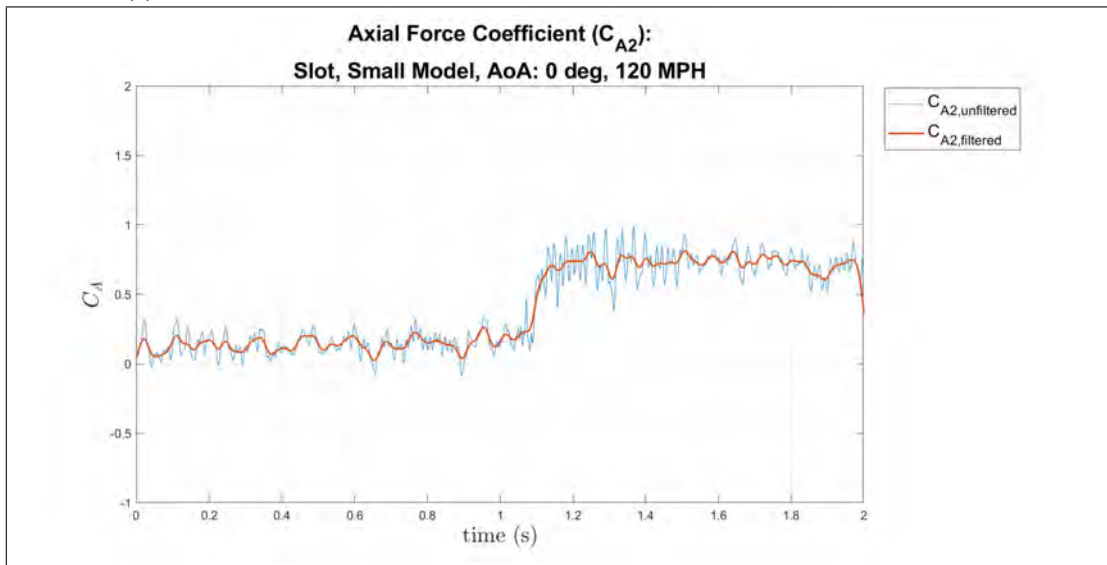


(b) Pitch Moment Coefficient, small model, 0° AoA, 120 MPH, release four, individual trial

Figure 276: Small model at 0° AoA of the pitch moment coefficient, release times three and four, 120 MPH, individual trial

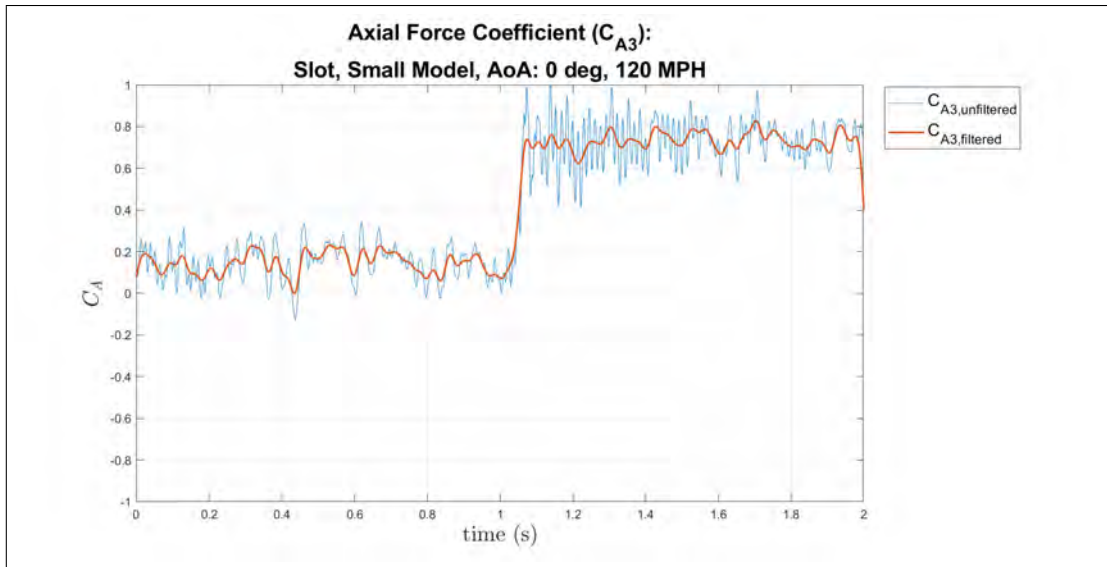


(a) Axial Force Coefficient, small model, 0° AoA, 120 MPH, release one, individual trial

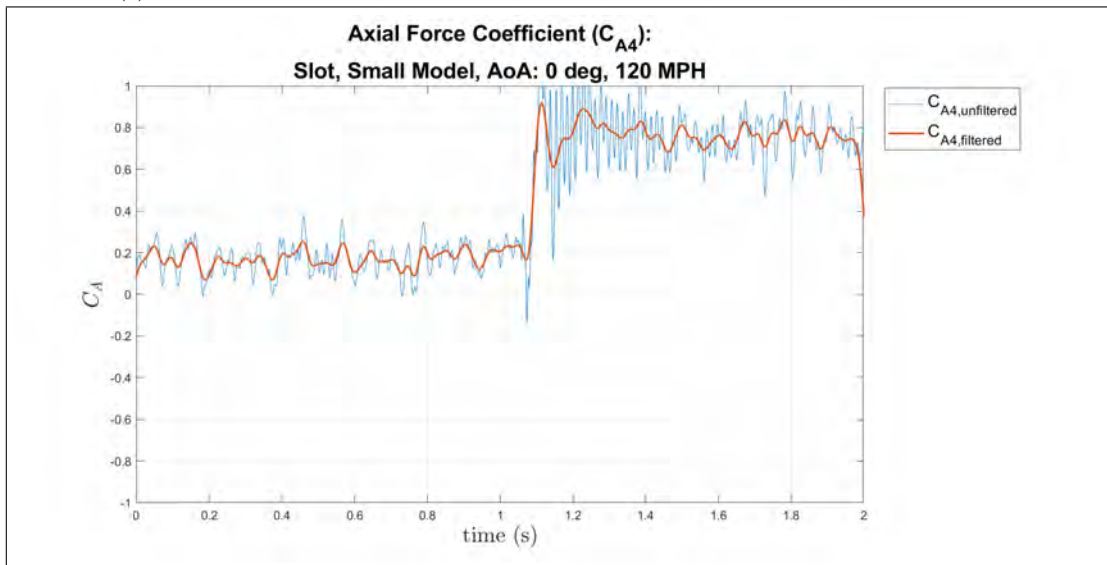


(b) Axial Force Coefficient, small model, 0° AoA, 120 MPH, release two, individual trial

Figure 277: Small model at 0° AoA of the axial force coefficient, release times one and two, 120 MPH, individual trial



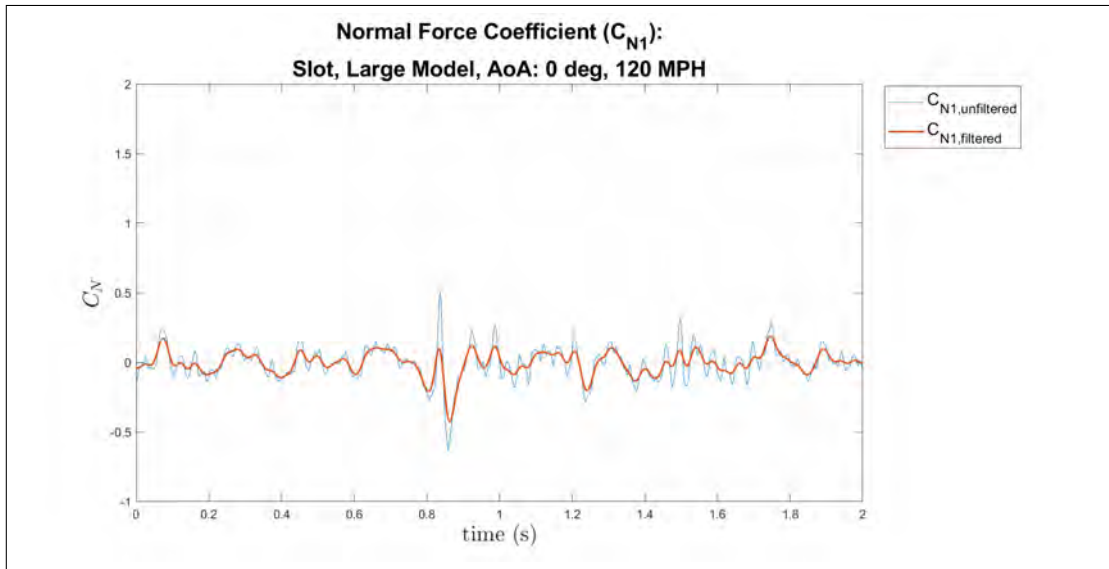
(a) Axial Force Coefficient, small model, 0° AoA, 120 MPH, release three, individual trial



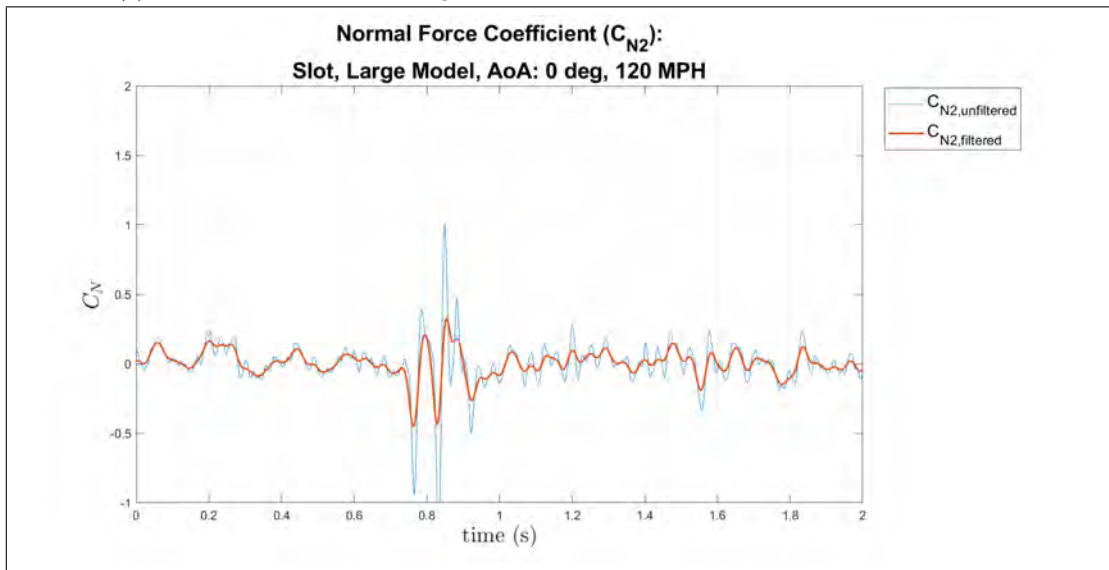
(b) Axial Force Coefficient, small model, 0° AoA, 120 MPH, release four, individual trial

Figure 278: Small model at 0° AoA of the axial force coefficient, release times three and four, 120 MPH, individual trial

Large Model, Dynamic Release, 0° AoA, 120 MPH

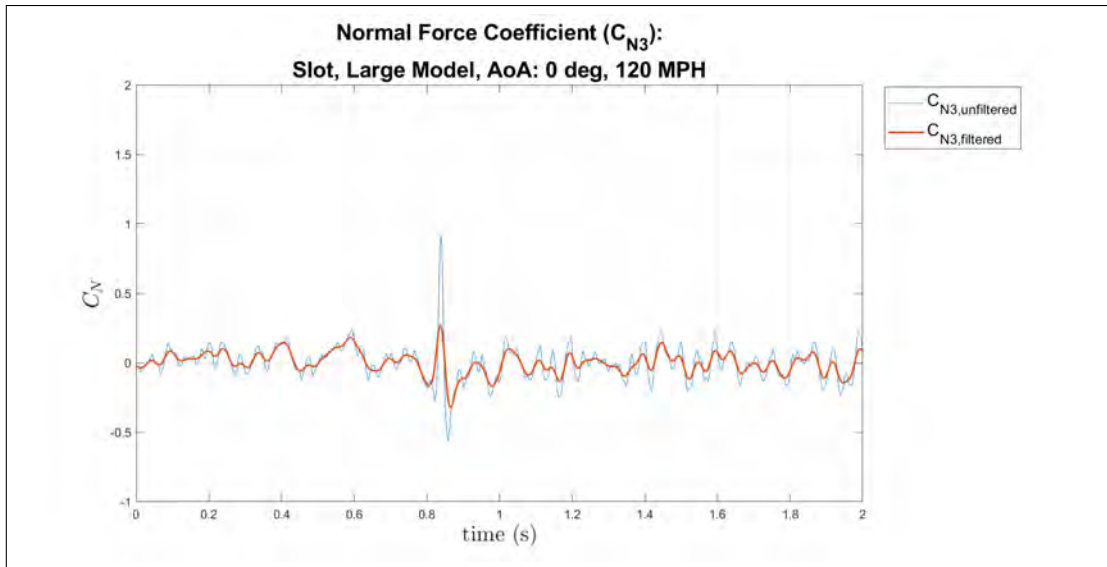


(a) Normal Force Coefficient, large model, 0° AoA, 120 MPH, release one, individual trial

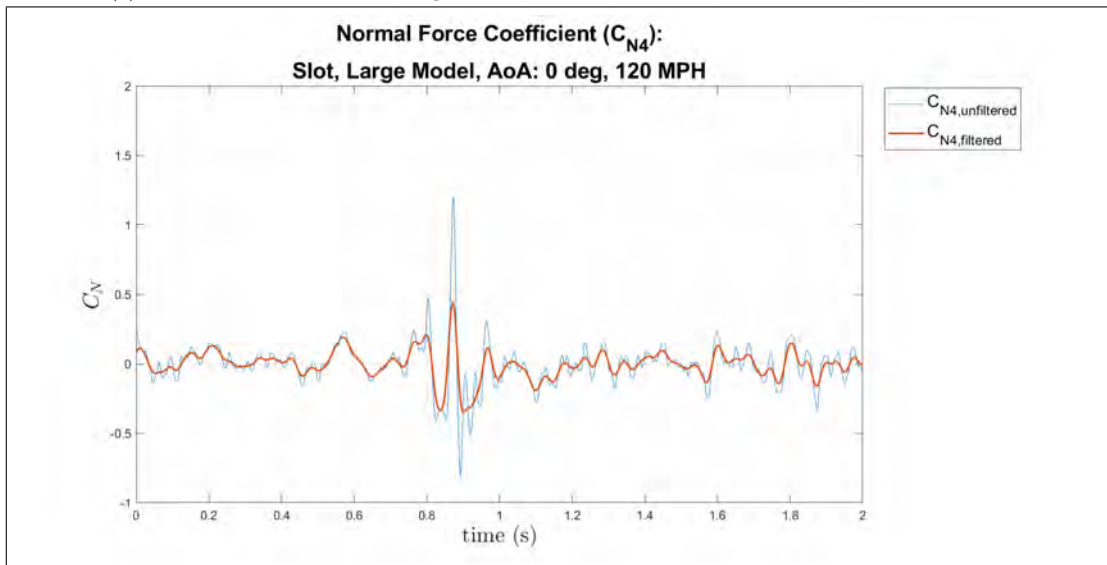


(b) Normal Force Coefficient, large model, 0° AoA, 120 MPH, release two, individual trial

Figure 279: Large model at 0° AoA of the normal force coefficient, release times one and two, 120 MPH, individual trial

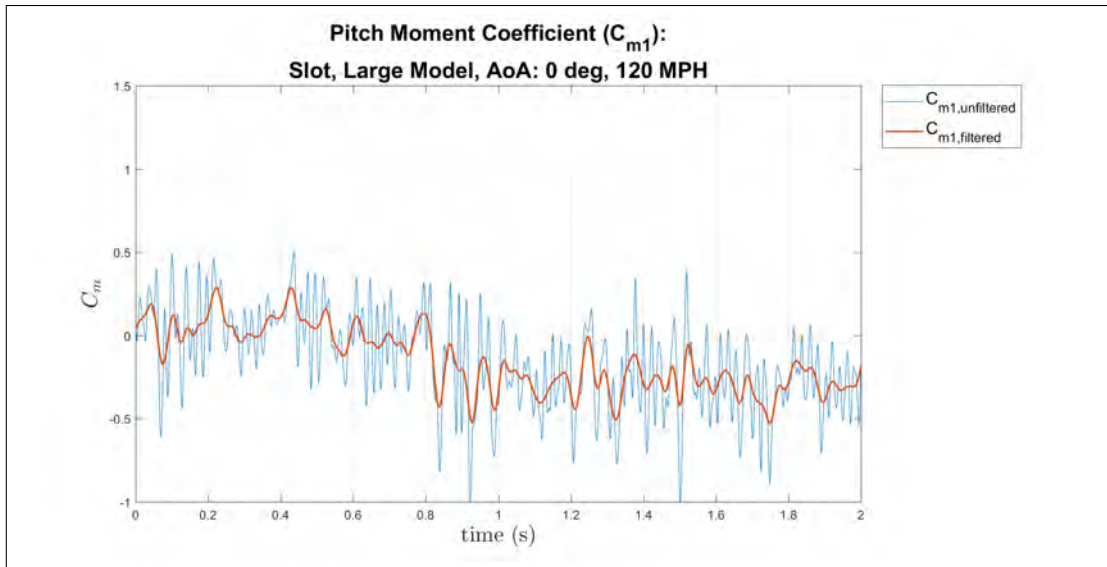


(a) Normal Force Coefficient, large model, 0° AoA, 120 MPH, release three, individual trial

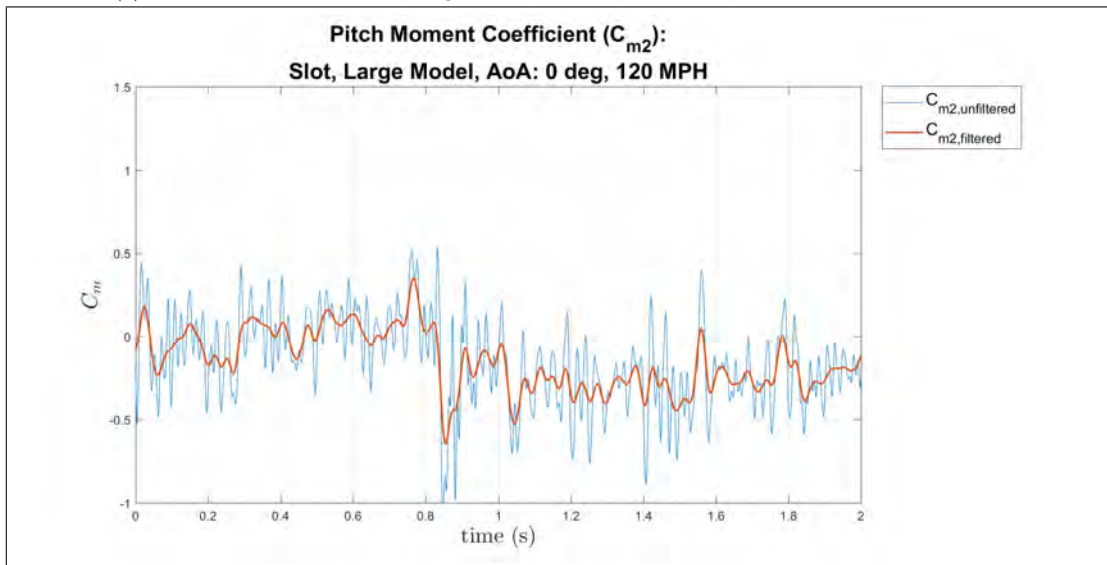


(b) Normal Force Coefficient, large model, 0° AoA, 120 MPH, release four, individual trial

Figure 280: Large model at 0° AoA of the normal force coefficient, release times three and four, 120 MPH, individual trial

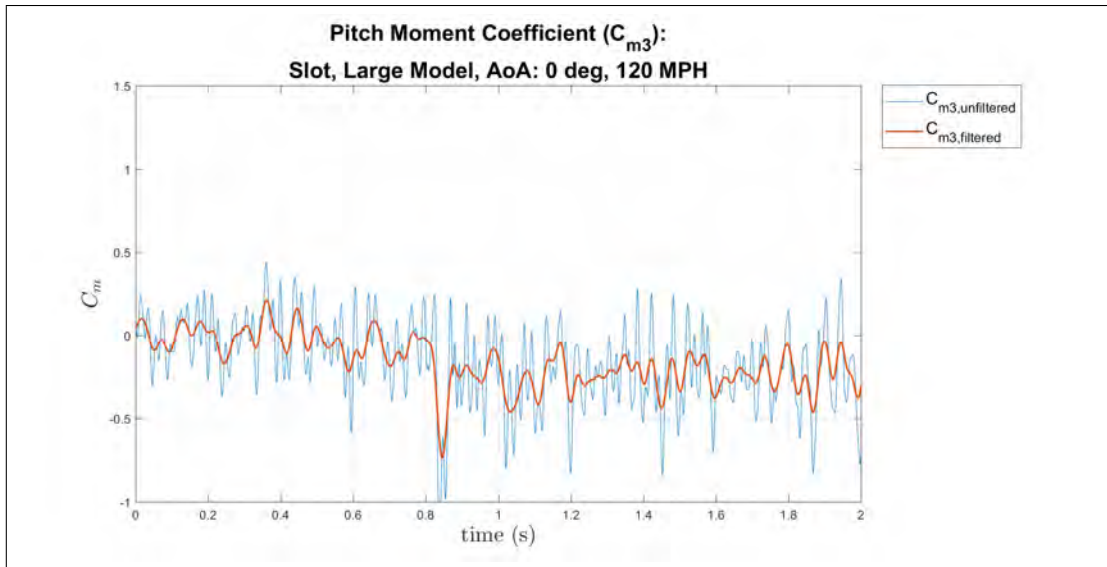


(a) Pitch Moment Coefficient, large model, 0° AoA, 120 MPH, release one, individual trial

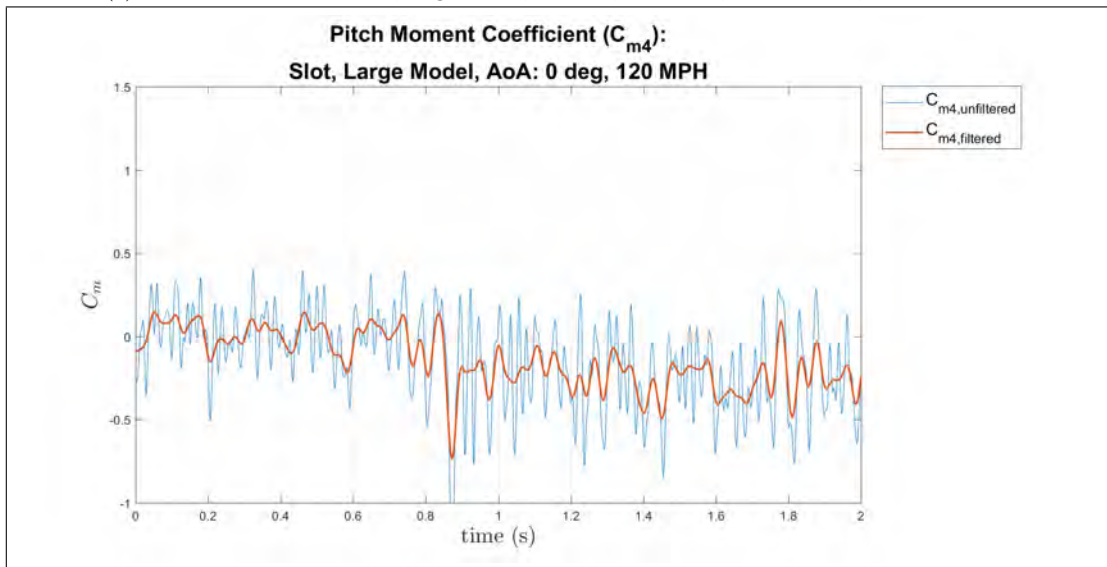


(b) Pitch Moment Coefficient, large model, 0° AoA, 120 MPH, release two, individual trial

Figure 281: Large model at 0° AoA of the pitch moment coefficient, release times one and two, 120 MPH, individual trial

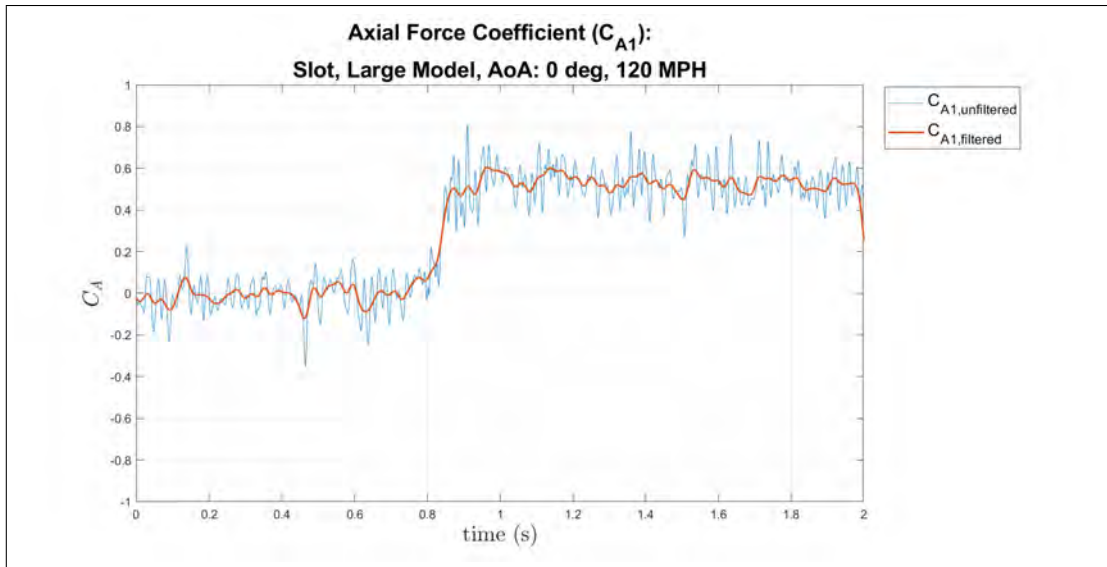


(a) Pitch Moment Coefficient, large model, 0° AoA, 120 MPH, release three, individual trial

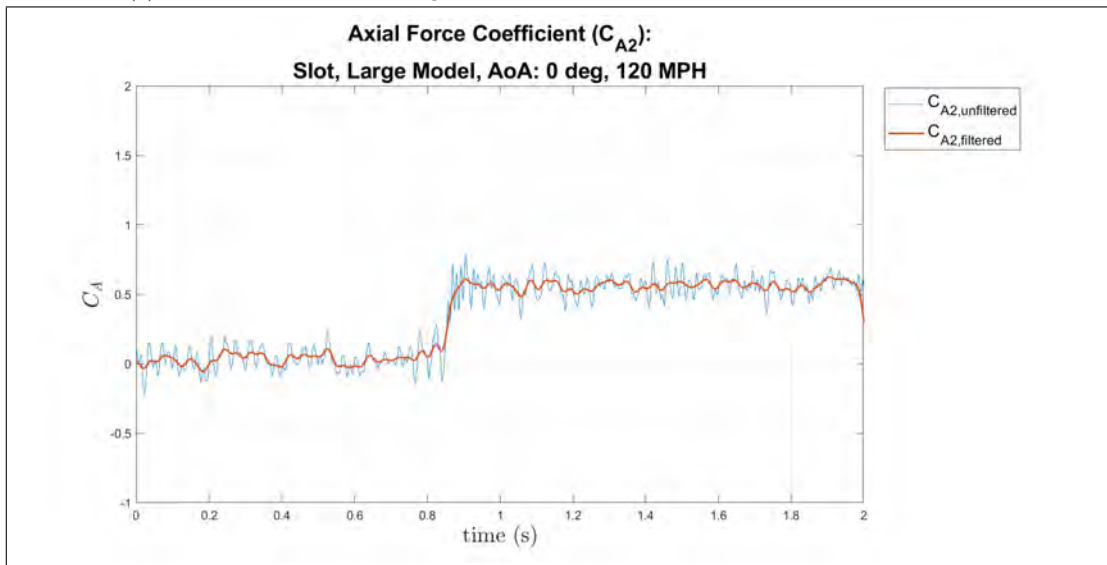


(b) Pitch Moment Coefficient, large model, 0° AoA, 120 MPH, release four, individual trial

Figure 282: Large model at 0° AoA of the pitch moment coefficient, release times three and four, 120 MPH, individual trial

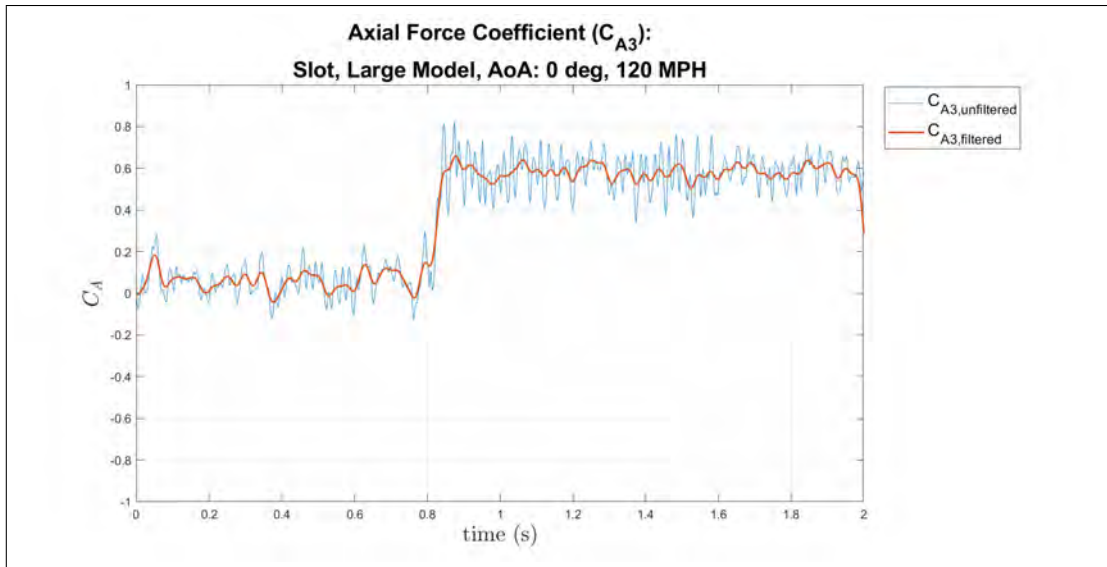


(a) Axial Force Coefficient, large model, 0° AoA, 120 MPH, release one, individual trial

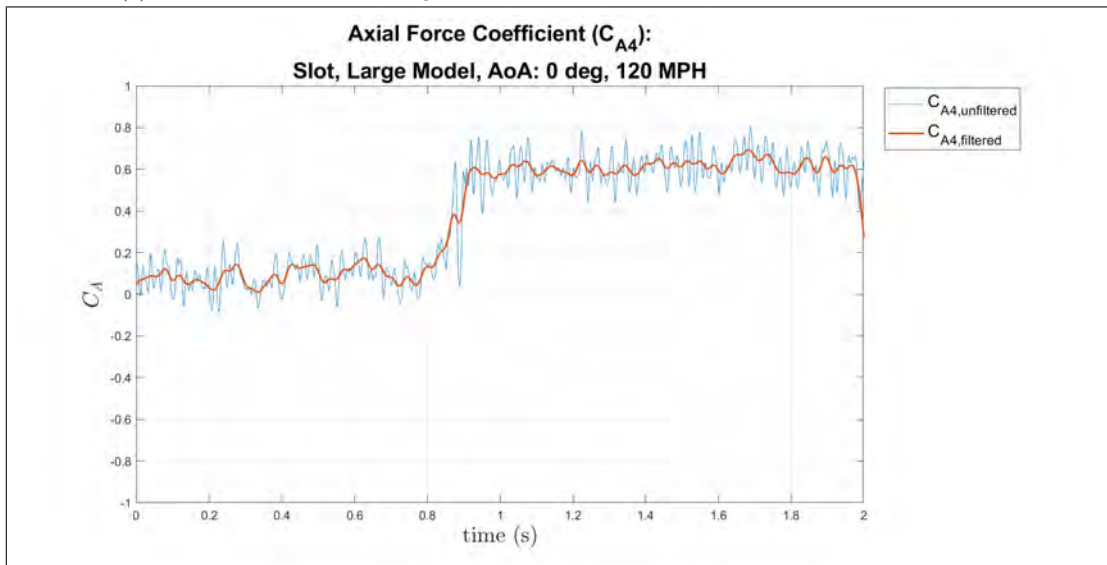


(b) Axial Force Coefficient, large model, 0° AoA, 120 MPH, release two, individual trial

Figure 283: Large model at 0° AoA of the axial force coefficient, release times one and two, 120 MPH, individual trial



(a) Axial Force Coefficient, large model, 0° AoA, 120 MPH, release three, individual trial



(b) Axial Force Coefficient, large model, 0° AoA, 120 MPH, release four, individual trial

Figure 284: Large model at 0° AoA of the axial force coefficient, release times three and four, 120 MPH, individual trial

Appendix C. Galil and Matlab Code

Index of Figures in Appendix C

Phase I: Matlab Code	(pg 382)
Freestream Apparatus Example Code	(pg 382)
Static: Cavity Apparatus Example Code	(pg 396)
Phase II: Matlab Code	(pg 412)
Dynamic Release Example Code	(pg 412)
Phase I: Matlab Code	(pg 427)
Reynolds Number Calculation	(pg 427)
Phase II: Matlab Code	(pg 430)
Reynolds Number Calculation	(pg 430)
Galil Codes	(pg 432)
Initialization of Motor A and B	(pg 432)
Jog Down, Jog Up, Jog Shear Layer	(pg 433)
Linear Jog Timing 1	(pg 434)
Linear Jog Timing 2	(pg 437)
Linear Jog Timing 3	(pg 440)
Linear Jog Timing 4	(pg 443)

Phase I: Matlab Code

Freestream Apparatus Example Code

```
%Tare, Force, and Coefficient Code, Freestream Code
%Authored by 2d Lt Ryan Saunders, USAF, and Capt Matt Wood, USMC
clear all;close all;clc

%% Set Values (only change values in this section -
%except axes on plots)
%ctrl+f 'set above' to find the below values, uncomment
%to run different
%sections by themselves
%must convert any .txt files to .csv (can use delimiting
%method in excel)
%can uncomment lines 100-112 to get encoder positions of
%_mph data
%can make single pitch coefficient and axial coefficient
%plots
%must make all folders used in fpath and fpathenc
mph = 120;
Fahrenheit = 69.2;
Inches_Hg = 29.2422;
d = 1.3; %diameter of model in inches
L = 2.0; % weapon bay length (ft)

begi = 1; %changes which items are plotted
endi = 1; %need to manually change name of plots if you care

name2 = 'Freestream, Small Model, AoA: 10 deg, 120 MPH';
fpath = 'F:\Thesis\Post Process\Freestream_1000\Small;...
Model\10AoA\figures\120mph';
fpathenc = 'F:\Thesis\Post Process\Freestream_1000\;...
Small Model\10AoA\figures\encoders';
%tare encoder indices
x1 = [2500];
x2 = [x1(1)-2000];
x3 = [50]; %uncomment lines 75-76 to use
div1 = [0.5]; %need to uncomment lines 61, 66 to use
%_mph indices
x4 = [2500];
x5 = [x4(1)-2000];
div2 = [0.5];
```

```

Fs = 1000;    % sample rate in Hz
cof = 15;     % cufoff frequency in Hz
order = 60;  % -th Order of lowpas filter

plot1 = 0; %encoder plot, 1 yes, 0 no
plot2 = 0; %unnecessary, mph encoder plot, 1 yes, 0 no
plot3 = 0; %Force and Taring plot, 1 yes, 0 no
plot4 = 1; %Normal Force Coeff plot, 1 yes, 0 no
plot5 = 0; %combined Normal Force Coeff plot, 1 yes, 0 no
plot6 = 0; %combined pitch moment Coeff plot, 1 yes, 0 no
plot7 = 0; %combined axial Force Coeff plot, 1 yes, 0 no

%line 178 Normal Force Tared
axes1 = {[0 2 -2.2 1]};
%line 253 Normal Force Coefficient
axes2 = {[0 2 1.35 1.6]};
%normal force coefficient combined
axesnc = [0 2 -0 2];
%pitch moment coefficient combined
axespc = [0 2 -0 1];
%axial force coefficient combined
axesac = [0 2 -2 0];

%% Missile and Wind Tunnel Properties

V_inf = mph*(1/3600)*(5280);
% MPH freestream vel converted to (ft/s)
%set above Fahrenheit = 77.2;
%set above Inches_Hg = 28.9845;
    %set above L = 2.0; % weapon bay length (ft)
    Dia = d/12; % missile diameter converted to (ft)
    Ref_Area = (pi/4)*Dia^2; % Model reference Area (ft^2)
        P_psi = Inches_Hg*0.49115420057253 ;
        % Inches Hg converted to psi
        P_psf = P_psi*12^2; %psi to psf
        T = Fahrenheit + 459.67;
        % temp deg F converted to Rankine
        R = 1716;
        % (lb-ft)/(slug-R) Imperial Gas constant for Dry Air
rho = P_psf/(R*T); % density from ideal gas law [slug/ft^3]

%% Importing and Plotting Encoder Positions

```

```

filename1 = {'0mph.csv'};
%set above x1 = [350,350,250,350,350,350,250,350];
%set above x2 = [250,250,150,250,250,250,150,250];
%set above x3 = [52,39,46,49,48,45,51,41];
%set above div1 = [0.5,0.8,0.6,0.8,0.5,0.75,0.3,1.8];

%0 mph Case Data Imported from .csv
%plot Encoder Data to line up timing
for i = 1:length(x1)
    voltage{i}.import1 = csvread(filename1{i});
    voltage{i}.use1 = voltage{i}.import1(end-x1(i):end-x2(i),:);
    voltage{i}.time1 = voltage{i}.use1(:,1);
    voltage{i}.encodera1 = voltage{i}.use1(:,8)/10^5;
    voltage{i}.encoderb1 = voltage{i}.use1(:,9)/10^5;
    voltage{i}.encoderb1 = voltage{i}.encoderb1/div1(i);
    if plot1 == 1
        figure
        plot(voltage{i}.time1, voltage{i}.encoderb1)
        %plot(voltage{i}.time1, voltage{i}.encodera1,;...
        voltage{i}.time1, voltage{i}.encoderb1);...
        hold on
        title(sprintf('Encoder Position %d',i))
        %turn off for final plots, figure description
        %in thesis names them
        line([voltage{i}.time1(x3(i)) ;...
        voltage{i}.time1(x3(i))],get(gca,;...
        'ylim'),'Color',[1 0 1])
        legend('Encoder B', 'Start of Release')
        legend('Encoder B')
        %legend('Encoder A', 'Encoder B', 'Start of Release')
        hold off
        movegui('northeast')
        filename = sprintf('encoder_%d',i);
        saveas(gca, fullfile(fpathenc, filename), 'png');
    end
end

%additional commands to manipulate figures
% [pks, locs] = findpeaks(enca_1);
% xx1 = t1(locs(1));
% line([xx1 xx1],get(gca,'ylim'),'Color',[1 0 1])
% x1 = t2(100);
% loc =;...

```

```

islocalmin(enca_2,1); locs = find(loc);
% xx1 = t2(locs(1));
% line([x1 x1],get(gca,'ylim'),'Color',[1 0 1])
% hold on
% line([xx1 xx1],get(gca,'ylim'),'Color',[0 1 0])
% title('Encoder Positions 2');...
% legend('Encoder A', 'Encoder B', 'start', 'min')

%% Importing For Force Data and Calibration Matrix

%Voltage Import
%_mph Case Data Imported from .csv
filename2 = {'120mph.csv'};
%set above x4 = [350,350,250,350,350,350,250,350];
%set above x5 = [250,250,150,250,250,250,150,250];
%set above div2 = [0.5,0.8,0.6,0.8,0.5,0.75,0.3,1.8];

for i = 1:length(x1)
    voltage{i}.import2 = csvread(filename2{i});
    %Data Imported from .csv
    voltage{i}.use2 = voltage{i}.import2;...
    (end-x4(i):end-x5(i),:);...
    %Taking the 2 seconds of data around the event
    voltage{i}.time2 = voltage{i}.use2(:,1);
    voltage{i}.encodera2 = voltage{i}.use2(:,8)/10^5;
    voltage{i}.encoderb2 = voltage{i}.use2(:,9)/10^5;
    voltage{i}.encoderb2 = voltage{i}.encoderb2/div2(i);
    if plot2 == 1
        figure
        plot(voltage{i}.time2, voltage{i}.encoderb2)
        %plot(voltage{i}.time2, voltage{i}.encodera2,;...
        voltage{i}.time2,
        voltage{i}.encoderb2)
        hold on
        title(sprintf('Encoder Position %d',i))
        %turn off for final;...
        plots, figure description in thesis names them
        line([voltage{i}.time2(x3(i)) voltage{i}.;...
        time2(x3(i))],;...
        get(gca,'ylim'),'Color',[1 0 1])
        legend('Encoder B', 'Start of Release')
        %legend('Encoder A', 'Encoder B', 'Start of Release')
        hold off
    end
end

```

```

        movegui('northeast')
        filename = sprintf('encoderb_%d',i);
        saveas(gca, fullfile(fpathenc, filename), 'png');
    end
end

%Calibration Matrix Nano-25
CalMat =;...
[ 0.01666, -0.00399, -0.31744,  2.98746,  0.42269, -3.00593;...
0.17884, -3.47015, -0.14035,  1.72288, -0.31903,  1.75159;...
5.26167, -0.04467,  5.59050,  0.20559,  5.32144, -0.10468;...
0.07209, -1.22529,  2.09820,  0.72446, -2.13718,  0.63742;...
-2.40927,  0.01016,  1.39990, -1.01331,  0.98241,  1.08087;...
0.03166, -1.11580,  0.14224, -1.09552,  0.16628, -1.10239];

%% Calculating the Force and Moment Tare Data at 0 mph

for i = 1:length(x1)
    plotting{i}.time1 = voltage{i}.use1(:,1) - voltage{i}.use1(1,1);
    voltage{i}.vfx1 = voltage{i}.use1(:,2);
    voltage{i}.vfy1 = voltage{i}.use1(:,3);
    voltage{i}.vfz1 = voltage{i}.use1(:,4);
    voltage{i}.vtx1 = voltage{i}.use1(:,5);
    voltage{i}.vty1 = voltage{i}.use1(:,6);
    voltage{i}.vtz1 = voltage{i}.use1(:,7);

    for j = 1:length(voltage{1}.vfx1)
        voltages_=[voltage{i}.vfx1(j);voltage{i}.vfy1(j);...
        voltage{i}.vfz1(j);voltage{i}.vtx1(j);...
        voltage{i}.vty1(j);voltage{i}.vtz1(j)];
        voltage{i}.forces1(:,j) = CalMat*voltages_;
    end

    %Converting the Nano-25 Coordinate System to conform
    with AIAA standard
    voltage{i}.tare_N1 = (-1)*voltage{i}.forces1(1,:);
    % AIAA Normal force N corresponds to Nano25 -Fx(lbf)
    voltage{i}.tare_Y1 = (-1)*voltage{i}.forces1(2,:);
    % AIAA Side Force Y corresponds to Nano25 -Fy(lbf)
    voltage{i}.tare_A1 = (-1)*voltage{i}.forces1(3,:);
    % AIAA Axial Force A corresponds to Nano25 -Fz(lbf)
    voltage{i}.tare_n1 = (1/12)*voltage{i}.forces1(4,:);
    % AIAA yaw moment n Corresponds to Nano25 Tx

```

```

    %converted to ft-lbs
    voltage{i}.tare_m1 = -(1/12)*voltage{i}.forces1(5,:);
    % AIAA pitch moment m Corresponds to Nano25 Ty
    %converted to ft-lbs
    voltage{i}.tare_l1 = (1/12)*voltage{i}.forces1(6,:); %L1
    % AIAA roll moment l Corresponds to Nano25 Tz
    %converted to ft-lbs
end

%% Calculating the Force and Moments at 60mph

for i = 1:length(x1)
    plotting{i}.time2 = voltage{i}.use2(:,1) - voltage{i}.use2(1,1);
    %%%%%%%%%%%%%%%%%%%%%%%%%%%%%%%%%%%%%%%%%%%%%%%%%%%%%%%%%%%%%%%%%%%%%%%%%
    voltage{i}.vfx2 = voltage{i}.use2(:,2);
    voltage{i}.vfy2 = voltage{i}.use2(:,3);
    voltage{i}.vfz2 = voltage{i}.use2(:,4);
    voltage{i}.vtx2 = voltage{i}.use2(:,5);
    voltage{i}.vty2 = voltage{i}.use2(:,6);
    voltage{i}.vtz2 = voltage{i}.use2(:,7);

    for j = 1:length(voltage{1}.vfx2)
        voltages_ = [voltage{i}.vfx2(j);voltage{i}.vfy2(j);...
            voltage{i}.vfz2(j);voltage{i}.vtx2(j);...
            voltage{i}.vty2(j);voltage{i}.vtz2(j)];
        voltage{i}.forces2(:,j) = CalMat*voltages_;
    end

    %Converting the Nano-25 Coordinate System to
    %conform with AIAA standard
    voltage{i}.tare_N2 = (-1)*voltage{i}.forces2(1,:);
    % AIAA Normal force N corresponds to Nano25 -Fx(lbf)
    voltage{i}.tare_Y2 = (-1)*voltage{i}.forces2(2,:);
    % AIAA Side Force Y corresponds to Nano25 -Fy(lbf)
    voltage{i}.tare_A2 = (-1)*voltage{i}.forces2(3,:);
    % AIAA Axial Force A corresponds to Nano25 -Fz(lbf)
    voltage{i}.tare_n2 = (1/12)*voltage{i}.forces2(4,:);
    % AIAA yaw moment n Corresponds to Nano25 Tx
    %converted to ft-lbs
    voltage{i}.tare_m2 = -(1/12)*voltage{i}.forces2(5,:);
    % AIAA pitch moment m Corresponds to Nano25 Ty
    %converted to ft-lbs
    voltage{i}.tare_l2 = (1/12)*voltage{i}.forces2(6,:);

```

```

        % AIAA roll moment 1 Corresponds to Nano25 Tz
        %converted to ft-lbs
end

% (-1) is for AIAA convention and F_ corresponds to Nano25(lbf)
%and T_ Corresponds to Nano25converted to ft-lb

%% Calculating/Plotting the TARED Data by subtracting
%the Tare Values from the
%Measured at Velocity, Normal Force Data

%set above axes1 = {[0 1 -2 1.5], [0 1 -2 1], [0 1 -2 2],;...
[0 1 -2 2], [0 1 -2 1], [0 1 -2.5 1], [0 1 -2 2], [0 1 -2 1]};

%Plots of the Data at Wind Tunnel Velocity vs. Tared
for i = 1:length(x1)
    plotting{i}.tared_N = voltage{i}.tare_N2 - voltage{i}.tare_N1;
    plotting{i}.tared_Y = voltage{i}.tare_Y2 - voltage{i}.tare_Y1;
    plotting{i}.tared_A = voltage{i}.tare_A2 - voltage{i}.tare_A1;
    plotting{i}.tared_n = voltage{i}.tare_n2 - voltage{i}.tare_n1;
    plotting{i}.tared_m = voltage{i}.tare_m2 - voltage{i}.tare_m1;
    plotting{i}.tared_l = voltage{i}.tare_l2 - voltage{i}.tare_l1;
    if plot3 == 1
        figure('Position',[100 100 1200 800]);
        plot(plotting{i}.time2,voltage{i}.tare_N2); hold on;
        plot(plotting{i}.time1,voltage{i}.tare_N1);
        plot(plotting{i}.time2,plotting{i}.tared_N);
        name1 = sprintf('Normal Force (F_{N%d}):',i);
        %set above %name2 = 'Missile, AoA: 10 deg, 60 MPH';
        title([name1,name2],'fontweight','bold','fontsize',18)
        xlabel('time (s)','Interpreter','latex','fontsize',18)
        % x-axis label
        ylabel('lbf','Interpreter','latex','fontsize',18)
        % y-axis label
        name3 = sprintf('F_{N%d}',i);
        name4 = sprintf('Tare F_{N%d}',i);
        name5 = sprintf('TARED F_{N%d}',i);
        legend({name3,name4,name5},'FontSize',12,'Location',;...
'bestoutside');...
        hold off
        axis(axes1{i}) %[0 1 -3 1])
        filename = sprintf('normalforcetare_%d',i);
        saveas(gca, fullfile(fpath, filename), 'png');
    end
end

```

```

end
if plot6 == 1
figure('Position',[100 100 1200 800]);
plot(plotting{i}.time2,voltage{i}.tare_m2); hold on;
plot(plotting{i}.time1,voltage{i}.tare_m1);
plot(plotting{i}.time2,plotting{i}.tared_m);
name1 = sprintf('Pitch Moment (F_{m%d}):',i);
%set above %name2 = 'Missile, AoA: 10 deg, 60 MPH';
title({name1,name2},'fontweight','bold','fontsize',18)
xlabel('time (s)','Interpreter','latex','fontsize',18)
% x-axis label
ylabel('lbf','Interpreter','latex','fontsize',18)
% y-axis label
name3 = sprintf('F_{m%d}',i);
name4 = sprintf('Tare F_{m%d}',i);
name5 = sprintf('TARED F_{m%d}',i);
legend({name3,name4,name5},'FontSize',12,'Location',;...
'bestoutside');...
hold off
axis(axespt{i}) %[0 1 -3 1])
filename = sprintf('pitchmomenttare_%d',i);
saveas(gca, fullfile(fpath, filename), 'png');
end
if plot9 == 1
figure('Position',[100 100 1200 800]);
plot(plotting{i}.time2,voltage{i}.tare_A2); hold on;...
plot(plotting{i}.time1,voltage{i}.tare_A1);...
plot(plotting{i}.time2,plotting{i}.tared_A);
name1 = sprintf('Axial Force (F_{A%d}):',i);
%set above %name2 = 'Missile, AoA: 10 deg, 60 MPH';
title({name1,name2},'fontweight','bold','fontsize',18)
xlabel('time (s)','Interpreter','latex','fontsize',18)
% x-axis label
ylabel('lbf','Interpreter','latex','fontsize',18)
% y-axis label
name3 = sprintf('F_{A%d}',i);
name4 = sprintf('Tare F_{A%d}',i);
name5 = sprintf('TARED F_{A%d}',i);
legend({name3,name4,name5},'FontSize',12,'Location',;...
'bestoutside');...
hold off
axis(axesat{i}) %[0 1 -3 1])
filename = sprintf('axialforcetare_%d',i);

```

```

        saveas(gca, fullfile(fpath, filename), 'png');
    end
end

%% Calculate Coefficients
q = (1/2)*rho*V_inf^2; %Dynamic Pressure

for i = 1:length(x1)
    voltage{i}.CN = (plotting{i}.tared_N) / (q*Ref_Area);
    %Normal Force Coeff
    voltage{i}.CY = (plotting{i}.tared_Y) / (q*Ref_Area);
    %Side Force Coeff
    voltage{i}.CA = (plotting{i}.tared_A) / (q*Ref_Area);
    %Axial Force Coeff
    voltage{i}.Cl = (plotting{i}.tared_n) / (q*Ref_Area*Dia);
    %Roll Moment Coeff
    voltage{i}.Cm = (plotting{i}.tared_m) / (q*Ref_Area*Dia);
    %Pitch Moment Coeff
    voltage{i}.Cn = (plotting{i}.tared_l) / (q*Ref_Area*Dia);
    %Yaw Moment Coeff
end

%% Filter for Coefficient Data Sets_Slot
%Transforming the noisy data array from a row into a column

for i = 1:length(x1)
    voltage{i}.CN = voltage{i}.CN';
    voltage{i}.CY = voltage{i}.CY';
    voltage{i}.CA = voltage{i}.CA';
    voltage{i}.Cl = voltage{i}.Cl';
    voltage{i}.Cm = voltage{i}.Cm';
    voltage{i}.Cn = voltage{i}.Cn';
end

%% Design a -th order lowpass FIR filter with
%cutoff frequency of (Hz)
%set above Fs = 100;    % sample rate in Hz
%set above cof = 25;    % cufoff frequency in Hz
%set above order = 60; % -th Order of lowpas filter
Fnorm = cof/(Fs/2); % Normalized frequency

%MATLAB digital filter Function

```

```

for i = 1:length(x1)
    df = designfilt('lowpassfir','FilterOrder',order,;...
        'CutoffFrequency',Fnorm);
    Delay = mean(grpdelay(df)); % filter delay in samples
    filtered{i}.CN = filter(df,[voltage{i}.CN; zeros(Delay,1)]);
    % Delay zeros concatenated with the input data
    filtered{i}.CN = filtered{i}.CN(Delay+1:end);
    % Shift data to compensate for delay
    filtered{i}.CY = filter(df,[voltage{i}.CY; zeros(Delay,1)]);
    filtered{i}.CY = filtered{i}.CY(Delay+1:end);
    filtered{i}.CA = filter(df,[voltage{i}.CA; zeros(Delay,1)]);
    filtered{i}.CA = filtered{i}.CA(Delay+1:end);
    filtered{i}.Cl = filter(df,[voltage{i}.Cn; zeros(Delay,1)]);
    filtered{i}.Cl = filtered{i}.Cl(Delay+1:end);
    filtered{i}.Cm = filter(df,[voltage{i}.Cm; zeros(Delay,1)]);
    filtered{i}.Cm = filtered{i}.Cm(Delay+1:end);
    filtered{i}.Cn = filter(df,[voltage{i}.Cl; zeros(Delay,1)]);
    filtered{i}.Cn = filtered{i}.Cn(Delay+1:end);
end

%% Plotting Normal Force Coefficients
%Normal Force Coeff

%set above axes2 = {[0 1 -15 15], [0 1 -6 5], [0 1 -5 15],;...
[0 1 -6 17], [0 1 -6 5], [0 1 -15 8], [0 1 -6 17], [0 1 -4 7]};

for i = begi:endi
    if plot4 == 1
        figure('Position',[100 100 1200 600]);
        plot(plotting{i}.time2(1:end),voltage{i}.CN(1:end)); hold on;
        plot(plotting{i}.time2(1:end),filtered{i}.CN(1:end),;...
            'Linewidth',1.5); grid on;
        name1 = sprintf('Normal Force Coefficient (C_{N%d}):',i);
        %set at top %name2 = 'Missile, AoA: 10 deg, 60 MPH';
        title({name1,name2},'fontweight','bold','fontsize',18);
        name3 = sprintf('C_{N%d},unfiltered',i);
        name4 = sprintf('C_{N%d},filtered',i);
        legend({name3,name4},'FontSize',14,'Location','bestoutside');
        xlabel('time (s)','Interpreter','latex','fontsize',18)
        % x-axis label
        ylabel('$C_{N}$','Interpreter','latex','fontsize',18)
        % y-axis label

```

```

        axis(axes2{i}); hold off; %axis([0 1 -10 10]); hold off;
        filename = sprintf('normalforcecoefficient_%d',i);
        saveas(gca, fullfile(fpath, filename), 'png');
    end
end

%% Plotting Normal Force Coefficients COMBINED
%COMBINED, zoomed in
if plot5 == 1
figure('Position',[100 100 1200 600]);
for i = begi:endi
    plot(plotting{i}.time2(1:end),filtered{i}.CN(1:end));...
    hold on; grid on; %plot(time_1(1:end),filtered_CN_1(1:end));
end
    name1 = 'Normal Force Coefficient (C_{N}): Combined';
    counti = 1;
for j = begi:endi
    legendi{counti} = sprintf('C_{N%d},filtered}',j);
    counti = counti + 1;
end
    title({name1,name2},...
        'fontweight','bold','fontsize',18);
    legend(legendi,'FontSize',12,'Location','bestoutside');
    xlabel('time (s)','Interpreter','latex','fontsize',18)
    % x-axis label
    ylabel('$C_{N}$','Interpreter','latex','fontsize',18)
    % y-axis label
    axis(axesnc); hold off;
    filename = 'normalforcecoefficient_all';
    saveas(gca, fullfile(fpath, filename), 'png');
end

%Averaging the Normal Force Coeff Data
% CN_avg = (filtered_CN_1 + filtered_CN_2 + filtered_CN_3;...
+ filtered_CN_4 + filtered_CN_5) / 5;
% figure('Position',[100 100 900 480]); plot(time_1(50:1900),;...
CN_avg(50:1900)); hold on; grid on;
%     title({'Average Normal Force Coefficient (C_{N});...
Slot, Max Stroke','Missile, AoA: 10 deg, 100 MPH'},...
%         'fontweight','bold','fontsize',16);
% %     legend({'C_{N1},filtered}','C_{N2},filtered'},;...
'C_{N3},filtered}','C_{N4},filtered}','C_{N5},filtered'}',...
% %         'FontSize',12,'Location','bestoutside');

```

```

%           xlabel('time (s)','Interpreter','latex',;...
'fontsize',18) % x-axis label
%           ylabel('$C_{N}$','Interpreter','latex','fontsize';...
,18) % y-axis label
%           hold off; axis([0.05 1.9 0 2.5]); set(findall;...
(gca, 'Type', 'Line'),'LineWidth',1.5);

%% Plotting Pitch Moment Coefficients

if plot7 == 1
for i = begi:endi
    figure('Position',[100 100 1200 600]);
    plot(plotting{i}.time2(1:end),voltage{i}.Cm(1:end));...
    hold on;
    plot(plotting{i}.time2(1:end),filtered{i}.Cm(1:end),;...
'Linewidth',1.5); grid on;
    name1 = sprintf('Pitch Moment Coefficient (C_{M%d}):',i);
    %set at top %name2 = 'Missile, AoA: 10 deg, 60 MPH';
    title({name1,name2},'fontweight','bold','fontsize',18);
    name3 = sprintf('C_{M%d,unfiltered}',i);
    name4 = sprintf('C_{M%d,filtered}',i);
    legend({name3,name4},'FontSize',14,'Location',;...
'bestoutside');
    xlabel('time (s)','Interpreter','latex','fontsize',18)
    % x-axis label
    ylabel('$C_{M}$','Interpreter','latex','fontsize',18)
    % y-axis label
    axis(axespc1{i}); hold off; %axis([0 1 -10 10]);...
    hold off;
    filename = sprintf('pitchmomentcoefficient_%d',i);
    saveas(gca, fullfile(fpath, filename), 'png');
end
end

%% Plotting Pitch Moment Coefficients Combined
%COMBINED, filtered, zoomed in
if plot8 == 1
figure('Position',[100 100 1200 600]);
for i = begi:endi
    plot(plotting{i}.time2(1:end),filtered{i}.Cm(1:end));
    hold on; grid on; %plot(time_1(1:end),filtered_CN_1(1:end));
end

```

```

        name1 = 'Pitch Moment Coefficient (C_{m}): Combined';
        counti = 1;
    for j = begi:endi
        legendi{counti} = sprintf('C_{m%d,filtered}',j);
        counti = counti + 1;
    end

    title({name1,name2},...
        'fontweight','bold','fontsize',16);
    legend(legendi,'FontSize',12,'Location','bestoutside');
    xlabel('time (s)','Interpreter','latex','fontsize',18)
    % x-axis label
    ylabel('$C_{m}$','Interpreter','latex','fontsize',18)
    % y-axis label
    axis(axespc); hold off; %set(findall(gca, 'Type',;...
        'Line'),'LineWidth',1.5);
    filename = 'pitchmomentcoefficient_all';
    saveas(gca, fullfile(fpath, filename), 'png');
end

%% Plotting Axial Force Coefficients
if plot10 == 1
    for i = begi:endi
        figure('Position',[100 100 1200 600]);
        plot(plotting{i}.time2(1:end),voltage{i}.CA(1:end));...
        hold on;
        plot(plotting{i}.time2(1:end),filtered{i}.CA(1:end),;...
            'Linewidth',1.5); grid on;
        name1 = sprintf('Axial Force Coefficient (C_{A%d}):',i);
        %set at top %name2 = 'Missile, AoA: 10 deg, 60 MPH';
        title({name1,name2},'fontweight','bold','fontsize',18);
        name3 = sprintf('C_{A%d,unfiltered}',i);
        name4 = sprintf('C_{A%d,filtered}',i);
        legend({name3,name4},'FontSize',14,'Location',;...
            'bestoutside');
        xlabel('time (s)','Interpreter','latex','fontsize',18)
        % x-axis label
        ylabel('$C_{A}$','Interpreter','latex','fontsize',18)
        % y-axis label
        axis(axesac1{i}); hold off; %axis([0 1 -10 10]);...
        hold off;
        filename = sprintf('axialforcecoefficient_%d',i);
        saveas(gca, fullfile(fpath, filename), 'png');
    end
end

```

```

end
%% Plotting Axial Force Coefficients Combined
%COMBINED, zoomed in
if plot11 == 1
figure('Position',[100 100 1200 600]);
for i = begi:endi
    plot(plotting{i}.time2(1:end),filtered{i}.CA(1:end));...
    hold on; grid on;
end
    name1 = 'Axial Force Coefficient (C_{A}): Combined';
    counti = 1;
for j = begi:endi
    legendi{counti} = sprintf('C_{A}%d,filtered}',j);
    counti = counti + 1;
end
    title({name1,name2},...
        'fontweight','bold','fontsize',16);
    legend(legendi,'FontSize',12,'Location',;...
        'bestoutside');
    xlabel('time (s)','Interpreter','latex',;...
        'fontsize',18) % x-axis label
    ylabel('$C_{A}$','Interpreter','latex',;...
        'fontsize',18) % y-axis label
    axis(axesac); hold off; %set(findall(gca, ;...
        'Type', 'Line'),'LineWidth',1.5);
    filename = 'axialforcecoefficient_all';
    saveas(gca, fullfile(fpath, filename), 'png');
end

```

Static: Cavity Apparatus Example Code

```
%Tare, Force, and Coefficient Code, Cavity Apparatus Code
%Authored by 2d Lt Ryan Saunders, USAF, and Capt Matt Wood, USMC
clear all;close all;clc

%% Set Values (only change values in this section -
%except axes on plots)
%ctrl+f 'set above' to find the below values,
%uncomment to run different
%sections by themselves
%must convert any .txt files to .csv (can use delimiting
%method in excel)
%can uncomment lines 100-112 to get encoder positions of _mph data
%can make single pitch coefficient and axial coefficient plots
%must make all folders used in fpath and fpathenc
mph1 = 60;
mph2 = 100;
mph3 = 120;
Fahrenheit = 71.6;
Inches_Hg = 29.0373;
d = 1.7; %diameter of model in inches
L = 2.0; % weapon bay length (ft)

begi = 1; %changes which items are plotted
endi = 3; %need to manually change name of plots if you care

name_base = 'No Oscillation, Large Model, AoA: 10 deg, In Cavity';
name2_1 = 'No Oscillation, Large Model, AoA: 10 deg,;...
In Cavity, 60 MPH';
name2_2 = 'No Oscillation, Large Model, AoA: 10 deg,;...
In Cavity, 100 MPH';
name2_3 = 'No Oscillation, Large Model, AoA: 10 deg,;...
In Cavity, 120 MPH';
fpath = 'F:\Thesis\Post Process\stilltests\Large Model\;...
10AoA\cavity\figures';
fpathenc = 'F:\Thesis\Post Process\stilltests\Large Model\;...
10AoA\cavity\figures\encoders';
%tare encoder indices
x1 = [3000,3000,3000];
x2 = [x1(1)-2000,x1(2)-2000,x1(3)-2000];
x3 = [50,50,50]; %uncomment lines 75-76 to use
div1 = [0.5,0.8,0.5]; %need to uncomment lines 61, 66 to use
```

```

%_mph indices
x4 = [3000,3000,3000];
x5 = [x4(1)-2000,x4(2)-2000,x4(3)-2000];
div2 = [0.5,0.8,0.5];

Fs = 1000;    % sample rate in Hz
cof = 15;     % cufoff frequency in Hz
order = 60;  % -th Order of lowpas filter

plot1 = 0; %encoder plot, 1 yes, 0 no
plot2 = 0; %unnecessary, mph encoder plot, 1 yes, 0 no
%
plot3 = 1; %Force and Taring plot, 1 yes, 0 no
plot4 = 1; %Normal Force Coeff plot, 1 yes, 0 no
plot5 = 1; %combined Normal Force Coeff plot, 1 yes, 0 no
%
plot6 = 1; %Pitch Moment Taring plot, 1 yes, 0 no
plot7 = 1; %Pitch Moment Coeff plot, 1 yes, 0 no
plot8 = 1; %Combined Pitch Moment Coeff plot, 1 yes, 0 no
%
plot9 = 1; %Axial Force Taring plot, 1 yes, 0 no
plot10 = 1; %Axial Force Coeff plot, 1 yes, 0 no
plot11 = 1; %Combined Axial Force Coeff plot, 1 yes, 0 no


%line 178 Normal Force Tared
axes1 = {[0 2 -3 0.5], [0 2 -3 0.5], [0 2 -3 0.5]};
%line 253 Normal Force Coefficient
axes2 = {[0 2 -0.2 0.5], [0 2 -0.2 0.5], [0 2 -0.4 0.5]};
%normal force coefficient combined
axesnc = [0 2 -0.4 0.4];

%Pitch Moment  Tared
axespt = {[0 2 -0.2 0.1], [0 2 -0.25 0.1], [0 2 -0.25 0.1]};
%pitch moment coefficient
axespc1 = {[0 2 -1 0.5], [0 2 -1 0.5], [0 2 -2 0.25]};
%pitch moment coefficient combined
axespc = [0 2 -1.6 0.3];

%Axial Moment  Tared
axesat = {[0 2 -0.2 1], [0 2 -0.2 1], [0 2 -0.2 1.2]};
%axial force coefficient

```

```

axesac1 = {[0 2 -0.2 0.4], [0 2 -0.2 0.4], [0 2 -0.2 0.4]};
%axial force coefficient combined
axesac = [0 2 -0.1 0.3];

%% Missile and Wind Tunnel Properties

V_inf1 = mph1*(1/3600)*(5280);
% MPH freestream velocity converted to (ft/s)
V_inf2 = mph2*(1/3600)*(5280);
% MPH freestream velocity converted to (ft/s)
V_inf3 = mph3*(1/3600)*(5280);
% MPH freestream velocity converted to (ft/s)
%set above Fahrenheit = 77.2;
%set above Inches_Hg = 28.9845;
    %set above L = 2.0; % weapon bay length (ft)
    Dia = d/12; % missile diameter converted to (ft)
    Ref_Area = (pi/4)*Dia^2; % Model reference Area (ft^2)
        P_psi = Inches_Hg*0.49115420057253 ;
        % Inches Hg converted to psi
        P_psf = P_psi*12^2; %psi to psf
        T = Fahrenheit + 459.67;
        % temp deg F converted to Rankine
        R = 1716;
        % (lb-ft)/(slug-R) Imperial Gas constant for Dry Air
rho = P_psf/(R*T); % density from ideal gas law [slug/ft^3]

%% Importing and Plotting Encoder Positions

filename1 = {'0mph.csv', '0mph.csv', '0mph.csv'};
%set above x1 = [350,350,250,350,350,350,250,350];
%set above x2 = [250,250,150,250,250,250,150,250];
%set above x3 = [52,39,46,49,48,45,51,41];
%set above div1 = [0.5,0.8,0.6,0.8,0.5,0.75,0.3,1.8];

%0 mph Case Data Imported from .csv
%plot Encoder Data to line up timing
for i = 1:length(x1)
    voltage{i}.import1 = csvread(filename1{i});
    voltage{i}.use1 = voltage{i}.import1(end-x1(i):end-x2(i),:);
    voltage{i}.time1 = voltage{i}.use1(:,1);
    voltage{i}.encodera1 = voltage{i}.use1(:,8)/10^5;
    voltage{i}.encoderb1 = voltage{i}.use1(:,9)/10^5;
    voltage{i}.encoderb1 = voltage{i}.encoderb1/div1(i);

```

```

    if plot1 == 1
    figure
    plot(voltage{i}.time1, voltage{i}.encoderb1)
    %plot(voltage{i}.time1, voltage{i}.encodera1,;...
    voltage{i}.time1, voltage{i}.encoderb1);...
    hold on
    title(sprintf('Encoder Position %d',i))
    %turn off for final plots, figure description
    %in thesis names them
    line([voltage{i}.time1(x3(i)) voltage{i}.time1(x3(i))],;...
    get(gca,'ylim'),'Color',[1 0 1])
    legend('Encoder B', 'Start of Release')
    legend('Encoder B')
    %legend('Encoder A', 'Encoder B', 'Start of Release')
    hold off
    movegui('northeast')
    filename = sprintf('encoder_%d',i);
    saveas(gca, fullfile(fpathenc, filename), 'png');
    end
end
%additional commands to manipulate figures
% [pks, locs] = findpeaks(enca_1); % xx1 = t1(locs(1));
% line([xx1 xx1],get(gca,'ylim'),'Color',[1 0 1])
% x1 = t2(100); % loc = islocalmin(enca_2,1); locs = find(loc);
% xx1 = t2(locs(1)); % line([x1 x1],get(gca,'ylim'),'Color',[1 0 1])
% hold on % line([xx1 xx1],get(gca,'ylim'),'Color',[0 1 0])
% title('Encoder Positions 2')
% legend('Encoder A', 'Encoder B', 'start', 'min')

%% Importing For Force Data and Calibration Matrix

%Voltage Import
%_mph Case Data Imported from .csv
filename2 = {'60mph.csv', '100mph.csv', '120mph.csv'};
%set above x4 = [350,350,250,350,350,350,250,350];
%set above x5 = [250,250,150,250,250,250,150,250];
%set above div2 = [0.5,0.8,0.6,0.8,0.5,0.75,0.3,1.8];

for i = 1:length(x1)
    voltage{i}.import2 = csvread(filename2{i});
    %Data Imported from .csv
    voltage{i}.use2 = voltage{i}.import2(end-x4(i):end-x5(i),:);
    %Taking the 2 seconds of data around the event

```

```

    voltage{i}.time2 = voltage{i}.use2(:,1);
    voltage{i}.encodera2 = voltage{i}.use2(:,8)/10^5;
    voltage{i}.encoderb2 = voltage{i}.use2(:,9)/10^5;
    voltage{i}.encoderb2 = voltage{i}.encoderb2/div2(i);
    if plot2 == 1
        figure
        plot(voltage{i}.time2, voltage{i}.encoderb2)
        %plot(voltage{i}.time2, voltage{i}.encodera2, ;...
        voltage{i}.time2, voltage{i}.encoderb2)
        hold on
        title(sprintf('Encoder Position %d',i))
        %turn off for final plots, figure description
        %in thesis names them
        line([voltage{i}.time2(x3(i)) voltage{i}.time2(x3(i))],;...
            get(gca,'ylim'),'Color',[1 0 1])
        legend('Encoder B', 'Start of Release')
        %legend('Encoder A', 'Encoder B', 'Start of Release')
        hold off
        movegui('northeast')
        filename = sprintf('encoderb_%d',i);
        saveas(gca, fullfile(fpathenc, filename), 'png');
    end
end

%Calibration Matrix Nano-25
CalMat = ;...
[ 0.01666, -0.00399, -0.31744, 2.98746, 0.42269, -3.00593;...
0.17884, -3.47015, -0.14035, 1.72288, -0.31903, 1.75159;...
5.26167, -0.04467, 5.59050, 0.20559, 5.32144, -0.10468;...
0.07209, -1.22529, 2.09820, 0.72446, -2.13718, 0.63742;...
-2.40927, 0.01016, 1.39990, -1.01331, 0.98241, 1.08087;...
0.03166, -1.11580, 0.14224, -1.09552, 0.16628, -1.10239];

%% Calculating the Force and Moment Tare Data at 0 mph

for i = 1:length(x1)
    plotting{i}.time1 = voltage{i}.use1(:,1) - voltage{i}.use1(1,1);
    voltage{i}.vfx1 = voltage{i}.use1(:,2);
    voltage{i}.vfy1 = voltage{i}.use1(:,3);
    voltage{i}.vfz1 = voltage{i}.use1(:,4);
    voltage{i}.vtx1 = voltage{i}.use1(:,5);
    voltage{i}.vty1 = voltage{i}.use1(:,6);
    voltage{i}.vtz1 = voltage{i}.use1(:,7);

```

```

for j = 1:length(voltage{1}.vfx1)
    voltages_=[voltage{i}.vfx1(j);voltage{i}.vfy1(j);...
    voltage{i}.vfz1(j);voltage{i}.vtx1(j);...
    voltage{i}.vty1(j);voltage{i}.vtz1(j)];
    voltage{i}.forces1(:,j) = CalMat*voltages_;
end

%Converting the Nano-25 Coordinate System to
%conform with AIAA standard
voltage{i}.tare_N1 = (-1)*voltage{i}.forces1(1,:);
% AIAA Normal force N corresponds to Nano25 -Fx(lbf)
voltage{i}.tare_Y1 = (-1)*voltage{i}.forces1(2,:);
% AIAA Side Force Y corresponds to Nano25 -Fy(lbf)
voltage{i}.tare_A1 = (-1)*voltage{i}.forces1(3,:);
% AIAA Axial Force A corresponds to Nano25 -Fz(lbf)
voltage{i}.tare_n1 = (1/12)*voltage{i}.forces1(4,:);
% AIAA yaw moment n Corresponds to Nano25 Tx
%converted to ft-lbs
voltage{i}.tare_m1 = -(1/12)*voltage{i}.forces1(5,:);
% AIAA pitch moment m Corresponds to Nano25 Ty
%converted to ft-lbs
voltage{i}.tare_l1 = (1/12)*voltage{i}.forces1(6,:);
%L1 % AIAA roll moment l Corresponds to Nano25 Tz
%converted to ft-lbs
end

%% Calculating the Force and Moments at 60mph

for i = 1:length(x1)
    plotting{i}.time2 = voltage{i}.use2(:,1) - voltage{i}.use2(1,1);
    %%%%%%%%%%%%%%%%%%%%%%%%%%%%%%%%%%%%%%%%%
    voltage{i}.vfx2 = voltage{i}.use2(:,2);
    voltage{i}.vfy2 = voltage{i}.use2(:,3);
    voltage{i}.vfz2 = voltage{i}.use2(:,4);
    voltage{i}.vtx2 = voltage{i}.use2(:,5);
    voltage{i}.vty2 = voltage{i}.use2(:,6);
    voltage{i}.vtz2 = voltage{i}.use2(:,7);

    for j = 1:length(voltage{1}.vfx2)
        voltages_ = [voltage{i}.vfx2(j);voltage{i}.vfy2(j);...
        voltage{i}.vfz2(j);voltage{i}.vtx2(j);...
        voltage{i}.vty2(j);voltage{i}.vtz2(j)];
    end
end

```

```

        voltage{i}.forces2(:,j) = CalMat*voltages_;
    end

    %Converting the Nano-25 Coordinate System to
    %conform with AIAA standard
    voltage{i}.tare_N2 = (-1)*voltage{i}.forces2(1,:);
    % AIAA Normal force N corresponds to Nano25 -Fx(lbf)
    voltage{i}.tare_Y2 = (-1)*voltage{i}.forces2(2,:);
    % AIAA Side Force Y corresponds to Nano25 -Fy(lbf)
    voltage{i}.tare_A2 = (-1)*voltage{i}.forces2(3,:);
    % AIAA Axial Force A corresponds to Nano25 -Fz(lbf)
    voltage{i}.tare_n2 = (1/12)*voltage{i}.forces2(4,:);
    % AIAA yaw moment n Corresponds to Nano25 Tx
    %converted to ft-lbs
    voltage{i}.tare_m2 = -(1/12)*voltage{i}.forces2(5,:);
    % AIAA pitch moment m Corresponds to Nano25 Ty
    %converted to ft-lbs
    voltage{i}.tare_l2 = (1/12)*voltage{i}.forces2(6,:);
    % AIAA roll moment l Corresponds to Nano25 Tz
    %converted to ft-lbs
end

% (-1) is for AIAA convention and F_ corresponds to Nano25(lbf)
%and T_ Corresponds to Nano25converted to ft-lb

%% Calculating and Plotting the TARED Data by subtracting the
%Tare Values from the
%Measured at Velocity, Normal Force Data

%set above axes1 = {[0 1 -2 1.5], [0 1 -2 1], [0 1 -2 2], ;...
[0 1 -2 2], [0 1 -2 1], [0 1 -2.5 1], [0 1 -2 2], [0 1 -2 1]};

%Plots of the Data at Wind Tunnel Velocity vs. Tared
for i = 1:length(x1)
    plotting{i}.tared_N = voltage{i}.tare_N2 - voltage{i}.tare_N1;
    plotting{i}.tared_Y = voltage{i}.tare_Y2 - voltage{i}.tare_Y1;
    plotting{i}.tared_A = voltage{i}.tare_A2 - voltage{i}.tare_A1;
    plotting{i}.tared_n = voltage{i}.tare_n2 - voltage{i}.tare_n1;
    plotting{i}.tared_m = voltage{i}.tare_m2 - voltage{i}.tare_m1;
    plotting{i}.tared_l = voltage{i}.tare_l2 - voltage{i}.tare_l1;
    if plot3 == 1
        figure('Position',[100 100 1200 800]);
        plot(plotting{i}.time2,voltage{i}.tare_N2); hold on;
    end
end

```

```

plot(plotting{i}.time1,voltage{i}.tare_N1);
plot(plotting{i}.time2,plotting{i}.tared_N);

name1 = sprintf('Normal Force (F_{N%d}): Slot',i);
%set above %name2 = 'Missile, AoA: 10 deg, 60 MPH';
if i == 1
    name2 = name2_1;
elseif i == 2
    name2 = name2_2;
elseif i == 3
    name2 = name2_3;
end
title({name1,name2},'fontweight','bold','fontsize',18)
xlabel('time (s)','Interpreter','latex','fontsize',18)
% x-axis label
ylabel('lbf','Interpreter','latex','fontsize',18)
% y-axis label
name3 = sprintf('F_{N%d}',i);
name4 = sprintf('Tare F_{N%d}',i);
name5 = sprintf('TARED F_{N%d}',i);
legend({name3,name4,name5},'FontSize',12,'Location',;...
'bestoutside');hold off
axis(axes1{i}) %[0 1 -3 1])
filename = sprintf('normalforce_%d',i);
saveas(gca, fullfile(fpath, filename), 'png');
end
if plot6 == 1
figure('Position',[100 100 1200 800]);
plot(plotting{i}.time2,voltage{i}.tare_m2); hold on;
plot(plotting{i}.time1,voltage{i}.tare_m1);
plot(plotting{i}.time2,plotting{i}.tared_m);

name1 = sprintf('Pitch Moment (F_{m%d}):',i);
%set above %name2 = 'Missile, AoA: 10 deg, 60 MPH';
if i == 1
    name2 = name2_1;
elseif i == 2
    name2 = name2_2;
elseif i == 3
    name2 = name2_3;
end
title({name1,name2},'fontweight','bold','fontsize',18)
xlabel('time (s)','Interpreter','latex','fontsize',18)

```

```

% x-axis label
ylabel('lbf','Interpreter','latex','fontsize',18)
% y-axis label
name3 = sprintf('F_{m%d}',i);
name4 = sprintf('Tare F_{m%d}',i);
name5 = sprintf('TARED F_{m%d}',i);
legend({name3,name4,name5},'Fontsize',12,'Location',;...
'bestoutside');hold off
axis(axespt{i}) %[0 1 -3 1])
filename = sprintf('pitchmomenttare_%d',i);
saveas(gca, fullfile(fpath, filename), 'png');
end
if plot9 == 1
figure('Position',[100 100 1200 800]);
plot(plotting{i}.time2,voltage{i}.tare_A2); hold on;
plot(plotting{i}.time1,voltage{i}.tare_A1);
plot(plotting{i}.time2,plotting{i}.tared_A);

name1 = sprintf('Axial Force (F_{A%d}):',i);
%set above %name2 = 'Missile, AoA: 10 deg, 60 MPH';
if i == 1
    name2 = name2_1;
elseif i == 2
    name2 = name2_2;
elseif i == 3
    name2 = name2_3;
end
title({name1,name2},'fontweight','bold','fontsize',18)
xlabel('time (s)','Interpreter','latex','fontsize',18)
% x-axis label
ylabel('lbf','Interpreter','latex','fontsize',18)
% y-axis label
name3 = sprintf('F_{A%d}',i);
name4 = sprintf('Tare F_{A%d}',i);
name5 = sprintf('TARED F_{A%d}',i);
legend({name3,name4,name5},'Fontsize',12,'Location',;...
'bestoutside');hold off
axis(axesat{i}) %[0 1 -3 1])
filename = sprintf('axialforcetare_%d',i);
saveas(gca, fullfile(fpath, filename), 'png');
end
end
end

```

```

%% Calculate Coefficients
q1 = (1/2)*rho*V_inf1^2; %Dynamic Pressure
q2 = (1/2)*rho*V_inf2^2; %Dynamic Pressure
q3 = (1/2)*rho*V_inf3^2; %Dynamic Pressure

for i = 1:length(x1)
    if i == 1
        q = q1;
    elseif i == 2
        q = q2;
    elseif i == 3
        q = q3;
    end
    voltage{i}.CN = (plotting{i}.tared_N) / (q*Ref_Area);
    %Normal Force Coeff
    voltage{i}.CY = (plotting{i}.tared_Y) / (q*Ref_Area);
    %Side Force Coeff
    voltage{i}.CA = (plotting{i}.tared_A) / (q*Ref_Area);
    %Axial Force Coeff
    voltage{i}.Cl = (plotting{i}.tared_n) / (q*Ref_Area*Dia);
    %Roll Moment Coeff
    voltage{i}.Cm = (plotting{i}.tared_m) / (q*Ref_Area*Dia);
    %Pitch Moment Coeff
    voltage{i}.Cn = (plotting{i}.tared_l) / (q*Ref_Area*Dia);
    %Yaw Moment Coeff
end

%% Filter for Coefficient Data Sets_Slot
%Transforming the noisy data array from a row into a column

for i = 1:length(x1)
    voltage{i}.CN = voltage{i}.CN';
    voltage{i}.CY = voltage{i}.CY';
    voltage{i}.CA = voltage{i}.CA';
    voltage{i}.Cl = voltage{i}.Cl';
    voltage{i}.Cm = voltage{i}.Cm';
    voltage{i}.Cn = voltage{i}.Cn';
end

%% Design a -th order lowpass FIR filter with cutoff;...
frequency of (Hz)
%set above Fs = 100;    % sample rate in Hz

```

```

%set above cof = 25;    % cufoff frequency in Hz
%set above order = 60; % -th Order of lowpas filter
Fnorm = cof/(Fs/2); % Normalized frequency

%MATLAB digital filter Function

for i = 1:length(x1)
    df = designfilt('lowpassfir','FilterOrder',order,;...
        'CutoffFrequency',Fnorm);
    Delay = mean(grpdelay(df)); % filter delay in samples
    filtered{i}.CN = filter(df,[voltage{i}.CN; zeros(Delay,1)]);
    % Delay zeros concatenated with the input data
    filtered{i}.CN = filtered{i}.CN(Delay+1:end);
    % Shift data to compensate for delay
    filtered{i}.CY = filter(df,[voltage{i}.CY; zeros(Delay,1)]);
    filtered{i}.CY = filtered{i}.CY(Delay+1:end);
    filtered{i}.CA = filter(df,[voltage{i}.CA; zeros(Delay,1)]);
    filtered{i}.CA = filtered{i}.CA(Delay+1:end);
    filtered{i}.Cl = filter(df,[voltage{i}.Cn; zeros(Delay,1)]);
    filtered{i}.Cl = filtered{i}.Cl(Delay+1:end);
    filtered{i}.Cm = filter(df,[voltage{i}.Cm; zeros(Delay,1)]);
    filtered{i}.Cm = filtered{i}.Cm(Delay+1:end);
    filtered{i}.Cn = filter(df,[voltage{i}.Cl; zeros(Delay,1)]);
    filtered{i}.Cn = filtered{i}.Cn(Delay+1:end);
end

%% Plotting Normal Force Coefficients
%Normal Force Coeff

%set above axes2 = {[0 1 -15 15], [0 1 -6 5], [0 1 -5 15], ;...
[0 1 -6 17], [0 1 -6 5], [0 1 -15 8], [0 1 -6 17], [0 1 -4 7]};

for i = begi:endi
    if plot4 == 1
        figure('Position',[100 100 1200 600]);
        plot(plotting{i}.time2(1:end),voltage{i}.CN(1:end));;...
        hold on;
        plot(plotting{i}.time2(1:end),filtered{i}.CN(1:end));;...
        'Linewidth',1.5); grid on;
        name1 = sprintf('Normal Force Coefficient (C_{N%d}):',i);
        %set at top %name2 = 'Missile, AoA: 10 deg, 60 MPH';
        if i == 1
            name2 = name2_1;

```

```

elseif i == 2
    name2 = name2_2;
elseif i == 3
    name2 = name2_3;
end
title({name1,name2},'fontweight','bold','fontsize',18);
name3 = sprintf('C_{N%d,unfiltered}',i);
name4 = sprintf('C_{N%d,filtered}',i);
legend({name3,name4},'Fontsize',14,'Location','bestoutside');
xlabel('time (s)','Interpreter','latex','fontsize',18)
% x-axis label
ylabel('$C_{N}$','Interpreter','latex','fontsize',18)
% y-axis label
axis(axes2{i}); hold off; %axis([0 1 -10 10]); hold off;
filename = sprintf('normalforcecoefficient_%d',i);
saveas(gca, fullfile(fpath, filename), 'png');
end
end

%% Plotting Normal Force Coefficients COMBINED
%COMBINED, zoomed in
if plot5 == 1
figure('Position',[100 100 1200 600]);
for i = begi:endi
    plot(plotting{i}.time2(1:end),filtered{i}.CN(1:end));...
    hold on; grid on; %plot(time_1(1:end),filtered_CN_1(1:end));
end
    name1 = 'Normal Force Coefficient (C_{N}): Combined';
    counti = 1;
    legend_s = [60,100,120];
for j = begi:endi
    legendi{counti} = sprintf('C_{N%d,filtered}',legend_s(j));
    counti = counti + 1;
end
    title({name1,name_base},...
        'fontweight','bold','fontsize',18);
    legend(legendi,'Fontsize',12,'Location','bestoutside');
    xlabel('time (s)','Interpreter','latex','fontsize',18)
    % x-axis label
    ylabel('$C_{N}$','Interpreter','latex','fontsize',18)
    % y-axis label
    axis(axesnc); hold off;

```

```

        filename = 'normalforcecoefficient_all';
        saveas(gca, fullfile(fpath, filename), 'png');
    end
    %Averaging the Normal Force Coeff Data
    % CN_avg = (filtered_CN_1 + filtered_CN_2 + filtered_CN_3 +;...
    filtered_CN_4 + filtered_CN_5) / 5;
    % figure('Position',[100 100 900 480]); plot(time_1(50:1900),;...
    CN_avg(50:1900)); hold on; grid on;
    %         title({'Average Normal Force Coefficient (C_{N}):;...
    Slot, Max Stroke','Missile, AoA: 10 deg, 100 MPH'},...
    %         'fontweight','bold','fontsize',16);
    % %         legend({'C_{N1,filtered}','C_{N2,filtered}',;...
    'C_{N3,filtered}','C_{N4,filtered}','C_{N5,filtered}',...
    % %         'FontSize',12,'Location','bestoutside');
    %         xlabel('time (s)','Interpreter','latex',;...
    'fontsize',18) % x-axis label
    %         ylabel('$C_{N}$','Interpreter','latex',;...
    'fontsize',18) % y-axis label
    %         hold off; axis([0.05 1.9 0 2.5]); set(findall;...
    (gca, 'Type', 'Line'),'LineWidth',1.5);

%% Plotting Pitch Moment Coefficients

if plot7 == 1
for i = begi:end
    figure('Position',[100 100 1200 600]);
    plot(plotting{i}.time2(1:end),voltage{i}.Cm(1:end));;...
    hold on;
    plot(plotting{i}.time2(1:end),filtered{i}.Cm(1:end),;...
    'Linewidth',1.5); grid on;
    name1 = sprintf('Pitch Moment Coefficient (C_{M%d}):',i);
    %set at top %name2 = 'Missile, AoA: 10 deg, 60 MPH';
    if i == 1
        name2 = name2_1;
    elseif i == 2
        name2 = name2_2;
    elseif i == 3
        name2 = name2_3;
    end
    title({name1,name2},'fontweight','bold','fontsize',18);
    name3 = sprintf('C_{M%d,unfiltered}',i);
    name4 = sprintf('C_{M%d,filtered}',i);
    legend({name3,name4},'FontSize',14,'Location',;...

```

```

        'bestoutside');
xlabel('time (s)','Interpreter','latex','fontsize',18)
% x-axis label
ylabel('$C_{M}$','Interpreter','latex','fontsize',18)
% y-axis label
axis(axespc1{i}); hold off; %axis([0 1 -10 10]);;...
hold off;
filename = sprintf('pitchmomentcoefficient_%d',i);
saveas(gca, fullfile(fpath, filename), 'png');
end
end

%% Plitting Pitch Moment Coefficients Combined
%COMBINED, filtered, zoomed in
if plot8 == 1
figure('Position',[100 100 1200 600]);
for i = begi:endi
    plot(plotting{i}.time2(1:end),filtered{i}.Cm(1:end));;...
    hold on; grid on; %plot(time_1(1:end),filtered_CN_1(1:end));
end
    name1 = 'Pitch Moment Coefficient (C_{m}): Combined';
    counti = 1;
    legend_s = [60,100,120];
for j = begi:endi
    legendi{counti} = sprintf('C_{m%d,filtered}',legend_s(j));
    counti = counti + 1;
end
    title({name1,name_base},...
        'fontweight','bold','fontsize',16);
    legend(legendi,'FontSize',12,'Location','bestoutside');
xlabel('time (s)','Interpreter','latex','fontsize',18)
% x-axis label
ylabel('$C_{m}$','Interpreter','latex','fontsize',18)
% y-axis label
axis(axespc); hold off; %set(findall(gca, 'Type',;...
'Line'),'LineWidth',1.5);
filename = 'pitchmomentcoefficient_all';
saveas(gca, fullfile(fpath, filename), 'png');
end

%% Plotting Axial Force Coefficients
if plot10 == 1
for i = begi:endi

```

```

figure('Position',[100 100 1200 600]);
plot(plotting{i}.time2(1:end),voltage{i}.CA(1:end));;...
hold on;
plot(plotting{i}.time2(1:end),filtered{i}.CA(1:end));;...
'Linewidth',1.5); grid on;
name1 = sprintf('Axial Force Coefficient (C_{A%d}):',i);
%set at top %name2 = 'Missile, AoA: 10 deg, 60 MPH';
if i == 1
    name2 = name2_1;
elseif i == 2
    name2 = name2_2;
elseif i == 3
    name2 = name2_3;
end
title({name1,name2},'fontweight','bold','fontsize',18);
name3 = sprintf('C_{A%d,unfiltered}',i);
name4 = sprintf('C_{A%d,filtered}',i);
legend({name3,name4},'FontSize',14,'Location',;...
'bestoutside');
xlabel('time (s)','Interpreter','latex','fontsize',18)
% x-axis label
ylabel('$C_{A}$','Interpreter','latex','fontsize',18)
% y-axis label
axis(axesac1{i}); hold off; %axis([0 1 -10 10]);;...
hold off;
filename = sprintf('axialforcecoefficient_%d',i);
saveas(gca, fullfile(fpath, filename), 'png');
end
end
%% Plotting Axial Force Coefficients Combined
%COMBINED, zoomed in
if plot11 == 1
figure('Position',[100 100 1200 600]);
for i = begi:endi
    plot(plotting{i}.time2(1:end),filtered{i}.CA(1:end));;...
    hold on; grid on;
end
    name1 = 'Axial Force Coefficient (C_{A}): Combined';
    counti = 1;
    legend_s = [60,100,120];
for j = begi:endi
    legendi{counti} = sprintf('C_{A%d,filtered}',legend_s(j));
    counti = counti + 1;
end

```

```

end
    title({name1,name_base},...
        'fontweight','bold','fontsize',16);
    legend(legendi,'FontSize',12,'Location','bestoutside');
    xlabel('time (s)','Interpreter','latex','fontsize',18)
    % x-axis label
    ylabel('$C_{A}$','Interpreter','latex','fontsize',18)
    % y-axis label
    axis(axesac); hold off; %set(findall(gca, 'Type', ;...
    'Line'),'LineWidth',1.5);
    filename = 'axialforcecoefficient_all';
    saveas(gca, fullfile(fpath, filename), 'png');
end

```

Phase II: Matlab Code

Dynamic Release Example Code

```
%Tare, Force, and Coefficient Code
%Authored by 2d Lt Ryan Saunders, USAF, and Capt Matt Wood, USMC
clear all;close all;clc

%% Set Values (only change values in this section -
%except axes on plots)
%ctrl+f 'set above' to find the below values, uncomment
%to run different
%sections by themselves
%must convert any .txt files to .csv (can use delimiting
%method in excel)
%can uncomment lines 100-112 to get encoder positions of
%_mph data
%can make single pitch coefficient and axial coefficient
%plots
%must make all folders used in fpath and fpathenc
mph = 120;
Fahrenheit = 79.7;
Inches_Hg = 29.1990;
d = 1.3; %diameter of model in inches
L = 2.0; % weapon bay length (ft)

begi = 1; %changes which items are plotted
endi = 4; %need to manually change name of plots if you care

name2 = 'Slot, Small Model, AoA: 10 deg, 120 MPH';
fpath = 'F:\Thesis\Post Process\Small Model\slot\10AoA\...\
120mph\figures';
fpathenc = 'F:\Thesis\Post Process\Small Model\slot\10AoA\120mph\...\
figures\encoders';
%tare encoder indices
x1 = [4000,3000,4000,3000]; %[349,348,249,351];
%x1 = x1+100;
%x1(4) = x1(4)-62;
x2 = [x1(1)-2000,x1(2)-2000,x1(3)-2000,x1(4)-2000];
x3 = [50,50,50,50]; %uncomment lines 75-76 to use
div1 = [0.5,0.8,0.6,0.8]; %need to uncomment lines 61, 66 to use
%_mph indices
x4 = [4003,3005,4008,3000]; %[354,354,256,352];
```

```

%x4 = x4+100;
%x4(4) = x4(4)-62;
x5 = [x4(1)-2000,x4(2)-2000,x4(3)-2000,x4(4)-2000];
div2 = [0.5,0.8,0.6,0.8];

Fs = 1000;    % sample rate in Hz +
cof = 15;     % cufoff frequency in Hz
order = 60;  % -th Order of lowpas filter

plot1 = 0; %encoder plot, 1 yes, 0 no
plot2 = 0; %unnecessary, mph encoder plot, 1 yes, 0 no
%
plot3 = 0; %Force and Taring plot, 1 yes, 0 no
plot4 = 0; %Normal Force Coeff plot, 1 yes, 0 no
plot5 = 0; %combined Normal Force Coeff plot, 1 yes, 0 no
%
plot6 = 1; %Pitch Moment Taring plot, 1 yes, 0 no
plot7 = 1; %Pitch Moment Coeff plot, 1 yes, 0 no
plot8 = 1; %Combined Pitch Moment Coeff plot, 1 yes, 0 no
%
plot9 = 0; %Axial Force Taring plot, 1 yes, 0 no
plot10 = 0; %Axial Force Coeff plot, 1 yes, 0 no
plot11 = 0; %Combined Axial Force Coeff plot, 1 yes, 0 no

%line 178 Normal Force Tared
axes1 = {[0 2 -4 1.5], [0 2 -4 1.5], [0 2 -4 1.5], [0 2 -4 1.5]};
%line 253 Normal Force Coefficient
axes2 = {[0 2 -1 2], [0 2 -1 2], [0 2 -1 2], [0 2 -1 2]};
%normal force coefficient combined
axesnc = [0 2 -1 2];

%Pitch Moment Tared
axespt = {[0 2 -0.1 0.25], [0 2 -0.1 0.25], [0 2 -0.1 0.25],;...
[0 2 -0.1 0.25]};
%pitch moment coefficient
axespc1 = {[0 2 -1 1], [0 2 -1 1], [0 2 -1 1], [0 2 -1 1]};
%pitch moment coefficient combined
axespc = [0 2 -0.6 0.75];

```

```

%Axial Moment Tared
axesat = {[0 2 -1 2], [0 2 -1 2], [0 2 -1 2], [0 2 -1 2]};
%axial force coefficient
axesac1 = {[0 2 -1 1], [0 2 -1 2], [0 2 -1 1], [0 2 -1 1]};
%axial force coefficient combined
axesac = [0 2 -1 1];

%% Missile and Wind Tunnel Properties

V_inf = mph*(1/3600)*(5280);
% MPH freestream vel converted to (ft/s)
%set above Fahrenheit = 77.2;
%set above Inches_Hg = 28.9845;
    %set above L = 2.0; % weapon bay length (ft)
    Dia = d/12; % missile diameter converted to (ft)
    Ref_Area = (pi/4)*Dia^2; % Model reference Area (ft^2)
    P_psi = Inches_Hg*0.49115420057253 ;
    % Inches Hg converted to psi
    P_psf = P_psi*12^2; %psi to psf
    T = Fahrenheit + 459.67;
    % temp deg F converted to Rankine
    R = 1716;
    % (lb-ft)/(slug-R) Imperial Gas constant for Dry Air
rho = P_psf/(R*T); % density from ideal gas law [slug/ft^3]

%% Importing and Plotting Encoder Positions

filename1 = {'1.csv', '2.csv', '3.csv', '4.csv'};
%set above x1 = [350,350,250,350,350,350,250,350];
%set above x2 = [250,250,150,250,250,250,150,250];
%set above x3 = [52,39,46,49,48,45,51,41];
%set above div1 = [0.5,0.8,0.6,0.8,0.5,0.75,0.3,1.8];

%0 mph Case Data Imported from .csv
%plot Encoder Data to line up timing
for i = 1:length(x1)
    voltage{i}.import1 = csvread(filename1{i});
    voltage{i}.use1 = voltage{i}.import1(end-x1(i):end-x2(i),:);
    voltage{i}.time1 = voltage{i}.use1(:,1);
    voltage{i}.encodera1 = voltage{i}.use1(:,8)/10^5;
    voltage{i}.encoderb1 = voltage{i}.use1(:,9)/10^5;
    voltage{i}.encoderb1 = voltage{i}.encoderb1/div1(i);

```

```

    if plot1 == 1
    figure
    plot(voltage{i}.time1, voltage{i}.encoderb1)
    %plot(voltage{i}.time1, voltage{i}.encodera1,;...
    voltage{i}.time1, voltage{i}.encoderb1);...
    hold on
    title(sprintf('Encoder Position %d',i))
    %turn off for final plots, figure description
    %in thesis names them
    line([voltage{i}.time1(x3(i)) ;...
    voltage{i}.time1(x3(i))],get(gca,;...
    'ylim'),'Color',[1 0 1])
    legend('Encoder B', 'Start of Release')
    legend('Encoder B')
    %legend('Encoder A', 'Encoder B', 'Start of Release')
    hold off
    movegui('northeast')
    filename = sprintf('encoder_%d',i);
    saveas(gca, fullfile(fpathenc, filename), 'png');
    end
end
%additional commands to manipulate figures
% [pks, locs] = findpeaks(enca_1);
% xx1 = t1(locs(1));
% line([xx1 xx1],get(gca,'ylim'),'Color',[1 0 1])
% x1 = t2(100);
% loc =;...
islocalmin(enca_2,1); locs = find(loc);
% xx1 = t2(locs(1));
% line([x1 x1],get(gca,'ylim'),'Color',[1 0 1])
% hold on
% line([xx1 xx1],get(gca,'ylim'),'Color',[0 1 0])
% title('Encoder Positions 2');...
% legend('Encoder A', 'Encoder B', 'start', 'min')

%% Importing For Force Data and Calibration Matrix

%Voltage Import
%_mph Case Data Imported from .csv
filename2 = {'1_.csv', '2_.csv', '3_.csv', '4_.csv'};
%set above x4 = [350,350,250,350,350,350,250,350];
%set above x5 = [250,250,150,250,250,250,150,250];
%set above div2 = [0.5,0.8,0.6,0.8,0.5,0.75,0.3,1.8];

```

```

for i = 1:length(x1)
    voltage{i}.import2 = csvread(filename2{i});
    %Data Imported from .csv
    voltage{i}.use2 = voltage{i}.import2;...
    (end-x4(i):end-x5(i),:);...
    %Taking the 2 seconds of data around the event
    voltage{i}.time2 = voltage{i}.use2(:,1);
    voltage{i}.encodera2 = voltage{i}.use2(:,8)/10^5;
    voltage{i}.encoderb2 = voltage{i}.use2(:,9)/10^5;
    voltage{i}.encoderb2 = voltage{i}.encoderb2/div2(i);
    if plot2 == 1
        figure
        plot(voltage{i}.time2, voltage{i}.encoderb2)
        %plot(voltage{i}.time2, voltage{i}.encodera2,;...
        voltage{i}.time2,
        voltage{i}.encoderb2)
        hold on
        title(sprintf('Encoder Position %d',i))
        %turn off for final;...
        plots, figure description in thesis names them
        line([voltage{i}.time2(x3(i)) voltage{i}.time2(x3(i))],;...
        time2(x3(i))],;...
        get(gca,'ylim'),'Color',[1 0 1])
        legend('Encoder B', 'Start of Release')
        %legend('Encoder A', 'Encoder B', 'Start of Release')
        hold off
        movegui('northeast')
        filename = sprintf('encoderb_%d',i);
        saveas(gca, fullfile(fpathenc, filename), 'png');
    end
end

%Calibration Matrix Nano-25
CalMat =;...
[ 0.01666, -0.00399, -0.31744, 2.98746, 0.42269, -3.00593;...
0.17884, -3.47015, -0.14035, 1.72288, -0.31903, 1.75159;...
5.26167, -0.04467, 5.59050, 0.20559, 5.32144, -0.10468;...
0.07209, -1.22529, 2.09820, 0.72446, -2.13718, 0.63742;...
-2.40927, 0.01016, 1.39990, -1.01331, 0.98241, 1.08087;...
0.03166, -1.11580, 0.14224, -1.09552, 0.16628, -1.10239];

%% Calculating the Force and Moment Tare Data at 0 mph

```

```

for i = 1:length(x1)
    plotting{i}.time1 = voltage{i}.use1(:,1) - voltage{i}.use1(1,1);
    voltage{i}.vfx1 = voltage{i}.use1(:,2);
    voltage{i}.vfy1 = voltage{i}.use1(:,3);
    voltage{i}.vfz1 = voltage{i}.use1(:,4);
    voltage{i}.vtx1 = voltage{i}.use1(:,5);
    voltage{i}.vty1 = voltage{i}.use1(:,6);
    voltage{i}.vtz1 = voltage{i}.use1(:,7);

    for j = 1:length(voltage{1}.vfx1)
        voltages_=[voltage{i}.vfx1(j);voltage{i}.vfy1(j);...
            voltage{i}.vfz1(j);voltage{i}.vtx1(j);...
            voltage{i}.vty1(j);voltage{i}.vtz1(j)];
        voltage{i}.forces1(:,j) = CalMat*voltages_;
    end

    %Converting the Nano-25 Coordinate System to conform
    with AIAA standard
    voltage{i}.tare_N1 = (-1)*voltage{i}.forces1(1,:);
    % AIAA Normal force N corresponds to Nano25 -Fx(lbf)
    voltage{i}.tare_Y1 = (-1)*voltage{i}.forces1(2,:);
    % AIAA Side Force Y corresponds to Nano25 -Fy(lbf)
    voltage{i}.tare_A1 = (-1)*voltage{i}.forces1(3,:);
    % AIAA Axial Force A corresponds to Nano25 -Fz(lbf)
    voltage{i}.tare_n1 = (1/12)*voltage{i}.forces1(4,:);
    % AIAA yaw moment n Corresponds to Nano25 Tx
    %converted to ft-lbs
    voltage{i}.tare_m1 = -(1/12)*voltage{i}.forces1(5,:);
    % AIAA pitch moment m Corresponds to Nano25 Ty
    %converted to ft-lbs
    voltage{i}.tare_l1 = (1/12)*voltage{i}.forces1(6,:); %L1
    % AIAA roll moment l Corresponds to Nano25 Tz
    %converted to ft-lbs
end

%% Calculating the Force and Moments at 60mph

for i = 1:length(x1)
    plotting{i}.time2 = voltage{i}.use2(:,1) - voltage{i}.use2(1,1);
    %%%%%%%%%%%%%%%%%%%%%%%%%%%%%%%%%%%%%%%%%%%%%%%%%%%%%%%%%%%%%%%%%%%%%%%%%
    voltage{i}.vfx2 = voltage{i}.use2(:,2);
    voltage{i}.vfy2 = voltage{i}.use2(:,3);

```

```

voltage{i}.vfz2 = voltage{i}.use2(:,4);
voltage{i}.vtx2 = voltage{i}.use2(:,5);
voltage{i}.vty2 = voltage{i}.use2(:,6);
voltage{i}.vtz2 = voltage{i}.use2(:,7);

for j = 1:length(voltage{1}.vfx2)
    voltages_ = [voltage{i}.vfx2(j);voltage{i}.vfy2(j);...
    voltage{i}.vfz2(j);voltage{i}.vtx2(j);...
    voltage{i}.vty2(j);voltage{i}.vtz2(j)];
    voltage{i}.forces2(:,j) = CalMat*voltages_;
end

%Converting the Nano-25 Coordinate System to
%conform with AIAA standard
voltage{i}.tare_N2 = (-1)*voltage{i}.forces2(1,:);
% AIAA Normal force N corresponds to Nano25 -Fx(lbf)
voltage{i}.tare_Y2 = (-1)*voltage{i}.forces2(2,:);
% AIAA Side Force Y corresponds to Nano25 -Fy(lbf)
voltage{i}.tare_A2 = (-1)*voltage{i}.forces2(3,:);
% AIAA Axial Force A corresponds to Nano25 -Fz(lbf)
voltage{i}.tare_n2 = (1/12)*voltage{i}.forces2(4,:);
% AIAA yaw moment n Corresponds to Nano25 Tx
%converted to ft-lbs
voltage{i}.tare_m2 = -(1/12)*voltage{i}.forces2(5,:);
% AIAA pitch moment m Corresponds to Nano25 Ty
%converted to ft-lbs
voltage{i}.tare_l2 = (1/12)*voltage{i}.forces2(6,:);
% AIAA roll moment l Corresponds to Nano25 Tz
%converted to ft-lbs
end

% (-1) is for AIAA convention and F_ corresponds to Nano25(lbf)
%and T_ Corresponds to Nano25converted to ft-lb

%% Calculating/Plotting the TARED Data by subtracting
%the Tare Values from the
%Measured at Velocity, Normal Force Data

%set above axes1 = {[0 1 -2 1.5], [0 1 -2 1], [0 1 -2 2],;...
[0 1 -2 2], [0 1 -2 1], [0 1 -2.5 1], [0 1 -2 2], [0 1 -2 1]};

%Plots of the Data at Wind Tunnel Velocity vs. Tared
for i = 1:length(x1)

```

```

plotting{i}.tared_N = voltage{i}.tare_N2 - voltage{i}.tare_N1;
plotting{i}.tared_Y = voltage{i}.tare_Y2 - voltage{i}.tare_Y1;
plotting{i}.tared_A = voltage{i}.tare_A2 - voltage{i}.tare_A1;
plotting{i}.tared_n = voltage{i}.tare_n2 - voltage{i}.tare_n1;
plotting{i}.tared_m = voltage{i}.tare_m2 - voltage{i}.tare_m1;
plotting{i}.tared_l = voltage{i}.tare_l2 - voltage{i}.tare_l1;
if plot3 == 1
figure('Position',[100 100 1200 800]);
plot(plotting{i}.time2,voltage{i}.tare_N2); hold on;
plot(plotting{i}.time1,voltage{i}.tare_N1);
plot(plotting{i}.time2,plotting{i}.tared_N);
name1 = sprintf('Normal Force (F_{N%d}):',i);
%set above %name2 = 'Missile, AoA: 10 deg, 60 MPH';
title({name1,name2},'fontweight','bold','fontsize',18)
xlabel('time (s)','Interpreter','latex','fontsize',18)
% x-axis label
ylabel('lbf','Interpreter','latex','fontsize',18)
% y-axis label
name3 = sprintf('F_{N%d}',i);
name4 = sprintf('Tare F_{N%d}',i);
name5 = sprintf('TARED F_{N%d}',i);
legend({name3,name4,name5},'Fontsize',12,'Location',;...
'bestoutside');...
hold off
axis(axes1{i}) %[0 1 -3 1])
filename = sprintf('normalforcetare_%d',i);
saveas(gca, fullfile(fpath, filename), 'png');
end
if plot6 == 1
figure('Position',[100 100 1200 800]);
plot(plotting{i}.time2,voltage{i}.tare_m2); hold on;
plot(plotting{i}.time1,voltage{i}.tare_m1);
plot(plotting{i}.time2,plotting{i}.tared_m);
name1 = sprintf('Pitch Moment (F_{m%d}):',i);
%set above %name2 = 'Missile, AoA: 10 deg, 60 MPH';
title({name1,name2},'fontweight','bold','fontsize',18)
xlabel('time (s)','Interpreter','latex','fontsize',18)
% x-axis label
ylabel('lbf','Interpreter','latex','fontsize',18)
% y-axis label
name3 = sprintf('F_{m%d}',i);
name4 = sprintf('Tare F_{m%d}',i);
name5 = sprintf('TARED F_{m%d}',i);

```

```

legend({name3,name4,name5},'FontSize',12,'Location',;...
'bestoutside');...
hold off
axis(axespt{i}) %[0 1 -3 1])
filename = sprintf('pitchmomenttare_%d',i);
saveas(gca, fullfile(fpath, filename), 'png');
end
if plot9 == 1
figure('Position',[100 100 1200 800]);
plot(plotting{i}.time2,voltage{i}.tare_A2); hold on;...
plot(plotting{i}.time1,voltage{i}.tare_A1);...
plot(plotting{i}.time2,plotting{i}.tared_A);
name1 = sprintf('Axial Force (F_{A%d}):',i);
%set above %name2 = 'Missile, AoA: 10 deg, 60 MPH';
title({name1,name2},'fontweight','bold','fontsize',18)
xlabel('time (s)','Interpreter','latex','fontsize',18)
% x-axis label
ylabel('lbf','Interpreter','latex','fontsize',18)
% y-axis label
name3 = sprintf('F_{A%d}',i);
name4 = sprintf('Tare F_{A%d}',i);
name5 = sprintf('TARED F_{A%d}',i);
legend({name3,name4,name5},'FontSize',12,'Location',;...
'bestoutside');...
hold off
axis(axesat{i}) %[0 1 -3 1])
filename = sprintf('axialforcetare_%d',i);
saveas(gca, fullfile(fpath, filename), 'png');
end
end

%% Calculate Coefficients
q = (1/2)*rho*V_inf^2; %Dynamic Pressure

for i = 1:length(x1)
voltage{i}.CN = (plotting{i}.tared_N) / (q*Ref_Area);
%Normal Force Coeff
voltage{i}.CY = (plotting{i}.tared_Y) / (q*Ref_Area);
%Side Force Coeff
voltage{i}.CA = (plotting{i}.tared_A) / (q*Ref_Area);
%Axial Force Coeff
voltage{i}.Cl = (plotting{i}.tared_n) / (q*Ref_Area*Dia);

```

```

    %Roll Moment Coeff
    voltage{i}.Cm = (plotting{i}.tared_m) / (q*Ref_Area*Dia);
    %Pitch Moment Coeff
    voltage{i}.Cn = (plotting{i}.tared_l) / (q*Ref_Area*Dia);
    %Yaw Moment Coeff
end

%% Filter for Coefficient Data Sets_Slot
%Transforming the noisy data array from a row into a column

for i = 1:length(x1)
    voltage{i}.CN = voltage{i}.CN';
    voltage{i}.CY = voltage{i}.CY';
    voltage{i}.CA = voltage{i}.CA';
    voltage{i}.Cl = voltage{i}.Cl';
    voltage{i}.Cm = voltage{i}.Cm';
    voltage{i}.Cn = voltage{i}.Cn';
end

%% Design a -th order lowpass FIR filter with
% cutoff frequency of (Hz)
%set above Fs = 100;    % sample rate in Hz
%set above cof = 25;    % cutoff frequency in Hz
%set above order = 60; % -th Order of lowpas filter
Fnorm = cof/(Fs/2); % Normalized frequency

%MATLAB digital filter Function

for i = 1:length(x1)
    df = designfilt('lowpassfir','FilterOrder',order,;...
        'CutoffFrequency',Fnorm);
    Delay = mean(grpdelay(df)); % filter delay in samples
    filtered{i}.CN = filter(df,[voltage{i}.CN; zeros(Delay,1)]);
    % Delay zeros concatenated with the input data
    filtered{i}.CN = filtered{i}.CN(Delay+1:end);
    % Shift data to compensate for delay
    filtered{i}.CY = filter(df,[voltage{i}.CY; zeros(Delay,1)]);
    filtered{i}.CY = filtered{i}.CY(Delay+1:end);
    filtered{i}.CA = filter(df,[voltage{i}.CA; zeros(Delay,1)]);
    filtered{i}.CA = filtered{i}.CA(Delay+1:end);
    filtered{i}.Cl = filter(df,[voltage{i}.Cn; zeros(Delay,1)]);
    filtered{i}.Cl = filtered{i}.Cl(Delay+1:end);
    filtered{i}.Cm = filter(df,[voltage{i}.Cm; zeros(Delay,1)]);

```

```

        filtered{i}.Cm = filtered{i}.Cm(Delay+1:end);
        filtered{i}.Cn = filter(df,[voltage{i}.Cl; zeros(Delay,1)]);
        filtered{i}.Cn = filtered{i}.Cn(Delay+1:end);
    end

%% Plotting Normal Force Coefficients
%Normal Force Coeff

%set above axes2 = {[0 1 -15 15], [0 1 -6 5], [0 1 -5 15],;...
[0 1 -6 17], [0 1 -6 5], [0 1 -15 8], [0 1 -6 17], [0 1 -4 7]};

for i = begi:endi
    if plot4 == 1
        figure('Position',[100 100 1200 600]);
        plot(plotting{i}.time2(1:end),voltage{i}.CN(1:end)); hold on;
        plot(plotting{i}.time2(1:end),filtered{i}.CN(1:end),;...
            'Linewidth',1.5); grid on;
        name1 = sprintf('Normal Force Coefficient (C_{N%d}):',i);
        %set at top %name2 = 'Missile, AoA: 10 deg, 60 MPH';
        title({name1,name2},'fontweight','bold','fontsize',18);
        name3 = sprintf('C_{N%d,unfiltered}',i);
        name4 = sprintf('C_{N%d,filtered}',i);
        legend({name3,name4},'FontSize',14,'Location','bestoutside');
        xlabel('time (s)','Interpreter','latex','fontsize',18)
        % x-axis label
        ylabel('$C_{N}$','Interpreter','latex','fontsize',18)
        % y-axis label
        axis(axes2{i}); hold off; %axis([0 1 -10 10]); hold off;
        filename = sprintf('normalforcecoefficient_%d',i);
        saveas(gca, fullfile(fpath, filename), 'png');
    end
end

%% Plotting Normal Force Coefficients COMBINED
%COMBINED, zoomed in
if plot5 == 1
    figure('Position',[100 100 1200 600]);
    for i = begi:endi
        plot(plotting{i}.time2(1:end),filtered{i}.CN(1:end));...
        hold on; grid on; %plot(time_1(1:end),filtered_CN_1(1:end));
    end
    name1 = 'Normal Force Coefficient (C_{N}): Combined';

```

```

        counti = 1;
    for j = begi:endi
        legendi{counti} = sprintf('C_{N%d,filtered}',j);
        counti = counti + 1;
    end
    title({name1,name2},...
        'fontweight','bold','fontsize',18);
    legend(legendi,'FontSize',12,'Location','bestoutside');
    xlabel('time (s)','Interpreter','latex','fontsize',18)
    % x-axis label
    ylabel('$C_{N}$','Interpreter','latex','fontsize',18)
    % y-axis label
    axis(axesnc); hold off;
    filename = 'normalforcecoefficient_all';
    saveas(gca, fullfile(fpath, filename), 'png');
end
%Averaging the Normal Force Coeff Data
% CN_avg = (filtered_CN_1 + filtered_CN_2 + filtered_CN_3;...
+ filtered_CN_4 + filtered_CN_5) / 5;
% figure('Position',[100 100 900 480]); plot(time_1(50:1900),;...
CN_avg(50:1900)); hold on; grid on;
%         title({'Average Normal Force Coefficient (C_{N}):;...
Slot, Max Stroke','Missile, AoA: 10 deg, 100 MPH'},...
%             'fontweight','bold','fontsize',16);
% %         legend({'C_{N1,filtered}','C_{N2,filtered}',;...
'C_{N3,filtered}','C_{N4,filtered}','C_{N5,filtered}'},...
% %             'FontSize',12,'Location','bestoutside');
%         xlabel('time (s)','Interpreter','latex',;...
'fontsize',18) % x-axis label
%         ylabel('$C_{N}$','Interpreter','latex','fontsize';...
,18) % y-axis label
%         hold off; axis([0.05 1.9 0 2.5]); set(findall;...
(gca, 'Type', 'Line'),'LineWidth',1.5);

%% Plotting Pitch Moment Coefficients

if plot7 == 1
for i = begi:endi
    figure('Position',[100 100 1200 600]);
    plot(plotting{i}.time2(1:end),voltage{i}.Cm(1:end));...
    hold on;
    plot(plotting{i}.time2(1:end),filtered{i}.Cm(1:end),;...

```

```

'Linewidth',1.5); grid on;
name1 = sprintf('Pitch Moment Coefficient (C_{M%d}):',i);
%set at top %name2 = 'Missile, AoA: 10 deg, 60 MPH';
title({name1,name2},'fontweight','bold','fontsize',18);
name3 = sprintf('C_{M%d,unfiltered}',i);
name4 = sprintf('C_{M%d,filtered}',i);
legend({name3,name4},'FontSize',14,'Location',;...
'bestoutside');
xlabel('time (s)','Interpreter','latex','fontsize',18)
% x-axis label
ylabel('$C_{M}$','Interpreter','latex','fontsize',18)
% y-axis label
axis(axespc1{i}); hold off; %axis([0 1 -10 10]);...
hold off;
filename = sprintf('pitchmomentcoefficient_%d',i);
saveas(gca, fullfile(fpath, filename), 'png');
end
end

%% Plotting Pitch Moment Coefficients Combined
%COMBINED, filtered, zoomed in
if plot8 == 1
figure('Position',[100 100 1200 600]);
for i = begi:endi
plot(plotting{i}.time2(1:end),filtered{i}.Cm(1:end));
hold on; grid on; %plot(time_1(1:end),filtered_CN_1(1:end));
end
    name1 = 'Pitch Moment Coefficient (C_{m}): Combined';
    counti = 1;
for j = begi:endi
    legendi{counti} = sprintf('C_{m%d,filtered}',j);
    counti = counti + 1;
end
    title({name1,name2},...
'fontweight','bold','fontsize',16);
    legend(legendi,'FontSize',12,'Location','bestoutside');
    xlabel('time (s)','Interpreter','latex','fontsize',18)
    % x-axis label
    ylabel('$C_{m}$','Interpreter','latex','fontsize',18)
    % y-axis label
    axis(axespc); hold off; %set(findall(gca, 'Type',;...
'Line'),'LineWidth',1.5);
    filename = 'pitchmomentcoefficient_all';

```

```

        saveas(gca, fullfile(fpath, filename), 'png');
end

%% Plotting Axial Force Coefficients
if plot10 == 1
for i = begi:endi
    figure('Position',[100 100 1200 600]);
    plot(plotting{i}.time2(1:end),voltage{i}.CA(1:end));...
    hold on;
    plot(plotting{i}.time2(1:end),filtered{i}.CA(1:end),;...
        'Linewidth',1.5); grid on;
    name1 = sprintf('Axial Force Coefficient (C_{A%d}):',i);
    %set at top %name2 = 'Missile, AoA: 10 deg, 60 MPH';
    title({name1,name2},'fontweight','bold','fontsize',18);
    name3 = sprintf('C_{A%d,unfiltered}',i);
    name4 = sprintf('C_{A%d,filtered}',i);
    legend({name3,name4},'Fontsize',14,'Location',;...
        'bestoutside');
    xlabel('time (s)','Interpreter','latex','fontsize',18)
    % x-axis label
    ylabel('$C_{A}$','Interpreter','latex','fontsize',18)
    % y-axis label
    axis(axesac1{i}); hold off; %axis([0 1 -10 10]);...
    hold off;
    filename = sprintf('axialforcecoefficient_%d',i);
    saveas(gca, fullfile(fpath, filename), 'png');
end
end

%% Plotting Axial Force Coefficients Combined
%COMBINED, zoomed in
if plot11 == 1
figure('Position',[100 100 1200 600]);
for i = begi:endi
    plot(plotting{i}.time2(1:end),filtered{i}.CA(1:end));...
    hold on; grid on;
end
    name1 = 'Axial Force Coefficient (C_{A}): Combined';
    counti = 1;
for j = begi:endi
    legendi{counti} = sprintf('C_{A%d,filtered}',j);
    counti = counti + 1;
end
    title({name1,name2},...

```

```

        'fontweight','bold','fontsize',16);
legend(legendi,'FontSize',12,'Location',;...
'bestoutside');
xlabel('time (s)','Interpreter','latex',;...
'fontsize',18) % x-axis label
ylabel('$C_{A}$','Interpreter','latex',;...
'fontsize',18) % y-axis label
axis(axesac); hold off; %set(findall(gca, ;...
'Type', 'Line'),'LineWidth',1.5);
filename = 'axialforcecoefficient_all';
saveas(gca, fullfile(fpath, filename), 'png');
end

```

Phase I: Matlab Code

Reynolds Number Calculation

```
%% Calculation of Re and Mach using SI units, Phase 1
clear all;clc; close all
%small model
V_inf = [60, 100, 120, 60, 100, 120, 60, 60,;...
        60, 100, 100, 100, 120, 120, 120, 60, 60,;...
        60, 100, 100, 100, 120, 120, 120];
V_inf = V_inf*0.44704;
%freestream velocity converted to (m/s)
%small
Fs = [74.0 75.0 76.0 72.2 73.5 74.0 80.3 80.3;...
     80.3 80.3 80.3 80.3 80.3 80.3 80.3 77.1;...
     77.1 77.1 77.1 77.1 77.1 77.1 77.1 77.1];
%temperature
%large
F1 = [75.0 75.9 76.5 75.5 77.0 77.8 80.8 80.8 ;...
     80.8 80.8 80.8 80.8 80.8 80.8 80.8 80.1;...
     80.1 80.1 80.1 80.1 80.1 80.1 80.1 80.1];
Celsius_s = (Fs-32)*5/9;
Celsius_l = (F1-32)*5/9;
%small
Inches_Hgs = [28.5183 28.5184 28.5186 28.5333;...
             28.5270 28.5275 29.1767 29.1767 29.1767;...
             29.1767 29.1767 29.1767 29.1767 29.1767;...
             29.1767 29.2193 29.2193 29.2193 29.2193;...
             29.2193 29.2193 29.2193 29.2193 29.2193];
%large
Inches_Hgl = [28.5064 28.5024 28.4995 28.4895;...
             28.4900 28.4900 29.1764 29.1764 29.1764;...
             29.1764 29.1764 29.1764 29.1764 29.1764;...
             29.1764 29.1861 29.1861 29.1861 29.1861;...
             29.1861 29.1861 29.1861 29.1861 29.1861];
L = 0.5969; % weapon bay length (m)
D = 0.1365; % weapon bay depth (m)
Dias = 1.29*0.0254;
% missile diameter converted to m
%1.7 for large model
Ref_Areas = (pi/4)*Dias^2;
% Model reference Area (m^2)
Dial = 1.7*0.0254;
```

```

% missile diameter converted to m
%1.7 for large model
Ref_Areal = (pi/4)*Dial^2;
% Model reference Area (m^2)
    P_Pas = Inches_Hgs*3386.39 ;
    % Inches Hg converted to Pa
    Ts = Celsius + 273.15;
    % temp deg F converted to Rankine
    P_Pal = Inches_Hgl*3386.39 ;
    % Inches Hg converted to Pa
    Tl = Celsiusl + 273.15;
    % temp deg F converted to Rankine
    R = 287.05;
    % [J / kg K] Specific Gas constant for Dry Air
rhos = P_Pas/(R*Tl); % density from ideal gas law [kg/m^3]
rhol = P_Pal/(R*Tl);
gamma = 1.4; %adiabatic gas constant
mu = 1.8372E-5; % kg/ (m-s)
nu = 1.5433E-5; % m^2/s

% dynamic and kinematic viscosity values are from
%http://www.mhtl.uwaterloo.ca/old/onlinetools;...
%/airprop/airprop.html

%% Re using cavity depth for empty cavity
%%Phase I and Re using missile diameter for Phase II

Re_depths = rhos*V_inf.*D / mu;
%Re number using cavity depth
Re_diameters = rhos*V_inf.*Dias / mu;
%Re number using store diameter
Re_depthl = rhol*V_inf.*D / mu;
%Re number using cavity depth
Re_diameterl = rhol*V_inf.*Dial / mu;
%Re number using store diameter
Re_depths = Re_depths';
Re_depthl = Re_depthl';
Re_diameters = Re_diameters';
Re_diameterl = Re_diameterl';

%% Mach number for the wind tunnel velocities
%%used in the experiment
as = sqrt(gamma*R*Ts);

```

```
Machs = V_inf / as;  
a1 = sqrt(gamma*R*T1);  
Machs = V_inf / a1;
```

Phase II: Matlab Code

Reynolds Number Calculation

```
%% Calculation of Re and Mach using SI units, Phase 2
clear all;clc; close all
%small model
V_inf = [60 100 120 60 100 120 60 100 120 60 100 120];
V_inf = V_inf*0.44704; %freestream velocity converted to (m/s)
%small
Fs = [75.8 78.5 79.9 75.3 77.3 79.7 76.5 78.9 80.0;...
      74.0 76.4 78.1]; %temperature
%large
Fl = [77.4 80.1 81.2 77.3 79.8 81.7 76.2 79.6 80.7;...
      77.5 80.1 82.1];
Celsius = (Fs-32)*5/9;
Celsiusl = (Fl-32)*5/9;
%small
Inches_Hgs = [29.1909 29.1915 29.1916 29.1961;...
              29.1954 29.1999 29.1794 29.1780 29.1779;...
              29.2018 29.1995 29.1990];
%large
Inches_Hgl = [29.1779 29.1788 29.1794 29.1843;...
              29.1863 29.1863 29.1764 29.1764 29.1765;...
              29.1842 29.1838 29.1832];
L = 0.5969; % weapon bay length (m)
D = 0.1365; % weapon bay depth (m)
Dias = 1.29*0.0254;
% missile diameter converted to m %1.7 for large model
Ref_Areas = (pi/4)*Dias^2;
% Model reference Area (m^2)
Dial = 1.7*0.0254;
% missile diameter converted to m %1.7 for large model
Ref_Areal = (pi/4)*Dial^2;
% Model reference Area (m^2)
P_Pas = Inches_Hgs*3386.39 ;
% Inches Hg converted to Pa
Ts = Celsius + 273.15;
% temp deg F converted to Rankine
P_Pal = Inches_Hgl*3386.39 ;
% Inches Hg converted to Pa
Tl = Celsiusl + 273.15;
% temp deg F converted to Rankine
R = 287.05;
```

```

        % [J / kg K] Specific Gas constant for Dry Air
rhos = P_Pas/(R*Tl);
% density from ideal gas law [kg/m^3]
rhol = P_Pal/(R*Tl);
gamma = 1.4; %adiabatic gas constant
mu = 1.8372E-5; % kg/ (m-s)
nu = 1.5433E-5; % m^2/s

% dynamic and kinematic viscosity values are from
%http://www.mhtl.uwaterloo.ca/old/onlinetools/airprop/airprop.html

%% Re using cavity depth for empty cavity Phase I
%%and Re using missile diameter for Phase II
Re_depths = rhos*V_inf.*D / mu;
%Re number using caviy depth
Re_diameters = rhos*V_inf.*Dias / mu;
%Re number using store diameter
Re_depthl = rhol*V_inf.*D / mu;
%Re number using caviy depth
Re_diameterl = rhol*V_inf.*Dial / mu;
%Re number using store diameter
Re_depths = Re_depths';
Re_depthl = Re_depthl';
Re_diameters = Re_diameters';
Re_diameterl = Re_diameterl';

%% Mach number for the wind tunnel velocities
%%used in the experiment
as = sqrt(gamma*R*Ts);
Machs = V_inf / as;
al = sqrt(gamma*R*Tl);
Machs = V_inf / al;

```

Galil Codes

Initializing Motor A

BA A
BMA=30720
TLA=6.75
TKA=9
ERA=5000
AUA=1
OEA=1
BZA=4
MTA=1
KDA=350.0
KPA=20
KIA=2
EN

Initializing Motor B

BA B
BMB=30720
TLB=6.75
TKB=9
ERB=10000
AUB=1
OEB=1
BZB=4
MTB=1
KDB=350
KPB=20
KIB=2
EN

Jog Down

```
#homeC; 'Home Routine
SH B
JG ,25000
BG B; 'Begin motion
AM B; 'After motion
MO A; MO B;
EN
```

Jog Up

```
#gravity
SH B
AC ,19620000 ;'acceleration
DC ,10240000 ;'deceleration
SP , rate ;'speed
PR ,-77000 ;'distance
BG B;' Begin the move
AM B;' After the move is over
EN
```

Jog Shear Layer

```
#gravity
SH B
AC ,19620000 ;'acceleration
DC ,10240000 ;'deceleration
SP , rate ;'speed
PR ,-40000 ;'distance
BG B;' Begin the move
AM B;' After the move is over
EN
```

Linear Jog Timing 1

i = 0

BA B; 'initializes B

BMB=30720;

TLB=6.75;

TKB=9;

ERB=10000;

AUB=1;

OEB=1;

BZB=4;

MTB=1;

KDB=350;

KPB=20;

KIB=2;

AMB;

;' pulls the horizontal motor out of the tube every time no matter
'where the end position is

PRA = 80000; 'sets position relative, + is to the right, - is to
'the left, max is 80000 in either direction

SHA; 'turns on motor

BGA; 'begins motion, actually executes motion

AMA; 'tells the computer there are more commands after the motion

#homeA; 'Home Routine

SH A

JG 25000

FI A; 'Find index

BG A; 'Begin motion

AM A; 'After motion

DP 0; 'set current position to 0

MG "Found Index"

WT 1000

#set

CO 2

CB 31;CB 32;

#homeB; 'Home Routine

SH B

JG ,25000

FI B; 'Find index

```

BG B; 'Begin motion
AM B; 'After motion
DP ,0; 'set current position to 0
MG "Found Index"

#reposit; 'Reposition to center
SH A
PR -19532 ; 'move to position
BG A; 'Begin Motion
AM A; 'After Motion
DP 0; 'Set current position to 0
MG "New Zero"

#sin;'Sine Wave Motion
SH A;      'turns on motor A
amp= 24736; 'amplitude in counts
freq= 5.0;  'frequency in Hz
rate= freq*amp*6.2832;    'calculates correct speed
VS rate
'set VA and VD if non-standard accel and decel are needed

#init
GO = 1
' sine wave on "A" axis
VM AN
CR amp,0,360; '1 sine wave to get started
BG S;      'starts motion

#loop
CR amp,0,360; 'add 1 sine wave continuously
VE

#wait
var1 = _LM;
var2 = _LM-var1;

IF (var2 > 0)
i = i + 1;
ENDIF

IF (i = 5)
SB 31
ENDIF

```

```

IF (i = 7)
counter = 1;
var4 = 1;
#while
var3 = _TPA; 'current position
diff = var3 - var4;
IF (diff > 0)&((_TPA<-24500)&(_TPA>-25000))
SB 32; XQ #gravity,1
counter = 2;
ENDIF
var4 = var3; 'previous position
JP #while,(counter = 1);
ENDIF

IF @OUT[32]=0
JP #loop,_LM>1;    '_LM shows how many segments are
'available in buffer
JP #wait,G0=1;    'continue adding sine waves until
'G0=0 is entered
ELSE
WT 3000; CB 32; CB 31; WT 5000; ST; JP #homeC;
ENDIF

#gravity
SH B
AC ,19620000 ;'acceleration
DC ,10240000 ;'deceleration
SP , rate ;'speed
PR ,-77000 ;'distance
BG B;' Begin the move
AM B;' After the move is over
EN

#homeC; 'Home Routine
SH B
JG ,25000
BG B; 'Begin motion
AM B; 'After motion
MO A; MO B;
EN

```

Linear Jog Timing 2: Minrange

i = 0

BA B; 'initializes B

BMB=30720;

TLB=6.75;

TKB=9;

ERB=10000;

AUB=1;

OEB=1;

BZB=4;

MTB=1;

KDB=350;

KPB=20;

KIB=2;

AMB;

;' pulls the horizontal motor out of the tube every time no matter
'where the end position is

PRA = 80000; 'sets position relative, + is to the right, - is to
'the left, max is 80000 in either direction

SHA; 'turns on motor

BGA; 'begins motion, actually executes motion

AMA; 'tells the computer there are more commands after the motion

#homeA; 'Home Routine

SH A

JG 25000

FI A; 'Find index

BG A; 'Begin motion

AM A; 'After motion

DP 0; 'set current position to 0

MG "Found Index"

WT 1000

#set

CO 2

CB 31;CB 32;

#homeB; 'Home Routine

SH B

JG ,25000

FI B; 'Find index

```

BG B; 'Begin motion
AM B; 'After motion
DP ,0; 'set current position to 0
MG "Found Index"

#reposit; 'Reposition to center
SH A
PR -19532 ; 'move to position
BG A; 'Begin Motion
AM A; 'After Motion
DP 0; 'Set current position to 0
MG "New Zero"

#sin;'Sine Wave Motion
SH A;      'turns on motor A
amp= 24736; 'amplitude in counts
freq= 5.0;  'frequency in Hz
rate= freq*amp*6.2832;    'calculates correct speed
VS rate
'set VA and VD if non-standard accel and decel are needed

#init
GO = 1
' sine wave on "A" axis
VM AN
CR amp,0,360; '1 sine wave to get started
BG S;      'starts motion

#loop
CR amp,0,360; 'add 1 sine wave continuously
VE

#wait
var1 = _LM;
var2 = _LM-var1;

IF (var2 > 0)
i = i + 1;
ENDIF

IF (i = 5)
SB 31
ENDIF

```

```

IF ((i = 7)&(_TPA > -400))
SB 32; XQ #gravity,1;
ENDIF

IF @OUT[32]=0
JP #loop,_LM>1;    '_LM shows how many segments are
'available in buffer
JP #wait,G0=1;    'continue adding sine waves until
'G0=0 is entered
ELSE
WT 2000; CB 32; CB 31; WT 5000; ST; JP #homeC;
ENDIF

#gravity
SH B
AC ,19620000 ;'acceleration
DC ,10240000 ;'deceleration
SP , rate ;'speed
PR ,-77000 ;'distance
BG B;' Begin the move
AM B;' After the move is over
EN

#homeC; 'Home Routine
SH B
JG ,25000
BG B; 'Begin motion
AM B; 'After motion
MO A; MO B;
EN

```

Linear Jog Timing 3

i = 0

BA B; 'initializes B

BMB=30720;

TLB=6.75;

TKB=9;

ERB=10000;

AUB=1;

OEB=1;

BZB=4;

MTB=1;

KDB=350;

KPB=20;

KIB=2;

AMB;

;' pulls the horizontal motor out of the tube every time no matter
'where the end position is

PRA = 80000; 'sets position relative, + is to the right, - is to
'the left, max is 80000 in either direction

SHA; 'turns on motor

BGA; 'begins motion, actually executes motion

AMA; 'tells the computer there are more commands after the motion

#homeA; 'Home Routine

SH A

JG 25000

FI A; 'Find index

BG A; 'Begin motion

AM A; 'After motion

DP 0; 'set current position to 0

MG "Found Index"

WT 1000

#set

CO 2

CB 31;CB 32;

#homeB; 'Home Routine

SH B

JG ,25000

FI B; 'Find index

```

BG B; 'Begin motion
AM B; 'After motion
DP ,0; 'set current position to 0
MG "Found Index"

#reposit; 'Reposition to center
SH A
PR -19532 ; 'move to position
BG A; 'Begin Motion
AM A; 'After Motion
DP 0; 'Set current position to 0
MG "New Zero"

#sin;'Sine Wave Motion
SH A;      'turns on motor A
amp= 24736; 'amplitude in counts
freq= 5.0;  'frequency in Hz
rate= freq*amp*6.2832;    'calculates correct speed
VS rate
'set VA and VD if non-standard accel and decel are needed

#init
GO = 1
' sine wave on "A" axis
VM AN
CR amp,0,360; '1 sine wave to get started
BG S;      'starts motion

#loop
CR amp,0,360; 'add 1 sine wave continuously
VE

#wait
var1 = _LM;
var2 = _LM-var1;

IF (var2 > 0)
i = i + 1;
ENDIF

IF (i = 5)
SB 31
ENDIF

```

```

IF (i = 7)
counter = 1;
var4 = -50000;
#while
var3 = _TPA; 'current position
diff = var3 - var4;
IF (diff < 0)&((_TPA<-24500)&(_TPA>-25000))
SB 32; XQ #gravity,1
counter = 2;
ENDIF
var4 = var3; 'previous position
JP #while,(counter = 1);
ENDIF

IF @OUT[32]=0
JP #loop,_LM>1;    '_LM shows how many segments are
'available in buffer
JP #wait,G0=1;    'continue adding sine waves until
'G0=0 is entered
ELSE
WT 3000; CB 32; CB 31; WT 5000; ST; JP #homeC;
ENDIF

#gravity
SH B
AC ,19620000 ;'acceleration
DC ,10240000 ;'deceleration
SP , rate ;'speed
PR ,-77000 ;'distance
BG B;' Begin the move
AM B;' After the move is over
EN

#homeC; 'Home Routine
SH B
JG ,25000
BG B; 'Begin motion
AM B; 'After motion
MO A; MO B;
EN

```

Linear Jog Timing 4: Maxrange

i = 0

BA B; 'initializes B

BMB=30720;

TLB=6.75;

TKB=9;

ERB=10000;

AUB=1;

OEB=1;

BZB=4;

MTB=1;

KDB=350;

KPB=20;

KIB=2;

AMB;

;' pulls the horizontal motor out of the tube every time no matter
'where the end position is

PRA = 80000; 'sets position relative, + is to the right, - is to
'the left, max is 80000 in either direction

SHA; 'turns on motor

BGA; 'begins motion, actually executes motion

AMA; 'tells the computer there are more commands after the motion

#homeA; 'Home Routine

SH A

JG 25000

FI A; 'Find index

BG A; 'Begin motion

AM A; 'After motion

DP 0; 'set current position to 0

MG "Found Index"

WT 1000

#set

CO 2

CB 31;CB 32;

#homeB; 'Home Routine

SH B

JG ,25000

FI B; 'Find index

```

BG B; 'Begin motion
AM B; 'After motion
DP ,0; 'set current position to 0
MG "Found Index"

#reposit; 'Reposition to center
SH A
PR -19532 ; 'move to position
BG A; 'Begin Motion
AM A; 'After Motion
DP 0; 'Set current position to 0
MG "New Zero"

#sin;'Sine Wave Motion
SH A;      'turns on motor A
amp= 24736; 'amplitude in counts
freq= 5.0;  'frequency in Hz
rate= freq*amp*6.2832;    'calculates correct speed
VS rate
'set VA and VD if non-standard accel and decel are needed

#init
GO = 1
' sine wave on "A" axis
VM AN
CR amp,0,360; '1 sine wave to get started
BG S;      'starts motion

#loop
CR amp,0,360; 'add 1 sine wave continuously
VE

#wait
var1 = _LM;
var2 = _LM-var1;

IF (var2 > 0)
i = i + 1;
ENDIF

IF (i = 5)
SB 31
ENDIF

```

```

IF ((i = 7)&(_TPA < -49000))
SB 32; XQ #gravity,1;
ENDIF

IF @OUT[32]=0
JP #loop,_LM>1;    '_LM shows how many segments are
'available in buffer
JP #wait,G0=1;    'continue adding sine waves until
'G0=0 is entered
ELSE
WT 2000; CB 32; CB 31; WT 5000; ST; JP #homeC;
ENDIF

#gravity
SH B
AC ,19620000 ;'acceleration
DC ,10240000 ;'deceleration
SP , rate ;'speed
PR ,-77000 ;'distance
BG B;' Begin the move
AM B;' After the move is over
EN

#homeC; 'Home Routine
SH B
JG ,25000
BG B; 'Begin motion
AM B; 'After motion
MO A; MO B;
EN

```

Appendix D. Drawings of Models

Index of Figures in Appendix D

Drawings

(pg 447)

Drawings

Drawings

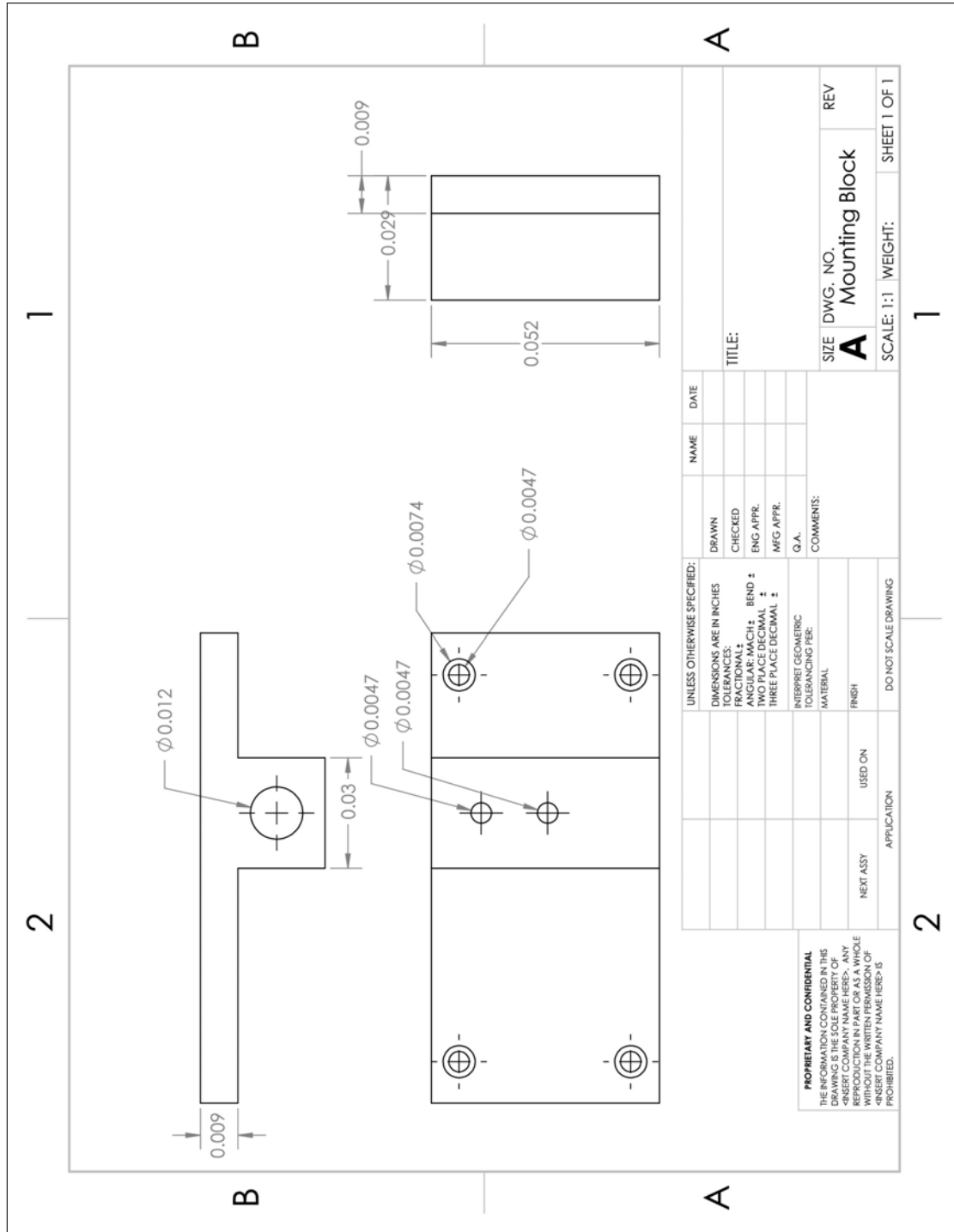


Figure 285: Drawing of Mounting Block for vertical rod and linear motor

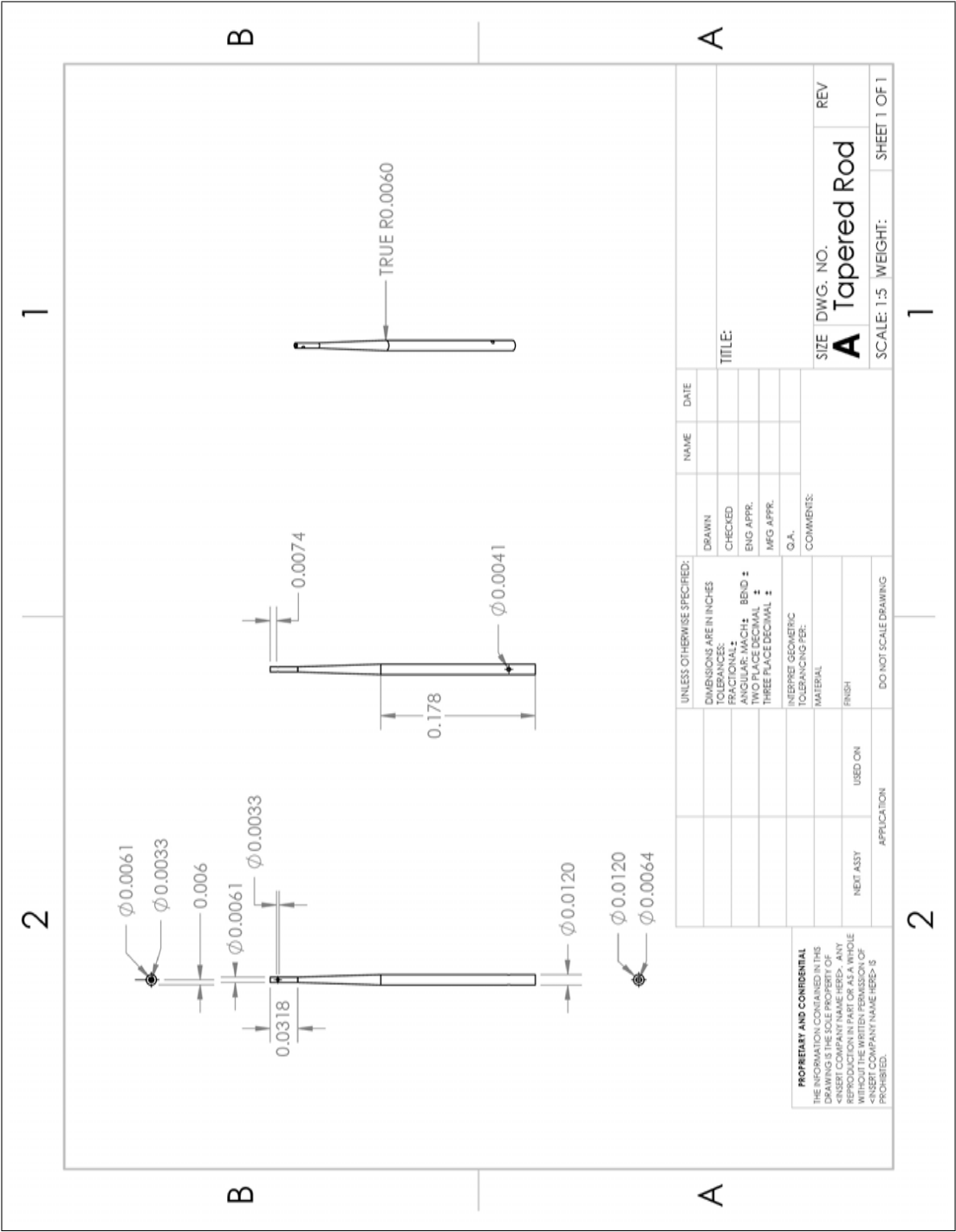


Figure 286: Drawing of Tapered Rod for vertical rod and linear motor

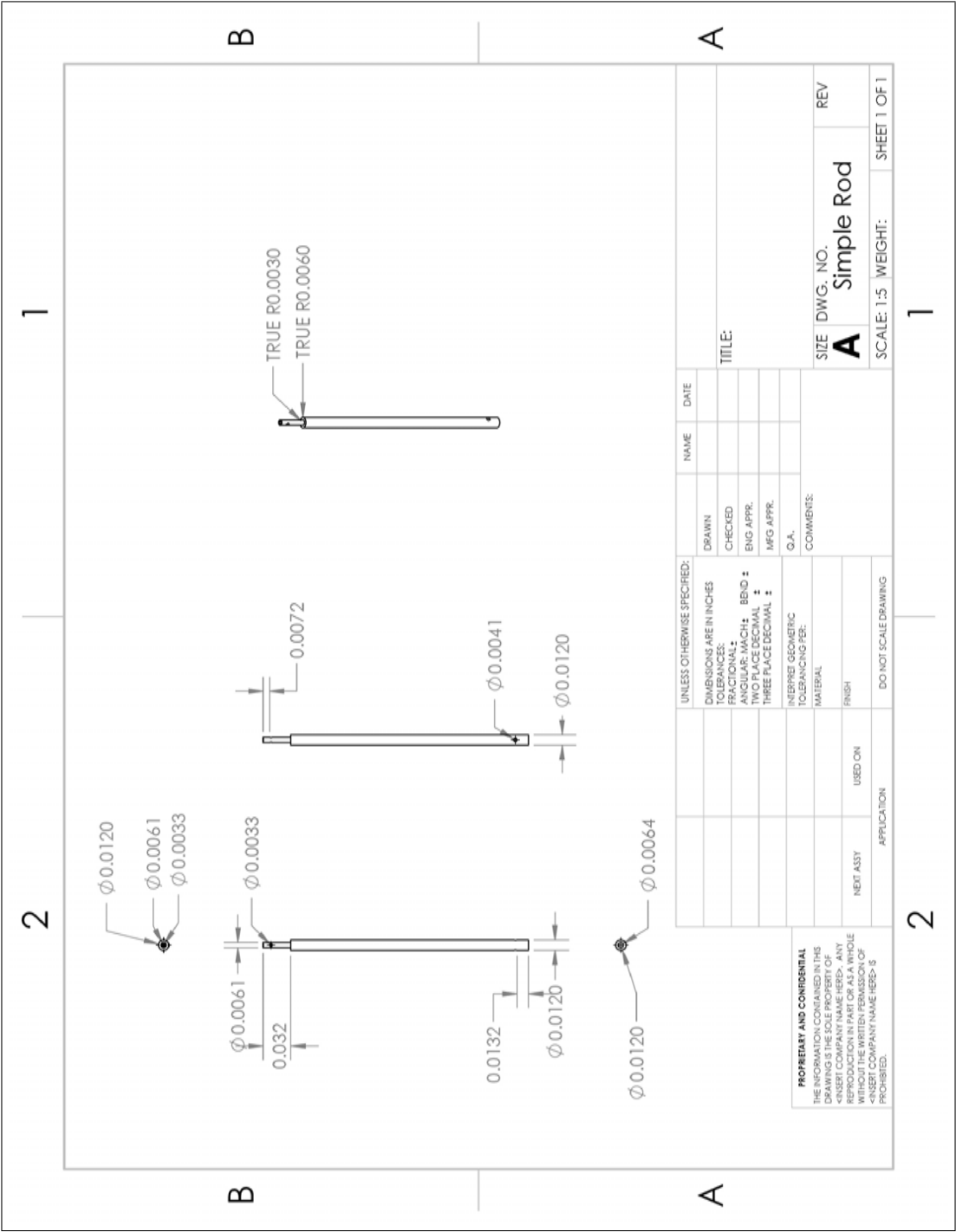


Figure 287: Drawing of Simple Rod for vertical rod and linear motor

Bibliography

1. M. Purdon, C. Hetreed, and M. Hudson, “F-35 Pre-Flight Store Separation Analyses: Innovative Techniques for Affordability,” in *47th AIAA Aerospace Sciences Meeting including The New Horizons Forum and Aerospace Exposition*, 2009.
2. K. Keen, “Equations for Store Separation Motion Simulations and Instrumented Model Data Reduction,” no. AEDC-TR-95-12, 1996.
3. L. N. Cattafesta III, D. R. Williams, C. W. Rowley, and F. S. Alvi, “Review of Active Control of Flow-Induced Cavity Resonance,” *33rd AIAA Fluid Dynamics Conference*, no. June, pp. 1–20, 2003.
4. R. A. Johnson, M. J. Stanek, and J. E. Grove, “Store Separation Trajectory Deviations Due to Unsteady Weapons Bay Aerodynamics,” *46th AIAA Aerospace Sciences Meeting and Exhibit*, no. January, pp. 1–15, 2008.
5. A. D. Bower, *Investigation of Dynamic Store Separation Out of a Weapons Bay Cavity Utilizing a Low Speed Wind Tunnel*. PhD thesis, Air Force Institute of Technology, 2017.
6. J. Sellers, *Force and Moment Measurements Applicable to a Flexible Weapons System*. PhD thesis, Air Force Institute of Technology, 2016.
7. Z. Probst, M. F. Reeder, R. Johnson, and J. Grove, “Flight Test Experiments on Cavity Flow in a SUU-41 Pod,” *AIAA Flight Testing Conference*, no. June, pp. 1–16, 2016.
8. M. L. Wood, *Leading Edge Oscillatory Blowing: Influence on Subsonic Cavity Flow and Application in Synchronized Dynamic Store Separation*. PhD thesis, Air Force Institute of Technology, 2018.
9. K. Krishnamurty, “Acoustic Radiation from Two-dimensional Rectangular Cutouts in Aerodynamic Surfaces,” *NACA*, no. 3487, 1955.
10. J. Rossiter, “Wind-tunnel experiments on the flow over rectangular cavities at subsonic and transonic speeds,” tech. rep., Ministry of Aviation, London, 1966.
11. G. B. Brown, “The vortex motion causing edge tones,” *Proceedings of the Physical Society*, vol. 49, no. 5, pp. 493–507, 1937.
12. H. H. Heller, D. G. Holmes, and E. E. Covert, “Flow-induced pressure oscillations in shallow cavities,” *Journal of Sound and Vibration*, vol. 18, no. 4, pp. 545–553, 1971.
13. H. H. Heller and D. B. Bliss, “The physical mechanism of flow-induced pressure fluctuations in cavities and concepts for their suppression,” *AIAA paper*, vol. 491, 1975.

14. D. B. Bliss and R. E. Hayden, "Landing Gear and Cavity Noise Prediction," tech. rep., 1976.
15. D. Rockwell and E. Naudascher, "Review - Self-Sustaining Oscillations of Flow Past Cavities," *Journal of Fluids Engineering*, vol. 100, no. June, p. 14, 1978.
16. R. Stallings and F. Wilcox, "Experimental Cavity Pressure Distributions at Supersonic Speeds," *NASA*, vol. 40, no. 4, 1987.
17. K. Yugulis, S. Hansford, J. W. Gregory, and M. Samimy, "Control of High Subsonic Cavity Flow Using Plasma Actuators," *AIAA Journal*, vol. 52, no. 7, pp. 1542–1554, 2014.
18. M. B. Tracy, E. B. Plentovich, and R. J. Stallings, "Experimental cavity pressure measurements at subsonic and transonic speeds," tech. rep., 1993.
19. M. B. Tracy and E. B. Plentovich, "Cavity Unsteady-Pressure Measurements at Subsonic and Transonic Speeds," tech. rep., 1997.
20. A. Cenko and P. River, "Unsteady Weapon Bay Aerodynamics - Urban Legend or Flight Clearance Nightmare," *Sciences-New York*, no. January, pp. 1–13, 2008.
21. P. Panickar and G. Raman, "Understanding the Mechanism of Cavity Resonance Suppression Using a Cylindrical Rod in Crossflow," *46th AIAA Aerospace Sciences Meeting and Exhibit*, no. January, 2008.
22. V. Shalaev, A. Fedorov, and N. Malmuth, "Dynamics of slender bodies separating from rectangular cavities," *15th AIAA Computational Fluid Dynamics Conference*, no. June, 2001.
23. Freeman J., Keen J., and Jolly B., "Quick-Reaction Computational Fluid Dynamics Support of Aircraft Store Compatibility," *ITEA Aircraft Store Compatibility Symposium*, pp. 19–24, 2006.
24. J. Jordan and A. Denny, "Approximation methods for computational trajectory predictions of a store released from a bay," *15th Applied Aerodynamics Conference*, 1997.
25. C. J. Coley and A. J. Lofthouse, "Correlation of Weapon Bay Resonance and Store Unsteady Force and Moment Loading," *AIAA*, no. 2012-0415, 2012.
26. L. H. Schindel, "Store Separation," tech. rep., National Technical Information Services, 1975.
27. L. Cattafesta, F. Alvi, D. Williams, and C. Rowley, "Review of Active Control of Flow-Induced Cavity Oscillations (Invited)," *33rd AIAA Fluid Dynamics Conference and Exhibit*, no. June, pp. 1–21, 2003.

28. J. Grove, L. Shaw, J. Leugers, and G. Akroyd, "USAF/RAAF F-111 flight test with active separation control," *AIAA paper*, no. January, 2003.
29. Y. Zhang, Y. Sun, N. Arora, and L. Cattafesta, "Suppression of Cavity Flow Oscillations via Three-Dimensional Steady Blowing," *American Institute of Aeronautics and Astronautics*, vol. 57, no. 1, pp. 90–105, 2018.
30. J. C. Lancaster, "Characterization of a Robotic Manipulator for Dynamic Wind Tunnel Applications," tech. rep., AFIT, 2015.
31. B. Stevens and F. Lewis, *Aircraft Control and Simulation*. Hoboken, NJ: John Wiley & Sons, second ed., 2003.
32. G. Lei, G. Xu, X. Zhang, Y. Zhang, Z. Song, and W. Xu, "Study on Dynamic Monitoring of Wire Rope Tension Based on the Particle Damping Sensor," *Sensors*, 2019.
33. D. Esposito, E. Andreozzi, A. Fratini, G. D. Gargiulo, S. Savino, V. Niola, and P. Bifulco, "A Piezoresistive Sensor to Measure Muscle Contraction and Mechanomyography," *Sensors*, 2018.
34. D. Giovanelli and E. Farella, "Force Sensing Resistor and Evaluation of Technology for Wearable Body Pressure Sensing," *Journal of Sensors*, 2016.
35. J. Pattinson, M. H. Lowenberg, and M. G. Goman, "Multi-Degree-of-Freedom Wind-Tunnel Maneuver Rig for Dynamic Simulation and Aerodynamic Model Identification," *Journal of Aircraft*, vol. 50, no. 2, pp. 551–566, 2013.
36. A. Bergmann, A. Huebner, and T. Loeser, "Experimental and numerical research on the aerodynamics of unsteady moving aircraft," *Progress in Aerospace Sciences*, vol. 44, no. 2, pp. 121–137, 2008.
37. B. Binkley and A. Vanderwyst, "Application of Statistical Techniques to Analyze and Model Trajectory Envelopes for Subscale Store Separation Testing," *30th AIAA Applied Aerodynamics Conference*, no. June, 2012.
38. K. Hufnagel and G. Schewe, *Springer Handbook of Experimental Fluid Mechanics - Force and Moment Measurement*. Springer Berlin Heidelberg, 2007.
39. E. T. Bird, A. J. Merrell, B. K. Anderson, C. N. Newton, P. G. Rosquist, D. T. Fullwood, A. E. Bowden, and M. K. Seeley, "Vibration monitoring via nanocomposite piezoelectric foam bushings," *Smart Materials and Structures*, 2016.
40. L. P. Erm, "Development and Use of a Dynamic-Testing Capability for the DSTO Water Tunnel," *Defence Science and Technology Organisation*, 2006.
41. Ultimaker, "Ultimaker 2+ Specifications Sheet," 2012.

42. Ultimaker, “Ultimaker 3 Specification Sheet,” pp. 1–4, 2009.
43. Ultimaker, “Technical data sheet PLA,” pp. 1–3, 2008.
44. Z. A. Probst, “PROJECT HAVE WASSP,” tech. rep., Air Force Institute of Technology, 2015.
45. RLS, “LM13 linear magnetic encoder system,” no. 11, p. 10, 2011.
46. G. M. Control, “GALIL Manual:DMC-30000,” 2016.
47. Galil, “Controllers: DMC - 4000,” tech. rep.
48. “NANO25,” tech. rep., ATI, 2013.
49. J. B. A. Sellers, A. Bower, I. Maatz, and M. F. Reeder, “Dynamic Measurement of Forces and Moments with the Motion Test Apparatus,”

REPORT DOCUMENTATION PAGE					Form Approved OMB No. 0704-0188	
<p>The public reporting burden for this collection of information is estimated to average 1 hour per response, including the time for reviewing instructions, searching existing data sources, gathering and maintaining the data needed, and completing and reviewing the collection of information. Send comments regarding this burden estimate or any other aspect of this collection of information, including suggestions for reducing this burden to Department of Defense, Washington Headquarters Services, Directorate for Information Operations and Reports (0704-0188), 1215 Jefferson Davis Highway, Suite 1204, Arlington, VA 22202-4302. Respondents should be aware that notwithstanding any other provision of law, no person shall be subject to any penalty for failing to comply with a collection of information if it does not display a currently valid OMB control number. PLEASE DO NOT RETURN YOUR FORM TO THE ABOVE ADDRESS.</p>						
1. REPORT DATE (DD-MM-YYYY)		2. REPORT TYPE		3. DATES COVERED (From — To)		
01-03-2019		Master's Thesis		Oct 2017 — Mar 2019		
4. TITLE AND SUBTITLE Influence of Leading Edge Oscillatory Blowing on Time-Accurate Dynamic Store Separation				5a. CONTRACT NUMBER		
				5b. GRANT NUMBER		
				5c. PROGRAM ELEMENT NUMBER		
6. AUTHOR(S) Saunders, Ryan G, 2d Lt, USAF				5d. PROJECT NUMBER 18Y245		
				5e. TASK NUMBER		
				5f. WORK UNIT NUMBER		
7. PERFORMING ORGANIZATION NAME(S) AND ADDRESS(ES) Air Force Institute of Technology Graduate School of Engineering and Management (AFIT/EN) 2950 Hobson Way WPAFB OH 45433-7765				8. PERFORMING ORGANIZATION REPORT NUMBER AFIT-ENY-MS-19-M-244		
9. SPONSORING / MONITORING AGENCY NAME(S) AND ADDRESS(ES) AFOSR/RTA 875 North Randolph Street, Suite 325 Arlington, VA 22203 COMM 703-588-1772 Email: brett.pokines.1@us.af.mil				10. SPONSOR/MONITOR'S ACRONYM(S)		
				11. SPONSOR/MONITOR'S REPORT NUMBER(S)		
12. DISTRIBUTION / AVAILABILITY STATEMENT Distribution Statement A: Approved for Public Release; distribution unlimited.						
13. SUPPLEMENTARY NOTES This work is declared a work of the U.S. Government and is not subject to copyright protection in the United States.						
14. ABSTRACT The primary objective of this research is to support the static and dynamic characterization and the time-accurate dynamic load data acquisition of store separation from a cavity with leading edge oscillatory blowing. Developing an understanding of, and potentially controlling, pitch bifurcation of a store release is a motivation for this research. The apparatus and data acquisition system was used in a two-part experiment to collect both static and dynamic testing data in the AFIT low speed wind tunnel in speeds of 60, 100, and 120 mph, from Reynolds numbers varying from 5.5e4 to 4.6e5, depending on reference length and tunnel speed. An ATI Nano25 6-DOF force and moment sensor was used to produce time-accurate force and moment measurements. Common aerodynamic trends were observed in the comparison of trials with different store model sizes and angles of attack which align with established aerodynamic analysis. The 5 Hz oscillatory flow control, using multiple flow control approaches, had a direct impact on the forces experienced by the mission store and a 5 Hz pattern in the data was observed in static positions as well as before and after store release. Data collected for the normal force, pitch moment, and axial force coefficients, depict the aerodynamic loads of a store release from a cavity environment with a developed shear layer. Phase manipulation of relative linear motor positions allowed for data collection under varying store release conditions and timings. A 180° out of phase phenomena was observed in the normal force coefficient in cases where the position of the motor was also 180° out of phase.						
15. SUBJECT TERMS Cavity Environment; Flow Control; Fluidic Diodes; Leading Edge Oscillatory Blowing; Low-Speed Wind Tunnel; Pitch Bifurcation; Store Release; Synchronized Dynamic Store Release; Time-Accurate Data Collection; Wind Tunnel; Weapons Bay Cavity						
16. SECURITY CLASSIFICATION OF:			17. LIMITATION OF ABSTRACT	18. NUMBER OF PAGES	19a. NAME OF RESPONSIBLE PERSON	
a. REPORT	b. ABSTRACT	c. THIS PAGE			Dr. Mark F. Reeder, AFIT/ENY	
U	U	U	UU	455	19b. TELEPHONE NUMBER (include area code) (937) 255-3636, x4530; mark.reeder@afit.edu	